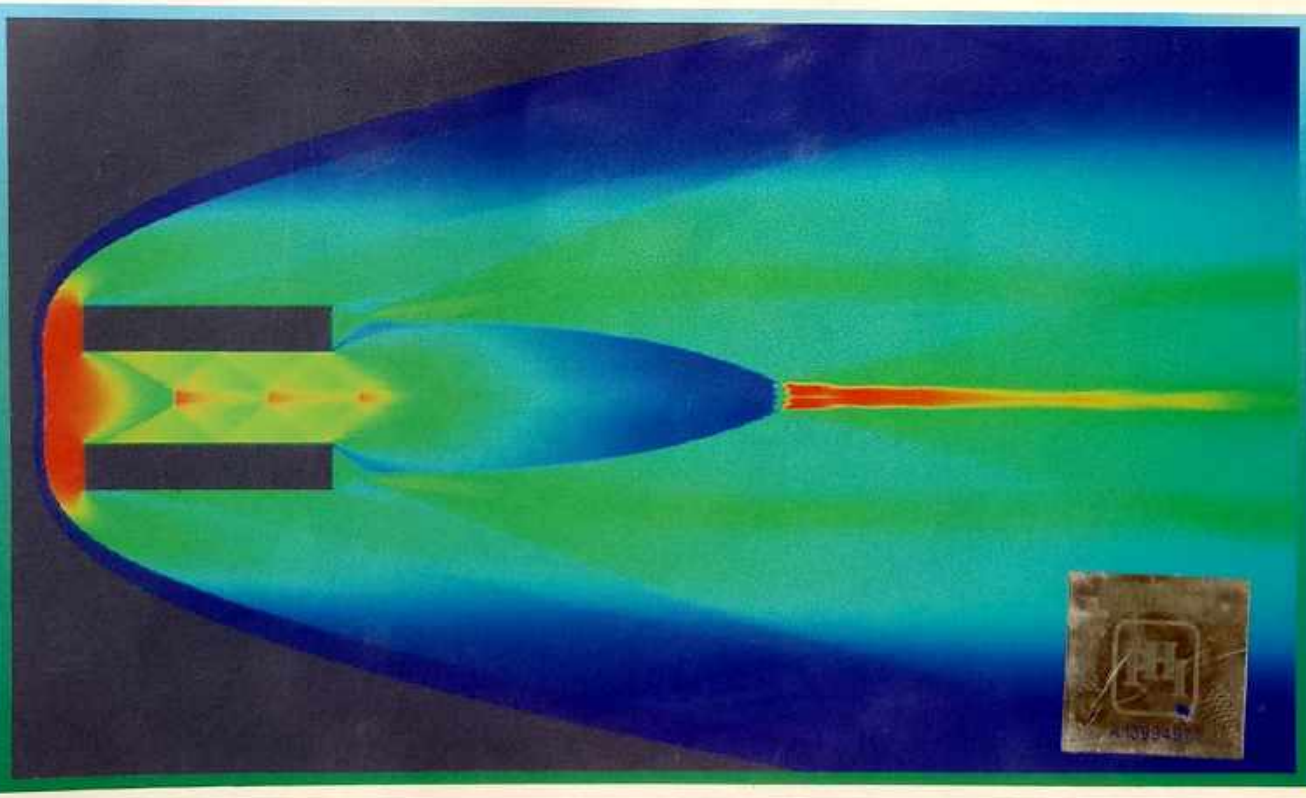
Eastern Economy Edition

GAS DYNAMICS

Sixth Edition



Ethirajan Rathakrishnan

Scanned by CamScanner

GAS DYNAMICS

SIXTH EDITION

Ethirajan Rathakrishnan
Indian Institute of Technology Kanpur

COMPLIMENTARY COPY
NOT FOR SALE

PHI Learning Private Limited
Delhi-110092
2017

Scanned by CamScanner

₹ 495.00

GAS DYNAMICS, Sixth Edition
Ethirajan Rathakrishnan

© 2017 by PHI Learning Private Limited, Delhi. All rights reserved. No part of this book may be reproduced in any form, by mimeograph or any other means, without permission in writing from the publisher.

ISBN-978-81-203-5316-9

The export rights of this book are vested solely with the publisher.

Fifteenth Printing (Sixth Edition) ... ... January, 2017

Published by Asoke K. Ghosh, PHI Learning Private Limited, Rimjhim House, 111, Patparganj Industrial Estate, Delhi-110092 and Printed by Rajkamal Electric Press, Plot No. 2, Phase IV, HSIDC, Kundli-131028, Sonepat, Haryana.

Scanned by CamScanner

To
my parents
Mr. Thammanur Shunmugam Ethirajan
and
Mrs. Aandaal Ethirajan

Scanned by CamScanner

Contents

Preface ..... *ix*
Preface to the Fifth Edition ..... *xi*
Preface to the Fourth Edition ..... *xiii*
Preface to the Third Edition ..... *xv*
Preface to the Second Edition ..... *xvii*
Preface to the First Edition ..... *xix*

1. Some Preliminary Thoughts 1–17

1.1 Gas Dynamics—A Brief History 1
1.2 Compressibility 2
1.3 Supersonic Flow—What Is It? 5
1.4 Speed of Sound 6
1.5 Temperature Rise 10
1.6 Mach Angle 12
1.7 Summary 15

2. Basic Equations of Compressible Flow 18–42

2.1 Thermodynamics of Fluid Flow 18
2.2 First Law of Thermodynamics (Energy Equation) 19
2.3 The Second Law of Thermodynamics (Entropy Equation) 23
2.4 Thermal and Calorical Properties 24
2.5 The Perfect Gas 26
2.6 Summary 35
Problems 39

3. Wave Propagation 43–46

3.1 Introduction 43
3.2 Wave Propagation 43
3.3 Velocity of Sound 44
3.4 Subsonic and Supersonic Flows 44
3.5 Summary 45

4. Steady One-Dimensional Flow 47–109

4.1 Introduction 47
4.2 The Fundamental Equations 47
4.3 Discharge from a Reservoir 51
4.4 Streamtube Area–Velocity Relation 61

Scanned by CamScanner

4.5 De Laval Nozzle 64
4.6 Supersonic Flow Generation 75
4.7 Diffusers 85
4.8 Dynamic Head Measurement in Compressible Flow 88
4.9 Pressure Coefficient 94
4.10 Summary 95
Problems 99

5. Normal Shock Waves 110–170

5.1 Introduction 110
5.2 Equations of Motion for a Normal Shock Wave 111
5.3 The Normal Shock Relations for a Perfect Gas 112
5.4 Change of Stagnation or Total Pressure across the Shock 116
5.5 Hugoniot Equation 123
5.6 The Propagating Shock Wave 126
5.7 Reflected Shock Wave 135
5.8 Centred Expansion Wave 143
5.9 Shock Tube 149
5.10 Summary 161
Problems 164

6. Oblique Shock and Expansion Waves 171–248

6.1 Introduction 171
6.2 Oblique Shock Relations 172
6.3 Relation between β and θ 177
6.4 Shock Polar 183
6.5 Supersonic Flow over a Wedge 187
6.6 Weak Oblique Shocks 189
6.7 Supersonic Compression 191
6.8 Supersonic Expansion by Turning 192
6.9 The Prandtl–Meyer Expansion 194
6.10 Simple and Nonsimple Regions 201
6.11 Reflection and Intersection of Shocks and Expansion Waves 202
6.12 Detached Shocks 218
6.13 Mach Reflection 219
6.14 Shock-Expansion Theory 223
6.15 Thin Aerofoil Theory 228
6.16 Summary 237
Problems 240

7. Potential Equation for Compressible Flow 249–270

7.1 Introduction 249
7.2 Crocco's Theorem 249
7.3 The General Potential Equation for Three-Dimensional Flow 253
7.4 Linearization of the Potential Equation 255

Scanned by CamScanner

7.5 Potential Equation for Bodies of Revolution 260
7.6 Boundary Conditions 263
7.7 Pressure Coefficient 265
7.8 Summary 266
Problems 270

8. Similarity Rule 271–308

8.1 Introduction 271
8.2 Two-Dimensional Flow: The Prandtl–Glauert Rule for Subsonic Flow 271
8.3 Prandtl–Glauert Rule for Supersonic Flow: Versions I and II 279
8.4 The von Karman Rule for Transonic Flow 282
8.5 Hypersonic Similarity 285
8.6 Three-Dimensional Flow: The Gothert Rule 288
8.7 Critical Mach Number 298
8.8 Summary 303
Problems 307

9. Two-Dimensional Compressible Flows 309–321

9.1 Introduction 309
9.2 General Linear Solution for Supersonic Flow 310
9.3 Flow along a Wave-Shaped Wall 315
9.4 Summary 319
Problems 320

10. Prandtl–Meyer Flow 322–328

10.1 Introduction 322
10.2 Thermodynamic Considerations 323
10.3 Prandtl–Meyer Expansion Fan 323
10.4 Reflections 326
10.5 Summary 327
Problems 327

11. Flow with Friction and Heat Transfer 329–358

11.1 Introduction 329
11.2 Flow in Constant-Area Duct with Friction 329
11.3 Adiabatic, Constant-Area Flow of a Perfect Gas 331
11.4 Flow with Heating or Cooling in Ducts 341
11.5 Summary 350
Problems 353

12. Method of Characteristics 359–383

12.1 Introduction 359
12.2 The Concepts of Characteristics 359
12.3 The Compatibility Relation 360
12.4 The Numerical Computational Method 363
12.5 Theorems for Two-Dimensional Flow 371

Scanned by CamScanner

12.6 Numerical Computation with Weak Finite Waves 373
12.7 Design of Supersonic Nozzle 377
12.8 Summary 382

13. Measurements in Compressible Flow 384–456

13.1 Introduction 384
13.2 Pressure Measurements 384
13.3 Temperature Measurements 391
13.4 Velocity and Direction 395
13.5 Density Problems 397
13.6 Compressible Flow Visualization 397
13.7 High-Speed Wind Tunnels 415
13.8 Instrumentation and Calibration of Wind Tunnels 441
13.9 Summary 448
Problems 456

14. Rarefied Gas Dynamics 457–464

14.1 Introduction 457
14.2 Knudsen Number 458
14.3 Slip Flow 461
14.4 Transition and Free Molecule Flow 461
14.5 Summary 463

15. High Temperature Gas Dynamics 465–467

15.1 Introduction 465
15.2 The Importance of High-Temperature Flows 465
15.3 The Nature of High-Temperature Flows 466
15.4 Summary 467

Appendix A 469–537

Table A1 Isentropic Flow of Perfect Gas ($\gamma = 1.4$) 469
Table A2 Normal Shock in Perfect Gas ($\gamma = 1.4$) 482
Table A3 Oblique Shock in Perfect Gas ($\gamma = 1.4$) 492
Table A4 One-Dimensional Flow with Friction ($\gamma = 1.4$) 526
Table A5 One-Dimensional Frictionless Flow with Change in Stagnation Temperature ($\gamma = 1.4$) 532

Appendix B 538–542

Listing of the Method of Characteristics Program 538

Appendix C 543–546

Output for Mach 2.0 Nozzle Contour 543

Appendix D 547–548

Oblique Shock Chart 1 547
Oblique Shock Chart 2 548

Selected References 549–550

Index 551–556

Scanned by CamScanner

Preface

The sixth edition of this book, developed to serve as the text for a course on *Gas Dynamics* at the introductory level for undergraduate courses and advanced level courses at the graduate level as well as for postgraduate courses, is well received all over the world because of its completeness and easy-to-follow style.

Over the years the feedback received from the faculties and students made the author realize the need for adding the derivation for the shock polar relation, expressions for the pressure and density ratio across an expansion fan, the relation between the Mach numbers of incident and reflected shocks and the mathematical steps in arriving at the θ–β–M relation of oblique shock. Some faculties conveyed that adding suitable solved numerical examples on 'moving shock' will be useful for understanding the theory.

Considering the feedback from faculties and students, the following material is added in this edition.

- Detailed analytical derivation of the above mentioned relations.
- Some examples showing derivations of some important analytical relations useful for theory are included in Chapters 4, 5, 6 and 7.
- A set of exercise problems in Chapters 2, 4, 5 and 6.

I would like to thank the faculties and students all over the world for adopting this book for their courses.

For instructors, a companion Solutions Manual that contains typed solutions to all the end-of-chapter problems for the complete book can be procured from the publisher, PHI Learning.

E. Rathakrishnan

Scanned by CamScanner

Preface to the Fifth Edition

My sincere thanks to the students and instructors who adopted this book for both undergraduate and postgraduate courses. In this edition, catchy worked examples are added to both stationary and moving shocks. Also, an example highlighting the application of shock-expansion theory and thin aerofoil theory is added. The new exercise problems added to different chapters will be of immense use to the students to practice application of the theory studied.

The computer program to calculate the coordinates of contoured nozzle, with the method of characteristics, has been given in C-language. This will be of immense value to the present generation of students. The program listing along with a sample output is given in the Appendix.

My sincere thanks to my undergraduate and postgraduate students at Indian Institute of Technology Kanpur and the University of Tokyo, who are directly and indirectly responsible for the development of this book. I sincerely thank Mr. Yasumasa Watanabe, doctoral student of Aerospace Engineering, the University of Tokyo, Japan, for writing the method of characteristics program in C-language.

For instructors, a companion Solutions Manual is available from the publisher that contains typed solutions to all the end-of-chapter problems. The financial support extended by the Continuing Education Centre of Indian Institute of Technology Kanpur for the preparation of the Solutions Manual is gratefully acknowledged.

E. Rathakrishnan

Scanned by CamScanner

Preface to the Fourth Edition

My sincere thanks to the students and instructors who adopted this book for both undergraduate and graduate courses. In the fourth edition, the subject matter has been given a fine tuning, clarifying the vital aspects of the flow processes associated with the compression and expansion waves. This exercise is made to make the book effective for both theory and application. A considerable number of worked examples are added, focusing attention on the design aspects. Some new problems along with answers are also added at the end of many chapters. A brief section on critical Mach number is added in Chapter 8, to gain an insight into this important parameter, which influences the aerodynamic efficiency of flying machines.

For instructors only, a companion Solutions Manual, which contains typed solutions to all the end-of-chapter problems, is available from PHI Learning, New Delhi. I am grateful for the financial support extended by the Continuing Education Centre of the Indian Institute of Technology Kanpur, for the preparation of the manuscript.

My sincere thanks to my undergraduate and graduate students at Indian Institute of Technology Kanpur and The University of Tokyo, who are directly and indirectly responsible for the development of this book.

E. Rathakrishnan

Scanned by CamScanner

Preface to the Third Edition

It gives me great pleasure to express my sincere thanks to the students and instructors who have been patronizing this book for both undergraduate and graduate courses. In the third edition, the subject matter has been appropriately revised throughout the book. Several new problems along with answers have been added at the end of many chapters. The chapter titled Measurements in Compressible Flow has been augmented with high speed wind tunnels, covering the types of supersonic tunnels, their design features, calibration and instrumentation and operating principles.

A companion Solutions Manual for instructors is available from PHI Learning, New Delhi. It contains typed solutions to all the chapter-end problems. The financial support extended by the Continuing Education Centre of Indian Institute of Technology Kanpur for the preparation of the Solutions Manual is gratefully acknowledged.

My heartfelt thanks to my undergraduate and graduate students at Indian Institute of Technology Kanpur, who have directly or indirectly contributed to the development and revision of this book. My special thanks go to my doctoral student Mrinal Kaushik for checking the Solutions Manual.

E. Rathakrishnan

Scanned by CamScanner

Preface to the Second Edition

This book was originally developed to serve as a text to introduce gas dynamics to students, engineers, and applied physicists. The book includes topics of interest to aerospace engineers, mechanical engineers, chemical engineers and applied physicists.

Throughout the book, considerable emphasis is placed on the physical phenomena of gas dynamics, and the limitations of applicability of such phenomena are stressed as well. A large number of solved numerical examples are presented to demonstrate the application of basic principles. Problems with answers are included at the end of each chapter to provide the students with an opportunity to test and augment their understanding of the fundamental principles of the subject. A list of selected references is given to serve as a guide for those students who wish to indulge in in-depth study of various branches of Gas Dynamics.

In this revised augmented edition, special attention has been given to the chapters on Basic Equations of Compressible Flows, Steady One-Dimensional Flow, Normal Shock Waves, Oblique Shock and Expansion Waves and Measurements in Compressible Flows. A number of new worked examples, direct definitions and descriptions of the concepts introduced are provided to let students gain an insight into the subject in an easy and effective manner.

For instructors only, a companion Solutions Manual is available from Prentice-Hall of India that contains typed solutions to all the end-of-chapter problems. The financial support extended by the Continuing Education Centre of Indian Institute of Technology Kanpur for the preparation of the Solutions Manual is gratefully acknowledged.

The first edition has been used as a text for a course on Gas Dynamics (or Compressible Flows or High-speed Aerodynamics) over a number of years, both by undergraduate and postgraduate students at several universities in the world. My sincere thanks to the students and instructors who adopted this book and inspired me with their feedback about the book. An important feedback has been that students and readers having a background of basic fluid mechanics are able to understand and apply the subject material covered in this text comfortably. Considerable additional details on the fundamentals have been included in this edition so that the text can be used for self study as well, extending its usefulness

Scanned by CamScanner

to scientists and engineers working in the field of gas dynamics in industries and research laboratories. In this context, a large number of new and involved exercise problems added to this edition would enable all categories of readers to enhance their understanding of the concepts discussed.

I wish to thank my colleagues and friends who are using this book as the text for their teaching, in particular, Professor S. Elangovan, Department of Aerospace Engineering, Madras Institute of Technology, Anna University, Chennai, India, who urged me to revise this book and helped me in checking the manuscript at various stages of its development. My sincere thanks to my undergraduate and postgraduate students at the Indian Institute of Technology Kanpur, who have been directly and indirectly responsible for the development of this second edition. My special thanks to my doctoral students Ignatius John, S. Elangovan, C. Senthilkumar, K. Vijayaraja, S. Thanigaiarasu, Sher Afgan Khan, P. Jeyajothiraj, P. Lovaraju, B. R. Vinoth, R. Kalimuthu, Dhananjaya Rao, K.L. Narayana, and V.N. Sukumar for their help during the course of development of this book. My appreciation goes to my graduate students Preveen Throvagunta, Hemant Sharma and Ashish Vashishtha for checking the Solutions Manual.

E. Rathakrishnan

Scanned by CamScanner

Preface to the First Edition

This book covers the subject of gas dynamics which deals with the behaviour of fluid flows where compressibility and temperature changes play a significant role. It is the outcome of a series of lectures delivered by me, over several years, to the undergraduate and postgraduate students of Aerospace Engineering at the Madras Institute of Technology, Madras and the Indian Institute of Technology Kanpur, besides the many invited lectures delivered by me at several universities and research laboratories in India and abroad. It is also in response to the keenly felt need to provide a basic text on gas dynamics, which clearly enunciates the fundamental principles associated with the subject.

Designed as a self-contained teaching instrument, this book treats a subject which has flourished during the past three decades due, in a large measure, to its applications in Aerospace Engineering. Besides, gas dynamics plays a key role in numerous non-aerospace applications too, for there is practically no limit to the variety of problems that need the application of principles of gas dynamics for their solution. The principles of gas dynamics have been applied to solve problems in a wide variety of areas, ranging from high speed aerodynamics to the transport of gases along considerable distances. It should be borne in mind that the principles of gas dynamics are based on the four basic laws, namely the conservation of mass, the conservation of momentum, the conservation of energy, and the second law of thermodynamics and, therefore, the notion that gas dynamics is a difficult subject is rather misconceived.

The book is organized in a logical order and the topics have been discussed in a systematic way. First, the various concepts are reviewed and some new ones are defined in order to establish a firm basis for the development of gas dynamic principles. Then the thermodynamics of the flow process is discussed. At this point the perfect gas approximation is introduced, together with the state equation. After the introduction of thermodynamic principles, the wave propagation, highlighting its characteristics, is described. Following a discussion of the basic principles and the thermodynamic concepts, steady one-dimensional isentropic flow processes are analyzed, developing the area-Mach number relation. The development of normal and oblique shock relations follow the same order, with special emphasis given to entropy generation. The concepts of potential flow and similarity rules are developed and applied to different flow problems. Following

Scanned by CamScanner

this, Fanno and Rayleigh flow processes are analyzed from one-dimensional point of view. The method of characteristics is introduced starting from basic principles, and the design of a supersonic nozzle is illustrated. The principles of pressure, temperature, velocity and flow direction measurements in compressible flow streams are discussed. Finally, some basic features of rarefied and high-temperature gas dynamics are outlined.

The order of coverage is gradual: it starts with the simplest case and then proceeds to the complex cases, one at a time. Thus, the basic principles are repeatedly applied to different problems, and the student is drilled in applying the principles. All derivations in the text are based on physical principles, and are easy to follow. A short summary is included at the end of each chapter for quickly recapturing the basic concepts and important relations. A large number of diagrams have been provided to illustrate the concepts introduced. The problems at the end of chapters are so arranged under specific topics that they correspond to the order in which they are covered. This makes problem selection easier for both instructors and students. Besides, my aim in this book has been to make the average student follow the text easily. It is self instructive, thus making the instructor free to use the lecture hours more effectively.

The book is intended primarily as an introductory text for undergraduate and postgraduate students offering courses on gas dynamics. In addition, it would be of assistance to professional engineers and physicists.

I wish to thank my colleagues who reviewed this text during the course of its development and, in particular, Professor S. Elangovan who assisted me in checking the manuscript as well as the proofs. The financial support provided by the Continuing Education Cell of The Indian Institute of Technology Kanpur for the preparation of the manuscript is gratefully acknowledged.

I also wish to thank my undergraduate and graduate students at Madras Institute of Technology, Madras and the Indian Institute of Technology Kanpur, who urged me to write this text; my Ph.D. students T.J. Ignatius, Himanshu Agrawal, K. Srinivasn and S. Elangovan, and my postgraduate students K. Selvaraj, Atul Rathore, R. Srikanth, K.S. Muralirajan, Khalid Sowaud, R. Kannan, A. Soliappan, and A. Palanisamy for the many useful suggestions and assistance given by them during the preparation of the manuscript. My sincere thanks are due to Himanshu Agrawal and K. Srinivasan for preparing detailed solutions to end-of-chapter problems. Finally, I would like to thank G. Narayanan and Sushil Kumar Tiwari for typing the manuscript and A.K. Ganguly for preparing the diagrams.

Any constructive comments for improving the contents will be highly appreciated.

E. Rathakrishnan

Scanned by CamScanner

1 Some Preliminary Thoughts

1.1 GAS DYNAMICS—A BRIEF HISTORY

Until the nineteenth century very little knowledge of gas dynamics had been assimilated by man. The motion of air, its effects and power were felt by human beings only through storms or from the disturbances created for lighting fires and other similar natural phenomena. Only those who were gifted with imagination beyond their times observed the flying of birds and dreamt of flying machines. Many efforts were made in those directions, costing priceless human lives. The early manned flights like those of Icarus and Bladud were not based on any aerodynamic concept.

The theory of air resistance was first proposed by Sir Isaac Newton in 1726. According to him, aerodynamic forces depend on the density and velocity of the fluid, and the shape and size of the displacing object. Newton's theory was soon followed by other theoretical solutions to fluid motion problems. Fluid motion was assumed to occur under idealized conditions, i.e. air was assumed to possess constant density and to move in response to pressure and inertia. Interest in gaining a deep understanding of dynamics of air motion arose because of its application to hot air balloon, windmill, ballistic devices (guns and cannons), and so on. Knowledge was mostly derived by trial and error, and codes of practice did not exist. The experimental techniques introduced for measurement during the eighteenth century provided a breakthrough in the study of aerodynamics. Benjamin Robins in the UK constructed a whirling arm to determine the air resistance of bodies, and a "ballistic pendulum" to find the velocity of a bullet or shell. In the former experiment, a horizontal arm was rotated about a vertical axis by the tension of a string holding a falling weight. After a few rotations the speed of the end of the whirling arm was constant, at approximately 7.6 m/s. Test objects were mounted at the end of the arm and their air resistance altered the speed of rotation. This device was used to compare the resistance of different shapes, and to show how the resistance of

Scanned by CamScanner

the plate changed with the angle of the airflow. In the ballistic pendulum experiment, a bullet was fired into a heavy suspended block which swung through a measurable angle. The bullet speed at impact was calculated from the angle of the swing of block, and the combined mass of the block and the bullet. From these tests, it was learnt that air resistance increases considerably as the air speed approaches the speed of sound.

Some uncertain progress towards heavier-than-air flight was made by gliders and powered models during the nineteenth century. In the same period, the introduction of blast furnaces required large quantities of gas to be pumped efficiently at high pressures and temperatures. In civil structures like large bridges and buildings, reliable calculation of wind forces was needed, and with the improvement in military artillery, greater precision was essential in measuring supersonic air resistance and designing bullets and shells for stable flight. All these developments emphasized the need for better understanding of gas dynamics.

In the twentieth century, the field of aeronautics made very rapid progress both in theory and experiment. In military operations, aerodynamics played its part not only with the airplanes, but also in ballistics, meteorology, and so on. The demand for designing vehicles, missiles, etc. to travel faster than sound gave rise to the challenging task of developing theory and experiments to describe the behaviour of the flows faster than sound wave. This kind of flow is called supersonic flow. There have been three major advances in aerodynamic theory; all of these emerged during the first-half of the twentieth century. They were: 1. Aerofoil theory; 2. boundary layer theory; and 3. theory to describe the behaviour of air when compressibility and temperature change become important as in supersonic flow—this is called *gas dynamics*.

1.2 COMPRESSIBILITY

Fluids such as water are incompressible at normal conditions. But under conditions of high pressure (e.g. 1000 atmospheres), they are compressible. The change in volume is the characteristic feature of a compressible medium under static conditions. Under dynamic conditions, i.e. when the medium is moving, the characteristic feature for incompressible and compressible flow situations are: the volume flow rate, $\dot{Q} = AV$ = constant, at any cross-section of a streamtube for incompressible flow, and the mass flow rate, $\dot{m} = \rho AV$ = constant, at any cross-section of a streamtube for compressible flow (Fig. 1.1). In this relation, A is the cross-sectional area of the streamtube, V and ρ are respectively the velocity and density of the fluid at that cross-section. The first equation is called the continuity equation for incompressible flows and the second is a special form of the general continuity equation.

Scanned by CamScanner

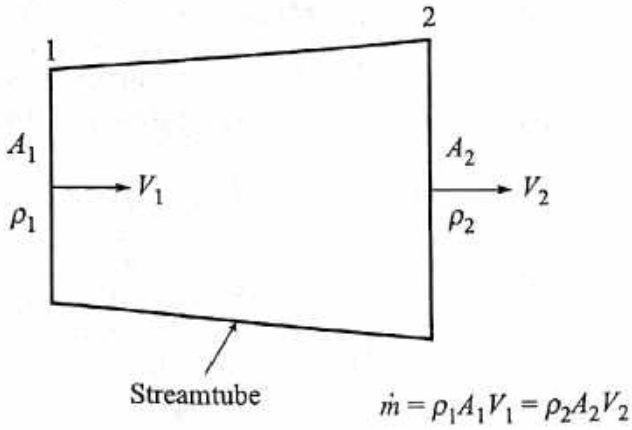


Fig. 1.1 Elemental streamtube.

In general, the flow of an incompressible medium is called *incompressible flow* and that of a compressible medium is called *compressible flow*. Though this statement is true for incompressible media at normal conditions of pressure and temperatures, for compressible medium like gases it has to be modified.

As long as a gas flows at a sufficiently low speed from one cross-section to another, the change in volume (or density) can be neglected and, therefore, the flow can be treated as an incompressible flow. Although the fluid is compressible, this property may be neglected when the flow is taking place at low speeds. In other words, although there is some density change associated with every physical flow, it is often possible (for low speed flows) to neglect it and to idealize the flow as incompressible. This approximation is applicable to many practical flow situations, such as low-speed flow around an airplane and flow through a vacuum cleaner.

From the above discussion it should be clear that compressibility is the phenomenon by virtue of which the flow changes its density with change in speed. Now, it may be asked as to what are the precise conditions under which density changes must be considered. We will try to answer this question now.

A quantitative measure of compressibility is the volume modulus of elasticity E, defined as

$$\Delta p = -E\frac{\Delta \mathbb{V}}{\mathbb{V}_i} \tag{1.1}$$

where Δp is change in static pressure, $\Delta \mathbb{V}$ is change in volume, and $\mathbb{V}_i$ is the initial volume. For ideal gases, the pressure can be expressed by the equation of state as

$$p = \rho RT$$

In particular, if the process is isothermal, then

$$p\mathbb{V} = p_i\mathbb{V}_i = \text{constant}$$

where p_i is the initial static pressure.

Scanned by CamScanner

The preceding equation may be written as

$$(p_i + \Delta p)(\mathbb{V}_i + \Delta\mathbb{V}) = p_i\mathbb{V}_i$$

Expanding the equation and neglecting the second order term ($\Delta p\,\Delta\mathbb{V}$), we get

$$\Delta p\mathbb{V}_i + \Delta\mathbb{V}p_i = 0$$

Therefore,

$$\Delta p = -p_i\frac{\Delta\mathbb{V}}{\mathbb{V}_i} \tag{1.2}$$

For gases, from Eqs. (1.1) and (1.2), we get

$$E = p_i \tag{1.3}$$

Hence by Eq. (1.2), the compressibility may be defined as the volume modulus of the pressure.

Limiting Conditions for Compressibility

By conservation of mass, we have $\dot{m} = \rho V = \text{constant}$, where $\dot{m}$ is mass flow rate per unit area, V is the flow velocity, and ρ is the corresponding density of the fluid. This can also be written as

$$(V_i + \Delta V)(\rho_i + \Delta\rho) = \rho_i V_i$$

After neglecting the second order term ($\Delta V\Delta\rho$), this simplifies to

$$\frac{\Delta\rho}{\rho_i} = -\frac{\Delta V}{V_i}$$

Substituting this relation in Eq. (1.1) and noting that $V = \mathbb{V}$ for unit area per unit time in the present case, we get

$$\Delta p = E\frac{\Delta\rho}{\rho_i} \tag{1.4}$$

From Eq. (1.4), it is seen that the compressibility may also be defined as the density modulus of the pressure.

For incompressible flows, from Bernoulli's equation,

$$\boxed{p + \frac{1}{2}\rho V^2 = \text{constant} = p_{\text{stag}}}$$

where the subscript "stag" refers to stagnation condition. The above equation may also be written as

$$p_{\text{stag}} - p = \Delta p = \frac{1}{2}\rho V^2$$

i.e. the change in pressure is $\frac{1}{2}\rho V^2$. Using Eq. (1.4) in the above relation, we obtain

$$\frac{\Delta p}{E} = \frac{\Delta\rho}{\rho_i} = \frac{\rho_i V_i^2}{2E} = \frac{q_i}{E} \tag{1.5}$$

Scanned by CamScanner

where $q_i = \frac{1}{2}\rho_i V_i^2$ is the dynamic pressure. Equation (1.5) relates the density change with flow speed.

The compressibility effects can be neglected if the density changes are very small, i.e. if

$$\frac{\Delta\rho}{\rho_i} << 1$$

From Eq. (1.5) it is seen that for neglecting compressibility,

$$\frac{q}{E} << 1$$

For gases, the speed of propagation of sound waves "a" may be expressed in terms of pressure and density changes as [see Eq. (1.11)]

$$\boxed{a^2 = \frac{\Delta p}{\Delta\rho}}$$

Using Eq. (1.4) in the above relation, we get

$$a^2 = \frac{E}{\rho_i}$$

With this, Eq. (1.5) reduces to

$$\frac{\Delta\rho}{\rho_i} = \frac{\rho_i}{2}\frac{V_i^2}{E} = \frac{1}{2}\left(\frac{V}{a}\right)^2 \qquad (1.6)$$

The ratio V/a is called the Mach number M. Therefore, the condition of incompressibility for gases is

$$\frac{M^2}{2} << 1$$

Thus, the criterion which determines the effect of compressibility for gases is M. It is widely accepted that compressibility can be neglected when

$$\boxed{\frac{\Delta\rho}{\rho_i} \le 0.05}$$

i.e. when $M \le 0.3$. In other words, the flow is treated as incompressible when $V \le 100$ m/s, i.e. when $V \le 360$ kmph under standard sea level conditions; The above values of M and V are the widely accepted values and they may be refixed at different levels, depending upon the flow situation and the degree of accuracy desired.

1.3 SUPERSONIC FLOW—WHAT IS IT?

The Mach number M is defined as the ratio of the local flow speed to the local speed of sound, i.e.

$$\boxed{M = \frac{V}{a}} \qquad (1.7)$$

Scanned by CamScanner

It is thus a dimensionless quantity. In general, both V and a are functions of position and time, therefore, the Mach number is not just the flow speed made nondimensional by dividing by a constant. Thus, we cannot write $M \propto V$. It is, however, almost always true that M increases monotonically with V.

A flow for which the Mach number is greater than unity is termed *supersonic flow* for which $V > a$. This means that the upstream flow remains unaffected by changes in conditions at a given point in a flow field.

1.4 SPEED OF SOUND

Sound waves are infinitely small pressure disturbances. The speed with which sound propagates in a medium is called *speed of sound* and is denoted by a.

If an infinitesimal disturbance is created by the piston, as shown in Fig. 1.2, the wave propagates through the gas at the velocity of sound relative to the gas into which the disturbance is moving. Let the stationary gas in the pipe at pressure p_i and density ρ_i be set in motion by the piston. The infinitesimal pressure wave created by piston movement travels with speed a, leaving the medium behind it at pressure p_1 and density ρ_1 to move with velocity V.

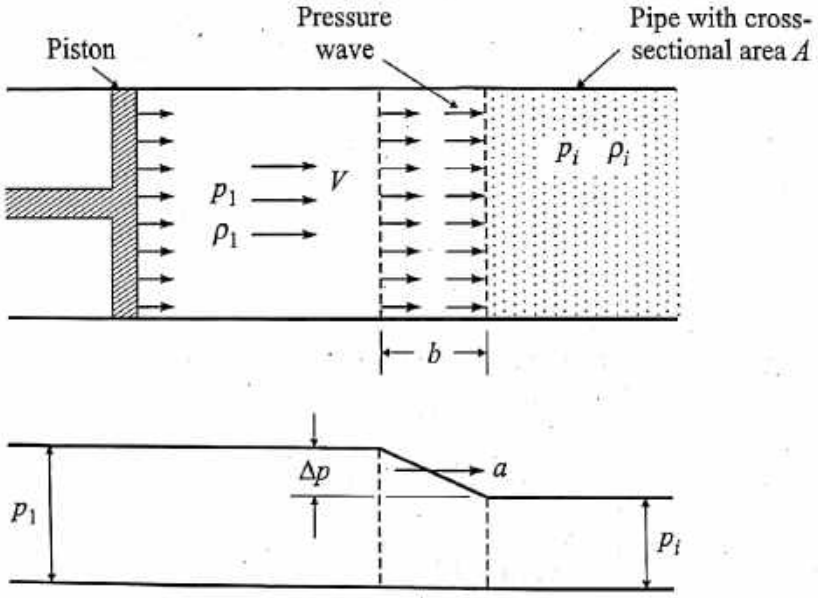


Fig. 1.2 Propagation of pressure disturbance.

As a result of the compression created by the piston, the pressure and density next to the piston are infinitesimally greater than the pressure and density of the gas at rest ahead of the wave. Therefore,

$$\Delta p = p_1 - p_i, \quad \Delta\rho = \rho_1 - \rho_i$$

are small.

Choose a control volume of length b, as shown in Fig. 1.2.

Scanned by CamScanner

Compression of volume Ab causes the density to rise from ρ_i to ρ_1 in time $t = b/a$. The mass flow into volume Ab is

$$\dot{m} = \rho_1 AV \tag{1.8}$$

For the conservation of mass, $\dot{m}$ must also be equal to the mass flow rate through the control volume, i.e. $Ab(\rho_1 - \rho_i)/t$. Thus,

$$\frac{Ab(\rho_1 - \rho_i)}{t} = \rho_1 AV$$

or

$$a(\rho_1 - \rho_i) = \rho_1 V \tag{1.9}$$

since $b/t = a$.

When the piston moves, the compression wave thus caused travels and accelerates the gas from zero velocity to V. The acceleration is given by

$$\frac{V}{t} = V\frac{a}{b}$$

The mass in the control volume Ab is

$$m = Ab\bar{\rho}$$

where

$$\bar{\rho} = \frac{\rho_i + \rho_1}{2}$$

The force acting on the control volume is $F = A(p_1 - p_i)$. Therefore, by Newton's law,

$$A(p_1 - p_i) = Ab\bar{\rho}\, V(a/b)$$

$$\bar{\rho} Va = p_1 - p_i \tag{1.10}$$

Since the disturbance is very weak, ρ_1 on the right-hand side of Eq. (1.9) may be replaced by $\bar{\rho}$ to give

$$a(\rho_1 - \rho_i) = \bar{\rho} V$$

Using this relation, Eq. (1.10) can be written as

$$a^2 = \frac{p_1 - p_i}{\rho_1 - \rho_i} = \frac{\Delta p}{\Delta \rho}$$

In the limiting case as Δp and $\Delta \rho$ approach zero, the above equation leads to

$$a^2 = \frac{dp}{d\rho} \tag{1.11}$$

This is Laplace's equation and is valid for any fluid.

The sound wave is a weak compression wave, across which only infinitesimal change in fluid properties occurs. Further, the wave itself is

Scanned by CamScanner

extremely thin, and changes in properties occur very rapidly. The rapidity of the process rules out the possibility of any heat transfer between the system of fluid particles and its surrounding.

For very strong pressure waves, the travelling speed of disturbance may be greater than that of sound. The pressure can be expressed as

$$p = p(\rho) \tag{1.12}$$

For isentropic process of a gas,

$$\boxed{\frac{p}{\rho^{\gamma}} = \text{constant}}$$

where the isentropic index γ is the ratio of specific heats and is a constant for a perfect gas. Using the above relation in Eq. (1.11), we get

$$a^2 = \frac{\gamma p}{\rho} \tag{1.13}$$

For a perfect gas, by the state equation

$$\boxed{p = \rho RT} \tag{1.14}$$

where R is the gas constant and T the static temperature of the gas in absolute units.

Equations (1.13) and (1.14) together lead to the following expression for the speed of sound:

$$\boxed{a = \sqrt{\gamma RT}} \tag{1.15}$$

The assumption of perfect gas is valid so long as the speed of gas stream is not too high. However, at hypersonic speeds the assumption of perfect gas is not valid and we must consider Eq. (1.13) to calculate the speed of sound.

Implication of variation of a with altitude Implication of speed of sound variation with altitude is explained in the following example.

EXAMPLE 1.1 For an aircraft flying at a speed of 1000 kmph the variations in speed of sound a, and Mach number M with altitude are as follows:

At sea level altitude From the International Standard Atmosphere (ISA), $T = 15°C$ at sea level. Therefore, the speed of sound $a = \sqrt{\gamma RT}$ is given by

$$a = \sqrt{1.4 \times 287 \times 288} \text{ m/s}$$

with $R = 287$ m^2/s^2-K and $\gamma = 1.4$ for air

i.e.

$$\boxed{a = 340.17 \text{ m/s}}$$

The Mach number of the aircraft at sea level is

Scanned by CamScanner

$$M = \frac{V}{a} = \left(\frac{1000}{3.6}\right)\left(\frac{1}{340.17}\right)$$

$$\boxed{M = 0.817}$$

At 11,000 metres altitude From ISA, temperature $T = -56.5°C$

$$T = (273 - 56.5) = 216.5 \text{ K}$$

The speed of sound, $a = \sqrt{1.4 \times 287 \times 216.5}$ m/s

i.e. $$\boxed{a = 294.94 \text{ m/s}}$$

The Mach number of the aircraft at 11,000 m altitude is

$$\boxed{M = 0.942}$$

Also,

$$\frac{\Delta\rho}{\rho_i} = \frac{1}{2}\left(\frac{V}{a}\right)^2 \approx \frac{M^2}{2}$$

Thus, the aircraft experiences different compressibility effects at the above two altitudes. The compressibility effects are particularly serious in this range (transonic range) of Mach numbers than any other range.

EXAMPLE 1.2 During a flight, a fighter aircraft attains its cruise speed of 600 m/s at 10 km altitude after taking off at 150 m/s from sea level. Assuming the speed to have increased linearly with altitude during the climb, compute the variation in Mach number with altitude.

Solution Let us consider increase in altitude in steps of 2 km. From ISA tables, we have the following variation in temperature with altitude:

Altitude, H(km)	0	2	4	6	8	10
Temperature, T(K)	288	275	262	249	236	223

For air, $\gamma = 1.4$ and $R = 287$ m^2/s^2-K. The flight velocity at any altitude H is given by

$$V = 150 + 45H$$

where V is in m/s and H in km. The velocity of sound at any altitude is given by

$$a = \sqrt{\gamma RT}$$

where T is the temperature at the altitude in kelvin.

$$a = \sqrt{1.4 \times 287 \times T} \text{ m/s}$$

i.e. $$a = 20.05\sqrt{T} \text{ m/s}$$

With the preceding expressions for flight speed and speed of sound, we get

Scanned by CamScanner

the following variation in Mach number with altitude:

H (km)	0	2	4	6	8	10
T (K)	288	275	262	249	236	223
V (m/s)	150	240	330	420	510	600
a (m/s)	340.3	332.5	324.5	316.4	308.0	299.4
M	0.44	0.72	1.02	1.33	1.66	2.0

1.5 TEMPERATURE RISE

For a perfect gas,

$$p = \rho RT, \quad R = c_p - c_v$$

where c_p and c_v are specific heats at constant pressure and constant volume, respectively. Also, $\gamma = c_p/c_v$; therefore,

$$R = \frac{\gamma - 1}{\gamma} c_p \tag{1.16}$$

For an isentropic change of state, an equation not involving T can be written as

$$\frac{p}{\rho^\gamma} = \text{constant}$$

Now, between state 1 and any other state, the relation between the pressures and densities can be written as

$$\left(\frac{p}{p_1}\right) = \left(\frac{\rho}{\rho_1}\right)^\gamma \tag{1.17}$$

Combining Eq. (1.17) and the equation of state, we get

$$\boxed{\frac{T}{T_1} = \left(\frac{\rho}{\rho_1}\right)^{\gamma-1} = \left(\frac{p}{p_1}\right)^{(\gamma-1)/\gamma}} \tag{1.18}$$

The above relations are very useful for gas dynamics and they can be expressed in terms of the Mach number.

Let us examine the flow around a symmetrical body, as shown in Fig. 1.3.

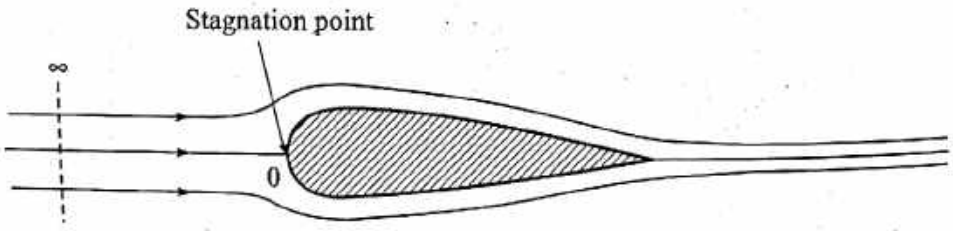


Fig. 1.3 Flow around a symmetrical body.

In a compressible medium, there will be change in density and temperature at

Scanned by CamScanner

point 0. The temperature rise at the stagnation point can be obtained from the energy equation.

The energy equation for an isentropic flow is

$$\boxed{h + \frac{V^2}{2} = \text{constant}} \tag{1.19}$$

where h is the enthalpy.

Equating the energy at far upstream ∞ and the stagnation point 0, we get

$$h_\infty + \frac{V_\infty^2}{2} = h_0 + \frac{V_0^2}{2}$$

Since $V_0 = 0$,

$$h_0 - h_\infty = \frac{V_\infty^2}{2}$$

For a perfect gas, substituting $h = c_p T$ in the above equation, we obtain

$$c_p(T_0 - T_\infty) = \frac{V_\infty^2}{2}$$

i.e.

$$\Delta T = T_0 - T_\infty = \frac{V_\infty^2}{2c_p} \tag{1.20}$$

Combining Eqs. (1.15) and (1.16), we get

$$c_p = \frac{1}{\gamma - 1}\frac{a_\infty^2}{T_\infty}$$

Hence,

$$\Delta T = \frac{\gamma - 1}{2} T_\infty M_\infty^2 \tag{1.21}$$

i.e.

$$\boxed{T_0 = T_\infty\left(1 + \frac{\gamma - 1}{2} M_\infty^2\right)} \tag{1.22}$$

For air, $\gamma = 1.4$, and hence

$$T_0 = T_\infty(1 + 0.2M_\infty^2) \tag{1.23}$$

This is the temperature at the stagnation point on the body. It is also referred to as total temperature.

EXAMPLE 1.3 A fighter aircraft attains its maximum speed of 2160 kmph at an altitude of 12 km. The take-off speed at sea level is 270 kmph. If the flight speed increases linearly with altitude, compute the variation in stagnation temperature with altitude for a climb up to the maximum speed.

Scanned by CamScanner

Solution For a compressible medium, the stagnation temperature T_0 is given by

$$T_0 = T_\infty + \frac{V_\infty^2}{2c_p} = T_\infty + \frac{\gamma - 1}{2} T_\infty M_\infty^2$$

where

T_∞ = freestream static temperature
V_∞ = freestream velocity
c_p = specific heat of fluid at constant pressure
γ = ratio of specific heats of the fluid
M_∞ = freestream Mach number.

For air,

$$c_p = 1005 \text{ m}^2/\text{s}^2\text{-K}$$

Therefore,

$$T_0 = T_\infty + \frac{V_\infty^2}{2010} \text{ K}$$

The variation of velocity with altitude may be expressed as

$$V_\infty = \left(270 + \frac{2160 - 270}{12} H\right) \text{ km/h}$$
$$= (270 + 157.5H) \text{ km/h}$$
$$= (75 + 43.75H) \text{ m/s}$$

Considering altitude increase in steps of 3 km, we obtain the values as given in the following table:

H (km)	0	3	6	9	12
T_∞ (K)	288.0	268.5	249.0	229.5	216.5
V_∞ (m/s)	75.00	206.25	337.50	468.75	600.0
$\frac{V_\infty^2}{2010}$ (K)	2.80	21.16	56.67	109.32	179.1
T_0 (K)	290.80	289.66	305.67	338.82	395.6

1.6 MACH ANGLE

We know that in a flow field the presence of a small disturbance is felt throughout the field by means of a wave travelling at the local velocity of sound relative to the medium.

Let us examine the propagation of pressure disturbance shown in Fig. 1.4. The propagation of disturbance waves created by an object moving with velocity $V = 0$, $V = a/2$, $V = a$ and $V > a$ is shown in Figs. 1.4(a), (b), (c), (d), respectively. The disturbance waves reach a stationary observer before the source of disturbance could reach him in subsonic flow, as shown in

Scanned by CamScanner

Figs. 1.4(a) and 1.4(b). But in supersonic flows, it takes considerable amount of time for an observer to perceive the pressure disturbance, after the source has passed him. This is one of the fundamental differences between subsonic and supersonic flows. Therefore, in a subsonic flow, the streamlines sense the presence of any obstacle in the flow field and adjust themselves ahead of it and flow around it smoothly. But in the supersonic flow field, the streamlines feel the obstacle only when they hit it. The obstacle acts as a source and so the streamlines deviate at the Mach cone as shown in Fig. 1.4(d). The disturbance due to obstacle is sudden and the flow behind the obstacle has to change abruptly.

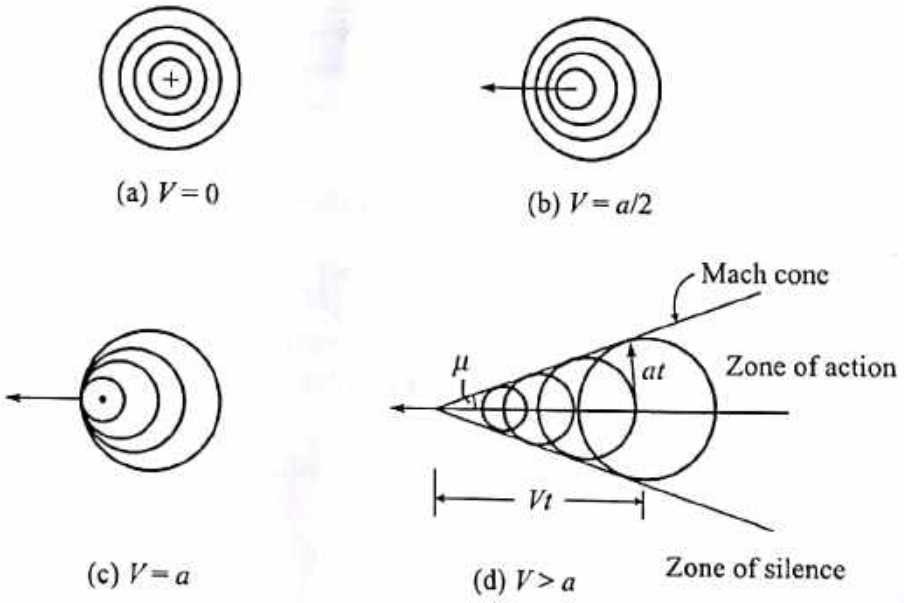


Fig. 1.4 Propagation of disturbance waves.

Flow around a wedge shown in Figs. 1.5(a) and 1.5(b) shows the smooth change and abrupt change in flow direction for subsonic and supersonic flow, respectively.

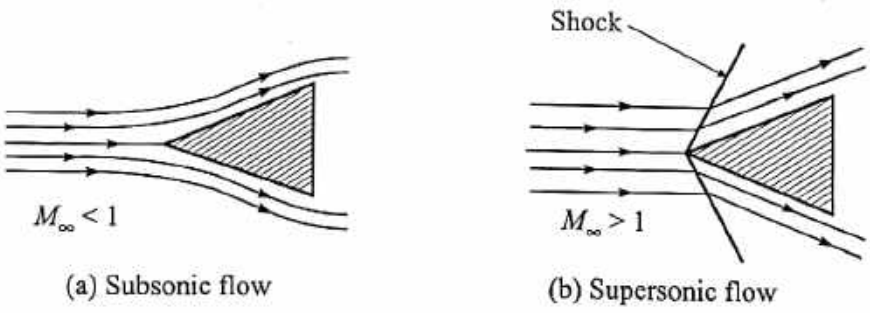


Fig. 1.5 Flow around a wedge.

For $M_\infty < 1$, the flow changes its direction smoothly and pressure decreases with acceleration; for $M_\infty > 1$, there is sudden change in flow direction at the body and pressure increases downstream of the shock.

Scanned by CamScanner

In Fig. 1.4(d), it is shown that for supersonic motion of an object there is a well-defined conical zone in the flow field with the object located at the nose of the cone, and the disturbance created by the moving object is confined only to the field included inside the cone. The flow field zone outside the cone does not even feel the disturbance.

For this reason, von Karman termed the region inside the cone as the *zone of action*, and the region outside the cone as the *zone of silence*. The lines at which the pressure disturbance is concentrated and which generate the cone are called *Mach waves* or *Mach lines*. The angle between the Mach line and the direction of motion of the body is called the Mach angle μ. From Fig. 1.4(d),

$$\sin \mu = \frac{at}{Vt} = \frac{a}{V} \tag{1.24}$$

i.e.

$$\boxed{\sin \mu = \frac{1}{M}} \tag{1.25}$$

From the disturbance waves propagation shown in Figure 1.4, we can infer the following features of the flow regimes.

- When the medium is *incompressible* [$M = 0$, Fig. 1.4(a)] or when the speed of the moving disturbance is negligibly small compared to the local sound speed, the pressure pulse created by the disturbance spreads uniformly in all directions.
- When the disturbance source moves with a *subsonic speed* [$M < 1$, Fig. 1.4(b)], the pressure disturbance is felt in all directions and at all points in space (neglecting viscous dissipation), but the pressure pattern is no longer symmetrical.
- For *sonic velocity* [$M = 1$, Fig. 1.4(c)] the pressure pulse is at the boundary between subsonic and supersonic flow and the wave front is in a plane.
- For *supersonic speeds* [$M > 1$, Fig. 1.4(d)] the disturbance wave phenomena are totally different from those at subsonic speeds. All the pressure disturbances are included in a cone which has the disturbance source at its apex, and the effect of the disturbance is not felt upstream of the disturbance source.

Small Disturbance

When the apex angle of wedge δ is vanishingly small, the disturbances will be small, and we can consider these to be identical to sound pulses. In such a case, the deviation of streamlines will be small and there will be infinitesimally small increase in pressure across the Mach cone, shown in Fig. 1.6.

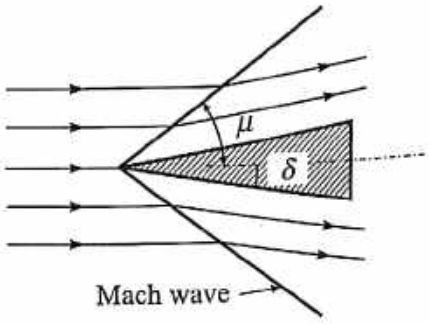


Fig. 1.6 Mach cone.

Scanned by CamScanner

Finite Disturbance

When the wedge angle δ is finite, the disturbances introduced are finite, and then the wave is not called Mach wave but a shock or shock wave (Fig. 1.7). The angle of shock, β, is always smaller than the Mach angle. The deviation of streamline is finite and there is finite pressure increase across the shock wave.

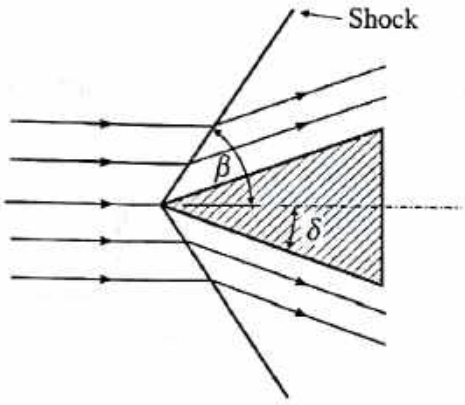


Fig. 1.7 Shock wave.

1.7 SUMMARY

In this chapter, the basic concepts of Gas Dynamics are introduced and discussed. *Gas Dynamics* is a science that primarily deals with the behaviour of gas flows in which compressibility and temperature change become significant. *Compressibility* is a phenomenon by virtue of which the flow changes its density with change in speed. Compressibility may also be defined as the volume modulus of the pressure.

Flows with significant compressibility are called *compressible flows*. To put it simply, compressible flow is defined as variable density flow; this is in contrast to incompressible flow, where the density is assumed to be invariant. In reality, every fluid is compressible to some greater or lesser extent; hence a truly incompressible flow is a hypothetical flow. However, when flow velocity is very small, the changes in density may be neglected and the assumption of constant density can be made with reasonable accuracy. Usually flows with Mach number less than 0.3 are treated as constant density (incompressible) flows.

The Mach number is defined as the ratio of the local flow speed to the local speed of sound, i.e.

$$M = \frac{V}{a} \tag{1.7}$$

Flows with Mach number greater than unity are called supersonic flows.

Scanned by CamScanner

Sound waves are infinitesimally small pressure disturbances. The speed with which sound waves propagate in a medium is called *speed of sound a*. The speed of sound is given by

$$a^2 = \frac{dp}{d\rho} \tag{1.11}$$

For a perfect gas, the speed of sound can be expressed as

$$a = \sqrt{\gamma RT} \tag{1.15}$$

where γ is the specific heats ratio, R is the gas constant, and T is the absolute static temperature.

For a perfect gas, the state equation is

$$p = \rho RT \tag{1.14}$$

and for an isentropic flow of a perfect gas, the relation between the pressure, temperature, and density between state 1 and any other state can be expressed as

$$\frac{T}{T_1} = \left(\frac{\rho}{\rho_1}\right)^{\gamma-1} = \left(\frac{p}{p_1}\right)^{(\gamma-1)/\gamma} \tag{1.18}$$

For supersonic motion of an object, there is a well-defined conical zone in the flow field with the object located at the nose of the cone. The region inside the cone is called the *zone of action*, and the region outside the cone is termed *zone of silence*. The lines at which the pressure difference is concentrated and which generate the cone are called *Mach waves* or *Mach lines*. Therefore, Mach waves may be defined as weak pressure waves across which there is only an infinitesimal change in flow properties. The angle between the Mach line and the direction of motion of the body (flow direction) is called the *Mach angle* μ, given by

$$\sin \mu = \frac{1}{M} \tag{1.25}$$

In classical literature, Fluid Mechanics is broadly divided into Hydrodynamics or incompressible flows with freestream Mach number negligibly small, and Gas Dynamics dealing with compressible flows. Gas Dynamics is further divided into subsonic flows in the Mach number range from 0 to 1, and supersonic flows with Mach numbers greater than 1.

The modern classification of the flow regimes is as follows:

1. Fluid flows with $0 < M < 0.8$ are called *subsonic flow*.
2. The flow in the Mach number range $0.8 < M < 1.2$ is called *transonic flow*.
3. The flow in the Mach number range $1.2 < M < 5$ is called *supersonic flow*.
4. The flow with $M > 5$ is called *hypersonic flow*.

Scanned by CamScanner

Linearized theory can be used for studying subsonic and supersonic flows; the study of transonic and hypersonic flows is, however, complicated.

Transonic Flow

When a body is kept in transonic flow, it experiences subsonic flow over some portions of its surface and supersonic flow over other portions. There is also a possibility of shock formation on the body. It is this mixed nature of the flow field which makes the study of transonic flows complicated.

Hypersonic Flow

The temperature at stagnation point and over the surface of an object in the hypersonic flow becomes very high and, therefore, it requires special treatment. That is, we must consider the thermodynamic aspects of the flow along with gas dynamic aspects. That is why hypersonic flow theory is also called aero-thermodynamic theory. Besides, because of high temperature, the specific heats become functions of temperature and hence the gas cannot be treated as perfect gas. If the temperature is quite high (of the order of more than 2000 K), even dissociation of gas can take place. The complexities due to high temperatures associated with hypersonic flow makes its study complicated.

Scanned by CamScanner

2 Basic Equations of Compressible Flow

2.1 THERMODYNAMICS OF FLUID FLOW

Entropy and temperature are the two fundamental concepts of thermodynamics. The energy changes associated with compressible flow, unlike low-speed or incompressible flow, are substantial enough to strongly interact with other properties of the flow. Hence, the energy concepts play an important role in the study of compressible flow. In other words, the study of thermodynamics which deals with energy (and entropy) is an essential component in the study of compressible flow.

The following are the broad divisions of the fluid flow studies classified, based on thermodynamic considerations: Fluid mechanics of perfect fluids, i.e. fluids without viscosity and heat (transfer) conductivity, is an extension of equilibrium thermodynamics to moving fluids. The kinetic energy of the fluid has to be considered in addition to the internal energy which the fluid possesses when at rest.

Fluid mechanics of real fluids goes beyond the scope of classical thermodynamics. The transport processes of momentum and heat are of primary interest here. But, even though thermodynamics is not fully and directly applicable to all phases of real fluid flow, it is often extremely helpful in relating the initial and final conditions.

For low speed flow problems, thermodynamic considerations are not needed because the heat content of the fluid flow is so large compared to the kinetic energy of the flow that the temperature remains nearly constant even if the whole kinetic energy is transformed into heat.

In modern high-speed problems, the kinetic energy content of the fluid can be so large compared to its heat content that the variations in temperature can become substantial. Hence, the emphasis on thermodynamic concepts assumes importance.

Scanned by CamScanner

2.2 FIRST LAW OF THERMODYNAMICS (ENERGY EQUATION)

Consider a closed system, which is a system of gas at rest, across whose boundaries no transfer of mass is possible. Let δQ be an incremental amount of heat added to the system across the boundary (by thermal conduction or by direct radiation). Also, let δW denote the work done on the system by the surroundings (or by the system on the surroundings). The sign convention is positive when the work is done by the system and negative when the work is done on the system. Due to the molecular motion of the gas, the system has an internal energy U. The First Law of Thermodynamics states that: *the heat added minus the work done by the system equals the change in the internal energy of the system,* i.e.

$$\boxed{\delta Q - \delta W = dU} \tag{2.1}$$

This is an empirical result confirmed by laboratory and practical experience. In Eq. (2.1), U is a state variable (thermodynamic property). Hence, dU is an exact differential, and its value depends only on the initial and final states of the system. In contrast (the nonthermodynamic properties), δQ and δW depend on the process in going from the initial to the final states.

In general, for any given dU, there are infinite number of ways (processes) by which heat can be added and work done on the system. In the present course of study, we will be mainly concerned with the following three types of processes only.

1. Adiabatic process—a process in which no heat is added to or taken away from the system.
2. Reversible process—a process which can be reversed without leaving any trace on the surroundings, i.e. both the system and the surroundings are returned to their initial states at the end of the reverse process.
3. Isentropic process—a process which is adiabatic and reversible.

For open systems (e.g. pipe flow), there is always a term $(U + p\mathbb{V})$ present instead of just U. This term is referred to as enthalpy or heat function H given by

$$\boxed{H = U + p\mathbb{V}} \tag{2.2}$$

$$H_2 - H_1 = U_2 - U_1 + p_2\mathbb{V}_2 - p_1\mathbb{V}_1 \tag{2.3}$$

where $(p_2\mathbb{V}_2 - p_1\mathbb{V}_1)$ is termed flow work and subscripts 1 and 2 represent states 1 and 2, respectively.

In general, we can say that the following are the major differences between open and closed systems:

Scanned by CamScanner

1. The mass which enters or leaves an open system has kinetic energy, whereas there is no mass transfer possible across closed system boundaries.
2. The mass can enter and leave the open systems at different levels of potential energy.
3. Open systems are able to deliver continuous work, because the medium which transforms energy is continuously replaced. This useful work, which the machine continuously delivers, is called the *shaft work*.

Energy Equation for an Open System

Consider the system shown in Fig. 2.1. The total energy E at inlet station 1 and outlet station 2 is given by

$$E_1 = U_1 + \frac{1}{2}mV_1^2 + mgz_1 \tag{2.4}$$

$$E_2 = U_2 + \frac{1}{2}mV_2^2 + mgz_2 \tag{2.5}$$

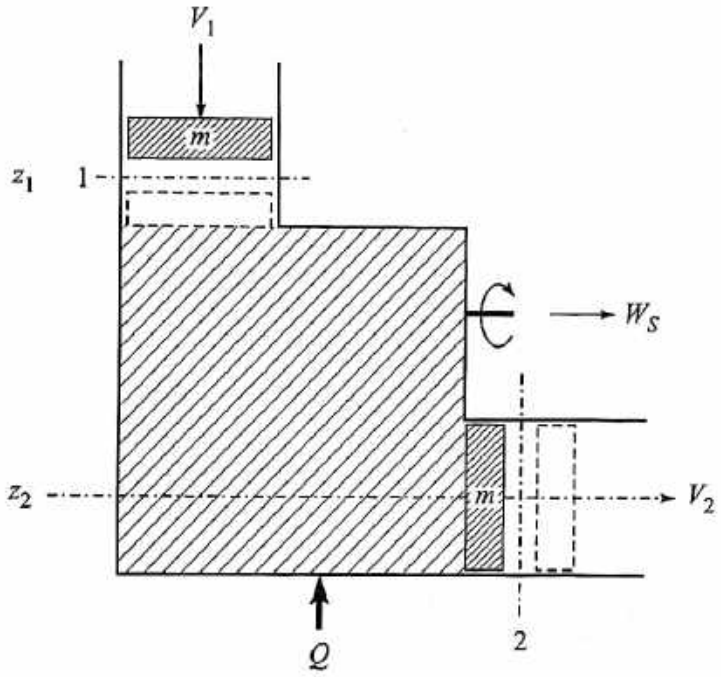


Fig. 2.1 Open system.

Comparing Eq. (2.1) with Eqs. (2.4) and (2.5) for an open system, U_2 and U_1 in Eq. (2.1) have to be replaced by E_1 and E_2 in Eqs. (2.4) and (2.5). Hence,

$$Q_{12} - W_{12} = E_2 - E_1 \tag{2.6}$$

or

$$Q_{12} - W_{12} = \left(U_2 + \frac{1}{2}mV_2^2 + mgz_2\right) - \left(U_1 + \frac{1}{2}mV_1^2 + mgz_1\right) \tag{2.7}$$

Scanned by CamScanner

For an open system, the shaft (useful) work is not just equal to W_{12}, but the work done to compress pistons at 1 and 2 must also be considered. Work done with respect to the system by the piston at state 1 is

$W_1' = -F_1\Delta_1$ (F_1 = force and Δ_1 = displacement)
$W_1' = -p_1A_1\Delta_1$ (p_1 = pressure at 1; A_1 = cross-sectional area of piston)
$W_1' = -p_1\mathbb{V}_1$

Work delivered at 2 is $W_2' = p_2\mathbb{V}_2$. Therefore,

$$W_{12} = W_S + p_2\mathbb{V}_2 - p_1\mathbb{V}_1 \tag{2.8}$$

In Eq. (2.8), W_S is the shaft work, which can be extracted from the system, and $(p_2\mathbb{V}_2 - p_1\mathbb{V}_1)$ is the flow work necessary to maintain the flow. Substituting Eq. (2.8) into Eq. (2.7), we get

$$Q_{12} - W_S = \left(U_2 + p_2\mathbb{V}_2 + \frac{1}{2}mV_2^2 + mgz_2\right) - \left(U_1 + p_1\mathbb{V}_1 + \frac{1}{2}mV_1^2 + mgz_1\right)$$

or

$$Q_{12} - W_S = \left(H_2 + \frac{1}{2}mV_2^2 + mgz_2\right) - \left(H_1 + \frac{1}{2}mV_1^2 + mgz_1\right)$$

The above equation is the fundamental equation for an open system. If there are any other forms of energy, e.g. electrical energy, magnetic energy, their initial and final values should be added properly to this equation. The energy equation

$$\boxed{H_1 + \frac{1}{2}mV_1^2 + mgz_1 = H_2 + \frac{1}{2}mV_2^2 + mgz_2 + W_S - Q_{12}} \tag{2.9}$$

is universally valid. This is the first law of thermodynamics for any open system. In most applications of gas dynamics, the gravitational energy is negligible compared to the kinetic energy. For working processes such as flow in turbines and compressors, the shaft work W_S in Eq. (2.9) is finite and, for flow processes like flow around an airplane, $W_S = 0$. Therefore, for a gas dynamic working process, Eq. (2.9) becomes

$$H_1 + \frac{1}{2}mV_1^2 = H_2 + \frac{1}{2}mV_2^2 + W_S - Q_{12} \tag{2.10}$$

This is usually the case with turbomachines, internal combustion engines, etc. where the process is assumed to be adiabatic. For a gas dynamic adiabatic flow process, the energy equation (2.9) becomes

$$H_1 + \frac{1}{2}mV_1^2 = H_2 + \frac{1}{2}mV_2^2 \tag{2.11}$$

or

$$H_1 + \frac{1}{2}mV_1^2 = H_0 = \text{constant} \tag{2.12}$$

where H_0 is called the stagnation enthalpy. That is, the sum of enthalpy and kinetic energy is constant in the case of adiabatic flow.

Scanned by CamScanner

Adiabatic Flow Process

For an adiabatic process, $Q = 0$. Therefore, the energy equation is given by Eqs. (2.11) and (2.12). Dividing Eqs. (2.11) and (2.12) by m, we can rewrite them as

$$h_1 + \frac{V_1^2}{2} = h_2 + \frac{V_2^2}{2} \tag{2.13}$$

$$h_1 + \frac{V_1^2}{2} = h_0 \tag{2.14}$$

or, in general

$$h + \frac{V^2}{2} = h_0 = \text{constant} \tag{2.15}$$

where $h = H/m$ is called specific enthalpy and h_0 is the specific stagnation enthalpy. With $h = p/\rho$, Eq. (2.15) represents Bernoulli's equation for incompressible flow, expressed as

$$p + \frac{1}{2}\rho V^2 = p_0 = \text{constant}$$

where p_0 is the stagnation pressure. That is, for incompressible flow of air, the energy equation happens to be the Bernoulli equation, because we are not interested in internal energy and temperature for such flows. In other words, Bernoulli's equation is the limiting case of the energy equation. Here it is important to realize that even though Bernoulli's equation for incompressible flow of a gas is shown to be the limiting case of the energy equation, it is essentially a momentum equation. For a closed system,

$$Q_{12} - W_{12} = U_2 - U_1$$

For the processes of a closed system there is no shaft work, i.e. no useful work can be extracted from the working medium. There will be only compressive or expansion work. Therefore, W_{12} may be expressed as

$$W_{12} = \int_1^2 p\,d\mathbb{V}$$

Thus,

$$du = \delta q - pdv \tag{2.16a}$$

But $h = u + pv$; $dh = du + pdv + vdp$. Using relation (2.16a), we can write

$$dh = \delta q + vdp \tag{2.16b}$$

and for adiabatic change of state,

$$du = -pdv, \quad dh = vdp \tag{2.16c}$$

where u, q and v in Eqs. (2.16) stand for specific quantities of internal energy, heat energy and volume, respectively.

Scanned by CamScanner

2.3 THE SECOND LAW OF THERMODYNAMICS (ENTROPY EQUATION)

Consider a cold body in contact with a hot body. From experience we can say that the cold body will get heated up and the hot body will cool down. However, Eq. (2.1) does not necessarily imply that this will happen. In fact, the first law allows the cold body to become cooler and the hot body to become hotter as long as energy is conserved during the process. However, in practice this does not happen; instead the law of nature imposes another condition on the process, a condition that stipulates in which direction a process should take place. To ascertain the proper direction of a process, let us define a new state variable, the entropy, as follows:

$$ds = \frac{\delta q_{\text{rev}}}{T} \tag{2.17}$$

where s is the entropy (amount of disorder) of the system, δq_{rev} is an incremental amount of heat added reversibly to the system, and T is the system temperature. The above definition gives the change in entropy in terms of a reversible addition of heat, δq_{rev}. Since entropy is a state variable, it can be used in conjunction with any type of process, reversible or irreversible. The quantity δq_{rev} is just an artifice; an effective value of δq_{rev} can always be assigned to relate the initial and final states of an irreversible process, where the actual amount of heat added is δq. Indeed, an alternative and probably more lucid relation is

$$\boxed{ds = \frac{\delta q}{T} + ds_{\text{irrev}}} \tag{2.18}$$

Equation (2.18) applies in general to all processes. It states that the change in entropy during any process is equal to the actual heat added, divided by the temperature, $\delta q/T$, plus a contribution from the irreversible dissipative phenomena of viscosity, thermal conductivity, and mass diffusion occurring within the system, ds_{irrev}. These dissipative phenomena always increase the entropy.

$$ds_{\text{irrev}} \geq 0 \tag{2.19}$$

The equal sign in inequality (2.19) denotes a reversible process where, by definition, the above dissipative phenomena are absent. Hence, a combination of Eqs. (2.18) and (2.19) yields

$$ds \geq \frac{\delta q}{T} \tag{2.20}$$

Further, if the process is adiabatic, $\delta q = 0$, and Eq. (2.20) reduces to

$$ds \geq 0 \tag{2.21}$$

Equations (2.20) and (2.21) are forms of the second law of thermodynamics. The second law gives the direction in which a process will take place.

Scanned by CamScanner

Equations (2.20) and (2.21) imply that a process will always proceed in a direction such that the entropy of the system plus surroundings always increases, or at least remains unchanged. That is, in an adiabatic process, the entropy can never decrease. This aspect of the second law of thermodynamics is important because it distinguishes between reversible and irreversible processes.

If $ds > 0$, the process is called an *irreversible process*, and when $ds = 0$, the process is called a *reversible process*. A reversible and adiabatic process is called an **isentropic process**. However, in a nonadiabatic process, we can extract heat and thus decrease the entropy.

2.4 THERMAL AND CALORICAL PROPERTIES

The equation $pv = RT$ or $p/\rho = RT$ is called the thermal equation of state, where p, T and $v(1/\rho)$ are called *thermal properties* and R is called the gas constant. A gas which obeys the thermal equation of state is called *thermally perfect gas*. Any relation between the calorical properties, u, h and s and any two thermal properties is called a calorical equation of state. In general, the thermodynamic properties (the properties which do not depend on process) can be grouped into thermal properties (p, T, v) and calorical properties (u, h, s). From Eqs. (2.16),

$$u = u(T, v), \quad h = h(T, p)$$

In terms of exact differentials, the above relations become

$$du = \left(\frac{\partial u}{\partial T}\right)_v dT + \left(\frac{\partial u}{\partial v}\right)_T dv \tag{2.22}$$

$$dh = \left(\frac{\partial h}{\partial T}\right)_p dT + \left(\frac{\partial h}{\partial p}\right)_T dp \tag{2.23}$$

For a constant volume process, Eq. (2.22) reduces to

$$du = \left(\frac{\partial u}{\partial T}\right)_v dT$$

where $\left(\frac{\partial u}{\partial T}\right)_v$ is the specific heat at constant volume represented as c_v and, therefore,

$$\boxed{du = c_v dT} \tag{2.24}$$

For an isobaric process, Eq. (2.23) reduces to

$$dh = \left(\frac{\partial h}{\partial T}\right)_p dT$$

where $\left(\frac{\partial h}{\partial T}\right)_p$ is the specific heat at constant pressure represented by c_p and, therefore,

$$\boxed{dh = c_p dT} \tag{2.25}$$

Scanned by CamScanner

From Eqs. (2.16) for a constant volume (isochoric) process, we get

$$\delta q = du = c_v dT \tag{2.26a}$$

and for a constant pressure (isobaric) process,

$$\delta q = dh = c_p dT, \quad \delta q = dh = c_v dT + pdv \tag{2.26b}$$

For an adiabatic ($q = 0$) flow process,

$$dh = vdp \tag{2.26c}$$

From Eqs. (2.26), it can be inferred that:

1. When heat is added at constant volume, it only raises the internal energy.
2. If heat is added at constant pressure, it not only increases the internal energy, but also does some external work, i.e. it increases the enthalpy.
3. If the change is adiabatic, the change in enthalpy is equal to external work vdp.

Thermally Perfect Gas

A gas is said to be thermally perfect when its internal energy and enthalpy are functions of temperature alone, i.e. for a thermally perfect gas,

$$u = u(T), \quad h = h(T) \tag{2.27a}$$

Therefore, from Eqs. (2.24) and (2.25), we get

$$c_v = c_v(T), \quad c_p = c_p(T) \tag{2.27b}$$

Further, from Eqs. (2.22), (2.23) and (2.27a), we obtain

$$\left(\frac{\partial u}{\partial v}\right)_T = 0, \quad \left(\frac{\partial h}{\partial p}\right)_T = 0 \tag{2.27c}$$

The important relations of this section are

$$du = c_v dT, \quad dh = c_p dT$$

These equations are universally valid so long as the gas is thermally perfect. Otherwise, in order to have equations of universal validity, we must add $\left(\frac{\partial u}{\partial v}\right)_T dv$ to the first equation and $\left(\frac{\partial h}{\partial p}\right)_T dp$ to the second equation.

The state equation for a thermally perfect gas is

$$pv = RT$$

In the differential form, this equation becomes

$$pdv + vdp = RdT$$

Scanned by CamScanner

Also,

$$h = u + pv$$
$$dh = du + pdv + vdp$$

Therefore,

$$dh - du = pdv + vdp = RdT$$

i.e.

$$RdT = c_p dT - c_v dT$$

Thus,

$$\boxed{R = c_p(T) - c_v(T)} \tag{2.28}$$

For thermally perfect gases, Eq. (2.28) shows that, though c_p and c_v are functions of temperature, their difference is a constant with reference to temperature.

2.5 THE PERFECT GAS

This is still more a specialization than the thermally perfect gas. For a perfect gas, both c_p and c_v are constants and are independent of temperature, i.e.

$$c_v = \text{constant} \neq c_v(T), \quad c_p = \text{constant} \neq c_p(T) \tag{2.29}$$

Such a gas with constant c_p and c_v is called a *calorically perfect gas*. Therefore, a perfect gas should be thermally as well as calorically perfect.

From the above discussions, it is evident that:

1. A perfect gas must be both thermally and calorically perfect.
2. A perfect gas must satisfy both *thermal equation of state*, $p = \rho RT$, and *caloric equations of state*, $c_p = \partial h/\partial T$, $c_v = \partial u/\partial T$.
3. A calorically perfect gas must be thermally perfect and a thermally perfect gas need not be calorically perfect. That is, thermal perfectness is a prerequisite for caloric perfectness.
4. For a thermally perfect gas, $c_p = c_p(T)$ and $c_v = c_v(T)$; i.e. both c_p and c_v are functions of temperature. But even though the specific heats c_p and c_v vary with temperature, their ratio, γ, becomes a constant and independent of temperature, i.e. $\gamma = \text{constant} \neq \gamma(T)$.
5. For a calorically perfect gas, c_p, c_v as well as γ are constants and independent of temperature.

Calculation of Entropy

Entropy is defined by the relation (for a reversible process)

$$\delta q = Tds$$

Scanned by CamScanner

Using Eqs. (2.16), we can write

$$Tds = du + pdv \tag{2.30}$$

$$Tds = dh - vdp \tag{2.31}$$

Equations (2.30) and (2.31) are as important and useful as the original form of the first law of thermodynamics, viz. Eq. (2.1).

For a thermally perfect gas, from Eq. (2.25), we have $dh = c_p dT$. Substituting this relation into Eq. (2.31), we obtain

$$ds = c_p \frac{dT}{T} - \frac{vdp}{T} \tag{2.32}$$

Substituting the perfect gas equation of state, $pv = RT$, into Eq. (2.32), we get

$$ds = c_p \frac{dT}{T} - R\frac{dp}{p} \tag{2.33}$$

Integrating Eq. (2.33) between states 1 and 2, we obtain

$$s_2 - s_1 = \int_{T_1}^{T_2} c_p \frac{dT}{T} - R \ln \frac{p_2}{p_1} \tag{2.34}$$

Equation (2.34) holds for a thermally perfect gas. The integral can be evaluated if c_p is known as function of T. Further, assuming the gas to be calorically perfect, for which c_p is constant, Eq. (2.34) reduces to

$$\boxed{s_2 - s_1 = c_p \ln \frac{T_2}{T_1} - R \ln \frac{p_2}{p_1}} \tag{2.35}$$

Using $du = c_v dT$ in Eq. (2.30), the change in entropy can also be expressed as

$$s_2 - s_1 = c_v \ln \frac{T_2}{T_1} + R \ln \frac{v_2}{v_1} \tag{2.36}$$

From the above discussions, we can summarize that a perfect gas is both thermally and calorically perfect. Further, a calorically perfect gas must also be thermally perfect, whereas a thermally perfect gas need not be calorically perfect.

For a thermally perfect gas, $p = \rho RT$, $c_v = c_v(T)$, $c_p = c_p(T)$, and for a perfect gas, $p = \rho RT$, c_v = const. c_p = const. Further, for a perfect gas, all equations get simplified, resulting in the following simple relations for u, h and s:

$$u = u_1 + c_v T \tag{2.37a}$$

$$h = h_1 + c_p T \tag{2.37b}$$

$$s = s_1 + c_v \ln \frac{p}{p_1} - c_p \ln \frac{\rho}{\rho_1} \tag{2.37c}$$

where the subscript '1' refers to the initial state.

Scanned by CamScanner

Equations (2.37a), (2.37b) and (2.28) combined with the equation of state result in

$$u = u_1 + \frac{1}{\gamma - 1}\frac{p}{\rho}, \quad h = h_1 + \frac{\gamma}{\gamma - 1}\frac{p}{\rho}$$

where γ is ratio of specific heats, c_p/c_v.

For the most simple molecular model, the kinetic theory of gases gives the specific heats ratio, γ, as

$$\boxed{\gamma = \frac{n+2}{n}}$$

where n is the number of degrees of freedom of the gas molecules. Thus, for monatomic gases with $n = 3$, the specific heats ratio becomes

$$\gamma = \frac{3+2}{3} = 1.67$$

Diatomic gases like oxygen, nitrogen, etc. have $n = 5$. Thus,

$$\gamma = \frac{5+2}{5} = 1.4$$

Gases with extremely complex molecules, such as freon and gaseous compounds of uranium have large values of n, resulting in values of γ only slightly greater than unity. Thus, the specific heats ratio value γ varies from 1 to 1.67, depending on the molecular nature of the gas, i.e.

$$\boxed{1 \le \gamma \le 1.67}$$

The preceding relations for u and h are important, because they connect the quantities used in thermodynamics with those used in gas dynamics. With the aid of these relations, the energy equation can be written in two different forms, as follows:

1. The energy equation for an adiabatic process, as given by Eq. (2.15), is

$$h + \frac{V^2}{2} = h_0 = \text{constant}$$

and when the gas is perfect, it becomes

$$c_p T + \frac{V^2}{2} = c_p T_0 = \text{constant} \qquad (2.38a)$$

2. Equation (2.38a), when combined with the state equation, yields

$$\boxed{\frac{\gamma}{\gamma - 1}\frac{p}{\rho} + \frac{V^2}{2} = \text{constant}} \qquad (2.38b)$$

Equation (2.38b) is the form of the energy equation commonly used in gas dynamics. This is popularly known as *compressible Bernoulli's* equation for isentropic flows.

Scanned by CamScanner

From Eq. (2.38a), we infer that for an adiabatic process of a perfect gas,

$$\boxed{T_{01} = T_{02} = T_0 = \text{constant}} \tag{2.39}$$

So far, we have not made any assumption about the reversibility or irreversibility of the process. Equation (2.39) implies that the stagnation temperature remains constant for an adiabatic process of a perfect gas, irrespective of the process being reversible or irreversible.

Consider the flow of gas in a tube with an orifice as shown in Fig. 2.2. In such a flow process, there will be pressure loss. But if the stagnation temperature is measured before and after the orifice plate and if it remains constant, then the gas can be treated as perfect gas and all the simplified equations (Eq. (2.37)) can be used. Otherwise, it cannot be treated as perfect gas, and Eq. (2.37c) can be rewritten as

$$\frac{p_2}{p_1} = \left(\frac{\rho_2}{\rho_1}\right)^{\gamma} \exp\left(\frac{s_2 - s_1}{c_v}\right) \tag{2.40}$$

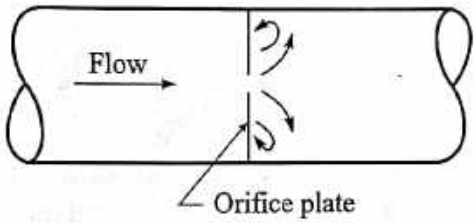


Fig. 2.2 Flow through an orifice plate.

Isentropic Relations

An adiabatic and reversible process is called an isentropic process. For an adiabatic proess, $\delta q = 0$, and for a reversible process, $ds_{\text{irrev}} = 0$. Hence, from Eq. (2.18), an isentropic process is one in which $ds = 0$, i.e. the entropy is constant. Important relations for an isentropic process can be directly obtained from Eqs. (2.35), (2.36) and (2.40), setting $s_2 = s_1$. For example, from Eq. (2.35), we have

$$0 = c_p \ln\frac{T_2}{T_1} - R \ln\frac{p_2}{p_1}$$

$$\ln\frac{p_2}{p_1} = \frac{c_p}{R} \ln\frac{T_2}{T_1}$$

$$\frac{p_2}{p_1} = \left(\frac{T_2}{T_1}\right)^{c_p/R} \tag{2.41}$$

From Eq. (2.28),

$$c_p - c_v = R$$

Scanned by CamScanner

$$1 - \frac{c_v}{c_p} = \frac{R}{c_p}$$

$$\frac{\gamma - 1}{\gamma} = \frac{R}{c_p}$$

since $c_p/c_v = \gamma$. Therefore,

$$\frac{c_p}{R} = \frac{\gamma}{\gamma - 1}$$

Substituting this relation into Eq. (2.41), we obtain

$$\frac{p_2}{p_1} = \left(\frac{T_2}{T_1}\right)^{\gamma/(\gamma-1)} \tag{2.42}$$

Similarly, from Eq. (2.36),

$$0 = c_v \ln\frac{T_2}{T_1} + R \ln\frac{v_2}{v_1}$$

$$\ln\frac{v_2}{v_1} = -\frac{c_v}{R} \ln\frac{T_2}{T_1}$$

$$\frac{v_2}{v_1} = \left(\frac{T_2}{T_1}\right)^{-c_v/R} \tag{2.43}$$

But, it can be shown that

$$\frac{c_v}{R} = \frac{1}{\gamma - 1}$$

Substituting the above relation into Eq. (2.43), we get

$$\frac{v_2}{v_1} = \left(\frac{T_2}{T_1}\right)^{-1/(\gamma-1)} \tag{2.44}$$

Since $\rho_2/\rho_1 = v_1/v_2$, Eq. (2.44) becomes

$$\frac{\rho_2}{\rho_1} = \left(\frac{T_2}{T_1}\right)^{1/(\gamma-1)} \tag{2.45}$$

Substituting $s_1 = s_2$ into Eq. (2.40), we obtain

$$\frac{p_2}{p_1} = \left(\frac{\rho_2}{\rho_1}\right)^{\gamma} \tag{2.46}$$

This relation is also called Poisson's equation. Summarizing Eqs. (2.42), (2.45), and (2.46), we can write

$$\boxed{\frac{p_2}{p_1} = \left(\frac{\rho_2}{\rho_1}\right)^{\gamma} = \left(\frac{T_2}{T_1}\right)^{\gamma/(\gamma-1)}} \tag{2.47}$$

Scanned by CamScanner

Equation (2.47) is an important equation and is used very frequently in the analysis of compressible flows.

Using the above discussed isentropic relations, several useful equations of total (stagnation) conditions can be obtained as follows: From Eqs. (2.38a) and (1.15),

$$\frac{T_0}{T} = 1 + \frac{V^2}{2c_pT} = 1 + \frac{V^2}{2\gamma RT/(\gamma-1)} = 1 + \frac{V^2}{2a^2/(\gamma-1)}$$

Hence,

$$\boxed{\frac{T_0}{T} = 1 + \frac{\gamma-1}{2}M^2} \tag{2.48}$$

Equation (2.48) gives the ratio of total to static temperature at a point in an isentropic flow field as a function of the flow Mach number M at that point. Combining Eqs. (2.47) and (2.48), we get

$$\boxed{\frac{p_0}{p} = \left(1 + \frac{\gamma-1}{2}M^2\right)^{\gamma/(\gamma-1)}} \tag{2.49}$$

$$\boxed{\frac{\rho_0}{\rho} = \left(1 + \frac{\gamma-1}{2}M^2\right)^{1/(\gamma-1)}} \tag{2.50}$$

Equations (2.49) and (2.50) give the ratios of total to static pressure and density, respectively, at a point in an isentropic flow field as a function of Mach number M at that point. Equations (2.48) – (2.50) form a set of most important equations for total properties, which are often used in gas dynamic studies. Their values as a function of M for $\gamma = 1.4$ (air at standard conditions) are tabulated in Table A1 of Appendix A.

At this stage, we may ask as to how Eq. (2.47) which is derived on the basis of the concept of isentropic change of state (which is so restrictive—adiabatic as well as reversible—that it may find only limited applications) is so important, and why it is frequently used. In the compressible flow processes such as flow through a rocket engine, flow over an airfoil, etc. large regions of the flow fields are isentropic. In the regions adjacent to the rocket nozzle walls and the airfoil surface, a boundary layer is formed wherein the dissipative mechanisms of viscosity, thermal conduction, and diffusion are strong. Hence, the entropy increases within these boundary layers. On the other hand, for fluid elements outside the boundary layer, the dissipative effects are negligible. Further, no heat is being added to or removed from the fluid element at these points; hence the flow is adiabatic. Therefore, the fluid elements outside the boundary layer experience adiabatic and reversible processes; hence the flow is isentropic. Moreover, the boundary layers are usually thin; hence large regions of the flow fields are isentropic. Therefore, a study of isentropic flow is directly applicable to many types of practical flow problems. Equation (2.47) is a powerful relation connecting pressure, density, and temperature, valid for a calorically perfect gas.

Scanned by CamScanner

Expressing all the quantities as stagnation quantities, Eq. (2.37c) can be written as

$$s_{02} - s_{01} = c_v \ln \frac{p_{02}}{p_{01}} - c_p \ln \frac{\rho_{02}}{\rho_{01}} \tag{2.51}$$

Also, by Eq. (2.28),

$$R = c_p - c_v$$

and by the state equation

$$\frac{p_{01}}{p_{02}} = \frac{\rho_{01}}{\rho_{02}} \frac{T_{01}}{T_{02}}$$

Substitution of the above relations into Eq. (2.51) yields

$$s_{02} - s_{01} = R \ln \frac{p_{01}}{p_{02}} + c_p \ln \frac{T_{02}}{T_{01}}$$

For an adiabatic process of a perfect gas,

$$T_{01} = T_{02}$$

Therefore,

$$s_{02} - s_{01} = R \ln \frac{p_{01}}{p_{02}} \tag{2.52}$$

From Eq. (2.52) it is obvious that the entropy changes only when there are losses in pressure. It does not change with velocity, and hence there is nothing like static and stagnation entropy. Also, by Eq. (2.39), the stagnation temperature does not change even when there are pressure losses. There is always an increase in entropy associated with pressure loss. In other words, when there are losses, there will be an increase in entropy, leading to a drop in stagnation pressure. These losses can be due to friction, separation, shock, etc.

EXAMPLE 2.1 Air flows through a duct. The pressure and temperature at station 1 are $p_1 = 0.7$ atmosphere and $T_1 = 30°C$, respectively. At a second station, the pressure is 0.5 atm. Calculate the temperature and density at the second station. Assume the flow to be isentropic.

Solution Given

$$p_1 = 0.7 \text{ atm} = 0.7 \times 1.0133 \times 10^5 \text{ N/m}^2$$

since in ISA, 1 atm = 1.0133×10^5 N/m^2 and $T_1 = 30°C$, i.e. $T_1 = 30 + 273 = 303$ K.

Using the state equation, we get

$$\rho_1 = \frac{p_1}{RT_1} = \frac{0.7 \times 1.0133 \times 10^5}{287 \times 303} = 0.8157 \text{ kg/m}^3$$

where the gas constant $R = 287$ m^2/s^2-K for air. By Eq. (2.42),

Scanned by CamScanner

$$\frac{p_2}{p_1} = \left(\frac{T_2}{T_1}\right)^{\gamma/(\gamma-1)}$$

Therefore,

$$\frac{T_2}{T_1} = \left(\frac{0.5}{0.7}\right)^{(\gamma-1)/\gamma} = \left(\frac{0.5}{0.7}\right)^{0.4/1.4} = 0.908$$

$$T_2 = (0.908)(303) = 275.12 \text{ K}$$

By Eq. (2.45),

$$\frac{\rho_2}{\rho_1} = \left(\frac{T_2}{T_1}\right)^{1/(\gamma-1)} = (0.908)^{1/0.4} = 0.786$$

Thus,

$$\rho_2 = (0.786)(0.8157) = 0.641 \text{ kg/m}^3$$

Hence, the temperature and density at the second station are

$$T_2 = \boxed{2.12°\text{C}}, \quad \rho_2 = \boxed{0.641 \text{ kg/m}^3}$$

EXAMPLE 2.2 Air is allowed to expand from an initial state A (where $p_A = 2.068 \times 10^5$ N/m^2 and $T_A = 333$ K) to state B (where $p_B = 1.034 \times 10^5$ N/m^2 and $T_B = 305$ K). Calculate the change in the specific entropy of the air, and show that the change in entropy is the same for (a) an isobaric process from A to some intermediate state C followed by an isovolumetric change from C to B, and (b) an isothermal change from A to some intermediate state D followed by an isentropic change from D to B.

Solution Given

$$p_A = 2.068 \times 10^5 \text{ N/m}^2, \quad T_A = 333 \text{ K}$$

and

$$p_B = 1.034 \times 10^5 \text{ N/m}^2, \quad T_B = 305 \text{ K}$$

(a) For an isobaric process from state A to state C:

$$p_A = p_C$$

For an isovolumetric process from state C to state B:

$$v_C = v_B$$

By the state equation, $pv = RT$,

$$v_A = \frac{RT_A}{p_A} = \frac{287 \times 333}{2.068 \times 10^5} = 0.462 \text{ m}^3/\text{kg}$$

$$v_B = \frac{RT_B}{p_B} = \frac{287 \times 305}{1.034 \times 10^5} = 0.847 \text{ m}^3/\text{kg}$$

Scanned by CamScanner

Now,

$$T_C = \frac{p_C v_C}{R} = \frac{p_A v_B}{R} \qquad (\because p_C = p_A,\ v_C = v_B)$$

$$T_C = \frac{2.068 \times 10^5 \times 0.847}{287} = 610 \text{ K}$$

By Eq. (2.34),

$$s_C - s_A = \int_{T_A}^{T_C} c_p \frac{dT}{T} - R \ln \frac{p_C}{p_A}$$

But, $p_C = p_A$ and, therefore,

$$s_C - s_A = c_p \ln \frac{T_C}{T_A}$$

For the isovolumetric process, by Eq. (2.36), we have

$$s_B - s_C = c_v \ln \frac{T_B}{T_C}$$

Hence,

$$s_B - s_A = c_p \ln \frac{T_C}{T_A} + c_v \ln \frac{T_B}{T_C}$$

Now,

$$c_p = \frac{\gamma}{\gamma - 1} R = \frac{1.4}{0.4} \times 287 = 1004.5 \text{ m}^2/\text{s}^2\text{-K}$$

$$c_v = \frac{1}{\gamma - 1} R = \frac{1}{0.4} \times 287 = 717.5 \text{ m}^2/\text{s}^2\text{-K}$$

Therefore,

$$s_B - s_A = 1004.5 \times \ln \frac{610}{333} + 717.5 \times \ln \frac{305}{610}$$
$$= 608 - 497.3$$
$$= \boxed{110.7 \text{ Nm/kg-K}}$$

(b) For an isothermal change from A to D, $T_A = T_D$. For an isentropic change from D to B, by Eq. (2.35), we have

$$s_B - s_A = c_p \ln \frac{T_B}{T_A} - R \ln \frac{p_B}{p_A}$$

$$= 1004.5 \times \ln \frac{305}{333} - 287 \times \ln \frac{1.034 \times 10^5}{2.068 \times 10^5}$$
$$= -88.23 + 198.93$$
$$= \boxed{110.7 \text{ Nm/kg-K}}$$

Scanned by CamScanner

Limitations of Air as a Perfect Gas

1. When the temperature is less than 500 K, air can be treated as a perfect gas and the ratio of specific heats, γ, takes a constant value of 1.4.
2. When the temperature lies between 500 K and 2000 K, air is only thermally perfect, and the state equation $p = \rho RT$ is valid, but c_p and c_v become function of temperature.
3. For temperatures more than 2000 K, air becomes both thermally and calorically imperfect.

In supersonic flight with Mach number, say 2.0 (at sea level), the temperature reached is already about 245°C (more than 500 K). But, for $500\ \text{K} \leq T \leq 700\ \text{K}$, we can still use perfect gas equations and the error involved in doing so will be negligible, i.e. for Mach number less than 2.68, perfect gas equations can be used with slight error. For temperatures more than 700 K, we must go for thermally perfect gas equations.

At this stage, we may have some doubt about the possible values of the isentropic index γ, when the flow medium is at a temperature which is quite high and the medium cannot be assumed as perfect. This doubt can be cleared if we consider that an ideal gas, which satisfies perfect gas equations, has γ = constant, independent of temperature. For a monatomic gas (He, Ar, Ne, etc.), the simplest possible molecular structure gives $\gamma = 5/3$. This prediction is well confirmed by experiment. At the other extreme of molecular complexity, very complicated molecules have large number of degrees of freedom, and γ may approach unity, which represents the minimum possible value, since $c_p \geq c_v$ by virtue of a general thermodynamic argument (see Eq. (B.6) in Appendix B of Thompson, 1972). Then γ necessarily has a range of values

$$\boxed{\frac{5}{3} \geq \gamma \geq 1}$$

Experimental results show that most diatomic gases, nitrogen and oxygen, in particular, have $\gamma = 7/5$ at room temperature, gradually tending to $\gamma = 9/7$ at a few thousand kelvin.

2.6 SUMMARY

In this chapter we introduced and discussed the basic concepts of thermodyamics. *Thermodynamics* is the science that primarily deals with energy. The *first law of thermodynamics* is simply an expression of the conservation of energy principle.

The second law of thermodynamics asserts that actual processes occur in the direction of increasing entropy.

A system of fixed mass is called a *closed system*, or *control mass*, and a system that involves mass transfer across its boundaries is called an *open system*, or *control volume*.

Scanned by CamScanner

For an open system, by the first law of thermodynamics, the energy equation can be expressed as

$$H_1 + \frac{1}{2}mV_1^2 + mgz_1 = H_2 + \frac{1}{2}mV_2^2 + mgz_2 + W_S - Q_{12} \quad (2.9)$$

where subscripts 1 and 2 refer to states 1 and 2. This equation is universally valid. For a gas dynamic working process, Eq. (2.9) becomes

$$H_1 + \frac{1}{2}mV_1^2 = H_2 + \frac{1}{2}mV_2^2 + W_S - Q_{12} \quad (2.10)$$

A process during which there is no heat transfer is called an adiabatic process. There are two ways a process can be adiabatic: Either the system is well insulated so that only a negligible amount of heat can pass through the boundary, or both the system and the surroundings are at the same temperature and therefore there is no driving thermal potential for heat transfer. For an adiabatic process the stagnation or total temperature remains unchanged.

A reversible process is defined as a process which can be reversed without leaving any trace on the surroundings. That is, both the system and the surroundings are returned to their initial states at the end of the reverse process. However, in reality it is not possible to have a process which can be reversed without leaving any trace on the surroundings. That is, in practice both the system and the surroundings returning to their initial states at the end of the process is impossible. Thus, the reversible process is only an idealized process. Processes that are not reversible are called *irreversible processes*.

A process which is adiabatic and reversible is called an *isentropic process*. As pointed out in Section 2.3, two factors can change the entropy of a system: heat transfer and irreversibility. Many engineering systems or devices such as nozzles, diffusers, and turbines are essentially adiabatic in their operation, and they perform best when the irreversibilities, such as the friction associated with the process, are minimized. Therefore, an isentropic process can serve as an appropriate model for actual processes.

A perfect gas is an *imaginary* substance that obeys the relation $p = \rho RT$. It is also called an ideal gas. It has been experimentally observed that the perfect gas relation given above closely approximates the p–ρ–T behaviour of real gases at low densities. At low pressures and high temperatures, the density of a gas decreases, and the gas behaves as perfect gas under these conditions. In the range of practical interest, many familiar gases such as air, nitrogen, oxygen, hydrogen, helium, argon, neon, krypton, and even heavier gases such as carbon dioxide can be treated as ideal gas with negligible error (often less than 1 per cent). Dense gases such as water vapour in steam power plants and refrigerant vapour in refrigerators, however, should not be treated as ideal gases.

The relation

$$p = \rho RT \quad \text{or} \quad pv = RT$$

is called the *perfect gas equation* of state or *ideal gas equation of state*. In this equation, p is the absolute pressure, T the absolute temperature, ρ the density,

Scanned by CamScanner

v the specific volume, and R is the gas constant. R is different for each gas and is determined from

$$R = \frac{R_u}{M} \text{ kJ/kg-K}$$

where R_u is the universal gas constant and M is the molar mass or molecular weight of the gas. The constant R_u is the same for all substances, and its value is

$$R_u = 8314 \text{ J/kg-K}$$

The amount of energy needed to raise the temperature of a unit mass of a substance by one degree is called the *specific heat at constant volume* c_v for a constant-volume process and the *specific heat at constant pressure* c_p for a constant-pressure process. They are defined as

$$c_v = \left(\frac{\partial u}{\partial T}\right)_v, \qquad c_p = \left(\frac{\partial h}{\partial T}\right)_p$$

For perfect gases, u and h are functions of temperature alone. The du and dh of perfect gases can be expressed as

$$du = c_v dT \tag{2.24}$$

$$dh = c_p dT \tag{2.25}$$

For perfect gases, c_v and c_p are related by

$$c_p - c_v = R \tag{2.28}$$

The specific heats ratio γ is defined as

$$\gamma = \frac{c_p}{c_v}$$

A gas is said to be perfect when it is thermally as well as calorically perfect. For a thermally perfect gas, u, h, c_v, and c_p are functions of temperature alone. That is,

$$u = u(T), \qquad h = h(T) \tag{2.27a}$$

$$c_v = c_v(T), \qquad c_p = c_p(T) \tag{2.27b}$$

For a calorically perfect gas, c_p and c_v are constants and are independent of temperature, i.e.

$$c_v = \text{constant} \neq c_v(T)$$

$$c_p = \text{constant} \neq c_p(T) \tag{2.29}$$

Therefore, a perfect gas has to be thermally as well as calorically perfect.

Entropy is a useful property and serves as a valuable tool in the second-law analysis of engineering devices. Entropy may be viewed as a measure of *disorder* or *randomness* in a system. The change in entropy can be expressed as

$$ds = \frac{\delta q}{T} + ds_{\text{irrev}} \tag{2.18}$$

Scanned by CamScanner

The value of ds can be used to determine whether a process is reversible, irreversible, or impossible:

$$ds \begin{cases} > 0 & \text{(irreversible process)} \\ = 0 & \text{(reversible process)} \\ < 0 & \text{(imposssible process)} \end{cases}$$

Entropy is a property, and it can be expressed in terms of more familiar properties through the Tds relations, expressed as

$$Tds = du + pdv \tag{2.30}$$

$$Tds = dh - vdp \tag{2.31}$$

These two relations have many uses and serve as the starting point in developing entropy change relations for processes.

For ideal gases with constant specific heats, the *entropy change* relations and isentropic relations for a process can be summarized as follows:

Any process

$$s_2 - s_1 = c_p \ln\frac{T_2}{T_1} - R \ln\frac{p_2}{p_1} \tag{2.35}$$

$$s_2 - s_1 = c_v \ln\frac{T_2}{T_1} + R \ln\frac{v_2}{v_1} \tag{2.36}$$

Isentropic process: s = constant

$$\frac{p_2}{p_1} = \left(\frac{\rho_2}{\rho_1}\right)^{\gamma} = \left(\frac{T_2}{T_1}\right)^{\gamma/(\gamma-1)} \tag{2.47}$$

$$\frac{T_0}{T} = 1 + \frac{\gamma-1}{2}M^2 \tag{2.48}$$

$$\frac{p_0}{p} = \left(1 + \frac{\gamma-1}{2}M^2\right)^{\gamma/(\gamma-1)} \tag{2.49}$$

$$\frac{\rho_0}{\rho} = \left(1 + \frac{\gamma-1}{2}M^2\right)^{1/(\gamma-1)} \tag{2.50}$$

For an adiabatic process of a perfect gas, $T_{01} = T_{02} = T_0$, and the entropy change in terms of stagnation pressure becomes

$$s_{02} - s_{01} = R \ln\frac{p_{01}}{p_{02}} \tag{2.52}$$

From this equation it is evident that the entropy changes only when there are losses in pressure. Entropy does not change with velocity and hence there is nothing like stagnation or static entropy.

The ratio of specific heats varies from 1 to 1.67. For monatomic gases like argon, $\gamma = 1.67$. Diatomic gases such as oxygen and nitrogen have $\gamma = 1.4$; for gases with extremely complex molecular structure, γ is slightly more than unity.

Scanned by CamScanner

From the discussions in this chapter, it is evident that, for the fluid motion of interest in gas dynamics the results of classical thermodynamics can be applied directly, provided the instantaneous local thermodynamic state is considered. The pressure, density, and temperature ratios are expressible in terms of Mach number for isentropic process and when the fluid is perfect, the isentropic tables are adequate for solving gas dynamic problems involving isentropic processes.

PROBLEMS

1. A stream of air drawn from a reservoir is flowing through an irreversible adiabatic process into a second reservoir in which the pressure is half of that in the first. Calculate the entropy difference between the two reservoirs at the beginning of the process.

   [**Ans.** 198.933 Nm/kg-K]

2. Air is expanded in an insulated cylinder equipped with a frictionless piston. The initial temperature of the air is 1400 K. The original volume is 1/10 of the final volume. Calculate (a) the change in temperature, (b) the work removed from the gas, and (c) the pressure ratio.

   [**Ans.** (a) −842.65 K; (b) 6.04×10^5 Nm/kg; (c) 25.1189]

3. A 15 m^3 tank contains air at $p_1 = 5.0 \times 10^5$ N/m^2 and $T_1 = 500$ K. The air is discharged into the atmosphere through a nozzle until the mass of the air contained in the tank is reduced to one-half of its original value. Assuming that the process is adiabatic and frictionless, calculate the pressure and the temperature of the air remaining in the tank. Consider a calorically perfect gas.

   [**Ans.** 1.8946×10^5 N/m^2, 378.92 K]

4. Air is compressed isentropically in a centrifugal compressor from a pressure of 1.0×10^5 N/m^2 to a pressure of 6.0×10^5 N/m^2. The initial temperature is 290 K. Calculate (a) the change in temperature, (b) the change in internal energy, and (c) the work imparted to the air, neglecting the velocity change.

   [**Ans.** (a) 193.868 K; (b) 1.39×10^5 Nm/kg; (c) 1.39×10^5 Nm/kg]

5. A perfect gas, enclosed by an insulated (upright) cylinder and piston, is at equilibrium at conditions p_1, v_1, T_1. A weight is placed on the piston. After a number of oscillations, the motion subsides and the gas reaches a new equilibrium at conditions p_2, v_2, T_2. Find the temperature ratio T_2/T_1 in terms of the pressure ratio $\lambda = p_2/p_1$. Show that the change in entropy is given by

$$s_2 - s_1 = R \ln \left[\left(\frac{1 + (\gamma - 1)\lambda}{\gamma} \right)^{\gamma/(\gamma-1)} \frac{1}{\lambda} \right]$$

Scanned by CamScanner

Show that, if the initial disturbance is small, i.e. $\lambda = 1 + \varepsilon$, $\varepsilon \ll 1$, then

$$\frac{s_2 - s_1}{R} \approx \frac{\varepsilon^2}{2\gamma}$$

$$\left[\textbf{Ans.}\ \frac{T_2}{T_1} = \frac{1 + (\gamma - 1)\lambda}{\gamma}\right]$$

6. The unit weight of air is compressed adiabatically from an initial state with $p_1 = 10^5$ N/m^2 and $T_1 = 303$ K to a final state of $p_2 = 2p_1$ and T_2. If the air enters and leaves the compressor with same velocities, calculate the shaft work necessary. Assume air as an ideal gas.

[**Ans.** $W_S = -66.66$ kN-m/kg]

7. A fluid in a cylinder at a pressure of 6 atm and volume 0.3 m^3 is expanded at constant pressure to a volume of 2 m^3. Determine the work done by this expansion.

[**Ans.** 1.0335 MJ]

8. A gas at pressure 150 kPa and density 1.5 kg/m^3 is compressed to 690 kPa isentropically. Determine the final density. Assume the isentropic index to be 1.3.

[**Ans.** 4.85 kg/m^3]

9. Air undergoes a change of state isentropically. The initial pressure and temperature are 101 kPa and 298 K, respectively. The final pressure is seven times the initial pressure. Determine the final temperature. Assume air to be an ideal gas with ratio of specific heats $\gamma = 1.4$.

[**Ans.** 519.9 K]

10. Air at 30°C is compressed isentropically to occupy a volume which is 1/30 of its initial volume. Assuming air as an ideal gas, determine the final temperature.

[**Ans.** 908.55°C]

11. An ideal gas is cooled under constant pressure from 200°C to 50°C. Assuming constant specific heats with $c_p = 1000$ J/kg-K, and $\gamma = 1.4$, determine, (a) the molecular weight of the gas and (b) the ratio of final to initial volume of the gas.

[**Ans.** (a) 29.1; (b) 0.683]

12. If the velocity of sound in an ideal gas with a molecular weight of 29 is measured to be 400 m/s at 100°C, determine the c_p and c_v of the gas at 100°C.

[**Ans.** $c_p = 860.1$ J/kg-K, $c_v = 573.4$ J/kg-K]

13. Air flows isentropically through a nozzle. If the velocity and the temperature at the exit are 390 m/s and 28°C, respectively, determine the Mach number and stagnation temperature at the exit. What will be the Mach number just upstream of a station where the temperature is 92.5°C?

[**Ans.** 1.12, 103.29°C, 0.387]

Scanned by CamScanner

14. Hydrogen gas in a cylinder at 7 atm and 300 K is expanded isentropically through a nozzle to a final pressure of 1 atm. Assuming hydrogen to be a perfect gas with $\gamma = 1.4$, determine the velocity and Mach number corresponding to the final pressure. Also, find the mass flow rate through the nozzle for an exit area of 10 cm^2.

[**Ans.** 1923 m/s, 1.93, 0.275 kg/s]

15. Air in a cylinder changes state from 101 kPa and 310 K to a pressure of 1100 kPa according to the process

$$pv^{1.32} = \text{constant}$$

Determine the entropy change associated with this process. Assume air to be an ideal gas with c_p = 1004 J/kg-K and $\gamma = 1.4$.

[**Ans.** −103.8 J/kg-K]

16. Oxygen gas is heated from 25°C to 125°C. Determine the increase in its internal energy and enthalpy. Take $\gamma = 1.4$.

[**Ans.** 64950 J/kg, 90930 J/kg]

17. Air enters a compressor at 100 kPa and 1.175 kg/m^3 and exits at 500 kPa and 5.875 kg/m^3. Determine the enthalpy difference between the outlet and inlet states. [**Ans.** 0]

18. Prove the following relation for an ideal gas.

$$ds = c_p \frac{dv}{v} + c_v \frac{dp}{p}$$

Using this result, show that for an ideal gas undergoing an isentropic change of state with constant specific heats, pv^γ = constant.

19. A quantity of air at 0.7 MPa and 150°C occupies a volume of 0.014 m^3. If the gas is expanded isothermally to a volume of 0.084 m^3, calculate the change in entropy.

[**Ans.** 513.4 J/kg-K]

20. 0.3 kg of air at 350 kPa and 35°C receives heat energy at constant volume until its pressure becomes 700 kPa. It then receives heat energy at constant pressure until its volume becomes 0.2289 m^3. Calculate the entropy change associated with each process.

[**Ans.** 149.2 J/K, 333 J/K]

21. Air flows through a frictionless diffuser. At a station in the diffuser the temperature, pressure and velocity are 0°C, 140 kPa and 900 m/s, respectively and at a downstream station the velocity decreases to 300 m/s. Assuming the flow to be adiabatic, calculate the increase in pressure and temperature of the flow between these stations.

[**Ans.** 358.39 K, 2.491 MPa]

22. Nitrogen gas is compressed reversibly and isothermally from 100 kPa and 25°C to a final pressure of 300 kPa. Calculate the entropy change associated with this compression process.

[**Ans.** − 0.3263 kJ/kg-K]

Scanned by CamScanner

23. Air undergoes a change of state isentropically from 300 K and 110 kPa to a final pressure of 550 kPa. Assuming ideal gas behavior, determine the change in enthalpy. [**Ans.** 176.29 kJ/kg]
24. Air at low pressure inside a rigid tank is heated from 50°C to 125°C. What is the change in entropy associated with this heating process? [**Ans.** 149.75 J/kg-K]
25. Compute the temperature rise at the nose of an aircraft flying with Mach number 2 at an altitude of 10,000 m. [**Ans.** 178.52]
26. A gas at an initial volume of 0.06 m^3 and 15°C is expanded to a volume of 0.12 m^3 while the pressure remains constant. Determine the final temperature of the gas. [**Ans.** 303.15°C]
27. If the speed of sound in a perfect gas stream at 300 K is 320 m/s, determine the specific heats ratio, if the molecular weight of the gas is 30. [**Ans.** 1.23]
28. A diatomic perfect gas is accelerated from state 1 to state 2. If the change in the internal energy associated with this process is –50 kJ/(kg-K), what will be the change in enthalpy? [**Ans.** –70 kJ/(kg-K)]
29. Helium gas at rest at 400 K is accelerated to a state where its enthalpy is 212 kJ/kg below the stagnation enthalpy. Determine the Mach number of the accelerated flow, assuming the specific heats ratio for helium is 1.66. [**Ans.** 0.585]
30. If the specific heat of a gas mixture at constant pressure is 1220 J/(kg-K), determine the molecular weight of the mixture, assuming it as a diatomic perfect gas. [**Ans.** 23.85]

Scanned by CamScanner

3 Wave Propagation

3.1 INTRODUCTION

We have studied that in incompressible flows the fluid particles are able to sense the presence of a body before actually reaching it. This fact suggests that a signalling mechanism exists, whereby fluid particles can be informed in advance about the presence of a body ahead of it. The velocity of propagation of this signal must be apparently greater than the fluid velocity, since the flow is able to adjust to the presence of a body before reaching it. On the other hand, if the fluid particles were to move faster than the signal waves as in the case of supersonic flows, the fluid would not be able to sense the body before actually reaching it, and very abrupt changes in velocity and other properties would take place.

An understanding of the mechanism by which the signal waves are propagated through fluid medium along with an expression for the velocity of propagation of the waves will be extremely useful in deriving significant conclusions concerning the fundamental differences between incompressible and compressible flows.

3.2 WAVE PROPAGATION

When a fluid medium is allowed to vary its density, the consequence is that the fluid elements can occupy varying volumes in space. This possibility means that a set of fluid elements can spread into a larger region of space without requiring a simultaneous shift to be made to all fluid elements in the flow, as would be required in the case of incompressible flow, in order to keep the density constant. In our preliminary studies of physics, we saw that a small shift of fluid elements in compressible media will induce in due course similar small movements in adjacent elements and in this way a disturbance, referred to as an acoustic wave, propagates at a relatively high speed through the medium. We

Scanned by CamScanner

know that in incompressible flows these waves propagate with infinitely large velocity; in other words, adjustments take place instantaneously throughout the flow and so in the conventional sense, there are no acoustic or elastic waves to be considered. With the introduction of compressibility, we thus permit the possibility of elastic waves having a finite velocity, and the magnitude of this wave velocity is of great importance in compressible flow theory.

3.3 VELOCITY OF SOUND

As seen in Chapter 1, the sound wave is a weak compression wave across which only infinitesimal changes in flow properties occur, i.e. across these waves there will be only infinitesimal pressure variations. In the ensuing chapters, we shall study waves where a comparatively large pressure variation occurs over a very narrow front. Such waves are called *shock waves,* and are nonisentropic, they move relative to the fluid at speeds that exceed the speed of sound. At this stage, one may think of the sound waves as limiting cases of shock waves where the change in pressure across the wave becomes infinitesimal.

By Eq. (1.15), we have the speed of sound a as $a = \sqrt{\gamma RT}$, where T is the static temperature of the medium in absolute unit. The speed of sound in perfect gas may be computed by employing Eq. (1.15) and for other fluids by employing Eq. (1.11).

3.4 SUBSONIC AND SUPERSONIC FLOWS

The velocity of sound is used as the limiting value for differentiating the subsonic flow from the supersonic flow. Flows with velocity more than the speed of sound are called *supersonic flows,* and those with velocities less than the speed of sound are called *subsonic flows.* Flows with velocity close to the speed of sound are classified under a special category called *transonic flows.*

In Chapter 1, we discussed the propagation of disturbance waves in flow fields with velocities from zero level to a level greater than the speed of sound, and that these disturbances will propagate along a "Mach-cone". For supersonic flow over two-dimensional objects, we will have a "Mach-wedge" instead of Mach-cone. The angle μ for such waves is measured in a counterclockwise manner from an axis taken parallel to the direction of freestream as shown in Fig. 3.1.

For an observer looking in the direction of flow towards the disturbance, the wave to his left is called a *left-running wave* and the wave to his right is called *right-running wave* (Fig. 3.1). In Chapter 1, we discussed the propagation of waves created by a disturbance without describing the source of disturbance. Usually, the disturbance arises at a solid boundary where the fluid, having

Scanned by CamScanner

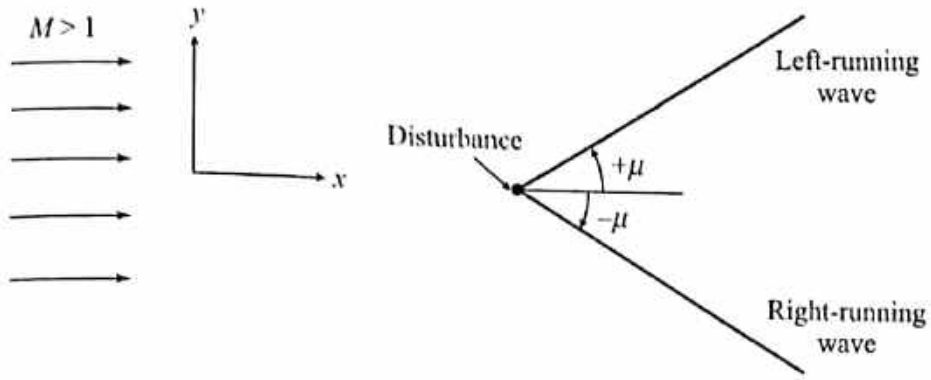


Fig. 3.1 Waves in supersonic flows.

arrived supersonically without previous warning through pressure or sound signals, is made to undergo a change in direction, thus initiating a disturbance at the boundary which propagates along the Mach waves.

For historical interest, we should mention that Newton was the first to calculate the propagation speed of pressure waves. Based on the assumed isothermal process in a perfect gas, he found the speed of propagation of sound to be equal to the square root of the ratio of the pressure to the corresponding density involved in the process, i.e.

$$a = \sqrt{p/\rho}$$

Since the science of thermodynamics was not known at Newton's time, the 18% difference between his theory and experiment was never justified.

Nearly a century later, Marquis de Laplace rectified Newton's calculation. The basic difference between Laplace's theory and Newton's theory is that the former considered an adiabatic process for propagation of pressure waves. This is fully justified since the compressions taking place in the propagation of pressure waves produce a very small temperature gradient, and hence it is not possible for heat due to compression to be transferred to the surrounding region. The correction by Laplace from adiabatic process model multiplied Newton's formula by $\sqrt{\gamma}$. The correct expression for speed of sound is $a = \sqrt{\gamma RT}$, which is the same as Eq. (1.15).

3.5 SUMMARY

In this chapter we discussed some of the basic features of the pressure wave propagation in a fluid medium. When an object moves through a fluid medium, waves are emitted from each point on the object and travel outwards at the velocity of sound. In an incompressible fluid, the velocity of sound is infinite; therefore, the entire flow field is able to feel the motion of the object instantaneously. In a compressible medium, the velocity of sound has a finite value, and hence, if a body travels at a velocity greater than that of sound, the

Scanned by CamScanner

fluid ahead of the body is not able to sense the motion of the object. However, for subsonic motion of an object the fluid ahead of the object is able to sense the motion of the object. Therefore, for subsonic motion, the fluid adjusts smoothly around the object, resulting in smooth, continuous streamline patterns. For the supersonic case, the fluid is forced to adjust rapidly to a moving object, resulting in shock wave formation.

Scanned by CamScanner

4 Steady One-Dimensional Flow

4.1 INTRODUCTION

The complications associated with compressible fluids are much more than those connected with incompressible fluids. Hence, it seems appropriate to begin with the simplest types of flow rather than with a general flow analysis. Therefore, in this chapter we shall consider steady flows with constant properties across the direction of the flow. The three state variables, p, ρ and T, and the flow speed V, of a particle now depend on a single parameter only, e.g. the arc length measured in the direction of the flow.

These conditions are approximately realised in flow through constant area ducts and ducts with gradually varying cross-section. The state of the fluid (including the speed) is often found constant over the whole cross-section except for a narrow zone in the immediate vicinity of the wall, so that the use of mean values in the calculations makes physical sense. The following remarks refer not only to the above case, but are also useful for steady flows of a more general spatial character.

Streamlines, in general, are imaginary curves in the flow field that have their tangents everywhere in the (instantaneous) direction of the flow. They can be bundled into streamtubes, and when sufficiently small cross-sections are chosen, the assumption of a uniform state of flow over the cross-section is almost satisfied. Also, in steady flows, a specified particle is at all times either inside or outside a specified streamtube. Therefore, the steady flow within a streamtube can be considered as strictly one dimensional. For flows with gradually varying finite cross-sections, we speak of quasi-one-dimensional flow in order to distinguish it from strictly one-dimensional flow.

4.2 THE FUNDAMENTAL EQUATIONS

Consider a streamtube differential in equilibrium in a one-dimensional flow field, as represented by the shaded area in Fig. 4.1. Here p is the pressure acting on

Scanned by CamScanner

the left face of the streamtube and $\left(p+\frac{\partial p}{\partial s}ds\right)$ is the pressure on the right face. Therefore, the pressure force in the positive s-direction, F_p, is given by

$$F_p = pdA - \left(p+\frac{\partial p}{\partial s}ds\right)dA = -\frac{\partial p}{\partial s}ds\ dA$$

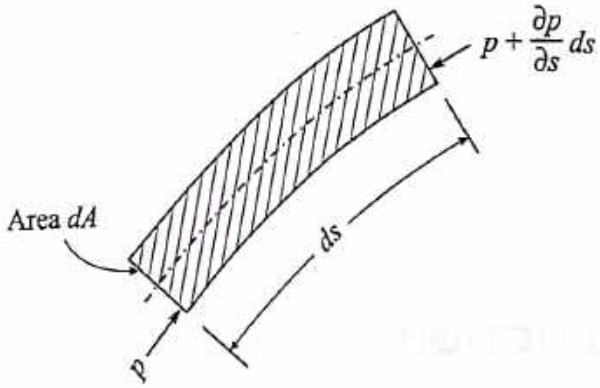


Fig. 4.1 Forces acting on streamtube.

For equilibrium, $dm\ (dV/dt)$ = sum of all the forces acting on the streamtube differential, where dm is the mass of fluid in the streamtube element considered and dV/dt is the substantial acceleration.

$$dV = \frac{\partial V}{\partial t}dt + \frac{\partial V}{\partial s}ds$$

$$\frac{dV}{dt} = \frac{\partial V}{\partial t}\frac{dt}{dt} + \frac{\partial V}{\partial s}\frac{ds}{dt}$$

In the above equation for substantial acceleration, $\partial V/\partial t$ is the local acceleration or acceleration at a point, i.e. the change in velocity at a fixed point in space with time. The convective acceleration $\frac{\partial V}{\partial s}\frac{ds}{dt} = V\frac{\partial V}{\partial s}$ is the acceleration between two points in space, i.e. change in velocity at a fixed time with space. It is present even in a steady flow.

The substantial derivative is expressed as

$$\frac{dV}{dt} = \frac{\partial V}{\partial t} + V\frac{\partial V}{\partial s} \tag{4.1}$$

Therefore, the equilibrium equation becomes

$$-\frac{\partial p}{\partial s}ds\ dA = dm\frac{dV}{dt}$$

But $dm = \rho\ dA\ ds$. Substituting this into the above equation, we get

$$\frac{dV}{dt} = -\frac{1}{\rho}\frac{\partial p}{\partial s}$$

Scanned by CamScanner

i.e.

$$\frac{\partial V}{\partial t} + V\frac{\partial V}{\partial s} + \frac{1}{\rho}\frac{\partial p}{\partial s} = 0 \tag{4.2}$$

Equation (4.2) is applicable for incompressible flows as well; the only difference comes in solution. For steady flow, Eq. (4.2) becomes

$$V\frac{\partial V}{\partial s} + \frac{1}{\rho}\frac{\partial p}{\partial s} = 0 \tag{4.3}$$

Integration of Eq. (4.3) yields

$$\boxed{\frac{V^2}{2} + \int \frac{1}{\rho}\frac{\partial p}{\partial s}ds = \text{constant}} \tag{4.4}$$

This equation is often called the compressible form of Bernoulli's equation for inviscid flows. If ρ is expressible as a function of p only, i.e. $\rho = \rho(p)$, the second expression is integrable. Fluids having this characteristic are called *barotropic fluids*. For isentropic flow process,

$$\frac{p}{\rho^\gamma} = \text{constant} \tag{4.5}$$

$$\frac{\rho_2}{\rho_1} = \left(\frac{p_2}{p_1}\right)^{1/\gamma} \tag{4.6}$$

where subscripts 1 and 2 refer to two different states. Therefore, integrating dp/ρ between pressure limits p_1 and p_2, we get

$$\int_{p_1}^{p_2} \frac{dp}{\rho} = \frac{\gamma}{\gamma-1}\frac{p_1}{\rho_1}\left[\left(\frac{p_2}{p_1}\right)^{(\gamma-1)/\gamma} - 1\right] \tag{4.7}$$

Using Eq. (4.7), Bernoulli's equation can be written as

$$\frac{V_2^2}{2} - \frac{V_1^2}{2} + \frac{\gamma}{\gamma-1}\frac{p_1}{\rho_1}\left[\left(\frac{p_2}{p_1}\right)^{(\gamma-1)/\gamma} - 1\right] = 0 \tag{4.8}$$

Equation (4.8) is a form of energy equation for isentropic flow process of gases.

For an adiabatic flow of gases, the energy equation can be written as

$$c_p T_2 + \frac{V_2^2}{2} = c_p T_1 + \frac{V_1^2}{2} \tag{4.9a}$$

or

$$\frac{\gamma}{\gamma-1}\frac{p_2}{\rho_2} + \frac{V_2^2}{2} = \frac{\gamma}{\gamma-1}\frac{p_1}{\rho_1} + \frac{V_1^2}{2} \tag{4.9b}$$

or

$$\frac{\gamma}{\gamma-1}\frac{p}{\rho} + \frac{V^2}{2} = \frac{\gamma}{\gamma-1}\frac{p_0}{\rho_0} \tag{4.9c}$$

Scanned by CamScanner

Equation (4.9) are more general in nature than Eq. (4.8): the restrictions on Eq. (4.8) are more severe than those on Eq. (4.9).

Equation (4.9) can be applied to shock, but not Eq. (4.8), as the flow across the shock is non-isentropic. With Laplace's equation $a^2 = \gamma p/\rho$, Eq. (4.9c) can be written as

$$\frac{V^2}{2} + \frac{a^2}{\gamma - 1} = \frac{\gamma}{\gamma - 1}\frac{p_0}{\rho_0} \tag{4.9d}$$

or

$$\frac{V^2}{2} + \frac{a^2}{\gamma - 1} = \frac{a_0^2}{\gamma - 1} \tag{4.9e}$$

The subscript '0' refers to stagnation condition when the flow is brought to rest isentropically or when the flow is connected to a large reservoir. All these relations are valid only for perfect gas.

EXAMPLE 4.1 Air at a stagnation state of 3 atm and 300 K is accelerated to 200 m/s. Determine the pressure, temperature and Mach number of the flow.

Solution Given, $p_0 = 3$ atm, $T_0 = 300$ K, $V = 200$ m/s. For air $\gamma = 1.4$ and $R = 287\ \text{m}^2/(\text{s}^2\ \text{K})$.

By compressible Bernoulli equation,

$$\frac{\gamma}{\gamma - 1}\frac{p}{\rho} + \frac{V^2}{2} = \frac{\gamma}{\gamma - 1}\frac{p_0}{\rho_0}$$

$$\frac{\gamma}{\gamma - 1}RT + \frac{V^2}{2} = \frac{\gamma}{\gamma - 1}RT_0$$

$$\frac{1.4}{1.4 - 1}RT + \frac{V^2}{2} = \frac{1.4}{1.4 - 1}RT_0$$

$$3.5RT + \frac{V^2}{2} = 3.5RT_0$$

$$\frac{V^2}{2} = 3.5R(T_0 - T)$$

$$T_0 - T = \frac{200^2}{2} \times \frac{1}{3.5 \times 287}$$

$$T = T_0 - 19.91 = 300 - 19.91$$

$$= 280.09\ \text{K}$$

$$= \boxed{6.94°\text{C}}$$

The speed of sound is

$$a = \sqrt{\gamma RT}$$

Scanned by CamScanner

$$= \sqrt{1.4 \times 287 \times 280.09}$$

$$= 335.47 \text{ m/s}$$

Therefore, the Mach number is

$$M = \frac{200}{335.47}$$

$$= \boxed{0.596}$$

By isentropic relation, we have

$$\frac{p_0}{p} = \left(1 + \frac{\gamma - 1}{2} M^2\right)^{\gamma/(\gamma-1)}$$

$$= (1 + 0.2 \times 0.596^2)^{3.5}$$

$$= 1.27$$

$$p = \frac{p_0}{1.27} = \frac{3}{1.27}$$

$$= 2.362 \text{ atm}$$

$$= 2.362 \times 1{,}01{,}325$$

$$= 2{,}39{,}330 \text{ Pa}$$

$$= \boxed{239.33 \text{ kPa}}$$

4.3 DISCHARGE FROM A RESERVOIR

Consider a reservoir as shown in Fig. 4.2, containing air at high pressure p_0. Let the density, temperature, speed of sound, and velocity of air be ρ_0, T_0, a_0 and V_0, respectively.

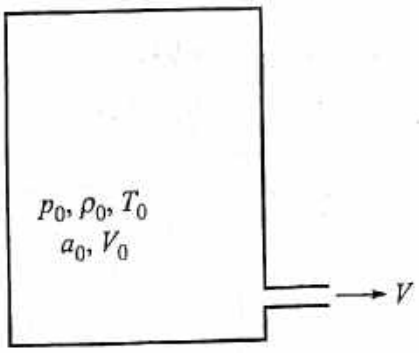


Fig. 4.2 Discharge of high pressure air through a small opening.

Scanned by CamScanner

Because of the large volume of the reservoir, the velocity of air inside is $V_0 = 0$. Let the high pressure air be discharged to ambient atmosphere at pressure p_a and velocity $V = 0$, through an opening as shown in Fig. 4.2. Now the velocity V at the opening, with which the air is discharged, can be obtained by substituting $V_1 = 0$, $p_1 = p_0$, $\rho_1 = \rho_0$, and $p_2 = p_a$ into Eq. (4.8) as

$$V = \sqrt{\frac{2\gamma}{\gamma-1}\frac{p_0}{\rho_0}\left[1-\left(\frac{p_a}{p_0}\right)^{(\gamma-1)/\gamma}\right]} \tag{4.10}$$

For discharge into vacuum, i.e. if $p_a = 0$, Eq. (4.10) results in the maximum velocity

$$V_{max} = \sqrt{\frac{2\gamma}{\gamma-1}\frac{p_0}{\rho_0}} = a_0\sqrt{\frac{2}{\gamma-1}} \tag{4.11}$$

V_{max} is the limiting velocity that may be achieved by expanding a gas at any given stagnation condition into vacuum. For air at $T_0 = 288$ K, $V_{max} = 760.7$ m/s = $2.236a_0$. This is the maximum velocity that can be obtained by discharge into vacuum in a frictionless flow. From Eq. (4.11), we can see that V_{max} is independent of reservoir pressure, but it depends only on the reservoir temperature. For incompressible flow, by Bernoulli's equation,

$$p + \frac{1}{2}\rho V^2 = p_0, \quad V = \sqrt{2\left(\frac{p_0 - p}{\rho}\right)} \tag{4.12}$$

Therefore,

$$V_{max} = \sqrt{2\left(\frac{p_0}{\rho_0}\right)} \tag{4.12a}$$

obtained by replacing ρ by ρ_0, since ρ is constant for incompressible flow. Combining Eqs. (4.11) and (4.12a), we get

$$\boxed{V_{max\,(comp.)} = \sqrt{\frac{\gamma}{\gamma-1}}\,V_{max\,(incomp.)}}$$

For air, with $\gamma = 1.4$,

$$V_{max\ (comp.)} \approx 1.9V_{max\ (incomp.)}$$

That is, the error involved in treating air as an incompressible medium is 90 per cent.

For the case when the flow is not into vacuum, $p_a/p_0 \neq 0$, and Eqs. (4.10) and (4.12) may be expressed by dividing them by a_0 as

$$\frac{V}{a_0} = \sqrt{\frac{2}{\gamma-1}\left[1-\left(\frac{p_a}{p_0}\right)^{(\gamma-1)/\gamma}\right]} \quad \text{(compressible)} \tag{4.13}$$

$$\frac{V}{a_0} = \sqrt{\frac{2}{\gamma}\left[1-\left(\frac{p_a}{p_0}\right)\right]} \quad \text{(incompressible)} \tag{4.14}$$

Scanned by CamScanner

Mass Flow per Unit Area

For a streamtube in compressible flow field,

$$\dot{m} = \rho A V = \text{constant}$$

or

$$\frac{\dot{m}}{A} = \rho V = \frac{\text{constant}}{A} \tag{4.15}$$

The mass flow rate per unit area $\propto \dfrac{1}{\text{sectional area of the streamtube}}$. With Eqs. (2.47), (4.13) and (4.15), we can write

$$\frac{\rho V}{\rho_0 a_0} = \sqrt{\frac{2}{\gamma - 1}} \left(\frac{p_a}{p_0}\right)^{1/\gamma} \sqrt{1 - \left(\frac{p_a}{p_0}\right)^{(\gamma-1)/\gamma}} \tag{4.16}$$

The peculiar shape of the curve represented by Eq. (4.16) is of utmost importance. $\rho V/(\rho_0 a_0)$ has a certain maximum, because, at $p_a/p_0 = 1.0$, $V/a_0 = 0$, and ρ/ρ_0 is finite as seen from Fig. 4.3. Therefore,

$$\frac{\rho V}{\rho_0 a_0} = 0$$

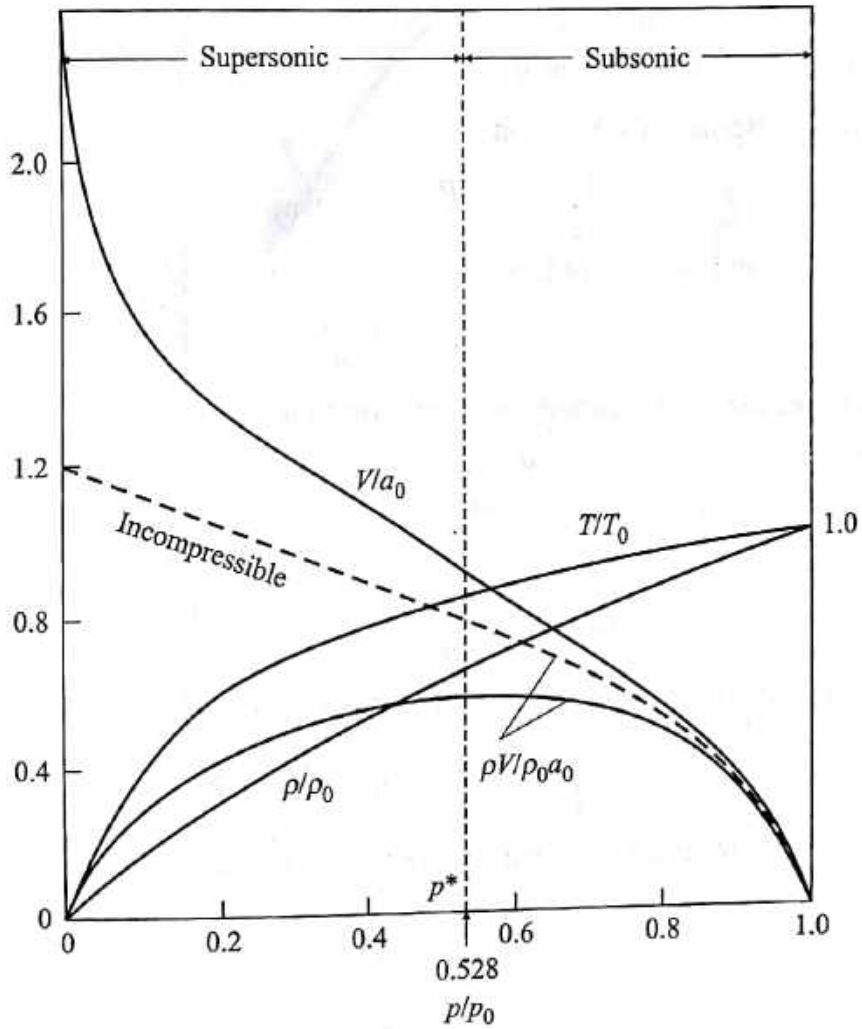


Fig. 4.3 Flow from a reservoir.

Scanned by CamScanner

At $p_a/p_0 = 0$, V/a_0 is finite and $\rho/\rho_0 = 0$, Thus,

$$\frac{\rho V}{\rho_0 a_0} = 0$$

That is, for the two limiting values of pressure ratio, $\rho V/(\rho_0 a_0)$ becomes zero and, therefore, it should have certain maximum value at a pressure ratio between the two limiting pressure ratios. Also, as p/p_0 decreases, V/a_0 increases, and ρ/ρ_0 decreases, therefore, there should be a point where their product $(\rho V)/(\rho_0 a_0)$ is a maximum. From the above discussions we can say that, in the range

(i) $\frac{p^*}{p_0} \leq \frac{p}{p_0} \leq 1$, V increases faster than ρ decreases and for

(ii) $0 \leq \frac{p}{p_0} \leq \frac{p^*}{p_0}$, the increase in V is slower than the decrease in ρ.

Also, at this point of maximum $\rho V/(\rho_0 a_0)$, the mass flow rate is maximum and the streamtube area is a minimum, i.e.

1. ρV is a maximum at $p = p^*$
2. A is a minimum at $p = p^*$
3. $V^* = a$ or $M^* = 1$ at $p = p^*$

Now, consider Bernoulli's equation

$$\frac{V^2}{2} + \int \frac{dp}{\rho} = \text{constant}$$

Differentiating and rearranging, we get

$$\rho V = -\frac{dp}{dV} \tag{4.17}$$

The condition for ρV maximum may be written as

$$\frac{d(\rho V)}{dp} = 0$$

i.e.

$$\rho \frac{dV}{dp} + V \frac{d\rho}{dp} = 0$$

Substituting for dV/dp from Eq. (4.17), we get

$$-\frac{1}{V} + V \frac{d\rho}{dp} = 0, \quad \frac{dp}{d\rho} = V^2$$

But $dp/d\rho = a^2$, from the Laplace equation (1.11). Therefore, $V^2 = a^2$ or

$$\begin{aligned} V^* &= a \\ M^* &= 1 \end{aligned} \tag{4.18}$$

Scanned by CamScanner

In Eq. (4.18), V is replaced with V^* in order to make this velocity correspond to the condition of ρV maximum. The values with * are called *critical values*, because if a reservoir at high pressure is connected to a pipe, then, depending on the backpressure (the pressure of the surrounding atmosphere to which the high pressure gas in the reservoir is discharged through the pipe), the velocity at the exit of the pipe changes. If the backpressure is more than p^*, the velocity at the pipe exit is subsonic; if it is equal to p^*, the velocity will be sonic, and if it is less than p^*, the velocity will be supersonic in the core region in the vicinity of the pipe exit. Variations in M, ρ_0/ρ, T/T_0, V/V_{max} and A^*/A with p/p_0 are illustrated in Fig. 4.4.

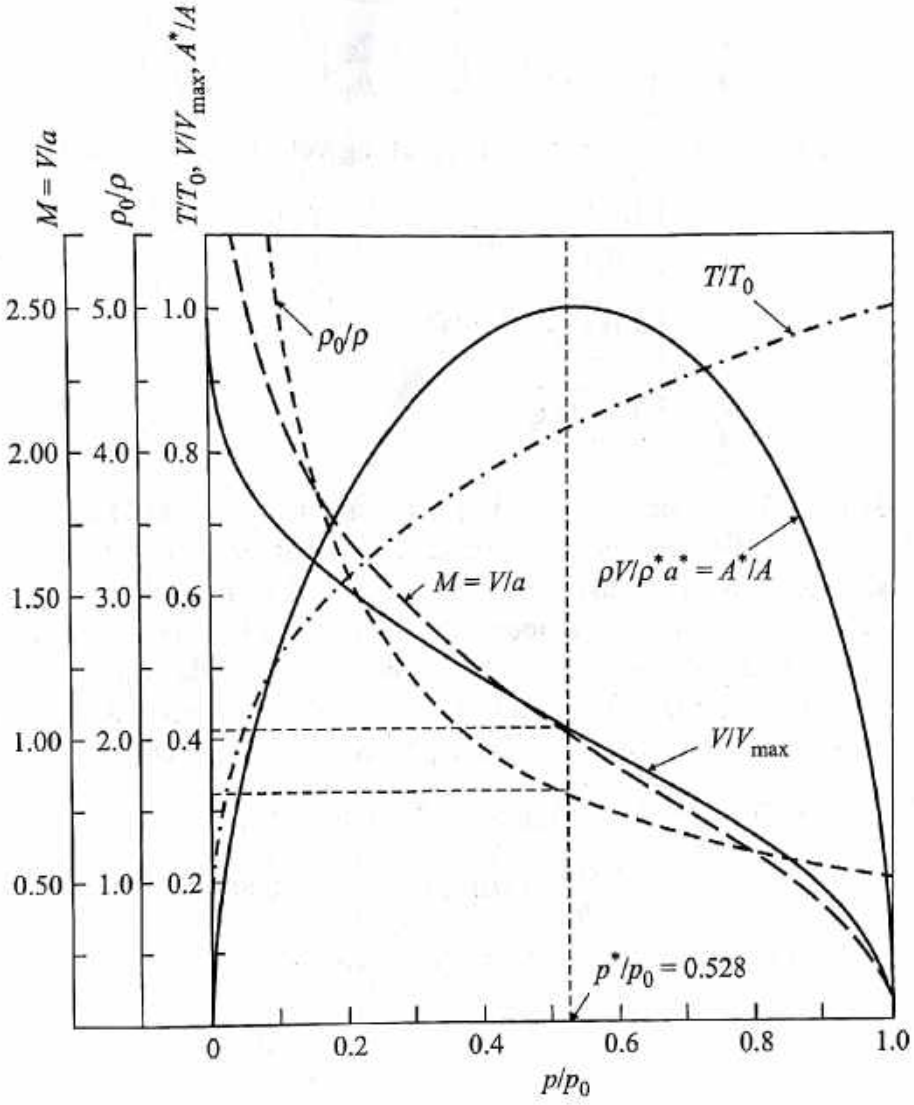


Fig. 4.4 Compressible flow relations.

EXAMPLE 4.2 A storage chamber of a compressor is maintained at 1.8 atmospheres absolute and 20°C. The surrounding ambient pressure is 1 atm. Calculate (a) the velocity with which airflow will take place from the chamber to the outside through a unit area hole, and (b) the mass flow rate per unit area. Assume air as a perfect gas.

Scanned by CamScanner

Solution Given $p_0 = 1.8$ atm, $T_0 = 293$ K. Assuming the flow to be isentropic, the velocity of airflow given by Eq. (4.10) is

$$\frac{V}{a_0} = \sqrt{\frac{2}{\gamma - 1}\left[1 - \left(\frac{p_a}{p_0}\right)^{(\gamma-1)/\gamma}\right]}$$

$$V = \sqrt{\frac{2\gamma}{\gamma - 1} RT_0\left[1 - \left(\frac{p_a}{p_0}\right)^{(\gamma-1)/\gamma}\right]}$$

The mass flow rate per unit area is given by Eq. (4.16) as

$$\frac{\dot{m}}{A} = \sqrt{\frac{2\gamma}{\gamma - 1}\left(\frac{p_0^2}{RT_0}\right)\left[1 - \left(\frac{p_a}{p_0}\right)^{(\gamma-1)/\gamma}\right]\left(\frac{p_a}{p_0}\right)^{1/\gamma}}$$

With $R = 287$ m^2/s^2-K and $\gamma = 1.4$, the resulting velocity and mass flow rate are

$$V = \left[\frac{2 \times 1.4}{0.4} \times 287 \times 293\left\{1 - \left(\frac{1}{1.8}\right)^{0.286}\right\}\right]^{1/2}$$

$$V = \boxed{301.8 \text{ m/s}}$$

$$\frac{\dot{m}}{A} = \boxed{430.0 \text{ kg/m}^2\text{-s}}$$

EXAMPLE 4.3 A ramjet flies at 11 km altitude with a flight Mach number of 0.9. In the inlet diffuser, the air is brought to the stagnation condition so that it is stationary just before the combustion chamber. Combustion takes place at constant pressure and a temperature increase of 1500 K results. The combustion products are then ejected through the nozzle. (a) Calculate the stagnation pressure and temperature. (b) What will be the nozzle exit velocity? (At inlet $p_\infty = 0.3$ atm and $T_\infty = 213$ K, at exit $p_{exit} = 0.3$ atm.)

Solution From Table A1 in Appendix A, at $M = 0.9$,

$$\frac{p_\infty}{p_0} = 0.5913, \quad \frac{T_\infty}{T_0} = 0.8606$$

Given $p_\infty = 0.3$ atm and $T_\infty = 213$ K, we have

$$p_0 = \frac{p_\infty}{0.5913} = \boxed{0.507 \text{ atm}}$$

$$T_0 = \frac{T_\infty}{0.8606} = \boxed{247.5 \text{ K}}$$

In the combustion process, temperature increase $\Delta T = 1500$ K. Therefore, the temperature after combustion $= T_{0c} = T_0 + \Delta T$; thus,

$$T_{0c} = \boxed{1747.5 \text{ K}}$$

Scanned by CamScanner

$$p_{exit} = p_\infty = 0.3 \text{ atm}$$
$$p_0 = 0.507 \text{ atm}$$

Hence,

$$\frac{p_{exit}}{p_0} = 0.5917$$

From Table A1 in Appendix A, at $\frac{p_{exit}}{p_0} = 0.5917$,

$$\frac{T_{exit}}{T_{0c}} = 0.8620$$

Therefore,

$$T_{exit} = \boxed{1506.35 \text{ K}}$$

By Eq. (4.9a),

$$h_{exit} + \frac{V_{exit}^2}{2} = h_{0c}$$

$$c_p T_e + \frac{V_e^2}{2} = c_p T_{0c}$$

$$V_e = \sqrt{2c_p (T_{0c} - T_e)}$$

$$= \sqrt{2\frac{\gamma}{\gamma - 1} R (T_{0c} - T_e)}$$

$$V_{exit} = \boxed{696 \text{ m/s}}$$

Critical Values

The critical value of pressure ratio, p^*/p_0, is obtained from Eq. (4.13) by replacing V by $V^* = a$. With $V = a$, Eq. (4.13) becomes

$$\frac{a}{a_0} = \sqrt{\frac{2}{\gamma - 1}\left[1 - \left(\frac{p_a}{p_0}\right)^{(\gamma-1)/\gamma}\right]}$$

With the speed of sound, $a = \sqrt{\gamma RT}$, we get

$$\sqrt{\frac{T}{T_0}} = \left[\frac{2}{\gamma - 1}\left\{1 - \left(\frac{p_a}{p_0}\right)^{(\gamma-1)/\gamma}\right\}\right]^{1/2}$$

By Eq. (2.47),

$$\frac{T}{T_0} = \left(\frac{p}{p_0}\right)^{(\gamma-1)/\gamma} = \left(\frac{a}{a_0}\right)^2 \qquad (4.19)$$

Scanned by CamScanner

Therefore,

$$\left(\frac{p}{p_0}\right)^{(\gamma-1)/\gamma} = \frac{2}{\gamma-1}\left[1-\left(\frac{p_a}{p_0}\right)^{(\gamma-1)/\gamma}\right]$$

or

$$\left(\frac{p^*}{p_0}\right)^{(\gamma-1)/\gamma} = \frac{2}{\gamma+1}$$

$$\frac{p^*}{p_0} = \left(\frac{2}{\gamma+1}\right)^{\gamma/(\gamma-1)} \tag{4.20}$$

Since Eq. (4.20) is derived with the assumption that $V = a$, which is the critical condition, the static pressure p is replaced by p^*. Also, note that the pressure p is the same as p_a in Eq. (4.13).

Equation (4.20) gives the value of critical pressure ratio; other critical values are obtained by introducing Eq. (4.20) into Eqs. (2.47), (4.16) and (4.19) as

$$\frac{\rho^*}{\rho_0} = \left(\frac{2}{\gamma+1}\right)^{1/(\gamma-1)} \tag{4.21}$$

$$\frac{T^*}{T_0} = \frac{2}{\gamma+1} \tag{4.22}$$

$$\frac{V^*}{a_0} = \frac{a^*}{a_0} = \sqrt{\frac{2}{\gamma+1}} \tag{4.23}$$

$$\frac{\rho^* V^*}{\rho_0 a_0} = \left(\frac{2}{\gamma+1}\right)^{(\gamma+1)/2(\gamma-1)} \tag{4.24}$$

All these critical values depend only on γ. For air at standard conditions, where $\gamma = 1.4$, these ratios are

$$\frac{p^*}{p_0} = 0.528$$

$$\frac{T^*}{T_0} = 0.833$$

$$\frac{\rho^*}{\rho_0} = 0.634$$

$$\frac{V^*}{a_0} = \frac{a^*}{a_0} = 0.913$$

$$\frac{\rho^* V^*}{\rho_0 a_0} = 0.578$$

It will be useful if we keep these values in mind for subsequent discussions. Some of the important relations of compressible flow are shown in graphical form in Fig. 4.4. Finally, from Eq. (2.38b), we have

$$\frac{a^2}{\gamma-1} + \frac{V^2}{2} = \frac{\gamma+1}{2(\gamma-1)}a^{*2}$$

Scanned by CamScanner

Dividing throughout by V^2, we get

$$\frac{(a/V)^2}{\gamma-1}+\frac{1}{2}=\frac{\gamma+1}{2(\gamma-1)}\left(\frac{a^*}{V}\right)^2$$

$$\frac{(1/M)^2}{\gamma-1}=\frac{\gamma+1}{2(\gamma-1)}\left(\frac{1}{M^*}\right)^2-\frac{1}{2}$$

$$\boxed{M^2=\frac{2}{((\gamma+1)/M^{*2})-(\gamma-1)}} \tag{4.25}$$

where M^*, which is the ratio of local flow speed and critical speed of sound, is called the *characteristic Mach number*. Equation (4.25) provides a direct relation between the actual Mach number M and the characteristic Mach number M^*. From Eq. (4.25), it is seen that

$$M^*=1 \quad \text{if } M=1$$
$$M^*<1 \quad \text{if } M<1$$
$$M^*>1 \quad \text{if } M>1$$
$$M^*\to\sqrt{\frac{\gamma+1}{\gamma-1}} \quad \text{if } M\to\infty$$

Hence, qualitatively, M^* behaves in the same manner as M, except when M goes to infinity. M^* will be a useful parameter for further building of the subject involving shocks and expansion waves because it approaches a finite value as M approaches infinity.

In the course of discussions in this section, we came across three speeds, namely, V_{max}, a_0, and $V^*(=a^*)$ repeatedly. These three speeds serve as standard reference speeds for gas dynamic study. We know that for an adiabatic flow of perfect gas, the velocity can be expressed as

$$V=\sqrt{2c_p(T_0-T)}=\sqrt{\frac{2\gamma}{\gamma-1}R(T_0-T)}$$

where T_0 is the stagnation temperature. Since negative temperatures on absolute scales are not attainable, it is evident from the above equation that there is a maximum velocity corresponding to a given stagnation temperature. This maximum velocity, which is often used for reference purposes, is given by

$$V_{max}=\sqrt{\frac{2\gamma}{\gamma-1}RT_0}$$

Another useful reference velocity is the speed of sound at the stagnation temperature, given by

$$a_0=\sqrt{\gamma RT_0}$$

Yet another convenient reference velocity is the critical speed V^*, i.e. velocity at Mach number unity, or

$$V^*=a^*$$

Scanned by CamScanner

This may also be written as

$$\sqrt{\frac{2\gamma}{\gamma-1}R(T_0-T^*)} = \sqrt{\gamma RT^*}$$

This results in

$$\frac{T^*}{T_0} = \frac{2}{\gamma+1}$$

Therefore, in terms of stagnation temperature, the critical speed becomes

$$V_0^* = a^* = \sqrt{\frac{2\gamma}{\gamma+1}RT_0}$$

From this equation, we may get the following relations between the three reference velocities (with $\gamma = 1.4$):

$$\frac{a^*}{a_0} = \sqrt{\frac{2}{\gamma+1}} = 0.913$$

$$\frac{V_{max}}{a_0} = \sqrt{\frac{2}{\gamma-1}} = 2.24$$

$$\frac{V_{max}}{a^*} = \sqrt{\frac{\gamma+1}{\gamma-1}} = 2.45$$

EXAMPLE 4.4 Determine the maximum speed and Mach number that can be achieved by accelerating stagnant air at standard sea level condition.

Solution At sea level state, the pressure and temperature are 1,01,325 Pa and 15°C, respectively. That is, the given stagnation state is at p_0 = 1,01,325 Pa and T_0 = 15°C. Also, for air, the gas constant R = 287 m^2/(s^2 K) and the specific heats ratio $\gamma = 1.4$.

By energy equation,

$$h + \frac{V^2}{2} = h_0$$

where h and h_0 are the static and stagnation enthalpies, respectively, and V is the flow speed. Treating the air as perfect gas, we have $h = c_pT$; therefore, the energy equation becomes

$$c_pT + \frac{V^2}{2} = c_pT_0$$

where T_0 is the stagnation temperature. For the limiting maximum speed of V_{max}, the temperature will become zero. Therefore,

$$0 + \frac{V_{max}^2}{2} = c_pT_0$$

Scanned by CamScanner

But,

$$c_p = \frac{\gamma}{\gamma - 1} R$$

Therefore,

$$\frac{V_{\max}^2}{2} = \frac{\gamma}{\gamma - 1} RT_0$$

$$V_{\max} = \sqrt{2 \frac{\gamma}{\gamma - 1} RT_0}$$

$$= \sqrt{2 \times \frac{1.4}{1.4 - 1} \times 287 \times (15 + 273.15)}$$

$$= \boxed{760.85 \text{ m/s}}$$

For air at $T = 0°C$, the speed of sound $a = \sqrt{\gamma RT} = 0$ m/s. This implies that the Mach number will tend to infinity. That is, the limiting case of M is $M \to \infty$.

4.4 STREAMTUBE AREA–VELOCITY RELATION

In this section, let us consider quasi-one-dimensional flow, allowing the streamtube area A to vary with distance x, as shown in Fig. 4.5.

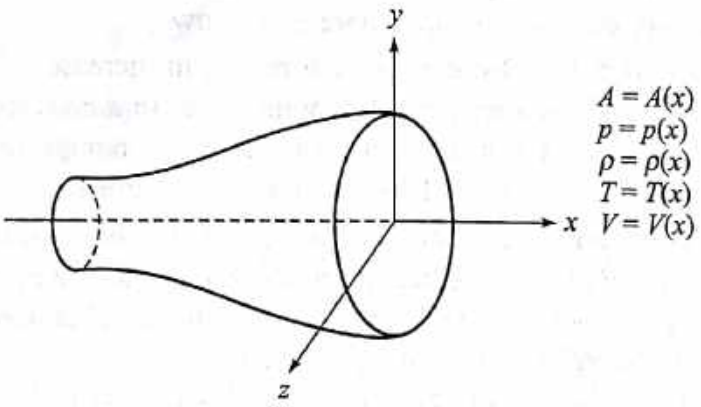


Fig. 4.5 Quasi-one-dimensional flow.

Let us continue to assume that all flow properties are uniform across any given cross-section of the streamtube, and hence are functions of x only for steady flows. Such a flow, where $A = A(x)$, $p = p(x)$, $\rho = \rho(x)$, and $V = V(x)$ for steady flow, is defined as quasi-one-dimensional flow. Algebraic equations for steady quasi-one-dimensional flow can be obtained by applying the integral form of the conservation equations.

For any streamtube of area A, the continuity equation is given by

$$\rho AV = \text{constant} \tag{4.26}$$

Scanned by CamScanner

Differentiating with respect to V, we obtain

$$\frac{d(\rho AV)}{dV} = \rho V\frac{dA}{dV} + A\frac{d(\rho V)}{dV} = 0$$

The term

$$A\frac{d(\rho V)}{dV} = A\left(\rho + V\frac{d\rho}{dp}\frac{dp}{dV}\right) = A\rho(1 - M^2)$$

Since, from Eq. (4.17),

$$\frac{dp}{dV} = -\rho V$$

and from the Laplace equation, we have

$$\frac{dp}{d\rho} = a^2$$

Therefore,

$$\rho V\frac{dA}{dV} + A\rho(1 - M^2) = 0$$

$$\boxed{\frac{dA}{dV} = -\frac{A}{V}(1 - M^2)} \qquad (4.27)$$

Equation (4.27) is an important result. It is called the area–velocity relation.

The following information can be derived from the area–velocity relation:

1. For incompressible flow limit, i.e. for $M \to 0$, Eq. (4.27) shows that AV = constant. This is the famous volume conservation equation or continuity equation for incompressible flow.
2. For $0 \leq M \leq 1$, a decrease in area results in increase of velocity, and vice versa. Therefore, the velocity increases in a convergent duct and decreases in a divergent duct. This result for compressible subsonic flows is the same as that for incompressible flow.
3. For $M > 1$, an increase in area results in increase of velocity and vice versa, i.e. the velocity increases in a divergent duct and decreases in a convergent duct. This is directly opposite to the behaviour of subsonic flow in divergent and convergent ducts.
4. For $M = 1$, by Eq. (4.27), $dA/A = 0$, which implies that the location where the Mach number is unity, the area of the passage is either minimum or maximum. We can easily show that the minimum in area is the only physically realistic solution.

The above results can be schematically shown as in Fig. 4.6.

From the above discussions, it is clear that for a gas to expand isentropically from subsonic to supersonic speeds, it must flow through a convergent-divergent duct, as shown in Fig. 4.7. The minimum area that divides the convergent and divergent sections of the duct is called the *throat*. From point 4 above, we know that the flow at the throat must be sonic with $M = 1$.

Scanned by CamScanner

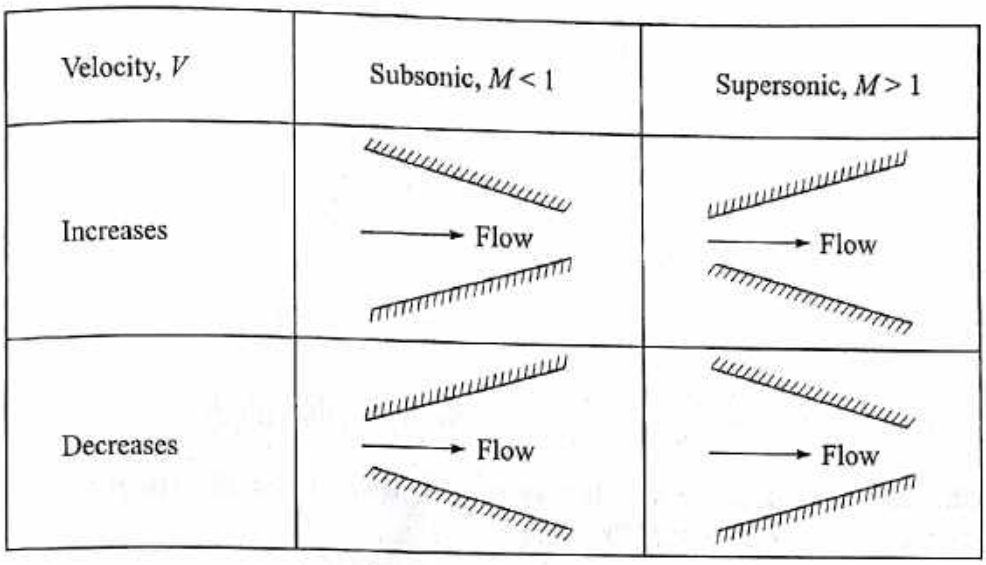


Fig. 4.6 Flow in convergent and divergent ducts.

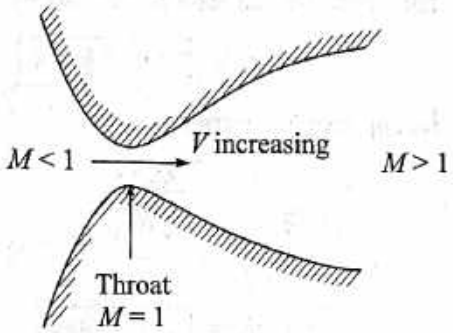


Fig. 4.7 Flow in a convergent-divergent duct.

Conversely, for a gas to get compressed isentropically from supersonic to subsonic speeds, it must again flow through a convergent-divergent duct, with a throat where sonic flow occurs.

EXAMPLE 4.5 A storage chamber supplies high pressure air to a pneumatic machine. It is found that there is an unavoidable leak at the joints and the total area through which leakage occurs is estimated to be 1 cm^2. Calculate the quantity of air leaking out of the chamber if the chamber is maintained at 5 atm and 20°C.

Solution For the reservoir,

$$\rho_0 = \frac{p_0}{RT_0}, \quad a_0 = \sqrt{\gamma RT_0}$$

and hence

$$\rho_0 a_0 = p_0 \sqrt{\frac{\gamma}{RT_0}}$$

Scanned by CamScanner

$$= 5 \times 1.0133 \times 10^5 \left(\frac{1.4}{287 \times 293}\right)^{1/2}$$

$$= \boxed{2067.27 \text{ kg/m}^2\text{-s}}$$

For the flow through joints,

$$\frac{p}{p_0} = \frac{1}{5} = 0.2$$

By Eq. (4.16), for $\frac{p}{p_0} = 0.2$, $\frac{\rho V}{\rho_0 a_0} = 0.43$. Note that the hole is not designed specifically and there cannot be supersonic flow. Even though $p/p_0 < p^*/p_0$, there will be only choking. Therefore,

$$\rho V = (0.43)(\rho_0 a_0) = 889 \text{ kg/m}^2\text{-s}$$

The mass flow rate through the joints (1 cm^2 area) will be

$$\dot{m} = \boxed{0.089 \text{ kg/s}}$$

In terms of p_0 and T_0, $\dot{m}$ can be expressed as

$$\dot{m} = \frac{0.6847}{\sqrt{RT_0}} p_0 A^*$$

Thus, we get

$$\dot{m} = \boxed{0.12 \text{ kg/s}}$$

4.5 DE LAVAL NOZZLE

Nozzle is a passage used to transform pressure energy into kinetic energy. A convergent-divergent nozzle used to generate supersonic flow is sometimes called De Laval Nozzle, after Carl G.P. De Laval, who first used such a configuration in his steam turbines in the late nineteenth century. Therefore, we can say that De Laval nozzle is the only means to produce supersonic flow.

A nozzle which does not have an expanding portion can never produce supersonic flow.

Consider the Laval nozzle shown in Fig. 4.8. At the throat, the flow is sonic. Hence, denoting conditions at sonic speed by an asterisk, we have at the throat, $M^* = 1$ and $V^* = a^*$. The area of the throat is A^*. At any other section of the duct, the local area, Mach number, and velocity are A, M and V, respectively. By continuity equation,

$$\rho^* V^* A^* = \rho V A \tag{4.28}$$

With $V^* = a^*$, Eq. (4.28) becomes

$$\frac{A}{A^*} = \frac{\rho^* a^*}{\rho V} = \frac{\rho^* \rho_0 a^*}{\rho_0 \rho V} \tag{4.29}$$

Scanned by CamScanner

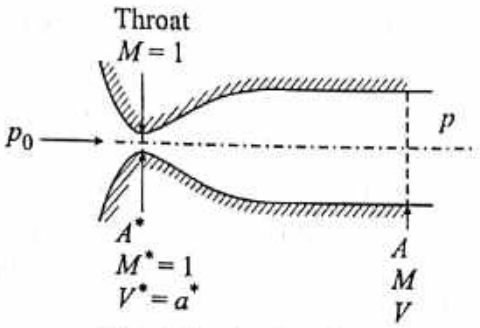


Fig. 4.8 De Laval nozzle.

where ρ_0 is the stagnation density and is constant throughout the isentropic flow. By Eq. (2.50),

$$\frac{\rho_0}{\rho} = \left(1 + \frac{\gamma - 1}{2} M^2\right)^{1/(\gamma-1)}$$

and applying this to sonic conditions, we get

$$\frac{\rho_0}{\rho^*} = \left(\frac{\gamma + 1}{2}\right)^{1/(\gamma-1)} \tag{4.30}$$

Also, by definition, $V/a^* = M^*$. From Eq. (4.25),

$$\boxed{M^{*2} = \frac{[(\gamma + 1)/2]M^2}{1 + [(\gamma - 1)/2]M^2}} \tag{4.31}$$

Squaring Eq. (4.29), and substituting for $\left(\frac{\rho^*}{\rho_0}\right)^2$, $\left(\frac{\rho_0}{\rho}\right)^2$, and $\left(\frac{a^*}{V}\right)^2$ from Eqs. (4.30), (2.50) and (4.31), respectively, we have

$$\left(\frac{A}{A^*}\right)^2 = \left(\frac{\rho^*}{\rho_0}\right)^2 \left(\frac{\rho_0}{\rho}\right)^2 \left(\frac{a^*}{V}\right)^2$$

$$\boxed{\left(\frac{A}{A^*}\right)^2 = \frac{1}{M^2}\left[\frac{2}{\gamma + 1}\left(1 + \frac{\gamma - 1}{2} M^2\right)\right]^{(\gamma+1)/(\gamma-1)}} \tag{4.32}$$

Equation (4.32) is called the *Area-Mach number relation*. From this equation we get the striking result $M = f(A/A^*)$, i.e. the Mach number at any location in the duct is a function of the ratio of the local area of the duct to the sonic throat area. As seen from Eq. (4.27), the local duct area, A, must be larger than or at least equal to A^*, the case in which $A < A^*$ is physically impossible in an isentropic flow. Further, from Eq. (4.32), for any given $A/A^* > 1$, two values of M are obtained: a subsonic value and a supersonic value. The plot given in Fig. 4.9 is the solution of Eq. (4.32) showing the subsonic and supersonic branches. The values of A/A^* as a function of M are tabulated in Table A1 of Appendix A, for both subsonic and supersonic flows. Once the

Scanned by CamScanner

variation of Mach number through the nozzle is known, the variations of static temperature, pressure, and density follow from Eqs. (2.48)–(2.50), respectively. The pressure, temperature, and density decrease continuously throughout the nozzle. Also, the exit pressure, density, and temperature ratios, p_e/p_0, ρ_e/ρ_0, and T_e/T_0 depend only on the exit area ratio A_e/A^*. That is, if the nozzle is part of a supersonic wind tunnel, then the test-section conditions are completely determined by A_e/A^* (geometry of the nozzle) and p_0 and T_0 (properties of the gas in the reservoir).

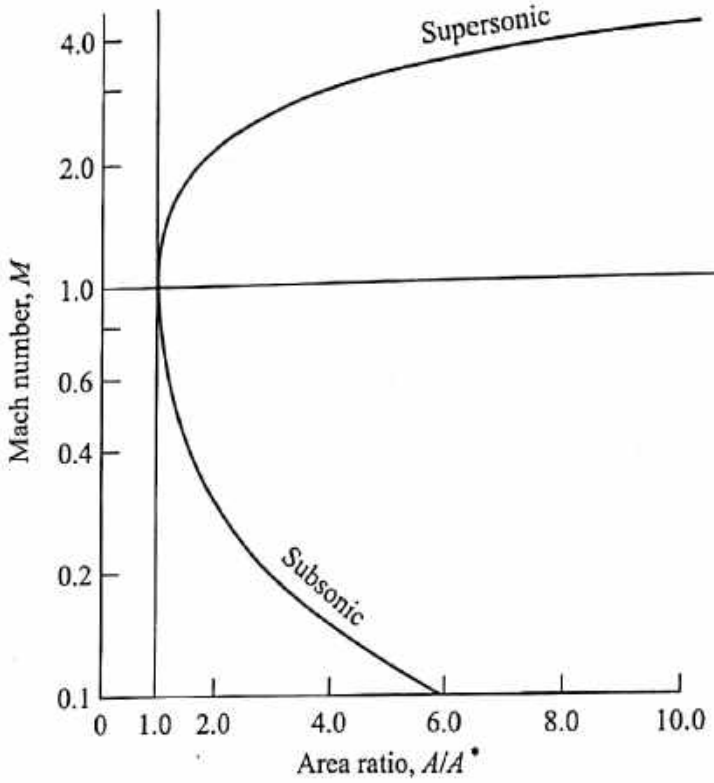


Fig. 4.9 Area-Mach number relation.

If a Laval nozzle, designed for a particular Mach number, is kept in still atmosphere, and nothing else is done, obviously the air will not start accelerating through the nozzle of its own accord. To accelerate the air, a favourable pressure gradient must be exerted across the nozzle. Therefore, in order to establish a flow through any duct, the pressure at the exit must be lower than the inlet pressure, i.e. $p_e/p_0 < 1$. Indeed, supersonic velocity can be reached only if $p_e/p_0 < 0.528$. For such pressure ratios, the contracting portion of the nozzle accelerates the flow up to $M = 1$, and the diverging portion further accelerates the flow beyond $M = 1$.

It is important to realize that the statement *supersonic velocity can be reached only if* $p_e/p_0 < 0.528$ is the essential requirement for the nozzle to choke at the throat (i.e. to have $M^* = 1$ at the throat). Thus, in the strict sense it should be stated that, a nozzle will have $M_{th} = 1$ at throat only if $p_{th}/p_0 \leq 0.528$, and the flow in the divergent portion of the nozzle will accelerate to increasing supersonic Mach numbers only if $p/p_{th} < 1$, where p is the local static pressure

Scanned by CamScanner

in the divergent portion of the nozzle. The flow after choking at the nozzle throat will continue to accelerate to progressively higher supersonic Mach numbers, in the divergent portion downstream of the throat, only if $p_e/p_{th} < 1$. In other words, for the flow to accelerate, a favourable pressure gradient should exist. Therefore, for a convergent-divergent nozzle to experience supersonic flow from downstream of the throat up to the exit, the limiting pressure ratio p_e/p_0 required across the nozzle is dictated by the presence of normal shock at the exit. Thus, p_e/p_0 required to choke the flow at a nozzle throat can also be greater than the isentropic limiting pressure ratio of 0.528 (for $\gamma = 1.4$).

A variety of flow fields can be generated in the convergent-divergent or Laval nozzle by independently governing the backpressure downstream of the nozzle exit. Consider the flow through a Laval nozzle as shown in Fig. 4.10. When $p_e = p_0$, there will be no flow through the nozzle. Let the exit pressure be reduced to a value (p_{e1}) slightly below p_0. This small favourable pressure gradient will cause a flow through the nozzle at low subsonic speeds. The local Mach number will increase continuously through the convergent portion of the nozzle, reaching a maximum at the throat. In other words, the static pressure will decrease continuously in the convergent portion of the nozzle, reaching a minimum at the throat, as shown by the curve *a* in the figure. Assume that p_e

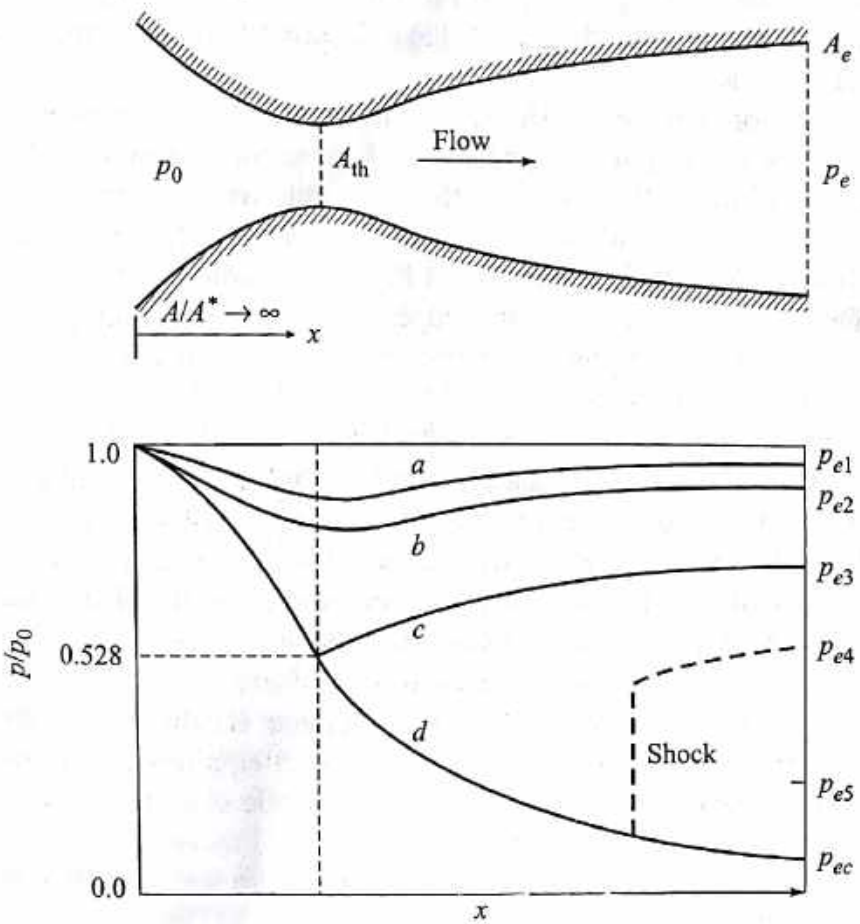


Fig. 4.10 Flow in a convergent-divergent nozzle.

Scanned by CamScanner

is reduced further (p_{e2}). Then the pressure gradient will be stronger, flow acceleration will be faster, and variation of Mach number and static pressure through the duct will be larger, as shown by curve *b*. Similarly, if p_e is reduced continuously, at some value of p_e, the flow will reach sonic velocity at the throat, as shown by curve *c*. For this case, $A_{th} = A^*$. Now, the sonic flow at the throat will expand further in the divergent portion of the nozzle as supersonic flow if $p_e/p_{th} < 1$, and will decelerate as a subsonic flow as shown by curve *c*, for $p_{e3}/p_{th} > 1$.

For the cases discussed above, the mass flow through the duct increases as p_e decreases. This mass flow can be calculated by evaluating Eq. (4.15) at the throat, $\dot{m} = \rho_{th} A_{th} V_{th}$. When p_e is equal to p_{e3}, where sonic flow is attained at the throat, $\dot{m} = \rho^* A^* a^*$; also, the Mach number at the throat is unity; this is dictated by Eq. (4.27). Hence, the flow properties at the throat, and indeed throughout the subsonic (convergent) section of the duct, become "frozen" when $p_e < p_{e3}$, i.e. the subsonic flow in the convergent portion of the nozzle remains unaffected and the mass flow remains constant for $p_e < p_{e3}$. This condition for sonic flow at the throat is called *choked flow*. For further reduction of p_e below p_{e3}, after the flow becomes choked, the mass flow remains constant.

At this stage it is important to realize that the choked mass flow rate $\dot{m}^*$ is the maximum only for a given p_0 and T_0. However, when the stagnation pressure and temperature are altered, $\dot{m}^*$ will have different maxima corresponding to every set of p_0 and T_0.

From the foregoing discussions, it is clear that in the convergent portion of the duct, flow remains unchanged for back pressures below p_{e3}. But, in the divergent portion of the duct the flow expands as a supersonic flow for $p_e < p_{e3}$. However, p_e should be adequately reduced to a specified low value, p_{ec}, for establishing isentropic expansion of flow throughout the divergent portion of the nozzle, resulting in shock-free supersonic flow; the variation in pressure for such an isentropic expansion is shown by curve *d* in Fig. 4.10.

For values of exit pressures between p_{ec} and p_{e3}, a normal shock wave exists inside the divergent portion of the nozzle. The flow behind the normal shock is subsonic; hence the static pressure increases to p_{e4} at the exit. The normal shock moves downstream with decrease in p_e below p_{e4} and will stand precisely at the exit when $p_e = p_{e5}$, where p_{e5} is the static pressure behind a normal shock at the design Mach number of the nozzle; this is shown in Fig. 4.11(a). When p_e is further reduced such that $p_{ec} < p_b < p_{e5}$, the flow inside the nozzle is fully supersonic and isentropic where p_b, the pressure of the ambient atmosphere to which the flow is discharged, is called the backpressure. Further increase in the flow pressure, resulting in equilibrium with p_b, takes place across an oblique shock attached to the nozzle exit outside the duct, as shown in Fig. 4.11(b). For further reduction in backpressure below p_{ec}, equilibration of the flow takes place across expansion waves outside the duct, as illustrated in Fig. 4.11(c).

When the flow situation is as shown in Fig. 4.11(b), the nozzle is said to be *overexpanded*, since the pressure at the exit has expanded below the

Scanned by CamScanner

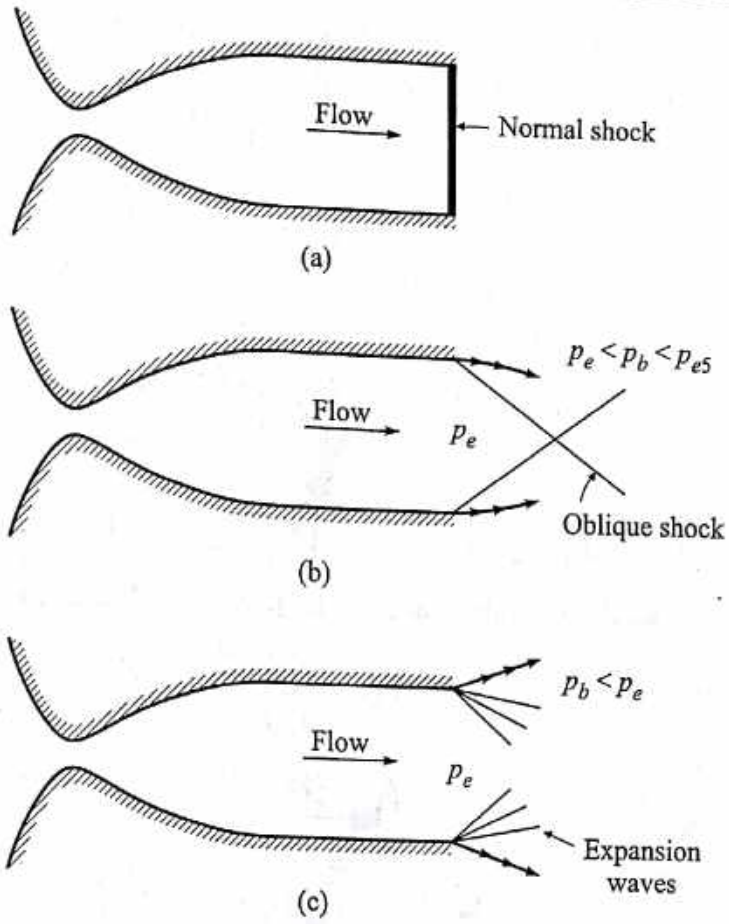


Fig. 4.11 Flow with shock and expansion waves at the exit of a convergent- divergent nozzle.

backpressure, $p_e < p_b$. Conversely, when the situation is as shown in Fig. 4.11(c), the nozzle is said to be *underexpanded*, since the exit pressure is higher than the backpressure, i.e. $p_e > p_b$, and hence the flow experiences additional expansion after leaving the nozzle.

The above results can be summarized as follows:

1. For $p_{e1}/p_0 < 1$, the flow is subsonic at the throat and so the divergent portion acts as a diffuser. This is the case of flow through venturi.
2. For $p_{e3}/p_0 < 1$, the pressure at the throat is p^* and so $M = 1$ at throat. But, $p_{e3}/p_{th} > 1$; therefore, the divergent portion acts as a diffuser and the flow does not become supersonic.
3. For pressure at the exit equal to p_{ec}, the flow expands isentropically in the nozzle and there is shock-free supersonic flow in the divergent portion of the nozzle.
4. For $p_{ec}/p_0 < p_e/p_0 < p_{e3}/p_0$, there will be supersonic velocity locally, but at the exit it cannot be supersonic, and so there will be a jump in static pressure at some section of the nozzle, i.e. there is a shock. Therefore, there is a certain backpressure p_{ec}, above which there cannot be supersonic flow at the exit. Only below p_{ec} there can be shock-free supersonic flow up to the exit.

Scanned by CamScanner

The equations which are useful for calculating the cross-sectional averaged properties inside a nozzle of a given shape are

$$\frac{p}{p_0} = \left(1+\frac{\gamma-1}{2}M^2\right)^{-\gamma/(\gamma-1)} \tag{4.33a}$$

$$\frac{\rho}{\rho_0} = \left(1+\frac{\gamma-1}{2}M^2\right)^{-1/(\gamma-1)} \tag{4.33b}$$

$$\frac{T}{T_0} = \left(1+\frac{\gamma-1}{2}M^2\right)^{-1} \tag{4.33c}$$

$$\frac{A}{A^*} = \frac{1}{M}\left(\frac{\gamma+1}{2}\right)^{-(\gamma+1)/2(\gamma-1)}\left(1+\frac{\gamma-1}{2}M^2\right)^{(\gamma+1)/2(\gamma-1)} \tag{4.33d}$$

For air at standard conditions ($\gamma = 1.4$), Eqs. (4.33) reduce to

$$\frac{p}{p_0} = \left(1+\frac{M^2}{5}\right)^{-7/2} \tag{4.34a}$$

$$\frac{\rho}{\rho_0} = \left(1+\frac{M^2}{5}\right)^{-5/2} \tag{4.34b}$$

$$\frac{T}{T_0} = \left(1+\frac{M^2}{5}\right)^{-1} \tag{4.34c}$$

$$\frac{A}{A^*} = \frac{1}{M}\left(\frac{5+M^2}{6}\right)^{3} \tag{4.34d}$$

From Eq. (4.34d), it is seen that for a required exit Mach number, there is only one ratio of exit area to throat area for De Laval nozzle, i.e. for a given Laval nozzle, there is only one exit Mach number that can be produced. Therefore, for a supersonic wind tunnel, it is necessary to have a separate nozzle for every test-section Mach number of interest. However, this requirement of a separate nozzle for every Mach number can be avoided if there is a provision in the tunnel to vary the exit area. Though this type of variable geometry nozzle will result in different test-section Mach numbers with a single nozzle, it is very expensive. Further, it is evident from Eq. (4.34d) that the higher the exit Mach number, the larger should be that exit area.

We see from Eqs. (4.34) that for high exit Mach numbers, the exit pressure, temperature, and density will be very small. Also, because the exit temperature is very low, it is sometimes necessary to heat the tunnel or increase the stagnation temperature of the air in the storage tanks so that there is reasonable temperature at the test-section. This requirement of maintaining moderate temperature becomes important if the temperature in the test-section goes to nearly –270°C, as no material can be used at such low temperatures. Therefore,

Scanned by CamScanner

for high Mach numbers, the air is heated to thousands of degree celsius before expanding into the tunnel. For example, consider the values of pressure and temperature at the exit section of a Laval nozzle for Mach numbers 2 and 4. From isentropic tables we have the following data:

M_{TS}	p_{TS}/p_0	T_{TS}/T_0
2	0.1278	0.5556
4	0.0066	0.2381

Let the stagnation temperature be 20°C. The corresponding test-section static temperatures are −110.2°C and −203.2°C for Mach numbers 2 and 4, respectively.

At $M = 4$, we are forced to heat the air since nitrogen in air liquefies at −180°C; for the air properties to be the same as those in atmosphere, heating the air becomes essential.

EXAMPLE 4.6 Using Area-Mach number relation, prove that $A < A^*$ is physically impossible.

Solution By Eq. (4.32), we have

$$\left(\frac{A}{A^*}\right)^2 = \frac{1}{M^2}\left[\frac{2}{\gamma+1}\left(1+\frac{\gamma-1}{2}M^2\right)\right]^{\frac{(\gamma+1)}{(\gamma-1)}}$$

Taking square root, this becomes

$$\left(\frac{A}{A^*}\right) = \frac{1}{M}\left[\frac{2}{\gamma+1}\left(1+\frac{\gamma-1}{2}M^2\right)\right]^{\frac{(\gamma+1)}{2(\gamma-1)}}$$

Differentiating with respect to M, we have

$$\frac{d(A/A^*)}{dM} = \left(\frac{2}{\gamma+1}\right)^{\frac{(\gamma+1)}{2(\gamma-1)}}\left[\frac{1}{M}\frac{(\gamma+1)}{2(\gamma-1)}\left(1+\frac{\gamma-1}{2}M^2\right)^{\left[\frac{\gamma+1}{2(\gamma-1)}-1\right]}(\gamma-1)M + \left(1+\frac{\gamma-1}{2}M^2\right)^{\frac{\gamma+1}{2(\gamma-1)}}\left(\frac{-1}{M^2}\right)\right] \quad \text{(i)}$$

For extremum, $\frac{d(A/A^*)}{dM} = 0$, therefore,

$$\left(\frac{2}{\gamma+1}\right)^{\frac{\gamma+1}{2(\gamma-1)}}\left[\frac{\gamma+1}{2}\left(1+\frac{\gamma-1}{2}M^2\right)^{\left[\frac{\gamma+1}{2(\gamma-1)}-1\right]}\right.$$

Scanned by CamScanner

$$-\left(1+\frac{\gamma-1}{2}M^2\right)^{\frac{\gamma+1}{2(\gamma-1)}}\left(\frac{1}{M^2}\right)\Bigg]=0 \qquad \text{(ii)}$$

Let

$$1+\frac{\gamma-1}{2}M^2=t \qquad \text{(iii)}$$

In terms of t, Eq. (ii) becomes

$$\left(\frac{\gamma+1}{2}\right)t^{\left[\frac{\gamma+1}{2(\gamma-1)}-1\right]}-\frac{t^{\frac{\gamma+1}{2(\gamma-1)}}}{M^2}=0$$

This simplifies to

$$\frac{\gamma+1}{2t}-\frac{1}{M^2}=0$$

or

$$t=\frac{\gamma+1}{2}M^2$$

Substituting for t from Eq. (iii), this become

$$\frac{\gamma+1}{2}M^2=1+\frac{\gamma-1}{2}M^2$$

or

$$\gamma M^2+M^2=2+\gamma M^2-M^2$$
$$2M^2=2$$
$$M=\pm 1$$

But $M=-1$ is an impractical solution, hence $M=1$ at the location in the nozzle where the local area is maximum or minimum.

Now, differentiating Eq. (i) with respective M, we have

$$\frac{d^2(A/A^*)}{dM^2}=\left(\frac{2}{\gamma+1}\right)^{\frac{\gamma+1}{2(\gamma-1)}}\left(\frac{\gamma+1}{2}\left(\frac{\gamma+1}{2(\gamma-1)}-1\right)t^{\left[\frac{\gamma+1}{2(\gamma-1)}-2\right]}(\gamma-1)M\right.$$
$$\left.-\left[\frac{\gamma+1}{2(\gamma-1)}t^{\frac{\gamma+1}{2(\gamma-1)}-1}\frac{(\gamma-1)M}{M^2}+t^{\frac{\gamma+1}{2(\gamma-1)}}\left(-\frac{2}{M^3}\right)\right]\right)$$

This reduces to

$$\frac{d^2(A/A^*)}{dM^2}=\left(\frac{2}{\gamma+1}\right)^{\frac{\gamma+1}{2(\gamma-1)}}\left(\frac{\gamma+1}{2}\left[\frac{3-\gamma}{2}t^{\left[\frac{\gamma+1}{2(\gamma-1)}-2\right]}M\right]\right.$$

Scanned by CamScanner

$$-\left[\frac{\gamma+1}{2M}t^{\left[\frac{\gamma+1}{2(\gamma-1)}-1\right]}-\frac{2t^{\frac{\gamma+1}{2(\gamma-1)}}}{M^3}\right]\Bigg) \qquad \text{(iv)}$$

or

$$\frac{d^2(A/A^*)}{dM^2}=\left(\frac{2}{\gamma+1}\right)^{\frac{\gamma+1}{2(\gamma-1)}}t^{\frac{\gamma+1}{2(\gamma-1)}}\left[\left(\frac{\gamma+1}{2}\right)\left(\frac{3-\gamma}{2}\right)\frac{M}{t^2}-\frac{\gamma+1}{2Mt}+\frac{2}{M^3}\right]$$

From Eq. (iii), for $M = 1$, we have $t=\frac{\gamma+1}{2}$. Therefore, for $M = 1$, Eq. (iv) simplifies to

$$\frac{d^2(A/A^*)}{dM^2}=\left(\frac{\gamma+1}{2}\right)\left(\frac{3-\gamma}{2}\right)\left(\frac{2}{\gamma+1}\right)^2-\left(\frac{\gamma+1}{2}\right)\left(\frac{2}{\gamma+1}\right)+2$$

or

$$\frac{d^2(A/A^*)}{dM^2}=\left(\frac{3-\gamma}{2}\right)\left(\frac{2}{\gamma+1}\right)+1$$

$$=\frac{4}{\gamma+1}$$

This shows that the second derivative of A/A^* is positive. Hence, the location where the area ratio is minimum is the choked location, thus the limiting minimum possible for A is A^*, i.e., A cannot be less than A^*.

Mass Flow Relation in Terms of Mach Number

From our discussions so far, it is clear that the flow Mach number M is the most convenient parameter in terms of which all other parameters can be expressed. Indeed, p/p_0, ρ/ρ_0, T/T_0 and A/A^* are all expressed in terms of M in Eq. (4.33). Therefore, the mass flow through the nozzle can also be expressed in terms of M. The mass flow rate per unit area is

$$\frac{\dot{m}}{A}=\rho V$$

$$=\frac{\rho}{\rho_0}\rho_0\frac{V}{a}a$$

$$=\frac{\rho}{\rho_0}\frac{p_0}{RT_0}M\sqrt{\gamma RT}$$

$$=\frac{\rho}{\rho_0}\sqrt{\frac{T}{T_0}}\sqrt{T_0}\frac{p_0M}{RT_0}\sqrt{\gamma R}$$

Scanned by CamScanner

$$= \frac{p_0 M\sqrt{\gamma/RT_0}}{\left(1+\frac{\gamma-1}{2}M^2\right)^{1/(\gamma-1)}\left(1+\frac{\gamma-1}{2}M^2\right)^{1/2}}$$

$$= \boxed{\frac{p_0 M\sqrt{\gamma/RT_0}}{\left(1+\frac{\gamma-1}{2}M^2\right)^{\frac{\gamma+1}{2(\gamma-1)}}}} \tag{4.35}$$

where the subscript 0 refers to the stagnation state. This relation shows that, the mass flow rate per unit area at a given Mach number is proportional to stagnation pressure and inversely proportional to the square root of the stagnation temperature.

Maximum Mass Flow Rate per Unit Area

To find the condition for maximum mass flow rate per unit area, we can differentiate $\dot{m}/A$ with respect to M and equate that derivative to zero. At this condition we find that, $M = 1$. That is, the mass flow rate per unit area is maximum at the location where the Mach number is unity. We know that, this can happen only at the throat of a convergent-divergent nozzle or at the exit of a convergent nozzle or orifice and it is referred to as the *choked state*. For this condition of $M = 1$, from Eq. (4.35), we get

$$\left(\frac{\dot{m}}{A}\right)_{\max} = \frac{\dot{m}}{A^*} = \boxed{\sqrt{\frac{\gamma}{RT_0}\left(\frac{2}{\gamma+1}\right)^{(\gamma+1)/(\gamma-1)}}\, p_0} \tag{4.36}$$

Equation (4.36) shows that, for a given gas (i.e. for a given γ), the maximum mass flow rate per unit area depends only on the ratio of $p_0/\sqrt{RT_0}$. This also implies that for a given stagnation state at p_0 and T_0 the mass flow through a passage with a given minimum area (given throat) is relatively large for gases of high molecular weight (i.e. for a gas of low gas constant, R) and relatively small for gases of low molecular weight. Also, doubling the stagnation pressure level would double the maximum flow, whereas doubling the stagnation temperature would reduce the maximum mass flow by about 29 per cent. For a gas with $\gamma = 1.4$, the maximum mass flow rate through a convergent-divergent nozzle becomes

$$\dot{m}_{\max} = \boxed{\frac{0.6847}{\sqrt{RT_0}} p_0 A^*}$$

The area A^* is the area at the choked location with $M = 1$, which is the minimum cross-sectional area of the passage. For a convergent-divergent nozzle, it is the throat.

Scanned by CamScanner

4.6 SUPERSONIC FLOW GENERATION

We saw in Section 4.5 that "a nozzle which does not have an expanding portion can never produce supersonic flow". Now, we may ask that "what will be the Mach number of a flow which comes out through a straight hole from a pressure tank at a high pressure, say $p_{01} = 10$ atm, to an environment at standard sea level condition, p_a, as shown in Fig. 4.12"? It is important to note that the pressure ratio across the hole is $p_a/p_{01} = 0.1$, which is much less than the isentropic choking pressure ratio of 0.528. Therefore, the flow leaving the hole would be choked and the exit velocity would be sonic. Also, the choked flow leaving the hole is highly underexpanded and finds a large space to expand further. Therefore, the flow on free expansion can attain a Mach number corresponding to the pressure ratio of 0.1. For this pressure ratio, isentropic expansion would result in Mach 2.15. This simply implies that the underexpanded flow exiting the hole at Mach 1 will pass through an expansion fan and attain Mach 2.15. At zones *a* and *b* the flow experiences only half the expansion compared to zone 2, and hence the Mach number in zones *a* and *b* would be less than the Mach number that the flow would attain at zone 2, after passing through double expansion. Soon after leaving the hole the sonic flow passes through the expansion fan and becomes supersonic. But at every point in the expansion fan the flow has a different supersonic Mach number. Also, since the flow at the apex of the expansion fan is turned almost suddenly to move away from the hole axis, it has to be turned towards the axis to become axial at a downstream distance. This turning is caused by the shock which is essentially an oblique shock. But on either side of the axis for a two-dimensional flow, and around the axis for axi-symmetric flow, the shape of the shock assumes the form of a "barrel" and thus, is termed *barrel shock*. Outside of the barrel shock, the flow has a mixture of supersonic and subsonic Mach numbers. The expansion rays get reflected from the free boundary as compression waves, since the reflection of a wave from a free boundary is *unlike*. The supersonic flow in zone 2 gets decelerated on passing through these reflected compression waves and hence the flow Mach number at *c* is less than that at 2. These compression waves may coalesce to form shock waves which cross each other at the axis and meet the barrel shock and reflect back as expansion waves, as shown in Fig. 4.12. The distance from the hole exit to the first kink-location on the barrel shock, where the shocks get reflected as expansion waves, is called a *shock-cell*, in jet literature. Therefore, what is meant by the statement in the beginning of Section 4.6, that "a nozzle which does not have an expanding portion cannot produce supersonic flow" is that, to generate a uniform supersonic flow of a specific Mach number, a divergent duct of specific exit area run by a convergent duct with choked throat, as shown in Fig. 4.13, is essential.

Scanned by CamScanner

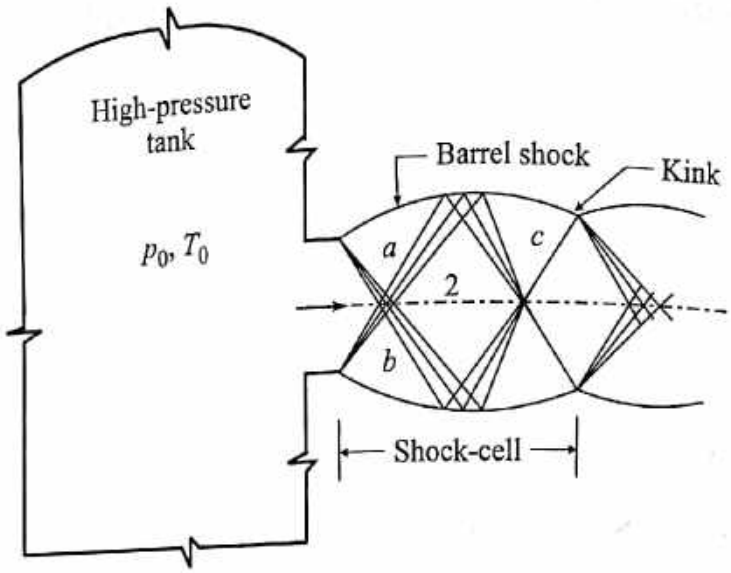
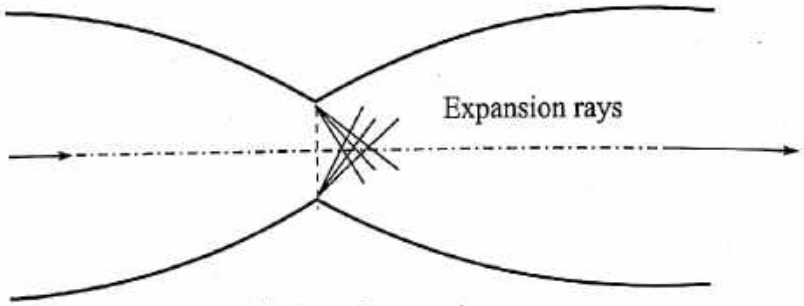
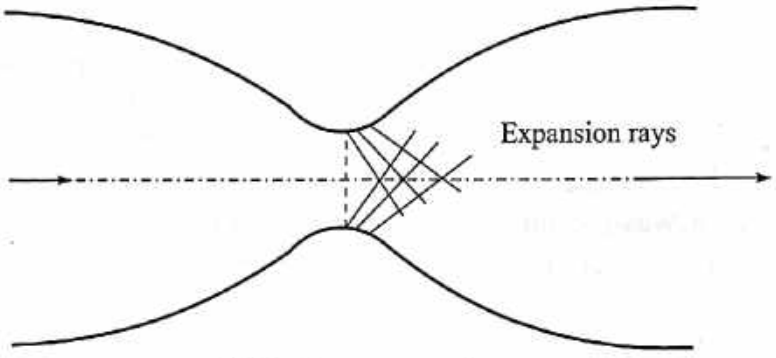


Fig. 4.12 Flow pattern of the discharge from a tank.



(a) Centred expansion



(b) Continuous expansion

Fig. 4.13 Contoured convergent-divergent (De Laval) nozzle.

If the nozzle has a shape with a contoured divergent duct, as in Fig. 4.13, it will deliver a uniform supersonic Mach number, M, corresponding to the area ratio A/A^*. Also, the supersonic flow coming out of a contoured nozzle will be a uniform flow parallel to the nozzle axis. This kind of contoured nozzle is called De Laval nozzle, in honour of De Laval who was the first to use such a configuration. The details of the design procedure and the associated wave cancellation process of contoured nozzles will be seen in our discussion on the method of characteristics dealt with in Chapter 12.

Scanned by CamScanner

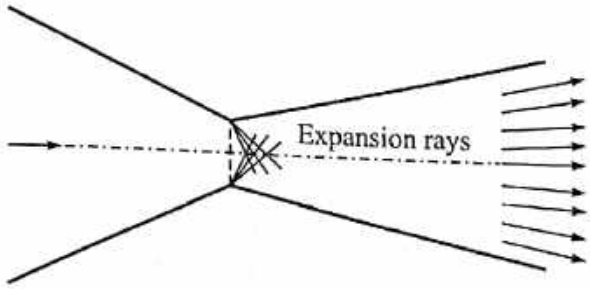


Fig. 4.14 Straight convergent-divergent nozzle.

A defined supersonic flow can also be generated using a convergent-divergent nozzle with straight walls, as shown in Fig. 4.14. But the flow exiting the straight C-D nozzle, even though will be of uniform Mach number, will be diverging away from the nozzle axis, as shown in Fig. 4.14. That is, a straight C-D nozzle can deliver a uniform supersonic Mach number but the flow will not be uni-directional. On the other hand, a contoured or De Laval nozzle can generate uniform flow as well as uni-directional supersonic flow.

Now, we may ask, what are the specific applications of these straight and contoured convergent-divergent nozzles? The answer to this question is the following.

- When the flow field has to be uniform as well as uni-directional as in the case of a wind tunnel test-section, only contoured or Laval nozzle can meet these requirements. Thus, in all supersonic tunnels, contoured nozzles are used to generate the desired flow field in the test-section.
- If thrust generation is the main requirement of the nozzle, as in the case of rocket engines, straight convergent-divergent nozzles can meet the requirement. In this case, definitely, there is some thrust loss due to the flow divergence at the nozzle exit. But this loss is not significant because of the low divergence angle of the nozzle geometry. Usually a semi-divergence angle of 7° is given for rocket nozzles. This angle is arrived at by considering the flow quality and engine weight. A smaller angle is preferred from the thrust loss minimization point of view, but a small angle will result in a longer nozzle for a specified Mach number, leading to increased weight. Larger angles will result in shorter nozzles but the flow will tend to separate inside the nozzle and cause many undesirable consequences. Thus, the 7° semi-divergence to a rocket nozzle is a compromise between weight and flow separation considerations.

EXAMPLE 4.7 A De Laval nozzle has to be designed for an exit Mach number of 1.5 with an exit diameter of 200 mm. Find the required ratio of throat area to exit area. The reservoir conditions are given as $p_0 = 1$ atmg; $T_0 = 20°C$. Find also the maximum mass flow rate through the nozzle. What will be the exit pressure and temperature?

Scanned by CamScanner

Solution Given $p_0 = 1$ atmg, $T_0 = 273 + 20 = 293$ K. We have

$$M_e = 1.5, \quad D_e = 200 \text{ mm} = 0.2 \text{ m}$$

By Eq. (4.34d),

$$\frac{A}{A^*} = \frac{1}{M}\left(\frac{5+M^2}{6}\right)^3$$

For $M_e = 1.5$,

$$\frac{A_e}{A^*} = 1.176$$

The maximum mass flow rate is

$$\dot{m}_{\max} = \rho^* A^* V^* = A^* \sqrt{\gamma\left(\frac{2}{\gamma+1}\right)^{(\gamma+1)/(\gamma-1)} p_0 \rho_0}$$

$$= A^* \sqrt{\gamma\left(\frac{2}{\gamma+1}\right)^{(\gamma+1)/(\gamma-1)} p_0^2 / RT_0} = \frac{0.6847}{\sqrt{RT_0}} p_0 A^*$$

$$\dot{m}_{\max} = \boxed{12.78 \text{ kg/s}}$$

By Eq. (4.34c),

$$\frac{T}{T_0} = \left(1+\frac{M^2}{5}\right)^{-1}$$

$$T = 293\left(1+\frac{2.25}{5}\right)^{-1}$$

$$T = \boxed{202.07 \text{ K}}$$

By Eq. (4.34a),

$$\frac{p}{p_0} = \left(1+\frac{M^2}{5}\right)^{-3.5}$$

$$p = 2\left(1+\frac{2.25}{5}\right)^{-3.5}$$

$$p = \boxed{0.545 \text{ atm}}$$

Thus,

$$A^*/A_e = 0.85$$
$$\dot{m}_{\max} = 12.78 \text{ kg/s}$$
$$p_{\text{exit}} = 0.545 \text{ atm}$$
$$T_{\text{exit}} = 202.07 \text{ K}$$

Scanned by CamScanner

EXAMPLE 4.8 A converging-diverging nozzle is designed to operate with an exit Mach number of 1.75. The nozzle is supplied from an air reservoir at 68×10^5 N/m^2 (abs). Assuming one-dimensional flow, calculate the following:

(a) Maximum backpressure to choke the nozzle
(b) Range of backpressure over which a normal shock will appear in the nozzle
(c) Backpressure for the nozzle to be perfectly expanded to the design Mach number M
(d) Range of backpressure for supersonic flow at the nozzle exit plane.

Solution Design $M = 1.75$

From isentropic table (Table A1 of Appendix A), at $M = 1.75$, $\frac{A}{A^*} = 1.386$

(a) The nozzle is choked with $M = 1$ at the throat, followed by subsonic flow in the diverging portion of the nozzle. Again, from Table A1 in Appendix A, at $A/A^* = 1.386$, $M = 0.48$, and $p/p_t = 0.854$. Therefore, the nozzle is choked for all backpressures below $\boxed{58 \text{ atm}}$.

(b) For normal shock at nozzle exit plane: from isentropic table (Table A1), for $M = 1.75$; $p_1 = 0.188 p_t = 12.78$ atm (subscript "1" refers to upstream of shock and the subscript "2" to downstream). From normal shock table (Table 2A of Appendix A) at $M_1 = 1.75$, $p_2/p_1 = 3.406$. For a normal shock at nozzle exit, the backpressure is $3.406 \times 12.78 = \boxed{43.53 \text{ atm}}$.

For a normal shock just downstream of the nozzle throat, the backpressure is 58 atm. Therefore, a normal shock will appear in the nozzle over the range of backpressures, $\boxed{43.53 - 58.0 \text{ atm}}$.

(c) From isentropic table, at $M = 1.75$, $p/p_t = 0.188$. Therefore, for a perfectly expanded nozzle, the backpressure is $\boxed{12.78 \text{ atm}}$.

(d) This nozzle will deliver supersonic flow for all backpressures below $\boxed{43.53 \text{ atm}}$.

From our discussions on nozzle flows, we may have the following doubt. When the backpressure p_b is more than the nozzle exit pressure p_e, it is termed overexpansion. An overexpanded nozzle could deliver supersonic flow. But under this condition, a normal shock can occur in the divergent section and the flow will become subsonic downstream of this normal shock and decelerate to backpressure. Then how does the flow experiences overexpansion? Does it mean that the normal shock will occur only under certain conditions? If so, what are those conditions? The answer to these questions are the following.

When $p_e < p_b$, the flow exiting the nozzle will be supersonic flow, provided within the nozzle the pressure gradient is favourable. That is, if $p_{i-1} > p_i$ from

Scanned by CamScanner

the choked throat to the exit. At any location inside the nozzle, if $p_{i-1} < p_i$, then a compression wave (a curved compression wave) will be established at the location and the flow will be locally separated from the nozzle wall. If $p_{i-1} << p_i$, a normal shock needs to be there to cause a steep increase in static pressure to overcome this strong adverse pressure gradient.

When the driving pressure p_0, namely the stagnation pressure in the settling chamber, is below a certain limiting value for a given Mach number, the static pressure p would encounter a low value inside the nozzle establishing an adverse pressure gradient, leading to flow separation in the divergent portion of the nozzle. Thus, for every design Mach number, there is a limiting p_0 for the nozzle to flow full, delivering a uniform Mach number throughout the exit plane. Otherwise, the nozzle will not have the uniform supersonic Mach number all over its exit plane. When there is a separation inside the nozzle, such that the compression wave formed is of curved shape, the flow along the nozzle axis may continue to be supersonic, but near the wall region the flow will be subsonic. Sometimes, by chance, the centreline Mach number may be the design value also. That is why a nozzle needs to be calibrated, by measuring the Mach number at least along a diameter at the exit, to ensure that the nozzle delivers supersonic flow throughout the exit plane.

EXAMPLE 4.9 A Mach 2 convergent-divergent nozzle, run by a settling chamber with air maintained at 300 K, is discharging to an environment at atmospheric pressure. Determine the settling chamber pressure required to run the nozzle (a) at correctly expanded state, (b) with maximum possible overexpansion, and (c) with normal shock at the exit. (d) Determine the settling chamber pressure required to position a normal shock in the divergent part of the nozzle, at the location where the area is 1.5 times the throat area. What will be the flow speed behind the normal shock?

Solution Given, the stagnation temperature $T_0 = 300$ K, backpressure $p_b = 1$ atm and the design Mach number $M_e = 2.0$.

(a) For correctly expanded operation, $p_e = p_b$. For $M_e = 2.0$, from the isentropic table,

$$\frac{p_e}{p_0} = 0.1278, \quad \frac{A_e}{A_{th}} = 1.688$$

where the subscripts e and th refer to the nozzle exit and throat, respectively.

For correct expansion, with $p_e = p_b$, the settling chamber pressure required is

$$p_0 = \frac{p_e}{0.1278}$$

$$= \frac{1}{0.1278}$$

$$= \boxed{7.82 \text{ atm}}$$

Scanned by CamScanner

(b) The maximum possible overexpansion corresponds to the stagnation pressure in the settling chamber, for which there will be the strongest possible oblique shock, for Mach 2 flow, positioned at the nozzle exit.

Let the subscripts 1 and 2 refer to the state ahead of and behind the oblique shock, respectively. For $M_1 = 2$, from the oblique shock table (or chart),

$$\frac{p_2}{p_1} = 3.971, \quad M_2 = 0.802$$

The flow behind the shock is subsonic; also this flow is a free flow outside the nozzle. Therefore, this flow has to be correctly expanded, with $p_2 = p_b$. Thus, the pressure ahead of the shock is

$$p_1 = \frac{p_2}{3.971}$$
$$= \frac{1}{3.971}$$
$$= 0.25 \text{ atm}$$

The flow from the inlet to the exit is isentropic, with $p_1/p_0 = 0.1278$. This gives the settling chamber pressure as

$$p_0 = \frac{p_1}{0.1278}$$
$$= \frac{0.25}{0.1278}$$
$$= \boxed{1.956 \text{ atm}}$$

(c) When there is a normal shock at the exit, the flow coming out of the nozzle will be subsonic. Therefore, the pressure p_2 behind the shock has to be equal to the backpressure, because subsonic free flows are always correctly expanded.

The Mach number ahead of the shock is $M_1 = 2$. From the normal shock table, for $M_1 = 2$, the pressure ratio across the shock is $p_2/p_1 = 4.5$. Therefore,

$$p_1 = \frac{p_2}{4.5}$$
$$= \frac{1}{4.5}$$
$$= 0.222 \text{ atm}$$

From the isentropic table, for $M_1 = 2$, $p_1/p_{01} = 0.1278$. Therefore,

$$p_{01} = \frac{p_1}{0.1278}$$

Scanned by CamScanner

$$= \frac{0.222}{0.1278}$$

$$= \boxed{1.74 \text{ atm}}$$

For a backpressure of 1 atm, if the settling chamber pressure is decreased below 1.74 atm, the normal shock will move upstream of the nozzle exit, and positioned in the divergent, portion, as long as the settling chamber pressure is sufficient to choke the throat. When the settling chamber pressure is reduced below this limiting value to choke the throat, the flow in the divergent portion will decelerate, and the divergent part of the duct will act as a subsonic diffuser.

(d) The normal shock is at $\frac{A}{A_{th}} = 1.5$. For this area ratio, from the isentropic table (supersonic solution), we have

$$M_1 = 1.85, \quad \frac{p_1}{p_{01}} = 0.1612, \quad \frac{T_1}{T_{01}} = 0.5936$$

For $M_1 = 1.85$, from the normal shock table,

$$\frac{T_2}{T_1} = 1.5693, \quad \frac{p_2}{p_1} = 3.8262, \quad \frac{p_{02}}{p_{01}} = 0.7902, \quad M_2 = 0.6057$$

where the subscripts 1 and 2 refer to the state ahead of and behind the shock, respectively.

The static temperature ahead of the shock is

$$T_1 = 0.5936\ T_{01}$$
$$= 0.5936 \times 300$$
$$= 178 \text{ K}$$

The static temperature behind the shock is

$$T_2 = 1.5693\ T_1$$
$$= 1.5693 \times 178$$
$$= 279.34 \text{ K}$$

The flow speed behind the shock is

$$V_2 = M_2 a_2$$
$$= M_2 \sqrt{\gamma R T_2}$$
$$= 0.6057 \times \sqrt{1.4 \times 287 \times 279.34}$$
$$= \boxed{203 \text{ m/s}}$$

Scanned by CamScanner

EXAMPLE 4.10 Sea level air is drawn through a convergent-divergent duct, connected to a vacuum chamber. (a) Determine the maximum velocity that can be achieved in the duct, and the location of the maximum velocity. (b) Is this a practically feasible process?

Solution (a) The maximum velocity in the convergent-divergent duct will be at the exit when it runs with choked throat, and the pressure gradient all over the nozzle length is favourable.

Given, the sea level air is drawn through the duct. Therefore, the total pressure and total temperature at the inlet of the duct are $p_0 = 1$ atm and $T_0 = 15°C = 15 + 273.15 = 288.15$ K, respectively.

By energy equation,

$$h_e + \frac{V_e^2}{2} = h_0$$

where h_e and V_e are the static enthalpy and velocity at the exit, respectively, and h_0 is the stagnation enthalpy. At the given temperature, air can be taken as a perfect gas. Therefore, we have

$$h_e = c_p T_e, \quad h_0 = c_p T_0$$

Substituting these, the energy equation becomes

$$c_p T_e + \frac{V_e^2}{2} = c_p T_0$$

This gives the exit velocity as

$$V_e = \sqrt{2c_p(T_0 - T_e)}$$

This will be maximum for $T_e = 0$. Thus,

$$V_{e,\,\max} = \sqrt{2c_p T_0}$$

For a perfect gas, with $\gamma = 1.4$, the specific heat c_p becomes

$$c_p = \frac{\gamma}{\gamma - 1} R$$

$$= \frac{1.4}{1.4 - 1} \times 287$$

$$= 1004.5 \text{ J/(kg K)}$$

Therefore, the maximum velocity becomes

$$V_{e,\,\max} = \sqrt{2 \times 1004.5 \times 288.15}$$

$$= \boxed{760.85 \text{ m/s}}$$

Scanned by CamScanner

(b) This acceleration process is practically not possible, because below certain temperature the moisture in the air will condense (Rathakrishnan, 2016).

For isentropic acceleration throughout the duct, the condensation of moisture in the air must be avoided. To ensure that the condensation will not be present in significant amounts, the air dew-point in the duct should be continuously monitored during the operation. The amount of moisture that can be held by a cubic metre of air increases with increasing temperature, but is independent of the pressure. The moist atmospheric air cools as it expands isentropically through the duct. The air may become supercooled (cooled to a temperature below the dew-point temperature) and the moisture will then condense out. If the moisture content is sufficiently high, it will appear as a dense fog in the duct.

Condensation causes changes in the local Mach number and other flow characteristics such that the data taken in a test may be erroneous. The flow changes depend on the amount of heat released through condensation.

At subsonic speeds, the Mach number decreases and the pressure increases with condensation, whereas at supersonic speeds, the reverse is taking place. It is important to note that, the presence of water vapour without condensation is of no significance as far as the temperature ratio, pressure ratio, and Mach number determination with the isentropic relations are concerned. The condensation depends on the amount of moisture in the air stream, the static temperature of the stream, the static pressure of the stream, and the time duration during which the stream is at a low temperature.

The amount of moisture that may be contained in normal atmospheric air usually varies in the range of 0.004 to 0.023 kg/(kg of dry air). The air temperature in the divergent portion of a convergent-divergent duct is usually quite low. For example, let us assume that the total temperature of the stored air is 40°C. From the isentropic table (for $\gamma = 1.4$), we can see that for a test-section Mach number of 1.0, the static temperature is –12°C, for $M = 1.5$, $T = -57$°C, and will go to a low value of –220°C at $M = 5.0$. The static temperatures reached during the expansion of air at a stagnation temperature of 40°C to the Mach number above 1 are considerably below the dew-point temperatures, normally found in the atmosphere. Hence, the static temperature in a convergent-divergent duct can easily be low enough to condense out normal atmospheric water vapour. The static pressure in a convergent-divergent duct drops more rapidly than the static temperature, with Mach number increase.

The condensation of moisture in an air stream is the result of molecules colliding and combining and eventually building up into droplet size. The likelihood of condensation in a convergent-divergent duct with supercooling (cooling of the air below the dew-point) of less than –12°C is negligible. Since condensation is a result of a gradual buildup from molecular to droplet size due to molecular collisions, it is obviously a time-dependent process.

Scanned by CamScanner

4.7 DIFFUSERS

Basically, diffusers are passages in which flow will decelerate. If the Laval nozzle shown in Fig. 4.10 discharges directly into a receiver, the minimum pressure ratio for full supersonic flow in the nozzle test-section is

$$\left(\frac{p_0}{p_e}\right)_{\min} = \frac{p_0}{p_{e5}}$$

where p_{e5} is the value of p_e at which the normal shock will stand at the nozzle exit [Fig. 4.11(a)]. However, if a diffuser is attached at the nozzle exit, as shown in Fig. 4.15, the nozzle can be operated to generate shock-free supersonic flow at a lower pressure ratio. This is because the subsonic flow downstream of the normal shock may be decelerated isentropically to the stagnation pressure p_{02}. The pressure ratio required then is the ratio of stagnation pressures across a normal shock wave at the test-section Mach number M_1, i.e.

$$\frac{p_{02}}{p_{01}} = \left(1 + \frac{2\gamma}{\gamma+1}(M_1^2 - 1)\right)^{-1/(\gamma-1)} \left(\frac{(\gamma+1)M_1^2}{(\gamma-1)M_1^2 + 2}\right)^{\gamma/(\gamma-1)}$$

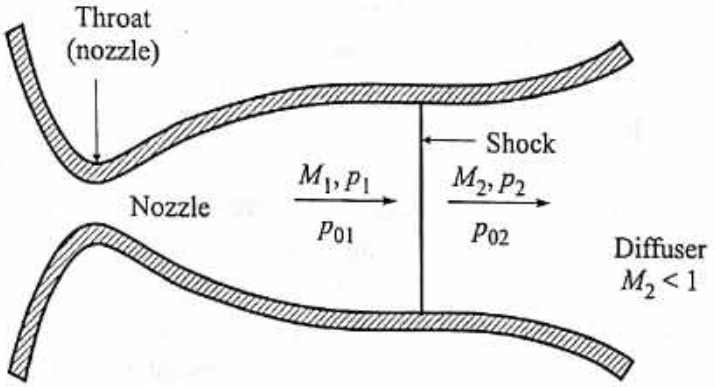


Fig. 4.15 Nozzle exhausting into a diffuser through a normal shock.

This ratio is given in Eq. (5.22).

It can be shown as follows that p_{02}/p_{01} is equal to the ratio of the first throat area A_1^* to that of the second throat A_2^*.

By continuity,

$$\dot{m}_1^* = \dot{m}_2^*$$

$$\rho_1^* A_1^* V_1^* = \rho_2^* A_2^* V_2^*$$

However, $V_1^* = V_2^* = a^*$; therefore,

$$\rho_1^* A_1^* = \rho_2^* A_2^*$$

$$\frac{A_1^*}{A_2^*} = \frac{\rho_2^*}{\rho_1^*} = \frac{p_2^*}{p_1^*}$$

Scanned by CamScanner

Since $T_1^* = T_2^*$, the second equation above can be written as

$$\frac{A_1^*}{A_2^*} = \frac{p_2^*}{p_{02}} \frac{p_{02}}{p_{01}} \frac{1}{p_1^*/p_{01}}$$

By isentropic relations, for $M = 1$,

$$\frac{p}{p_0} = \left(\frac{\gamma+1}{2}\right)^{-\gamma/(\gamma-1)}$$

Hence,

$$\frac{p_2^*}{p_{02}} = \frac{p_1^*}{p_{01}}$$

Thus,

$$\boxed{\frac{A_1^*}{A_2^*} = \frac{p_{02}}{p_{01}}}$$

This pressure ratio is based on the assumption of isentropic expansion of the subsonic flow in the diffuser and hence it does not account for losses in the diffuser. But in practice, the diffuser of Fig. 4.15 does not give the expected recovery due to the interaction of shock wave and boundary layer which produces a flow different from the above isentropic model. Therefore, the design of a perfect isentropic diffuser is impossible. In other words, the design of a diffuser which can give complete pressure recovery (i.e. which can expand the flow isentropically so that the tunnel can be run with stagnation pressure ratio p_{02}/p_{01}) is physically not possible. The other way of looking at it is: no diffuser can expand the flow with a stagnation pressure p_{02} at its entrance (just behind the shock in Fig. 4.15), taking the static pressure value from p_2 at its entrance to the ambient atmospheric pressure value p_a (also called the backpressure) at its exit. Hence the stagnation pressure required for practical operation is definitely much larger than the pressure p_{01} required for isentropic operation.

From the above discussion, it is clear that a perfect diffuser cannot be built. However, we can visualize, with our basic knowledge about shocks, that the normal shock is the strongest one, and the flow experiences more pressure loss across it compared to an oblique shock. Therefore, modification of the diffuser in such a manner as to compress the supersonic flow to subsonic level through a series of oblique shocks instead of through a single normal shock, as shown in Fig. 4.15, before it is being actually expanded as a subsonic flow, will result in a better pressure recovery. Therefore, it would be advantageous to replace the normal shock diffuser in Fig. 4.15 with an oblique shock diffuser as illustrated in Fig. 4.16, where the test-section Mach number M_1 is slowed down through a series of oblique shock waves initiated by a compression corner at the diffuser inlet and finally by a weak normal shock at the end of the constant area section before entering the subsonic portion of the diffuser, where it is

Scanned by CamScanner

subsonically compressed by the divergent section which exhausts to the atmosphere. At the diffuser exit, the static pressure p_e, in principle, can be made equal to the ambient atmospheric pressure p_a, by suitably designing the diffuser. Conceptually, this oblique shock diffuser should provide a better pressure recovery (lesser loss in total pressure) than a normal shock diffuser. But, in practice, the interaction of the shock waves (Fig. 4.16) with the viscous boundary layer on the diffuser walls creates an additional total pressure loss which tends to partially reduce the advantages of an oblique shock diffuser. The net effect is that the full potential of an oblique shock diffuser is never achieved.

For a better understanding of the arguments given in this section, the reader is advised to consult Chapters 5 and 6.

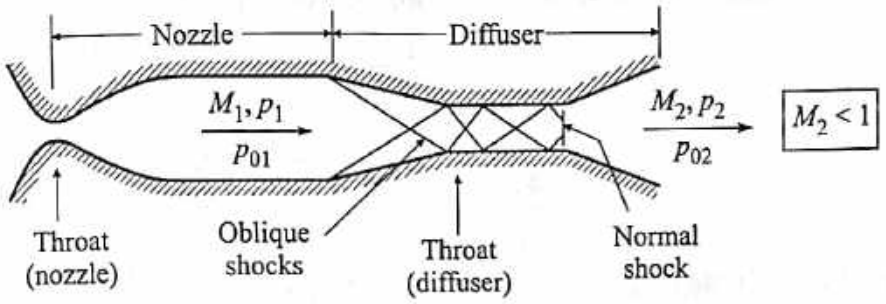


Fig. 4.16 Nozzle exhausting into a diffuser through oblique shocks.

EXAMPLE 4.11 A supersonic converging-diverging diffuser, shown in Fig. 4.17, is designed to operate at a Mach number of 1.7. To what Mach number should the inlet be accelerated in order to swallow the shock during the start-up?

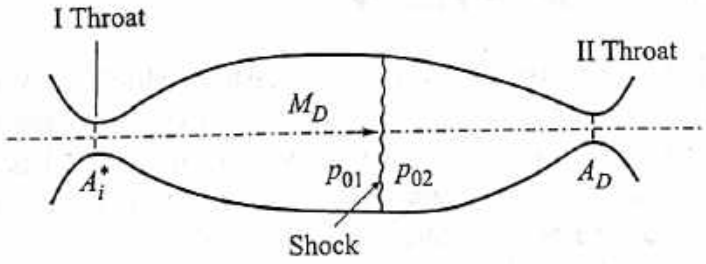


Fig. 4.17 Example 4.11.

Solution Let A_1^* and A_D be the area of first and second throats respectively. The area at the entry to the diffuser where $M_D = 1.7$ is given by the isentropic area ratio for $M_D = 1.7$. From isentropic Table A1 of Appendix A, for $M_D = 1.7$, $A/A_1^* = 1.338$. If $A \rightarrow A_D$, then the shock will be swallowed. Therefore,

$$\frac{A_D}{A_1^*} = \frac{A}{A_1^*} = 1.338$$

This ratio is also equal to the stagnation pressure ratio p_{01}/p_{02}. Therefore, $p_{02}/p_{01} = 0.747$. For this value of stagnation pressure ratio, from normal shock

Scanned by CamScanner

table, $M = 1.94$. Thus, the Mach number to which the inlet should be accelerated to swallow the shock during the start-up is $M = 1.94$.

EXAMPLE 4.12 A convergent-divergent diffuser is to be used at Mach 3.0. The diffuser has to use a variable throat area so as to swallow the starting shock. What percentage increase in throat area will be necessary?

Solution Let A_1^* and A_2^* be the area of first and second throat respectively. The minimum starting area for the second throat is given by

$$\frac{A_2^*}{A_1^*} = \frac{p_{01}}{p_{02}}$$

From normal shock Table A2 of Appendix A, for $M_1 = 3.0$,

$$\frac{p_{01}}{p_{02}} = \frac{1}{0.3283} = 3.046$$

Therefore,

$$\frac{A_2^*}{A_1^*} = 3.046$$

Hence, the percentage increase in the area required to swallow the starting shock is

$$\boxed{\frac{A_2^* - A_1^*}{A_1^*} \times 100 = 204.6\%}$$

4.8 DYNAMIC HEAD MEASUREMENT IN COMPRESSIBLE FLOW

In any flow field, basically there are three pressures which are of interest to gas dynamic studies. However, in fluid mechanics we use yet a fourth pressure in parallel flow studies, which we call the *geometric pressure*. Also, we know that this pressure is due only to the gravitational action on a static fluid having the same geometry as the actual flow.

The three pressures which are of interest in gas dynamics are (i) total or stagnation pressure, (ii) static pressure, and (iii) dynamic pressure. The *total pressure* is the pressure which results when the flow is brought to rest isentropically, i.e. at a position in the flow where the actual fluid velocity is zero; the total pressure corresponds to the undisturbed static pressure p.

The *static pressure* is that pressure which acts equally in all directions in space.

The third pressure, viz. *dynamic pressure*, may be associated with the flow conditions at a point by taking the difference between the stagnation pressure and the undisturbed static pressures.

For incompressible flows, these three pressures are linked together by Bernoulli's equation

Scanned by CamScanner

$$p_0 - p = \frac{1}{2}\rho V^2 = q \text{ (incomp.)} \tag{4.37}$$

where p_0 is the total pressure, p the static pressure, and $(1/2)\rho V^2$ the dynamic pressure. p_0 will be the same everywhere in an incompressible flow with no losses. For a constant p_0, it is seen from Eq. (4.37) that increase in flow velocity results in decrease in static pressure and vice versa. The dynamic pressure q is linked to the kinetic energy of the flow and it has the same direction as that of the flow. Also, we know that the static pressure of a flow is that pressure which is acting normal to the flow direction. Therefore, the total pressure also has a definite direction. The total pressures are measured by using a simple device called a Pitot (total) probe. The Pitot probe is simply a tube with a blunt end facing into the gas stream. The tube will normally have an inside-to-outside diameter ratio of 1/2 to 3/4, and a length aligned with the gas stream of 15 to 20 tube diameters. The pressure hole is formed by the inside diameter of the tube at the blunt end. A typical Pitot tube is shown in Fig. 4.18.

The open-ended tube facing into the flow always measures the stagnation pressure it sees. But for supersonic flows, there will be a detached shock formed and standing in front of the blunt end. This means that the tube does not measure the actual stagnation pressure but only the stagnation pressure behind a normal shock. This new value is called *Pitot pressure* and in modern terminology denotes the total pressure in supersonic streams.

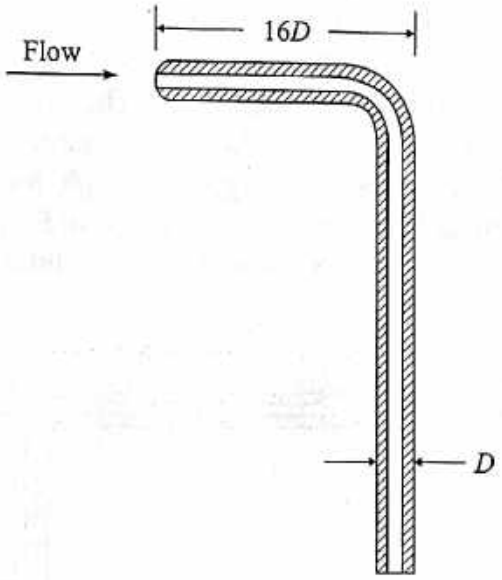


Fig. 4.18 Pitot-pressure probe.

This indicated Pitot pressure p_{02}, the stagnation pressure behind the normal shock, may be used for calculating Mach number, as follows: Multiply the equation

$$\frac{p_{01}}{p_1} = \left(1 + \frac{\gamma - 1}{2} M_1^2\right)^{\gamma/(\gamma-1)}$$

Scanned by CamScanner

by Eq. (5.22) to obtain

$$\frac{p_1}{p_{02}} = \frac{\left(\frac{2\gamma}{\gamma+1} M_1^2 - \frac{\gamma-1}{\gamma+1}\right)^{1/(\gamma-1)}}{\left(\frac{\gamma+1}{2} M_1^2\right)^{\gamma/(\gamma-1)}}$$

This relation is called the *Rayleigh supersonic Pitot formula*. Once the static pressure p and Pitot pressure p_{02} are known, M can be calculated.

When the Reynolds number of the flow (based on probe diameter) is very low (< 500), the measured Pitot pressures are unreliable. However, this effect is seldom a problem is supersonic tunnels, because a reasonable sized probe will usually have a Reynolds number well above 500.

The measurement of static pressures in supersonic flow are much more difficult than in subsonic flow. Though static probes are not used extensively for calibrating supersonic tunnels, considerable amount of study has been made for the development of accurate static pressure probes for other applications. The major problem in the use of static probes at supersonic speeds is that any probe will have a shock wave at its nose which causes a rise in static pressure.

In subsonic flow if the probe has a conical tip followed by a cylinder, the air passing the shoulder will be expanded to a pressure below static. Then, as the distance from the shoulder is increased, the pressure on the probe will approach the true static pressure of the stream. The sharp nosed tip of the probe facing the flow is closed and holes are drilled perpendicular to the axis of the tube at a specified distance from the sharp nose. The included angle of the sharp cone should be small for good results. Also, it is established that the static hole located beyond $8D$ from the nose is good enough for reasonably accurate measurements. A typical L-shaped probe is shown in Fig. 4.19. Static pressure measurements are very sensitive to inclination of the tube to the flow direction.

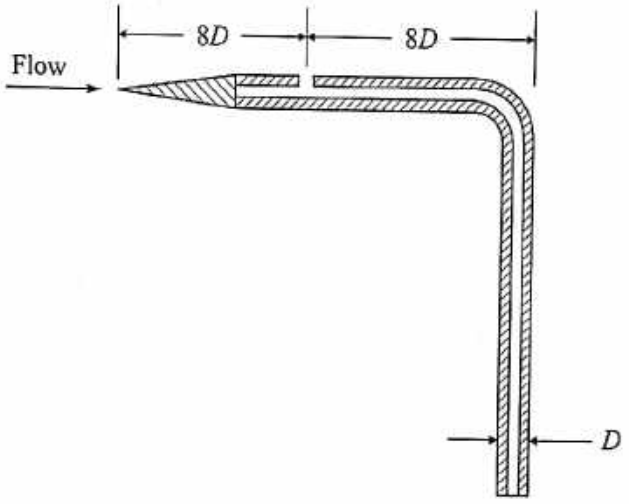


Fig. 4.19 Static pressure probe.

Scanned by CamScanner

Inclinations beyond 5° result in a large error in the measured pressures. In order to minimize this error, it is a common practice to have static probes with four holes in mutually perpendicular directions. When a static pressure probe is placed in the flow field, the flow is accelerated because of the horizontal portion of the probe and decelerated because of the vertical stem of the probe; therefore, the holes are located at such a location that these two effects cancel each other and the probe measures the correct pressure.

For measurement of static pressures in supersonic flow, the hole should be located beyond $8D$ from the nose and the acceleration due to the probe should be kept to a minimum; for this the nose should be very sharp with included angle less than 10°. Also, it is a usual practice to employ a straight probe for measurement in supersonic flows.

The dynamic pressure of a subsonic flow can be measured directly by a special probe called Pitot-static probe, which is a combination of Pitot and static probes. A typical Pitot-static probe is shown in Fig. 4.20.

Compressibility Correction to Dynamic Pressure

For an incompressible flow, the velocity of the flow can be calculated from the measured dynamic pressure q, by the relation

$$V = \sqrt{\frac{2}{\rho} q}$$

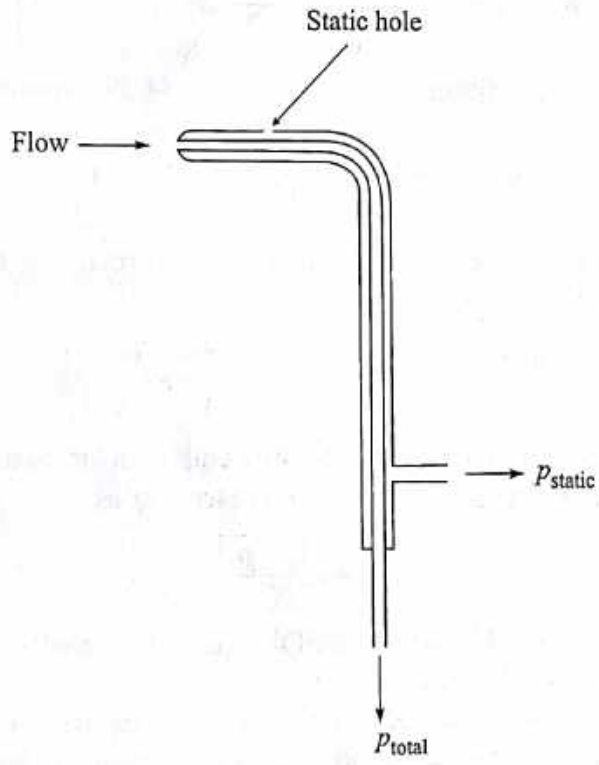


Fig. 4.20 Pitot-static tube.

Scanned by CamScanner

However, for compressible flow, the above formula cannot be used for calculating the flow velocity, because in compressible flow the relation $p_0 - p = q$ is not valid. Also, it may be noted that in supersonic regime of the compressible flow, the Mach number is more important than the velocity itself. For compressible flows, the dynamic pressure can be expressed in terms of M as follows:

$$q = \frac{1}{2}\rho V^2 = \frac{\rho}{2}M^2a^2 = \frac{\rho}{2}M^2\gamma RT$$

$$= \frac{\gamma p}{2}M^2 \tag{4.38}$$

From Eq. (4.38), we get

$$p = \frac{2}{\gamma M^2}q \tag{4.38a}$$

Also, by Eq. (2.49),

$$p_0 = p\left(1 + \frac{\gamma - 1}{2}M^2\right)^{\gamma/(\gamma-1)}$$

$$p_0 - p = p\left[\left(1 + \frac{\gamma - 1}{2}M^2\right)^{\gamma/(\gamma-1)} - 1\right]$$

Now, replacing the p on the RHS by Eq. (4.38a), we get

$$p_0 - p = \frac{2}{\gamma M^2}q\left[\left(1 + \frac{\gamma - 1}{2}M^2\right)^{\gamma/(\gamma-1)} - 1\right] \tag{4.39}$$

For air at standard conditions, i.e. $\gamma = 7/5$, Eq. (4.39) becomes

$$p_0 - p = q\frac{2}{\gamma M^2}\left[\left(1 + \frac{M^2}{5}\right)^{7/2} - 1\right] \tag{4.39a}$$

Expanding Eq. (4.39a) as per Binomial series and retaining terms only up to fourth power in M, we get

$$p_0 - p = q\left(1 + \frac{M^2}{4} + \frac{M^4}{40}\right) \tag{4.40}$$

For $M = 0$, Eq. (4.40) gives the Bernoulli's equation for incompressible flow. From this equation, we get the dynamic pressure q as

$$\boxed{q = \frac{p_0 - p}{K}} \tag{4.41}$$

where $K = 1 + M^2/4 + M^4/40$ is called the correction coefficient for dynamic pressure in compressible flow.

It is essential to note that, $M = 0$ giving rise to incompressible Bernoulli's equation is only a mathematical solution and not a physically possible one, since at $M = 0$ the flow velocity is also zero and hence there is no flow. In actual flows

Scanned by CamScanner

we treat $M < 0.3$ as incompressible, since under standard atmospheric conditions the density change associated with the Mach number ranging from 0 to 0.3 is less than 5 per cent, which can be regarded as incompressible, as discussed in Section 1.2.

Equation (4.40) is accurate enough up to $M = 2$ and for Mach numbers up to 1; even without the last term the equation should be proved to be reasonable accurate.

For any Mach number more than 2, Eq. (4.39) should be used for proper estimation of dynamic pressure. With a Pitot-static tube,

error in q with Eq. (4.41) = 20% at $M = 1$, with $K = 1$

error in $q = 2.5\%$ at $M = 1$, with $K = \left(1 + \frac{M^2}{4}\right)$

error in $q = 4\%$ at $M = 2$, with $K = 1 + \frac{M^2}{4} + \frac{M^4}{40}$

Beyond $M = 2$, use of Eq. (4.41) results in a large error in q.

EXAMPLE 4.13 Calculate the dynamic pressure of the flow if $V_\infty = 175$ m/s, $p_\infty = 1$ atm and $T_\infty = 298$ K. What will be the percentage error if the flow is treated as incompressible?

Solution (a) *Compressible flow:*

By Eq. (4.40), the dynamic pressure is given by

$$p_0 - p_\infty = q_\infty \left(1 + \frac{M_\infty^2}{4} + \frac{M_\infty^4}{40}\right)$$

where

$$q_\infty = \frac{1}{2}\rho_\infty V_\infty^2$$

(b) *Incompressible flow:*

For this, $q_\infty = \frac{1}{2}\frac{p_\infty}{RT_\infty}V_\infty^2 = 18142 \text{ N/m}^2 = 18.142 \text{ kPa}$ ($\because$ 1 Pa = 1 N/m^2)

$$M_\infty = \frac{V_\infty}{a_\infty} = \frac{175}{346} = 0.506$$

Therefore,

$$p_0 - p_\infty = 18142(1 + 0.064 + 0.00164)$$

$$= \boxed{19.333 \text{ kPa}}$$

Thus, the error involved in considering the flow to be incompressible is $\boxed{6.16\%}$.

Scanned by CamScanner

4.9 PRESSURE COEFFICIENT

The pressure coefficient C_p, an extremely useful quantity in fluid dynamics, is defined as

$$\boxed{C_p = \frac{p - p_\infty}{(1/2)\rho_\infty V_\infty^2}} \tag{4.42}$$

where p is the static pressure and p_∞, ρ_∞ and V_∞ are the pressure, density, and velocity in the freestream. The pressure coefficient is a nondimensional pressure difference.

An alternative form of the pressure coefficient, convenient for compressible flows, can be obtained be re-writing Eq. (4.42) as follows:

$$C_p = \frac{p - p_\infty}{(\gamma/2) p_\infty M_\infty^2} = \frac{p_\infty (p/p_\infty - 1)}{(\gamma/2) p_\infty M_\infty^2}$$

Therefore,

$$C_p = \frac{2}{\gamma M_\infty^2}\left(\frac{p}{p_\infty} - 1\right) \tag{4.43}$$

Equation (4.43) is an exact representation of Eq. (4.42) expressed in terms of M_∞.

We now proceed to obtain an expression for pressure coefficient at stagnation point in a compressible flow. Let us recall that, in an incompressible flow, the pressure coefficient at a stagnation point is $C_{p0} = 1$. But in compressible flows, because of the basic fact that, unlike incompressible flows, the dynamic pressure is not simply the difference between the stagnation and static pressures, it is given from Eq. (4.39) as

$$q = \frac{\gamma M^2 (p_0 - p)}{2\left[\left(1 + \dfrac{\gamma - 1}{2} M^2\right)^{\gamma/(\gamma-1)} - 1\right]} \tag{4.44}$$

Therefore, the stagnation pressure coefficient for compressible flow can be expressed as

$$C_{p0} = \frac{p_0 - p}{q} = \frac{2}{\gamma M^2}\left[\left(1 + \frac{\gamma - 1}{2} M^2\right)^{\gamma/(\gamma-1)} - 1\right] \tag{4.45}$$

By Eq. (4.40), C_{p0} can also be expressed as

$$C_{p0} = 1 + \frac{M^2}{4} + \frac{M^4}{40} \tag{4.46}$$

Equation (4.46) is accurate enough only for Mach numbers up to 2. For Mach numbers less than 1, it may further be simplified without loss of accuracy as

$$C_{p0} = 1 + \frac{M^2}{4} \tag{4.47}$$

Scanned by CamScanner

Equation (4.43) may also be expressed in another form in terms of velocities and Mach number as follows: From Eq. (4.43), we get

$$\frac{p}{p_\infty} = 1 + \frac{\gamma}{2} M_\infty^2 C_p$$

Combining this with Eq. (4.8), we can obtain

$$C_p = \frac{2}{\gamma M_\infty^2}\left[\left(\frac{\gamma-1}{2} M_\infty^2 \left\{1 - \left(\frac{V}{V_\infty}\right)^2\right\} + 1\right)^{\gamma/(\gamma-1)} - 1\right] \tag{4.48}$$

where V and V_∞ are the local and freestream velocities, respectively. For small values of the factor $\frac{\gamma-1}{2} M_\infty^2\left[1 - \left(\frac{V}{V_\infty}\right)^2\right]$, Eq. (4.48) may be simplified further to result in

$$C_p = \left[1 - \left(\frac{V}{V_\infty}\right)^2\right]\left[1 + \frac{M_\infty^2}{4}\left\{1 - \left(\frac{V}{V_\infty}\right)^2\right\}\right] \tag{4.49}$$

The first term on the right-hand side of Eq. (4.49) gives the pressure coefficient for incompressible flows in terms of velocity, namely

$$\boxed{C_{p_{\text{inc}}} = 1 - \left(\frac{V}{V_\infty}\right)^2} \tag{4.50}$$

4.10 SUMMARY

In this chapter the equations of continuity, momentum, and energy are applied to one-dimensional and quasi-one-dimensional isentropic flow through constant area ducts and ducts with gradually varying cross-section. The effects of Mach number on pressure, temperature, and density are demonstrated; the variations of pressure, velocity, and temperature with area for supersonic flow are totally different from those for subsonic flow.

For supersonic flow in a divergent channel, decrease in density is so rapid that both the area and velocity must increase together in order to keep the mass conservation rule, ρAV = constant, which is an essential feature for continuum flows.

The phenomenon of choking is discussed in detail, and the reason why choking should occur only at the minimum area and the reason for maximum mass flow rate per unit area at the throat are analyzed with different arguments. As the backpressure on a nozzle is lowered for a constant reservoir pressure, mass flow through the nozzle keeps increasing until a maximum flow rate is reached. Further decrease in backpressure has no effect on the mass flow rate, and at this condition the nozzle is said to be *choked*. That is, after choking, the

Scanned by CamScanner

decrease in backpressure cannot be sensed by the fluid in the reservoir. For subsonic flow, any change in backpressure is sensed in the reservoir by means of signal waves which are travelling with speed equal to *velocity of sound*. Once the flow velocity at a point in the nozzle becomes equal to the velocity of sound, the signals carrying the information about backpressure changes are not able to travel to the reservoir crossing the sonic speed location. This is because the *effective velocity* with which the signals can travel back into the convergent portion of the nozzle becomes zero at sonic location. Therefore, the reservoir is unable to sense any further decrease in backpressure.

The *nozzles* whose flow area decreases in the flow direction are called *converging nozzles*. The nozzles whose flow area first decreases and then increases are called *converging-diverging nozzles*. The converging-diverging nozzle with a *contoured* shape that leads to a uniform parallel flow at the exit is called a *Laval nozzle*. The location of the smallest flow area of a nozzle is called the throat. The highest velocity to which the flow can be accelerated in a convergent nozzle is the sonic velocity. Accelerating a flow to supersonic velocities is possible only in converging-diverging nozzles. In all supersonic converging-diverging nozzles, the flow velocity at the throat is the velocity of sound.

A defined supersonic flow can also be generated using a convergent-divergent nozzle with straight walls. But the flow exiting the straight C-D nozzle, even though of uniform Mach number, will be diverging away from the nozzle axis. That is, a straight C-D nozzle can deliver uniform supersonic Mach number but the flow will not be uni-directional. Whereas, a contoured or De Laval nozzle can generate uniform flow as well as uni-directional supersonic flow.

For steady inviscid flows the *compressible form of Bernoulli's equation* is given by

$$\int \frac{1}{\rho}\frac{\partial p}{\partial s}\,ds + \frac{V^2}{2} = \text{const.} \tag{4.4}$$

The limiting velocity that may be achieved by expanding a gas at any given stagnation condition into vacuum is

$$V_{\max} = a_0\sqrt{\frac{2}{\gamma - 1}} \tag{4.11}$$

When $M = 1$, the resulting static-to-stagnation property ratios for pressure, density, and temperature are called *critical ratios* and are denoted by the superscript asterisk:

$$\frac{p^*}{p_0} = \left(\frac{2}{\gamma + 1}\right)^{\gamma/(\gamma-1)} \tag{4.20}$$

$$\frac{\rho^*}{\rho_0} = \left(\frac{2}{\gamma + 1}\right)^{1/(\gamma-1)} \tag{4.21}$$

Scanned by CamScanner

$$\frac{T^*}{T_0} = \frac{2}{\gamma + 1} \tag{4.22}$$

The pressure outside the exit plane of a nozzle is called the *backpressure*. For all backpressures lower than p^*, the pressure of the exit plane of the converging nozzle is equal to p^*, the Mach number at the exit plane is unity, and the mass flow rate is the maximum (or choked) flow rate. Under steady-flow conditions, the mass flow rate through the nozzle is constant and can be expressed as

$$\dot{m} = \frac{AMp_0\sqrt{\gamma/(RT_0)}}{[1 + (\gamma - 1)M^2/2]^{(\gamma+1)/[2(\gamma-1)]}}$$

For air with $\gamma = 1.4$, the maximum mass flow rate becomes

$$\dot{m}_{\max} = \frac{0.6847\, p_0 A^*}{\sqrt{RT_0}}$$

The variation of flow area A through the nozzle relative to the throat area A^* for the same mass flow rate and stagnation properties of a perfect gas is

$$\frac{A}{A^*} = \frac{1}{M}\left[\left(\frac{2}{\gamma + 1}\right)\left(1 + \frac{\gamma - 1}{2}M^2\right)\right]^{(\gamma+1)/[2(\gamma-1)]} \tag{4.32}$$

This is called the *area-Mach number relation.*

The parameter M^* is defined as the ratio of the local velocity to the velocity of sound at the throat ($M = 1$). It can be expressed as

$$M^* = M\sqrt{\frac{\gamma + 1}{2 + (\gamma - 1)M^2}} \tag{4.31}$$

The three standard reference speeds for gas dynamic study are the $V_{\max}$ corresponding to a given stagnation state, the speed of sound a_0 at the stagnation temperature, and the critical speed V^*. They can be expressed as

$$V_{\max} = \sqrt{\frac{2\gamma}{\gamma - 1}RT_0}$$

$$a_0 = \sqrt{\gamma RT_0}$$

$$V^* = a^* = \sqrt{\gamma RT^*}$$

A nozzle is said to be *overexpanded* when the pressure at the nozzle exit p_e is less than the backpressure p_b. When the exit pressure is higher than the backpressure, the nozzle is said to be *underexpanded.*

Basically, diffusers are passages in which flow decelerates. In a diffuser with a normal shock, it can be shown that

Scanned by CamScanner

$$\frac{p_{02}}{p_{01}} = \frac{A_1^*}{A_2^*}$$

where p_{01} and p_{02} are stagnation pressures just upstream and downstream of the normal shock, respectively, and A_1^* is the area of first throat and A_2^* that of the second throat.

The pressures which are of interest in Gas Dynamics are the total or stagnation pressure, the static pressure, and the dynamic pressure. In incompressible flows, these three pressures are linked by *incompressible Bernoulli's equation*

$$p_0 - p = \frac{1}{2}\rho V^2 \tag{4.37}$$

This equation is used for the measurement of flow velocity with Pitot-static tube in incompressible flows. But in compressible flows, Bernoulli's equation becomes

$$\frac{\gamma}{\gamma-1}\frac{p}{\rho} + \frac{1}{2}V^2 = \frac{\gamma}{\gamma-1}\frac{p_0}{\rho_0} \tag{4.9c}$$

This is the *compressible Bernoulli's equation* for isentropic flow of perfect fluids.

In a supersonic flow, the indicated Pitot pressure p_{02} is measured by a Pitot probe; the stagnation pressure behind a normal shock may be used for calculating the flow Mach number with the relation

$$\frac{p_1}{p_{02}} = \frac{\left(\frac{2\gamma}{\gamma+1}M_1^2 - \frac{\gamma-1}{\gamma+1}\right)^{1/(\gamma-1)}}{\left(\frac{\gamma+1}{2}M_1^2\right)^{\gamma/(\gamma-1)}}$$

The relation is called the *Rayleigh supersonic Pitot formula.*

The dynamic pressure q in compressible flow can be expressed as

$$q = \frac{p_0 - p}{K} \tag{4.41}$$

where

$$K = 1 + \frac{M^2}{4} + \frac{M^4}{40}$$

is called the *correction coefficient.*

For compressible flows, the pressure coefficient, which is a dimensionless pressure difference, can be expressed as

$$C_p = \frac{2}{\gamma M_\infty^2}\left(\frac{p}{p_\infty} - 1\right) \tag{4.43}$$

Scanned by CamScanner

PROBLEMS

1. In an intermittently operated supersonic wind tunnel, atmospheric air at stationary conditions is taken into a constant pressure heat exchanger, where it is heated to T_1 K. The air leaves the heat exchanger with a velocity $V_1 = 15$ m/s and is then expanded in a Laval nozzle to attain the test-section Mach number $M_T = 2.5$ and temperature T_T K. Calculate the necessary temperature rise in the heat exchanger so that $T_T = T_0$. Given $T_0 = 300$ K and $\rho_0 = 1.25$ kg/m^3.

[**Ans.** $T_1 - T_0 = 375$ K]

2. Dry heated air is supplied from a storage chamber to a blowdown type wind tunnel through a suitable nozzle. The nozzle throat area is 80 cm^2 and is designed for $M = 2.0$. The storage chamber conditions are $p_0 = 3.12$ atm and $T_0 = 100°C$. Find the test-section temperature and the mass flow rate.

[**Ans.** $T_{TS} = 207.3$ K, $\dot{m} = 5.288$ kg/s]

3. A supersonic stream at $M_1 = 3.0$ has to be decelerated in a convergent nozzle to sonic conditions at the exit of the nozzle. Calculate the pressure and temperature at the entry and the mass flow rate. What will be the temperature indicated by a thermocouple held in the flow direction at the entry? The conditions at nozzle exit are: $p_e = 0.8$ atm; $T_e = 293$ K; $A_e = 40$ cm^2.

[**Ans.** $p_1 = 0.04123$ atm, $T_1 = 125.57$ K, $\dot{m} = 1.323$ kg/s, $T_0 = 351.6$ K]

4. In a continuous-operation supersonic wind tunnel, the inlet area $A_1 = 600 \times 400$ mm^2, the throat area of the nozzle is 300×400 mm^2, and the test-section is $h_2 \times 400$ mm^2. The test-section conditions are $M_2 = 2.5$, $T_2 = -10°C$, $p_2 = 0.15$ atm. Calculate h_2, T_1, M_1, V_1 and the temperature at the stagnation point of a model in the test-section.

[**Ans.** $h_2 = 791$ mm, $T_1 = 581.5$ K, $M_1 = 0.3$, $V_1 = 145$ m/s, $T_0 = 592$ K]

5. For the operation of a supersonic test-section, an air flow at the conditions p_1, T_1 and M_1 is led through an inlet section of area A_1 to a Laval nozzle which expands the flow to a pressure of p_2 at the test-section. Given $p_1 = 6.5$ atm, $T_1 = 440$ K, $M_1 = 0.5$, $A_1 = 160$ cm^2, $p_2 = 1.0$ atm. What will be M_2, A^*/A_2 and $\dot{m}$?

[**Ans.** $M_2 = 2.0$, $A^*/A_2 = 0.6$, $\dot{m} = 17.54$ kg/s]

6. To find the flow Mach number in a pipe, a venturi nozzle is built into the pipe, the measured values of pressures p_1 and p_2 at inlet and throat of venturi are 1.5 atm and 1.2 atm, respectively. Inlet area/throat area = 4/3. Find M_1 and M_{throat}.

[**Ans.** $M_1 = 0.46$, $M_{\text{throat}} = 0.74$]

Scanned by CamScanner

7. A Pitot-static tube shows a pressure difference of 490 mm of mercury, when placed in a flow. The static pressure is measured separately to be 0.35 atm (gauge). The stagnation temperature is 25°C. Calculate the flow velocity.

[**Ans.** $V = 253.7$ m/s]

8. Air is compressed isentropically in a centrifugal compressor from a pressure of 1 atm to a pressure of 6 atm. The initial temperature is 290 K. Calculate (a) the change in temperature, (b) the change in internal energy, and (c) the work imparted to the air, neglecting the velocity change.

[**Ans.** (a) $\Delta T = 194$ K; (b) $\Delta e = 1.39 \times 10^5$ Nm/kg; (c) $\Delta w = 1.39 \times 10^5$ Nm/kg]

9. Air at atmospheric pressure and at a temperature of 300 K expands in an ideal diffuser. The entrance speed is 180 m/s. Calculate the maximum pressure (ram pressure) that can be achieved if the air is diffused to zero speed.

[**Ans.** $p_0 = 1.217 \times 10^5$ N/m^2]

10. Air at a stagnation temperature and pressure of 200.9 K and 6.895×10^5 N/m^2, respectively, flows from a reservoir through a converging nozzle that exhausts into an atmosphere where the pressure is 1.014×10^5 N/m^2. Calculate (a) the pressure in the nozzle exit plane, (b) the minimum stagnation pressure for which the flow is choked, and (c) the exit plane pressure if the stagnation pressure is reduced to 1.724×10^5 N/m^2.

[**Ans.** (a) 3.64×10^5 N/m^2; (b) 1.92×10^5 N/m^2; (c) 1.014×10^5 N/m^2]

11. A diffuser of a turbojet engine operating at 10,000 m passes a mass flow rate of 25 kg/s. The inlet velocity is 200 m/s, the inlet static pressure is 0.35×10^5 N/m^2, and the inlet static temperature is 230 K. The exit area of the diffuser is 0.5 m^2. Assuming frictionless flow, calculate the reaction force acting on the diffuser if the exit Mach number is 0.2.

[**Ans.** 10.815 kN]

12. Air enters a tank at a speed of 100 m/s and leaves it at 200 m/s. If no heat is added to, and no work is done by the air, show that the temperature of the air at the exit is 15°C below that at the entrance.

13. Air enters a machine at 373 K with a speed of 200 m/s, and leaves at standard sea level temperature (15°C). Show that, in order to have the machine deliver 100,000 Nm/kg of work without any heat input, the exit air speed is 103.3 m/s, and the exit speed becomes 459 m/s when the machine is idling.

Scanned by CamScanner

14. Two jets of air of equal mass flow rate mix thoroughly before entering a large reservoir. One jet is at 400 K and 100 m/s, and the other is at 200 K and 300 m/s. In the absence of heat addition or work done, show that the temperature of air in the reservoir is 324.9 K.

15. When air is released adiabatically from a tyre, the temperature of the air at the exit is 37°C below that inside the tyre. Show that the exit speed of air is 272.57 m/s.

16. An airplane flies at an altitude of 15,000 m with a velocity of 800 km/h. Calculate (a) the maximum possible temperature at the airplane skin, (b) the maximum possible pressure intensity on the airplane body, (c) the critical velocity of the air relative to the airplane, and (d) the maximum possible velocity of the air relative to the airplane.

[**Ans.** (a) 241.12 K; (b) 1.751×10^4 N/m^2; (c) 283.97 m/s; (d) 695.9 m/s]

17. A perfect gas having $c_p = 1017$ Nm/kg-K and $\gamma = 1.4$ flows adiabatically in a converging passage with a mass flow rate $\dot{m} = 29.188$ kg/s. At a particular cross-section, $M = 0.6$, $T_0 = 550$ K, and $p_0 = 2.0 \times 10^5$ N/m^2. Calculate the area of the cross-section of the passage at the point considered.

[**Ans.** 0.10125 m^2]

18. Sea level air is being drawn isentropically through a duct into a vacuum tank. The cross-sectional areas of the duct at the mouth, throat and the entrance to the vacuum tank are 2 m^2, 1 m^2, 4 m^2, respectively. Show that (a) the maximum of air that can be drawn into the vacuum tank is 241 kg/s, and (b) if the maximum flow rate is to be attained, the pressure in the vacuum tank must be 3018.7 N/m^2.

19. A supersonic wind tunnel nozzle is to be designed for $M = 2$ with a throat 1 m^2 in area. The supply pressure and the temperature at the nozzle inlet, where the velocity is negligible, are 7×10^5 N/m^2 and 40°C, respectively. The preliminary design is to be based on the assumption that the flow is one-dimensional at the throat and at the test-section. Compute the mass flow, the test-section area, and the flow properties at the throat and at the test-section.

[**Ans.** $\dot{m} = 1599.13$ kg/s, $A = 1.6875$ m^2
At throat: $p = 3.7 \times 10^5$ N/m^2, $T = 261$ K, $\rho = 4.944$ kg/m^3
At test-section: $p = 8.946 \times 10^4$ N/m^2, $T = 173.9$ K, $\rho = 1.794$ kg/m^3]

20. Air at 300 K and 1×10^5 N/m^2 enters a diffuser with a velocity of 245 m/s. The diffuser is to be designed to reduce the velocity of the air to 60 m/s. The mass flow rate through the diffuser is 13.6 kg/s. Assuming the flow to be isentropic, determine (a) the inlet diameter, (b) the outlet diameter, and (c) the rise in static temperature.

[**Ans.** (a) 0.2467 m; (b) 1.0143 m; (c) 28.2 K]

Scanned by CamScanner

21. A blunt nose Pitot tube is placed in a supersonic wind tunnel to estimate the flow Mach number. The stagnation pressure p_0 at the entrance to the Pitot tube is 2.0×10^5 N/m^2. The freestream static pressure p_1 ahead of the shock wave is measured by a static pressure tap in the wall of the tunnel, and is 0.15×10^5 N/m^2. Estimate the Mach number in the tunnel.

[**Ans.** $M = 3.16$]

22. Consider Problem 18. If a normal shock is detected (by Schlieren photography) in the divergence portion of the duct where the cross-sectional area is 3 m^2, show that the pressure in the reservoir is 41442.5 N/m^2.

23. A subsonic diffuser operating under isentropic conditions has an inlet area of 0.15 m^2. The inlet conditions are $V_1 = 240$ m/s, $T_1 = 300$ K, $p_1 = 0.70 \times 10^5$ N/m^2. The velocity leaving the diffuser is 120 m/s. Calculate (a) the mass flow rate, (b) the stagnation pressure at the exit, (c) the stagnation temperature at the exit, (d) the static pressure at the exit, (e) the entropy change across the diffuser, and (f) the exit area.

[**Ans.** (a) 29.26 kg/s; (b) 0.9624×10^5 N/m^2; (c) 328.6 K; (d) 8.91×10^4 N/m^2; (e) 0.0; (f) 0.252 m^2]

24. The working section of a wind tunnel of cross-sectional area 0.6 m^2 has a Mach number of 0.80. In the settling chamber of cross-sectional area 4.0 m^2 the pressure, density and temperature are 0.1014 MPa, 1.144 kg/m^3 and 35°C, respectively. Calculate the pressure, density and temperature in the working section, neglecting the effects of viscosity and treating the flow as one-dimensional.

[**Ans.** 0.665×10^5 Pa, 0.847 kg/m^3, 273 K]

25. Air flows through a frictionless adiabatic convergent-divergent nozzle. The air stagnation pressure and temperature are 7.0×10^5 N/m^2 and 500 K, respectively. The diverging portion of the nozzle has an area ratio of $A_{exit}/A_{throat} = 11.91$. A normal shock wave stands in the divergent portion of nozzle where the Mach number is 3.0. Determine the Mach number and the static pressure and temperature at the nozzle exit plane.

[**Ans.** $M_e = 0.15$, $p_e = 2.2622 \times 10^5$ N/m^2, $T_e = 497.8$ K]

26. A supersonic wind tunnel nozzle is to be designed for $M = 2.5$ with a test-section 1 m^2 in area. The supply pressure and the temperature at the nozzle inlet, where the velocity is negligible, are 7×10^5 N/m^2 and 27°C, respectively. The preliminary design is to be based on the assumption that the flow is isentropic, with $\gamma = 1.4$, and that the flow is one-dimensional at the throat and at the test-section. Compute (a) the throat area, (b) the temperature at the throat in degrees celsius, (c) the flow velocity in test-section, and (d) the mass flow rate through the test-section.

[**Ans.** (a) 0.38 m^2; (b) −23.1°C; (c) 578.75 m/s; (d) 620 kg/s]

Scanned by CamScanner

27. The pressure coefficient $C_p = (p - p_\infty)/q_\infty$ is used to denote the local pressure coefficient near a body placed in a freestream under conditions p_∞, V_∞, M_∞. Show that the value of C_p at which the critical velocity occurs somewhere on the body can be written as

$$C_p^* = \frac{[(2 + (\gamma - 1) M_\infty^2)/(\gamma + 1)]^{\gamma/(\gamma-1)} - 1}{(\gamma/2) M_\infty^2}$$

28. Air at 500 kPa and 30°C from a storage tank exhausts through a convergent nozzle of exit area 0.5 cm^2 to an environment at 1 atm pressure. Compute the mass flow rate at the beginning of discharge.

[Ans. 0.058 kg/s]

29. Air at a stagnation state of 700 kPa and 180°C expands isentropically through a nozzle. If the pressure at the nozzle exit is 100 kPa, determine the flow velocity at the nozzle exit. Assume the air to be a perfect gas with $\gamma = 1.4$.

[Ans. 623.4 m/s]

30. Calculate the maximum mass flow rate possible through a frictionless, insulated convergent nozzle of exit area 6.5 cm^2 operating at sea level, if the stagnation conditions are 5 bar and 15°C. Also, calculate the exit temperature.

[Ans. 0.774 kg/s, 240.12 K]

31. Air at 101 kPa and 20°C is drawn isentropically through a convergent-divergent nozzle of exit area 0.033 m^2. If the pressure at the nozzle exit is 91.4 kPa, determine the mass flow rate through the nozzle. What is the pressure at the location with area 0.022 m^2?

[Ans. 4.74 kg/s, 73.5 kPa]

32. A rocket nozzle has to generate 9 kN thrust at an altitude of 16 km above the earth, with its chamber pressure and temperature of 15 atm and 2600°C, respectively. Calculate its exit and throat areas and the velocity and temperature at the exit. Take $\gamma = 1.4$, $R = 287$ J/kg-K, and assume the nozzle to be operating at the adapted condition.

[Ans. 0.0394 m^2, 0.00374 m^2, 2094.6 m/s, 689.33 K]

33. Determine the stagnation pressure p_0, temperature T_0, and density ρ_0 of an air stream flowing at 200 m/s, 15°C and 101 kPa.

[Ans. 127.8 kPa, 308.2 K, 1.445 kg/m^3]

34. Air flows through a convergent duct. At a station 1 in the duct, $A_1 = 10$ cm^2, $p_1 = 100$ kPa, $T_1 = 30$°C, and $V_1 = 90.5$ m/s. Calculate M_2, p_2 and T_2 at a station 2 where $A_2 = 6.9$ cm^2. Assume the flow to be one-dimensional and isentropic.

[Ans. 0.4, 93.86 kPa, 297.72 K]

Scanned by CamScanner

35. Carbon dioxide from a large reservoir maintained at 6 atm and 30°C is discharged to ambient atmosphere through an orifice of diameter 1 mm. Determine the temperature of the carbon dioxide stream and the mass flow rate.

[**Ans.** −9.55°C, 0.00133 kg/s]

36. Air flows isentropically through a convergent-divergent nozzle of inlet area 12 cm^2 at a rate of 0.7 kg/s. The conditions at the inlet and exit of the nozzle are 8 kg/m^3 and 400 K and 4 kg/m^3 and 300 K, respectively. Find the cross-sectional area, the pressure and the Mach number at the nozzle exit.

[**Ans.** 3.9 cm^2, 344.4 kPa, 1.29]

37. Air stream at 200 kPa and 400 K enters a convergent axisymmetric nozzle at a velocity of 100 m/s and expands isentropically to an exit pressure of 150 kPa. If the inlet diameter is 75 mm, find the temperature, the Mach number and the diameter at the nozzle exit. Also, estimate the mass flow rate through the nozzle.

[**Ans.** 368.85 K, 0.7, 50.7 mm, 0.77 kg/s]

38. Air enters a nozzle at 3 MPa and 400°C. At the nozzle exit, $A_2 = 5000$ mm^2 and $p_2 = 0.5$ MPa. Expansion through the nozzle is isentropic according to the law pV^γ = constant. Determine (a) the Mach number at nozzle exit, (b) the throat area, and (c) the mass flow through the nozzle.

[**Ans.** (a) 1.83, (b) 3415 mm^2, (c) 15.89 kg/s]

39. Air flows through a convergent nozzle, as shown in Fig. P4.39 at the rate of 5 kg/s. Determine the force experienced by the inner surface of the nozzle.

[**Ans.** 36414.15 N]

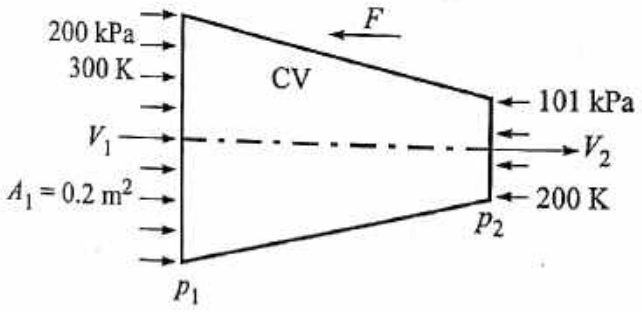


Fig. P4.39.

40. An aircraft flies at Mach 0.8 at an altitude where the pressure and temperature are 44 kPa and −15°C, respectively. Determine the isentropic stagnation pressure and temperature recorded on the aircraft. Assume air to be an ideal gas. Solve the problem using property relations as well as gas tables.

[**Ans.** 67.07 kPa, 291.2 K]

Scanned by CamScanner

41. The pressure and temperature in the test-section of a supersonic wind tunnel are 0.55 atm and 216 K, respectively. If the total temperature is 40°C, calculate the test-section Mach number and the total pressure.

[**Ans.** 1.5, 2.019 atm]

42. Air flow in a duct has $V_1 = 100$ m/s, $T_1 = 70°C$, $p_1 = 2.5$ atm at station 1. At a downstream station 2, if $V_2 = 400$ m/s and $p_2 = 0.5$ atm, compute M_2, V_{max}, and p_{02}/p_{01}. Treat the flow to be isentropic.

[**Ans.** 1.218, 836.3 m/s, 0.471]

43. Air from a high pressure tank at 350 kPa and 420 K expands isentropically through a nozzle of exit area $A_e = 0.22$ m^2. If $V_e = 525$ m/s, determine M_e, p_e, $\dot{m}_e$, and A^*.

[**Ans.** 1.56, 87.35 kPa, 124.3 kg/s, 0.18 m^2]

44. Air flows through a convergent-divergent nozzle of throat area 25 cm^2. At station 1 upstream of the throat, $V_1 = 150$ m/s, $T_1 = 315$ K and $p_1 = 152$ kPa. If the flow velocity at the nozzle exit is supersonic, compute the nozzle cross-sectional area at station 1 and the mass flow rate $\dot{m}$. Assume the flow to be isentropic.

[**Ans.** 38.22 cm^2, 0.9637 kg/s]

45. Compressed dry air at 40°C from a large reservoir exhausts through a nozzle with an exit velocity of 200 m/s. A mercury manometer (with standard sea level pressure reference) reads the corresponding pressure as 2.27 cm compression. Determine the exit Mach number, the reservoir pressure and the atmospheric pressure. Assume the flow through the nozzle to be isentropic.

[**Ans.** 0.583, 131.381 kPa, 104.354 kPa]

46. At a particular station of a duct, air at 32°C and 80 kPa flows with a velocity of 365 m/s. Assuming the process to be isentropic, calculate the temperature and velocity at the station where the pressure is 120 kPa. Determine the Mach number at both the stations.

[**Ans.** 69.91°C, 237.6 m/s, 1.04, 0.64]

47. Calculate the mass flow rate, the nozzle throat area, and the reservoir pressure and temperature required for a supersonic wind tunnel operation with test-section conditions of Mach 3, static pressure of 0.2 atm and static temperature of 300 K. The test-section area is 0.05 m^2. Assume the flow to be isentropic.

[**Ans.** 12.25 kg/s, 0.0118 m^2, 744.4 kPa, 840 K]

48. Air enters the Laval nozzle of a Mach 2 tunnel at 1 MPa and 300 K with a very low velocity. The nozzle exit area $A_e = 0.15$ m^2, which is same as the test-section area A_{TS}. Calculate the pressure, temperature, velocity in the test-section and the mass flow rate $\dot{m}$ through the nozzle.

[**Ans.** 127.8 kPa, 166.67 K, 517.56 m/s, 207.43 kg/s]

Scanned by CamScanner

49. Air at a stagnation state of 3.5 MPa and 500°C is expanded isentropically through a Laval nozzle to a pressure of 0.7 MPa at the nozzle exit. If the mass flow rate through the nozzle is 1.3 kg/s, determine (a) the exit Mach number, (b) the exit area, and (c) the throat area.

[**Ans.** 1.71, 3.5 cm^2, 2.6 cm^2]

50. Subsonic air flow from a nozzle of exit area 15 cm^2 strikes a vertical plate, as shown in Fig. P4.50. A force F of 100 N is required to hold the plate in position. If the stagnation temperature of the nozzle flow is 25°C, determine the Mach number M_e and the velocity V_e at the nozzle exit, and the stagnation pressure of the flow p_0.

[**Ans.** 0.69, 228.2 m/s, 1.37 atm]

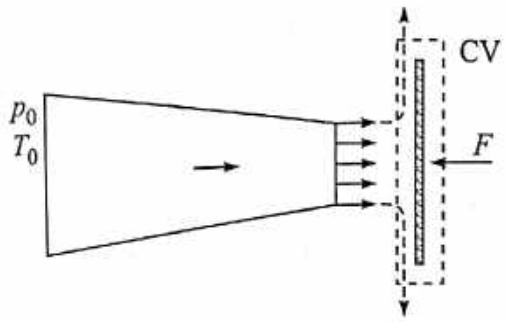


Fig. P4.50.

51. Air at $p_0 = 700$ kPa and $T_0 = 325$ K flows isentropically through a Laval nozzle with a mass flow rate of 1 kg/s. If the nozzle is correctly expanded to standard atmosphere, determine A^*, M_e, and V_e.

[**Ans.** 6.37 cm^2, 1.92, 526.27 m/s]

52. Air flows isentropically through a convergent–divergent nozzle. The flow conditions at the inlet are $V_1 = 100$ m/s, $p_1 = 1$ atm, $T_1 = 300$ K and $A_1 = 5$ cm^2. If the nozzle delivers supersonic flow, find p_{02} and T_{02} at the exit. Also determine the static pressure, temperature and area at the throat.

[**Ans.** 1.06 atm, 305K, 0.56 atm, 254 K, 2.36 cm^2]

53. Determine the exit area of an ideal convergent nozzle for a mass flow rate of air at 0.5 kg/s flowing from a reservoir at 6 atm and 30°C and discharging into a second reservoir maintained at a pressure of 3 atm.

[**Ans.** 3.544 cm^2]

54. A convergent–divergent nozzle discharges air from a reservoir at 1 MPa to a surrounding at 100 kPa. The throat and exit areas of the nozzle are 8 cm^2 and 13.5 cm^2, respectively. Determine the exit Mach number.

[**Ans.** 2.0]

55. Air initially at standard sea–level pressure and temperature flows into an evacuated tank through a convergent nozzle of exit diameter 0.04 m. What pressure must be maintained in the tank to produce a sonic jet? What will be the corresponding mass flow rate?

[**Ans.** 53.5 kPa, 0.303 kg/s]

Scanned by CamScanner

56. A converging–diverging nozzle fed from a reservoir has an exit area 4 times the throat area. What is the ratio of the exit pressure to reservoir pressure for isentropic flow of air if the Mach number at the exit is supersonic and correctly expanded?

[**Ans.** 0.0298]

57. A convergent–divergent nozzle is designed to operate at an exit Mach number of 1.63. If the stagnation pressure is maintained at 10 atm, assuming one–dimensional flow, calculate (a) the backpressure for correct expansion, (b) the range of backpressure for supersonic flow at the nozzle exit, and (c) the maximum backpressure up to which the flow will remain choked.

[**Ans.** (a) 228 kPa, (b) < 228 kPa, (c) 830.87 kPa]

58. Show that the limiting values of density ratio and downstream Mach number for a normal shock in air when the upstream Mach number becomes very large are 6 and 0.378, respectively.

59. Determine the suction indicated by a mercury manometer connected to a wall static pressure located in a Mach 2 supersonic tunnel test-section, if the stagnation pressure and atmospheric pressure are 3 atm and 760 mm of mercury, respectively. Treat the flow to be one-dimensional and isentropic.

[**Ans.** 468.61 mm]

60. The barometer of a mountain hiker reads 1000 mbar at the beginning of a hiking trip and 500 mbar at the end. Determine the vertical distance climbed by the hiker. Neglect the effect of altitude on local gravitational acceleration. Take an average air density of 1.10 kg/m^3 and gravitational acceleration $g = 9.81$ m/s^2.

[**Ans.** 4633.49 m]

61. Air in a high-pressure tank at pressure p_0 is suddenly accelerated through a nozzle to maximum possible velocity. What will be the error in the maximum velocity calculated by assuming this flow as incompressible?

[**Ans.** 87%]

62. Air flow at 60 m/s enters a nozzle kept horizontal. The specific enthalpies at the nozzle inlet and exit are 3025 kJ/kg and 2790 kJ/kg, respectively. Neglecting the heat loss from the nozzle, calculate (a) the flow velocity at the nozzle exit, (b) mass flow rate through the nozzle, if the inlet area is 0.1 m^2 and the specific volume at inlet is 0.19 m^3/kg, and (c) the exit area of the nozzle, when the specific volume at the exit is 0.5 m^3/kg.

[**Ans.** (a) 688.2 m/s, (b) 31.58 kg/s, (c) 0.0229 m^2]

63. A Mach 2 uniform airstream enters a convergent duct. If the exit area is 70 percent of the inlet area, determine the Mach number at the duct exit, treating the flow to be one-dimensional and isentropic. Also, verify the validity of the answer.

[**Ans.** 1.51]

Scanned by CamScanner

64. A uniform airstream with Mach angle 40° flows past a symmetrical wedge. If the freestream temperature and pressure are 10°C and 101.3 kPa, respectively,
    (a) Determine the pressure coefficient at the nose of the wedge.
    (b) Calculate the pressure coefficient with
    $$C_p = 1 + \frac{M^2}{4} + \frac{M^4}{40}$$
    (c) What will be the percentage error involved in C_p obtained using this expression?

    [**Ans.** (a) 1.765, (b) 1.756, (c) 0.51%]

65. A Venturi-meter of throat diameter 50 mm is used to measure the flow rate of superheated steam with specific heats ratio 1.3. If the stagnation pressure and the temperature at the entry to the Venturi-meter are 200 kPa and 150°C, respectively, determine the maximum mass flow rate that can be measured by this meter, treating the flow process to be isentropic.

    [**Ans.** 0.593 kg/s]

66. Sea level air is drawn through a convergent duct. If the velocity at the inlet is 4 m/s, determine the exit area required to accelerate the flow to 75 m/s.

    [**Ans.** $0.05516A_1$]

67. If the maximum speed that can be achieved by expanding a monatomic gas mixture in a reservoir at 350 K is 600 m/s, find the molecular weight of the mixture.

    [**Ans.** 40.31]

68. Air at 425 K in a reservoir is expanded through a nozzle. If the Mach number at the nozzle exit is 0.7, determine the flow velocity.

    [**Ans.** 276.06 m/s]

69. The maximum mass flow rate of air through a Laval nozzle of throat area 78.54 mm^2, run by a settling chamber is 0.2 kg/s. If the speed of sound in the settling chamber is 360 m/s, determine the settling chamber pressure.

    [**Ans.** 11.17 atm]

70. A settling chamber with air at a stagnation state of 82 atm and 740 K, runs a Mach 8 wind tunnel. Treating the expansion through the wind tunnel nozzle as isentropic, determine (a) the static temperature, (b) static pressure, (c) velocity, (d) unit Reynolds number of the flow, and (e) dynamic pressure, of the test-section flow.

    [**Ans.** (a) –219.53°C, (b) 851.03 Pa, (c) 1174.24 m/s, (d) 18.649×10^6 per unit length, (e) 38124.91 Pa]

Scanned by CamScanner

71. Air at 8 atm from a storage tank leaks through a joint in the tank. If the area through which air leaks is 20 mm^2 and the rate of leak when the air begins to leak is 0.036 kg/s, determine the temperature in the tank at the beginning of leak.

[Ans. 58.12°C]

72. Oxygen gas from a reservoir at 35°C is discharged through a nozzle. If the enthalpy of the gas released is 40% of the enthalpy in the tank, determine the velocity and Mach number of the oxygen released.

[Ans. 579.87 m/s, 2.74]

Scanned by CamScanner

5 Normal Shock Waves

5.1 INTRODUCTION

The shock may be described as a compression front in a supersonic flow field, and the flow process across the front results in an abrupt change in fluid properties. The thickness of the shocks is comparable to the mean free path of the gas molecules in the flow field. To have some physical feel about the formation of such shock waves, consider a cylinder placed in a flow as shown in Fig. 5.1.

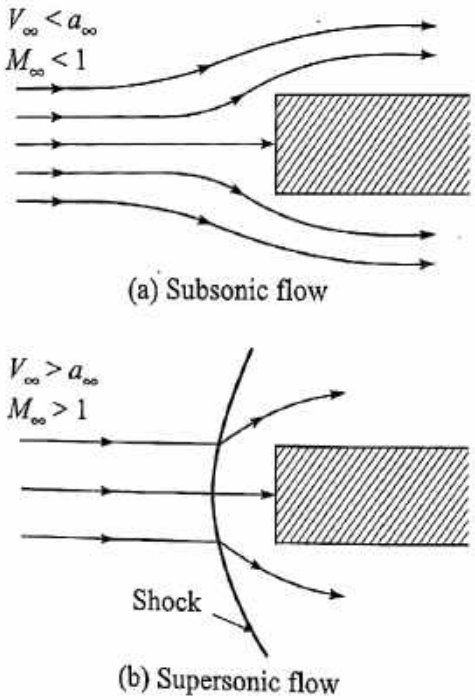


Fig. 5.1 Streamlines around a blunt-faced cylinder in subsonic and supersonic flows.

We know from the kinetic theory that the flow consists of a large number of fluid molecules in unit volume and the transport of mass, momentum and

Scanned by CamScanner

energy takes place through the motion of these molecules. Also, the molecules carry the signals about the presence of the cylinder around the flow field at a speed equal to the speed of sound. In Fig. 5.1(a), the incoming stream is subsonic, $V_\infty < a_\infty$, and the molecules far upstream of the cylinder get the information about the presence of the body through the signals which travel with speed, a_∞, well in advance before reaching the cylinder. Therefore, the molecules orient themselves in order to flow around the cylinder as shown in Fig. 5.1(a). But when the incoming stream is supersonic, the molecules travel faster than the signals, and there is no possibility that they will be informed of the presence of the body, before they reach the cylinder. Also, the reflected signals from the face of the cylinder tend to coalesce a short distance ahead of the body. Their coalescence forms a thin compression front called shock wave, as shown in Fig. 5.1(b). Upstream of the shock, the flow has no information about the presence of the body. However, the streamlines behind the normal shock quickly compensate for the obstruction, since the flow is subsonic after a normal shock. Although the shock formation discussed above is for a specific situation, the mechanism described is, in general, valid. However, we should realize that, when the flow just starts, there is no shock. The formation of shock takes place after the fluid molecules impinge on to the face of the cylinder and rebound.

5.2 EQUATIONS OF MOTION FOR A NORMAL SHOCK WAVE

For a quantitative analysis of changes across a normal shock wave, let us consider an adiabatic, constant-area flow through a nonequilibrium region, as shown in Fig. 5.2(a). Let sections 1 and 2 be sufficiently away from the nonequilibrium region so that we can define flow properties at these stations, as shown in Fig. 5.2(a). Now we can write the equations of motion for the flow considered, as follows: By continuity,

$$\rho_1 V_1 = \rho_2 V_2 \tag{5.1}$$

The momentum equation

$$p_1 + \rho_1 V_1^2 = p_2 + \rho_2 V_2^2 \tag{5.2}$$

The energy equation

$$h_1 + \frac{1}{2} V_1^2 = h_2 + \frac{1}{2} V_2^2 \tag{5.3}$$

Equations (5.1)–(5.3) are general and apply to all gases. Also, there is no restriction on the size or details of the nonequilibrium region as long as the reference sections 1 and 2 are outside of it. The solution of these equations gives the relations that must exist between the flow parameters at these two sections.

Since there is no restriction on the size or details of the nonequilibrium region, it may be idealized by a vanishingly thin region, as shown in Fig. 5.2(b),

Scanned by CamScanner

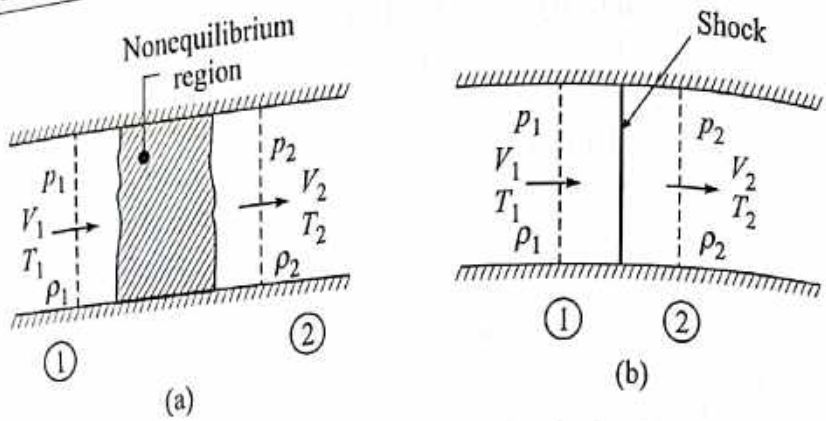


Fig. 5.2 Flow through a normal shock.

across which the flow parameters are said to *jump*. The control sections 1 and 2 may also be brought arbitrarily close to it. Such a front or discontinuity across which there is sudden change in flow properties is called a *shock wave*. There is no heat added or taken away from the flow as it traverses the shock wave; hence the flow across the shock wave is adiabatic.

At this stage, the question obviously arises: Is it possible to have a discontinuity in a continuum flow field of a real fluid? We should realize that the above consideration is only an idealization of the very high gradients that actually occur in a shock wave, in the transition from state 1 to state 2. These severe gradients produce viscous stress and heat transfer, i.e. nonequilibrium conditions inside the shock. The processes taking place inside the shock wave itself are extremely complex, and cannot be studied on the basis of equilibrium thermodynamics. Temperature and velocity gradients internal to the shock provide heat conduction and viscous dissipation that render the shock process internally irreversible. In most of the practical applications, the primary interest is not generally focused on the internal mechanism of the shock wave, but on the net changes in fluid properties taking place across the wave. However, there are situations where the detailed information about the flow mechanism inside the shock describing its structure is essential for studying practical problems. But, since such conditions occur only in flow regimes like rarefied flow fields, it is not of any interest for the present study.

5.3 THE NORMAL SHOCK RELATIONS FOR A PERFECT GAS

For a calorically perfect gas, we have the equation of state, viz.

$$p = \rho RT \tag{5.4}$$

and

$$h = c_p T \tag{5.5}$$

Equations (5.1)–(5.5) form a set of five equations with five unknowns: p_2, ρ_2, T_2, V_2 and h_2. Hence, they can be solved algebraically. In other words,

Scanned by CamScanner

Eqs. (5.1)–(5.3) are the general equations for a normal shock wave, and for a perfect gas it is possible to obtain explicit solutions in terms of Mach number, M_1, ahead of the shock using Eqs. (5.4) and (5.5) along with Eqs. (5.1)–(5.3), as follows: Dividing Eq. (5.2) by Eq. (5.1), we get

$$\frac{p_1}{\rho_1 V_1} - \frac{p_2}{\rho_2 V_2} = V_2 - V_1 \tag{5.6}$$

Recalling that the speed of sound $a = \sqrt{\gamma p/\rho}$, Eq. (5.6) becomes

$$\frac{a_1^2}{\gamma V_1} - \frac{a_2^2}{\gamma V_2} = V_2 - V_1 \tag{5.7}$$

Now, a_1^2 and a_2^2 in Eq. (5.7) may be replaced with energy equation for a perfect gas as follows: By energy equation, we have

$$\frac{V_1^2}{2} + \frac{a_1^2}{\gamma - 1} = \frac{V_2^2}{2} + \frac{a_2^2}{\gamma - 1} = \frac{1}{2}\frac{\gamma + 1}{\gamma - 1} a^{*2}$$

From the above relation, a_1^2 and a_2^2 can be expressed as

$$a_1^2 = \frac{\gamma + 1}{2} a^{*2} - \frac{\gamma - 1}{2} V_1^2$$

$$a_2^2 = \frac{\gamma + 1}{2} a^{*2} - \frac{\gamma - 1}{2} V_2^2$$

since the flow is adiabatic across the shock wave, a^* in the above relations for a_1^2 and a_2^2 has the same constant value.

Substituting these relations into Eq. (5.7), we get

$$\frac{\gamma + 1}{2}\frac{a^{*2}}{\gamma V_1} - \frac{\gamma - 1}{2\gamma} V_1 - \frac{\gamma + 1}{2}\frac{a^{*2}}{\gamma V_2} + \frac{\gamma - 1}{2\gamma} V_2 = V_2 - V_1$$

$$\frac{\gamma + 1}{2\gamma V_1 V_2}(V_2 - V_1) a^{*2} + \frac{\gamma - 1}{2\gamma}(V_2 - V_1) = V_2 - V_1$$

Dividing this equation by $(V_2 - V_1)$, we obtain

$$\frac{\gamma + 1}{2\gamma V_1 V_2} a^{*2} + \frac{\gamma - 1}{2\gamma} = 1$$

This may be solved to result in

$$a^{*2} = V_1 V_2 \tag{5.8}$$

which is called the *Prandtl relation.*

In terms of the speed ratio $M^* = V/a^*$, Eq. (5.8) can be expressed as

$$\boxed{M_2^* = \frac{1}{M_1^*}} \tag{5.9}$$

Equation (5.9) implies that the velocity change across a normal shock must be from supersonic to subsonic and vice versa. But, it will be shown later in this

Scanned by CamScanner

section that only the former is possible. Hence, the *Mach number behind a normal shock is always subsonic*. This is a general result, not limited just to a calorically perfect gas.

The relation between M^* and M is given by Eq. (4.25) as

$$M^{*2} = \frac{(\gamma+1)M^2}{(\gamma-1)M^2+2} \tag{5.10}$$

Using Eq. (5.10) to replace M_1^* and M_2^* in Eq. (5.9), we get

$$\boxed{M_2^2 = \frac{1+\frac{\gamma-1}{2}M_1^2}{\gamma M_1^2 - \frac{\gamma-1}{2}}} \tag{5.11}$$

Equation (5.11) shows that, for a perfect gas, the Mach number behind the shock is a function of only the Mach number ahead of the shock. It also shows that when $M_1 = 1$, $M_2 = 1$. This is the case of an infinitely weak normal shock, which is defined as a Mach wave. But, as M_1 increases above 1, the normal shock becomes stronger and M_2 becomes progressively less than 1, and in the limit, as $M_1 \to \infty$, M_2 approaches a finite minimum value, $M_2 \to \sqrt{(\gamma-1)/2\gamma}$, which for air (at standard conditions), with $\gamma = 1.4$ is 0.378.

The ratio of velocities may also be written as

$$\frac{V_1}{V_2} = \frac{V_1^2}{V_1 V_2} = \frac{V_1^2}{a^{*2}} = M_1^{*2} \tag{5.12}$$

Equations (5.10) and (5.12) are useful for the derivation of other normal shock relations.

From Eq. (5.1), we can write

$$\boxed{\frac{\rho_2}{\rho_1} = \frac{V_1}{V_2} = \frac{(\gamma+1)M_1^2}{(\gamma-1)M_1^2+2}} \tag{5.13}$$

To obtain the pressure relation, consider the momentum Eq. (5.2),

$$p_2 - p_1 = \rho_1 V_1^2 - \rho_2 V_2^2$$

which, combined with Eq. (5.1), gives

$$p_2 - p_1 = \rho_1 V_1 (V_1 - V_2) = \rho_1 V_1^2 \left(1 - \frac{V_2}{V_1}\right)$$

Dividing throughout by p_1, we get

$$\frac{p_2 - p_1}{p_1} = \frac{\rho_1 V_1^2}{p_1}\left(1 - \frac{V_2}{V_1}\right)$$

Now, recalling $a_1^2 = \frac{\gamma p_1}{\rho_1}$, we obtain

$$\frac{p_2 - p_1}{p_1} = \gamma M_1^2 \left(1 - \frac{V_2}{V_1}\right) \tag{5.14}$$

Scanned by CamScanner

Substituting for V_2/V_1 from Eq. (5.13), we get

$$\frac{p_2 - p_1}{p_1} = \gamma M_1^2 \left[1 - \frac{2 + (\gamma - 1) M_1^2}{(\gamma + 1) M_1^2} \right] \tag{5.15}$$

Equation (5.15) may also be written as

$$\boxed{\frac{p_2}{p_1} = 1 + \frac{2\gamma}{\gamma + 1}(M_1^2 - 1)} \tag{5.16}$$

The ratio $(p_2 - p_1)/p_1 = \Delta p/p_1$ is called the *shock strength*.

The state equation $p = \rho RT$ can be used to get the temperature ratio. With the state equation, we can write

$$\frac{T_2}{T_1} = \left(\frac{p_2}{p_1} \right) \left(\frac{\rho_1}{\rho_2} \right) \tag{5.17}$$

Substituting Eqs. (5.16) and (5.13) into Eq. (5.17) and rearranging, we get

$$\boxed{\frac{T_2}{T_1} = \frac{h_2}{h_1} = \frac{a_2^2}{a_1^2} = 1 + \frac{2(\gamma - 1)}{(\gamma + 1)^2} \frac{(\gamma M_1^2 + 1)}{M_1^2} (M_1^2 - 1)} \tag{5.18}$$

By Eq. (2.35), we have

$$s_2 - s_1 = c_p \ln \frac{T_2}{T_1} - R \ln \frac{p_2}{p_1}$$

From Eqs. (5.16) and (5.18),

$$s_2 - s_1 = c_p \ln \left[1 + \frac{2(\gamma - 1)}{(\gamma + 1)^2} \frac{(\gamma M_1^2 + 1)}{M_1^2} (M_1^2 - 1) \right] - R \ln \left(1 + \frac{2\gamma}{\gamma + 1} (M_1^2 - 1) \right) \tag{5.19}$$

From Eqs. (5.11), (5.13), (5.16), (5.18), and (5.19), it is obvious that, for a perfect gas with a given γ, M_2, ρ_2/ρ_1, p_2/p_1, T_2/T_1, and $(s_2 - s_1)$ are all functions of M_1 only. This explains the importance of Mach number in the quantitative governance of compressible flows. At this stage, we should realize that the simplicity of the above equations arises from the fact that the gas is assumed to be perfect. For high temperature gas dynamic problems, closed form expressions such as Eqs. (5.11)–(5.18) are generally not possible, and the normal shock properties must be computed numerically. The results of this section hold reasonably accurately up to about $M_1 = 5$ for air at standard conditions. Beyond Mach 5, the temperature behind the normal shock becomes high enough that γ is no longer constant.

The limiting case of $M_1 \to \infty$ can be considered either as $V_1 \to \infty$, where, because of high temperatures the perfect gas assumption becomes invalid, or as $a_1 \to 0$ where, because of extremely low temperatures the perfect gas assumption becomes invalid. That is, when $M_1 \to \infty$ (either by $V_1 \to \infty$ or by $a_1 \to 0$), the perfect gas assumption becomes invalid. But, it is interesting to

Scanned by CamScanner

examine the variation of properties across the normal shock, for this limiting case. When $M_1 \to \infty$, we find, for $\gamma = 1.4$,

$$\lim_{M_1 \to \infty} M_2 = \sqrt{\frac{\gamma - 1}{2\gamma}} = 0.378$$

$$\lim_{M_1 \to \infty} \frac{\rho_2}{\rho_1} = \frac{\gamma + 1}{\gamma - 1} = 6$$

$$\lim_{M_1 \to \infty} \frac{p_2}{p_1} = \infty$$

$$\lim_{M_1 \to \infty} \frac{T_2}{T_1} = \infty$$

At the other extreme case of an infinitely weak normal shock degenerating into a Mach wave, i.e. at $M_1 = 1$, Eqs. (5.11), (5.13), (5.16) and (5.18) yield $M_2 = \rho_2/\rho_1 = p_2/p_1 = T_2/T_1 = 1$. That is, when $M_1 = 1$, no finite changes occur across the wave.

It should be noted that the limiting value of the density ratio, $\rho_2/\rho_1 = 6$ as $M \to \infty$, is valid only for perfect gases with $\gamma = 1.4$. For high-temperature gases, the density ratio across a normal shock can be higher than 6.

Equation (5.19) justifies the statements we made earlier in this section: "from Prandtl equation, although it is possible for the flow to decelerate from supersonic to subsonic and vice versa across a normal shock wave, only the former is physically feasible". From Eq. (5.19), if $M_1 = 1$, then $\Delta s = 0$; if $M_1 < 1$, $\Delta s < 0$; and if $M_1 > 1$, $\Delta s > 0$. Therefore, since it is necessary that $\Delta s \geq 0$ from the second law of thermodynamics, M_1 must be greater than or equal to 1. When M_1 is subsonic, the entropy across the wave decreases, which is impossible. Therefore, the only physically possible flow is $M_1 > 1$, and from the above results we have $M_2 < 1$, $\rho_2/\rho_1 > 1$, $p_2/p_1 > 1$ and $T_2/T_1 > 1$.

The changes in flow properties across the shock take place over a very short distance, of the order of 10^{-5} cm. Hence, the velocity and temperature gradients inside the shock structure are very large. These large gradients result in increase in entropy across the shock. Also, these gradients internal to the shock provide heat conduction and viscous dissipation that render the shock process internally irreversible.

5.4 CHANGE OF STAGNATION OR TOTAL PRESSURE ACROSS THE SHOCK

There is no heat added to or taken away from the flow as it traverses the shock wave; i.e. the flow process across the shock wave is adiabatic. Therefore, the total temperature remains the same ahead and behind the wave, i.e.

$$T_{02} = T_{01} \tag{5.20}$$

Scanned by CamScanner

Now, it is important to note that Eq. (5.20), valid for a perfect gas, is a special case of the more general result that the total enthalpy is constant across a normal shock, as given by Eq. (5.3). For a stationary normal shock, the total enthalpy is always constant across the wave which, for calorically or thermally perfect gases, translates into a constant total temperature across the shock. However, for a chemically reacting gas, the total temperature is not constant across the shock. Also, if the shock wave is not stationary, neither the total enthalpy nor the total temperature are constant across the shock wave.

For an adiabatic process of a perfect gas, by Eq. (2.52) we have

$$s_{02} - s_{01} = R \ln \frac{p_{01}}{p_{02}}$$

In the above equation, all the quantities are expressed as stagnation quantities. It is seen from the equation that the entropy varies only when there are losses in pressure. It is independent of velocity, and hence there is nothing like stagnation entropy. Therefore,

$$s_2 - s_1 = R \ln \frac{p_{01}}{p_{02}} \tag{5.21}$$

The exact expression for the ratio of total pressures may be obtained from Eqs. (5.21) and (5.19) as

$$\boxed{\frac{p_{02}}{p_{01}} = \left(1 + \frac{2\gamma}{\gamma+1}(M_1^2 - 1)\right)^{-1/(\gamma-1)} \left(\frac{(\gamma+1)M_1^2}{(\gamma-1)M_1^2 + 2}\right)^{\gamma/(\gamma-1)}} \tag{5.22}$$

Equation (5.22) is an important and useful equation, since it connects the stagnation pressures on either side of a normal shock to flow Mach number ahead of the shock. Also, we can see the usefulness of Eq. (5.22) from the application aspect. When a Pitot probe is placed in a supersonic flow facing the flow, there is a detached shock standing ahead of probe nose and, therefore, the probe measures the total pressure behind that normal shock. Knowing the stagnation pressure ahead of the shock, which is the pressure in the reservoir, for isentropic flow up to the shock, we can determine the flow Mach number ahead of the shock with Eq. (5.22).

The variations in p_2/p_1, ρ_2/ρ_1, T_2/T_1, p_{02}/p_{01} and M_2 with M_1 as obtained from the above equations are tabulated in Table A2 of Appendix A. These variations are also given in graphical form in Fig. 5.3. From the figure it is seen that as M_1 becomes very large, T_2/T_1 and p_2/p_1 also become very large, whereas ρ_2/ρ_1 and M_2 approach finite limits, as already stated.

Scanned by CamScanner

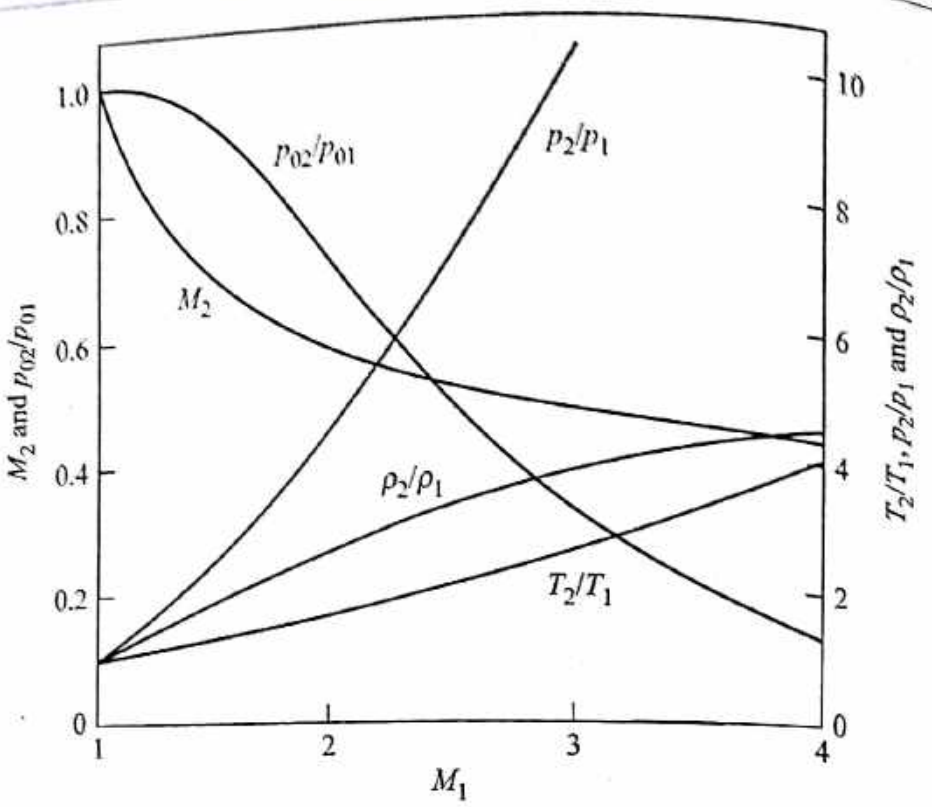


Fig. 5.3 Properties behind a normal shock wave as a function of upstream Mach number.

EXAMPLE 5.1 Derive the relation for total pressure ratio across a normal shock in a perfect gas, in terms of upstream Mach number M_1.

Solution Let subscripts 1 and 2 refer to the state ahead of and behind the shock, respectively.

The entropy change caused by the shock is

$$ds = \frac{dq}{T}$$

$$= \frac{du + pdv}{T}$$

or

$$ds = \frac{dh - vdp}{T}$$

where u, h, p, and v, respectively, are the internal energy, enthalpy, pressure and specific volume.

For a perfect gas,

$$h = c_p T, \text{ and } u = c_v T$$

Therefore,

$$ds = \frac{dh}{T} - \frac{v}{T} dp$$

$$= c_p \frac{dT}{T} - \frac{v}{T} dp$$

Scanned by CamScanner

For a perfect gas,

$$c_p = \frac{\gamma}{\gamma - 1} R$$

Also, by thermal state equation

$$v = \frac{RT}{p}$$

Therefore,

$$ds = \frac{c_p dT}{T} - R\frac{dp}{p}$$

Integrating between 1 and 2, we have

$$s_2 - s_1 = c_p \ln\frac{T_2}{T_1} - R\ln\frac{p_2}{p_1} \qquad \text{(i)}$$

In terms of stagnation pressure and temperature, the entropy change is

$$s_2 - s_1 = c_p \ln\frac{T_{02}}{T_{01}} - R\ln\frac{p_{02}}{p_{01}}$$

The flow process across the shock is adiabatic hence $T_{02} = T_{01}$. Thus,

$$s_2 - s_1 = R\ln\frac{p_{01}}{p_{02}} \qquad \text{(ii)}$$

Equating Eqs. (i) and (ii), we have

$$R\ln\frac{p_{01}}{p_{02}} = c_p \ln\frac{T_2}{T_1} - R\ln\frac{p_2}{p_1}$$

This can be arranged as

$$\ln\frac{p_{01}}{p_{02}} = \frac{c_p}{R}\ln\frac{T_2}{T_1} - \ln\frac{p_2}{p_1}$$

$$= \frac{\gamma}{\gamma - 1}\ln\frac{T_2}{T_1} - \ln\frac{p_2}{p_1}$$

$$= \ln\left(\frac{T_2}{T_1}\right)^{\frac{\gamma}{\gamma-1}} - \ln\frac{p_2}{p_1}$$

$$\frac{p_{02}}{p_{01}} = \frac{p_2}{p_1}\left(\frac{T_2}{T_1}\right)^{-\frac{\gamma}{\gamma-1}}$$

$$= \frac{p_2}{p_1}\left(\frac{p_2}{p_1}\frac{\rho_1}{\rho_2}\right)^{-\frac{\gamma}{\gamma-1}}$$

Scanned by CamScanner

$$= \left(\frac{p_2}{p_1}\right)^{1-\frac{\gamma}{\gamma-1}} \left(\frac{\rho_2}{\rho_1}\right)^{\frac{\gamma}{\gamma-1}}$$

$$= \left(\frac{p_2}{p_1}\right)^{\frac{1}{\gamma-1}} \left(\frac{\rho_2}{\rho_1}\right)^{\frac{\gamma}{\gamma-1}}$$

By Eq. (5.16),

$$\frac{p_2}{p_1} = 1 + \frac{2\gamma}{\gamma+1}(M_1^2 - 1)$$

By Eq. (5.13),

$$\frac{\rho_2}{\rho_1} = \frac{(\gamma+1)M_1^2}{2+(\gamma-1)M_1^2}$$

Substituting these we have the total pressure ratio across the shock as

$$\boxed{\frac{p_{02}}{p_{01}} = \left[1 + \frac{2\gamma}{\gamma+1}(M_1^2 - 1)\right]^{\frac{1}{\gamma-1}} \left[\frac{(\gamma+1)M_1^2}{2+(\gamma-1)M_1^2}\right]^{\frac{\gamma}{\gamma-1}}}$$

EXAMPLE 5.2 The flow Mach number, pressure, and temperature ahead of a normal shock are given as 2.0, 0.5 atm, and 300 K, respectively. Determine M_2, p_2, T_2 and V_2 behind the wave.

Solution From Table A2 of Appendix A, for $M_1 = 2.0$,

$$\frac{p_2}{p_1} = 4.5, \quad \frac{T_2}{T_1} = 1.687, \quad M_2 = \boxed{0.5774}$$

Therefore,

$$p_2 = (4.500)(0.5) = \boxed{2.250 \text{ atm}}$$

$$T_2 = (1.687)(300) = \boxed{506.1 \text{ K}}$$

For $T_2 = 506.1$ K the speed of sound $a_2 = \sqrt{\gamma R T_2}$, i.e.

$$a_2 = \sqrt{1.4 \times 287 \times 506.1} = 450.94 \text{ m/s}$$

Thus,

$$V_2 = M_2 a_2 = (0.5774)(450.94) = \boxed{260.37 \text{ m/s}}$$

EXAMPLE 5.3 A re-entry vehicle (RV) is at an altitude of 15,000 m and has a velocity of 1850 m/s. A bow shock wave envelops the RV. Neglecting dissociation, determine the static and stagnation pressure and temperature just behind the shock wave on the RV centre line where the shock wave may be treated as normal shock. Assume that the air behaves as perfect gas, with $\gamma = 1.4$ and $R = 287$ J/kg-K.

Scanned by CamScanner

Solution Let subscripts 1 and 2 stand for conditions before and after the shock. At 15,000 m altitude,

$$p_1 = 1.2108 \times 10^4 \text{ N/m}^2, \quad T_1 = -56.5^\circ\text{C} = 216.5 \text{ K}$$

The speed of sound

$$a_1 = \sqrt{\gamma R T_1} = 295 \text{ m/s}$$

Therefore,

$$M_1 = \frac{V_1}{a_1} = 6.27$$

By supersonic Rayleigh relation (Section 4.8),

$$\frac{p_1}{p_{02}} = \frac{\left(\dfrac{2\gamma}{\gamma+1}M_1^2 - \dfrac{\gamma-1}{\gamma+1}\right)^{1/(\gamma-1)}}{\left(\dfrac{\gamma+1}{2}M_1^2\right)^{\gamma/(\gamma-1)}} = \frac{1}{51.08}$$

$$p_{02} = 51.08 p_1 = \boxed{6.18 \times 10^5 \text{ N/m}^2}$$

$$T_{01} = T_{02} = T_1\left(1 + \frac{\gamma-1}{2}M_1^2\right) \text{ from isentropic relation}$$

$$T_{01} = T_{02} = 216.5(1 + 0.2M_1^2) = \boxed{1918.75 \text{ K}}$$

By Eq. (5.16),

$$\frac{p_2}{p_1} = 1 + \frac{2\gamma}{\gamma+1}(M_1^2 - 1) = 45.7$$

Therefore,

$$p_2 = 45.7 p_1 = \boxed{5.53 \times 10^5 \text{ N/m}^2}$$

By Eq. (5.18),

$$\frac{T_2}{T_1} = 1 + \frac{2(\gamma-1)}{(\gamma+1)^2}\frac{\gamma M_1^2 + 1}{M_1^2}(M_1^2 - 1) = 8.59$$

Thus,

$$T_2 = \boxed{1859.74 \text{ K}}$$

EXAMPLE 5.4 If the entropy change caused by a normal shock in an airstream is 200 J/(kg K), determine the Mach number ahead of the shock and the shock strength.

Solution Given, $\Delta s = 200$ J/(kg K).
The entropy change across a normal shock in terms of pitot pressures on either side of the shock is

Scanned by CamScanner

$$\Delta s = R \ln\left(\frac{p_{01}}{p_{02}}\right)$$

where p_{01} and p_{02} are the pitot pressures upstream and downstream of the shock, respectively.

Thus,

$$R \ln\left(\frac{p_{01}}{p_{02}}\right) = 200$$

$$\ln\left(\frac{p_{01}}{p_{02}}\right) = \frac{200}{R}$$

$$= \frac{200}{287}$$

$$= 0.697$$

$$\frac{p_{01}}{p_{02}} = e^{0.697}$$

$$= 2$$

$$\frac{p_{02}}{p_{01}} = \frac{1}{2}$$

$$= 0.5$$

For $\frac{p_{02}}{p_{01}} = 0.5$, from normal shock table,

$$M_1 = \boxed{2.5}$$

and

$$\frac{p_2}{p_1} = 7.125$$

Therefore, the shock strength becomes

$$\frac{p_2 - p_1}{p_1} = \frac{p_2}{p_1} - 1$$

$$= 7.125 - 1$$

$$= \boxed{6.125}$$

EXAMPLE 5.5 A convergent–divergent nozzle is designed to deliver Mach 1.8 helium stream. If this nozzle has to run with air, with a normal shock at the exit, determine the stagnation pressure required if the backpressure is 30 kPa. Also, find the Mach number ahead of the shock.

Solution Given, $M_e = 1.8$, $p_b = 30$ kPa.

For helium, $\gamma = 1.67$, from isentropic table for $\gamma = 1.67$; for $M_e = 1.8$,

Scanned by CamScanner

$$\frac{A_e}{A_{th}} = 1.35$$

Now, from isentropic table for $\gamma = 1.4$, $A_e/A_{th} = 1.35$,

$$\frac{p_e}{p_{0e}} = \frac{p_1}{p_{01}} = 0.1996, M_e = 1.71$$

Thus, the Mach number ahead of the shock at the nozzle exit is

$$M_1 = \boxed{1.71}$$

From normal shock table, for $M_1 = 1.71$,

$$\frac{p_2}{p_1} = 3.2448$$

The subsonic flow leaving the nozzle has to be correctly expanded (because subsonic jets are always correctly expanded). Thus, $p_2 = p_b$. Therefore,

$$p_1 = \frac{p_2}{3.2448}$$
$$= \frac{30}{3.2448}$$
$$= 9.25 \text{ kPa}$$

The stagnation pressure required is

$$p_{01} = \frac{p_1}{0.1996}$$
$$= \frac{9.25}{0.1996}$$
$$= \boxed{46.34 \text{ kPa}}$$

5.5 HUGONIOT EQUATION

As already discussed, the static pressure always increases across a shock wave; therefore, the shock can be visualized as a thermodynamic device which compresses the gas. With this consideration, the changes across a normal shock wave can be expressed purely in terms of thermodynamic variables, without explicit reference to a velocity or Mach number, as follows: By the continuity Eq. (5.1),

$$V_2 = V_1\left(\frac{\rho_1}{\rho_2}\right) \tag{5.23}$$

Scanned by CamScanner

Substituting Eq. (5.23) into Eq. (5.2), we get

$$p_1 + \rho_1 V_1^2 = p_2 + \rho_2 \left(\frac{\rho_1}{\rho_2} V_1\right)^2 \tag{5.24}$$

Solving Eq. (5.24) for V_1^2, we obtain

$$V_1^2 = \frac{p_2 - p_1}{\rho_2 - \rho_1}\left(\frac{\rho_2}{\rho_1}\right) \tag{5.25}$$

Also, substituting $V_1 = V_2(\rho_2/\rho_1)$ from Eq. (5.1) into Eq. (5.2) and solving for V_2, we get

$$V_2^2 = \frac{p_2 - p_1}{\rho_2 - \rho_1}\left(\frac{\rho_1}{\rho_2}\right) \tag{5.26}$$

Replacing h by $\left(e + \frac{p}{\rho}\right)$ in the energy Eq. (5.3), we obtain

$$e_1 + \frac{p_1}{\rho_1} + \frac{V_1^2}{2} = e_2 + \frac{p_2}{\rho_2} + \frac{V_2^2}{2} \tag{5.27}$$

Substituting for V_1 and V_2 from Eqs. (5.25) and (5.26) into Eq. (5.27), we get

$$e_1 + \frac{p_1}{\rho_1} + \frac{1}{2}\left(\frac{p_2 - p_1}{\rho_2 - \rho_1}\right)\left(\frac{\rho_2}{\rho_1}\right) = e_2 + \frac{p_2}{\rho_2} + \frac{1}{2}\left(\frac{p_2 - p_1}{\rho_2 - \rho_1}\right)\left(\frac{\rho_1}{\rho_2}\right) \tag{5.28}$$

On simplification, Eq. (5.28) yields

$$e_2 - e_1 = \frac{p_1 + p_2}{2}\left(\frac{1}{\rho_1} - \frac{1}{\rho_2}\right) \tag{5.29}$$

Replacing ρ_1 and ρ_2 in Eq. (5.29) by specific volumes v_1 and v_2, we obtain

$$\boxed{e_2 - e_1 = \frac{p_1 + p_2}{2}(v_1 - v_2)} \tag{5.30}$$

Equation (5.30) is called the *Hugoniot equation*. It has certain advantages because it relates only thermodynamic quantities across the shock. Also, since there was no assumption made about the type of gas in deriving Eq. (5.30), it is a general relation that holds for a perfect gas, a real gas, and a chemically reacting gas. Further, the form of Eq. (5.30), $\Delta e = -p_{av}\Delta v$, implies that the change in internal energy is equal to the mean pressure across the shock times the change in specific volume, and this strongly reminds us of the first law of thermodynamics in the form of Eq. (2.1), with $\delta q = 0$ for an adiabatic process across the shock.

We know that in equilibrium thermodynamics any state variable can be expressed as a function of any other two state variables. Therefore, the specific energy, e, can be expressed as

$$e = e(p, v)$$

Scanned by CamScanner

Substituting this into Eq. (5.30), we get

$$p_2 = f(p_1, v_1, v_2) \tag{5.31}$$

For given p_1 and v_1, Eq. (5.31) represents p_2 as a function of v_2. A plot of this relation on a pv diagram is called the *Hugoniot curve*, shown in Fig. 5.4. This curve is the locus of all possible pressure-volume conditions behind normal shocks of different strengths for a given set of upstream values for p_1 and v_1 (point 1 in Fig. 5.4). Therefore, each point on the Hugoniot curve in Fig. 5.4 corresponds to a shock with a specific upstream velocity V_1.

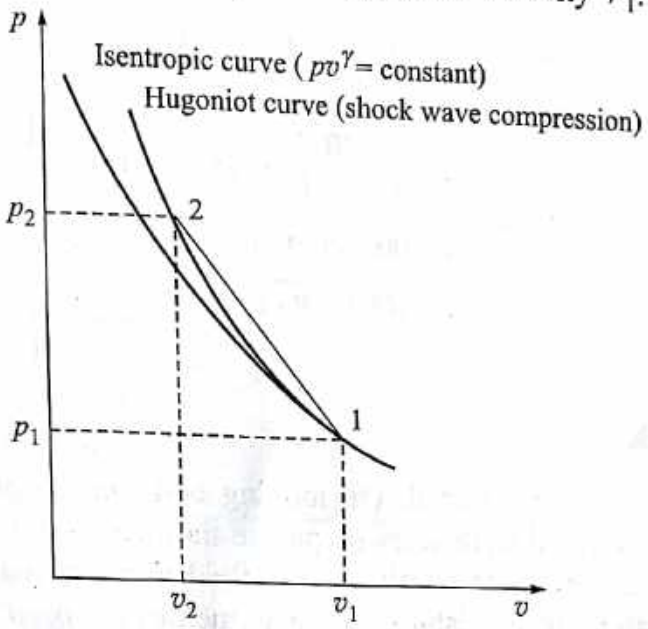


Fig. 5.4 Hugoniot curve.

Now, choosing a specific shock with a specific upstream velocity V_1, we can locate the specific point on the Hugoniot curve, point 2, which corresponds to this particular shock, as follows: Replacing $1/\rho$ by v in Eq. (5.25), we get

$$V_1^2 = \frac{p_2 - p_1}{1/v_2 - 1/v_1}\left(\frac{v_1}{v_2}\right)$$

This equation may be expressed as

$$\frac{p_2 - p_1}{v_2 - v_1} = -\left(\frac{V_1}{v_1}\right)^2 \tag{5.32}$$

In Eq. (5.32), the left-hand side gives the slope of the straight line through points 1 and 2 in Fig. 5.4. The right-hand side is a known value, given by the upstream velocity and specific volume. That is, Eq. (5.32) connects the geometry of the Hugoniot curve to the flow velocity and specific volume upstream of the shock. Further, for calorically perfect gas, it is possible to write Eq. (5.30) as

$$\frac{p_2}{p_1} = \frac{\left(\frac{\gamma+1}{\gamma-1}\right)\left(\frac{v_1}{v_2}\right) - 1}{\left(\frac{\gamma+1}{\gamma-1}\right) - \left(\frac{v_1}{v_2}\right)}$$

noting $e = c_v T$ and $T = pv/R$.

Scanned by CamScanner

EXAMPLE 5.6 A gas flow with velocity 400 m/s and specific volume 1.11 m^3/kg passes through a normal shock. If the specific volume behind the shock is 0.333 m^3/kg, deter mine the pressure increase caused by the shock.

Solution Let subscripts 1 and 2, respectively, refer to the condition ahead of and behind the shock.

Given, $V_1 = 400$ m/s, $v = 1.11$ m^3/kg.

By Eq. (5.32), the pressure difference across the shock is

$$p_2 - p_1 = -\left(\frac{V_1^2}{v_1}\right)^2 (v_2 - v_1)$$

$$= -\left(\frac{400}{1.11}\right)^2 (0.333 - 1.11)$$

$$= 100,900.9 \text{ Pa}$$

$$= \boxed{100.9 \text{ kPa}}$$

Moving Shocks

We are familiar with the fact that a moving body in a flow field creates disturbances and these disturbances propagate throughout the flow field. The motion of these disturbances relative to the fluid is called *wave motion*. The speed of propagation of the disturbances is termed *wave speed*. Through these waves only the various parts of the body interact with the fluid and with each other, and by which the forces on the body are established.

For our discussion, let us consider the case of one-dimensional motion of a shock wave in a tube of constant area. These waves are called *plane waves*. Since this sort of waves may be generated by the motion of a piston in a tube, they are also referred to as *piston problems*.

5.6 THE PROPAGATING SHOCK WAVE

The study of equations of motion for a normal shock wave in Section 5.2 assumed the shock to be stationary, as shown in Fig. 5.5(a). The fluid flows through the shock with velocity V_1. We may say that relatively the shock is propagating through the fluid with speed V_1. Let us call this as shock speed, C_s. This situation is shown in Fig. 5.5(b) where the shock is moving with speed C_s and the fluid ahead of it is at rest. Therefore, we have

$$C_s = V_1 \tag{5.33a}$$

The fluid behind the shock wave is following the shock with speed

$$V_p = V_1 - V_2 \tag{5.33b}$$

Scanned by CamScanner

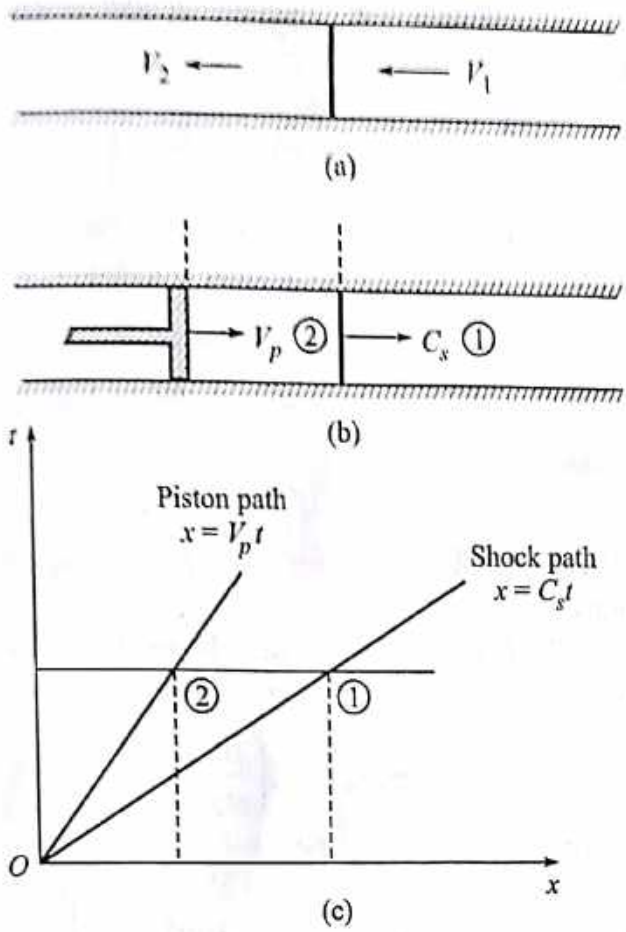


Fig. 5.5 Stationary and moving shock waves.

For stationary normal shock wave shown in Fig. 5.5(a), we know from Eqs. (5.1) to (5.3) that the continuity, momentum, and energy equations are, respectively,

$$\rho_1 V_1 = \rho_2 V_2 \tag{5.1}$$

$$p_1 + \rho_1 V_1^2 = p_2 + \rho_2 V_2^2 \tag{5.2}$$

$$h_1 + \frac{1}{2} V_1^2 = h_2 + \frac{1}{2} V_2^2 \tag{5.3}$$

From Fig. 5.5(c), it is seen that

V_1 = velocity of the fluid ahead of the shock wave, relative to the wave

V_2 = velocity of the fluid behind the shock wave, relative to the wave

Equations (5.1)–(5.3) always hold for flow velocities relative to the shock wave, whether the shock is stationary or moving. Therefore, from Fig. 5.5(b), we deduce from the geometry of a moving shock that

C_s = velocity of the gas ahead of the shock wave, relative to the wave

$C_s - V_p$ = velocity of the gas behind the shock wave, relative to the wave

It may be assumed that the fluid behind the shock wave is followed by a driving piston, moving at the speed V_p, as illustrated in Fig. 5.5(b).

Scanned by CamScanner

In Fig. 5.5(c), the position-time diagram of piston and shock wave is illustrated. At time $t = 0$ the piston is started impulsively with speed V_p. It establishes a shock wave which runs ahead at the speed C_s. The pressure on the piston face is p_2. The region of compressed fluid between the shock wave and the piston increases in length at the rate $(C_s - V_p)$. Therefore, the normal shock continuity, momentum, and energy equations, viz. Eqs. (5.1)–(5.3), for the moving shock wave, shown in Fig. 5.5(b), become

$$\rho_1 C_s = \rho_2 (C_s - V_p) \tag{5.34}$$

$$p_1 + \rho_1 C_s^2 = p_2 + \rho_2 (C_s - V_p)^2 \tag{5.35}$$

$$h_1 + \frac{C_s^2}{2} = h_2 + \frac{(C_s - V_p)^2}{2} \tag{5.36}$$

Equations (5.34)–(5.36) are the governing normal shock equations for a shock moving with velocity C_s into a stagnant gas.

For convenience, the above equations may be rearranged as follows: From Eq. (5.34), we get

$$C_s - V_p = C_s \left(\frac{\rho_1}{\rho_2} \right) \tag{5.37}$$

Substitution of Eq. (5.37) into (5.35) yields

$$p_1 + \rho_1 C_s^2 = p_2 + \rho_2 C_s^2 \left(\frac{\rho_1}{\rho_2} \right)^2$$

i.e.

$$p_2 - p_1 = \rho_1 C_s^2 \left(1 - \frac{\rho_1}{\rho_2} \right)$$

$$C_s^2 = \frac{p_2 - p_1}{\rho_1 (1 - \rho_1/\rho_2)}$$

$$C_s^2 = \frac{p_2 - p_1}{\rho_2 - \rho_1} \left(\frac{\rho_2}{\rho_1} \right) \tag{5.38}$$

Equation (5.34) can also be expressed as

$$C_s = (C_s - V_p) \left(\frac{\rho_2}{\rho_1} \right) \tag{5.39}$$

Substituting Eq. (5.39) into Eq. (5.38), we get

$$(C_s - V_p)^2 \left(\frac{\rho_2}{\rho_1} \right)^2 = \frac{p_2 - p_1}{\rho_1 - \rho_2} \left(\frac{\rho_2}{\rho_1} \right)$$

$$(C_s - V_p)^2 = \frac{p_2 - p_1}{\rho_2 - \rho_1} \left(\frac{\rho_1}{\rho_2} \right) \tag{5.40}$$

Substitution of Eqs. (5.38) and (5.40) into relation (5.36), with $h = e + p/\rho$, results in

Scanned by CamScanner

$$e_1 + \frac{p_1}{\rho_1} + \frac{1}{2}\left[\frac{p_2 - p_1}{\rho_2 - \rho_1}\left(\frac{\rho_2}{\rho_1}\right)\right] = e_2 + \frac{p_2}{\rho_2} + \frac{1}{2}\left[\frac{p_2 - p_1}{\rho_2 - \rho_1}\left(\frac{\rho_1}{\rho_2}\right)\right] \quad (5.41)$$

On simplification, Eq. (5.41) reduces to

$$e_2 - e_1 = \frac{p_1 + p_2}{2}\left(\frac{1}{\rho_1} - \frac{1}{\rho_2}\right)$$

or

$$e_2 - e_1 = \frac{p_1 + p_2}{2}(v_1 - v_2) \quad (5.42)$$

Equation (5.42) is the Hugoniot equation, and is identically of the same form as Eq. (5.30) for a stationary shock. This is naturally expected, since the Hugoniot equation relates changes of thermodynamic variables across a normal shock wave, and these are physically independent of shock motion.

In general, Eqs. (5.34)–(5.36) must be solved numerically. However, for the special case of calorically perfect gas with $e = c_v T$, and $v = RT/p$, Eq. (5.42) becomes

$$\frac{T_2}{T_1} = \frac{p_2}{p_1}\left(\frac{\dfrac{\gamma+1}{\gamma-1} + \dfrac{p_2}{p_1}}{1 + \dfrac{\gamma+1}{\gamma-1}\dfrac{p_2}{p_1}}\right) \quad (5.43)$$

Similarly, the density ratio ρ_2/ρ_1 becomes

$$\frac{\rho_2}{\rho_1} = \frac{1 + \dfrac{\gamma+1}{\gamma-1}\left(\dfrac{p_2}{p_1}\right)}{\dfrac{\gamma+1}{\gamma-1} + \dfrac{p_2}{p_1}} \quad (5.44)$$

The temperature ratio and the density ratio across a moving shock wave is given as a function of the pressure ratio. Unlike a stationary shock wave where it is conventional to think of Mach number M_1, upstream of shock wave as the governing parameter for changes across the wave, for a moving shock wave it now becomes convenient to keep p_2/p_1 as the basic parameter governing changes across the wave.

Now, even the moving shock Mach number M_s, defined as

$$M_s = \frac{C_s}{a_1}$$

where $a_1^2 = (dp/d\rho)_1$ can also be expressed in terms of p_2/p_1.

With Eq. (5.16) to relate p_2/p_1 to the Mach number, the shock velocity for a perfect gas can be expressed as

$$C_s = a_1\sqrt{\frac{\gamma+1}{2\gamma}\left(\frac{p_2}{p_1} - 1\right) + 1} \quad (5.45)$$

Scanned by CamScanner

Equation (5.45) is important; it relates the wave velocity of the moving shock wave to the pressure ratio across the wave and the *speed of sound* in the gas into which the wave is moving. The fluid velocity behind the shock is

$$V_p = V_1 - V_2 = C_s\left(1 - \frac{V_2}{V_1}\right)$$

or

$$V_p = C_s\left(1 - \frac{\rho_1}{\rho_2}\right)$$

since $\rho_1/\rho_2 = V_2/V_1$ from continuity. Substituting Eqs. (5.44) and (5.45) for density ratio and shock speed in the equation for V_p, we get

$$V_p = \frac{a_1}{\gamma}\left(\frac{p_2}{p_1} - 1\right)\left(\frac{\frac{2\gamma}{\gamma+1}}{\frac{p_2}{p_1} + \frac{\gamma-1}{\gamma+1}}\right)^{1/2} \tag{5.46}$$

It is seen from Eq. (5.46) that, like the shock velocity C_s, the fluid velocity behind the shock, which is sometimes called *mass-motion velocity* V_p, also depends on the pressure ratio across the shock wave and the speed of sound ahead of the wave.

Now let us study the above jump relations and shock speed and mass-motion velocity for the moving shock wave for the extreme cases of weak and strong shocks.

EXAMPLE 5.7 A shock of strength 0.382 is generated by a piston which moves in still air at 300 K. Determine the shock speed and the piston speed.

Solution Given, $\Delta p/p_1 = (p_2 - p_1) = 0.382$, $T_1 = 300$ K, where subscripts 1 and 2, respectively, refer to the states ahead of and behind the shock. Therefore,

$$\frac{p_2 - p_1}{p_1} = 0.382$$

$$\frac{p_2}{p_1} - 1 = 0.382$$

$$\frac{p_2}{p_1} = 1.382$$

$$a_2 = \sqrt{1.4 \times 287 \times 300}$$
$$= 347.19 \text{ m/s}$$

From Eq. (5.16),

$$\frac{p_2}{p_1} = 1 + \frac{2\gamma}{\gamma+1}(M_s^2 - 1)$$

Scanned by CamScanner

$$M_s^2 - 1 = \left(\frac{p_2}{p_1} - 1\right) \times \frac{\gamma + 1}{2\gamma}$$

$$= 0.382 \times \frac{2.4}{2.8}$$

$$= 0.3274$$

$$M_s = \sqrt{1.3274}$$

$$= 1.152$$

Therefore,

$$C_s = M_s a_1 = 1.152 \times 347.19$$

$$= \boxed{400 \text{ m/s}}$$

By Eq. (5.46), we have

$$V_p = \frac{a_1}{\gamma}\left(\frac{p_2}{p_1} - 1\right)\left[\frac{\frac{2\gamma}{\gamma+1}}{\frac{p_2}{p_1} + \frac{\gamma-1}{\gamma+1}}\right]^{1/2}$$

$$= \frac{347.19}{1.4} \times 0.382 \times \left[\frac{2.8/2.4}{1.382 + 0.4/2.4}\right]^{1/2}$$

$$= 248 \times 0.382 \times \left[\frac{1.167}{1.549}\right]^{1/2}$$

$$= \boxed{82.23 \text{ m/s}}$$

The piston speed is also given by

$$V_p = C_s\left(1 - \frac{\rho_1}{\rho_2}\right)$$

From Eq. (5.44), we have

$$\frac{\rho_2}{\rho_1} = \frac{1 + \frac{\gamma+1}{\gamma-1}\left(\frac{p_2}{p_1}\right)}{\frac{\gamma+1}{\gamma-1} + \frac{p_2}{p_1}}$$

$$= \frac{1 + \frac{2.4}{0.4} \times 1.382}{\frac{2.4}{0.4} + 1.382}$$

$$= \frac{9.292}{7.382}$$

$$= 1.259$$

Scanned by CamScanner

Thus,

$$V_p = C_s\left(1-\frac{1}{1.259}\right)$$
$$= 400\times\left(1-\frac{1}{1.259}\right)$$
$$= \boxed{82.29 \text{ m/s}}$$

Weak Shock

A weak shock is that for which the normalized *pressure jump is very small*, i.e.

$$\frac{\Delta p}{p_1} = \frac{p_2 - p_1}{p_1} \ll 1$$

The other jumps are then correspondingly small, as may be seen by expanding Eqs. (5.43) and (5.44) in series and retaining only the first-order terms in $\Delta p/p_1$. This gives

$$\frac{\Delta T}{T_1} \approx \frac{\gamma-1}{\gamma}\frac{\Delta p}{p_1} \tag{5.47a}$$

$$\frac{\Delta \rho}{\rho_1} \approx \frac{1}{\gamma}\frac{\Delta p}{p_1} \approx \frac{V_p}{a_1} \tag{5.47b}$$

Similarly, from Eq. (5.45), we get

$$C_s \approx a_1\left(1+\frac{\gamma+1}{4\gamma}\frac{\Delta p}{p_1}\right) \tag{5.47c}$$

Note from Eq. (5.47c) that the speed of very weak shocks is nearly equal to a_1.

EXAMPLE 5.8 A weak shock is generated by a piston in a tube containing still air at 300 K. If the temperature of the air traversed by the shock is 5 per cent more than the initial temperature, determine the piston speed and the shock Mach number.

Solution Let subscripts 1 and 2 refer to the initial and final states, respectively.

Given, $T_1 = 300$ K, $T_2 = 1.05T_1$.

By Eq. (5.47a),

$$\frac{\Delta T}{T} \approx \frac{\gamma-1}{\gamma}\left(\frac{\Delta p}{p_1}\right)$$
$$\frac{T_2 - T_1}{T_1} = \frac{1.4-1}{1.4}\left(\frac{\Delta p}{p_1}\right)$$
$$\frac{T_2}{T_1} - 1 = \frac{1.4-1}{1.4}\left(\frac{\Delta p}{p_1}\right)$$

Scanned by CamScanner

$$1.05 - 1 = \frac{0.4}{1.4}\frac{\Delta p}{p_1}$$

$$\frac{\Delta p}{p_1} = \frac{1.4 \times 0.05}{0.4}$$

$$\frac{p_2 - p_1}{p_1} = 0.175$$

$$\frac{p_2}{p_1} = 1.175$$

By Eq. (5.47b),

$$\frac{V_p}{a_1} \approx \frac{1}{\gamma}\frac{\Delta p}{p_1}$$

$$= \frac{1}{1.4} \times 1.175 = 0.8393$$

$$V_p = 0.8393\sqrt{\gamma R T_1}$$

$$= 0.8393\sqrt{1.4 \times 287 \times 300}$$

$$= \boxed{291.40 \text{ m/s}}$$

By Eq. (5.47c),

$$C_s = a_1\left(1 + \frac{\gamma + 1}{4\gamma}\frac{\Delta p}{p_1}\right)$$

$$= \sqrt{1.4 \times 287 \times 300}\left(1 + \frac{2.4}{4 \times 1.4} \times 0.175\right)$$

$$= 373.23 \text{ m/s}$$

The shock Mach number is

$$M_s = \frac{C_s}{a_1}$$

$$= \frac{373.23}{347.19} = \boxed{1.075}$$

Strong Shock

A strong shock is one for which p_2/p_1 is *very large*. For this case we can show that

$$\frac{T_2}{T_1} \to \frac{\gamma - 1}{\gamma + 1}\frac{p_2}{p_1} \tag{5.48a}$$

Scanned by CamScanner

$$\frac{\rho_2}{\rho_1} \to \frac{\gamma+1}{\gamma-1} \tag{5.48b}$$

$$C_s \to a_1\left(\frac{\gamma+1}{2\gamma}\frac{p_2}{p_1}\right)^{1/2} \tag{5.48c}$$

$$V_p \to a_1\left(\frac{2}{\gamma(\gamma+1)}\frac{p_2}{p_1}\right)^{1/2} \tag{5.48d}$$

EXAMPLE 5.9 A normal shock moves in a constant area tube as shown in Fig. 5.6(a). In region 1, $V_1 = 100$ m/s, $T_1 = 30°C$, and $p_1 = 0.7$ atm. The shock speed C_s with respect to a fixed coordinate system is 600 m/s. Find the fluid properties in region 2.

Solution Referring to a coordinate system which is moving at velocity 600 m/s to the left, the flow field becomes as in Fig. 5.6(b) with shock stationary. The speed of sound is given by

$$a_1 = \sqrt{\gamma R T_1} = 348.9 \text{ m/s}$$

$$V_1 = 500 \text{ m/s}$$

$$M_1 = \frac{500}{348.9} = 1.433$$

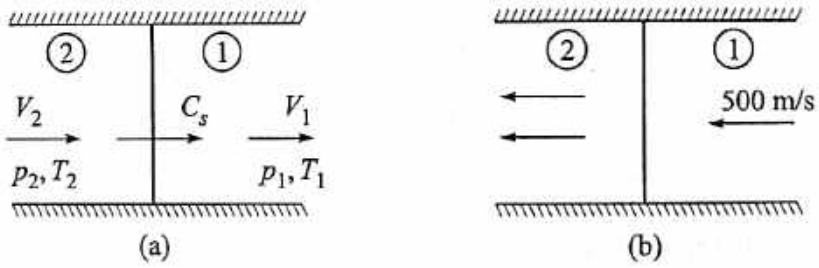


Fig. 5.6 Example 5.9.

From Eq. (5.11), we have

$$M_2^2 = \frac{1+0.2M_1^2}{1.4M_1^2-0.2} = 0.527$$

Hence, $M_2 = 0.726$. From Eq. (5.13),

$$\frac{\rho_2}{\rho_1} = \frac{2.4M_1^2}{0.4M_1^2+2} = 1.748$$

Again, from Eq. (5.16),

$$\frac{p_2}{p_1} = 1 + \frac{2.8}{2.4}(M_1^2-1) = 2.229$$

Scanned by CamScanner

Further, from Eq. (5.17),

$$\frac{T_2}{T_1} = \frac{p_2}{p_1}\frac{\rho_1}{\rho_2} = 1.275$$

Therefore,

$$p_2 = \boxed{1.56 \text{ atm}}, \qquad T_2 = \boxed{386.33 \text{ K}}$$

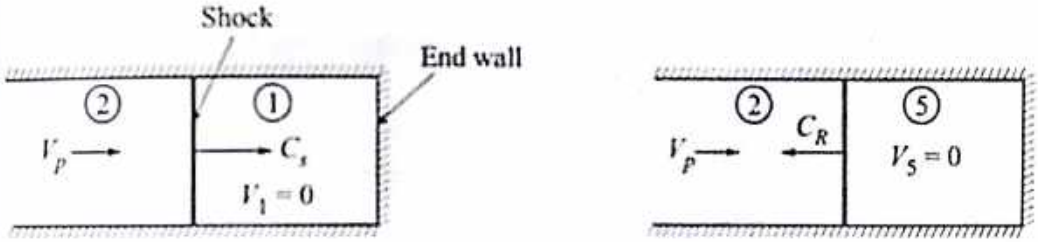
$$V_2 = M_2 a_2 = 0.726\sqrt{1.4 \times 287 \times 386.33}$$

$V_2 = 286$ m/s to the left w.r.t. the fixed coordinate system

$V_2 = -286 + 600 = \boxed{314 \text{ m/s}}$ to the right

5.7 REFLECTED SHOCK WAVE

Consider a normal shock wave moving with velocity C_s to the right inside a tube as shown in Fig. 5.7(a). Let the shock be incident on a flat end wall. Upstream of the incident shock, the mass motion $V_1 = 0$. Behind the incident shock, the mass velocity is V_p towards the end wall. The shock gets reflected from the wall and travels to the left with velocity C_R, as shown in Fig. 5.7(b).



(a) Incident shock (b) Reflected shock

Fig. 5.7 Incident and reflected shock waves.

The strength of this reflected shock is such that the originally induced mass motion with velocity V_p is stopped completely in its tracks. The mass motion behind the reflected shock should be zero, i.e. $V_5 = 0$ in Fig. 5.7(b). Thus, the zero-velocity boundary condition is kept by the reflected shock wave. Indeed, for an incident normal shock of specified strength, the reflected normal shock strength is completely determined by imposing the boundary condition $V_5 = 0$.

The shock wave reflection considered above is illustrated as x–t diagram in Fig. 5.8. The plot showing the wave motion on a graph of x vs. t is called *wave diagram*. At time $t = 0$, the incident shock just starts from the diaphragm location.

Therefore, at $t = 0$, the incident shock is at location $x = 0$. The shock wave travels to the right with increasing t and is located at $x = x_1$, at $t = t_1$. This is marked as point 1 in the x–t diagram. After hitting the wall at $x = x_2$, the shock reflects towards the left with velocity C_R. At time $t = t_3$, the reflected shock is

Scanned by CamScanner

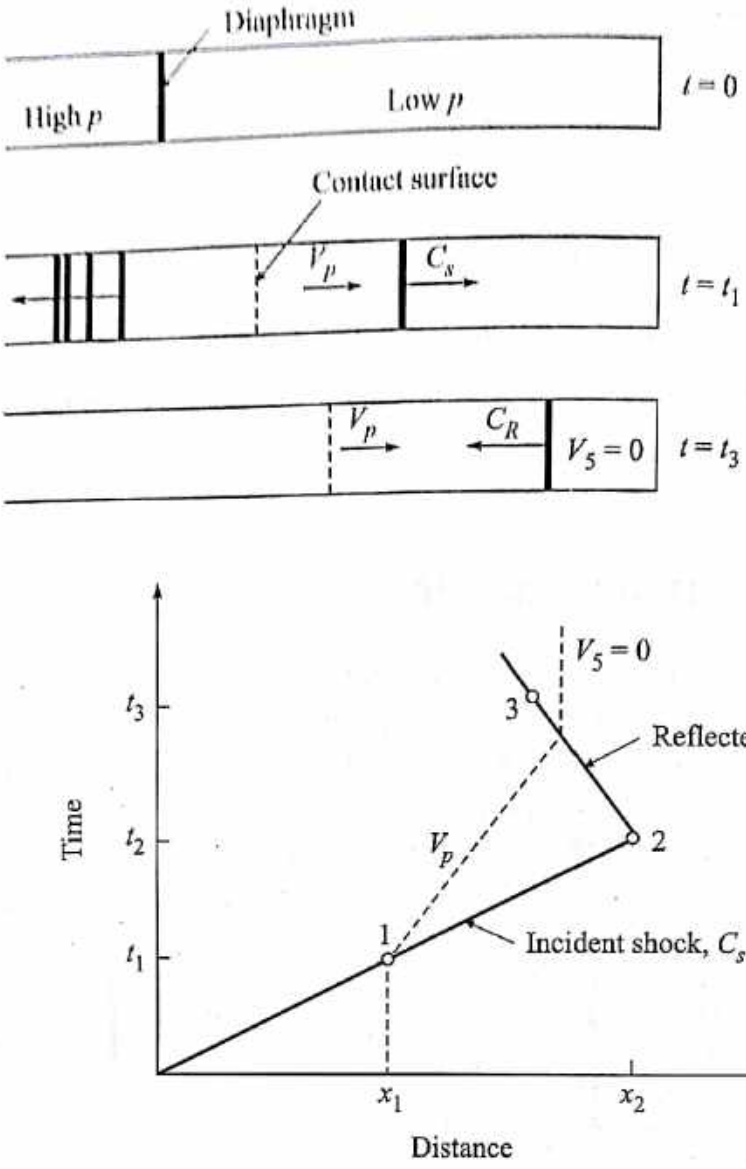


Fig. 5.8 x–t diagram.

at $x = x_3$. The incident and reflected shock paths are straight in the wave diagram. The slopes of the incident and reflected shock paths are $1/C_s$ and $1/C_R$, respectively. Also, $C_R < C_s$ because of the general characteristic of reflected shock; therefore, the reflected shock path is more steeply inclined than the incident shock path.

The path of the fluid particles behind the shock, travelling with velocity V_p, is shown by the dashed lines in Fig. 5.8. In Fig. 5.7(b), we note that

$C_R + V_p$ = velocity of the gas ahead of the shock wave relative to the wave
C_R = velocity of the gas behind the shock wave relative to the wave

Hence, following Eqs. (5.1)–(5.3), for the reflected shock, we have

$$\rho_2(C_R + V_p) = \rho_5 C_R \tag{5.49}$$

$$p_2 + \rho_2(C_R + V_p)^2 = p_5 + \rho_5 C_R^2 \tag{5.50}$$

Scanned by CamScanner

$$h_2 + \frac{(C_R + V_p)^2}{2} = h_5 + \frac{C_R^2}{2} \tag{5.51}$$

Equations (5.49)–(5.51) are the continuity, momentum, and energy equations, respectively, for a reflected shock wave.

The incident shock propagates into the gas ahead of it with a Mach number $M_s = C_s/a_1$. The reflected shock propagates into the gas ahead of it with a Mach number $M_R = (C_R + V_p)/a_2$. With the incident shock equations (5.1)–(5.3), and the reflected shock equations (5.49)–(5.51), for a perfect gas, a relation between M_R and M_s can be obtained as follows:

By Eq. (5.33b), we have the piston speed V_p, in terms of the flow speed V_1 ahead of and V_2 behind the incident shock, as

$$V_p = V_1 - V_2$$

But $V_1 = C_s$, therefore,

$$\begin{aligned} V_p &= C_s - V_2 \\ &= C_s\left(1 - \frac{V_2}{C_s}\right) \\ &= C_s\left(1 - \frac{C_s V_2}{C_s^2}\right) \end{aligned}$$

By Eq. (5.8), $C_s V_2 = a_1^{*2}$, therefore,

$$\begin{aligned} V_p &= C_s\left(1 - \frac{a_1^{*2}}{C_s^2}\right) \\ &= C_s\left(1 - \frac{1}{M_1^{*2}}\right) \end{aligned}$$

By Eq. (4.31),

$$M_1^{*2} = \frac{(\gamma+1)M_1^2}{2 + (\gamma-1)M_1^2}$$

and $M_1 = M_s$, therefore,

$$\begin{aligned} V_p &= C_s\left[1 - \frac{2 + (\gamma-1)M_s^2}{(\gamma+1)M_s^2}\right] \\ &= C_s\left[\frac{(\gamma+1)M_s^2 - 2 - (\gamma-1)M_s^2}{(\gamma+1)M_s^2}\right] \\ &= C_s\left[\frac{2M_s^2 - 2}{(\gamma+1)M_s^2}\right] \end{aligned}$$

Scanned by CamScanner

$$= \frac{2}{\gamma+1} C_s \left[\frac{M_s^2 - 1}{M_s^2} \right]$$

But $Cs = a_1 M_s$, therefore,

$$V_p = \frac{2a_1 M_s}{\gamma+1} \left(\frac{M_s^2 - 1}{M_s^2} \right)$$

$$= \frac{2a_1}{\gamma+1} \left(\frac{M_s^2 - 1}{M_s} \right)$$

For the reflected shock, by Eq. (5.49),

$$\rho_2 (C_R + V_p) = \rho_5 C_R$$

This can be expressed as

$$\rho_2 (C_R + V_p) = \rho_5 [(C_R + V_p) - V_p]$$

Dividing by a_2, we have

$$\rho_2 \frac{(C_R + V_p)}{a_2} = \rho_5 \left[\frac{(C_R + V_p)}{a_2} - \frac{V_p}{a_2} \right]$$

$$\rho_2 M_R = \rho_5 \left(M_R - \frac{V_p}{a_2} \right)$$

$$\frac{\rho_2}{\rho_5} M_R = M_R - \frac{V_p}{a_2}$$

$$\frac{V_p}{a_2} = M_R \left(1 - \frac{\rho_2}{\rho_5} \right)$$

But

$$\frac{\rho_2}{\rho_5} = \frac{C_R}{C_R + V_p}$$

or

$$\frac{\rho_2}{\rho_5} = \frac{C_R (C_R + V_p)}{(C_R + V_p)^2}$$

By Prandtl equation, $C_R (C_R + V_p) = a_2^{*2}$, thus

$$\frac{\rho_2}{\rho_5} = \frac{a_2^{*2}}{(C_R + V_p)^2}$$

$$= \frac{1}{M_R^{*2}}$$

Scanned by CamScanner

By Eq. (4.25),

$$M_R^{*2} = \frac{(\gamma+1)M_R^2}{2+(\gamma-1)M_R^2}$$

Thus

$$\frac{V_p}{a_2} = M_R\left(1 - \frac{1}{M_R^{*2}}\right)$$

$$= M_R\left[1 - \frac{2+(\gamma-1)M_R^2}{(\gamma+1)M_R^2}\right]$$

$$= M_R\left[\frac{(\gamma+1)M_R^2 - 2 - (\gamma-1)M_R^2}{(\gamma+1)M_R^2}\right]$$

$$= M_R\left(\frac{2(M_R^2-1)}{(\gamma+1)M_R^2}\right)$$

$$V_p = \frac{2a_2}{\gamma+1}\left(\frac{M_R^2-1}{M_R}\right)$$

Equating the above expressions for V_p, we have

$$\frac{2a_1}{\gamma+1}\left(\frac{M_s^2-1}{M_s}\right) = \frac{2a_2}{\gamma+1}\left(\frac{M_R^2-1}{M_R}\right)$$

$$a_1\left(\frac{M_s^2-1}{M_s}\right) = a_2\left(\frac{M_R^2-1}{M_R}\right)$$

$$\frac{M_R}{M_R^2-1} = \frac{a_2}{a_1}\frac{M_s}{M_s^2-1}$$

$$= \sqrt{\frac{T_2}{T_1}}\frac{M_s}{M_s^2-1}$$

By Eq. (5.18),

$$\frac{T_2}{T_1} = 1 + \frac{2(\gamma-1)\gamma M_s^2+1}{(\gamma+1)^2 \quad M_s^2}(M_s^2-1)$$

Scanned by CamScanner

Thus

$$\frac{M_R}{M_R^2-1}=\frac{M_s}{M_s^2-1}\left[1+\frac{2(\gamma-1)}{(\gamma+1)^2}\frac{\gamma M_s^2+1}{M_s^2}(M_s^2-1)\right]^{1/2} \tag{5.52}$$

EXAMPLE 5.10 A normal shock wave with pressure ratio of 4.5 impinges on a plane wall. Determine the static pressure ratio for the reflected normal shock wave [see Fig. 5.9(a)]. The air temperature in front of the incident wave is 280 K.

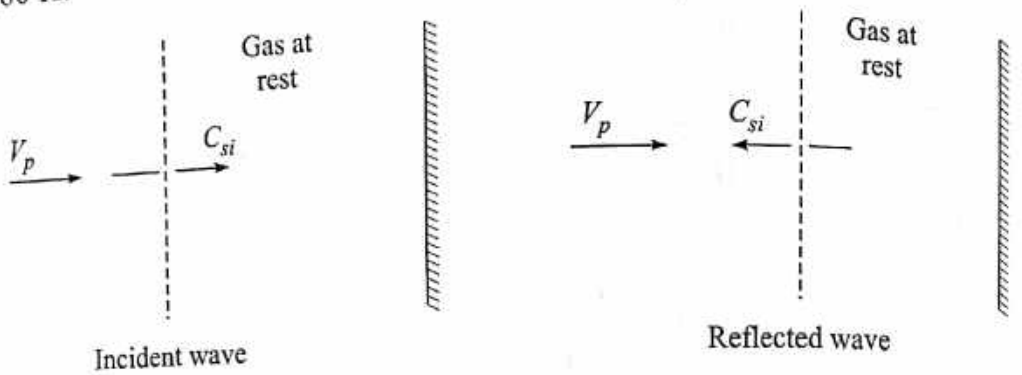


Fig. 5.9(a) Example 5.10.

Solution The flow field for incident shock is equivalent to one with velocities as shown in Fig. 5.9(b).

$$\frac{p_2}{p_1}=4.5$$

$$a_1=\sqrt{\gamma RT_1}=335.4 \text{ m/s}$$

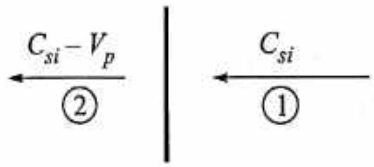


Fig. 5.9(b) Example 5.10.

From normal shock table, for $p_2/p_1 = 4.5$,

$$M_1 = 2.0, \quad T_2/T_1 = 1.688$$

$$T_2 = 472.64 \text{ K}$$

Therefore, $C_{si} = M_1 a_1 = 670.8$ m/s. From Eqs. (5.33a) and (5.13), we get

$$\frac{C_{si}-V_p}{C_{si}}=\frac{2+(\gamma-1)M_1^2}{(\gamma+1)M_1^2}=0.375$$

Scanned by CamScanner

$$C_{si} - V_p = 251.55 \text{ m/s}$$

Therefore,

$$V_p = 419.25 \text{ m/s}$$

The flow field for the reflected shock is equivalent to that shown in Fig. 5.9(c). The speed of sound in zone 3 is given by

$$a_3 = \sqrt{\gamma R T_2} = 435.78 \text{ m/s}$$

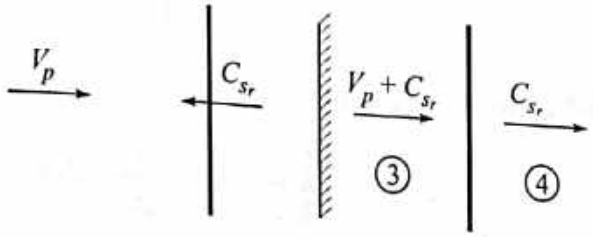


Fig. 5.9(c) Example 5.10.

Therefore,

$$M_3 = \frac{C_{sr} + 419.25}{435.78} \tag{i}$$

From Eq. (5.13),

$$\frac{V_3}{V_4} = \frac{(\gamma+1) M_3^2}{2 + (\gamma-1) M_3^2} = \frac{C_{sr} + 419.25}{C_{sr}} \tag{ii}$$

Substituting for C_{sr} from Eq. (i) into Eq. (ii), we obtain

$$\frac{2.4 M_3^2}{2 + 0.4 M_3^2} = \frac{435.78 M_3}{435.78 M_3 - 419.25}$$

This results in $M_3 = 1.73$. Therefore,

$$\frac{p_4}{p_3} = 1 + \frac{2\gamma}{\gamma+1}(M_3^2 - 1) = \boxed{3.32}$$

EXAMPLE 5.11 A normal shock, generated by impulsively moving the piston in a cylinder piston device with stagnant air at 300 K and 1 atm, moves towards the closed end of the piston and reflects back. If the pressure losses caused by the incident and reflected shocks are 23.26% and 14.01%, respectively, determine (a) the speed of the incident shock and piston speed, and (b) the pressure behind the reflected shock and the speed of sound ahead of the reflected shock.

Solution (a) Let the subscripts 1 and 2, respectively, refer to the fields ahead of and behind the incident shock and the subscripts 3 and 4 refer to the fields ahead of and behind the reflected shock, respectively.

Scanned by CamScanner

Given, $T_1 = 300$ K and $p_1 = 1$ atm and

$$\frac{p_{01} - p_{02}}{p_{01}} \times 100 = 23.26$$

$$1 - \frac{p_{02}}{p_{01}} = 0.2326$$

$$\frac{p_{02}}{p_{01}} = 0.7674$$

For $p_{02}/p_{01} = 0.7674$, from the normal shock table, we have

$$M_1 = 1.9, \frac{p_2}{p_1} = 4.045, \frac{T_2}{T_1} = 1.6079, \frac{\rho_2}{\rho_1} = 2.5157$$

Thus,

$$V_1 = M_1 a_1 = 1.9 \times \sqrt{\gamma R T_1}$$

$$= 1.9 \times \sqrt{1.4 \times 287 \times 300}$$

$$= \boxed{659.66 \text{ m/s}}$$

$$\frac{V_1}{V_2} = \frac{V_1}{V_1 - V_p} = \frac{\rho_2}{\rho_1} = 2.5157$$

$$V_p = V_1 - \frac{V_1}{2.5157}$$

$$= 659.66 - \frac{659.66}{2.5157}$$

$$= \boxed{397.44 \text{ m/s}}$$

(b) Temperature T_3 ahead of the reflected shock is the same as T_2, the temperature behind the incident shock. Thus,

$$T_3 = 1.6079 \times T_1 = 1.6079 \times 300$$

$$= 482.37 \text{ K}$$

Thus, the speed of sound ahead of the reflected shock is

$$a_3 = \sqrt{\gamma R T_3} = \sqrt{1.4 \times 287 \times 482.37}$$

$$= \boxed{440.25 \text{ m/s}}$$

Scanned by CamScanner

Given,

$$\frac{p_{04}}{p_{03}} = 1 - 0.1401 = 0.8599$$

For $p_{04}/p_{03} = 0.8599$, from the normal shock table,

$$\frac{p_4}{p_3} = 3.1654$$

But the pressure p_3 ahead of the reflected shock is equal to the pressure p_2 behind the incident shock. Therefore,

$$p_4 = 3.1654 \times p_2 = 3.1654 \times 4.045$$
$$= 12.804 \text{ atm}$$
$$= 12.804 \times 101325$$
$$= \boxed{1.297 \text{ MPa}}$$

5.8 CENTRED EXPANSION WAVE

If, instead of moving the piston into the fluid, the piston is withdrawn, an expansion wave is produced. The wave diagram of such a motion is shown in Fig. 5.10. The front of the expansion wave travels with speed a_4 into the undisturbed fluid, i.e. in the direction opposite to the piston and fluid motion (note any isentropic wave will travel at the speed of sound in the undisturbed fluid).

The wave speed in the portions of the wave behind the front is given by (Section 3.9 of Ref. 1)

$$C_e = a_4 + \frac{\gamma + 1}{2} V$$

Here, $V < 0$ and, therefore, C_e decreases continuously through the wave. The fan of straight lines shown are lines of constant C_e, and thus of constant V and ρ. These lines are called *characteristics*.

With increasing time the fan becomes wider, i.e. the gradients of V, ρ, etc. become smaller. Thus, the wave *remains isentropic*. The terminating characteristic is given by

$$\frac{x}{t} = C_{e3} = a_4 - \frac{\gamma + 1}{2} |V_p|$$

and slopes to right or left, depending on whether $a_4 >$ or $< \frac{\gamma + 1}{2} |V_p|$.

Scanned by CamScanner

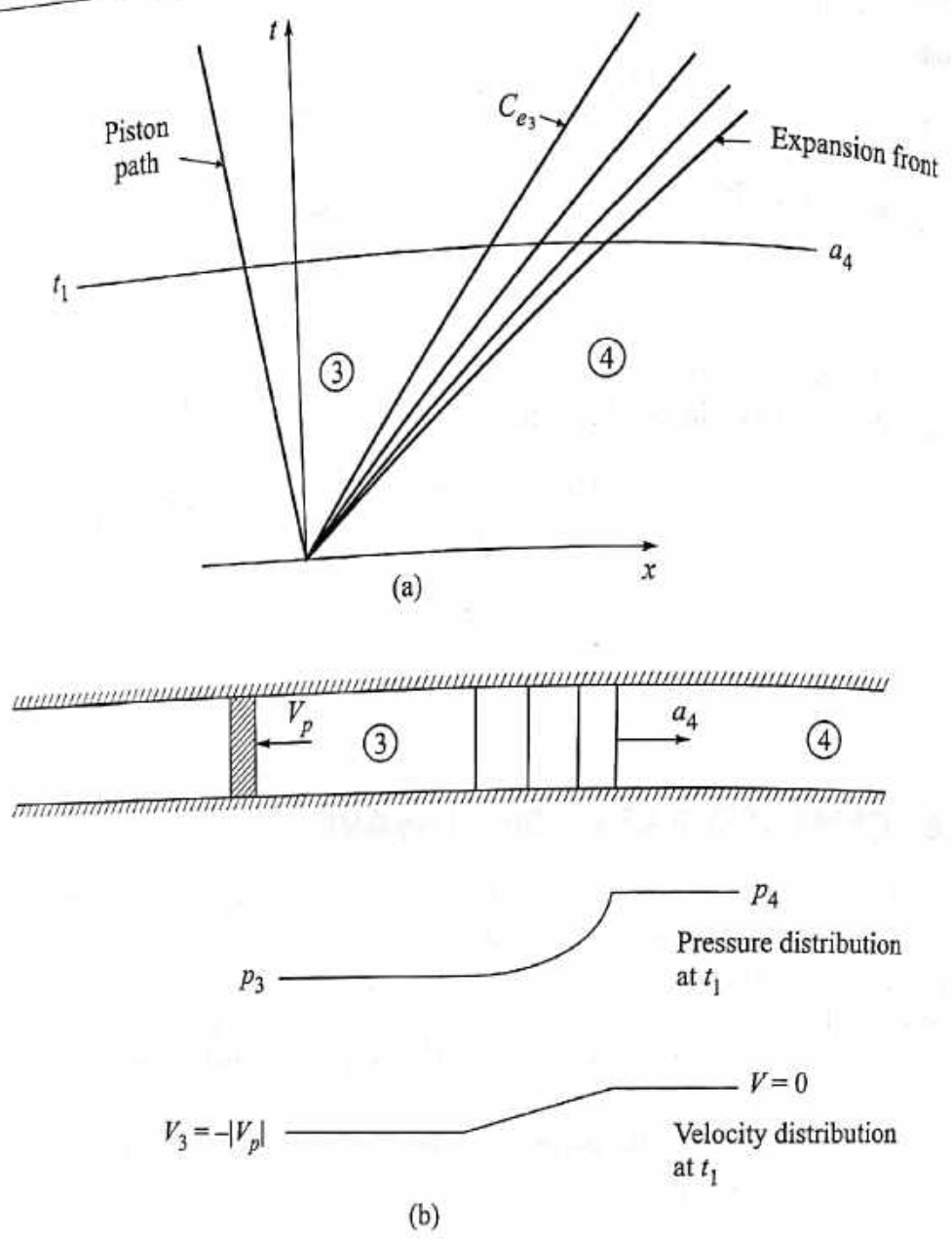


Fig. 5.10 (a) x–t diagram of the centred expansion,
(b) variation of pressure and velocity across the expansion zone.

Between the terminating characteristic and piston, the fluid properties have the uniform values p_3, ρ_3, a_3, etc. For a perfect gas, they are given by the isentropic relations

$$\frac{\rho_3}{\rho_4} = \left(1 - \frac{\gamma - 1}{2}\frac{|V_p|}{a_4}\right)^{2/(\gamma-1)} \tag{5.53}$$

$$\frac{p_3}{p_4} = \left(1 - \frac{\gamma - 1}{2}\frac{|V_p|}{a_4}\right)^{2\gamma/(\gamma-1)} \tag{5.54}$$

The density ratio ρ_3/ρ_4 and pressure ratio p_3/p_4 across a centered expansion wave, in a perfect gas, given in Eqs. (5.53) and (5.54) can be derived as follows.

Scanned by CamScanner

Let us consider a single ray of the expansion fan, as shown in the Fig. 5.11.

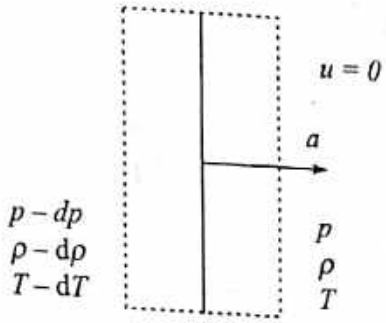


Figure 5.11 Flow properties on either side of an expansion ray.

By continuity equation, the mass flow across an acoustic wave is

$$\rho a = (\rho - d\rho)\,(a - du)$$

$$\rho a = \rho a - \rho du - a d\rho + dp du$$

The product term $dp du \approx 0$, since both $d\rho$ and du are very small. Thus

$$\rho a = \rho a - \rho du - a d\rho$$

$$du = -a\frac{d\rho}{\rho}$$

The velocity decreases from V_4 to V_3, across the expansion waves, thus

$$\sum du = \int_0^u du = -\int_{\rho_4}^{\rho_3} a\frac{d\rho}{\rho}$$

By process relation,

$$\frac{a}{a_4} = \left(\frac{\rho}{\rho_4}\right)^{(\gamma-1)/2}$$

Therefore,

$$u = -\frac{a_4}{(\rho_4)^{(\gamma-1)/2}}\int_{\rho_4}^{\rho_3}\rho^{(\gamma-3)/2}d\rho$$

$$= -a_4\frac{1}{(\rho_4)^{(\gamma-1)/2}}\left[\rho^{(\gamma-1)/2}\times\frac{2}{(\gamma-1)}\right]_{\rho_4}^{\rho_3}$$

$$= -\frac{2a_4}{\gamma-1}\left[\left(\frac{\rho_3}{\rho_4}\right)^{(\gamma-1)/2} - 1\right]$$

$$1 - \frac{\gamma-1}{2}\frac{u}{a_4} = \left(\frac{\rho_3}{\rho_4}\right)^{(\gamma-1)/2}$$

Scanned by CamScanner

$$= \frac{a_3}{a_4}$$

Thus,

$$\left[1 - \frac{\gamma - 1}{2}\frac{u_3}{a_4}\right] = \left(\frac{\rho_3}{\rho_4}\right)^{(\gamma-1)/2}$$

where $u = u_3$. This gives

$$\boxed{\frac{\rho_3}{\rho_4} = \left(1 - \frac{\gamma - 1}{2}\frac{u_3}{a_4}\right)^{2/(\gamma-1)}}$$

For the case of piston problem, $u_3 = |V_p|$, thus

$$\boxed{\frac{\rho_3}{\rho_4} = \left(1 - \frac{\gamma - 1}{2}\frac{|V_p|}{a_4}\right)^{2/(\gamma-1)}}$$

By isentropic relation,

$$\frac{p_3}{\rho_3^\gamma} = \frac{p_4}{\rho_4^\gamma}$$

$$\frac{p_3}{p_4} = \left(\frac{\rho_3}{\rho_4}\right)^\gamma$$

$$= \left(1 - \frac{(\gamma - 1)}{2}\frac{|V_p|}{a_4}\right)^{2\gamma/(\gamma-1)}$$

ALITER

The pressure ratio p_3/p_4 and density ratio ρ_3/ρ_4 across the expansion fan in a perfect gas can be expressed in terms of $|V_p|/a_4$ can also be obtained as follows.

The leading characteristic of the expansion fan travels with speed of sound a_4 corresponding to the temperature in zone 4. The terminating characteristic travel with speed C_{e3}. Thus

$$C_{e3} = a_4 - \frac{\gamma + 1}{2}|V_p|$$

$$C_{e4} = a_4$$

The total density across the expansion fan is invariant, thus $\rho_{03} = \rho_{04}$. Therefore,

$$\frac{\rho_3}{\rho_{03}} = \left(1 + \frac{\gamma - 1}{2}\frac{C_{e3}^2}{a_4^2}\right)^{\frac{1}{\gamma-1}}$$

Scanned by CamScanner

$$= \left[1 + \frac{\gamma-1}{2}\left(a_4 - \frac{\gamma+1}{2}|V_p|\right)^2 \frac{1}{a_4^2}\right]^{\frac{1}{\gamma-1}}$$

$$= \left[1 + \frac{\gamma-1}{2}\left(1 - 2\frac{\gamma+1}{2}\frac{|V_p|}{a_4}\right)\right]^{\frac{1}{\gamma-1}}$$

$$= \left(1 + \frac{\gamma-1}{2} - \frac{(\gamma-1)}{2}(\gamma+1)\frac{|V_p|}{a_4}\right)^{\frac{1}{\gamma-1}}$$

$$= \left(\frac{\gamma+1}{2} - \frac{(\gamma-1)}{2}(\gamma+1)\frac{|V_p|}{a_4}\right)^{\frac{1}{\gamma-1}}$$

$$= \left(\frac{\gamma+1}{2}\right)^{\frac{1}{\gamma-1}}\left(1 - \frac{(\gamma-1)}{2}\frac{|V_p|}{a_4}\right)^{\frac{2}{\gamma-1}}$$

$$\frac{\rho_4}{\rho_{04}} = \left(1 + \frac{\gamma-1}{2}\frac{C_{e4}^2}{a_4^2}\right)^{\frac{1}{\gamma-1}}$$

$$= \left(1 + \frac{\gamma-1}{2}\right)^{\frac{1}{\gamma-1}}$$

$$= \left(\frac{\gamma+1}{2}\right)^{\frac{1}{\gamma-1}}$$

Therefore,

$$\frac{\rho_3}{\rho_4} = \frac{\rho_3/\rho_{03}}{\rho_4/\rho_{04}}$$

$$= \frac{\left(\frac{\gamma+1}{2}\right)^{\frac{1}{\gamma-1}}\left[1 - \frac{(\gamma-1)}{2}\frac{|V_p|}{a_4}\right]^{\frac{2}{\gamma-1}}}{\left(\frac{\gamma+1}{2}\right)^{\frac{1}{\gamma-1}}}$$

$$\boxed{= \left[1 - \frac{(\gamma-1)}{2}\frac{|V_p|}{a_4}\right]^{\frac{2}{\gamma-1}}}$$

Scanned by CamScanner

By isentropic relation,

$$\frac{p_3}{\rho_3^\gamma} = \frac{p_4}{\rho_4^\gamma}$$

$$\frac{p_3}{p_4} = \left(\frac{\rho_3}{\rho_4}\right)^\gamma$$

$$= \left[1 - \frac{(\gamma-1)}{2}\frac{|V_p|}{a_4}\right]^{\frac{2\gamma}{\gamma-1}}$$

The pressure ratio p_3/p_4 is called the *strength of the expansion fan*. The maximum expansion that can be obtained corresponds to $\rho_3 = 0$, and is obtained when $|V_p| = 2a_4/(\gamma - 1)$. For this case, $p_3 = T_3 = 0$, i.e. all the fluid energy is converted into kinetic energy of flow. If the piston velocity is more than this limiting value, it has no further effect on the flow.

EXAMPLE 5.12 If the piston in the device shown in Fig. 5.12 is withdrawn suddenly with a speed of 120 m/s, determine the temperature of the air traversed by the expansion caused due to the piston motion, before reflection from the end wall. Also, find whether the expansion waves will slant to the right or left.



Fig. 5.12 Example 5.12.

Solution Given, $T_4 = 30 + 273.15 = 303.15$ K, $V_p = 120$ m/s. Therefore, the speed of the leading ray of the expansion (refer Fig. 5.10) is

$$a_4 = \sqrt{1.4 \times 287 \times 303.15}$$
$$= 349 \text{ m/s}$$

The speed of terminating characteristic is given by

$$a_3 = a_4 - \frac{\gamma+1}{2}|V_p|$$

Thus,

$$a_3 = 349 - \frac{2.4}{2} \times 120$$
$$= 205 \text{ m/s}$$

But $a_3 = \sqrt{\gamma R T_3}$. Therefore, the temperature T_3 of the air traversed by the expansion waves is

$$T_3 = \frac{205^2}{1.4 \times 287}$$
$$= 104.59 \text{ K}$$

Scanned by CamScanner

$$= 104.59 - 273.15$$

$$= \boxed{-168.56°C}$$

In this case, $a_4 > \frac{\gamma+1}{2}|V_p|$. Therefore, the expansion waves will slant to the right.

EXAMPLE 5.13 The piston cylinder device, shown in Fig. 5.13, initially has stagnant air at 300 K and 1 atm. If the piston is suddenly withdrawn at 200 m/s, determine the strength of the expansion caused by the piston movement.

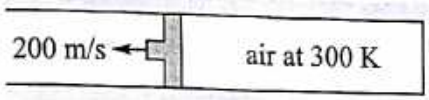


Fig. 5.13 Example 5.13.

Solution Given, $T_4 = 300$ K, therefore (refer Fig. 5.10),

$$a_4 = \sqrt{\gamma R T_4} = \sqrt{1.4 \times 287 \times 300}$$

$$= 347.19 \text{ m/s}$$

The expansion strength is given by

$$\frac{p_4}{p_3} = \left(1 - \frac{\gamma-1}{2}\frac{|V_p|}{a_4}\right)^{2\gamma/(\gamma-1)}$$

Thus,

$$\frac{p_4}{p_3} = \left(1 - 0.2 \times \frac{200}{347.19}\right)^7$$

$$= \boxed{0.4245}$$

5.9 SHOCK TUBE

The shock tube is a device to produce high speed flow with high temperatures, by traversing normal shock waves which are generated by the rupture of a diaphragm separating a high-pressure gas from a low-pressure gas. The shock tube is a very useful research tool for investigating not only the shock phenomena, but also the behaviour of materials and objects when subjected to extreme conditions of pressure and temperature. Thus, problems like the kinetics of a chemical reaction taking place at high temperature, the performance, for example, of a body during re-entry into the earth's atmosphere and so on, can be studied with shock tube.

In general, shock tubes are thick walled tubes made out of stainless steel or aluminium alloy with circular or square or rectangular cross-section, with a very smooth inner surface, which is divided by a membrane or diaphragm into two

Scanned by CamScanner

chambers in which the pressures are different. When the membrane is suddenly removed, a wave motion is set up. A shock tube and fluid motion in it are shown in Fig. 5.14. The studies made in the preceding sections, for shock waves and expansion wave, may be used to analyze flow conditions in the shock tube.

For shock tube operation, it is of prime importance to develop an expression for shock strength p_2/p_1 as a function of the diaphragm pressure ratio p_4/p_1. Once the shock strength is known, all other flow quantities are easily determined from the normal shock relations.

A diaphragm at $x = 0$ separates the high-pressure (compression) and low-pressure (expansion) regions in a tube, as shown in Fig. 5.14(b).

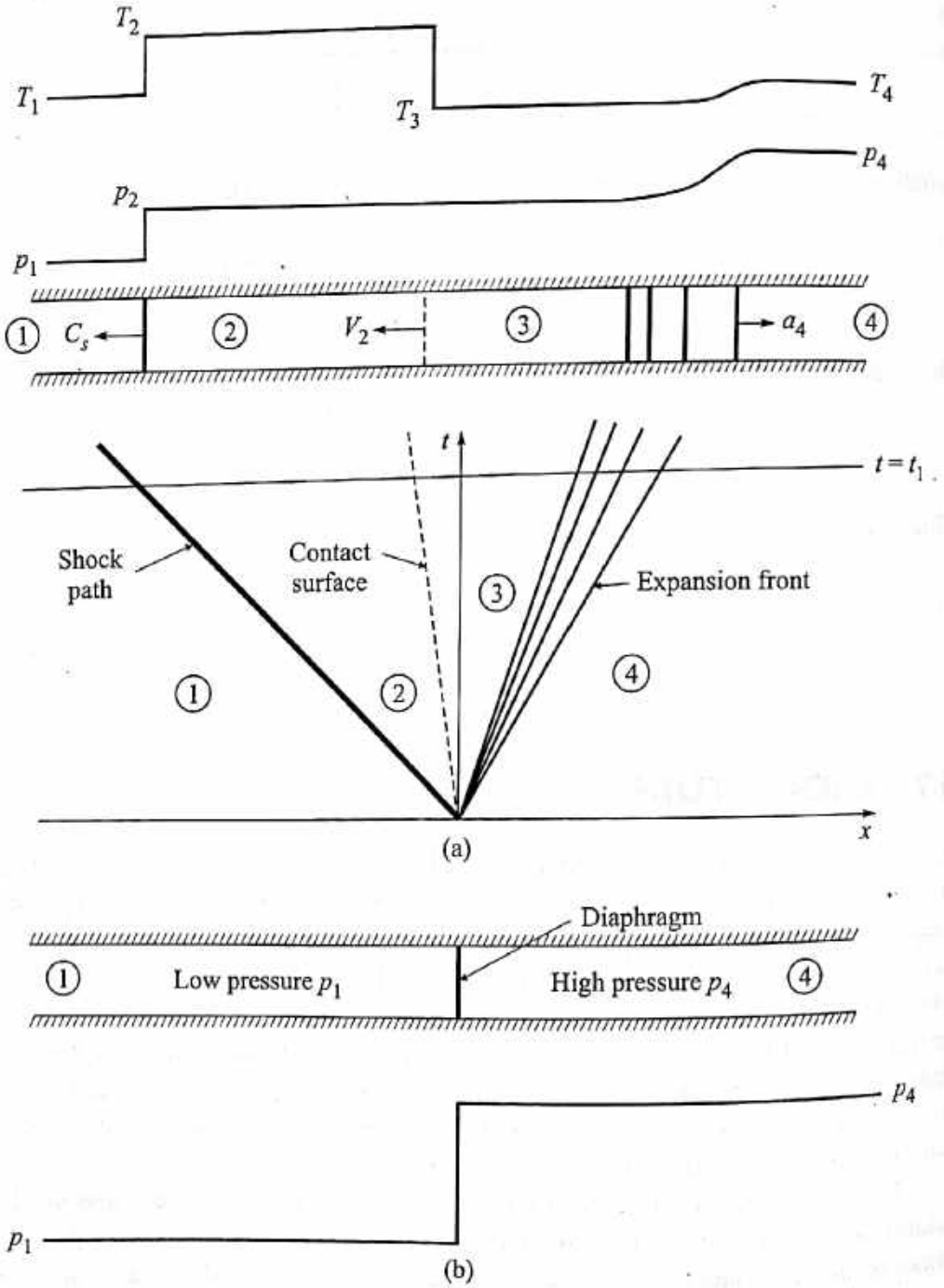


Fig. 5.14 Flow motion in a shock tube.

Scanned by CamScanner

The basic parameter of the shock tube is the *diaphragm pressure ratio* p_4/p_1. The two chambers may be at different temperatures, T_1 and T_4, and may contain different gases with gas constants R_1 and R_4.

At time $t = 0$ when the diaphragm is burst, the pressure distribution is a step as illustrated in Fig. 5.14(b). The shock wave propagates into the low-pressure chamber with speed C_s, and an expansion wave propagates into the high-pressure chamber with the speed a_4 at its front.

The condition of the fluid which is traversed by the shock is denoted by (2), and that of the fluid traversed by the expansion wave is denoted by (3). The interface between the regions 2 and 3 [Fig. 5.14(a)] is called the *contact surface*. It makes the boundary between the fluids which were initially on either side of the diaphragm. Neglecting diffusion, the high-pressure gas and low-pressure gas do not mix, but are permanently separated by the contact surface, which is like the front of a piston, driving into the low-pressure chamber.

On either side of the contact surface, the temperatures, T_2 and T_3, and the densities, ρ_2 and ρ_3, may be different, but it is necessary that the pressure and fluid velocity be the same, i.e.

$$p_2 = p_3, \quad V_2 = V_3$$

Thus, V_2 is the velocity of the contact surface. With the above two conditions, the shock strength p_2/p_1, and the expansion strength p_3/p_4, in terms of the diaphragm pressure ratio p_4/p_1 are determined as follows:

The values of V_2 and V_3 may be calculated from Eqs. (5.46), (5.53), and (5.54), which are for shock and expansion waves. By rearranging the above equations, and with subscripts to correspond to the present case, we get

$$V_2 = a_1\left(\frac{p_2}{p_1} - 1\right)\left[\frac{2/\gamma_1}{(\gamma_1+1)p_2/p_1 + (\gamma_1 - 1)}\right]^{1/2} \tag{5.55}$$

$$V_3 = \frac{2a_4}{\gamma_4 - 1}\left[1 - \left(\frac{p_3}{p_4}\right)^{(\gamma_4-1)/2\gamma_4}\right] \tag{5.56}$$

But $V_2 = V_3$ and $p_2 = p_3$; therefore, from Eqs. (5.55) and (5.56) we can write the basic shock tube equation as

$$\frac{p_4}{p_1} = \frac{p_2}{p_1}\left[1 - \frac{(\gamma_4 - 1)\left(\frac{a_1}{a_4}\right)\left(\frac{p_2}{p_1} - 1\right)}{\sqrt{2\gamma_1}\sqrt{2\gamma_1 + (\gamma_1+1)(p_2/p_1 - 1)}}\right]^{-2\gamma_4/(\gamma_4-1)} \tag{5.57}$$

Equation (5.57) gives the shock strength p_2/p_1 as a function of the diaphragm pressure ratio p_4/p_1. The expansion strength is obtained from

$$\frac{p_3}{p_4} = \frac{p_3}{p_1}\frac{p_1}{p_4} = \frac{p_2/p_1}{p_4/p_1} \tag{5.58}$$

From the above shock tube relations it is evident that once the shock strength p_2/p_1 is known, all other flow quantities can be determined from the normal shock relations.

Scanned by CamScanner

The thermodynamic properties immediately behind the expansion fan can be found from the isentropic relations

$$\frac{p_3}{p_4} = \left(\frac{\rho_3}{\rho_4}\right)^{\gamma_4} = \left(\frac{T_3}{T_4}\right)^{\gamma_4/(\gamma_4-1)}$$

$$\frac{T_3}{T_4} = \left(\frac{p_3}{p_4}\right)^{(\gamma_4-1)/\gamma_4} = \left(\frac{p_2/p_1}{p_4/p_1}\right)^{(\gamma_4-1)/\gamma_4} \tag{5.59}$$

The temperature T_2 behind the shock is given by Eq. (5.43), as

$$\frac{T_2}{T_1} = \frac{1+\dfrac{\gamma_1-1}{\gamma_1+1}\dfrac{p_2}{p_1}}{1+\dfrac{\gamma_1-1}{\gamma_1+1}\dfrac{p_1}{p_2}} \tag{5.60}$$

The velocity of contact surface may be obtained from either Eq. (5.55) or Eq. (5.56).

Applications

The shock tube being a device capable of producing established flow with uniform temperatures and pressures at high values, which cannot be achieved with conventional tunnels, finds for instance, application in numerous fields in science and engineering.

1. The uniform flow behind the shock wave may be used as a short duration wind tunnel. In this role, the shock tube is similar to an intermittent or blow-down tunnel, but the duration of flow is much shorter, usually of the order of a millisecond. But the operating conditions (particularly the high stagnation enthalpies) which are possible, cannot be easily obtained with other types of facility.
2. The abrupt changes of flow condition at the shock front may be utilized for studying transient aerodynamic effects, and for studies of dynamic and thermal response.
3. Shock tubes can also be used for studies on relaxation effects, reaction rates, dissociation, ionization, etc.

Finally, note that in the shock tube relations we use a different γ for every flow zone. This is because in most of the applications, the temperatures experienced by the gas at these zones are appreciably above the level mentioned in Section 2.5, describing perfect gas. Therefore, the gas does not behave as perfect gas, and hence γ takes different values corresponding to the local temperature.

EXAMPLE 5.14 A shock tube may be used as a short-duration wind tunnel by utilizing the flow behind the shock wave. Show that, in terms of the shock speed $M_s = C_s/a_1$, the density ratio $\eta = \rho_2/\rho_1$, and conditions in the expansion chamber (1), the flow conditions behind the shock in region (2) are given by the following:

Scanned by CamScanner

(a) $\dfrac{p_2}{p_1} = 1 + \gamma_1 M_s^2\left(1 - \dfrac{1}{\eta}\right)$

(b) $\dfrac{h_2}{h_1} = 1 + \dfrac{\gamma_1 - 1}{2} M_s^2\left(1 - \dfrac{1}{\eta^2}\right)$

(c) $\dfrac{V_p}{a_1} = M_s\left(1 - \dfrac{1}{\eta}\right)$

(d) $\dfrac{h_{02}}{h_1} = 1 + (\gamma_1 - 1) M_s^2\left(1 - \dfrac{1}{\eta}\right)$

Solution The flow field is shown in Fig. 5.15(a).

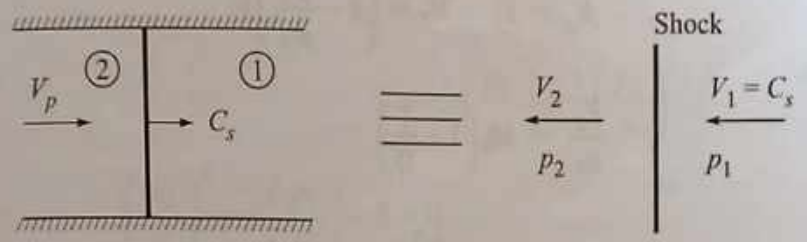


Fig. 5.15(a) Example 5.14.

(a) By the momentum equation,

$$p_2 - p_1 = \rho_1 V_1^2 - \rho_2 V_2^2$$

From the continuity equation, we have

$$\rho_1 V_1 = \rho_2 V_2, \quad \frac{V_2}{V_1} = \frac{\rho_1}{\rho_2} = \frac{1}{\eta}$$

$$p_2 - p_1 = \rho_1 V_1 (V_1 - V_2) = \rho_1 V_1^2\left(1 - \frac{V_2}{V_1}\right) = \rho_1 V_1^2\left(1 - \frac{1}{\eta}\right)$$

Dividing throughout by p_1, we get

$$\frac{p_2}{p_1} - 1 = \frac{\gamma_1 \rho_1}{\gamma_1 p_1} V_1^2\left(1 - \frac{1}{\eta}\right) = \gamma_1 M_s^2\left(1 - \frac{1}{\eta}\right)$$

since $\gamma p/\rho = a^2$. Therefore,

$$\frac{p_2}{p_1} = 1 + \gamma_1 M_s^2\left(1 - \frac{1}{\eta}\right)$$

(b) By the energy equation,

$$h_1 + \frac{V_1^2}{2} = h_2 + \frac{V_2^2}{2}$$

$$h_2 - h_1 = \frac{V_1^2 - V_2^2}{2} = \frac{V_1^2}{2}\left(1 - \frac{V_2^2}{V_1^2}\right) = \frac{a_1^2}{2} M_s^2\left(1 - \frac{1}{\eta^2}\right)$$

Dividing throughout by h_1, we get

$$\frac{h_2}{h_1} = 1 + \frac{a_1^2}{2 h_1} M_s^2\left(1 - \frac{1}{\eta^2}\right)$$

Scanned by CamScanner

h_1 can be written as

$$h_1 = c_p T_1 = \frac{\gamma_1}{\gamma_1 - 1} RT_1 = \frac{a_1^2}{\gamma_1 - 1}$$

Therefore,

$$\frac{h_2}{h_1} = 1 + \frac{\gamma_1 - 1}{2} M_s^2 \left(1 - \frac{1}{\eta^2}\right)$$

(c) By continuity,

$$\rho_1 V_1 = \rho_2 V_2, \quad V_2 = \frac{\rho_1}{\rho_2} V_1$$

The piston speed

$$V_p = V_1 - V_2 = \left(1 - \frac{\rho_1}{\rho_2}\right) V_1$$

Therefore,

$$\frac{V_p}{a_1} = M_s \left(1 - \frac{1}{\eta}\right)$$

(d)

$$h_{02} = h_2 + \frac{V_p^2}{2}$$

$$\frac{h_{02}}{h_1} = \frac{h_2}{h_1} + \frac{1}{2}\frac{V_p^2}{h_1} = \frac{h_2}{h_1} + \frac{\gamma_1 - 1}{2}\frac{V_p^2}{a_1^2}$$

$$= 1 + \frac{\gamma_1 - 1}{2} M_s^2 \left(1 - \frac{1}{\eta^2}\right) + \frac{\gamma_1 - 1}{2} M_s^2 \left(1 - \frac{1}{\eta}\right)^2$$

$$\frac{h_{02}}{h_1} = 1 + (\gamma_1 - 1) M_s^2 \left(1 - \frac{1}{\eta}\right)$$

Refer Fig. 5.15(b) for the above solution.

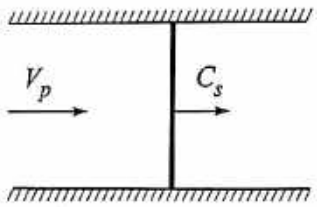


Fig. 5.15(b) Example 5.14.

EXAMPLE 5.15 If a shock tube filled with air at 300 K and 400 K in its low- and high-pressure chambers, respectively, has to generate a shock to traverse air to attain 600 K, what should be the shock strength? Also, determine the velocity of the contact surface and the shock speed.

Solution Given $T_1 = 300$ K, $T_4 = 400$ K, $T_2 = 600$ K. Also, $\gamma_1 = \gamma_4 = 1.4$. By Eq. (5.60),

$$\frac{T_2}{T_1} = \frac{1 + \dfrac{\gamma_1 - 1}{\gamma_1 + 1}\dfrac{p_2}{p_1}}{1 + \dfrac{\gamma_1 - 1}{\gamma_1 + 1}\dfrac{p_1}{p_2}}$$

Scanned by CamScanner

$$2 = \frac{1 + \frac{0.4}{1.4}\frac{p_2}{p_1}}{1 + \frac{0.4}{1.4}\frac{p_1}{p_2}}$$

$$2\left(1 + \frac{1}{6}\frac{p_1}{p_2}\right) = 1 + \frac{1}{6}\frac{p_2}{p_1}$$

$$2\left(6 + \frac{p_1}{p_2}\right) = 6 + \frac{p_2}{p_1}$$

$$\frac{p_1}{p_2} = -6 + 3 + \frac{1}{2}\frac{p_2}{p_1}$$

$$1 = -3\left(\frac{p_2}{p_1}\right) + \frac{1}{2}\left(\frac{p_2}{p_1}\right)^2$$

$$\left(\frac{p_2}{p_1}\right)^2 - 6\left(\frac{p_2}{p_1}\right) - 2 = 0$$

$$\frac{p_2}{p_1} = \frac{6 \pm \sqrt{36+8}}{2}$$

$$= \frac{6 + 6.633}{2} = 6.32$$

Note That the negative values of p_2/p_1 is not a feasible solution.
Thus the shock strength is

$$\frac{\Delta p}{p_1} = \frac{p_2 - p_1}{p_1}$$

$$= \frac{p_2}{p_1} - 1$$

$$= 6.32 - 1$$

$$= \boxed{5.32}$$

The contact surface speed, by Eq. (5.55), is

$$V_2 = a_1\left(\frac{p_2}{p_1} - 1\right)\left[\frac{2/\gamma_1}{(\gamma_1 + 1)\frac{p_2}{p_1} + (\gamma_1 - 1)}\right]^{1/2}$$

$$= \sqrt{1.4 \times 287 \times 300} \times (6.32 - 1) \times \left[\frac{2/1.4}{2.4 \times 6.32 + 0.4}\right]^{1/2}$$

Scanned by CamScanner

$$= 347.19 \times 5.32 \times \sqrt{\frac{1.429}{15.568}}$$

$$= \boxed{559.60 \text{ m/s}}$$

By Eq. (5.45), the shock speed is

$$C_s = a_1 \sqrt{\frac{\gamma_1 + 1}{2\gamma_1}\left(\frac{p_2}{p_1} - 1\right) + 1}$$

$$= 347.19 \times \sqrt{\frac{2.4}{2.8}(6.32 - 1) + 1}$$

$$= \boxed{818.66 \text{ m/s}}$$

EXAMPLE 5.16 A shock tube has still air at 0.1 atm and 270 K in its low-pressure chamber. A normal shock generated, by rupturing the diaphragm separating the high-pressure chamber from the low-pressure chamber, moves at 2100 m/s. Determine the pressure in the high-pressure chamber at the time of diaphragm rupture, and the pressure, temperature and Mach number of the air traversed by the shock, treating air as a perfect gas.

Solution Let subscripts 1 and 2 refer to the state ahead of and behind the shock, respectively.
Given, $p_1 = 0.1$ atm, $T_1 = 270$ K. The shock speed is $C_s = 2100$ m/s.
The speed of sound ahead of the shock is

$$a_1 = \sqrt{\gamma RT}$$

$$= \sqrt{1.4 \times 287 \times 270}$$

$$= 329.37 \text{ m/s}$$

The shock Mach number is

$$M_s = \frac{C_s}{a_1}$$

$$= \frac{2100}{329.37}$$

$$= 6.38$$

For $M_s = 6.38$, from normal shock table,

$$\frac{p_{02}}{p_{01}} = 0.023$$

Therefore, the pressure in the high-pressure chamber is

$$p_{01} = \frac{0.1}{0.023}$$

Scanned by CamScanner

$$= \boxed{4.35\,\text{atm}}$$

By Eq. (5.48c),

$$C_s = a_1 \left(\frac{\gamma+1}{2\gamma} \frac{p_2}{p_1} \right)^{1/2}$$

Therefore,

$$\left(\frac{\gamma+1}{2\gamma} \frac{p_2}{p_1} \right)^{1/2} = \frac{C_s}{a_1}$$

$$\left(\frac{\gamma+1}{2\gamma} \frac{p_2}{p_1} \right) = 6.38^2$$

$$\frac{p_2}{p_1} = 6.38^2 \times \left(\frac{2 \times 1.4}{1+1.4} \right)$$

$$= 47.49$$

$$p_2 = 47.49 \times 0.1$$

$$= \boxed{4.749\,\text{atm}}$$

By Eq. (5.48a),

$$\frac{T_2}{T_1} = \left(\frac{\gamma-1}{\gamma+1} \right) \left(\frac{p_2}{p_1} \right)$$

$$= \frac{0.4}{2.4} \times 47.49$$

$$= 7.915$$

$$T_2 = 7.915\, T_1$$

$$= 7.915 \times 270$$

$$= \boxed{2137\,\text{K}}$$

By Eq. (5.48d),

$$V_2 = V_p = a_1 \left(\frac{2}{\gamma(\gamma+1)} \frac{p_2}{p_1} \right)^{1/2}$$

$$= 329.37 \left(\frac{2}{1.4 \times 2.4} \times 47.49 \right)^{1/2}$$

$$= 1751.18 \text{ m/s}$$

Scanned by CamScanner

The Mach number of the flow traversed by the shock is

$$M_2 = \frac{V_2}{a_2}$$

$$= \frac{1751.18}{\sqrt{1.4 \times 287 \times 2137}}$$

$$= 1.89$$

EXAMPLE 5.17 A shock tube is filled with air. The temperature in the low-pressure chamber is atmospheric. (a) If the shock generated by rupturing the diaphragm moves at Mach 10, treating the air traversed by the shock as perfect gas, determine the stagnation temperature of the air behind the shock. (b) What will be the test time available for testing a model located at 8 m from the diaphragm?

Solution (a) Given, $M_s = 10$, $T_1 = 15°C = 288.15$ K, $\gamma = 1.4$.
The speed of sound in the low-pressure chamber is

$$a_1 = \sqrt{\gamma R T_1}$$

$$= \sqrt{1.4 \times 287 \times 288.15}$$

$$= 340.3 \text{ m/s}$$

Thus the shock speed is

$$C_s = M_s a_1$$

$$= 10 \times 340.3$$

$$= 3403 \text{ m/s}$$

The pressure ratio across the shock is

$$\frac{p_2}{p_1} = 1 + \frac{2\gamma}{\gamma + 1}(M_s^2 - 1)$$

$$= 1 + \frac{2 \times 1.4}{1.4 + 1}(10^2 - 1)$$

$$= 116.5$$

For $M_s = 10$, from normal shock table,

$$\frac{\rho_2}{\rho_1} = 5.71429, \quad \frac{T_2}{T_1} = 20.387$$

The flow speed of the field traversed by the shock, by Eq. (5.45), is

$$V_2 = C_s \left(1 - \frac{\rho_1}{\rho_2}\right)$$

Scanned by CamScanner

$$= 3403 \times \left(1 - \frac{1}{5.71429}\right)$$

$$= 2807.48 \text{ m/s}$$

The temperature of air stream traversed by the shock is

$$T_2 = 20.387\, T_1$$

$$= 20.387 \times 288.15$$

$$= 5874.5 \text{ K}$$

The Mach number of the air stream traversed by the shock is

$$M_2 = \frac{V_2}{a_2}$$

$$= \frac{V_2}{\sqrt{\gamma R T_2}}$$

$$= \frac{2807.48}{\sqrt{1.4 \times 287 \times 5874.5}}$$

$$= 1.83$$

From $M_2 = 1.83$, from isentropic table,

$$\frac{T_2}{T_{02}} = 0.599$$

The flow across the shock is adiabatic, hence $T_{02} = T_{01}$. Thus, the stagnation temperature of air behind the shock is

$$T_{02} = \frac{T_2}{0.599}$$

$$= \frac{5874.5}{0.599}$$

$$= \boxed{9807.2 \text{K}}$$

(b) Let l be the distance between the model and the diaphragm. The test time t is equal to $(1/V_2 - 1/C_s)$. Thus

$$t = \frac{l}{V_2} - \frac{l}{C_s}$$

$$= \frac{8}{2807.48} - \frac{8}{3403}$$

$$= \boxed{4.99 \times 10^{-4} s}$$

Scanned by CamScanner

EXAMPLE 5.18 If the shock created by piston motion moves into still air at 23°C causing an enthalpy jump of 2, determine the shock strength and the piston speed.

Solution Let subscripts 1 and 2 refer to the states ahead of and behind the shock, respectively.

Given, $h_2/h_1 = 2$ and $T_1 = 23°C$. Treating the air as perfect gas, we have $h = c_p T$, thus

$$\frac{h_2}{h_1} = \frac{c_p T_2}{c_p T_1} = \frac{T_2}{T_1} = 2$$

For $\frac{T_2}{T_1} = 2$, from normal shock table, we have

$$M_1 = 2.36,\ M_2 = 0.5275,\ \frac{p_2}{p_1} = 6.3312$$

The shock strength is

$$\frac{\Delta p}{p_1} = \frac{p_2 - p_1}{p_1}$$

$$= \frac{p_2}{p_1} - 1$$

$$= 6.3312 - 1$$

$$= \boxed{5.3312}$$

The shock speed is

$$C_s = M_1 a_1$$

$$= M_1 \times \sqrt{\gamma R T_1}$$

$$= 2.36 \times \sqrt{1.4 \times 287 \times 296.15}$$

$$= \boxed{814.09 \text{ m/s}}$$

The piston speed is

$$V_p = C_s - V_2$$

where

$$V_2 = M_2 a_2$$

$$= M_2 \times \sqrt{\gamma R T_2}$$

Scanned by CamScanner

$$= 0.5275 \times \sqrt{1.4 \times 287 \times (2 \times T_1)}$$

$$= 0.5275 \times \sqrt{1.4 \times 287 \times (2 \times 296.15)}$$

$$= 0.5275 \times 487.84$$

$$= 257.33 \text{ m/s}$$

Thus

$$V_p = 814.09 - 257.33$$

$$= \boxed{556.76 \text{ m/s}}$$

5.10 SUMMARY

In this chapter we examined the dynamic and thermodynamic aspects of high-speed flow with normal shocks. The shock may be described as a compression front in a supersonic flow field across which there is abrupt change in flow properties. The flow process through the shock wave is highly irreversible and cannot be approximated as being isentropic. The flow is supersonic upstream of the shock and subsonic downstream of it. Therefore, the flow must change from supersonic to subsonic if a normal shock is to occur. The larger the Mach number before the shock, the stronger the shock will be. In the limiting case of $M_1 = 1$, the shock wave simply becomes a sonic wave. The flow through the shock wave is adiabatic and irreversible.

The conservation of energy principle (Eq. (5.3)) requires that the stagnation enthalpy remain constant across the shock, i.e. $h_{01} = h_{02}$. For ideal gas, $h_0 = c_p T_0$, and hence

$$T_{01} = T_{02} \tag{5.20}$$

That is, the stagnation temperature of a perfect gas also remains constant across the shock. However, it should be noted that the stagnation pressure decreases across the shock because of irreversibilities.

In terms of the speed ratio $M^* = V/a^*$, the Prandtl equation (5.8) can be expressed as

$$M_2^* = \frac{1}{M_1^*} \tag{5.9}$$

This implies that the velocity change across a normal shock must be from supersonic to subsonic and vice versa. But from entropy consideration it can be shown that only the former is the practical solution. Hence, *the Mach number behind a normal shock is always subsonic*. This is a general result, not limited to calorically perfect gases alone.

Scanned by CamScanner

The Mach number behind a normal shock is given by

$$M_2^2 = \frac{1 + \frac{\gamma - 1}{2} M_1^2}{\gamma M_1^2 - \frac{\gamma - 1}{2}} \tag{5.11}$$

The ratios of density, pressure, and temperature across a normal shock are given by

$$\frac{\rho_2}{\rho_1} = \frac{(\gamma + 1) M_1^2}{(\gamma - 1) M_1^2 + 2} \tag{5.13}$$

$$\frac{p_2}{p_1} = 1 + \frac{2\gamma}{\gamma + 1}(M_1^2 - 1) \tag{5.16}$$

$$\frac{T_2}{T_1} = 1 + \frac{2(\gamma - 1)}{(\gamma + 1)^2} \frac{\gamma M_1^2 + 1}{M_1^2} (M_1^2 - 1) \tag{5.18}$$

The entropy change across the shock is given by

$$s_2 - s_1 = c_p \ln \frac{T_2}{T_1} - R \ln \frac{p_2}{p_1}$$

The variations in properties across a normal shock, for the limiting case of $M_1 \to \infty$, in a gas with $\gamma = 1.4$ are

$$\lim_{M_1 \to \infty} M_2 = \sqrt{\frac{\gamma - 1}{2\gamma}} = 0.378$$

$$\lim_{M_1 \to \infty} \frac{\rho_2}{\rho_1} = \frac{\gamma + 1}{\gamma - 1} = 6$$

$$\lim_{M_1 \to \infty} \frac{p_2}{p_1} = \infty$$

$$\lim_{M_1 \to \infty} \frac{T_2}{T_1} = \infty$$

The ratio of stagnation pressures across a normal shock is

$$\frac{p_{02}}{p_{01}} = \left(1 + \frac{2\gamma}{\gamma + 1}(M_1^2 - 1)\right)^{-1/(\gamma - 1)} \left[\frac{(\gamma + 1) M_1^2}{(\gamma - 1) M_1^2 + 2}\right]^{\gamma/(\gamma - 1)} \tag{5.22}$$

The change in flow properties across a normal shock can also be expressed only in terms of thermodynamic variables, without explicit reference to velocity or Mach number, as

$$e_2 - e_1 = \frac{p_1 + p_2}{2}(v_1 - v_2) \tag{5.30}$$

This is called the *Hugoniot equation*. It is a general relation valid for perfect gases, real gases, chemically reacting gases, etc. since there is no assumption made about the type of gas in deriving it.

Scanned by CamScanner

A moving body in a flow field creates disturbances. The motion of these disturbances relative to the fluid is called *wave motion*. The speed of propagation of the disturbances is known as wave speed.

The wave or shock velocity for a perfect gas can be expressed as

$$C_s = a_1\sqrt{\frac{\gamma+1}{2\gamma}\left(\frac{p_2}{p_1}-1\right)+1} \tag{5.45}$$

The fluid velocity behind a moving shock, also called the *mass-motion velocity* V_p, is given by

$$V_p = \frac{a_1}{\gamma}\left(\frac{p_2}{p_1}-1\right)\left(\frac{\frac{2\gamma}{\gamma-1}}{\frac{p_2}{p_1}+\frac{\gamma-1}{\gamma+1}}\right)^{1/2} \tag{5.46}$$

The wave produced by an impulsive withdrawal of the piston is called a *centred expansion wave*. The front of the wave propagates in the direction opposite to the piston and fluid motion. The maximum expansion that can be obtained corresponds to the state with *zero density* behind the terminating characteristic. This situation corresponds to the state where all the fluid energy is converted into kinetic energy of flow.

The shock tube consists of a long duct of constant cross-section divided into two chambers by a diaphragm. The high-pressure chamber is called the driver section and the low-pressure chamber is called the expansion section. The low-pressure gas may be the same as or different from the high-pressure gas. Also, the temperature of the gases at the two chambers may be the same or different. The *basic equation for a shock tube* is

$$\frac{p_4}{p_1} = \frac{p_2}{p_1}\left[1-\frac{(\gamma_4-1)\left(\frac{a_1}{a_4}\right)\left[\frac{p_2}{p_1}-1\right]}{\sqrt{2\gamma_1}\sqrt{2\gamma_1+(\gamma_1+1)(p_2/p_1-1)}}\right]^{-2\gamma_4/(\gamma_4-1)} \tag{5.57}$$

This equation gives the shock strength p_2/p_1 as a function of the diaphragm pressure ratio p_4/p_1. The expansion strength is given by

$$\frac{p_3}{p_4} = \frac{p_2/p_1}{p_4/p_1} \tag{5.58}$$

The shock tube is used for studying unsteady short-duration phenomena in varied fields of aerodynamics, physics and chemistry. Because of the high stagnation enthalpies that are attained, the shock tube provides means to study phenomena such as the thermodynamic properties of gases at high temperatures, dissociation, ionization, and chemical kinetics. Temperatures as high as 8000°C have been attained in shock tubes. The high speed of shock waves necessitates that experimental measurements be accomplished in a very short duration. This demands high-speed photography and optical methods for collection of data.

Scanned by CamScanner

The flow process across a normal shock is shown to be adiabatic. But we have seen that there are large gradients of flow properties across the shock. We also know that these severe gradients produce viscous stress and heat transfer, i.e. nonequilibrium conditions inside the shock. No wonder then we ask as to how the process across a shock can be treated as adiabatic. The answer to this question is the following: The shock is a very thin compression front with thickness of the order of 10^{-5} cm. Also, the flow crosses the shock wave with a very high velocity. The combination of this high velocity of the flow and extremely small thickness of the wave makes the fluid particles cross the wave in an infinitesimal time, thereby ruling out the possibility of any exchange of energy of the fluid particles with the surroundings. In other words, even though the fluid particles attain high temperature while passing through the shock, they do not have any significant energy exchange with the surroundings since they have only an infinitesimal contact time with the surroundings, while passing through the shock.

It is interesting to recall that the flow through a normal shock is one-dimensional. The change of flow properties occurs in the same direction as that of the flow. The flow properties and their derivatives across a shock wave are discontinuous. Shock waves propagate faster than Mach waves do, and they show large gradients in pressure, temperature, and density. Finally, we should realize that the formation of proper normal shock (the shock front which is strictly normal to the flow) is possible only in internal flows such as flow in a wind tunnel and shock-tubes. Normal shocks formed without a solid confinement are only close to normal shock and are not strictly normal to the flow.

PROBLEMS

1. A normal shock moves at a constant speed of 500 m/s into still air at 0°C and 0.7 atm. Determine the static and stagnation conditions present in the air after passage of the wave.

   [**Ans.** $p = 1.745$ atm, $T = 362.27$ K, $V = 233.9$ m/s, $p_t = 2.25$ atm, $T_t = 389.5$ K]

2. A horizontal tube contains stationary air at 1 atm and 300 K. The left end of the tube is closed by a movable piston, which at time $t = 0$ is moved impulsively at a speed of $V_p = 100$ m/s to the right. Find the wave speed and the pressure on the face of the piston.

   [**Ans.** $C_s = 413$ m/s, $p_{\text{piston face}} = 1.505 \times 10^5$ N/m^2]

3. A horizontal tube contains stationary air at 1 atm and 300 K. The left end of the tube is closed by a movable piston, which at time $t = 0$ is moved impulsively at a speed of 120 m/s to the left. Find the pressure on the face of the piston, if (a) the piston motion is to the left, and (b) the piston motion is to the right.

   [**Ans.** (a) 0.606 atm; (b) 1.595 atm]

Scanned by CamScanner

4. Consider a pipe in which air at 300 K and 1.50×10^5 N/m^2 flows uniformly with a speed of 150 m/s. The end of the pipe is suddenly closed by a valve, and a shock wave is propagated back into the pipe. Compute the speed of the wave and the pressure and temperature of the air which has been brought to rest.

[**Ans.** $C_s = 298.5$ m/s, $p_{02} = 2.66 \times 10^5$ N/m^2, $T_{02} = 355.5$ K]

5. A shock wave is formed in a tube of initially stagnant air (state 1) by the sudden acceleration of a piston to the speed V_p. Show that the following relation holds between the dimensionless shock speed C_s/a_1 and the dimensionless piston speed V_p/a_1:

$$\frac{C_s}{a_1} = \frac{\gamma+1}{4}\frac{V_p}{a_1} + \left[1 + \frac{1}{4}\left(\frac{\gamma+1}{2}\right)^2 \left(\frac{V_p}{a_1}\right)^2\right]^{1/2}$$

Determine the limiting form of this relation as

$$\frac{V_p}{a_1} \to \infty, \quad \frac{V_p}{a_1} \to 0$$

$$\left[\textbf{Ans.}\ \text{As}\ \frac{V_p}{a_1} \to \infty, \frac{C_s}{a_1} \to \infty; \text{as}\ \frac{V_p}{a_1} \to 0, \frac{C_s}{a_1} \to 1\right]$$

6. A horizontal tube contains stationary air at 1 atm and at a temperature such that the velocity of sound is 360 m/s. It has a movable piston which at instant $t = 0$ is withdrawn impulsively from the tube with a constant velocity of 300 m/s. If the piston is suddenly stopped after a travel of 30 m, a shock runs into the tube. Calculate (a) the pressure on the face of the piston, and (b) the time for the shock to hit the terminating characteristic after stoppage of the piston. Draw the x–t diagram for the above process, showing the piston path, the shock path, the expansion wave and the particle path.

[**Ans.** (a) 0.969 atm; (b) 0.0566 s]

7. Calculate the pressure required in the driver (or higher pressure) section of a shock tube to produce a shock of $M_s = 5.0$ in the driven section which contains air (perfect gas) at an initial temperature of 27°C and pressure 0.01 atm if the driver gas is air at 27°C, $\gamma = 1.4$, $R = 287$ m^2/s^2-K.

[**Ans.** 2.26×10^4 atm]

8. If the flow behind the shock wave in Problem 7 is to be used as a short duration wind tunnel flow, calculate (a) the static temperature and pressure, (b) the stagnation temperature and pressure, (c) the testing time available, given that the test-section is 8 m from the bursting diaphragm (assume that the contact surface is disturbance which limits the testing time), and (d) the angle of a Mach line in this flow.

[**Ans.** (a) 1740 K, 0.29 atm; (b) 2699 K, 1.349 atm; (c) 1.15×10^{-3} s; (d) 37°]

Scanned by CamScanner

9. If the conditions behind the shock after its reflection from the end of the tube are denoted by (5) and the shock speed relative to the tube U_R, show that, in terms of the density ratios $\eta = \rho_2/\rho_1$ and $\zeta = \rho_5/\rho_1$,

$$\frac{U_R}{C_s} = \frac{\eta - 1}{\xi - \eta}$$

$$\frac{p_5}{p_1} = 1 + \gamma_1 M_s^2 \frac{(\eta - 1)(\zeta - 1)}{\zeta - \eta}$$

$$\frac{h_5}{h_1} = 1 + (\gamma_1 - 1) M_s^2 \frac{(\eta - 1)(\zeta - 1)}{\zeta - \eta} \frac{1}{\eta}$$

10. An intermittent wind tunnel is operated by expanding atmospheric air at 15°C through the test-section into an evacuated tank. Determine the static pressure and the pressure that a Pitot tube placed in the test-section would measure, if the Mach number there is 3.0.

[**Ans.** 2758 Pa, 33.265 kPa]

11. Upstream of a normal shock in air, $M_1 = 2.5$, $p_1 = 1$ atm, $\rho_1 = 1.225$ kg/m^3. Determine p_2, ρ_2, T_2, M_2, V_2, p_{02} and T_{02} downstream of it.

[**Ans.** 7.125 atm, 4.083 kg/m^3, 616.03 K, 0.51299, 255.22 m/s, 8.5261 atm, 648.45 K]

12. Nitrogen gas passes through a normal shock with upstream conditions of $p_1 = 300$ kPa, $T_1 = 303$ K and $V_1 = 923$ m/s. Determine the velocity V_2 and pressure p_2 downstream of the shock. If the same deceleration from V_1 to V_2 takes place isentropically what will be the resultant p_2?

[**Ans.** 2.316 MPa, 267.64 m/s, 5.036 MPa]

13. A blunt nosed model is placed in a Mach 3 supersonic tunnel test-section. If the settling chamber pressure and temperature of the tunnel are 10 atm and 315 K, respectively, calculate the pressure, temperature and density at the nose of the model. Assume the flow to be one-dimensional.

[**Ans.** 332.69 kPa, 315 K, 3.68 kg/m^3]

14. A normal shock travels with velocity C_s in a still atmosphere at 101 kPa and 330 K. If the pressure just downstream of the shock is 5000 kPa, determine the velocity C_s and the velocity of the field traversed by the shock, just downstream of it.

[**Ans.** 2374.16 m/s, 1932.24 m/s]

15. There is a normal shock in a uniform air stream. The properties upstream of the shock are $V_1 = 412$ m/s, $p_1 = 92$ kPa, and $T_1 = 300$ K. Determine V_2, p_2, T_2, T_{02} and p_{02} downstream of the shock. Also, calculate the entropy increase across the shock.

[**Ans.** 311.98 m/s, 136.66 kPa, 336.51 K, 384.96 K, 218.83 kPa, 1.8042 J/kg-K]

Scanned by CamScanner

16. A convergent-divergent nozzle of exit area 4.0 cm^2 is to be designed to generate Mach 2.5 air stream. If the nozzle is correctly expanded and discharging into atmosphere, and the stagnation temperature at the entry is 500 K, determine the backpressure required to position a normal shock at the nozzle exit plane.

[**Ans.** 863.91 kPa]

17. Suppose the backpressure were to be increased for the nozzle in Problem 16 until a normal shock wave was formed in the divergent section where $M = 1.5$. What backpressure would be necessary to accomplish this, and what would be the resulting velocity and temperature at the nozzle exit?

[**Ans.** 15.89 atm, 108.71 m/s, 490 K]

18. Air from a storage tank at 700 kPa and 530 K is expanded through a frictionless convergent-divergent duct of throat area 5 cm^2 and exit area 12.5 cm^2. The backpressure is 350 kPa. There is a normal shock in the divergent portion and the Mach number just upstream of the shock is 2.32. Determine (a) the cross-sectional area at the shock location, (b) the exit Mach number, and (c) the backpressure for the flow to be isentropic throughout the duct.

[**Ans.** (a) 11.15 cm^2; (b) 0.45; (c) 44.98 kPa]

19. A normal shock wave forms in an air stream at a static temperature of 22 K. If the total temperature is 400 K, determine the Mach number and static temperature behind the shock.

[**Ans.** 0.3893, 382.8 K]

20. The flow properties upstream of a normal shock are 500 m/s, 100 kPa and 300 K. Determine the velocity, pressure and temperature of the gas downstream of the shock and the increase in entropy. Take the gas to be air.

[**Ans.** 284.25 m/s, 225.25 kPa, 384.21 K, 15.432 J/kg-K]

21. Air at 1 MPa and 300 K enters the Mach 2 Laval nozzle of a supersonic wind tunnel at a low velocity. If a normal shock wave is formed at the nozzle exit plane, determine the pressure, temperature, Mach number, velocity and the stagnation pressure of the flow just behind the shock.

[**Ans.** 0.5751 MPa, 281.3 K, 0.57735, 194.1 m/s, 0.72087 MPa]

22. Air at 30°C and 101 kPa is drawn through a convergent-divergent nozzle which discharges into a large vacuum tank. Determine the conditions upstream and downstream of a normal shock which is located at the nozzle exit. The nozzle throat and exit have areas of 0.025 m^2 and 0.0724 m^2, respectively.

[**Ans.** 2.6, 5.06 kPa, 128.9 K, 101 kPa, 0.504, 39.06 kPa, 288.5 K, 46.47 kPa]

23. Air from a reservoir at 200 kPa and 350 K is expanded through a convergent-divergent nozzle of throat area 0.2 m^2 and exit area 0.8 m^2.

Scanned by CamScanner

If a normal shock wave is positioned in the nozzle where the cross-sectional area is 0.6 m^2, compute the static and stagnation pressures on either side of the shock. What will be the static and stagnation pressures and temperatures at the nozzle exit?

[**Ans.** $p_1 = 9.422$ kPa, $p_{01} = 200$ kPa, $p_2 = 75.04$ kPa, $p_{02} = 89.04$ kPa, $p_3 = 81.81$ kPa, $p_{03} = 89.04$ kPa, $T_3 = 341.63$ K]

24. A convergent-divergent nozzle connects two reservoirs at pressures 5 atm and 3.6 atm. If a normal shock has to stand at the nozzle exit, find the pressure at the nozzle exit, just downstream of the shock.

[**Ans.** 2.876 atm]

25. A Pitot tube is placed in an air stream of static pressure 0.95 atm. Determine the flow Mach number if the Pitot tube records (i) 1.1 atm, (ii) 2.5 atm, and (iii) 10 atm.

[**Ans.** (i) 0.465, (ii) 1.275, (iii) 2.79]

26. A convergent-divergent nozzle with $A_{th} = 1000$ mm^2 and $A_e = 3000$ mm^2 operates under a stagnation condition of 200 kPa and 45°C. If a normal shock is present in the nozzle at a location with area 2000 mm^2, determine the exit pressure and the pressure loss experienced by the nozzle flow.

[**Ans.** 116.76 kPa, 74.37 kPa]

27. An Mach 2 air stream at 80 kPa and 290 K enters a divergent channel with a ratio of inlet to exit area of 0.25. Determine the backpressure required to position a normal shock in the channel at an area equal to twice the inlet area.

[**Ans.** 243.8 kPa]

28. In a supersonic wind tunnel test-section a wall pressure tap and a Pitot tube are used to measure the pressures. They indicate 112 kPa and 2895 kPa, respectively. If the stagnation temperature is 500 K, determine the test-section Mach number and velocity.

[**Ans.** 4.44, 895.1 m/s]

29. A continuous supersonic wind tunnel is designed to operate at a test-section Mach number of 2.4, with static conditions corresponding to those at 10,000 m altitude. The test-section is of circular cross-section with 250 mm in diameter. Neglecting friction and boundary layer effects, determine the power requirements of the compressor (a) during steady-state operation and (b) during start-up. Assume isentropic compression, with cooler located between the compressor and the nozzle, so that the compressor inlet temperature is maintained equal to the test-section stagnation temperature.

[**Ans.** (a) 376.3 hp, (b) 1815 hp]

30. Compute the Mach number and pressure at a section downstream of a normal shock in a nozzle where the cross-sectional area is twice the

Scanned by CamScanner

area at the normal shock location. Upstream of the normal shock, the air stream has $p_{01} = 400$ kPa and $M_1 = 1.85$.

[**Ans.** 0.25, 302.65 kPa]

31. The mass flow rate through a convergent-divergent duct run by a settling chamber with air at 4 atm and 30°C is 0.9 kg/s. If a normal shock of strength 2 is positioned at the duct exit for this stagnation state, determine (a) the exit area, and (b) the velocity of the flow leaving the duct.

[**Ans.** (a) 12.35 cm^2, (b) 219 m/s]

32. In a piston cylinder device containing stagnant air at 300 K, a normal shock of strength $[(p_2 - p_1)/p_1]$ 3.5 has to be generated by moving the piston impulsively. (a) Determine the speed with which the piston has to be moved. (b) If the shock strength has to be doubled, what should be the piston speed?

[**Ans.** (a) 434 m/s, (b) 657.56 m/s]

33. A normal shock is positioned inside a convergent-divergent nozzle of throat area 5 cm^2, run by a settling chamber with air at 5 atm and 330 K. If the pressure loss caused by the shock is 12.4% and the temperature at the nozzle exit is 300 K, determine (a) the Mach number ahead of the shock, (b) the flow speed behind the shock and at the nozzle exit, and (c) the mass flow rate through the nozzle.

[**Ans.** (a) 1.65, (b) $V_2 = 228.57$ m/s, $V_e = 245.5$ m/s, (c) 0.5636 kg/s]

34. For a perfect case, show that, beginning with the Hugoniot equation, the pressure ratio across a shock can be expressed as

$$\frac{p_2}{p_1} = \frac{\left(\frac{\gamma+1}{\gamma-1}\right)\left(\frac{v_1}{v_2}\right) - 1}{\left(\frac{\gamma+1}{\gamma-1}\right) - \left(\frac{v_1}{v_2}\right)}$$

35. For a normal shock with pressures p_1 and p_2, ahead of and behind it, respectively, show that

$$\frac{\rho_2}{\rho_1} = \frac{1 + \left(\frac{\gamma+1}{\gamma-1}\right)\left(\frac{p_2}{p_1}\right)}{\left(\frac{\gamma+1}{\gamma-1}\right) + \frac{p_2}{p_1}}$$

36. In a piston-cylinder device containing helium at 10 kPa and 50 K, the piston is suddenly moved with 1000 m/s. Find the shock speed, pressure, density and temperature behind the shock.

[**Ans.** 1454.62 m/s, 150 kPa, 0.308 kg/m^3, 234.31 K]

Scanned by CamScanner

37. If the entropy increase across a normal shock in an air stream is 0.45 kJ/(kg-K), determine the enthalpy ratio across the shock.

[**Ans.** 3.35]

38. Show that, only the deceleration of a supersonic to subsonic level is possible through a normal shock and the reverse is impossible.

39. If the density ratio across a normal shock moving in air is 1.6, determine the shock Mach number.

[**Ans.** 1.35]

40. If the density ratio across the shock at the nose of a vehicle flying at a very high hypersonic speed is 18, assuming fluid as perfect gas, determine the value of specific heats ratio.

[**Ans.** 1.12]

Scanned by CamScanner

6 Oblique Shock and Expansion Waves

6.1 INTRODUCTION

In Chapters 4 and 5, the normal shock wave, a compression wave normal to the flow direction, was studied in some detail. However, in a wide variety of physical situations, a compression wave inclined at an angle to the flow occurs. Such a wave is called an *oblique shock*.

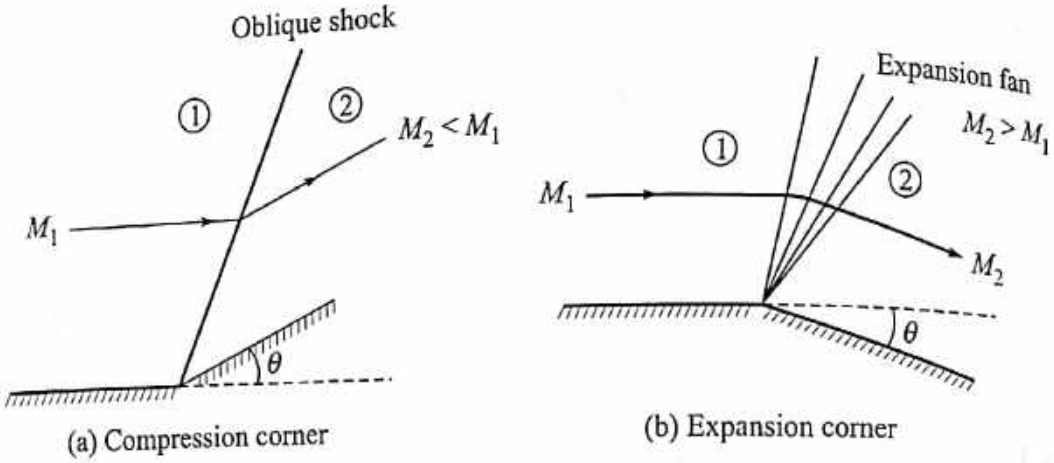
For steady subsonic flows, we generally do not think in terms of wave motion. It is usually much simpler to view the motion from a frame of reference system in which the body is stationary and the fluid flows over it. If the relative speed is supersonic, the disturbance waves cannot propagate ahead of the immediate vicinity of the body, and the wave system travels with the body. Thus, in the reference system in which the body is stationary, the wave system is also stationary; then the correspondence between the wave system and the flow field is direct.

The normal shock wave is a special case of oblique shock waves. Also, it can be shown that the superposition of a uniform velocity, which is normal to the upstream flow, on the flow field of the normal shock will result in a flow field through an oblique shock wave. This phenomenon will be employed later in this chapter to get the oblique shock relations. Oblique shocks usually occur when a supersonic flow is turned into itself. The opposite of this, i.e. when a supersonic flow is turned away from itself, results in the formation of an expansion fan. These two families of waves play a dominant role in all flow fields involving supersonic velocities. Typical flows with oblique shock and expansion fan are illustrated in Fig. 6.1.

In Fig. 6.1(a) the flow is deflected into itself by the oblique shock. All the streamlines are deflected to the same angle θ at the shock, resulting in uniform parallel flow downstream of shock. The angle θ is referred to as *flow deflection angle*. Across the shock wave, the Mach number decreases, and the pressure, density, and temperature increase. The corner which turns the flow into itself

Scanned by CamScanner

is called compression or concave corner. In contrast, in an expansion or convex corner, the flow is turned away from itself through an expansion fan. All the streamlines are deflected to the same angle θ after the expansion fan, resulting in uniform parallel flow downstream of the fan. Across the expansion wave, the



(a) Compression corner (b) Expansion corner

Fig. 6.1 Supersonic flow over corners.

Mach number increases, and the pressure, density and temperature decrease. From Fig. 6.1, it is seen that the flow turns suddenly across the shock and the turning is gradual across the expansion fan, and hence all flow properties through the expansion fan change smoothly, with the exception of the wall streamline which changes suddenly.

Oblique shock and expansion waves prevail in two- and three-dimensional supersonic flows, in contrast to normal shock waves, which are one-dimensional. In this chapter, we shall focus our attention on steady, two-dimensional (plane) supersonic flow.

6.2 OBLIQUE SHOCK RELATIONS

The flow through an oblique shock is given in Fig. 6.2. The flow through a normal shock has been modified to result in flow through an oblique shock, by superimposing a uniform velocity V_y (parallel to the normal shock) on the flow field of the normal shock (Fig. 6.2(a)). The resultant velocity upstream of the shock is $V_1 = \sqrt{V_{x1}^2 + V_y^2}$ and is inclined at an angle $\beta (= \tan^{-1}(V_{x1}/V_y))$ to the shock. This angle β is called *shock angle*. The velocity component V_{x2} is always less than V_{x1}; therefore, the inclinations of the flow to the shock ahead of the shock and after the shock are different. The inclination ahead is always more than that behind the shock wave, i.e. the flow is turned suddenly at the shock. Since V_{x1} is always more than V_{x2}, the turn is always towards the shock. The angle θ by which the flow turns towards the shock is called the flow deflection angle and is positive as shown in Fig. 6.2. The rotation of the flow field in Fig. 6.2(a) by an angle β results in the field shown in Fig. 6.2(b), with V_1 in

Scanned by CamScanner

the horizontal direction. The shock in that field inclined at an angle β to the incoming supersonic flow is called the *oblique shock*.

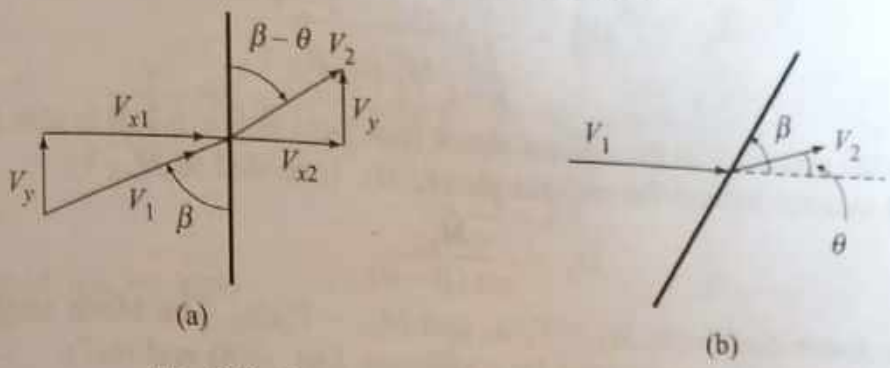


Fig. 6.2 Flow through an oblique shock wave.

The relations between the flow parameters upstream and downstream of the flow field through the oblique shock, illustrated in Fig. 6.2(b), can be obtained from the normal shock relations in Chapter 5, since the superposition of uniform velocity V_y on the normal shock flow field in Fig. 6.2(a) does not affect the flow parameters (e.g. static pressure) defined for normal shock. The only change is that in the present case the upstream Mach number is

$$\boxed{M_1 = \frac{\text{resultant velocity}}{\text{speed of sound}} = \frac{V_1}{a_1}}$$

The component of M_1 normal to the shock wave is

$$M_{n1} = M_1 \sin \beta \tag{6.1}$$

Thus, the replacement of M_1 in normal shock relations (5.13), (5.16), (5.18) and (5.19) with $M_1 \sin \beta$ results in corresponding relations for the oblique shock, giving thereby

$$\frac{\rho_2}{\rho_1} = \frac{(\gamma+1)M_1^2 \sin^2\beta}{(\gamma-1)M_1^2 \sin^2\beta + 2} \tag{6.2}$$

$$\frac{p_2}{p_1} = 1 + \frac{2\gamma}{\gamma+1}(M_1^2 \sin^2\beta - 1) \tag{6.3}$$

$$\frac{T_2}{T_1} = \frac{a_2^2}{a_1^2} = 1 + \frac{2(\gamma-1)}{(\gamma+1)^2}\frac{M_1^2 \sin^2\beta - 1}{M_1^2 \sin^2\beta}(\gamma M_1^2 \sin^2\beta + 1) \tag{6.4}$$

$$\frac{s_2 - s_1}{R} = \ln\left\{\left[1 + \frac{2\gamma}{\gamma+1}(M_1^2 \sin^2\beta - 1)\right]^{1/(\gamma-1)}\left[\frac{(\gamma+1)M_1^2 \sin^2\beta}{(\gamma-1)M_1^2 \sin^2\beta + 2}\right]^{-\gamma/(\gamma-1)}\right\}$$

$$= \ln \frac{p_{01}}{p_{02}} \tag{6.5}$$

Scanned by CamScanner

The normal component of Mach number behind the shock M_{n2} is given by

$$M_{n2}^2 = \frac{M_1^2 \sin^2\beta + \dfrac{2}{\gamma - 1}}{\dfrac{2\gamma}{\gamma - 1} M_1^2 \sin^2\beta - 1} \tag{6.6}$$

From the geometry of the oblique shock flow field in Fig. 6.2, it is seen that the Mach number behind the oblique shock, M_2, is related to M_{n2} by

$$M_2 = \frac{M_{n2}}{\sin(\beta - \theta)} \tag{6.7}$$

In the above equations, $M_2 = V_2/a_2$ and $M_{n2} = V_{x2}/a_2$. The Mach number M_2 after a shock can be obtained by combining Eqs. (6.6) and (6.7).

Numerical values of the oblique shock relations for a perfect gas, with $\gamma = 1.4$, are presented in graphical form (Appendix D) and tabular form (Table A3) in Appendix A.

It is seen from the oblique shock relations (6.1)–(6.5) that the ratios of thermodynamic variables depend only on the normal component of velocity ahead of the shock. But, we are already familiar with the fact from normal shock analysis that this component must be supersonic, i.e. $M_1 \sin\beta \geq 1$. This requirement imposes the restriction on the wave angle β that it cannot go beyond a minimum value for any given M_1. The maximum value of β is that for a normal shock, $\beta = \pi/2$. Thus for a given initial Mach number M_1, the possible range of wave angles is

$$\boxed{\sin^{-1}\left(\frac{1}{M_1}\right) \leq \beta \leq \frac{\pi}{2}} \tag{6.8}$$

EXAMPLE 6.1 Derive the Prandtl relation for oblique shock in perfect gas.

Solution The resultant velocities ahead of and behind oblique shock, shown in Fig. 6.2, are

$$V_1 = \sqrt{V_{x1}^2 + V_{t1}^2}$$

$$V_2 = \sqrt{V_{x2}^2 + V_{t2}^2}$$

where subscripts 1 and 2 refer to states ahead of and behind the shock and V_{x1}, V_{x2} are the normal components and V_{t1}, V_{t2} are the tangential components of velocity.

By energy equation,

$$h_1 + \frac{V_1^2}{2} = h_2 + \frac{V_2^2}{2} = h_0$$

For perfect gas

$$h = c_p T;\ c_p = \frac{\gamma}{\gamma - 1} R$$

Scanned by CamScanner

Therefore

$$c_p T_1 + \frac{(V_{x1}^2 + V_{t1}^2)}{2} = c_p T_2 + \frac{(V_{x2}^2 + V_{t2}^2)}{2} = c_p T_0$$

$$\frac{\gamma}{\gamma - 1} RT_1 + \frac{(V_{x1}^2 + V_{t1}^2)}{2} = \frac{\gamma}{\gamma - 1} RT_2 + \frac{(V_{x2}^2 + V_{t2}^2)}{2}$$

$$= \frac{\gamma}{\gamma - 1} RT_0$$

By Eq. (4.9c), we have

$$\frac{\gamma}{\gamma - 1} \frac{p}{\rho} + \frac{V^2}{2} = \frac{\gamma}{\gamma - 1} \frac{p_0}{\rho_0}$$

At critical state, this becomes

$$\frac{a^{*2}}{\gamma - 1} + \frac{a^{*2}}{2} = \frac{a_0^2}{\gamma - 1}$$

$$a^{*2} \left(\frac{1}{\gamma - 1} + \frac{1}{2} \right) = \frac{a_0^2}{\gamma - 1}$$

$$\frac{\gamma + 1}{2(\gamma - 1)} a^{*2} = \frac{a_0^2}{\gamma - 1}$$

Substituting this into the energy equation, we get

$$\frac{\gamma}{\gamma - 1} \frac{p_1}{\rho_1} + \frac{(V_{x1}^2 + V_{t1}^2)}{2} = \frac{\gamma + 1}{2(\gamma - 1)} a^{*2}$$

and

$$\frac{\gamma}{\gamma - 1} \frac{p_2}{\rho_2} + \frac{(V_{x2}^2 + V_{t2}^2)}{2} = \frac{\gamma + 1}{2(\gamma - 1)} a^{*2}$$

Solving for p_1 and p_2, we have

$$p_1 = \rho_1 \left[\frac{\gamma + 1}{2\gamma} a^{*2} - \frac{\gamma - 1}{2\gamma} (V_{x1}^2 + V_{t1}^2) \right]$$

$$p_2 = \rho_2 \left[\frac{\gamma + 1}{2\gamma} a^{*2} - \frac{\gamma - 1}{2\gamma} (V_{x2}^2 + V_{t2}^2) \right]$$

By momentum equation,

$$p_1 + \rho_1 V_{x1}^2 = p_2 + \rho_2 V_{x2}^2$$

Scanned by CamScanner

Substituting for p_1 and p_2, we have

$$\rho_1\left[\frac{\gamma+1}{2\gamma}a^{*2}-\frac{\gamma-1}{2\gamma}(V_{x1}^2+V_{t1}^2)+V_{x1}^2\right]$$

$$=\rho_2\left[\frac{\gamma+1}{2\gamma}a^{*2}-\frac{\gamma-1}{2\gamma}(V_{x2}^2+V_{t2}^2)+V_{x2}^2\right]$$

$$\rho_1\left[\frac{\gamma+1}{2\gamma}(V_{x1}^2+a^{*2})-\frac{\gamma-1}{2\gamma}V_{t1}^2\right]=\rho_2\left[\frac{\gamma+1}{2\gamma}(V_{x2}^2+a^{*2})-\frac{\gamma-1}{2\gamma}V_{t2}^2\right]$$

But $V_{t1}=V_{t2}$ and $\rho_1V_{x1}=\rho_2V_{x2}$, therefore,

$$\frac{\gamma+1}{2\gamma}\rho_1V_{x1}^2+\frac{\gamma+1}{2\gamma}\rho_1a^{*2}-\frac{\gamma+1}{2\gamma}\rho_2V_{x2}^2-\frac{\gamma+1}{2\gamma}\rho_2a^{*2}$$

$$=\frac{\gamma-1}{2\gamma}(\rho_1V_{t_1}^2-\rho_2V_{t_2}^2)$$

$$\frac{\gamma+1}{2\gamma}\left(\rho_1V_{x1}\frac{\rho_2}{\rho_1}V_{x2}-\rho_2V_{x2}\frac{\rho_1}{\rho_2}V_{x1}\right)+\frac{\gamma+1}{2\gamma}a^{*2}(\rho_1-\rho_2)$$

$$=\frac{\gamma-1}{2\gamma}V_t^2(\rho_1-\rho_2)$$

$$\frac{\gamma+1}{2\gamma}(\rho_2V_{x1}V_{x2}-\rho_1V_{x1}V_{x2})+\frac{\gamma+1}{2\gamma}a^{*2}(\rho_1-\rho_2)=\frac{\gamma-1}{2\gamma}V_t^2(\rho_1-\rho_2)$$

$$-\frac{\gamma+1}{2\gamma}V_{x1}V_{x2}(\rho_1-\rho_2)+\frac{\gamma+1}{2\gamma}a^{*2}(\rho_1-\rho_2)=\frac{\gamma-1}{2\gamma}V_t^2(\rho_1-\rho_2)$$

$$-\frac{\gamma+1}{2\gamma}V_{x1}V_{x2}+\frac{\gamma+1}{2\gamma}a^{*2}=\frac{\gamma-1}{2\gamma}V_t^2$$

$$-V_{x1}V_{x2}+a^{*2}=\frac{\gamma-1}{\gamma+1}V_t^2$$

or

$$\boxed{V_{x1}V_{x2}=a^{*2}-\frac{\gamma-1}{\gamma+1}V_t^2}$$

EXAMPLE 6.2 An oblique shock in air causes an entropy increase of 11.5 J/(kg K). If the shock angle is 25°, determine the Mach number ahead of the shock and the flow deflection angle.

Solution Given, $s_2-s_1=11.5$ J/(kg K) and $\beta=25°$.

Scanned by CamScanner

But,

$$s_2 - s_1 = R \ln\left(\frac{p_{01}}{p_{02}}\right)$$

Therefore,

$$R \ln\left(\frac{p_{01}}{p_{02}}\right) = 11.5$$

$$\ln\left(\frac{p_{01}}{p_{02}}\right) = \frac{11.5}{287}$$

$$\frac{p_{01}}{p_{02}} = e^{(11.5/287)}$$

$$\frac{p_{02}}{p_{01}} = 1/e^{(11.5/287)}$$

$$= 0.9607$$

From the normal shock table, for $p_{02}/p_{01} = 0.9607$,

$$M_{1n} = 1.39$$

Thus, the Mach number ahead of the shock is

$$M_1 = \frac{M_{1n}}{\sin \beta}$$

$$= \frac{1.39}{\sin 25°}$$

$$= \boxed{3.29}$$

For $M_1 = 3.29$ and $\beta = 25°$, from the oblique shock chart I,

$$\theta = \boxed{9°}$$

6.3 RELATION BETWEEN β AND θ

It is seen from Eq. (6.7) that for determining M_2, the deflection angle θ must be known. Further, for each wave angle β at a given M_1 there is a corresponding flow turning angle θ, i.e. θ can also be expressed as a unique function of M_1 and β. From Fig. 6.2, we have

$$\tan \beta = \frac{V_{x1}}{V_y} \tag{6.9}$$

$$\tan(\beta - \theta) = \frac{V_{x2}}{V_y} \tag{6.10}$$

Scanned by CamScanner

Combining Eqs. (6.9) and (6.10), we get

$$\frac{\tan(\beta-\theta)}{\tan\beta} = \frac{V_{x2}}{V_{x1}} \tag{6.11}$$

By continuity,

$$\frac{V_{x2}}{V_{x1}} = \frac{\rho_1}{\rho_2}$$

Now, substituting for ρ_1/ρ_2 from Eq. (6.2), we get

$$\frac{\tan(\beta-\theta)}{\tan\beta} = \frac{(\gamma-1)M_1^2\sin^2\beta+2}{(\gamma+1)M_1^2\sin^2\beta} \tag{6.12}$$

Equation (6.12) is an implicit relation between θ and β, for a given M_1.

Expanding $\tan(\beta-\theta)$, we have

$$\tan(\beta-\theta) = \frac{\tan\beta-\tan\theta}{(1+\tan\beta\tan\theta)}$$

Therefore,

$$\frac{\tan\beta-\tan\theta}{(1+\tan\beta\tan\theta)\tan\beta} = \frac{(\gamma-1)M_1^2\sin^2\beta+2}{(\gamma+1)M_1^2\sin^2\beta}$$

$$\tan\beta-\tan\theta = (\tan\beta+\tan^2\beta\tan\theta)\left[\frac{(\gamma-1)M_1^2\sin^2\beta+2}{(\gamma+1)M_1^2\sin^2\beta}\right]$$

$$\tan\theta\left\{\tan^2\beta\left[\frac{(\gamma-1)M_1^2\sin^2\beta+2}{(\gamma+1)M_1^2\sin^2\beta}\right]+1\right\} = \tan\beta\left[1-\frac{(\gamma-1)M_1^2\sin^2\beta+2}{(\gamma+1)M_1^2\sin^2\beta}\right]$$

$$\tan\theta\{\tan^2\beta[(\gamma-1)M_1^2\sin^2\beta+2]+(\gamma+1)M_1^2\sin^2\beta\}$$

$$= \tan\beta[(\gamma+1)M_1^2\sin^2\beta-(\gamma-1)M_1^2\sin^2\beta-2]$$

$$\tan\theta\frac{\sin^2\beta[(\gamma-1)M_1^2\sin^2\beta+2]+\cos^2\beta(\gamma+1)M_1^2\sin^2\beta}{\cos^2\beta}$$

$$= \tan\beta(2M_1^2\sin^2\beta-2)$$

$$\tan\theta\{\sin^2\beta[(\gamma-1)M_1^2\sin^2\beta+(\gamma+1)M_1^2\cos^2\beta]+2\sin^2\beta\}$$

$$= \tan\beta\cos^2\beta(2M_1^2\sin^2\beta-2)$$

$$\tan\theta\{\sin^2\beta[\gamma M_1^2(\sin^2\beta+\cos^2\beta)+(\cos^2\beta-\sin^2\beta)M_1^2]+2\sin^2\beta\}$$

Scanned by CamScanner

$$= 2 \tan \beta \cos^2 \beta (M_1^2 \sin^2 \beta - 1)$$

$$\tan \theta [\sin^2 \beta (\gamma M_1^2 + M_1^2 \cos 2\beta) + 2 \sin^2 \beta] = 2 \sin \beta \cos \beta (M_1^2 \sin^2 \beta - 1)$$

$$\tan \theta = \frac{2 \sin \beta \cos \beta (M_1^2 \sin^2 \beta - 1)}{M_1^2 \sin^2 \beta (\gamma + \cos 2\beta) + 2 \sin^2 \beta}$$

$$\tan \theta = 2(\cos \beta / \sin \beta) \left[\frac{(M_1^2 \sin^2 \beta - 1)}{M_1^2 (\gamma + \cos 2\beta) + 2} \right]$$

$$\boxed{\tan \theta = 2 \cot \beta \left[\frac{M_1^2 \sin^2 \beta - 1}{M_1^2 (\gamma + \cos 2\beta) + 2} \right]} \qquad (6.13)$$

Equation (6.13) is called the *θ–β–M relation.*

This relation is important for the analysis of oblique shocks. The expression on the right-hand side of Eq. (6.13) becomes zero at $\beta = \pi/2$ and at $\beta = \sin^{-1}(1/M_1)$, which are the limiting values of β, defined in Eq. (6.8). The deflection angle θ is positive in this range, and must therefore have a maximum value. The results obtained from Eq. (6.13) are plotted in Fig. 6.3 for $\gamma = 1.4$. From the plot of *θ–β–M* (Fig. 6.3) curves, the following observations can be made:

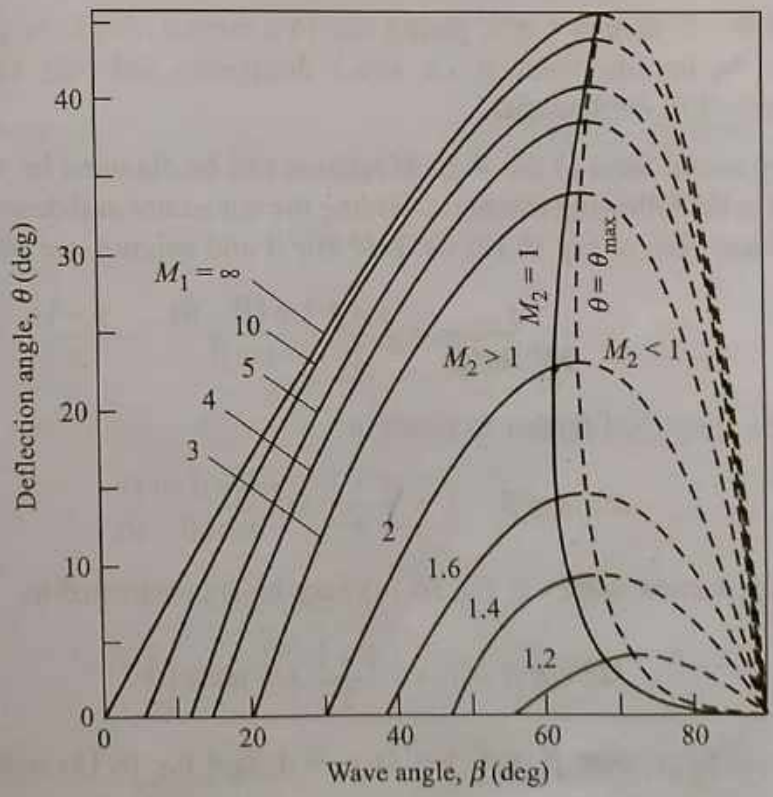


Fig. 6.3 Oblique shock solution.

Scanned by CamScanner

1. For any given M_1, there is a maximum value of θ. Therefore, at a given M_1, if $\theta > \theta_{max}$, then no solution is possible for a straight oblique shock wave. In such cases, the shock will be curved and detached, as shown in Fig. 6.4.
2. When $\theta < \theta_{max}$, there are two possible solutions, for each value of θ and M, having two different wave angles. The large value of β is called the *strong shock solution* and the small value of β is referred to as the *weak shock solution*. For strong shock solution the flow behind the shock becomes subsonic. For weak shock solution the flow remains supersonic, except for a small range of θ values slightly smaller than θ_{max}.

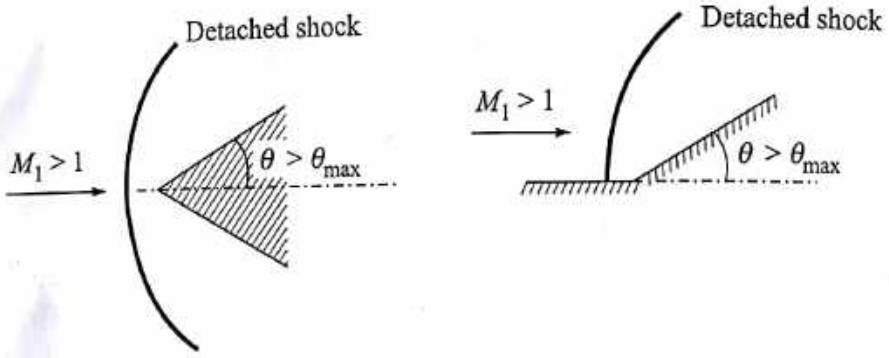


Fig. 6.4 Detached shocks.

3. If $\theta = 0$, then $\beta = \pi/2$, giving rise to a normal shock, or β decreases to the limiting value μ, i.e. shock disappears and only Mach waves prevail in the flow field.

A very useful form of the θ–β–M relation can be obtained by rearranging Eq. (6.12) in the following manner: Dividing the numerator and denominator on the right-hand side of Eq. (6.12) by $2M_1^2 \sin^2\beta$ and solving, we obtain

$$\frac{1}{M_1^2 \sin^2\beta} = \frac{\gamma+1}{2}\frac{\tan(\beta-\theta)}{\tan\beta} - \frac{\gamma-1}{2}$$

This can be simplified further to result in

$$M_1^2 \sin^2\beta - 1 = \frac{\gamma+1}{2} M_1^2 \frac{\sin\beta \sin\theta}{\cos(\beta-\theta)} \tag{6.14}$$

For small deflection angles θ, Eq. (6.14) may be approximated by

$$M_1^2 \sin^2\beta - 1 \approx \left(\frac{\gamma+1}{2} M_1^2 \tan\beta\right)\theta \tag{6.15}$$

If M_1 is very large, then $\beta \ll 1$, but $M_1\beta \gg 1$, and Eq. (6.15) reduces to

$$\beta = \frac{\gamma+1}{2}\theta \tag{6.16}$$

Scanned by CamScanner

It is important to note that oblique shocks are essentially compression fronts across which the flow decelerates and the pressure, temperature and density jump to higher values. If the deceleration is such that the Mach number behind the shock continues to be greater than unity, the shock is termed *weak oblique shock*. If the downstream Mach number becomes less than unity, then the shock is called *strong oblique shock*. It is essential to note that only the weak oblique shocks are usually formed and it calls for special arrangements to generate strong oblique shocks. One such situation where strong oblique shocks are generated with special arrangements is the engine intakes of supersonic flight vehicles, where the engine has provision to control its backpressure. When the backpressure is increased to an appropriate value, the oblique shock at the engine inlet will become a strong shock and decelerate the supersonic flow passing through it to subsonic level.

EXAMPLE 6.3 A Mach 1.8 Laval nozzle connected to a settling chamber, maintained at 400 kPa, discharges air into a very large tank provided with pressure control device (vacuum pump) to maintain the tank pressure at any desired level. (a) If a shock of 5 per cent strength is formed at the nozzle exit, determine the static pressure behind the shock and the tank pressure. (b) What should be the limiting minimum pressure in the tank to make the oblique shock strong? Find the Mach number behind this strong shock.

Solution Let subscripts 1 and 2 refer to the states ahead of and behind the shock and 01 and 02 refer to the states of the settling chamber and the tank, respectively.

(a) Given, $p_{01} = 400$ kPa, $M_1 = 1.8$, $\dfrac{p_2 - p_1}{p_1} = 0.05$. Therefore,

$$\frac{p_2}{p_1} - 1 = 0.05$$

$$\frac{p_2}{p_1} = 1.05$$

For $p_2/p_1 = 1.05$, from normal shock table,

$$M_{1n} = 1.02,\ M_{2n} = 0.98$$

Therefore,

$$M_{1n} = M_1 \sin\beta = 1.02$$

$$\sin\beta = \frac{1.02}{M_1}$$

$$= \frac{1.02}{1.8} = 0.567$$

$$\beta = \sin^{-1}(0.567)$$

$$= 34.54^\circ$$

Scanned by CamScanner

For $M_1 = 1.8$ and $\beta = 34.54°$, from oblique shock table, the flow deflection angle $\theta \approx 1°$. Therefore, the Mach number behind the shock becomes

$$M_2 = \frac{M_{2n}}{\sin(\beta - \theta)}$$

$$= \frac{0.98}{\sin(34.54 - 1)}$$

$$= 1.77$$

From $M_1 = 1.8$, from isentropic table,

$$\frac{p_1}{p_{01}} = 0.174$$

Thus the pressure ahead of the shock becomes

$$p_1 = 0.174 \times 400$$

$$= 69.6 \text{ kPa}$$

The pressure behind the shock is

$$p_2 = 1.05 \times p_1$$

$$= 1.05 \times 69.6$$

$$= \boxed{73.08 \text{ kPa}}$$

For $M_2 = 1.77$, from isentropic table,

$$\frac{p_2}{p_{02}} = 0.1822$$

This gives the tank pressure as

$$p_{02} = \frac{p_2}{0.1822}$$

$$= \frac{73.08}{0.1822}$$

$$= \boxed{401.1 \text{ kPa}}$$

(b) For $M_1 = 1.8$, from weak shock solution of oblique shock table, we have the shock angle for the limiting minimum pressure in the tank at which the shock is strong enough to decelerate the flow Mach number to slightly less than unity as

$$\beta = 62.30°$$

The corresponding values of Mach number and flow turning angle are

$$M_2 = 0.977, \ \theta = 19°$$

Therefore,

$$M_{1n} = M_1 \sin \beta$$

$$= 1.8 \times \sin 62.30°$$

$$= 1.59$$

Scanned by CamScanner

For $M_{1n} = 1.59$, from normal shock table,

$$M_{2n} = 0.6715, \frac{p_{02}}{p_{01}} = 0.8989$$

Therefore,

$$M_2 = \frac{M_{2n}}{\sin(\beta - \theta)}$$
$$= \frac{0.6715}{\sin(62.30 - 19)}$$
$$= \boxed{0.98}$$
$$p_{02} = 0.8989 \times p_{01}$$
$$= 0.8989 \times 400$$
$$= \boxed{359.56 \text{ kPa}}$$

6.4 SHOCK POLAR

Shock polar is a graphical representation of oblique shock properties. We have seen in Section 6.3 that, in general, for any specified turning angle θ there are two possible shock angles, giving rise to strong and weak solutions.

The shock polar for the oblique shock geometry illustrated in Fig. 6.5 may be drawn as follows:

An oblique shock with upstream velocity V_1 in the xy-Cartesian coordinate system as shown in Fig. 6.5 has the velocity components V_{x2} and V_{y2} in the downstream field, as shown. The xy-plane in Fig. 6.5 is called the *physical plane*. Let V_{x1}, V_{y2}, V_{x2}, and V_{y2} be the x and y components of flow velocity ahead of and behind the shock. Now, let us represent the oblique shock field in a plane with V_x and V_y as the axes, as shown in Fig. 6.6. This plane is called the *hodograph plane*.

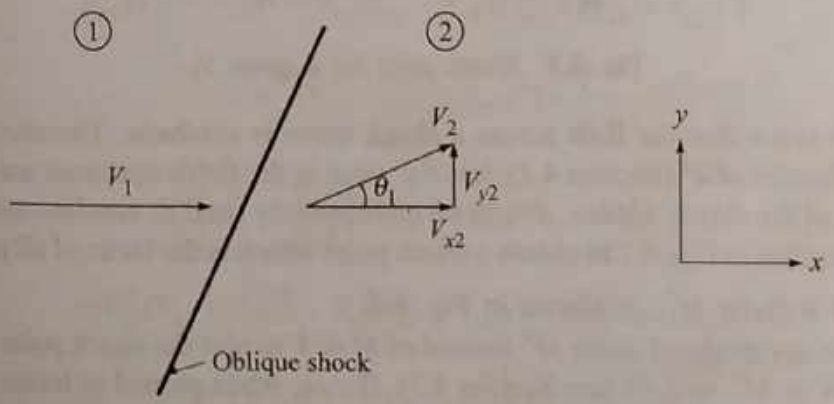


Fig. 6.5 Oblique shock in physical plane.

Scanned by CamScanner

In the hodograph plane, the point A represents the flow field ahead of the shock marked as region 1 in the physical plane of Fig. 6.5. Similarly, region 2 in the physical plane is represented by point B in the hodograph plane. If the deflection angle θ_1 in Fig. 6.6 is increased, then the shock becomes stronger and, therefore, the velocity V_2 decreases. One such point for θ_2 is shown by point C in Fig. 6.7. The loci of all such points for θ values from zero to θ_{max} representing all possible velocities behind the shock are given in Fig. 6.7. Such a locus is defined as a *shock polar*.

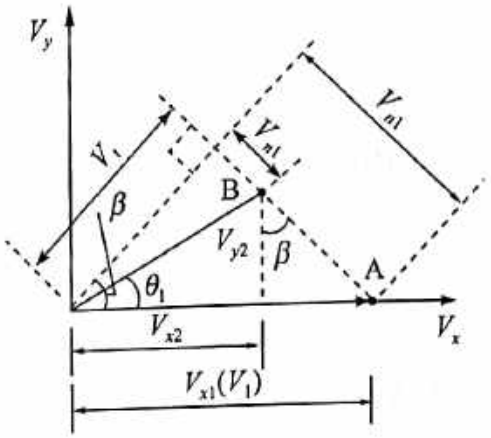


Fig. 6.6 Oblique shock geometry in hodograph plane.

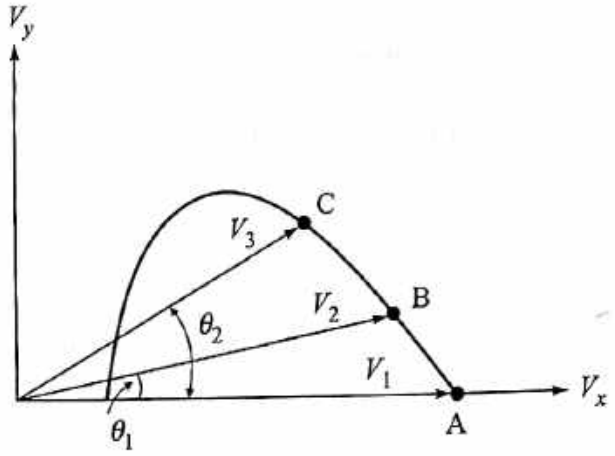


Fig. 6.7 Shock polar for a given V_1.

We know that the flow across a shock wave is adiabatic. Therefore, from our definition of a^* (Section 4.2), it is the same in the fields upstream and downstream of the shock. Hence, a^* can be conveniently used to nondimensionalise the velocities in Fig. 6.7 to obtain a shock polar which is the locus of all possible M_2^* for a given M_1^*, as shown in Fig. 6.8.

The advantage of using M^* instead of M or V to plot the shock polar is that, as $M \to \infty$, $M^* \to 2.45$ (see Section 4.3). Hence, when plotted in terms of M^*, the shock polar becomes compact. Note that in Fig. 6.8, the circle with radius

Scanned by CamScanner

$M^* = 1$ is called the *sonic circle*; inside the circle all velocities are subsonic; outside it, all velocities are supersonic.

The shock polar can also be described by an analytical equation called the *shock polar relation*.

The shock polar relation can be derived using the Prandtl relation for oblique shock, derived in Example 6.1.

Prandtl equation for oblique shock is

$$V_{n1}V_{n2} = a^{*2} - \frac{\gamma - 1}{\gamma + 1}V_t^2$$

From Fig. 6.6,

$$V_{n1} = V_{x1} \sin \beta$$

$$V_{n2} = V_{n1} - \sqrt{V_{y2}^2 + (V_{x1} - V_{x2})^2}$$

$$V_t = V_{x1} \cos \beta$$

But $V_{y2} = V_y$. Substituting these into Prandtl equation, we have

$$V_{x1} \sin\beta\left[V_{n1} - \sqrt{V_{y2}^2 + (V_{x1} - V_{x2})^2}\right] = a^{*2} - \frac{\gamma - 1}{\gamma + 1}V_{x1}^2 \cos^2 \beta$$

$$V_{x1}^2 \sin^2 \beta - V_{x1} \sin \beta\sqrt{V_{y2}^2 + (V_{x1} - V_{x2})^2} = a^{*2} - \frac{\gamma - 1}{\gamma + 1}V_{x1}^2 \cos^2 \beta$$

Substituting for $\sin \beta$ and $\cos \beta$, we have

$$\frac{V_{x1}^2(V_{x1} - V_{x2})^2}{V_y^2 + (V_{x1} - V_{x2})^2} - V_{x1}(V_{x1} - V_{x2})$$

$$= a^{*2} - \frac{\gamma - 1}{\gamma + 1}V_{x1}^2 \frac{V_y^2}{V_y^2 + (V_{x1} - V_{x2})^2}$$

$$V_{x1}^2(V_{x1} - V_{x2})^2 - V_{x1}(V_{x1} - V_{x2})[V_y^2 + (V_{x1} - V_{x2})^2]$$

$$= a^{*2}[V_y^2 + (V_{x1} - V_{x2})^2] - \frac{\gamma - 1}{\gamma + 1}(V_{x1}^2 V_y^2)$$

$$V_y^2\left[a^{*2} - \frac{\gamma - 1}{\gamma + 1}(V_{x1})^2 + V_{x1}(V_{x1} - V_{x2})\right]$$

$$= V_{x1}^2(V_{x1} - V_{x2})^2 - V_{x1}(V_{x1} - V_{x2})^3 - a^{*2}(V_{x1} - V_{x2})^2$$

$$V_y^2\left[a^{*2} + V_{x1}^2\left(1 - \frac{\gamma - 1}{\gamma + 1}\right) - V_{x1}V_{x2}\right]$$

Scanned by CamScanner

$$= (V_{x1} - V_{x2})^2 [V_{x1}^2 - V_{x1}(V_{x1} - V_{x2}) - a^{*2}]$$

$$V_y^2 \left(a^{*2} + \frac{2}{\gamma + 1} V_{x1}^2 - V_{x1} V_{x2} \right)$$

$$= (V_{x1} - V_{x2})^2 [V_{x1} V_{x2} - a^{*2}]$$

Dividing throughout by a^{*2}, we get

$$V_y^2 \left(1 + \frac{2}{\gamma + 1} \frac{V_{x1}^2}{a^{*2}} - \frac{V_{x1}}{a^*} \frac{V_{x2}}{a^*} \right)$$

$$= \left(\frac{V_{x1}}{a^*} - \frac{V_{x2}}{a^*} \right)^2 \left(\frac{V_{x1}}{a^*} \frac{V_{x2}}{a^*} - 1 \right) a^{*2}$$

Expressing V_{x1}/a^* as M_1^*, we have

$$V_y^2 \left[1 + \frac{2}{\gamma + 1} M_1^{*2} - M_1^* \left(\frac{V_{x2}}{a^*} \right) \right]$$

$$= \left(M_1^* - \frac{V_{x2}}{a^*} \right)^2 \left[M_1^* \left(\frac{V_{x2}}{a^*} \right) - 1 \right] a^{*2}$$

or

$$\boxed{\left(\frac{V_y}{a^*} \right)^2 = \frac{\left(M_1^* - \frac{V_{x2}}{a^*} \right)^2 \left[\left(\frac{V_{x2}}{a^*} \right) M_1^* - 1 \right]}{\frac{2}{\gamma + 1} M_1^{*2} - \left(\frac{V_{x2}}{a^*} \right) M_1^* + 1}} \tag{6.17}$$

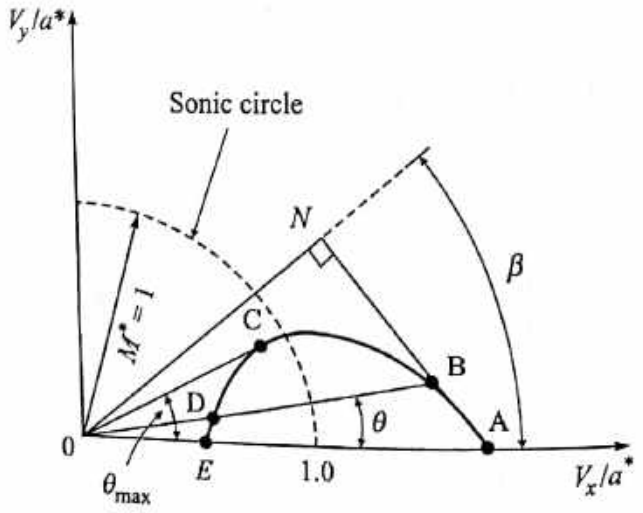


Fig. 6.8 Dimensionless shock polar.

Scanned by CamScanner

The shock polars for different Mach numbers form a family of curves, as shown in Fig. 6.9. Note that for $M_1^* = 2.45$ ($M_1 \to \infty$), the shock polar is a circle.

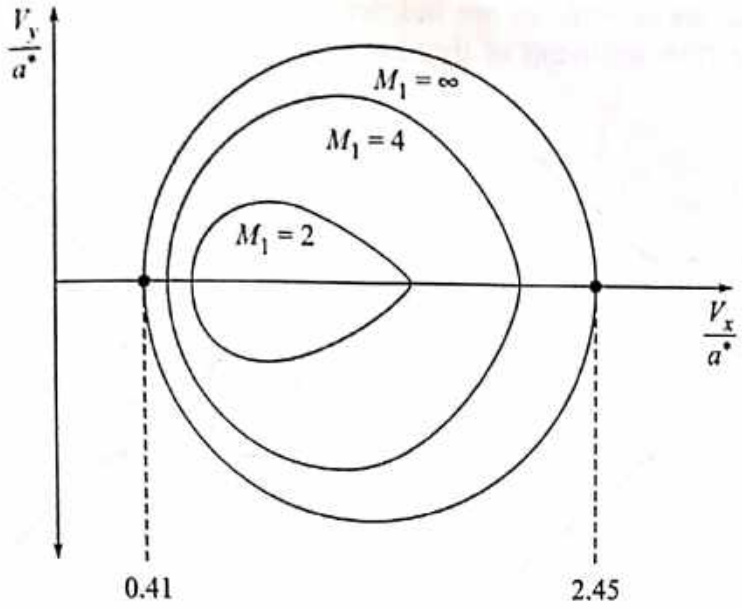


Fig. 6.9 Shock polars for different Mach numbers.

6.5 SUPERSONIC FLOW OVER A WEDGE

From studies on inviscid flows, we know that any streamline can be replaced by a solid boundary. In our present study, we treat the supersonic flow as inviscid and, therefore, here also the streamlines can be assumed as solid boundaries. Thus the oblique shock flow results already described can be used for solving practical problems like supersonic flow in a corner, as shown in Fig. 6.10. For any given values of M_1 and θ, the values of M_2 and β can be determined from oblique shock charts (Appendix D) or Table A3 (Appendix A).

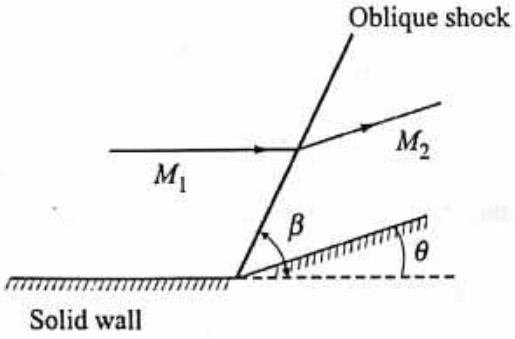


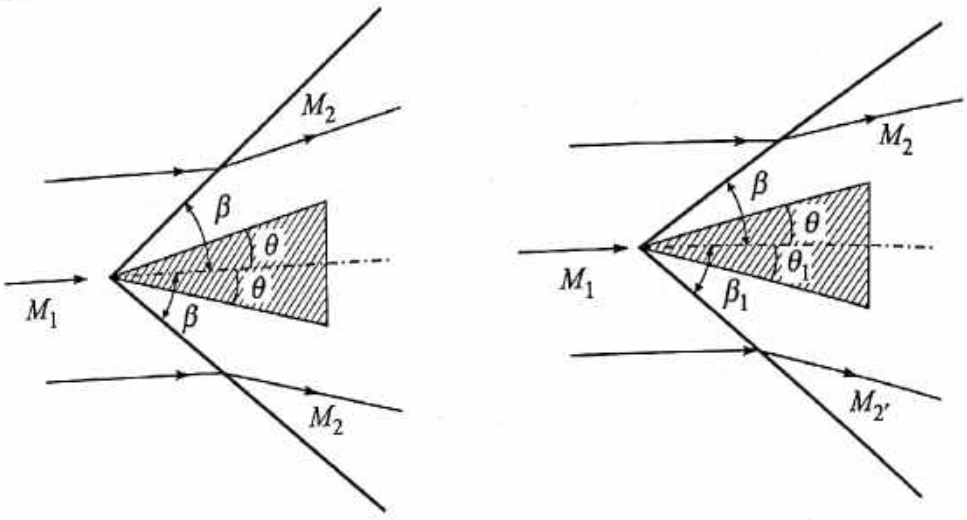
Fig. 6.10 Supersonic flow in a corner.

In a similar fashion, problems like supersonic flow over symmetrical [Fig. 6.11(a)] and unsymmetrical wedges [Fig. 6.11(b)], and so on can also be

Scanned by CamScanner

solved with oblique shock relations, assuming the solid surfaces of the objects as streamlines in accordance with the nonviscous flow theory.

In Fig. 6.11(b), the flow on each side of the wedge is determined only by the inclination of the surface on that side. If the shocks are attached to the nose, the upper and lower surfaces are independent, and there is no influence of wedge on the flow upstream of the shock waves.



(a) Symmetric wedge (b) Unsymmetric wedge

Fig. 6.11 Flow past wedge.

In our discussion on β and θ (Section 6.3), we have seen that when θ decreases to zero, β [Fig. 6.12(a)] decreases to the limiting value μ [Fig. 6.12(b)] giving rise to Mach waves in the field (see Fig. 6.12), which is given from Eq. (6.14) as

$$M_1^2 \sin^2\mu - 1 = 0 \tag{6.18}$$

Also, the jump quantities given by Eqs. (6.2)–(6.5) reach zero. There is, in fact, no disturbance in the flow. The point P in Fig. 6.12(b) may be any point in the flow. Then the angle μ is simply a characteristic angle associated with the Mach number M by the relation

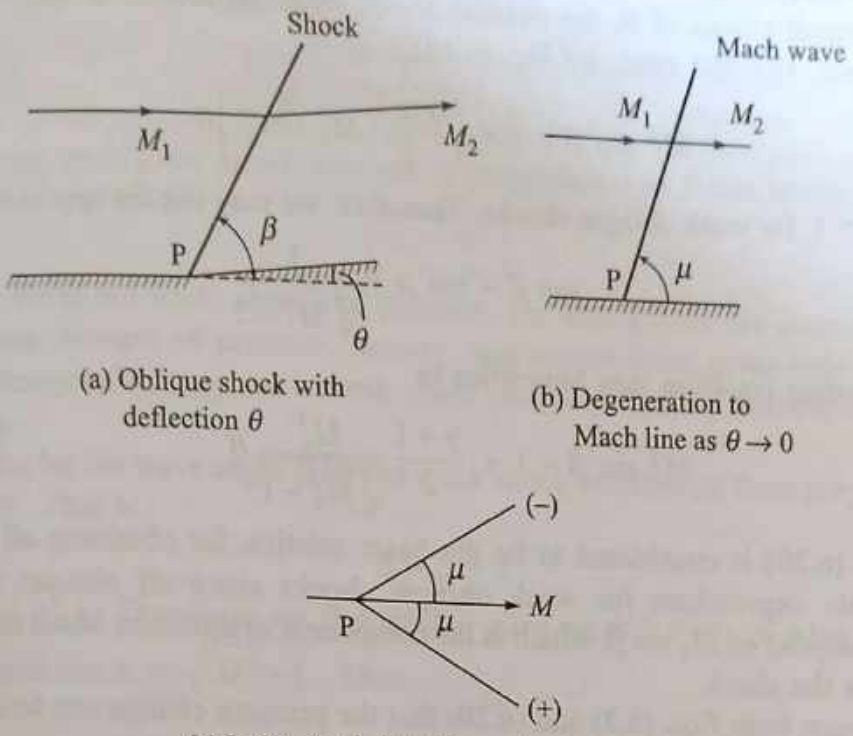
$$\mu = \sin^{-1}\left(\frac{1}{M}\right) \tag{6.19}$$

This is called the *Mach angle–Mach number relation*. These lines which may be drawn at any point in the flow field with inclination μ are called *Mach lines* or *Mach waves*. In nonuniform flow fields, μ varies with M and the Mach lines are curved.

In the flow field at any point P [Fig. 6.12(c)], there are always two lines which intersect the streamline at the angle μ. In a three-dimensional flow, the Mach wave is in the form of a conical surface, with vertex at P. Thus, a two-dimensional flow of supersonic stream is always associated with two families of Mach lines. These are represented with plus and minus signs in Fig. 6.12(c) (see also Section 3.4). The Mach lines with "+" sign run to the right

Scanned by CamScanner

of the streamline when viewed through the flow direction and those lines with "–" run to the left. These Mach lines are also called *characteristics*.



(a) Oblique shock with deflection θ

(b) Degeneration to Mach line as $\theta \to 0$

(c) Left (–) and right (+) running Mach lines at an arbitrary point in the flow

Fig. 6.12 Waves in a supersonic stream.

The characteristic lines introduce an infinitesimal, but finite change to flow properties when a flow passes through them. At this stage it is essential to note the difference between the Mach, characteristic, and expansion waves. Even though all are isentropic waves, there is a distinct difference between them. Mach waves are weak isentropic waves across which the flow experiences *insignificant* change in its properties. Whereas, the expansion and characteristic waves are isentropic waves which introduce small, but *finite* property changes to a flow passing them.

The characteristic lines play an important role in the compression and expansion processes in the sense that it is only through these lines that it is possible to retard or accelerate a supersonic flow isentropically. Also, this concept will be employed in Chapter 12 for designing supersonic nozzles with the Method of Characteristics.

6.6 WEAK OBLIQUE SHOCKS

In Section 6.5, we have seen that the compression of supersonic flow without entropy increase is possible only through the Mach waves. In the present discussion on weak shocks as well, it will be shown that these weak shocks, which result when the deflection angle θ is small and Mach number downstream

Scanned by CamScanner

of shock $M_2 > 1$, can also compress the flow with entropy increase almost closer to zero.

For small values of θ, the oblique shock relations reduce to very simple expressions. For this case, by Eq. (6.14),

$$M_1^2 \sin^2\beta - 1 \approx \left(\frac{\gamma+1}{2} M_1^2 \tan\beta\right)\theta$$

Also, $M_2 > 1$, for weak oblique shocks. Therefore, we may use the approximation

$$\tan\beta \approx \tan\mu = \frac{1}{\sqrt{M_1^2 - 1}}$$

The preceding equation then simplifies to

$$M_1^2 \sin^2\beta - 1 \approx \frac{\gamma+1}{2} \frac{M_1^2}{\sqrt{M_1^2-1}}\theta \tag{6.20}$$

Equation (6.20) is considered to be the basic relation for obtaining all other appropriate expressions for weak oblique shocks since all oblique shock relations depend on $M_1 \sin\beta$, which is the component of upstream Mach number normal to the shock.

It is seen from Eqs. (6.3) and (6.20) that the pressure change can be easily expressed as

$$\frac{p_2 - p_1}{p_1} = \frac{\Delta p}{p_1} \approx \frac{\gamma M_1^2}{\sqrt{M_1^2-1}}\theta \tag{6.21}$$

Equation (6.21) shows that the strength of the shock wave is proportional to the deflection angle.

Similarly, it can be shown that the changes in density and temperature are also proportional to θ. But the change in entropy, on the other hand, is proportional to the third power of shock strength as shown now: By Eq. (6.5), we have

$$\frac{s_2 - s_1}{R} = \ln\left[\left(1 + \frac{2\gamma}{\gamma+1} m\right)^{1/(\gamma-1)} (1+m)^{-\gamma/(\gamma-1)} \left(\frac{\gamma-1}{\gamma+1} m + 1\right)^{\gamma/(\gamma-1)}\right] \tag{6.22}$$

where $m = M_1^2 - 1$ [Note that for weak oblique shocks under consideration, $M_1^2 \sin^2\beta$ is approximated as M_1^2]. For values of M_1 close to unity, m is small, and the terms in the parentheses are like $1 + \varepsilon$, with $\varepsilon \ll 1$. Expanding the terms as logarithmic series, we get

$$\frac{s_2 - s_1}{R} = \frac{2\gamma}{(\gamma+1)^2} \frac{m^3}{3} + \text{higher-order terms}$$

or

$$\frac{s_2 - s_1}{R} \approx \frac{2\gamma}{(\gamma+1)^2} \frac{(M_1^2-1)^3}{3} \tag{6.23}$$

Scanned by CamScanner

Since the entropy cannot decrease in adiabatic flow, Eq. (6.23) shows that $M_1 \geq 1$. The increase in entropy is of *third order* in $(M_1^2 - 1)$. This may be written in terms of shock strength with Eq. (5.16) as

$$\frac{s_2 - s_1}{R} \approx \frac{\gamma + 1}{12\gamma^2}\left(\frac{\Delta p}{p_1}\right)^3 \tag{6.24}$$

But by Eq. (6.21), the shock strength is proportional to θ and hence

$$\boxed{\Delta s \sim \theta^3} \tag{6.25}$$

Thus, a small but finite change of pressure, for which there are corresponding first-order changes of pressure, density, and temperature, gives only a third-order change of entropy, i.e. a weak shock produces a nearly isentropic change of state.

Now, let the wave angle β for the weak shock be different from μ by a small angle $\varepsilon°$. That is,

$$\beta = \mu + \varepsilon$$

where $\varepsilon \ll \mu$. Therefore, $\sin\beta = \sin(\mu + \varepsilon) = \sin\mu + \varepsilon\cos\mu$. Also, $\sin\mu = 1/M_1$, and $\cot\mu = \sqrt{M_1^2 - 1}$. Thus,

$$M_1 \sin\beta \approx 1 + \varepsilon\sqrt{M_1^2 - 1} \tag{6.26}$$

or

$$M_1^2 \sin^2\beta \approx 1 + 2\varepsilon\sqrt{M_1^2 - 1} \tag{6.27}$$

From Eqs. (6.20) and (6.27), we obtain

$$\varepsilon = \frac{\gamma + 1}{4}\frac{M_1^2}{M_1^2 - 1}\theta \tag{6.28}$$

That is, for a finite deflection angle θ, the direction of weak oblique shock wave differs from the Mach wave direction μ by an amount ε, which is of the same order as θ.

6.7 SUPERSONIC COMPRESSION

Compressions in supersonic flow are not usually isentropic. Generally, they take place through shock waves and are nonisentropic. But there are certain cases, for which the compression is isentropic. A case in point is the one shown in Fig. 6.13, where the turning of the flow is achieved through a large number of weak oblique shocks.

The weak oblique shocks divide the field near the wall into segments of uniform flow. Away from the wall the weak shocks might coalesce and form a strong shock. As already seen in Section 6.6, the entropy increase across a weak wave is of the order of third power of deflection angle. Let the flow turning through an angle θ, shown in Fig. 6.13, be taking place through n weak waves, each wave turning the flow by $\Delta\theta$. Then the overall entropy change is

Scanned by CamScanner

$$s_n - s_1 \sim n(\Delta\theta)^3 \sim n\,\Delta\theta(\Delta\theta)^2 \sim \theta(\Delta\theta)^2$$

Thus, if the compression is achieved through a large number of weak waves, the entropy increase can be reduced to a very large extent compared to a single shock giving the same net deflection. When $\Delta\theta$ is made vanishingly small, the smooth turn shown in Fig. 6.13 is obtained. The entropy increase in such a case is vanishingly small, i.e. the compression can be treated as isentropic.

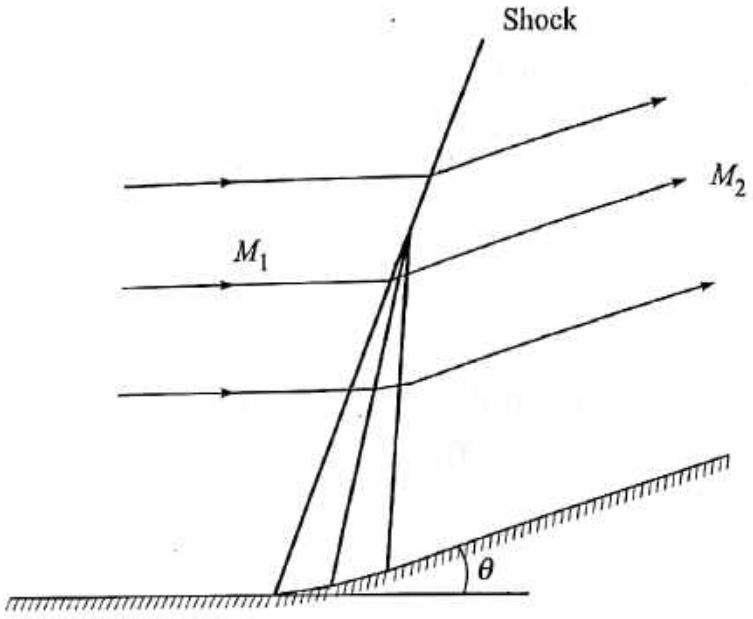


Fig. 6.13 Smooth continuous compression.

6.8 SUPERSONIC EXPANSION BY TURNING

Consider the turning of a two-dimensional supersonic flow through a finite angle at a convex corner, as illustrated in Fig. 6.14. Let us assume that the flow is turned by an oblique shock at the corner, as shown in the figure.

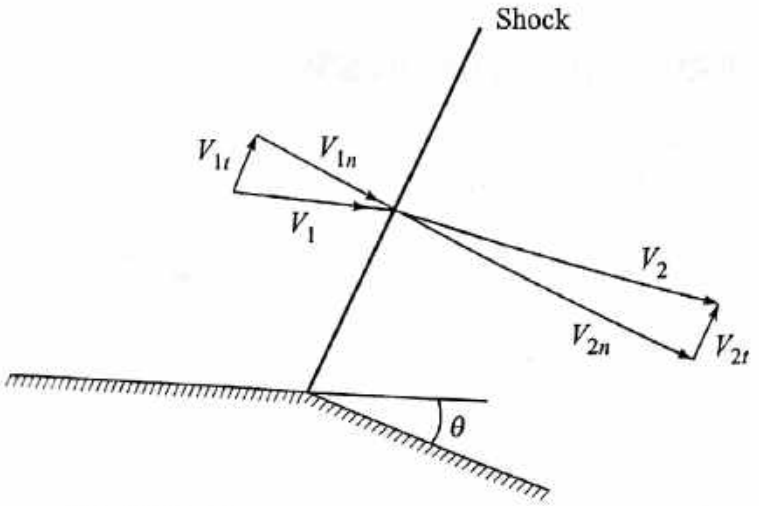


Fig. 6.14 Supersonic flow over convex corner.

Scanned by CamScanner

If the turn shown in Fig. 6.14 has to be made possible, then the normal component of velocity V_{2n} after the shock has to be greater than the normal component ahead of the shock, since V_{1t} and V_{2t} on either side of the shock must be equal. Although this would satisfy the equations of motion, it would lead to a decrease in entropy across the shock and, therefore, is not physically possible. From the geometry of the flow shown in Fig. 6.14, it follows that V_{2n} must be greater than V_{1n}. The normal momentum equation yields

$$p_1 + \rho_1 V_{1n}^2 = p_2 + \rho_2 V_{2n}^2$$

Combining this with continuity equation, we obtain

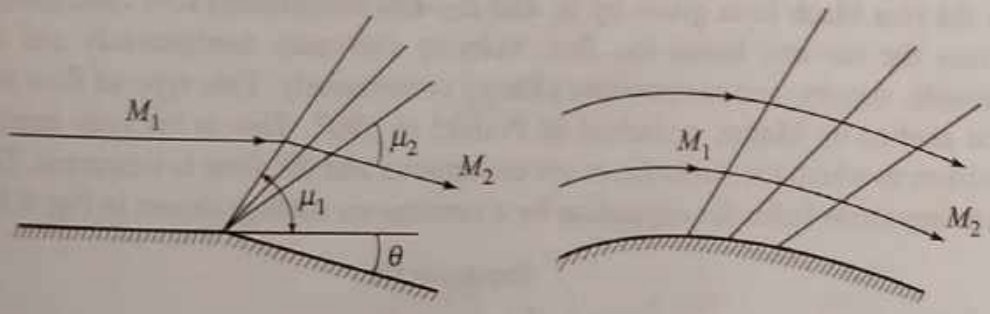
$$p_2 - p_1 = \rho_1 V_{1n}(V_{1n} - V_{2n})$$

Since $V_{2n} > V_{1n}$, it follows that $p_2 < p_1$, indicating that the resultant flow must be an expansion.

In an expansion process, the Mach lines are divergent, as shown in Fig. 6.15 and, consequently, there is a tendency to decrease the gradients of pressure, density, and temperature. In other words, an expansion is isentropic throughout of a simple continuous expansion [Fig. 6.15(b)], whereas it is isentropic everywhere except at the vertex for centred expansion [Fig. 6.15(a)].

The expansion at a corner [Fig. 6.15(a)] occurs through a centred wave, defined by a 'fan' of straight Mach lines. This centred wave, also called a Prantdl–Meyer expansion fan, is the counterpart, for a convex corner, of the oblique shock at a concave corner.

A typical expansion over a continuous convex turn is shown in Fig. 6.15(b). Since the flow is isentropic, it is reversible.



(a) Centred expansion (b) Simple expansion

Fig. 6.15 Expanding flows.

The expansion rays in Figure 6.15 are referred to as Mach lines in a loose sense. Essentially they are "expansion waves" or expansion rays. Even though, like Mach waves, the Mach lines are also isentropic waves, they distinctly differ from Mach waves in the sense that the change in flow properties across a Mach line (expansion wave) is small but finite, whereas across a Mach wave the change in flow properties is negligibly small.

Scanned by CamScanner

6.9 THE PRANDTL–MEYER EXPANSION

Now, we are familiar with the fact that the supersonic flow around a convex corner involves a smooth, gradual change in flow properties. The Prandtl–Meyer fan consists of an infinite number of Mach waves, centred at the convex corner. There are two Mach lines, one at an angle μ_1 to the initial flow (upstream of fan) direction and the other at an angle μ_2 to the final flow (downstream of fan) direction. The change in Mach number from M_1 to M_2 takes place through an infinite number of Mach waves. There is a wedge-like space with the corner as the apex, as shown in Fig. 6.16, bounded

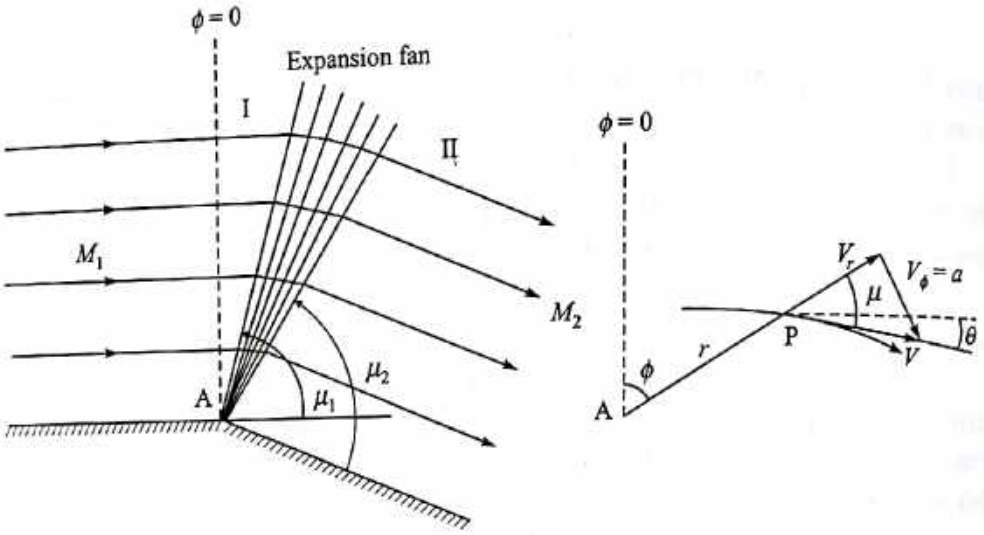


Fig. 6.16 Prandtl–Meyer corner flow.

by the two Mach lines given by μ_1 and μ_2. The streamlines turn continuously across the fan and hence the flow velocity increases continuously and the pressure, density, and temperature change continuously. This type of flow was first studied by Meyer, a student of Prandtl in 1907. This is the only turning problem in which the streamlines are continuous and the flow is isentropic. The same argument holds for expansion by a continuous surface shown in Fig. 6.17.

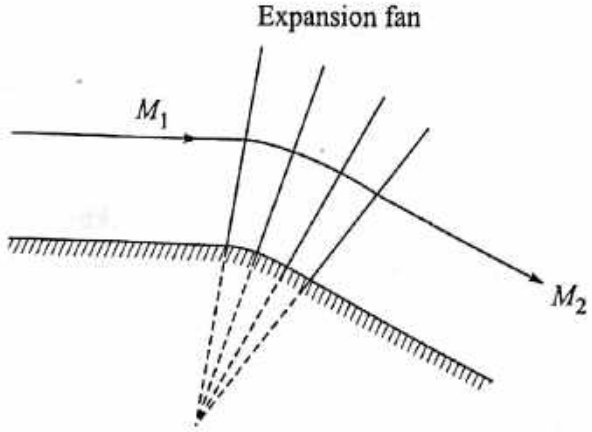


Fig. 6.17 Expansion in a continuous corner.

Scanned by CamScanner

This type of flow is important from the mathematical point of view, since it is the only problem where an exact solution to the nonlinear compressible flow equation exists. In polar coordinates, the equations of motion for such flow can be written as

$$\frac{\partial}{\partial r}(\rho r V_r) + \frac{\partial}{\partial \phi}(\rho V_\phi) = 0 \tag{6.29}$$

$$V_r \frac{\partial V_r}{\partial r} + \frac{V_\phi}{r}\frac{\partial V_r}{\partial \phi} - \frac{V_\phi^2}{r} = -\frac{1}{\rho}\frac{\partial p}{\partial r} \tag{6.30}$$

$$V_r \frac{\partial V_\phi}{\partial r} + \frac{V_\phi}{r}\frac{\partial V_\phi}{\partial \phi} + \frac{V_r V_\phi}{r} = -\frac{1}{\rho}\frac{1}{r}\frac{\partial p}{\partial \phi} \tag{6.31}$$

Equation (6.29) is the continuity equation, and Eqs. (6.30) and (6.31) are the r and ϕ momentum equations, respectively. The momentum equations of this type for inviscid flow are also called Euler's equations. Note that in the above equations, r and ϕ are used as the variables for polar coordinates instead of the conventional r and θ to avoid clash with the flow deflection angle θ.

From the geometry of the flow it is reasonable to assume that the flow properties do not change along any radial line, i.e. they vary only with ϕ and are independent of r. This is a reasonable (also valid) assumption and considerably simplifies the equations.

By the above assumption, the derivatives of flow properties with respect to r are zero and so Eqs. (6.29)–(6.31) are no more partial, i.e.

$$\frac{\partial V_r}{\partial r} = \frac{\partial p}{\partial r} = \frac{\partial V_\phi}{\partial r} = 0$$

Equations (6.29)–(6.31) now become

$$\rho V_r + \frac{d}{d\phi}(\rho V_\phi) = 0 \tag{6.32}$$

$$V_\phi = \frac{dV_r}{d\phi} \tag{6.33}$$

$$V_\phi\left(\frac{dV_\phi}{d\phi} + V_r\right) = -\frac{1}{\rho}\frac{dp}{d\phi} \tag{6.34}$$

But $dp/d\phi$ can be expressed as

$$\frac{dp}{d\phi} = \frac{dp}{d\rho}\frac{d\rho}{d\phi} = a^2\frac{d\rho}{d\phi}$$

Using this equation and relation (6.32), Eq. (6.34) can be rewritten as

$$\left(V_r + \frac{dV_\phi}{d\phi}\right)\left(1 - \frac{V_\phi^2}{a^2}\right) = 0 \tag{6.35}$$

Scanned by CamScanner

This is the governing equation for the Prandtl–Meyer flow. First, let the term in the first set of parentheses in Eq. (6.35) be zero, i.e.

$$V_r + \frac{dV_\phi}{d\phi} = 0$$

Then from Eq. (6.34), we get

$$\frac{dp}{d\phi} = 0$$

This implies that the pressure is constant throughout the flow field and so there can be no expansion. But the basic geometry considered is an expansion field and, therefore, the above solution is impossible. Hence, from Eq. (6.35) we have

$$1 - \frac{V_\phi^2}{a^2} = 0$$

i.e.

$$\boxed{V_\phi = a} \tag{6.36}$$

The velocity is constant along the radial lines and is equal to the local speed of sound. This means that the radial lines must correspond to *Mach lines*. The Mach angle is given by

$$\sin \mu = \frac{V_\phi}{V} = \frac{a}{V} = \frac{1}{M}$$

Hence, all rays in an expansion field are Mach lines and the entire flow is isentropic.

Velocity Components V_r and V_ϕ

By compressible Bernoulli's equation, we have

$$\frac{\gamma}{\gamma-1}\frac{p}{\rho} + \frac{V^2}{2} = \frac{\gamma}{\gamma-1}\frac{p_0}{\rho_0} = \frac{V_{\max}^2}{2}$$

where p_0 and ρ_0 are stagnation pressure and density respectively. The resultant velocity V and the ϕ-component of velocity are given by

$$V^2 = V_r^2 + V_\phi^2$$

$$V_\phi^2 = a^2 = \frac{\gamma p}{\rho}$$

With the above two relations, Bernoulli's equation may be rewritten as

$$V_r^2 + \frac{\gamma+1}{\gamma-1}V_\phi^2 = V_{\max}^2 \tag{6.37}$$

For the present flow, the velocity and pressure are constants along the radial lines and, therefore, Eq. (6.30) reduces to

Scanned by CamScanner

$$\frac{dV_r}{d\phi} = V_\phi$$

Substituting the above expression for V_ϕ into Eq. (6.37), we get

$$\frac{dV_r}{d\phi} = V_{max}\sqrt{\frac{\gamma-1}{\gamma+1}}\sqrt{1-\left(\frac{V_r}{V_{max}}\right)^2}$$

Integration of the above equations by separation of variables gives

$$\phi\sqrt{\frac{\gamma-1}{\gamma+1}} = \text{arc sin}\left(\frac{V_r}{V_{max}}\right) + \text{constant} \tag{6.38}$$

From Fig. 6.16, when $\phi = 0$, constant = 0. Therefore, Eq. (6.38) yields

$$V_r = V_{max}\sin\left(\phi\sqrt{\frac{\gamma-1}{\gamma+1}}\right) \tag{6.39}$$

From Eqs. (6.39) and (6.33), we obtain

$$V_\phi = V_{max}\sqrt{\frac{\gamma-1}{\gamma+1}}\cos\left(\phi\sqrt{\frac{\gamma-1}{\gamma+1}}\right) \tag{6.40}$$

For $\phi = 0$, Eq. (6.40) gives

$$V_\phi = V_{max}\sqrt{\frac{\gamma-1}{\gamma+1}}$$

Substituting for V_{max} from Bernoulli's equation, we get

$$V_\phi = \sqrt{\frac{2\gamma}{\gamma+1}\frac{p_0}{\rho_0}} = \sqrt{\frac{2}{\gamma+1}}a_0 = a^*$$

i.e. at the beginning of the fan the ϕ-component of velocity corresponds to the speed of sound at sonic condition.

We can also express the pressure at any point in the Prandtl–Meyer flow in terms of ϕ as follows: With the resultant velocity $V^2 = V_r^2 + V_\phi^2$, Bernoulli's equation can be expressed as

$$V_r^2 + V_\phi^2 = V_{max}^2\left[1-\left(\frac{p}{p_0}\right)^{(\gamma-1)/\gamma}\right]$$

Replacing V_r and V_ϕ by Eqs. (6.39) and (6.40), we get

$$\left(\frac{p}{p_0}\right)^{(\gamma-1)/\gamma} = \frac{1}{\gamma+1}\left[1+\cos\left(2\phi\sqrt{\frac{\gamma-1}{\gamma+1}}\right)\right] \tag{6.41}$$

The derivation of Eq. (6.41) is left as an exercise to the reader.

From Eq. (6.41), it is seen that the flow can be turned by an angle ϕ_{max} where the pressure p will become zero. This condition results in

Scanned by CamScanner

$$\phi_{max} = \frac{\pi}{2}\sqrt{\frac{\gamma+1}{\gamma-1}} \tag{6.42}$$

For this situation,

$$V_r = V_{max}, \quad V_\phi = 0$$

For air as perfect gas with $\gamma = 1.4$,

$$\boxed{\phi_{max} = 220.5^\circ}$$

$$\boxed{\theta = 130.5^\circ}$$

From the foregoing discussion, it is seen that the beginning of the Prandtl–Meyer expansion is marked by $\phi = 0$, where the radial component of flow velocity is zero and the expansion can go to a maximum extent where the static pressure of the flow goes to zero and the ϕ-component of flow velocity also vanishes. The values of expansion angle and flow deflection angle are 220.5° and 130.5°, respectively. The expansion described can be shown graphically as shown in Fig. 6.18. The normal direction to the hodograph curve in the figure gives the Mach line direction in the physical plane.

The Prandtl–Meyer Function

It is known from basic studies on fluid flows that a motion which preserves its own geometry in space or time or both is called *self-similar*. In the simplest cases of flows, such motions are described by a single independent variable, referred to as similarity variable. The Prandtl–Meyer expansion is one such self-similar motion, and hence the *Prandtl–Meyer function is a similarity variable.*

From the geometry of flow in Fig. 6.16, $\theta = \phi + \mu - \pi/2$, where θ is the isentropic turning angle.

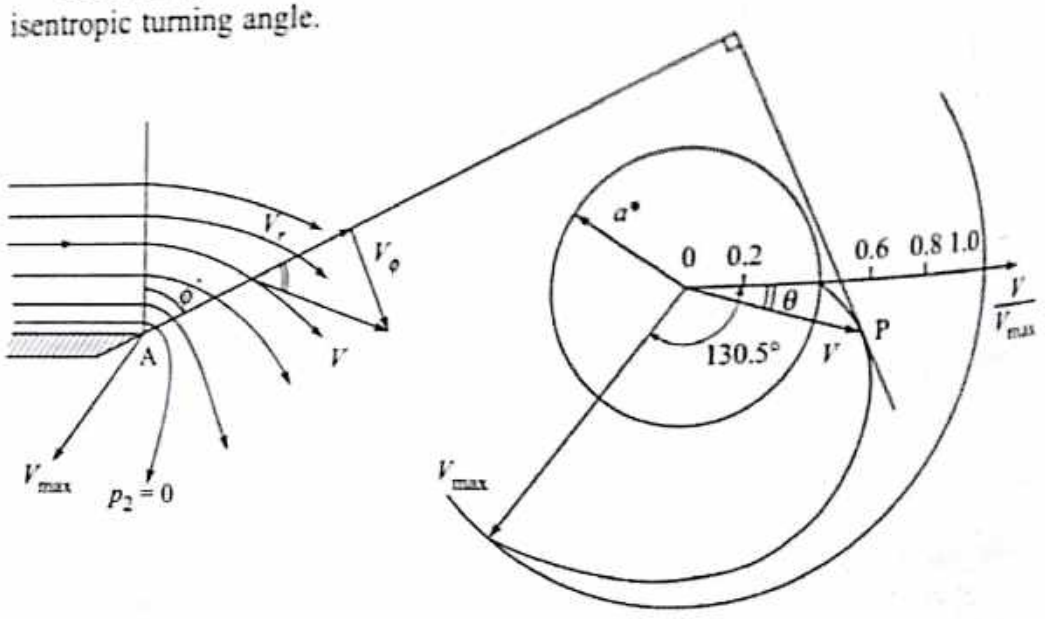


Fig. 6.18 Expansion around a corner.

Scanned by CamScanner

Now, we define the quantity ν such that $\nu = \pm\theta$, where "+" holds across a *right-running characteristic* and "–" across a *left-running characteristic*. This function ν is called the Prandtl–Meyer function. From the above definition,

$$\nu = \phi + \mu - \pi/2 \tag{6.43}$$

or

$$\phi = \pi/2 + \nu - \mu \tag{6.44}$$

From the flow geometry of Fig. 6.16,

$$\tan \mu = V_\phi / V_r$$

Substituting for V_ϕ and V_r from Eqs. (6.39) and (6.40), we get

$$\tan \mu = \sqrt{\frac{\gamma-1}{\gamma+1}} \cot\left(\phi\sqrt{\frac{\gamma-1}{\gamma+1}}\right) \tag{6.45a}$$

or

$$\cot \mu = \sqrt{\frac{\gamma+1}{\gamma-1}} \tan\left(\phi\sqrt{\frac{\gamma-1}{\gamma+1}}\right) \tag{6.45b}$$

However,

$$\cot \mu = \sqrt{M^2-1} \tag{6.46}$$

With this the above equation can be expressed as

$$\sqrt{\frac{\gamma-1}{\gamma+1}(M^2-1)} = \tan\left(\phi\sqrt{\frac{\gamma-1}{\gamma+1}}\right)$$

or

$$\phi = \sqrt{\frac{\gamma+1}{\gamma-1}} \arctan\sqrt{\frac{\gamma-1}{\gamma+1}(M^2-1)}$$

Substitution of ϕ from Eq. (6.44) into the above equation results in

$$\nu = \sqrt{\frac{\gamma+1}{\gamma-1}} \arctan\sqrt{\frac{\gamma-1}{\gamma+1}(M^2-1)} + \mu - \frac{\pi}{2}$$

From Eq. (6.46), we have the Mach angle

$$\mu = \operatorname{arccot}\sqrt{(M^2-1)}$$

Also, $\operatorname{arccot}\sqrt{(M^2-1)} = \pi/2 - \arctan\sqrt{(M^2-1)}$.

Using the above relations, we obtain

$$\boxed{\nu = \sqrt{\frac{\gamma+1}{\gamma-1}} \arctan\sqrt{\frac{\gamma-1}{\gamma+1}(M^2-1)} - \arctan\sqrt{(M^2-1)}} \tag{6.47}$$

Equation (6.47), expressing the Prandtl–Meyer function ν in terms of the Mach number, is a very important result of supersonic flow. From this relation, it is

Scanned by CamScanner

seen that for a given M, there is a fixed ν. Physically, ν is the flow inclination from $M = 1$ (i.e. $\phi = 0$) line.

If the wall inclination is θ, then ν_2 can be obtained by adding θ to ν_1, i.e. $\nu_2 = \nu_1 + \theta$. As M varies from 1 to ∞, ν increases from 0 to ν_{max}. When $\phi = 0$, $M_1 = 1$ and $\nu = 0$. When $\phi_1 = 220.5°$ or $\theta_{max} = 130.5°$, $M_2 = \infty$ and $\nu = \nu_{max}$. This maximum for ν is

$$\nu_{max} = \frac{\pi}{2}\left(\sqrt{\frac{\gamma+1}{\gamma-1}} - 1\right) \tag{6.48}$$

For air with $\gamma = 1.4$, $\nu_{max} = 130.5°$ for $M = \infty$. The Prandtl–Meyer function is tabulated in the isentropic flow tables (Table A1 of the Appendix A).

EXAMPLE 6.4 (ISENTROPIC EXPANSION) A uniform flow at $M_1 = 2.0$ passes over an expansion corner with wall inclination of 10°. Find the Mach number of the flow downstream of the expansion fan.

Solution Given

$$M_1 = 2, \qquad \theta = 10°$$

From Table A1 of Appendix A for $M_1 = 2$,

$$\nu_1 = 26.38°$$

Therefore,

$$\nu_2 = \nu_1 + \theta = 26.38° + 10° = 36.38°$$

Again, from Table A1, for $\nu_2 = 36.38°$

$$M_2 = \boxed{2.386}$$

Compression

The supersonic flow over a continuous compression corner, discussed in Section 6.7, resulting in isentropic compression of flow is similar to the Prandtl–Meyer expansion except that compression results in isentropic deceleration of flow and expansion accelerates the flow isentropically. In expansion, all Mach lines diverge, whereas in compression, all Mach lines converge. The purpose of Mach lines is to change the direction of streamlines in such a way that they are parallel to the solid boundary. For isentropic compression too, the Prandtl–Meyer function can be used, but this is restricted to the flow near the wall only.

EXAMPLE 6.5 (ISENTROPIC COMPRESSION) A uniform flow at $M_1 = 2.0$ passes over an isentropic compression corner. Find the downstream Mach number of the flow following a 10° turn.

Solution Given

$$M_1 = 2, \quad \theta = 10°$$

Scanned by CamScanner

From Table A1 of Appendix A for $M_1 = 2$,

$$\nu_1 = 26.38°$$

After the compression, the Prandtl–Meyer function becomes

$$\nu_2 = \nu_1 - \theta = 16.381°$$

Again, from Table A1, for $\nu_2 = 16.38°$

$$M_2 = \boxed{1.652}$$

Instead of continuous change, if the compression is caused by only one kink of the wall of about 10°, the compressions cannot be isentropic and the turning of the flow will take place through a shock as shown in Fig. 6.19. Only when the compression is continuous, the process can be treated as isentropic. However, for small values of θ, it can still be treated as isentropic, and reasonably accurate results can be obtained. $\theta \leq 5°$ may be taken as the limit for considering the compression to be isentropic.

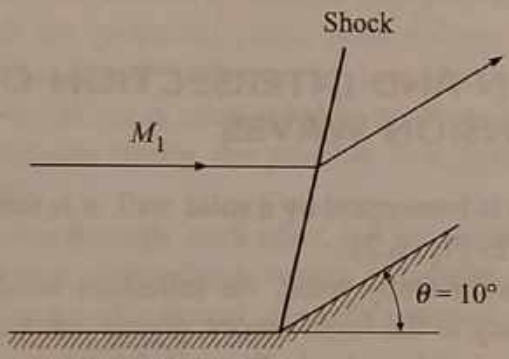


Fig. 6.19 Example 6.5.

From the above discussion it is clear that the relation between the Prandtl–Meyer function and the flow turning angle may be expressed as

$$\nu_n = \nu_{n-1} + |\theta_n - \theta_{n-1}| \quad \text{(expansion)} \qquad (6.49a)$$

$$\nu_n = \nu_{n-1} - |\theta_n - \theta_{n-1}| \quad \text{(compression)} \qquad (6.49b)$$

6.10 SIMPLE AND NONSIMPLE REGIONS

The waves causing isentropic expansion and compression discussed in Section 6.9 are called *simple waves*. A simple wave is a straight Mach line, with constant flow conditions, and is governed by the simple relations (Eqs. (6.49)) between the flow direction and the Prandtl–Meyer function.

A supersonic flow field with simple and nonsimple regions is shown in Fig. 6.20. Supersonic expansion or compression with Mach lines which are straight is called a *simple region*. The simple equations (6.49a) and (6.49b) are not applicable to nonsimple regions. Such a region may be treated by the method

Scanned by CamScanner

of characteristics. The method of characteristics is discussed in detail in Chapter 12.

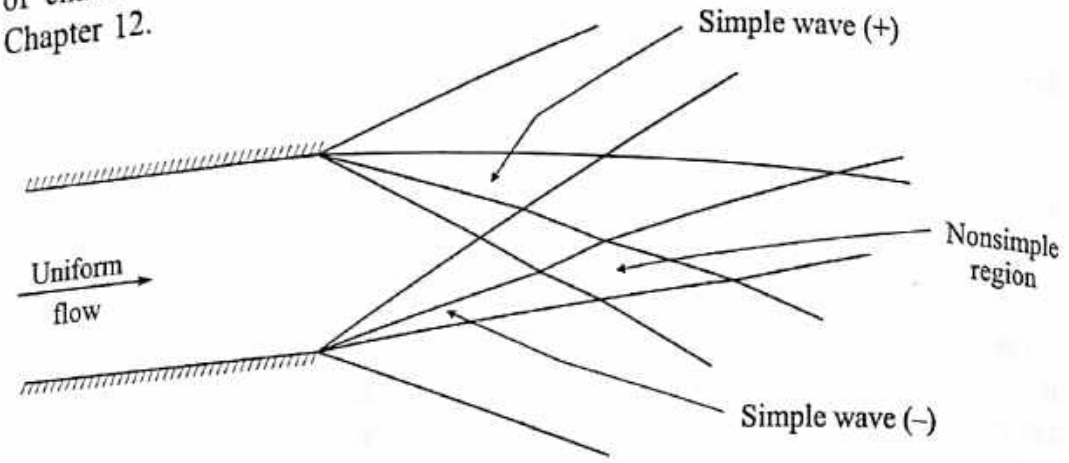


Fig. 6.20 Regions in isentropic supersonic flow.

The Mach lines which are straight in the simple region become curved in the nonsimple region, after intersection with other Mach lines.

6.11 REFLECTION AND INTERSECTION OF SHOCKS AND EXPANSION WAVES

When an oblique shock is intercepted by a solid wall, it is reflected. A possible flow field is as shown in Fig. 6.21.

If the shock were sufficiently weak, the reflection would be regular and could be treated according to the linear theory, giving just a reflected shock of the same strength as the incident shock. For a shock which is not necessarily weak, the incident shock deflects the flow through an angle θ towards the wall.

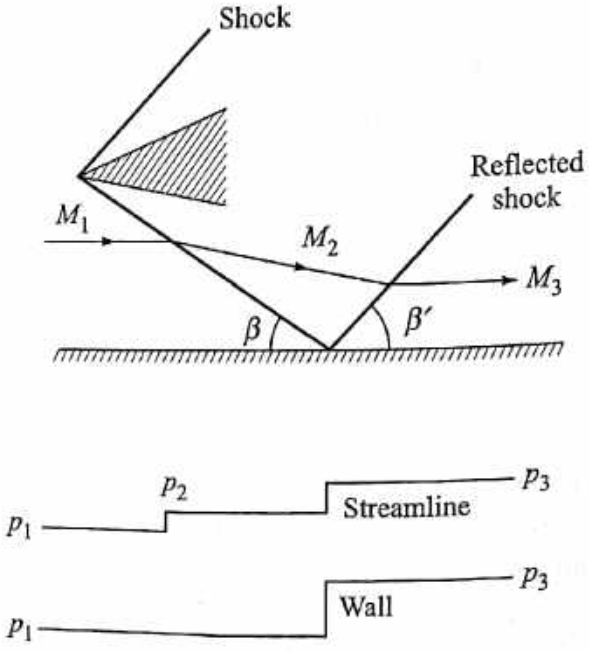


Fig. 6.21 Shock reflection from a rigid wall.

Scanned by CamScanner

A second reflected shock of opposite family is required to turn the flow back again by an amount θ, to satisfy the constraint of the wall.

Although the flow deflection θ, produced by the incident and reflected shocks, are equal in magnitude, the pressure ratios are not, since $M_2 < M_1$. The pressure distribution along a streamline and along the wall are as shown in Fig. 6.21. The strength of the reflection may be defined by the overall pressure ratio.

$$\frac{p_3}{p_1} = \frac{p_3}{p_2}\frac{p_2}{p_1}$$

But p_3/p_2 and p_2/p_1 are the strengths of reflected and incident shocks, respectively. Therefore, the strength of reflection is given by the product of individual shock strengths.

The reflection from a rigid surface, in general, is not specular, i.e. the reflected shock inclination (β') is not equal to the incident shock inclination (β). Now there exists one of the two possibilities. i.e. either $\beta > \beta'$ or $\beta < \beta'$. These two cases are opposite, and the net result depends on the particular values of M_1 and θ. These results cannot be written explicitly in general form but may easily be obtained, for particular cases, from oblique shock charts. For high Mach numbers (M_1), $\beta > \beta'$, whereas for low Mach numbers, $\beta < \beta'$.

When an oblique shock is intercepted by another oblique shock of the same strength but of opposite family, the possible flow field will look like the one shown in Fig. 6.22.

The shocks 'pass through' each other, but are slightly 'bent' in the process. The flow downstream of the shock system is parallel to the initial flow.

When two shocks of unequal strength intersect, a new flow geometry appears as shown in Fig. 6.23.

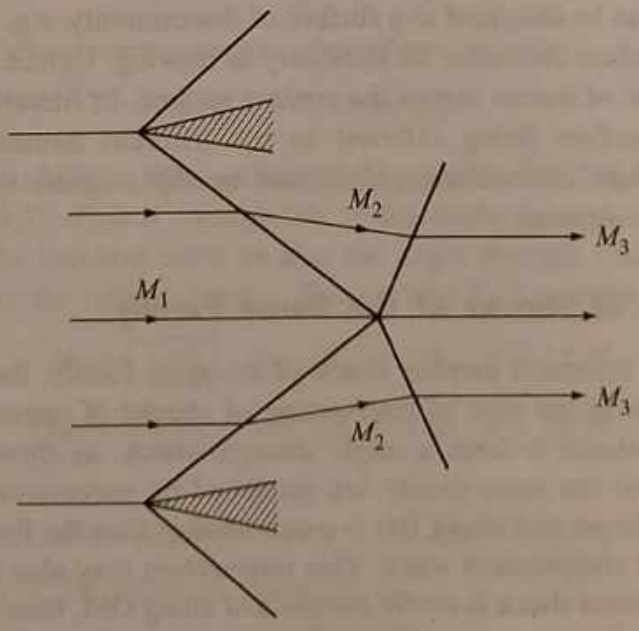


Fig. 6.22 Interaction of two shocks of opposite families with equal strengths.

Scanned by CamScanner

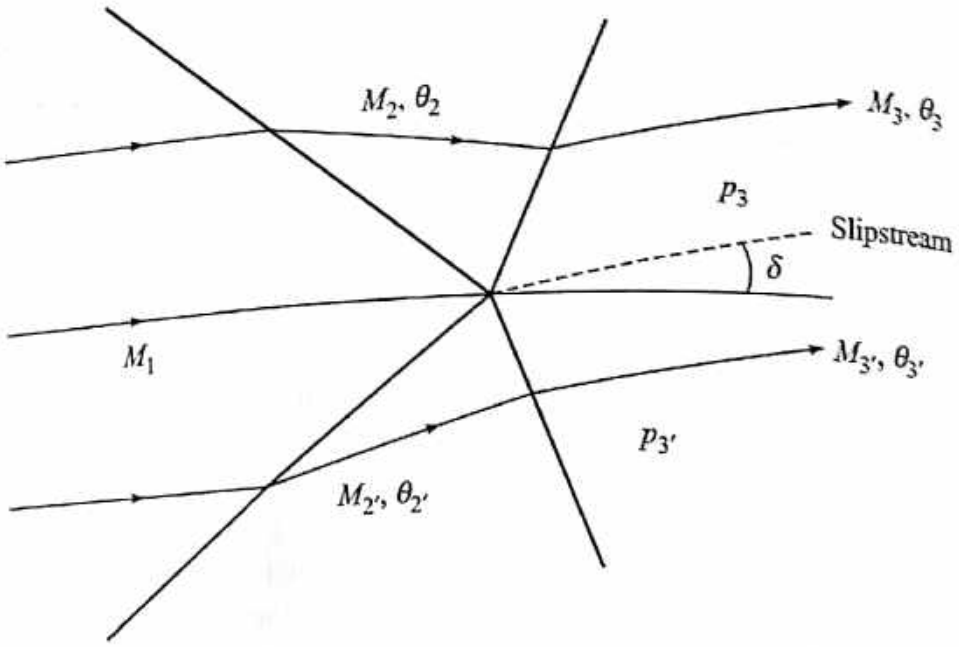


Fig. 6.23 Interaction of two shocks of opposite families with different strengths.

The flow field is divided into two portions by the streamline through the intersection points. The two portions experience different changes in traversing the shock wave system. The overall results must be such that the two portions have the same pressure and the same flow direction, i.e. $p_3 = p_{3'}$ and $\theta_3 = \theta_{3'}$. The flow downstream of the reflected shocks (zone 3) need not be in the freestream direction. These two requirements determine the final direction δ and the final pressure p_3.

The streamline shown with dashed line, having two flow fields of different parameters (T and ρ) on either side of it, is called *contact surface*. The contact surface may also be *idealized* as a surface of discontinuity, e.g. the shock wave. The contact surface can either be stationary or moving. Unlike the shock wave, there is no flow of matter across the contact surface. In literature, we can find this contact surface being referred to by different names, e.g. *material boundary, entropy discontinuity, slipstream* or *slip surface, vortex sheet,* and *tangential discontinuity.*

Intersection of Shocks of the Same Family

When a shock intersects another shock of the same family, the shocks cannot pass through as in the case of intersection of shocks of opposite family. The shocks will coalesce to form a single stronger shock, as shown in Fig. 6.24, where shocks of the same family are produced by successive corners in the same wall. If the second shock BO is much weaker than the first one AO, then OC will be the compression wave. This intersection may also be described as follows: the second shock is partly *transmitted* along OM, thus augmenting the strength of the first one, and partly reflected along OC.

Scanned by CamScanner

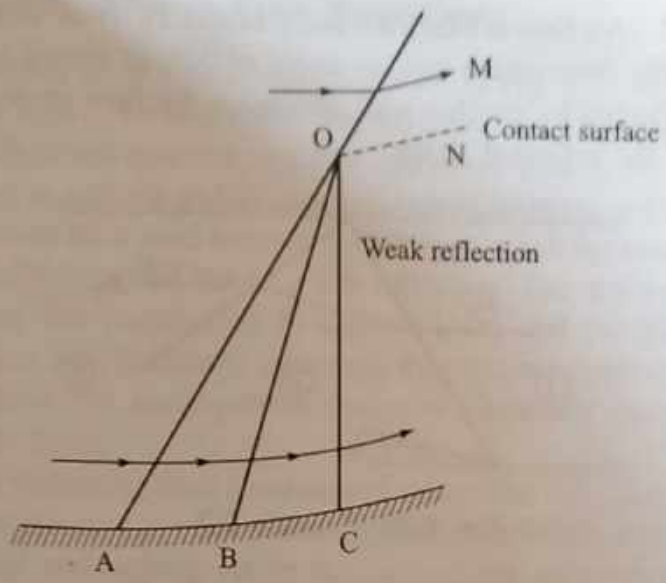


Fig. 6.24 Intersection of waves of the same family.

EXAMPLE 6.6 For the flow field shown in Fig. 6.25, determine β_r, M_2 and M_3 if $M_1 = 2.0$ and $\beta_i = 40°$.

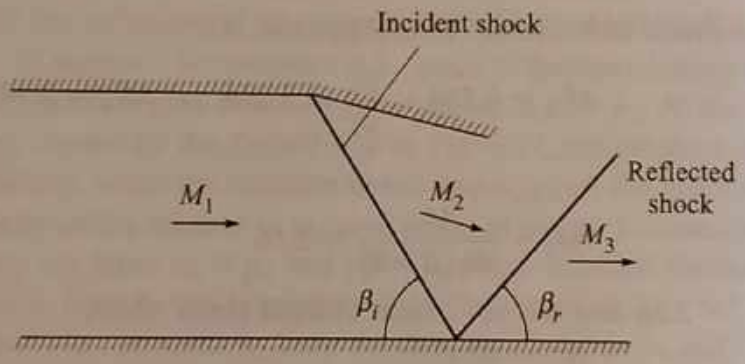


Fig. 6.25 Example 6.6.

Solution From oblique shock Chart 1 (Appendix D), for $M_1 = 2.0$ and $\beta_i = 40°$, $\theta = 10.5°$. This θ corresponds to the angle through which the flow is turned after the incident wave as also the angle through which the flow is turned back after the reflected wave. From Chart 2 (Appendix D),

$$M_2 = \boxed{1.63} \quad \text{for } M_1 = 2.0, \quad \theta = 10.5°$$

$$M_3 = \boxed{1.3} \quad \text{for } M_2 = 1.63, \ \theta = 10.5°$$

From Chart 1,

the shock wave angle $\beta = 50.2°$ for $M_2 = 1.63$, $\theta = 10.5°$

The wave angle of the reflected shock, β_r, is

$$\beta_r = 50.2 - 10.5 = \boxed{39.7°}$$

Scanned by CamScanner

EXAMPLE 6.7 Air flow at Mach 4.0 and pressure 10^5 N/m^2 is turned abruptly by a wall into the flow with a turning angle of 20°, as shown in Fig. 6.26. If the shock is reflected by another wall determine the flow properties M and p downstream of the reflected shock.

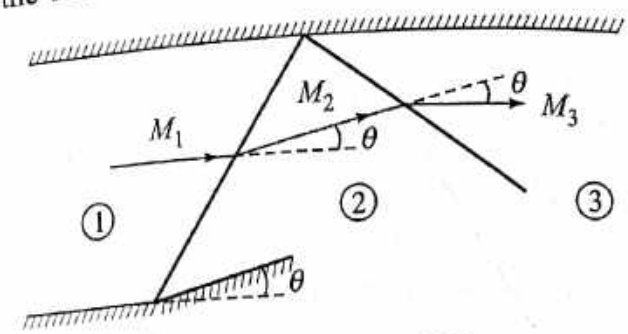


Fig. 6.26 Example 6.7.

Solution From the oblique shock chart (Appendix D),

$$\beta_{12} = 32.5° \quad \text{for } M_1 = 4.0,\ \theta = 20°$$

Hence,

$$M_{1n} = M_1 \sin \beta = 2.149$$

From normal shock table (Table A1 of Appendix A),

$$M_{2n} = 0.554, \quad \frac{p_2}{p_1} = 5.226 \quad \text{at } M_{1n} = 2.149$$

Therefore,

$$M_2 = \frac{M_{2n}}{\sin(\beta - \theta)} = 2.56$$

Now, for $M_2 = 2.56$ and $\theta = 20°$, from oblique shock chart,

$$\beta_{23} = 42.11°$$

$$M_{2n} = M_2 \sin \beta_{23} = 1.70$$

For $M_{2n} = 1.70$, normal shock table gives

$$M_{3n} = 0.64, \quad \frac{p_3}{p_2} = 3.205$$

Hence,

$$M_3 = \frac{0.64}{\sin(42.11° - 20°)} = \boxed{1.7}$$

Thus,

$$\frac{p_3}{p_1} = \frac{p_3}{p_2}\frac{p_2}{p_1} = 3.205 \times 5.226 = 16.75$$

$$p_3 = \boxed{16.75 \times 10^5 \text{ N/m}^2}$$

Note: Problems involving oblique shocks can also be solved using the oblique shock tables instead of oblique shock charts.

Scanned by CamScanner

Wave Reflection from a Free Boundary

Reflection of shock from a solid wall is shown in Fig. 6.21 and based on the analysis of that figure, we also know that the reflection from a solid boundary, though generally is not specular, is a *like reflection*. That is, an incident shock will be reflected as a shock and an incident expansion wave will be reflected as an expansion wave by a solid boundary. However, when the boundary is a free boundary the reflection will not be a like reflection. The wave patterns shown emanating from the nozzle exit in Figs. 4.11(b) and (c) experience such reflection from a free boundary. Although they are not inherently quasi-one-dimensional flows, the wave pattern shown is frequently encountered in the study of nozzle flows.

The gas jet emanating from a nozzle and exhausting into the surrounding still atmosphere (of pressure p_a) has a boundary surface which interfaces with the surrounding still atmosphere. As in the case of the slipstreams discussed in Section 6.11, the pressure across this boundary must be preserved, i.e. the jet boundary pressure must be equal to p_a along its complete length. Therefore, the waves must reflect from the jet boundary in such a manner as to preserve the pressure at the boundary downstream of the nozzle exit. The free boundary, unlike a solid boundary, can change its size and direction.

Examine the reflection of an oblique shock from a free boundary, as shown in Fig. 6.27. In region 1, the pressure is p_1, equal to the surrounding atmosphere. The pressure in the region downstream of shock is $p_2 > p_1$. At the edge of the jet boundary, shown by the dashed line in Fig. 6.27, the pressure must always be p_1. Therefore, when the incident shock impinges on the boundary, it must be reflected in such a manner as to result in p_1, in region 3 behind the reflected wave. Hence we have $p_3 = p_1$ and $p_1 < p_2$. This situation demands that the reflected wave must be an expansion wave, as shown in Fig. 6.27. The flow in turn is deflected upwards by both the incident shock wave and the reflected expansion fan, resulting in the upward deflection of the free boundary.

Reflection of an expansion fan from a free boundary is shown in Fig. 6.28. The expansion fan is reflected from the free boundary as compression waves.

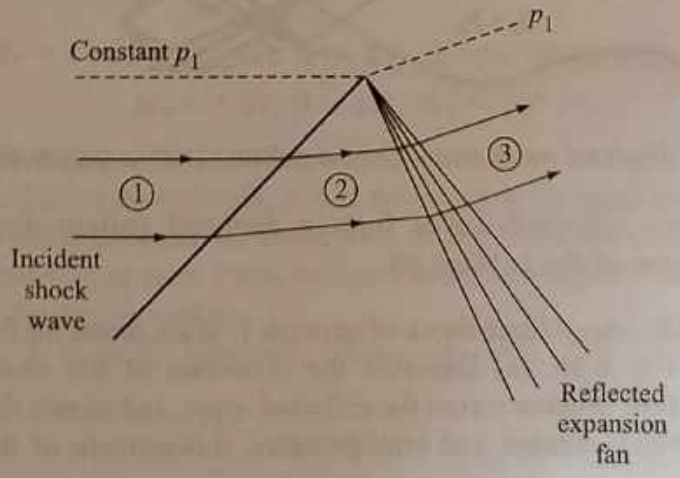


Fig. 6.27 Shock wave reflection from a free boundary.

Scanned by CamScanner

These waves coalesce into a shock wave, as shown. The wave interaction shown in Fig. 6.28 should be analysed by the method of characteristics, which will be discussed in Chapter 12.

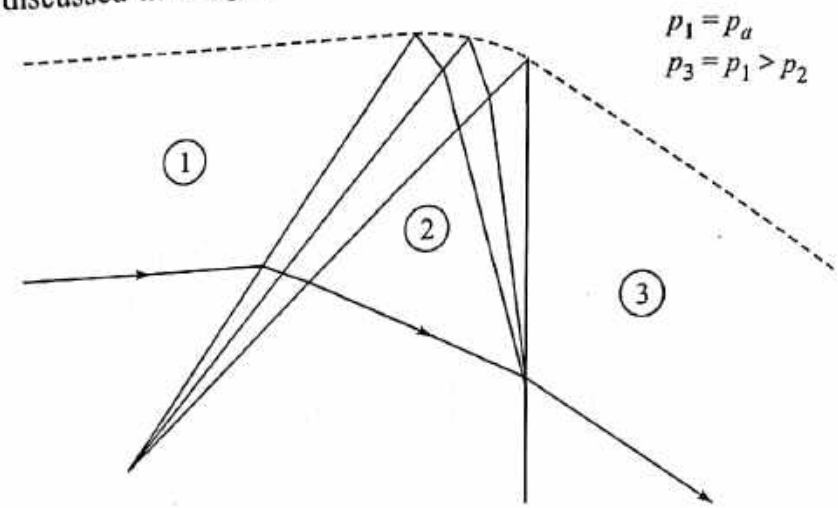


Fig. 6.28 Reflection of an expansion fan from a free boundary.

From the above discussion, the following two observations can be made:

1. The reflection of an incident shock wave from a solid boundary is called a *like reflection* i.e. a shock wave reflects as a shock and an expansion wave reflects as an expansion wave.
2. The reflection of an incident shock wave from a free boundary is called an *unlike reflection* (opposite manner), i.e. a shock wave reflects as an expansion wave and an expansion wave reflects as a shock (a compression wave).

Consider the overexpanded nozzle flow in Fig. 4.11(b). The flow pattern downstream of the nozzle exit will appear as shown in Fig. 6.29.

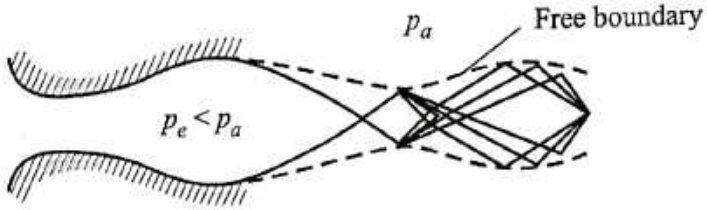


Fig. 6.29 Diamond wave pattern in the exhaust from a supersonic nozzle.

The various reflected waves form a diamond pattern throughout the supersonic region of the exhaust jet.

EXAMPLE 6.8 An oblique shock of strength 1, in air, meets the free boundary as shown in Fig. 6.30. (a) Describe the reflection of the shock from the boundary, the flow process across the reflected wave, and sketch the reflection. (b) Find the Mach number and total pressure, downstream of the reflection

Scanned by CamScanner

zone, and (c) find the fan angle of the expansion. (d) Determine the deflection angle of the free boundary with reference to the freestream direction, upstream of the shock, and check whether the flow downstream of the expansion satisfies the streamline concept.

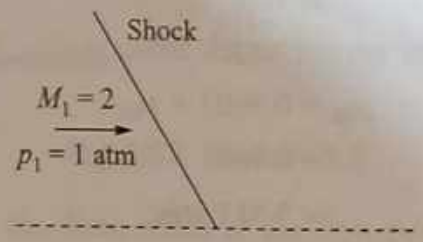


Fig. 6.30 Example 6.8.

Solution (a) The reflection of shock from the free boundary is unlike. Thus, the oblique shock will reflect as an expansion fan, as shown in Fig. 6.31. The flow process across the expansion fan will be isentropic everywhere, except at the vertex of the fan, where the flow is nonisentropic.

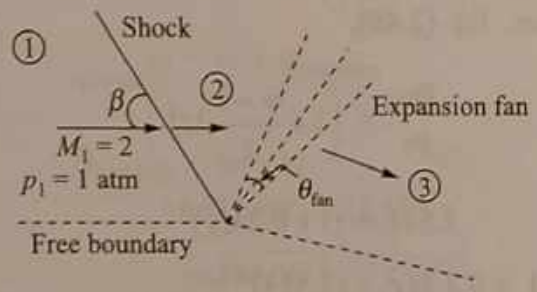


Fig. 6.31 Example 6.8.

Given, the shock strength is 1. That is, $\Delta p/p_1 = 1$; therefore,

$$\frac{p_2 - p_1}{p_1} = 1$$

$$\frac{p_2}{p_1} = 2$$

(b) For $M_1 = 2$ and $p_2/p_1 = 2$, from the oblique shock table,

$$M_2 = 1.49,\ \beta \approx 44^\circ,\ \theta_{12} = 14^\circ$$

The shock gets reflected as an expansion fan, as shown in Fig. 6.31. The free boundary is deflected downwards. A free boundary is identical to a slipstream; therefore, the static pressure on either side of the boundary should be equal. Thus, the pressure p_3 at zone 3 will be equal to the atmospheric pressure on the other side of the free boundary.

For $M_1 = 2$, from the isentropic table, $p_1/p_{01} = 0.1278$. Therefore,

$$p_{01} = \frac{1}{0.1278}$$

$$= 7.82 \text{ atm}$$

Scanned by CamScanner

The Mach number normal to the shock is

$$M_{1n} = M_1 \sin \beta$$
$$= 2 \times \sin 44°$$
$$= 1.39$$

For $M_{1n} = 1.39$, from the normal shock table, $p_{02}/p_{01} = 0.9607$. Therefore,

$$p_{02} = 0.9607 \times p_{01}$$
$$= 0.9607 \times 7.82$$
$$= 7.513 \text{ atm}$$

The flow through the expansion fan is isentropic; therefore,

$$p_{03} = p_{02} = \boxed{7.513 \text{ atm}}$$

Thus,

$$\frac{p_{03}}{p_3} = 7.513$$

By isentropic relation, Eq. (2.49),

$$\frac{p_{03}}{p_3} = \left(1 + \frac{\gamma - 1}{2} M_3^2\right)^{\gamma/(\gamma-1)}$$

$$7.513 = (1 + 0.2M_3^2)^{3.5}$$

$$1 + 0.2\, M_3^2 = (7.513)^{1/3.5}$$

$$1 + 0.2M_3^2 = 1.779$$

$$M_3 = \sqrt{\frac{0.779}{0.2}}$$

$$= \boxed{1.974}$$

(c) From the isentropic table,

for $M_2 = 1.49$, $\mu_2 = 42.155°$.

for $M_3 = 1.97$, $\mu_3 = 30.35°$.

The first leading ray of the expansion fan is the Mach line corresponding to Mach 1.49 and the terminating ray of the fan is the Mach line corresponding to Mach 1.97. Thus, the fan angle of the expansion is

$$\theta_{\text{fan}} = \mu_2 - \mu_3$$
$$= 42.155 - 30.55$$
$$= \boxed{11.805°}$$

(d) The flow field ahead of and behind the shock, and downstream of the expansion fan are as shown in Fig. 6.32.

Scanned by CamScanner

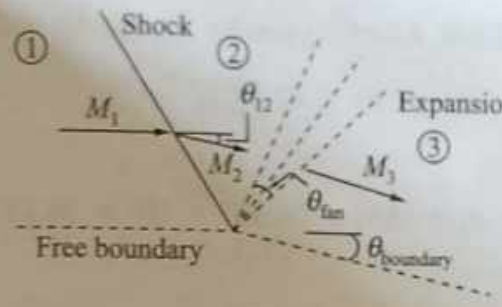


Fig. 6.32 Example 6.8.

The Mach numbers in the three zones of the flow field are

$$M_1 = 2,\ M_2 = 1.49,\ M_3 = 1.974$$

For $M_2 = 1.49$, from the isentropic table, the Prandtl–Meyer function is

$$\nu_2 = 11.61°$$

For $M_3 = 1.974$, from the isentropic table, the Prandtl–Meyer function is

$$\nu_3 = 25.66°$$

But

$$\nu_3 = \nu_2 + \theta_{boundary}$$

Thus,

$$\begin{aligned}\theta_{boundary} &= \nu_3 - \nu_2 \\ &= 25.66° - 11.61° \\ &= \boxed{14.05°}\end{aligned}$$

This is the deflection angle of the boundary, with reference to the flow direction in zone 1. This shows that the boundary is deflected by the same angle by which the shock has deflected the flow ($\theta_{12} = \theta_{boundary}$). It is seen that the shock turned the flow by θ_{12}, downwards, and the boundary has also been turned downwards by the same angle. This turning of the free boundary ensures that the flow from zone 2 coming downwards has been made to flow parallel to the boundary. Thus, the streamlines in zone 3 are parallel to the boundary, satisfying the streamline concept.

EXAMPLE 6.9 Consider a two-dimensional duct carrying a perfect gas with uniform conditions $p_1 = 1$ atm and $M_1 = 2.0$. Design a 10° turning elbow to achieve a uniform downstream state 2 for each of the following cases:

(a) $M_2 > M_1,\ s_2 = s_1$; (b) $M_2 < M_1,\ s_2 = s_1$
(c) $M_2 < M_1,\ s_2 > s_1$; (d) $M_2 = M_1,\ s_2 = s_1$

In each case find the numerical values for M, p and duct area (compared to that of state 1).

Solution (a) Given

$$M_2 > M_1,\ s_2 = s_1$$

Scanned by CamScanner

From isentropic table (Table A1 of Appendix A), for $M_1 = 2.0$,

$$\nu_1 = 26.38°$$

Hence,

$$\nu_2 = \nu_1 + |\Delta\theta| = 26.38° + 10° = 36.38°$$

For $\nu_2 = 36.38°$,

$$M_2 = \boxed{2.387}$$

For $M_1 = 2.0$,

$$\frac{p_1}{p_0} = 0.1278, \quad \frac{A^*}{A_1} = 0.5924$$

For $M_2 = 2.387$,

$$\frac{p_2}{p_0} = 0.06948, \quad \frac{A^*}{A_2} = 0.4236$$

Therefore,

$$\frac{p_2}{p_1} = 0.544, \quad p_2 = \boxed{0.544 p_1}$$

$$\frac{d_2^2}{d_1^2} = \frac{A_2}{A_1} = \frac{A_2}{A^*}\frac{A^*}{A_1} = 1.40, \quad d_2 = \boxed{\sqrt{1.4}\, d_1}$$

(b) Given $M_2 < M_1$, $s_2 = s_1$. It is a compression corner, therefore,

$$\nu_2 = \nu_1 - |\Delta\theta| = \boxed{16.38°}$$

From isentropic table, for $\nu_2 = 16.38°$, $M_2 = 1.655$,

$$\frac{p_2}{p_0} = 0.2168, \quad \frac{A^*}{A_2} = 0.7713$$

Therefore,

$$p_2 = \boxed{1.7 p_1}, \quad d_2 = \boxed{\sqrt{0.768}\, d_1}$$

(c) Given $M_2 < M_1$, $s_2 > s_1$.

Unlike cases (a) and (b), case (c) is nonisentropic since $s_2 > s_1$. Therefore, there should be a shock in the duct to decelerate the flow from M_1 to M_2. From oblique shock Chart 1 (Appendix D), for $M_1 = 2.0$ and $\theta = 10°$, $\beta = 39.5°$. Thus,

$$M_{1n} = M_1 \sin\beta = 1.27$$

From normal shock table (Table A2 of Appendix A), at $M_{1n} = 1.27$, we have

$$M_{2n} = 0.8016, \quad \frac{p_2}{p_1} = 1.715$$

$$\frac{\rho_2}{\rho_1} = 1.463, \quad \frac{a_2}{a_1} = 1.083$$

Scanned by CamScanner

Hence,

$$M_2 = \frac{M_{2n}}{\sin(\beta - \theta)} = \boxed{1.628}$$

$$p_2 = \boxed{1.715 p_1}$$

By continuity,

$$\rho_2 A_2 V_2 = \rho_1 A_1 V_1$$

Therefore,

$$\frac{d_2^2}{d_1^2} = \frac{A_2}{A_1} = \frac{\rho_1 V_1}{\rho_2 V_2} = \frac{\rho_1}{\rho_2}\frac{M_1}{M_2}\frac{a_1}{a_2} = 0.775$$

$$d_2 = \boxed{\sqrt{0.775}\, d_1}$$

(d) Given $M_2 = M_1$, $s_2 = s_1$.

Thus there is no change in area and flow properties from state 1 to state 2.

EXAMPLE 6.10 A uniform supersonic flow at $M_1 = 2.0$, $p_1 = 0.8 \times 10^5$ N/m^2 and temperature 270 K expands through two convex corners of 10° each as shown in Fig. 6.33. Determine the downstream Mach number M_3, p_2, T_2 and the angle of the second fan.

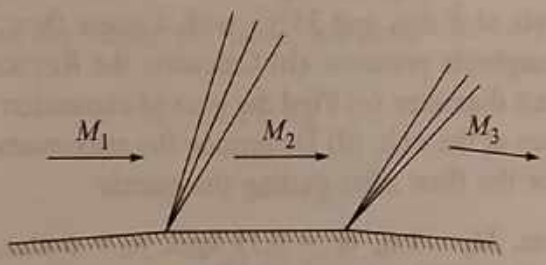


Fig. 6.33 Example 6.10.

Solution From isentropic table (Appendix A),

$$\nu_1 = 26.38° \quad \text{for } M_1 = 2.0$$

Therefore, the Prandtl–Meyer function after the first fan is

$$\nu_2 = \nu_1 + 10° = 36.38°$$

From Table A1 of Appendix A, for $\nu_2 = 36.38°$, $M_2 = 2.38$. The Prandtl–Meyer function after the second fan is

$$\nu_3 = \nu_2 + 10° = 46.38°$$

for $\nu_3 = 46.38°$, $M_3 = \boxed{2.83}$. From isentropic table,

$$\frac{p_1}{p_{01}} = 0.1278, \quad \frac{T_1}{T_{01}} = 0.5556 \quad \text{at } M_1 = 2.0$$

$$\frac{p_2}{p_{02}} = 0.0706, \quad \frac{T_2}{T_{02}} = 0.4688 \quad \text{at } M_2 = 2.38$$

Scanned by CamScanner

But for isentropic flow, $p_{01} = p_{02}$, $T_{01} = T_{02}$. Therefore,

$$p_2 = \frac{0.0706}{0.1278} \times p_1$$

$$p_2 = \boxed{0.4419 \times 10^5 \text{ N/m}^2}$$

$$T_2 = \frac{0.4688}{0.5556} \times 270 = \boxed{227.82 \text{ K}}$$

After the second fan, following the same procedure as above and using the isentropic table, we get

$$p_3 = 0.2203 \times 10^5 \text{ N/m}^2, \quad T_3 = 186.8 \text{ K}$$

The fan angle for the second fan

$$\mu_{23} = \theta + \mu_2 - \mu_3 = 10° + 24.85° - 20.69°$$

i.e. $$\mu_{23} = \boxed{14.16°}$$

EXAMPLE 6.11 (a) Design a nozzle to deliver Mach 1.6 air flow with inlet diameter 40 mm, semi-convergence angle 30° and semi-divergence angle 7°, to be run by a reservoir at 6 atm and 35°C, with a mass flow rate of 0.11 kg/s, discharging to atmospheric pressure. (b) Calculate the Reynolds number at the exit, based on the exit diameter. (c) Find the type of expansion at the nozzle exit, and sketch the waves at the exit. (d) Determine the maximum theoretical Mach number possible for the flow after exiting the nozzle.

Solution (a) Given, $M_e = 1.6$, $\dot{m} = 0.11$ kg/s, $p_0 = 6$ atm, $T = 35 + 273 = 308$ K, $\theta_c = 30°$C, $\theta_d = 7°$C and $p_b = 1$ atm.

The mass flow rate is given by

$$\dot{m} = \frac{0.6847 p_0 A_{th}}{\sqrt{RT_0}}$$

Therefore,

$$A_{th} = \frac{\dot{m}\sqrt{RT_0}}{0.6847 p_0}$$

$$= \frac{0.11 \times \sqrt{287 \times 308}}{0.6847 \times (6 \times 1,01,325)}$$

$$= 7.857 \times 10^{-5} \text{ m}^2$$

$$d_{th} = \sqrt{\frac{(7.857 \times 10^{-5}) \times 4}{\pi}}$$

$$= 0.01 \text{ m}$$

$$= 10 \text{ mm}$$

Scanned by CamScanner

The convergent portion is shown in Fig. 6.34.

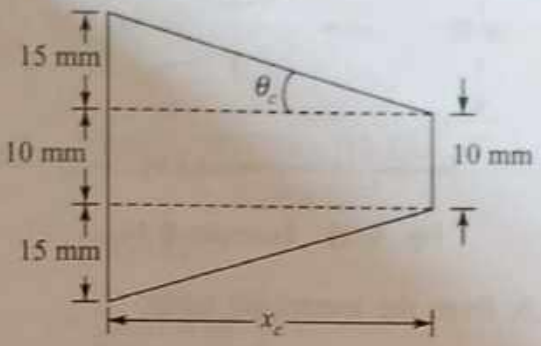


Fig. 6.34 Example 6.11.

The length of the convergent portion is

$$x_c = \frac{15}{\tan\theta_c} = \frac{15}{\tan 30^\circ}$$

$$= 26 \text{ mm}$$

For $M_e = 1.6$, from the isentropic table, we have $\frac{A_e}{A_{th}} = 1.25$. Thus,

$$A_e = 1.25\ A_{th}$$

$$d_e = \sqrt{1.25}\, d_{th}$$

$$= \sqrt{1.25} \times 10$$

$$= 11.18 \text{ mm}$$

The divergent portion of the nozzle is shown in Fig. 6.35.

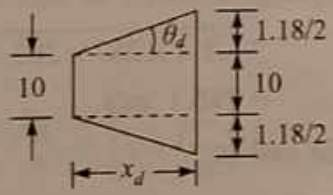


Fig. 6.35 Example 6.11.

The length of the divergent portion is

$$x_d = \frac{1.18/2}{\tan\theta_d} = \frac{0.59}{\tan 7^\circ}$$

$$= 4.805 \text{ mm}$$

The dimensions of the desired nozzle are shown in Fig. 6.36.

Scanned by CamScanner

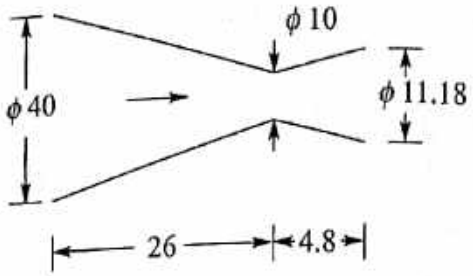


Fig. 6.36 Example 6.11.

(b) For $M_e = 1.6$, from the isentropic table,

$$\frac{T_e}{T_0} = 0.6614, \quad \frac{\rho_e}{\rho_0} = 0.3557, \quad \frac{p_e}{p_0} = 0.2353$$

Therefore, the exit temperature is

$$T_e = 0.6614 T_0 = 0.6614 \times 308$$
$$= 203.7 \text{ K}$$

The viscosity of the flow at the nozzle exit, by Sutherland relation, is

$$\mu = 1.46 \times 10^{-6} \frac{T_e^{3/2}}{T_e + 111}$$

$$= (1.46 \times 10^{-6}) \times \frac{203.7^{3/2}}{203.7 + 111}$$

$$= 1.35 \times 10^{-5} \text{ kg/(m s)}$$

The speed of sound at the nozzle exit is

$$a_e = \sqrt{\gamma R T_e}$$
$$= \sqrt{1.4 \times 287 \times 203.7}$$
$$= 286.1 \text{ m/s}$$

The flow speed at the nozzle exit is

$$V_e = M_e a_e = 1.6 \times 286.1$$
$$= 457.76 \text{ m/s}$$

The flow density at the nozzle exit is

$$\rho_e = 0.3557 \rho_0 = 0.3557 \frac{p_0}{R T_0}$$

$$= 0.3557 \times \frac{6 \times 101325}{287 \times 308}$$
$$= 2.446 \text{ kg/m}^3$$

Scanned by CamScanner

Thus, the Reynolds number of the flow delivered by the nozzle, based on d_e, is

$$\mathrm{Re}_{d_e} = \frac{\rho_e V_e d_e}{\mu_e}$$

$$= \frac{2.446 \times 457.76 \times (11.18 \times 10^{-3})}{1.35 \times 10^{-5}}$$

$$= 927262$$

$$= \boxed{9.27 \times 10^5}$$

(c) The flow pressure at the nozzle exit is

$$p_e = 0.2353, \quad p_0 = 0.2353 \times (6 \times 101325)$$

$$= 1{,}43{,}050.6 \text{ Pa}$$

The backpressure p_b = 1,01,325 Pa, thus, $p_e > p_b$ and the nozzle is underexpanded. Therefore, there will be an expansion fan at the nozzle exit, as shown in Fig. 6.37.

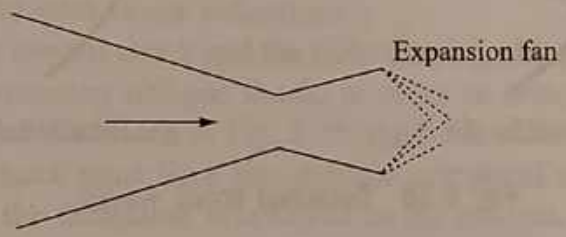


Fig. 6.37 Example 6.11.

(d) The theoretical Mach number M_{max} possible for the flow leaving the nozzle is the Mach number that can be achieved by expanding the stagnation air at 6 atm to 1 atm. Thus, $(p_0/p) = 6$. By the isentropic relation, we have

$$\frac{p_0}{p} = \left(1 + \frac{\gamma - 1}{2} M^2\right)^{\gamma/(\gamma-1)}$$

That is,

$$6 = (1 + 0.2 M_{max}^2)^{3.5}$$

$$1 + 0.2 M_{max}^2 = 6^{1/3.5} = 1.668$$

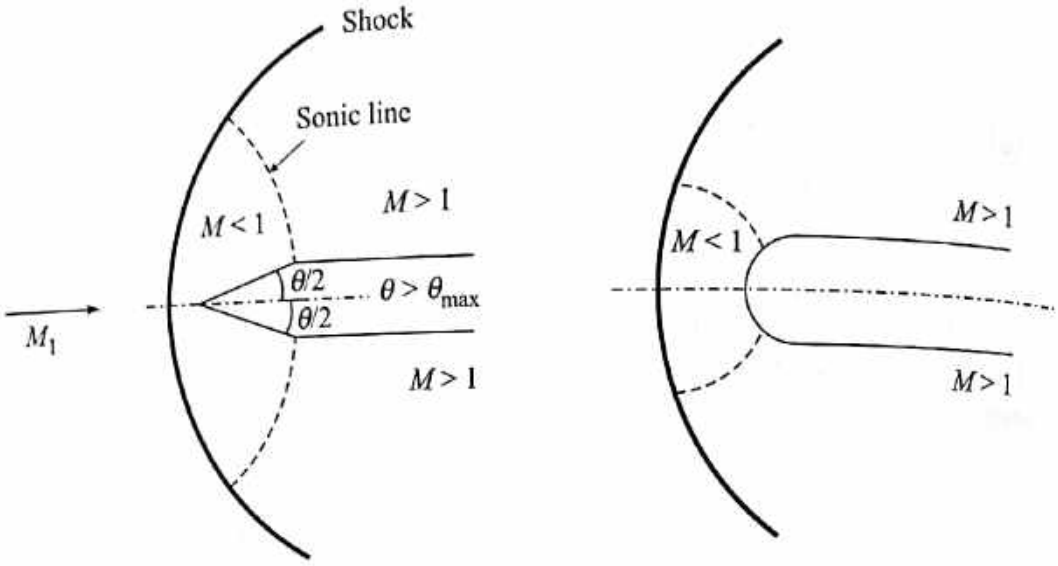
$$M_{max} = \sqrt{\frac{1.668 - 1}{0.2}}$$

$$= \boxed{1.83}$$

Scanned by CamScanner

6.12 DETACHED SHOCKS

This is the shock which results when the wall deflection angle θ is greater than θ_{max} (Section 6.3). We know from the discussions of Section 6.3 that there is in fact no rigorous analytical treatment for problems in which the deflection angles are more than θ_{max}. Experimentally, it is observed that the flow with $\theta > \theta_{max}$ will have a configuration as shown in Fig. 6.38. The shape of the



(a) Detached shock for $\theta > \theta_{max}$ (b) Detached shock at blunt body

Fig. 6.38 Detached shock waves.

detached shock and its detachment distance depend on the geometry of the object facing the flow and the Mach number M_1.

For an object with a blunt-nose, the shock wave is detached at all supersonic Mach numbers. Therefore, even a streamlined body like a cone is a 'blunt-nosed' body as for as the oncoming flow is concerned, when $\theta > \theta_{max}$.

From Fig. 6.38, it is seen that the shock portion at the nose of the object can be approximated to a normal shock. So, immediately behind it there will be subsonic flow. Hence, the wedge portion gives rise to acceleration of the flow from subsonic to supersonic. Therefore, there will be a sonic line, which will emanate from the shoulder of the wedge. For blunt bodies, it is difficult to determine the position of the sonic line.

For a given wedge angle θ, when M_1 is high enough, the shock is attached to the nose. As M_1 decreases, the shock angle increases; with further decrease in Mach number, a value is reached for which the conditions after the shock are subsonic. The shoulder now has an effect on the whole shock, which may be curved, even though attached. These conditions correspond to the region between the lines with $M_2 = 1$ and $\theta = \theta_{max}$ in Fig. 6.3. At the Mach number

Scanned by CamScanner

corresponding to θ_{max}, the shock wave starts detaching. This is called the detachment Mach number. With further decrease in M_1, the detached shock moves upstream of the nose.

The analysis of the flow field associated with detached shock becomes very difficult because of the transonic flow, which prevails behind the shock. In this case, we mainly look for the shape of the shock, the detachment distance, and the shape of the sonic line. But such a solution does not exist. The approximation we usually make is that the sonic line is linear.

The strength of the detached shock is maximum near the stagnation streamline, where it is approximated as a normal shock, and then it continuously decreases by becoming oblique until finally it becomes a Mach line, far away from the object.

6.13 MACH REFLECTION

A look at the detached shock field will show that the complications are due to the appearance of subsonic regions in the flow. Similar complications leading to a condition where no solution with simple oblique shock waves is possible will arise in a flow field with shock reflections.

Intersection of normal shock and the right-running oblique shock gives rise to a reflected left-running oblique shock, in order to bring the flow into the original direction, as illustrated in Fig. 6.39; these are called Mach reflections. The left-running shock must have less strength compared to the right-running shock because of the deflection θ involved in the process, but $M_1 > M_2$.

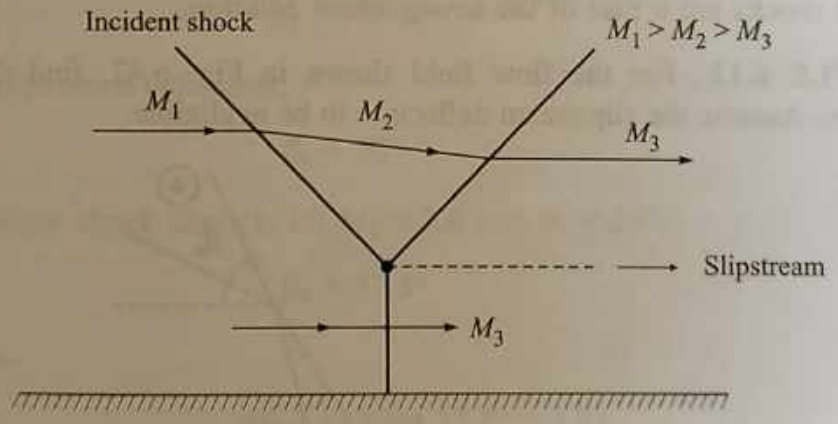


Fig. 6.39 Mach reflection.

It may so happen that M_2 is less than the detachment M for the wall deflection required; in such a case, the entire picture of the flow field changes, all the shocks become curved, and the flow behind the shock system need not be parallel to the wall as shown in Fig. 6.40. Some other phenomenon might take place later on to bring the flow parallel to the wall.

Scanned by CamScanner

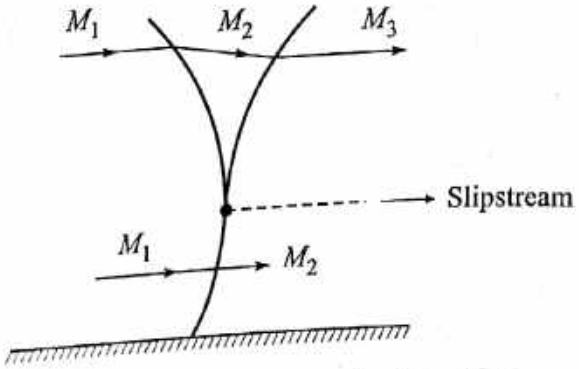


Fig. 6.40 Flow past a shock system.

A similar phenomenon also occurs when two oblique shocks of opposite family intersect with a normal shock bridging them, as shown in Fig. 6.41.

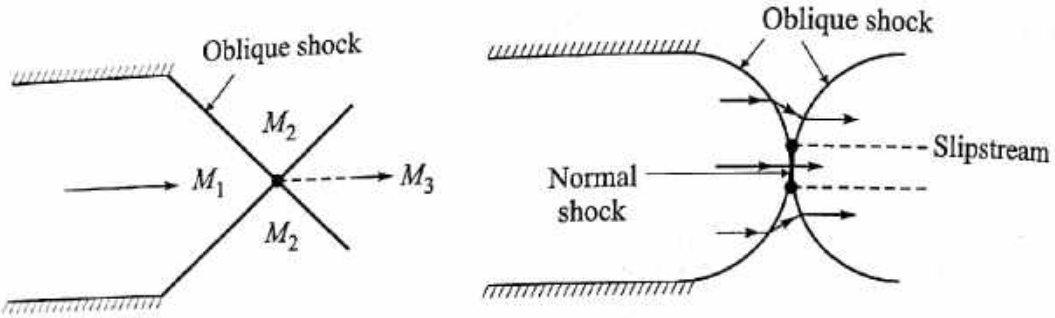


Fig. 6.41 Intersection of oblique shocks.

From the discussions on oblique shocks we notice that, in the case of oblique shocks, the strong shock solution is physically impossible. But the detached shocks are a part of the *strong shock solution*.

EXAMPLE 6.12 For the flow field shown in Fig. 6.42, find the flow properties. Assume the slipstream deflection to be negligible.

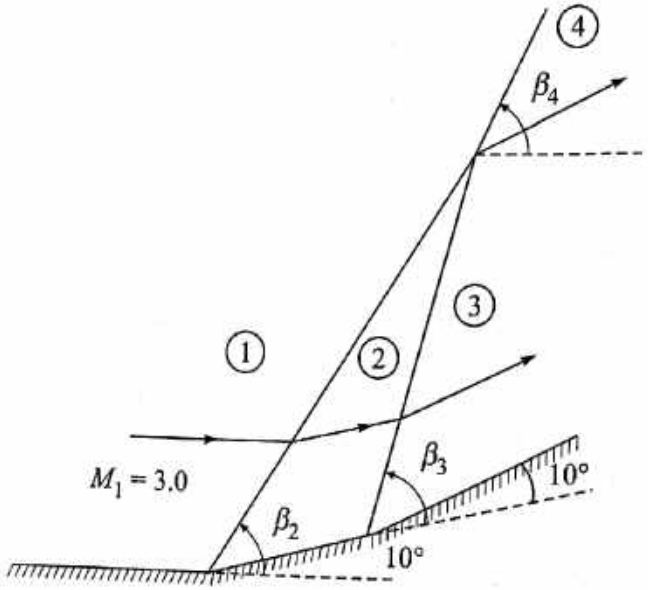


Fig. 6.42 Example 6.12.

Scanned by CamScanner

Solution From oblique shock chart 1 (Appendix D), for $M_1 = 3.0$ and $\theta_2 = 10°$, we have

$$\beta_2 = 27.5°$$

Therefore,

$$M_{1n2} = 3 \sin 27.5° = 1.38$$

From normal shock table (Table A2 of Appendix A), for $M_{1n2} = 1.38$, we have

$$\frac{p_2}{p_1} = 2.055; \quad M_{2n1} = 0.7483$$

Therefore,

$$M_2 = \frac{M_{2n1}}{\sin(\beta_2 - \theta_2)} = 2.49$$

From $M_2 = 2.49$ and $\theta_3 = 10°$, from oblique shock chart, $\beta_3 = 32°$

$$M_{2n3} = 2.49 \sin 32° = 1.32$$

From normal shock table, for $M_{2n3} = 1.32$, $p_3/p_2 = 1.866$; $M_{3n2} = 0.7760$. Therefore,

$$M_3 = \boxed{2.07}$$

Thus,

$$\frac{p_3}{p_1} = 1.866 \times 2.055 = 3.835$$

With no slipstream deflection,

$$\theta_4 = 20°$$

From oblique shock chart 1, fro $M_1 = 3.0$ and $\theta_4 = 20°$,

$$\beta_4 = 37.5°$$

Therefore,

$$M_{1n4} = 3 \sin 37.5° = 1.83$$

From normal shock table, for $M_{1n4} = 1.83$

$$\frac{p_4}{p_1} = 3.74, \quad M_{4n} = 0.6099$$

Therefore, $M_4 = \boxed{2.03}$.

Scanned by CamScanner

EXAMPLE 6.13 Find the flow properties for the flow field shown in Fig. 6.43.

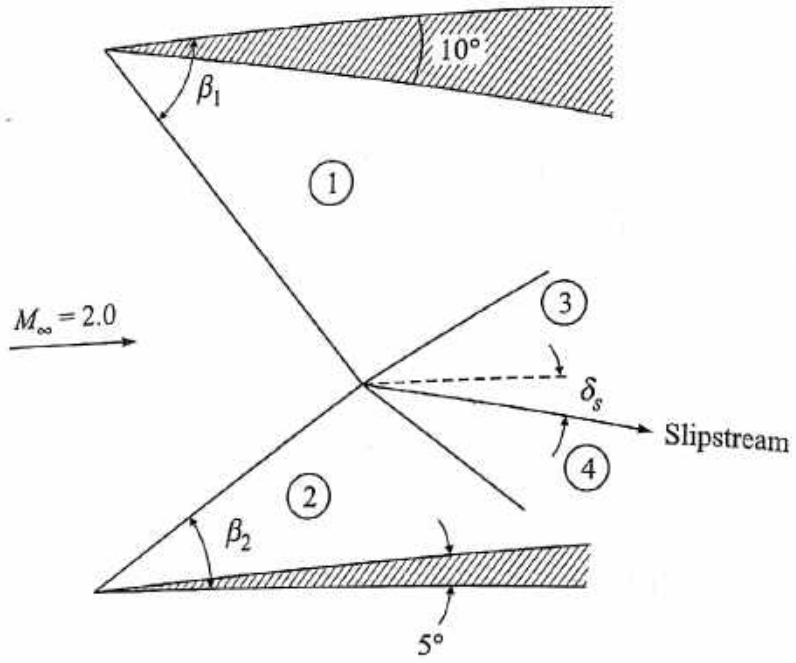


Fig. 6.43 Example 6.13.

Solution From oblique shock chart 1, for $M_\infty = 2.0$ and $\theta_1 = 10°$, $\beta_1 = 39°$,

$$M_1 = 1.665, \quad \frac{p_1}{p_\infty} = 1.686$$

For $M_\infty = 2.0$ and $\theta_2 = 5°$,

$$\beta_2 = 34.5°, \quad M_2 = 1.805, \quad \frac{p_2}{p_\infty} = 1.323$$

Because of the slipstream, the properties in the regions (3) and (4) can be calculate by trial and error only.

Trial 1 Let the downstream flow be parallel to upstream flow. For $\theta_3 = 10°$ and $M_1 = 1.665$, from oblique shock chart 1, $\beta_3 = 48.5°$; $M_{1n3} = M_1 \sin \beta_3 = 1.247$; $p_3/p_1 = 1.656$. Hence,

$$\frac{p_3}{p_\infty} = 2.79$$

For $\theta_4 = 5°$ and $M_2 = 1.805$,

$$\beta_4 = 38°, \quad M_{2n4} = 1.111, \quad \frac{p_4}{p_\infty} = 1.271$$

Therefore,

$$\frac{p_4}{p_\infty} = 1.68$$

Since $p_3/p_\infty > p_4/p_\infty$, the slipstream has to be deflected downwards so that the two pressures become equal.

Scanned by CamScanner

Trial 2 Let

$$\frac{p_3}{p_\infty} = \frac{p_4}{p_\infty} = 2.25, \quad \frac{p_3}{p_1} = 1.334,$$

$$M_{1n3} = 1.135, \quad M_1 = 1.665$$

$$\beta_3 = \sin^{-1}\frac{1.135}{1.665} = 43°$$

For $M_1 = 1.665$ and $\beta_3 = 43°$, from oblique shock chart 1, $\theta_3 = 6.5°$, i.e. 3.5° below freestream direction. Similarly,

$$\frac{p_4}{p_2} = 1.7, \quad M_{2n} = 1.27, \quad M_2 = 1.805$$

$$\beta_4 = 44.7°, \ \theta_4 = 11°, \text{ i.e. } 6° \text{ below freestream direction}$$

Trial 3 With downstream flow 4.5° below upstream flow,

$$\theta_3 = 5.5°, \qquad M_1 = 1.665$$

$$\beta_3 = 42.5°, \quad M_{1n3} = 1.125, \quad \frac{p_3}{p_1} = 1.31$$

Therefore,

$$\frac{p_3}{p_\infty} = 2.21$$

For $\theta_4 = 9.5°$ and $M_2 = 1.805$,

$$\beta_4 = 43.5°, \quad M_{2n4} = 1.242, \quad \frac{p_4}{p_2} = 1.63$$

Thus,

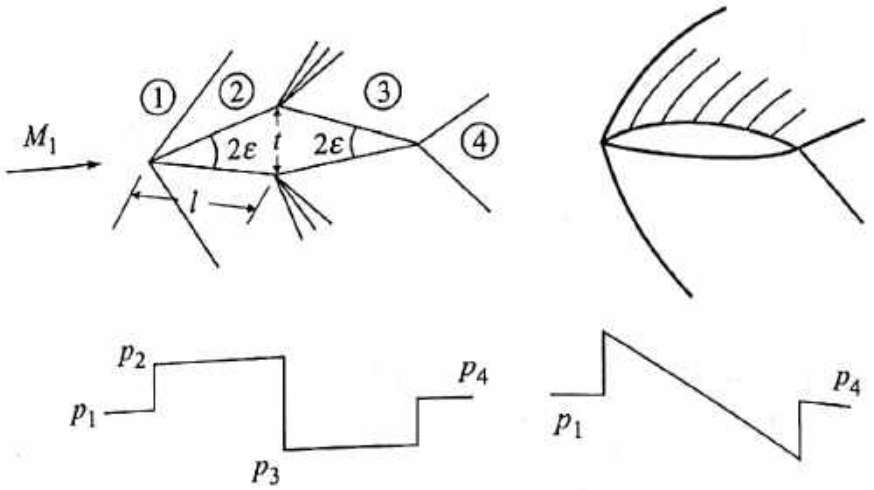
$$\frac{p_4}{p_\infty} = 1.63 \times 1.322 = 2.16$$

In trial 3, it is seen that the pressures p_3 and p_4 are nearly equal, i.e. the assumed slipstream deflection of 4.5° (δ_s) is correct.

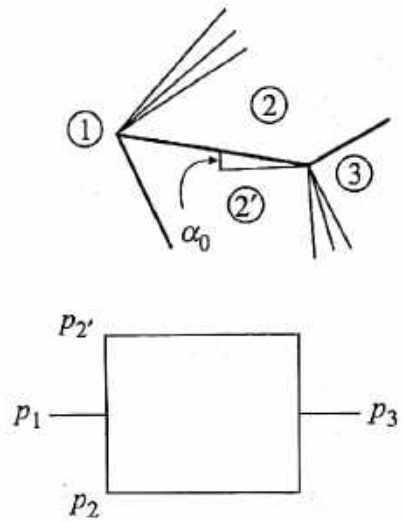
6.14 SHOCK-EXPANSION THEORY

The shocks and expansion waves discussed in this chapter are the basis for analysing a large number of problems in two-dimensional, supersonic flow by simply 'patching' together appropriate combinations of two or more solutions. That is, aerodynamic forces on a body present in a supersonic flow are governed by the shocks and expansion waves formed at the surface of the body. This can be easily seen from the basic fact that the aerodynamic forces on a body depend on the pressure distribution around it, and in supersonic flow, the pressure distribution over an object depends on the wave pattern over it, as shown in Figs. 6.44(a)–(c).

Scanned by CamScanner



(a) Diamond wedge aerofoil (b) Circular arc aerofoil



(c) Flat plate at an angle of attack

Fig. 6.44 Wave pattern over objects.

Consider the two-dimensional supersonic aerofoil shown in Fig. 6.44(a). It is at zero angle of attack to the flow. The supersonic flow at M_1 is first compressed and deflected through an angle ε by the oblique shock wave at the leading edge. At the shoulder located at midchord, the flow is expanded through an angle 2ε by the expansion fan. At the trailing edge, the flow is again deflected through an angle ε, in order to bring it back to the original direction. Therefore, the surface pressure on segments ahead and after the shoulder, will be at a constant level over each segment for supersonic flow, according to oblique shock and the Prandtl–Meyer expansion theory.

On the diamond aerofoil, at zero angle of attack, the lift is zero because the pressure distributions on the top and bottom surfaces are the same. Therefore, the only aerodynamic force on the aerofoil is due to the overpressure on the forward face and underpressure on the rearward face. The drag per unit span is

$$D = 2(p_2 l \sin \varepsilon - p_3 l \sin \varepsilon) = 2(p_2 - p_3)(t/2)$$

Scanned by CamScanner

i.e.

$$\boxed{D = (p_2 - p_3)t} \tag{6.50}$$

Equation (6.50) gives an expression for drag experienced by a two-dimensional aerofoil, kept at zero angle of attack in an inviscid flow. This is in contrast with the familiar result from studies on subsonic flow that, for two-dimensional inviscid flow over a wing of infinite span at subsonic velocity, one obtains zero drag—a theoretical result called D'Alembert's paradox. In contrast with this, for supersonic flow, drag exists even in the idealized, nonviscous fluid. This new component of drag encountered when the flow is supersonic is called *wave drag*, and is fundamentally different from the frictional drag and separation drag which are associated with boundary layers in a viscous fluid. The wave drag is related to loss of total pressure and increase in entropy across the oblique shock waves generated by the aerofoil.

For the flat plate shown in Fig. 6.44(c), from the uniform pressures on the two sides, the lift and drag are computed very easily, with the following equations:

$$L = (p_{2'} - p_2)\, c \cos \alpha_0$$
$$D = (p_{2'} - p_2)\, c \sin \alpha_0 \tag{6.51}$$

where c is the chord.

EXAMPLE 6.14 A flat plate is kept at 15° angle of attack to a supersonic stream at Mach 2.4 as shown in Fig. 6.45. Solve the flow field around the plate and determine the inclination of slipstream to the freestream direction using shock-expansion theory.

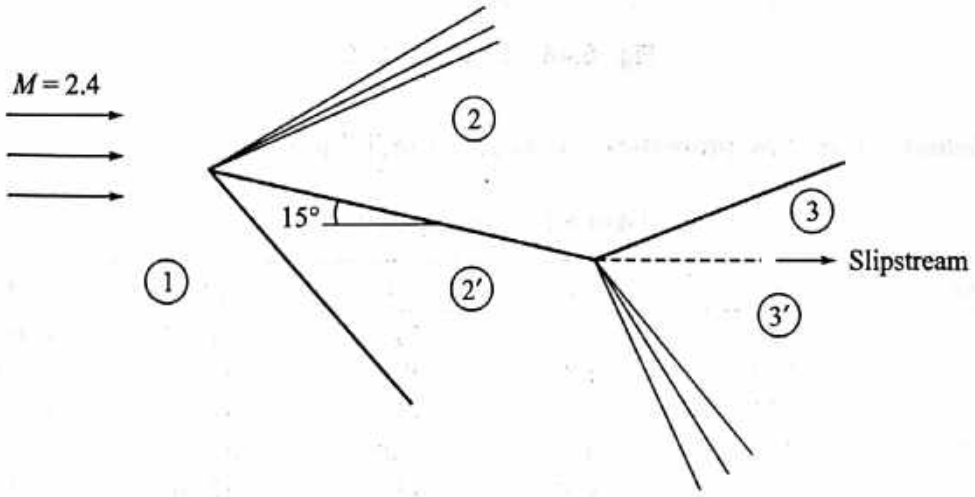


Fig. 6.45 Example 6.14.

Solution Using the shock and expansion wave properties, Table 6.1 can be formed.

Scanned by CamScanner

TABLE 6.1 Example 6.14

Region	M	ν	μ	p/p_{01}	T/T_{01}
1	2.40	36.8°	24.6°	0.0684	0.465
2	3.11	51.8°	18.8°	0.0231	0.341
3	2.33	35.0°	25.4°	0.0675	0.480
2′	1.80	20.7°	33.8°	0.1629	0.607
3′	2.36	35.7°	25.1°	0.0679	0.473

The above table gives the flow properties around the flat plate. Slip surface inclination relative to freestream is negligibly small. The velocity jump across the slip surface is found to be 1 m/s.

EXAMPLE 6.15 Determine the flow field around a symmetric double wedge of 20° included angle kept at 15° angle of attack to a supersonic stream of Mach number 2.4 and stagnation temperature 300 K, shown in Fig. 6.46, by the shock-expansion theory.

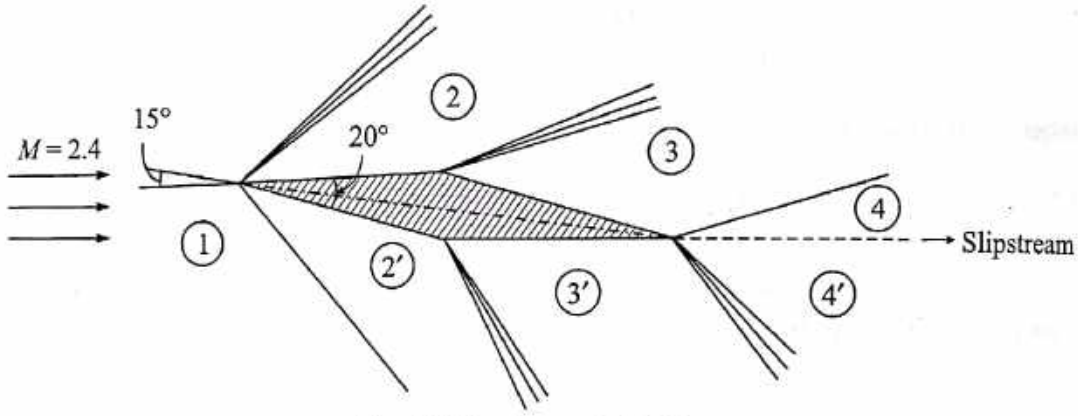


Fig. 6.46 Example 6.15.

Solution The flow properties are as given in Table 6.2.

TABLE 6.2 Example 6.15

Region	M	ν	μ	p/p_{01}	T/T_{01}
1	2.40	36.8°	24.6°	0.0684	0.465
2	2.62	41.8°	22.5°	0.0486	0.421
3	3.71	61.8°	15.6°	0.0098	0.267
4	2.00	26.5°	30.0°	0.0707	0.555
2′	1.31	6.5°	49.7°	0.2736	0.745
3′	2.00	26.5°	30.0°	0.0986	0.555
4′	2.23	32.5°	26.6°	0.0689	0.501

Scanned by CamScanner

From the above values, we get (with $T_{01} = 300$ K)

$$a_4 = 258.7 \text{ m/s}, \qquad V_4 = 517.4 \text{ m/s}$$
$$a_{4'} = 245.8 \text{ m/s}, \qquad V_{4'} = 548.1 \text{ m/s}$$

Slipstream surface: Inclination $\approx 1°$ upwards relative to freestream.

$$\text{Velocity jump} = 30.7 \text{ m/s}$$

EXAMPLE 6.16 For the flow over the half-diamond wedge shown in Fig. 6.47, find the inclinations of shocks and expansion waves and the pressure distributions.

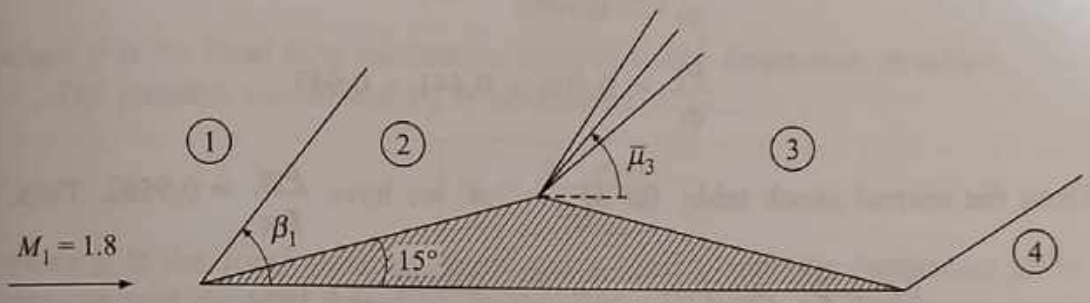


Fig. 6.47 Example 6.16.

Solution From oblique shock chart 1, for $M_1 = 1.8$ and $\theta = 15°$, $\beta_1 = \boxed{51.5°}$. By Eq. (6.3),

$$\frac{p_2}{p_1} = 1 + \frac{2\gamma}{\gamma + 1}(M_1^2 \sin^2\beta - 1) = 2.149$$

$$C_{p2} = \frac{p_2 - p_1}{q_1} = \frac{2(p_2/p_1 - 1)}{\gamma M_1^2} = 2 \times 0.253 = \boxed{0.506}$$

By Eq. (6.7),

$$M_2 = \frac{M_{n2}}{\sin(\beta_1 - \theta)}$$

From normal shock table, for $M_{1n} = M_1 \sin\beta_1 = 1.4$, we have $M_{2n} = 0.7397$. Therefore, $M_2 = 1.24$. From isentropic table, for $M_2 = 1.24$, we have $\nu_2 = 4.569°$, $\mu_2 = 53.751°$. Now, $\nu_3 = \nu_2 + \theta_3 = 4.569° + 30° = 34.569°$. Hence, $M_3 = 2.315$, $\mu_3 = 25.6°$. Thus

$$\bar{\mu}_3 = \frac{\mu_2 + \mu_3}{2} = \boxed{39.68°}$$

Region 3 From isentropic table, for $M_1 = 1.8$,

$$\frac{p_1}{p_{01}} = 0.1740$$

Scanned by CamScanner

For $M_3 = 2.315$,

$$\frac{p_3}{p_{02}} = 0.0780 \text{ since } p_{02} = p_{03}$$

$$q_1 = \frac{1}{2}\rho_1 V_1^2 = \frac{\gamma p_1 M_1^2}{2}$$

Therefore,

$$\frac{q_1}{p_{01}} = \frac{\gamma M_1^2}{2} \times 0.1740 = 0.3946$$

$$\frac{p_1}{q_1} = \frac{0.1740}{0.3946} = 0.441$$

$$\frac{p_2}{q_1} = 0.506 + 0.441 = 0.947$$

From the normal shock table, for $M_{1n} = 1.4$, we have $\frac{p_{02}}{p_{01}} = 0.9582$. Thus,

$$\frac{p_3}{q_1} = \frac{p_3}{p_{02}}\frac{p_{02}}{p_{01}}\frac{p_{01}}{q_1} = \frac{0.0780 \times 0.9582}{0.3946} = 0.1894$$

$$C_{p3} = \frac{p_3 - p_1}{q_1} = \boxed{-0.2516}$$

Note: It is important to note that the solutions to problems involving oblique shock, obtained using oblique shock chart or table, are only close to the correct results and are not 100 per cent accurate. For accurate results we have to use the appropriate relations directly. However, the use of chart and table results in considerable saving in time and also the resulting accuracies are good enough for any application.

6.15 THIN AEROFOIL THEORY

We have seen in Section 6.14 that the shock-expansion theory gives a simple method for computing *lift* and *drag*. This theory is applicable as long as the shocks are attached. This theory may be further simplified by approximating it by using the approximate relations for the weak shocks and expansion, when the aerofoil is thin and is kept at a small angle of attack, i.e. if the flow inclinations are small. This approximation will result in simple analytical expressions for lift and drag.

From our studies on weak oblique shocks in Section 6.6, we know that the basic approximate expression (Eq. (6.21)) for calculating pressure change across a weak shock is

$$\frac{\Delta p}{p_1} = \frac{\gamma M_1^2}{\sqrt{M_1^2 - 1}}\Delta\theta$$

Scanned by CamScanner

Since the wave is weak, the pressure p behind the shock will not be significantly different from p_1, nor will M be appreciably different from M_1. Therefore, we can write

$$\frac{\Delta p}{p} = \frac{\gamma M^2}{\sqrt{M^2 - 1}} \Delta\theta$$

Now, assuming all direction changes to the freestream direction to be zero and freestream pressure to be p_1, we can write

$$\frac{p - p_1}{p_1} = \frac{\gamma M_1^2}{\sqrt{M_1^2 - 1}} (\theta - 0)$$

where θ is the local flow inclination relative to the freestream direction.

The pressure coefficient C_p is defined as

$$\boxed{C_p = \frac{p - p_1}{q_1}}$$

where p is the local static pressure and p_1 and q_1 are the freestream static pressure and dynamic pressure, respectively. In terms of freestream Mach number M_1, C_p can be expressed as

$$C_p = \frac{p - p_1}{q_1} = \frac{2}{\gamma M_1^2} \frac{p - p_1}{p_1}$$

Substituting the expression for $(p - p_1)/p_1$ in terms of θ and M_1, we get

$$\boxed{C_p = \frac{2\theta}{\sqrt{M_1^2 - 1}}} \tag{6.52}$$

The above equation, which states that the pressure *coefficient is proportional to the local flow direction*, is the basic relation for thin aerofoil theory.

Application of Thin Aerofoil Theory

Applying the thin aerofoil theory relation to the flat plate shown in Fig. 6.44(c) at a small angle of attack α_0, the C_p on the upper and lower surfaces can be expressed as

$$C_p = \mp \frac{2\alpha_0}{\sqrt{M_1^2 - 1}} \tag{6.53}$$

where the minus sign is for C_p on the upper surface and the plus sign is for C_p on the lower surface. The lift and drag coefficients are respectively given by

$$C_L = \frac{(p_l - p_u)c \cos\alpha_0}{q_1 c} = (C_{p_l} - C_{p_u}) \cos\alpha_0$$

$$C_D = \frac{(p_l - p_u)c \sin\alpha_0}{q_1 c} = (C_{p_l} - C_{p_u}) \sin\alpha_0$$

Scanned by CamScanner

In the above expressions for C_L and C_D, $\cos \alpha_0 = 1$ and $\sin \alpha_0 \approx \alpha_0$, since α_0 is small and the subscripts l and u refer to lower and upper surfaces. Therefore,

$$C_L = (C_{p_l} - C_{p_u}), \quad C_D = (C_{p_l} - C_{p_u})\alpha_0$$

Using Eq. (6.53), the C_L and C_D of the flat plate at small angle of attack may be expressed as

$$\boxed{C_L = \frac{4\alpha_0}{\sqrt{M_1^2 - 1}}}$$

$$\boxed{C_D = \frac{4\alpha_0^2}{\sqrt{M_1^2 - 1}}} \tag{6.54}$$

Now, consider the diamond section aerofoil shown in Fig. 6.44(a), with nose angle 2ε, at zero angle of attack. The expressions for C_p on the front and rear faces are given by

$$C_p = \pm \frac{2\varepsilon}{\sqrt{M_1^2 - 1}}$$

This can be rewritten in terms of pressure difference to give

$$p_2 - p_3 = \frac{4\varepsilon}{\sqrt{M_1^2 - 1}} q_1$$

Therefore, the drag is given by

$$D = (p_2 - p_3)t = (p_2 - p_3)\varepsilon c$$

i.e.

$$D = \frac{4\varepsilon^2}{\sqrt{M_1^2 - 1}} q_1 c$$

In terms of the drag coefficient, the above drag equation becomes

$$C_D = \frac{D}{q_1 c} = \frac{4\varepsilon^2}{\sqrt{M_1^2 - 1}} \tag{6.55a}$$

or

$$C_D = \frac{4}{\sqrt{M_1^2 - 1}} \left(\frac{t}{c}\right)^2 \tag{6.55b}$$

In the above two applications, the thin aerofoil theory was used for specific profiles to get expressions for C_L and C_D. A general result applicable to any thin aerofoil may be obtained as follows: Consider a cambered aerofoil with finite thickness at a small angle of attack treated by linear resolution into three components, each of which contributing to lift and drag, as shown in Fig. 6.48.

Scanned by CamScanner

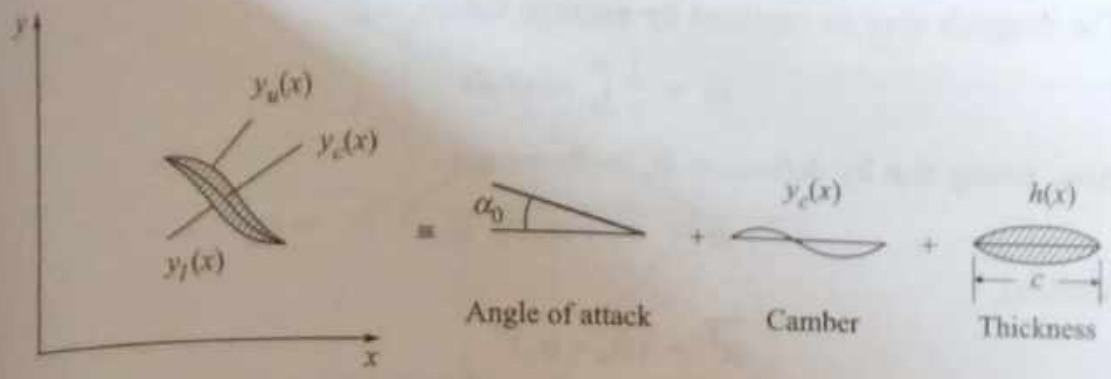


Fig. 6.48 Linear resolution of aerofoil into angle of attack, camber, and thickness.

By thin aerofoil theory, the expressions for C_p on the upper and lower surfaces are obtained as

$$C_{p_u} = \frac{2}{\sqrt{M_1^2 - 1}}\left(\frac{dy_u}{dx}\right)$$
$$C_{p_l} = \frac{2}{\sqrt{M_1^2 - 1}}\left(-\frac{dy_l}{dx}\right) \tag{6.56}$$

where y_u and y_l are the upper and lower profiles of the aerofoil. The profile may be resolved into a symmetrical thickness distribution $h(x)$ and a camber line of zero thickness $y_c(x)$. Thus, we have

$$\frac{dy_u}{dx} = \frac{dy_c}{dx} + \frac{dh}{dx} = -\alpha(x) + \frac{dh}{dx}$$
$$\frac{dy_l}{dx} = \frac{dy_c}{dx} - \frac{dh}{dx} = -\alpha(x) - \frac{dh}{dx} \tag{6.57}$$

where $\alpha(x) = \alpha_0 + \alpha_c(x)$ is the local angle of attack of the camber line. The lift and drag are given by

$$L = q_1 \int_0^c (C_{pl} - C_{p_u})dx$$
$$D = q_1 \int_0^c \left[C_{pl}\left(-\frac{dy_l}{dx}\right) + C_{p_u}\left(\frac{dy_u}{dx}\right)\right]dx \tag{6.58}$$

Substituting Eqs. (6.56) and (6.57) into Eqs. (6.58), we get

$$L = \frac{2q_1}{\sqrt{M_1^2 - 1}} \int_0^c \left(-2\frac{dy_c}{dx}\right)dx = \frac{4q_1}{\sqrt{M_1^2 - 1}} \int_0^c \alpha(x)\, dx$$

$$D = \frac{2q_1}{\sqrt{M_1^2 - 1}} \int_0^c \left[\left(\frac{dy_l}{dx}\right)^2 + \left(\frac{dy_u}{dx}\right)^2\right]dx$$

$$D = \frac{4q_1}{\sqrt{M_1^2 - 1}} \int_0^c \left[\{\alpha(x)\}^2 + \left(\frac{dh}{dx}\right)^2\right]dx$$

Scanned by CamScanner

The integrals may be replaced by average values, e.g.

$$\overline{\alpha} = \frac{1}{c}\int_0^c \alpha(x)\, dx$$

Also, noting that by definition $\overline{\alpha}_c = 0$, we get

$$\overline{\alpha} = \overline{\alpha_0 + \alpha_c} = \overline{\alpha}_0 + \overline{\alpha}_c = \alpha_0$$

Similarly,

$$\begin{aligned}\overline{\alpha^2} &= \overline{(\alpha_0 + \alpha_c)^2} \\ &= \overline{\alpha_0^2} + \overline{2\alpha_0 \alpha_c} + \overline{\alpha_c^2} \\ &= \alpha_0^2 + \overline{\alpha_c^2}\end{aligned}$$

Using the above averages in the lift and drag expressions, we obtain the lift and drag coefficients as

$$\boxed{C_L = \frac{4\overline{\alpha}}{\sqrt{M_1^2 - 1}} = \frac{4\alpha_0}{\sqrt{M_1^2 - 1}}} \tag{6.59a}$$

$$C_D = \frac{4}{\sqrt{M_1^2 - 1}}\left[\overline{\left(\frac{dh}{dx}\right)^2} + \overline{\alpha^2(x)}\right]$$

$$\boxed{C_D = \frac{4}{\sqrt{M_1^2 - 1}}\left[\overline{\left(\frac{dh}{dx}\right)^2} + \alpha_0^2 + \overline{\alpha_c^2(x)}\right]} \tag{6.59b}$$

Equations (6.59) give the general expressions for lift and drag coefficients of a thin aerofoil in supersonic flow. In thin aerofoil theory, the drag is split into *drag due to lift*, *drag due to camber*, and *drag due to thickness* as given by Eq. (6.59b). But the lift coefficient depends only on the mean angle of attack.

EXAMPLE 6.17 A supersonic, circular arc aerofoil, shown in Fig. 6.49, has chord c and thickness-to-chord ratio of 0.12. Determine the lift and drag coefficient of the aerofoil in terms of the angle of attack, α.

Solution Let O, the origin of the xy-coordinate system, be at the leading edge of the aerofoil. Now, the equation of the circular arc is given by

$$\left(x - \frac{c}{2}\right)^2 + (y + K)^2 = R^2 \tag{i}$$

Substituting $x = 0$, $y = 0$ in Eq. (i), we get

$$\frac{c^2}{4} + K^2 = R^2$$

Also,

$$R - K = t$$

Scanned by CamScanner

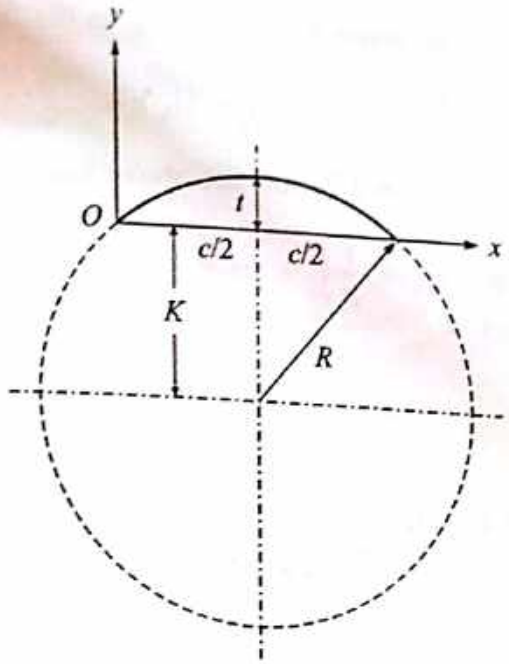


Fig. 6.49 Example 6.17.

Simplifying the above two equations, we can write

$$R = \frac{1}{8}\frac{c^2}{t}\left[1+\left(\frac{2t}{c}\right)^2\right]$$

$$K = \frac{1}{8}\frac{c^2}{t}\left[1-\left(\frac{2t}{c}\right)^2\right]$$

Differentiating Eq. (i), the slope dy/dx can be obtained as

$$\frac{dy}{dx} = \frac{\frac{c}{2}\left(1-2\frac{x}{c}\right)}{y+K}$$

For small y, this can be approximated as

$$\frac{dy}{dx} \approx \left(\frac{dy}{dx}\right)_{y=0} = \frac{4\frac{t}{c}\left(1-\frac{2x}{c}\right)}{(1-(2t/c)^2)} = 0.509\left(1-\frac{2x}{c}\right)$$

For the aerofoil considered,

$$\frac{dy_u}{dx} = \frac{dy_c}{dx}, \quad \frac{dy_l}{dx} = \frac{dy_c}{dx}, \quad \frac{dh}{dx} = 0$$

Therefore, when the aerofoil is at an angle of attack α, we have

$$\frac{dy_c}{dx} = -\alpha(x) + \frac{dh}{dx} = -\alpha(x) + 0.509\left(1-\frac{2x}{c}\right)$$

Scanned by CamScanner

The coefficient of lift C_L is given by Eq. (6.58), in the form

$$\frac{L}{q_1 c} = \frac{1}{c}\int_0^c (C_{p_l} - C_{p_u})dx$$

Substituting Eqs. (6.56) and (6.57) into the above equation, we get

$$C_L = \frac{1}{c}\int_0^c -\frac{4}{\sqrt{M_1^2 - 1}}\left(\frac{dy_c}{dx}\right)dx$$

$$= -\frac{4}{c\sqrt{M_1^2 - 1}}\int_0^c \left(-\alpha(x) + 0.509\left(1 - \frac{2x}{c}\right)\right)dx$$

On integrating, we obtain the result

$$C_L = \boxed{\frac{4\alpha}{\sqrt{M_1^2 - 1}}}$$

This result of C_L also implies that the lift goes to zero when the angle of attack is zero. The drag coefficient is given by

$$C_D = \frac{1}{c}\int_0^c \left[C_{pl}\left(-\frac{dy_l}{dx}\right)dx + C_{p_u}\left(\frac{dy_u}{dx}\right)\right]dx$$

$$= \frac{2}{c\sqrt{M_1^2 - 1}}\int_0^c \left[\left(\frac{dy_l}{dx}\right)^2 + \left(\frac{dy_u}{dx}\right)^2\right]dx$$

$$= \frac{4}{c\sqrt{M_1^2 - 1}}\int_0^c \left(\frac{dy_c}{dx}\right)^2 dx$$

$$= \frac{4}{c\sqrt{M_1^2 - 1}}\int_0^c \left[-\alpha(x) + 0.509\left(1 - \frac{2x}{c}\right)\right]^2 dx$$

$$= \frac{4}{c\sqrt{M_1^2 - 1}}\int_0^c \left[\alpha^2(x) + 0.509^2\left(1 - \frac{4x}{c} + \frac{4x^2}{c^2}\right)\right.$$

$$\left. -2\alpha(x) \times 0.509\left(1 - \frac{2x}{c}\right)\right]dx$$

$$\boxed{C_D = \frac{4\alpha^2(x)}{\sqrt{M_1^2 - 1}} + \frac{0.3451}{\sqrt{M_1^2 - 1}}}$$

Scanned by CamScanner

EXAMPLE 6.18 A symmetric diamond aerofoil of sides 1 m and maximum thickness 150 mm is at zero angle of attack to a Mach 1.6 airstream at pressure 50 kPa. Determine the drag coefficient using (a) shock-expansion theory and (b) thin aerofoil theory. Also, determine the percentage error involved in assuming the aerofoil as thin.

Solution Given, $l = 1$ m, $t = 0.15$ m, $M_1 = 1.6$, $\alpha = 0°$, $p_1 = 50$ kPa. The aerofoil and the waves over that are as shown in Fig. 6.50.

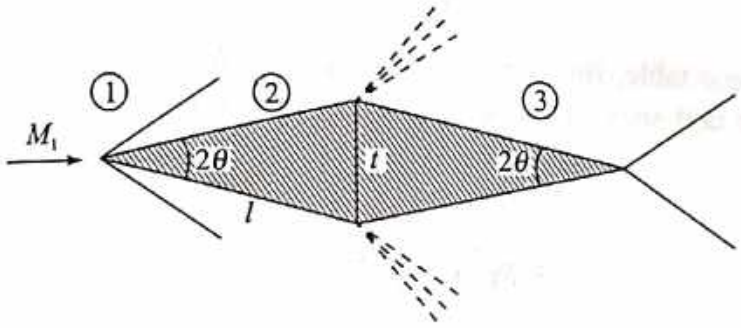


Fig. 6.50 A symmetric diamond aerofoil in a supersonic flow.

The semi-angle at the nose is

$$\theta = \sin^{-1}\left(\frac{t/2}{l}\right)$$

$$= \sin^{-1}\left(\frac{0.15/2}{1}\right)$$

$$= 4.3°$$

(a) For $M_1 = 1.6$ and $\theta = 4.3°$, from oblique shock chart 1,

$$\beta \approx 44°$$

Therefore,

$$M_{1n} = M_1 \sin(44°)$$

$$= 1.6 \times \sin(44°)$$

$$= 1.11$$

For $M_{1n} = 1.11$, from normal shock table,

$$M_{2n} = 0.9041, \frac{p_2}{p_1} = 1.2708$$

Therefore,

$$M_2 = \frac{M_{2n}}{\sin(\beta - \theta)}$$

$$= \frac{0.9041}{\sin(44 - 4.3)}$$

$$= 1.41$$

Scanned by CamScanner

For $M_2 = 1.41$, from isentropic table,

$$\nu_2 = 9.276°, \frac{p_2}{p_{02}} = 0.3098$$

The flow from zone 2 to zone 3 is expanded by $2\theta = 8.6°$. Therefore,

$$\begin{aligned}\nu_3 &= \nu_2 + 8.6 \\ &= 9.276 + 8.6 \\ &= 17.876°\end{aligned}$$

From isentropic table, for $\nu_3 = 17.876°$, $p_3/p_{03} \approx 0.1996$.
The drag per unit span of the wing, by Eq. (6.50), is

$$\begin{aligned}D &= (p_2 - p_3)t \\ &= p_2\left(1 - \frac{p_3}{p_2}\right)t \\ &= p_2\left(1 - \frac{p_3/p_{03}}{p_2/p_{02}}\right)t \\ &= 1.2708p_1\left(1 - \frac{p_3/p_{03}}{p_2/p_{02}}\right)t \\ &= 1.2708p_1\left(1 - \frac{0.1996}{0.3098}\right)t \\ &= 1.2708p_1 \times 0.3557t\end{aligned}$$

The drag coefficient is

$$C_D = \frac{D}{q_1 S}$$

where $S = c \times 1 = c$ is the planform area per unit span. The dynamic pressure q_1 can be expressed as

$$q_1 = \frac{\gamma}{2}p_1 M_1^2$$

Therefore,

$$\begin{aligned}C_D &= \frac{1.2708p_1 \times 0.3557 \times t}{\left(\frac{1.4}{2}\right)p_1 \times (1.6)^2 \times (2 \times l \times \cos(4.3°))} \\ &= \frac{1.2708 \times 0.3557 \times 0.15}{0.7 \times (1.6)^2 \times 1.994} \\ &= \boxed{0.019}\end{aligned}$$

Scanned by CamScanner

(b) The drag coefficient given by thin aerofoil theory, Eq. (6.55b), is

$$C_D = \frac{4}{\sqrt{M_1^2 - 1}} \left(\frac{t}{c}\right)^2$$

$$= \frac{4}{\sqrt{1.6^2 - 1}} \times \left(\frac{0.15}{1.994}\right)^2$$

$$= \boxed{0.0181}$$

The thin aerofoil theory understimates the drag. The error committed in assuming the aerofoil as thin is

$$\% \text{ error} = \frac{0.019 - 0.0181}{0.019} \times 100$$

$$= \boxed{4.74\%}$$

6.16 SUMMARY

In this chapter we discussed the flow processes through oblique shock and expansion waves. A shock wave which is inclined at an angle to the flow direction is called an *oblique shock wave*. Oblique shocks usually occur when a supersonic flow is turned into itself. The opposite of this, namely, when a supersonic flow is turned away from itself, results in the formation of an *expansion fan*. Oblique shock and expansion waves prevail in two- and three-dimensional supersonic flows, in contrast to normal shock waves, which are one-dimensional.

The density, pressure, and temperature ratios across an oblique shock wave are given by

$$\frac{\rho_2}{\rho_1} = \frac{(\gamma + 1) M_1^2 \sin^2 \beta}{(\gamma - 1) M_1^2 \sin^2 \beta + 2} \tag{6.2}$$

$$\frac{p_2}{p_1} = 1 + \frac{2\gamma}{\gamma + 1} (M_1^2 \sin^2 \beta - 1) \tag{6.3}$$

$$\frac{T_2}{T_1} = 1 + \frac{2(\gamma - 1)}{(\gamma + 1)^2} \frac{M_1^2 \sin^2 \beta - 1}{M_1^2 \sin^2 \beta} (\gamma M_1^2 \sin^2 \beta + 1) \tag{6.4}$$

where subscripts 1 and 2 refer to the conditions ahead of and behind the oblique shock and β is the shock angle.

The Mach number behind the oblique shock M_2 is given by

$$M_2 = \frac{M_{n2}}{\sin(\beta - \theta)} \tag{6.7}$$

Scanned by CamScanner

where M_{n2} is the normal component of Mach number behind the shock and θ is the flow turning angle.

The maximum and minimum values of shock angle correspond to those for normal shock—$\beta = \pi/2$ and Mach wave, μ. Thus the possible range of β is

$$\sin^{-1}\left(\frac{1}{M_1}\right) \leq \beta \leq \frac{\pi}{2} \tag{6.8}$$

The relation between the Mach number, shock angle, and flow turning angle is given by

$$\tan\,\theta = 2\,\cot\,\beta\left(\frac{M_1^2\,\sin^2\beta - 1}{M_1^2(\gamma + \cos 2\beta) + 2}\right) \tag{6.13}$$

This is known as the *θ–β–M relation.*

The graphical representation of oblique shock properties is known as *shock polar.*

A two-dimensional flow of supersonic stream is always associated with two families of Mach lines. The Mach lines with (+) sign which run to the right of the streamline, when viewed through the flow direction, are called right-running characteristics, and the Mach lines with (–) sign which run to the left of the streamline are called left-running characteristics.

Supersonic flow expansion around a convex corner, involving a smooth, gradual change in flow properties is known as *Prandtl–Meyer expansion.* The expansion fan or the Prandtl–Meyer fan consists of an infinite number of Mach waves, centred at the convex corner. All rays in an expansion fan are Mach lines and the entire flow, except the flow at the vertex of the fan, is isentropic.

The maximum turning of the flow corresponds to the situation where p goes to zero. This corresponds to a flow turning angle of $\theta = 130.5°$.

The Prandtl–Meyer expansion is a self-similar motion and the *Prandtl–Meyer function is a similarity parameter.* The Prandtl–Meyer function in terms of Mach number is given by

$$\nu = \sqrt{\frac{\gamma+1}{\gamma-1}}\,\arctan\sqrt{\frac{\gamma-1}{\gamma+1}(M^2-1)} - \arctan\sqrt{(M^2-1)} \tag{6.47}$$

The waves causing isentropic expansion and compression are called *simple waves.* Zones of supersonic expansion or compression with Mach lines which are straight are called *simple regions.* Zones with curved Mach lines are called *non-simple regions.*

An incident shock gets reflected as a shock from a solid boundary. This kind of reflection is called *like reflection.* On the other hand, an incident shock gets reflected as an expansion fan and the expansion fan gets reflected as compression waves from a free boundary. This kind of reflection is called *unlike reflection.*

For supersonic flows, drag exists even in the idealized, nonviscous fluid. This new component of drag encountered when the flow is supersonic is called

Scanned by CamScanner

wave drag, and it is fundamentally different from the frictional drag and separation drag which are associated with boundary layers in a viscous fluid.

Thin aerofoil theory gives an expression for the pressure coefficient as

$$C_p = \frac{2\theta}{\sqrt{M_1^2 - 1}} \tag{6.52}$$

It states that the pressure coefficient is proportional to the local flow direction.

For a flat plate at a small angle of attack α_0, the lift and drag coefficients may be expressed as

$$\left.\begin{aligned} C_L &= \frac{4\alpha_0}{\sqrt{M_1^2 - 1}} \\ C_D &= \frac{4\alpha_0^2}{\sqrt{M_1^2 - 1}} \end{aligned}\right\} \tag{6.54}$$

The general expressions of lift and drag coefficients of a thin aerofoil in supersonic flow may be written as

$$C_L = \frac{4\alpha_0}{\sqrt{M_1^2 - 1}} \tag{6.59a}$$

$$C_D = \frac{4}{\sqrt{M_1^2 - 1}} \left[\overline{\left(\frac{dh}{dx}\right)^2} + \alpha_0^2 + \overline{\alpha_c^2(x)} \right] \tag{6.59b}$$

where $h(x)$ gives the symmetrical thickness distribution, α_0 is the freestream angle of attack, and $\alpha_c(x)$ is the angle of attack due to camber. It is seen from Eq. (6.59b) that the drag is split into *drag due to lift*, *drag due to camber*, and *drag due to thickness*. But the lift coefficient depends only on the mean angle of attack.

From the discussions of shock and expansion waves in this chapter, it is clear that any problem in supersonic flow, in principle, can be analysed with the relations developed for the oblique shock and expansion fans. However, it must be realized that all relations we have developed are for flow fields with simple regions. For the nonsimple regions with nonlinear wave net there is no exact analytical approach developed so far. But when the wave net pattern is made with tiny segments, the relation developed for linear waves can be applied to nonlinear wave segments in the nonsimple region, without introducing a significant error. This kind of approach is adopted in Chapter 12 while designing contoured nozzles to generate supersonic flows. Experimental results with such nozzles prove that assuming the nonlinear waves to be straight waves within a small wave net does not introduce any significant error. It is essential to realize that in Method of Characteristics the above approximation is made for expansion waves which are isentropic. When the wave net involves crossing of shocks or

Scanned by CamScanner

compression waves, this assumption is bound to introduce significant errors in our calculations. The development of a theory involving nonsimple regions with shocks or compression waves is still an open question.

PROBLEMS

1. A uniform supersonic air flow at Mach 2.0 passes over a wedge. An oblique shock, making an angle of 40° with the flow direction, is attached to the wedge. If the static pressure and temperature in the freestream are 0.5×10^5 N/m^2 and 0°C, determine the static pressure and temperature behind the wave, the Mach number of the flow passing over the wedge, and the wedge angle.

   [**Ans.** 0.8875×10^5 N/m^2, 323.5 K, 1.61 and 21.14°]

2. Air stream at Mach 2.0 is isentropically deflected by 5° in the clockwise direction. If the pressure and temperature before deflection are 98 kN/m^2 and 17°C, determine the final state after deflection.

   [**Ans.** $M = 2.18$, $p = 74$ kN/m^2, $T = 276.8$ K, $\rho = 0.9315$ kg/m^3]

3. A two-dimensional wind tunnel nozzle is designed to give a uniform parallel flow at a Mach 3.0 with air as the flowing fluid. The test gas is supplied from a blow down air supply initially at a pressure of 70×10^5 N/m^2 and the nozzle exhausts to the atmosphere ($p_e = 1$ atm). During the operation, the pressure in the supply reservoir decreases.

   (a) At what supply pressure will oblique shock waves first appear in the exhaust jet? A test region extending one diameter downstream and 10% of the diameter in height is required, in which the flow is shock free.

   (b) What is the minimum supply pressure for obtaining the desired test region?

   (c) What is the minimum supply pressure for which a normal shock will appear at the nozzle exit?

   [**Ans.** (a) $\leq 37.2 \times 10^5$ N/m^2; (b) 23.3×10^5 N/m^2; (c) 3.6×10^5 N/m^2]

4. Air approaches a symmetrical wedge with semi-vertex angle 15° at Mach 2.0. Determine for the strong and weak waves (a) wave angle with respect to freestream direction, (b) pressure ratio across the wave, (c) temperature ratio across the wave, (d) density ratio across the wave, and (e) Mach number downstream of shock.

   [**Ans.** *Strong Shock Solution*
   (a) 79.8°; (b) 4.354; (c) 1.662; (d) 2.615; (e) 0.644
   Weak Shock Solution
   (a) 45.3°; (b) 2.191; (c) 1.267; (d) 1.729; (e) 1.446]

Scanned by CamScanner

5. An underexpanded, two-dimensional, supersonic nozzle exhausts into a region where $p = 0.75$ atm. Flow at nozzle exit plane is uniform, with $p = 1.6$ atm and $M = 2.0$. Calculate the flow direction and Mach number after initial expansion.

[**Ans.** Flow turning angle = 12.275°, $M = 2.48$]

6. (a) Compute the maximum deflection angles for which the oblique shock remains attached to the wedge when $M_1 = 2.0$ and 3.0.

(b) Compute the minimum values of Mach number M_1 for which the oblique shock remains attached to the wedge for deflection angles of $\theta_d = 15°$, 25° and 40°.

[**Ans.** (a) 22°, 34°; (b) 1.65, 2.11, 4.45]

7. An oblique shock wave is incident on a solid boundary as shown in Fig. P6.7. The boundary is to be turned through such an angle that there will be no reflected wave. Determine the angle θ, and the flow Mach number M.

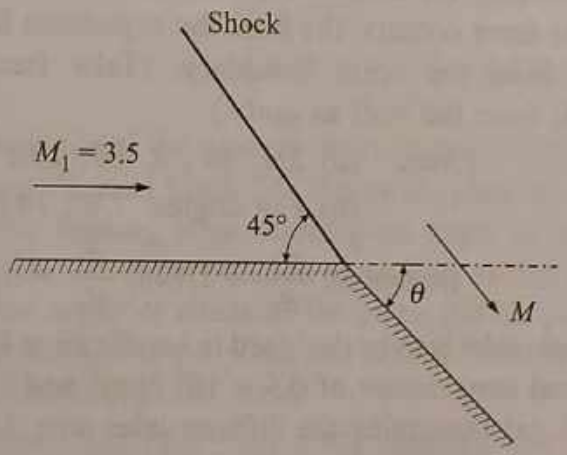


Fig. P6.7

[**Ans.** 28.158°, 1.78]

8. Air flows above a frictionless surface having a sharp corner. The flow angle and Mach number downstream from the corner are −60° and 4.0, respectively. Calculate the upstream Mach number for the flow angle of (a) 15° clockwise, (b) 30° clockwise, (c) 60° clockwise, and (d) 15° counterclockwise.

[**Ans.** (a) 1.8022; (b) 2.360; (c) 4.0; (d) For this case ν is negative, which is not physically possible. Flow can exist only up to $|\Delta\theta| = 65.785$, for which $\nu_1 = 0$ and $M_1 = 1.0$]

9. A steady supersonic flow expands from Mach number $M_1 = 2.0$ and pressure p_1 to pressure $p_2 = p_1/2$ from a centred rarefaction. Find the Mach number M_2 and flow direction θ_2.

[**Ans.** 2.444, 11.43°]

Scanned by CamScanner

10. (a) A wind tunnel nozzle is designed to yield a parallel uniform flow of air with a Mach number $M = 3.0$. The stagnation pressure of the air supply reservoir $p_0 = 70 \times 10^5$ N/m^2, and the nozzle exhausts into the atmosphere. (a) Calculate the flow angle at the exit lip of the nozzle if the atmospheric pressure $p_e = 1.0$ atm. (b) For the wind tunnel in (a), determine the stagnation pressure of the air supply for which the flow angle at the exit lip is zero

[**Ans.** (a) 7.67°; (b) 3.723 MPa]

11. Air at $p_1 = 0.3 \times 10^5$ N/m^2, $T_1 = 350$ K and $M_1 = 1.5$ is to be expanded isentropically to 0.13×10^5 N/m^2. Determine (a) the flow deflection angle, (b) final Mach number, and (c) the temperature of air after expansion.

[**Ans.** (a) 15.75°; (b) 2.05; (c) 275.7 K]

12. Air with an initial Mach number $M_1 = 2.0$ flows over three sharp corners in succession, having clockwise turning angles of 5°, 10° and 15°, respectively. (a) Calculate the Mach number and flow angle after each of the three corners. (b) Find the expansion fans, and streamline distances from the solid boundary. (Take freestream streamline distance d_1 from the wall as unity.)

[**Ans.** (a) 2.0, 30°, 2.187, 27.2°, 2.6, 22.62°

(b) Fan angles: 7.8°, 14.6°, 20.34°

Distances: $\frac{d_2}{d_1} = 1.173$, $\frac{d_3}{d_1} = 1.716$, $\frac{d_4}{d_1} = 3.562$]

13. A supersonic inlet is to be designed to handle air at Mach 2.4 with static pressure and temperature of 0.5×10^5 N/m^2 and 280 K, as shown in Fig. P6.13. (a) Determine the diffuser inlet area A_i if the device is to handle 20 kg/s of air. (b) The diffuser has to further decelerate the flow behind the normal shock so that the velocity entering the compressor is not to exceed 30 m/s. Assuming isentropic flow behind the normal shock, determine the area A_e required, and the static pressure p_e there.

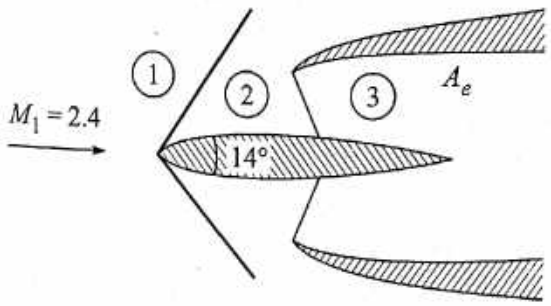


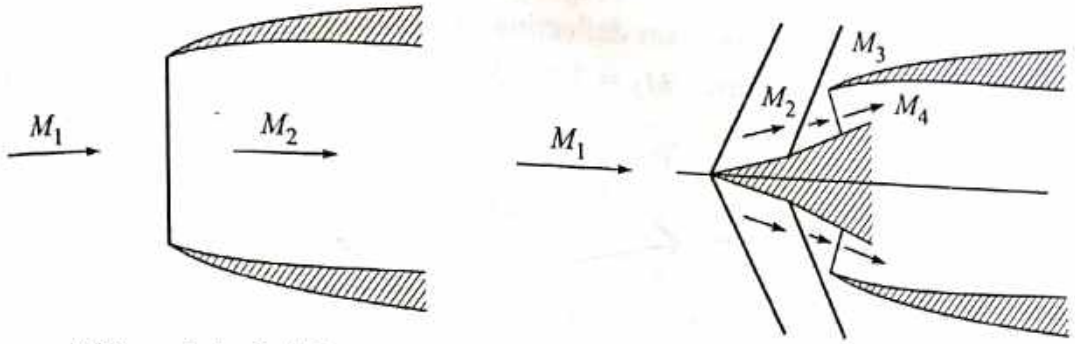
Fig. P6.13

[**Ans.** (a) $A_i = 0.0313$ m^2; (b) $A_e = 0.240$ m^2, $p_e = 4.82 \times 10^5$ N/m^2]

14. A supersonic inlet is to be designed to operate at Mach 3.0. Two possibilities are considered, as shown in Fig. P6.14. In one, the

Scanned by CamScanner

compression and deceleration of the flow takes place through a single normal shock [Fig. P6.14(a)]; in the other, a wedge-shaped diffuser [Fig. P6.14(b)] is used and the deceleration is through two weak oblique shocks followed by a normal shock wave. The wedge turning angles are 8° each. Compare the loss in stagnation pressure for the two cases.



(a) Normal shock diffuser (b) Wedge-shaped diffuser

Fig. P6.14

[**Ans.** (a) $\frac{p_{02}}{p_{01}} = 0.3283$; (b) $\frac{p_{04}}{p_{01}} = 0.5804$]

15. A two-dimensional flat plate is inclined at a positive angle of attack in supersonic stream of Mach 2.0. Below the plate, an oblique shock wave starts at the leading edge, making an angle of 42° with the stream direction. On the upper side, an expansion occurs at the leading edge. Find (a) the angle of attack of the plate, (b) the pressure on the lower and upper surface of the plate, and (c) the pressure at the trailing edge after the flow leaves the plate.

[**Ans.** (a) 12.3°; (b) 1.928 atm and 0.473 atm; (c) 1.0 atm]

16. Air, which is assumed to be a perfect gas, flows in a blow-down wind tunnel with constant stagnation parameters $T_0 = 300$ K and $p_0 = 70 \times 10^5$ N/m^2. A symmetrical wedge having a semi-angle $\theta/2 = 15°$ is placed in the test-section where $M = 3.0$. Calculate the following flow properties on the face of the wedge: (a) static pressure, density, and temperature, (b) stagnation pressure, (c) flow velocity, and flow Mach number.

[**Ans.** (a) 5.37×10^5 N/m^2, 12.57 kg/m^3 and 148.7 K; (b) 66.66×10^5 N/m^2; (c) 552.3 m/s and 2.26]

17. The two-dimensional aerofoil shown in Fig. P6.17 is travelling at a Mach number of 3 and at an angle of attack of 2°. The thickness-to-chord ratio of the aerofoil is 0.1, and the maximum thickness occurs at 30 per cent of the chord downstream from the leading edge. Using the linearized theory, show that the moment coefficient about the aerodynamic centre is – 0.0354, the centre of pressure is at $1.217c$, and the drag coefficient is 0.0354. Show also that the angle of zero lift is 0°.

Scanned by CamScanner

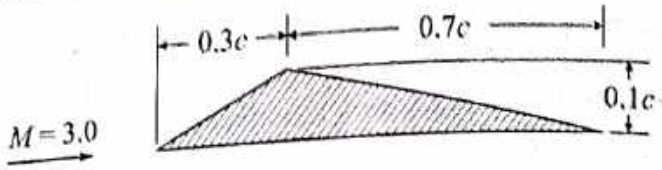


Fig. P6.17

18. For the flat plate shown in Fig. P6.18, calculate the flow Mach numbers assuming the slipstream deflection to be negligible.

[**Ans.** $M_2 = 3.71$, $M_3 = 2.726$, $M_{2'} = 2.4$, $M_{3'} = 2.95$]

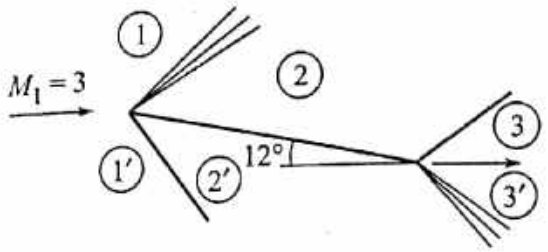


Fig. P6.18

19. For the double wedge shown in Fig. P6.19, calculate the flow Mach numbers and the slipstream.

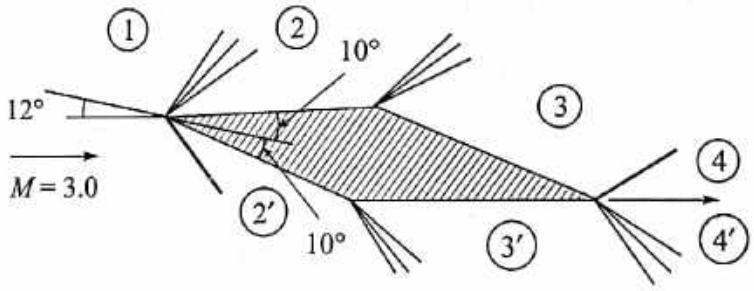


Fig. P6.19

[**Ans.** $M_2 = 3.105$, $M_3 = 4.493$, $M_4 = 2.580$
$M_{2'} = 1.910$, $M_{3'} = 2.710$, $M_{4'} = 2.806$]
Comparing p_4/p_{01} and $p_{4'}/p_{01}$ it can be seen that the slipstream is very weak]

20. A two-dimensional wedge shown in Fig. P6.20 moves through the atmosphere at sea-level, at zero angle of attack with $M_\infty = 3.0$. Calculate C_L and C_D using the shock-expansion theory.

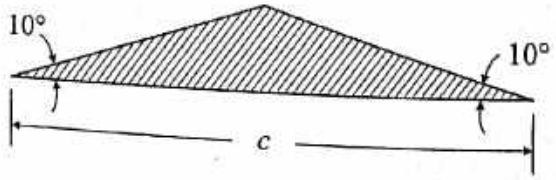


Fig. P6.20

[**Ans.** $C_L = -0.0389$, $C_D = 0.02267$]

Scanned by CamScanner

21. For a Prandtl–Meyer expansion, the upstream Mach number is 2 and the pressure ratio across the fan is 0.5. Determine the angles of the front and end Mach lines of the expansion fan relative to the freestream.

[**Ans.** 30°, 12.86°]

22. Calculate the ratios of static and total pressures across the shock wave emanating from the leading edge of a wedge of 5° half-angle flying at Mach 2.2.

[**Ans.** 1.3397, 0.99726]

23. An uniform supersonic flow of air at Mach 3.0 and $p_1 = 0.05$ atm passes over a cone of semi-vertex angle 8° kept in line with the flow. Determine the shock angle and the static pressure at the cone surface, just behind the shock.

[**Ans.** 25.61°, 9.1 kPa]

24. A supersonic stream of air at Mach 3 and 1 atm passes through a sudden convex and then a sudden concave corner of turning angle 15° each. Determine the Mach number and pressure of the flow downstream of the concave corner.

[**Ans.** 2.7, 1.019 atm]

25. A flat plate wing of chord 1 m experiences a lift of 10.2 kN per metre of width. If the flow Mach number and pressure are 1.6 and 25 kPa, respectively, determine the angle of attack and the aerodynamic efficiency of the wing.

[**Ans.** 4°, 14]

26. For an oblique shock wave with a wave angle of 33° and upstream Mach number 2.4, calculate the flow deflection angle θ, the pressure and temperature ratios across the shock wave and the Mach number behind the wave.

[**Ans.** 10°, 1.8354, 1.1972, 2.0]

27. Show that the pressure difference across a oblique shock wave with wave angle β may be expressed in the form

$$\frac{p_2 - p_1}{\frac{1}{2}\rho_1 u_1^2} = \frac{4}{\gamma + 1}\left(\sin^2\beta - \frac{1}{M_1^2}\right)$$

where the subscripts 1 and 2 refer to states upstream and downstream of the shock.

28. Air flow with Mach number 3.0 and pressure 1 atm passes over a compression corner. If the pressure downstream of the corner is 5 atm, determine the flow turning angle.

[**Ans.** 25.5°]

Scanned by CamScanner

29. A Mach 2 air stream passes over a 10° compression corner. The oblique shock from the corner is reflected from a flat wall which is parallel to the freestream, as shown in Fig. P6.29. Compute the angle of the reflected shock wave relative to the flat wall and the Mach number downstream of the reflected shock.

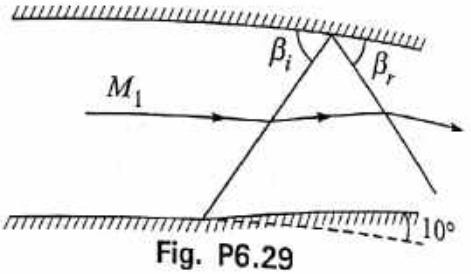


Fig. P6.29

[**Ans.** 39.5°, 1.28]

30. Air at Mach 2 passes over two compression corners of angles 7° and θ, as shown in Fig. P6.30. Determine the value of θ up to which the second shock will remain attached.

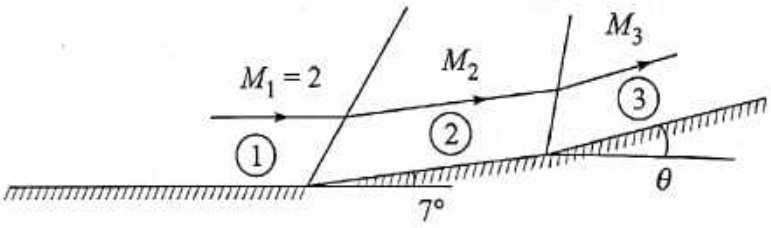


Fig. P6.30

[**Ans.** 18°]

31. Air flow at Mach 2 is compressed by turning it through 15°. For each of the possible solutions calculate (a) the shock angle, (b) the Mach number downstream of the shock and (c) the change in entropy. What is the maximum deflection angle up to which the shock will remain attached?

[**Ans.** Weak solution: 45.34°, 1.45, 13.73 J/kg-K,
Strong solution: 79.83°, 0.64, 88.25 J/kg-K, 22.97°]

32. A Mach 3 air flow with pressure and temperatures of 1 atm and 200 K, respectively, is deflected at a compression corner through 10°. Calculate the Mach number, static and stagnation pressure and temperatures downstream the corner.

[**Ans.** 2.5, 2.06 atm, 248.36 K, 35.37 atm, 560 K]

33. Determine the wave angle and Mach number behind and the pressure ratio across the oblique shock with $M_1 = 3.0$ and $\theta = 10°$, treating the shock as weak and strong.

[**Ans.** Weak solution: $\beta = 27.4°$, 2.5, 2.05,
Strong solution: $\beta = 86.41°$, 0.49, 10.3]

34. Compare the pressure loss experienced by the (a) one-shock and (b) two-shock spikes shown in Figs. P6.34(a) and (b).

Scanned by CamScanner

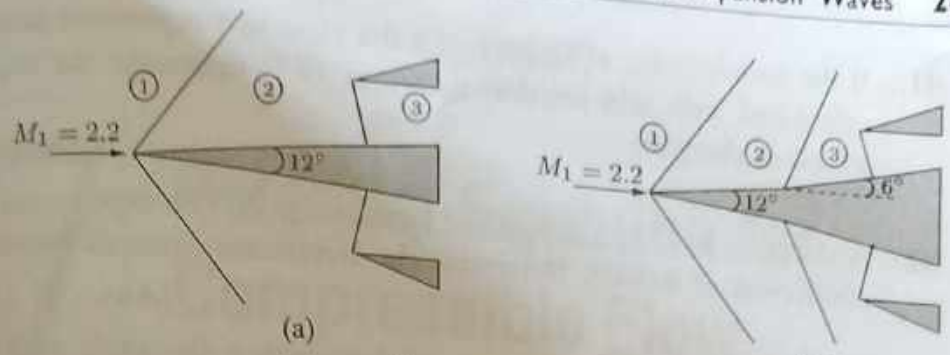


Fig. P6.34

[**Ans.** 27.3 per cent, 17.2 per cent]

35. An oblique shock created by the flow of air over a sharp corner, as shown in Fig. P6.35, is with wave angle 30°. If the Mach number upstream of the incident wave is 2.4, determine the Mach number upstream and downstream of the reflected shock wave.

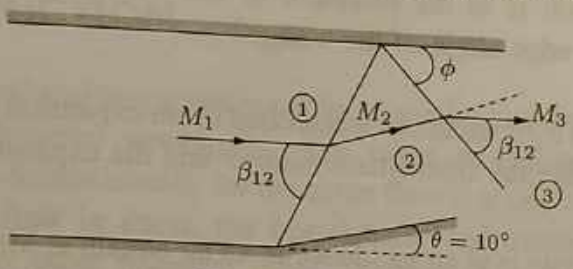


Fig. P6.35

[**Ans.** 2.09, 1.84]

36. A two-stage ramp of an intake compresses Mach 2.3 air stream. If the pressure loss caused by the second shock is half of the pressure loss of the first shock at the step of semi-angle 8°, determine the semi-angle of the second ramp.

[**Ans.** 7°]

37. If the entropy increase across an oblique shock causing 9° flow turning is 150 J/(kg K), determine the shock strength.

[**Ans.** 0.699]

38. The entropy increase across an oblique shock in air is 150 J/(kg K). If the shock angle is 29°, determine the flow deflection caused by the shock wave.

[**Ans.** 19°]

39. A flat plate aerofoil in a Mach 2 freestream experiencing a lift coefficient of 0.16 has an aerodynamics efficiency of 14.65. Determine the drag coefficient and angle of attack.

[**Ans.** 0.0109, 3.97°]

40. The temperature and flow speed ahead of an oblique shock of wave angle 38° is 238 K and 773 m/s, respectively. Find the flow deflection caused by the shock, the Mach number behind the shock and the shock strength.

[**Ans.** 16°, 1.83, 1.6]

Scanned by CamScanner

41. If the aerodynamic efficiency of a flat plate in a supersonic airstream calculated with thin aerofoil theory is 19.1, determine the angle of attack of the plate.

[**Ans.** 3°]

42. A flat plate at 2° to a supersonic airstream at 20 kPa experiences a lift coefficient of 0.0609. Determine the freestream dynamic pressure.

[**Ans.** 87.5 kPa]

43. A Mach 2.2 air stream is expanded through a fan angle of 2.412°. Determine the Mach number and the flow turning angle.

[**Ans.** 2.4, 5.015°]

44. A semi diamond wedge of nose angle 5° is kept at zero incidence in a Mach 1.6 air stream at atmospheric pressure. If the shock at the trailing edge has to be 1.7 times stronger than the shock at the nose, and the slipstream is in the direction of the freestream, what should be the trailing edge angle of the wedge?

[**Ans.** 7.308°]

45. A Mach 2 air stream is accelerated by an expansion corner of angle 10°. Determine the final Mach number and the expansion fan angle.

[**Ans.** 2.39, 16°]

46. A flat plate is at an incidence in an air stream at Mach 1.8 and 0.5 atm. (a) If the pressure coefficient over the lower surface of the plate is 0.222, determine the angle of incidence. (b) Find the pressure coefficient over the upper surface of the plate.

[**Ans.** (a) 8°, (b) –0.157]

47. If an oblique shock of strength 0.25 is positioned at the exit of a Mach 2.35 nozzle discharging air to an environment at 1 atm, determine Mach number behind the shock, the shock angle and the total pressure at the nozzle inlet.

[**Ans.** 1.97, 29.9°, 10.81 atm]

48. A shock of wave angle 18° deflects the flow by 3.5°. If the Mach number behind the shock is 1.8, determine the Mach number ahead of the shock and the shock strength.

[**Ans.** 11.42, 13.371]

49. Show that the following are the limiting relations for $\beta/\tan(\beta-\theta)$ and M_2^2 for oblique shocks when M_1 ahead of the shock becomes very large.

$$\frac{\tan\beta}{\tan(\beta-\theta)} \to \frac{\gamma+1}{\gamma-1}$$

$$M_2^2 \to \frac{\gamma-1}{2\gamma\sin^2(\beta-\theta)}$$

Scanned by CamScanner

7 Potential Equation for Compressible Flow

7.1 INTRODUCTION

The one-dimensional analyses given in earlier chapters are valid only for the flow through an infinitesimal streamtube. For other real flow situations, the assumption of one-dimensionality for the entire flow is at best an approximation. In problems like flow in ducts, the one-dimensional treatment is adequate. However, in many other practical cases, the one-dimensional methods are neither adequate nor do they provide information about important aspects of the flow. For example, in the case of flow past the wings of an aircraft, the flow through the blade passages of turbines and compressors, and the flow through ducts of rapidly varying cross-sectional area the flow field must be thought of as two dimensional or three dimensional in order to obtain results of practical interest.

Because of the mathematical difficulties associated with the treatment of the most general case of three-dimensional motion—including shocks, friction, and heat transfer—it becomes necessary to conceive simple models of flow, which lend themselves to analytical treatment but at the same time furnish valuable information concerning the real and difficult flow patterns. We know that by using Prandtl's boundary layer concept, it is possible to neglect friction and heat transfer for the region of potential flow outside the boundary layer (see Section 2.5).

In this chapter, we discuss the differential equations of motion for irrotational, inviscid, adiabatic, and shock-free motion of a perfect gas.

7.2 CROCCO'S THEOREM

Consider two-dimensional, steady, inviscid flow in natural coordinates (l, n) such that l is along the streamline direction and n is perpendicular to the direction of the streamline. The advantage of using the natural coordinate system—a

Scanned by CamScanner

coordinate system in which one coordinate is along the streamline direction and the other normal to it—is that the flow velocity is always along the streamline direction and the velocity normal to streamline is zero.

Though this is a two-dimensional flow, we can apply one-dimensional analysis, by considering the portion between the two streamlines 1 and 2 (as shown in Fig. 7.1) as a streamtube and taking the third dimension to be unity.

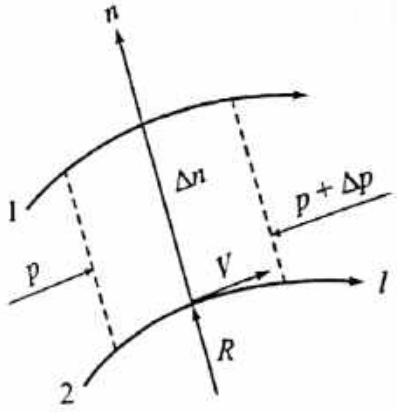


Fig. 7.1 Flow between two streamlines.

Let us consider a unit width in the third direction, for the present study. For this flow, the equation for continuity is

$$\rho V \, \Delta n = \text{constant} \tag{7.1}$$

The l-momentum equation* is

$$\rho V \, \Delta n \, dV = -dp \, \Delta n$$

The l-momentum equation can also be expressed as

$$\rho V \frac{\partial V}{\partial l} = -\frac{\partial p}{\partial l} \tag{7.2}$$

The n-momentum equation is

$$dV = 0$$

But there will be a centrifugal force acting in the n-direction. Therefore,

$$\frac{\rho V^2}{R} = -\frac{\partial p}{\partial n} \tag{7.3}$$

*Momentum equation. For incompressible flow,

$$\Sigma F_i = \rho \int V_x \, dQ$$

where Q is the volume flow rate. For compressible flow,

$$\Sigma F_i = \int \rho V_x \, dQ$$

$$\Sigma dF_i = \rho V_x \, dQ = \dot{m} \, V_x$$

Scanned by CamScanner

The energy equation is

$$h + \frac{V^2}{2} = h_0 \tag{7.4}$$

Also, by Eq. (2.31),

$$Tds = dh - \frac{dp}{\rho}$$

Differentiation of Eq. (7.4) gives $dh + VdV = dh_0$. Therefore, the entropy equation becomes

$$Tds = -\left(VdV + \frac{dp}{\rho}\right) + dh_0$$

This equation can be split as follows:

(i) $$T\frac{\partial s}{\partial l} = -\left(V\frac{\partial V}{\partial l} + \frac{1}{\rho}\frac{\partial p}{\partial l}\right)$$

since $\dfrac{dh_0}{dl} = 0$ along the streamlines.

(ii) $$T\frac{\partial s}{\partial n} = -\left(V\frac{\partial V}{\partial n} + \frac{1}{\rho}\frac{\partial p}{\partial n}\right) + \frac{dh_0}{dn}$$

Introducing $\partial p/\partial l$ from Eq. (7.2) and $\partial p/\partial n$ from Eq. (7.3) into the above two equations, we get

$$T\frac{\partial s}{\partial l} = 0 \tag{7.5a}$$

$$T\frac{\partial s}{\partial n} = -V\left(\frac{\partial V}{\partial n} - \frac{V}{R}\right) + \frac{dh_0}{dn} \tag{7.5b}$$

i.e.

$$\boxed{T\frac{\partial s}{\partial n} = \frac{dh_0}{dn} + V\zeta} \tag{7.6}$$

This is known as Crocco's theorem for two-dimensional flows. From this it is seen that the rotation depends on the rate of change of entropy and stagnation enthalpy normal to the streamlines.

Crocco's theorem essentially relates entropy gradients to vorticity, in steady, frictionless, non-conducting, adiabatic flows. In this form Crocco's equation shows that if s is a constant, the vorticity ζ must be zero. Likewise, if vorticity ζ is zero, ds/dn must be zero, implying that the entropy s is a constant. That is, isentropic flows are irrotational and irrotational flows are isentropic. This result is true, in general, only for steady flows of inviscid fluids in which there are no body forces acting and the stagnation enthalpy is a constant.

From Eq. (7.5a) it is seen that the entropy does not change along a streamline. Also, Eq. (7.5b) shows how entropy varies normal to the streamlines.

Scanned by CamScanner

In Eq. (7.6), $\zeta = \frac{V}{R} - \frac{\partial V}{\partial n}$ is the vorticity of the flow. The circulation is

$$\Gamma = \oint_c V dl = \iint_s \text{curl } V \, ds = \iint_s \zeta \, ds \tag{7.7}$$

By Stokes' theorem, the vorticity ζ is given by

$$\boxed{\zeta = \text{curl } V} \tag{7.8}$$

$$\zeta_x = \left(\frac{\partial V_z}{\partial y} - \frac{\partial V_y}{\partial z} \right)$$

$$\zeta_y = \left(\frac{\partial V_x}{\partial z} - \frac{\partial V_z}{\partial x} \right)$$

$$\zeta_z = \left(\frac{\partial V_y}{\partial x} - \frac{\partial V_x}{\partial y} \right)$$

where ζ_x, ζ_y, ζ_z are the vorticity components. The two conditions that are necessary for a frictionless flow to be isentropic throughout are:

1. h_0 = constant, throughout the flow
2. $\zeta = 0$, throughout the flow

From Eq. (7.8), $\zeta = 0$ for irrotational flow. That is, if a frictionless flow is to be isentropic, the total enthalpy should be constant throughout and the flow should be irrotational.

When $\zeta \neq 0$ Since h_0 = constant, T_0 = constant (perfect gas). For this type of flow we can show that

$$\zeta = \frac{T}{V} \frac{ds}{dn} = -\frac{RT_0}{Vp_0} \frac{dp_0}{dn} \tag{7.9}$$

From Eq. (7.9), it is seen that in an irrotational flow, the stagnation pressure does not change normal to the streamlines. Even, when there is a shock in the flow field, p_0 changes along the streamlines at the shock, but does not change normal to the streamlines.

Let h_0 = constant (isoenergic flow). Then Eq. (7.6) can be written in vector form as

$$T \text{ grad } s + V \times \text{curl } V = \text{grad } h_0 \tag{7.10a}$$

where grad s stands for increase of s in the n-direction. For a steady, inviscid, and isoenergic flow,

$$T \text{ grad } s + V \times \text{curl } V = 0$$

$$V \times \text{curl } V = -T \text{ grad } s \tag{7.10b}$$

If s = constant, $V \times$ curl $V = 0$. This implies that (a) the flow is irrotational, i.e. curl $V = 0$, or (b) V is parallel to curl V.

Scanned by CamScanner

Irrotational flow For irrotational flows (curl $V = 0$), a potential function ϕ exists such that

$$\boxed{V = \text{grad}\ \phi} \tag{7.11}$$

Therefore, the velocity components are given by

$$V_x = \frac{\partial \phi}{\partial x}, \qquad V_y = \frac{\partial \phi}{\partial y}, \qquad V_z = \frac{\partial \phi}{\partial z}$$

The advantage of introducing ϕ is the three unknowns V_x, V_y and V_z in a general three-dimensional flow are reduced to a single unknown ϕ. With ϕ, the irrotationality conditions defined by Eq. (7.8) may be expressed as follows:

$$\zeta_x = \frac{\partial V_z}{\partial y} - \frac{\partial V_y}{\partial z} = 0 = \frac{\partial}{\partial y}\left(\frac{\partial \phi}{\partial z}\right) - \frac{\partial}{\partial z}\left(\frac{\partial \phi}{\partial y}\right) = 0$$

Also, the incompressible continuity equation $\text{div}\,(V) = 0$ becomes

$$\boxed{\frac{\partial^2 \phi}{\partial x^2} + \frac{\partial^2 \phi}{\partial y^2} + \frac{\partial^2 \phi}{\partial z^2} = 0}$$

This is Laplace's equation. With the introduction of ϕ, the three equations of motion can be replaced, at least for incompressible flow, by one Laplace's equation, which is a linear equation.

Basic solutions of Laplace's equation We know from our basic studies on fluid flows (Shames, 1962) that

1. $\phi = V_\infty x$ — for uniform parallel flow (towards $+x$-direction)
2. $\phi = \dfrac{Q}{2\pi} \ln r$; Q is the strength of source — for source
3. $\phi = \dfrac{\mu \cos \theta}{\pi}$; μ is the moment of doublet — for doublet (issuing in the $-x$-direction)
4. $\phi = \dfrac{\Gamma}{2\pi}\theta$; Γ is circulation — for potential vortex (counterclockwise)

7.3 THE GENERAL POTENTIAL EQUATION FOR THREE-DIMENSIONAL FLOW

By continuity equation, $\text{div}\,(\rho V) = 0$, i.e.

$$\frac{\partial (\rho V_x)}{\partial x} + \frac{\partial (\rho V_y)}{\partial y} + \frac{\partial (\rho V_z)}{\partial z} = 0 \tag{7.12}$$

Scanned by CamScanner

Euler's equations of motion (neglecting body forces) are:

$$\rho\left(V_x\frac{\partial V_x}{\partial x}+V_y\frac{\partial V_x}{\partial y}+V_z\frac{\partial V_x}{\partial z}\right)=-\frac{\partial p}{\partial x} \tag{7.13a}$$

$$\rho\left(V_x\frac{\partial V_y}{\partial x}+V_y\frac{\partial V_y}{\partial y}+V_z\frac{\partial V_y}{\partial z}\right)=-\frac{\partial p}{\partial y} \tag{7.13b}$$

$$\rho\left(V_x\frac{\partial V_z}{\partial x}+V_y\frac{\partial V_z}{\partial y}+V_z\frac{\partial V_z}{\partial z}\right)=-\frac{\partial p}{\partial z} \tag{7.13c}$$

For incompressible flow, ρ is a constant. Therefore, the above four equation are sufficient for solving the four unknowns V_x, V_y, V_z and p. But for a compressible flow, ρ is also an unknown. Therefore, the unknowns are ρ, V_x, V_y, V_z, and p. Hence the additional equation, namely, the isentropic process equation, is used. That is, p/ρ^γ = constant is the additional equation used along with continuity and momentum equations..

Introducing the potential function ϕ, we have the velocity components as

$$V_x=\frac{\partial\phi}{\partial x}=\phi_x,\qquad V_y=\frac{\partial\phi}{\partial y}=\phi_y,\qquad V_z=\frac{\partial\phi}{\partial z}=\phi_z \tag{7.14}$$

Equation (7.12) may also be written as

$$\rho\left(\frac{\partial V_x}{\partial x}+\frac{\partial V_y}{\partial y}+\frac{\partial V_z}{\partial z}\right)+V_x\frac{\partial\rho}{\partial x}+V_y\frac{\partial\rho}{\partial y}+V_z\frac{\partial\rho}{\partial z}=0 \tag{7.12a}$$

From isentropic process relation, $\rho=\rho(p)$. Hence,

$$\frac{\partial\rho}{\partial x}=\frac{d\rho}{dp}\frac{\partial p}{\partial x}=-\frac{1}{a^2}\rho\left(V_x\frac{\partial V_x}{\partial x}+V_y\frac{\partial V_x}{\partial y}+V_z\frac{\partial V_x}{\partial z}\right)$$

because from Eq. (7.13a),

$$\frac{\partial p}{\partial x}=-\rho\left(V_x\frac{\partial V_x}{\partial x}+V_y\frac{\partial V_x}{\partial y}+V_z\frac{\partial V_x}{\partial z}\right),\quad \frac{dp}{d\rho}=a^2$$

Similarly,

$$\frac{\partial\rho}{\partial y}=-\frac{1}{a^2}\rho\left(V_x\frac{\partial V_y}{\partial x}+V_y\frac{\partial V_y}{\partial y}+V_z\frac{\partial V_y}{\partial z}\right)$$

$$\frac{\partial\rho}{\partial z}=-\frac{1}{a^2}\rho\left(V_x\frac{\partial V_z}{\partial x}+V_y\frac{\partial V_z}{\partial y}+V_z\frac{\partial V_z}{\partial z}\right)$$

With the above relations for $\frac{\partial\rho}{\partial x}$, $\frac{\partial\rho}{\partial y}$ and $\frac{\partial\rho}{\partial z}$, Eq. (7.12a) can be expressed as

$$\frac{\partial V_x}{\partial x}\left(1-\frac{V_x^2}{a^2}\right)+\frac{\partial V_y}{\partial y}\left(1-\frac{V_y^2}{a^2}\right)+\frac{\partial V_z}{\partial z}\left(1-\frac{V_z^2}{a^2}\right)$$

$$-\frac{V_xV_y}{a^2}\left(\frac{\partial V_x}{\partial y}+\frac{\partial V_y}{\partial x}\right)-\frac{V_yV_z}{a^2}\left(\frac{\partial V_y}{\partial z}+\frac{\partial V_z}{\partial y}\right)-\frac{V_zV_x}{a^2}\left(\frac{\partial V_z}{\partial x}+\frac{\partial V_x}{\partial z}\right)=0$$

Scanned by CamScanner

Using Eq. (7.14), the above equation can also be written as

$$\left(1-\frac{\phi_x^2}{a^2}\right)\phi_{xx}+\left(1-\frac{\phi_y^2}{a^2}\right)\phi_{yy}+\left(1-\frac{\phi_z^2}{a^2}\right)\phi_{zz}$$
$$-2\left(\frac{\phi_x\phi_y}{a^2}\phi_{xy}+\frac{\phi_y\phi_z}{a^2}\phi_{yz}+\frac{\phi_z\phi_x}{a^2}\phi_{zx}\right)=0 \qquad (7.15)$$

This is the *basic potential equation for compressible flow*; it is nonlinear.

The difficulties with compressible flow stem from the fact that the basic equation is nonlinear. Hence the superposition of solutions is not valid. Further, in Eq. (7.15) the local speed of sound "a" is also a variable. By Eq. (4.9e), we have

$$\left(\frac{a}{a_\infty}\right)^2=1-\frac{\gamma-1}{2}M_\infty^2\left(\frac{V_x^2+V_y^2+V_z^2}{V_\infty^2}-1\right) \qquad (7.16)$$

To solve a compressible flow problem, we have to solve Eq. (7.15) using Eq. (7.16), but this is not possible analytically. However, a numerical solution is possible for the given boundary conditions.

7.4 LINEARIZATION OF THE POTENTIAL EQUATION

The general equation for compressible flows, namely Eq. (7.15), can be simplified for flow past slender or planar bodies. Aerofoil, slender bodies of revolution, and so on are typical examples of slender bodies. Bodies like wing, where one dimension is smaller than others, are called planar bodies. These bodies introduce small disturbances. The aerofoil contour becomes the stagnation streamline.

For the aerofoil shown in Fig. 7.2, with the exception of nose region, the perturbation velocity w is small everywhere.

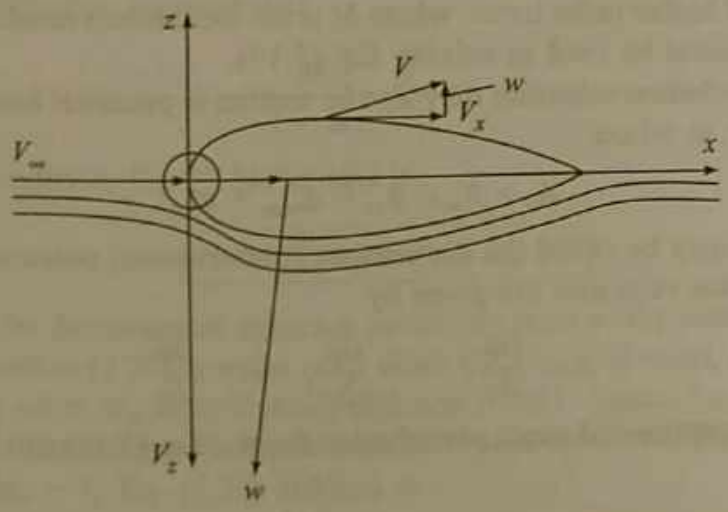


Fig. 7.2 Aerofoil in uniform flow.

Scanned by CamScanner

Small Perturbation Theory

Assume the velocity components around the aerofoil in Fig. 7.2 to be

$$V_x = V_\infty + u, \quad V_y = v, \quad V_z = w \tag{7.17}$$

where V_x, V_y, V_z are the main flow velocity components and u, v, w are the perturbation (disturbance) velocity components along the x, y, and z directions, respectively.

The small perturbation theory postulates that the perturbation velocities are small compared to main velocity components, i.e.

$$u \ll V_\infty, \quad v \ll V_\infty, \quad w \ll V_\infty \tag{7.18a}$$

Therefore,

$$V_x \approx V_\infty, \quad V_y \ll V_\infty, \quad V_z \ll V_\infty \tag{7.18b}$$

Now, consider a flow at a small angle of attack or yaw as shown in Fig. 7.3. Here,

$$V_x = V_\infty \cos \alpha + u, \quad V_y = V_\infty \sin \alpha + v$$

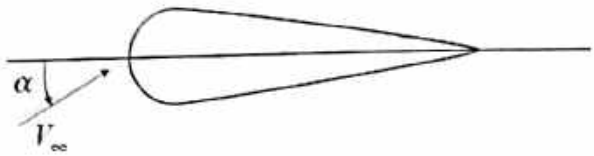


Fig. 7.3 Aerofoil at an angle of attack.

Since α is small, the above equations reduce to

$$V_x = V_\infty + u, \quad V_y = v$$

Thus, Eq. (7.17) can be used for this case as well.

With Eq. (7.17), linearization of Eq. (7.15) gives

$$(1 - M^2)\phi_{xx} + \phi_{yy} + \phi_{zz} = 0 \tag{7.19}$$

neglecting all higher order terms, where M is the local Mach number. Therefore, Eq. (7.16) should be used in solving Eq. (7.19).

The perturbation velocities may also be written in potential form, as follows: Let $\phi = \phi_\infty + \varphi$, where

$$\phi_\infty = V_\infty x: \quad \phi_{xx} = \overset{0}{\phi_{\infty xx}} + \varphi_{xx}$$

Therefore, ϕ may be called the disturbance (perturbation) potential, and hence the perturbation velocities are given by

$$u = \frac{\partial \phi}{\partial x}, \quad v = \frac{\partial \phi}{\partial y}, \quad w = \frac{\partial \phi}{\partial z} \tag{7.20}$$

With the assumptions of small perturbation theory, Eq. (7.16) can be expressed as

$$\left(\frac{a}{a_\infty}\right)^2 = 1 - (\gamma - 1)M_\infty^2 \frac{u}{V_\infty} \tag{7.21}$$

Scanned by CamScanner

$$\left(\frac{a_\infty}{a}\right)^2 = \left(1-(\gamma-1)\,M_\infty^2\,\frac{u}{V_\infty}\right)^{-1}$$

Using Binomial theorem, $(a_\infty/a)^2$ can be expressed as

$$\left(\frac{a_\infty}{a}\right)^2 = 1+(\gamma-1)\,\frac{u}{V_\infty}M_\infty^2 + O\left(M_\infty^4\,\frac{u^2}{V_\infty^2}\right) \tag{7.22}$$

Substituting the above expression for (a_∞/a) in the equation

$$M = \left(1+\frac{u}{V_\infty}\right)\left(\frac{a_\infty}{a}\right)M_\infty$$

the relation between M and M_∞ may be expressed as (neglecting small terms)

$$M^2 = \left[1+2\frac{u}{V_\infty}\left(1+\frac{\gamma-1}{2}M_\infty^2\right)\right]M_\infty^2 \tag{7.23}$$

The combination of Eqs. (7.23) and (7.19) gives

$$\boxed{(1-M_\infty^2)\phi_{xx}+\phi_{yy}+\phi_{zz}=\frac{2}{V_\infty}M_\infty^2\,\phi_x\,\phi_{xx}\left(1+\frac{\gamma-1}{2}M_\infty^2\right)} \tag{7.24}$$

Equation (7.24) is a nonlinear equation and is valid for subsonic, transonic, and supersonic flow under the framework of small perturbations with $u \ll V_\infty$, $v \ll V_\infty$, and $w \ll V_\infty$. It is, however, not valid for hypersonic flow even for slender bodies (since $u \approx V_\infty$). The equation is called the *linearized potential flow equation*, though it is not linear.

Equation (7.24) may also be written as

$$(1-M_\infty^2)\phi_{xx}+\phi_{yy}+\phi_{zz} = 2\,\frac{M_\infty^2}{1-M_\infty^2}\,\frac{u}{V_\infty}\left(1+\frac{\gamma-1}{2}M_\infty^2\right)(1-M_\infty^2)\phi_{xx} \tag{7.25}$$

Further linearization is possible if

$$\frac{M_\infty^2}{1-M_\infty^2}\,\frac{u}{V_\infty} \ll 1 \tag{7.26}$$

With this condition, Eq. (7.25) results in

$$\boxed{(1-M_\infty^2)\phi_{xx}+\phi_{yy}+\phi_{zz}=0} \tag{7.27}$$

This is the fundamental equation governing most of the compressible flow regime. Equation (7.27) is valid only when Eq. (7.26) is valid, and Eq. (7.26) is valid only when M_∞ is sufficiently different from 1. Hence, Eq. (7.26) is valid for subsonic and supersonic flows only. For transonic flows, Eq. (7.24) can be used. For $M_\infty \approx 1$, Eq. (7.24) reduces to

$$\boxed{-\frac{\gamma+1}{V_\infty}\phi_x\,\phi_{xx}+\phi_{yy}+\phi_{zz}=0} \tag{7.28}$$

Scanned by CamScanner

The nonlinearity of Eq. (7.28) makes the transonic flow problems much more difficult than subsonic or supersonic flow problems.

Equation (7.27) is elliptic (i.e. all terms are positive) for $M_\infty < 1$ and hyperbolic (i.e. not all terms are positive) for $M_\infty > 1$. But in both the cases, the governing differential equation is linear. This is the advantage of Eq. (7.27).

EXAMPLE 7.1 Show that with small perturbation theory assumption

$$\left(\frac{a}{a_\infty}\right)^2 = 1 - \frac{(\gamma-1)}{2} M_\infty^2 \left(\frac{V_x^2 + V_y^2 + V_z^2}{V_\infty^2} - 1\right)$$

will reduce to

$$\left(\frac{a}{a_\infty}\right)^2 = 1 - (\gamma-1)\, M_\infty^2 \frac{u}{V_\infty}$$

Solution By Eq. (7.16),

$$\left(\frac{a}{a_\infty}\right)^2 = 1 - \frac{(\gamma-1)}{2} M_\infty^2 \left(\frac{V_x^2 + V_y^2 + V_z^2}{V_\infty^2} - 1\right)$$

where V_x, V_y, V_z are the main velocity components along x, y and z directions. By small perturbation theory,

$$V_x = V_\infty + u, V_y = v, V_z = w$$

where u, v and w are the perturbation velocities along along x, y and z directions. Also, u, v and w are very small compared to V_∞.

Substituting these in to Eq. (7.16), we have

$$\left(\frac{a}{a_\infty}\right)^2 = 1 - \frac{(\gamma-1)}{2} M_\infty^2 \left(\frac{(V_\infty + u)^2 + v^2 + w^2}{V_\infty^2} - 1\right)$$

Neglecting v^2 and w^2 being small, this reduces to

$$\left(\frac{a}{a_\infty}\right)^2 = 1 - \frac{(\gamma-1)}{2} M_\infty^2 \left(\frac{(V_\infty + u)^2}{V_\infty^2} - 1\right)$$

$$= 1 - \frac{(\gamma-1)}{2} M_\infty^2 \left(\frac{V_\infty^2 + 2uV_\infty + u^2}{V_\infty^2} - 1\right)$$

$$= 1 - \frac{(\gamma-1)}{2} M_\infty^2 \left(1 + 2\frac{u}{V_\infty} + \frac{u^2}{V_\infty^2} - 1\right)$$

But $\frac{u^2}{V_\infty^2}$ is very small, therefore,

Scanned by CamScanner

$$\left(\frac{a}{a_\infty}\right)^2 = 1 - \frac{(\gamma-1)}{2} M_\infty^2 \left(2\frac{u}{V_\infty}\right)$$

or

$$\boxed{\left(\frac{a}{a_\infty}\right)^2 = 1 - (\gamma-1) M_\infty^2 \frac{u}{V_\infty}}$$

EXAMPLE 7.2 Show that using small perturbation theory assumption the local Mach number M in terms of freestream Mach number M_∞ can be expressed as

$$M^2 = \left[1 + 2\frac{u}{V_\infty}\left(1 + \frac{\gamma-1}{2} M_\infty^2\right)\right] M_\infty^2$$

Solution The local Mach number is

$$M = \frac{V}{a}$$

where V is the local flow speed and a is the local speed of sound. With small perturbation assumption V can be expressed as

$$V \approx V_\infty + u$$

Therefore,

$$M = \frac{V_\infty + u}{a}$$

Multiplying and dividing the right-hand side by $V_\infty a_\infty$, we have

$$M = \frac{V_\infty + u}{V_\infty a_\infty} \frac{V_\infty a_\infty}{a}$$

$$= \left(1 + \frac{u}{V_\infty}\right)\left(\frac{V_\infty}{a_\infty}\right)\left(\frac{a_\infty}{a}\right)$$

$$= \left(1 + \frac{u}{V_\infty}\right)\left(\frac{a_\infty}{a}\right) M_\infty$$

In the frame of small perturbation assumption we have

$$\left(\frac{a}{a_\infty}\right)^2 = 1 - (\gamma-1) M_\infty^2 \frac{u}{V_\infty}$$

Therefore,

$$M^2 = \left(1 + \frac{u}{V_\infty}\right)^2 \left(\frac{a_\infty}{a}\right)^2 M_\infty^2$$

$$= \left(1 + \frac{u}{V_\infty}\right)^2 \left[1 - (\gamma-1)\frac{u}{V_\infty} M_\infty^2\right]^{-1} M_\infty^2$$

Scanned by CamScanner

Expanding the first groups on the right-hand side, we have

$$\left(1+\frac{u}{V_\infty}\right)^2=\left(1+2\frac{u}{V_\infty}+\frac{u^2}{V_\infty^2}\right)$$

Expanding the second group on the right-hand side, retaining only the first order terms of u/V_∞, we have

$$\left[1-(\gamma-1)\frac{u}{V_\infty}M_\infty^2\right]^{-1}=\left[1+(\gamma-1)\frac{u}{V_\infty}M_\infty^2\right]$$

Substituting, we have

$$M^2=\left(1+2\frac{u}{V_\infty}\right)\left[1+(\gamma-1)\frac{u}{V_\infty}M_\infty^2\right]M_\infty^2$$

or

$$M^2=\left[1+(\gamma-1)\frac{u}{V_\infty}M_\infty^2+2\frac{u}{V_\infty}+2\frac{u}{V_\infty}(\gamma-1)\frac{u}{V_\infty}M_\infty^2\right]M_\infty^2$$

$$=\left[1+(\gamma-1)\frac{u}{V_\infty}M_\infty^2+2\frac{u}{V_\infty}+2(\gamma-1)\frac{u^2}{V_\infty^2}M_\infty^2\right]M_\infty^2$$

Neglecting the term with $\frac{u^2}{V_\infty^2}$, being small, this reduces to

$$M^2=\left[1+(\gamma-1)\frac{u}{V_\infty}M_\infty^2+2\frac{u}{V_\infty}\right]M_\infty^2$$

or

$$\boxed{M^2=\left[1+2\frac{u}{V_\infty}\left(1+\frac{\gamma-1}{2}M_\infty^2\right)\right]M_\infty^2}$$

7.5 POTENTIAL EQUATION FOR BODIES OF REVOLUTION

Fuselage of aeroplanes, rocket shells, missile bodies, and circular ducts are the few bodies of revolutions which are commonly used in practice. The general three-dimensional Cartesian equations can be used for these problems. But it is much simpler to use cylindrical polar coordinates than Cartesian coordinates. Cartesian coordinates are x, y, z and the corresponding velocities V_x, V_y, V_z.

The cylindrical polar coordinates are x, r, θ, and the corresponding velocities are V_x, V_r, V_θ.

Scanned by CamScanner

For axi-symmetric flows with cylindrical coordinates, the equations will be independent of θ. Thus, mathematically, cylindrical coordinates reduce the problem to two dimensional. However, for flows which are not axially symmetric (e.g. missile at an angle of attack), θ will be involved. The continuity equation in cylindrical coordinates is

$$\frac{\partial(\rho V_x)}{\partial x} + \frac{1}{r}\frac{\partial(\rho r V_r)}{\partial r} + \frac{1}{r}\frac{\partial(\rho V_\theta)}{\partial \theta} = 0 \tag{7.29}$$

Expressing the velocity components in terms of the potential function ϕ as

$$V_x = \frac{\partial \phi}{\partial x}, \quad V_r = \frac{\partial \phi}{\partial r}, \quad V_\theta = \frac{1}{r}\frac{\partial \phi}{\partial \theta} \tag{7.30}$$

The potential Eq. (7.25) can be written, in cylindrical polar coordinates, as

$$\left(1 - \frac{\phi_x^2}{a^2}\right)\phi_{xx} + \left(1 - \frac{\phi_r^2}{a^2}\right)\phi_{rr} + \left(1 - \frac{1}{r^2}\frac{\phi_\theta^2}{a^2}\right)\frac{1}{r^2}\phi_{\theta\theta}$$

$$-2\left(\frac{\phi_x \phi_r}{a^2}\phi_{xr} + \frac{\phi_x \phi_\theta}{a^2}\frac{1}{r^2}\phi_{x\theta} + \frac{\phi_r \phi_\theta}{a^2}\frac{1}{r^2}\phi_{r\theta}\right) + \left(1 + \frac{1}{r^2}\frac{\phi_\theta^2}{a^2}\right)\frac{1}{r}\phi_r = 0 \tag{7.31}$$

Also,

$$\left(\frac{a}{a_\infty}\right)^2 = 1 - \frac{\gamma - 1}{2}M_\infty^2\left(\frac{V_x^2 + V_r^2 + V_\theta^2}{V_\infty^2} - 1\right) \tag{7.32}$$

The small perturbation assumptions are:

$$V_x = V_\infty + u, \quad V_r = v_r, \quad V_\theta = v_\theta$$
$$u \ll V_\infty, \quad v_r \ll V_\infty, \quad v_\theta \ll V_\infty$$

where V_x, V_r, V_θ are the mean velocity components and u, v_r, v_θ are the perturbation velocities along the x-, r- and θ-direction, respectively. Introduction of these relations in Eq. (7.31) results in

$$(1 - M^2)\phi_{xx} + \phi_{rr} + \frac{1}{r}\phi_r + \frac{1}{r^2}\phi_{\theta\theta} = 0 \tag{7.33}$$

where M is the local Mach number after Eq. (7.23). The relations for u, v_r, v_θ in polar coordinates, under the small perturbation assumption are

$$u = \frac{\partial \phi}{\partial x} = \phi_x, \quad v_r = \frac{\partial \phi}{\partial r} = \phi_r, \quad v_\theta = \frac{1}{r}\frac{\partial \phi}{\partial \theta} = \frac{1}{r}\phi_\theta$$

With these expressions for u, v_r and v_θ, Eq. (7.24) can be written as

$$(1 - M_\infty^2)\phi_{xx} + \phi_{rr} + \frac{1}{r}\phi_r + \frac{1}{r^2}\phi_{\theta\theta} = \frac{2}{V_\infty}M_\infty^2\,\phi_x\,\phi_{xx}\left(1 + \frac{\gamma - 1}{2}M_\infty^2\right) \tag{7.34}$$

Scanned by CamScanner

This equation corresponds to Eq. (7.24) with the same term on the right-hand side. Therefore, with

$$\frac{M_\infty^2}{1 - M_\infty^2} \frac{u}{V_\infty} \ll 1$$

Eq. (7.34) simplifies to

$$(1 - M_\infty^2)\phi_{xx} + \phi_{rr} + \frac{1}{r}\phi_r + \frac{1}{r^2}\phi_{\theta\theta} = 0 \tag{7.35}$$

This is the governing equation for subsonic and supersonic flows in cylindrical coordinates. For transonic flow, Eq. (7.35) becomes

$$-\frac{\gamma + 1}{V_\infty}\phi_x \phi_{xx} + \phi_{rr} + \frac{1}{r}\phi_r + \frac{1}{r^2}\phi_{\theta\theta} = 0 \tag{7.36}$$

For axially symmetric subsonic and supersonic flows, $\phi_{\theta\theta} = 0$. Therefore, Eq. (7.35) reduces to

$$(1 - M_\infty^2)\phi_{xx} + \phi_{rr} + \frac{1}{r}\phi_r = 0 \tag{7.37}$$

Similarly, Eq. (7.36) reduces to

$$-\frac{\gamma + 1}{V_\infty}\phi_x \phi_{xx} + \phi_{rr} + \frac{1}{r}\phi_r = 0 \tag{7.38}$$

Equation (7.38) is the equation for axially symmetric transonic flows. All these equations are valid only for small perturbations, i.e. for small values of angle of attack and angle of yaw (< 15°).

Conclusions

From the above discussions on potential flow theory for compressible flows, we can draw the following conclusions:

1. The small perturbation equations for subsonic and supersonic flows are linear, but for transonic flows the equation is nonlinear.
2. Subsonic and supersonic flow equations do not contain γ; but the transonic flow equation contains γ. This shows that the results obtained for subsonic and supersonic flows, with small perturbation equations, can be applied to any gas, but this cannot be done for transonic flows.
3. All these equations are valid for slender bodies. This is true of rockets, missiles, etc.
4. These equations can also be applied to aerofoils, but not to bluff shapes like circular cylinder, etc.
5. For nonslender bodies, the flow can be calculated by using the original nonlinear equation.

Scanned by CamScanner

Solution of Nonlinear Potential Equation

(i) *Numerical methods* The nonlinearity of Eq. (7.24) makes it tedious to solve the equation analytically. However, the solution to the equation can be obtained by numerical methods. But a numerical solution is not a general solution, and is valid only for a specific configuration in a flow field with a fixed Mach number and specified geometry.

(ii) *Transformation (Hodograph) methods* When one velocity component is plotted against another velocity component, the resulting curve may be linear, whereas in the physical plane, the relation may be nonlinear. This method is used for solving certain transonic flow problems.

(iii) *Similarity methods* In these methods, the boundary conditions need to be specified for solving the equation. (This method is discussed in detail in Chapter 8.)

7.6 BOUNDARY CONDITIONS

Examine the aerofoil kept in a flow field as shown in Fig. 7.4.

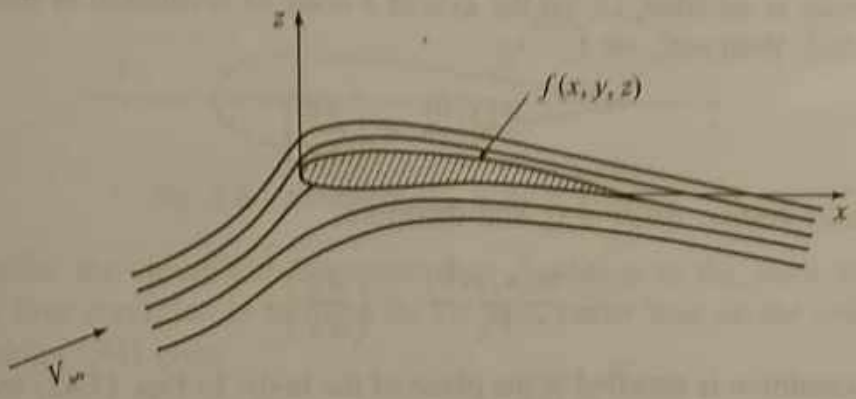


Fig. 7.4 Cambered aerofoil at an angle of attack.

In inviscid flow the streamline near the boundary is similar to the body contour. The flow must satisfy the following boundary conditions (BCs):

Boundary condition 1: *Kinetic flow condition* The velocities are tangential on the body contour. Normal to the body contour the velocities are zero.

Boundary condition 2: At $z \to \pm\infty$, perturbation velocities are zero or finite. The kinematic flow condition for the aerofoil shown in Fig. 7.4, with small perturbation assumptions, may be written as follows: Body contour: $f = f(x, y, z)$.

The velocity vector is V. Therefore, on the surface, $(V \cdot \text{grad } f) = 0$, i.e.

$$(V_\infty + u)\frac{\partial f}{\partial x} + v\frac{\partial f}{\partial y} + w\frac{\partial f}{\partial z} = 0 \qquad (7.39)$$

Scanned by CamScanner

but $u/V_\infty \ll 1$. Therefore, Eq. (7.39) becomes

$$V_\infty \frac{\partial f}{\partial x} + v\frac{\partial f}{\partial y} + w\frac{\partial f}{\partial z} = 0 \tag{7.40}$$

For two-dimensional flows, $v = 0$; $\partial f/\partial y = 0$. Then Eq. (7.39) reduces to

$$\frac{w}{V_\infty + u} = -\frac{\partial f/\partial x}{\partial f/\partial z} = \left(\frac{\partial z}{\partial x}\right)_c \tag{7.41}$$

where the subscript "c" refers to the body contour and $(\partial z/\partial x)$ is the slope of the body. Expressing u and w as power series of z, we get

$$u(x, z) = u(x, 0) + a_1 z + a_2 z^2 + \ldots$$
$$w(x, z) = w(x, 0) + b_1 z + b_2 z^2 + \ldots$$

where a's and b's are the functions of x. If the body is sufficiently slender, then

$$\frac{w(x, 0)}{V_\infty + u(x, 0)} = \left(\frac{dz}{dx}\right)_c$$

i.e. for sufficiently slender bodies, it is not necessary to fulfil the boundary condition on the contour. It is sufficient if the boundary condition on the x-axis of the body is satisfied, i.e. on the axis of a body of revolution or the chord of an aerofoil. With $u/V_\infty \ll 1$,

$$\frac{w(x, 0)}{V_\infty} = \left(\frac{dz}{dx}\right)_c \tag{7.42}$$

For *planar bodies*: $\partial f/\partial y = 0$, and therefore,

$$\frac{w(x, y, 0)}{V_\infty} = \left(\frac{dz}{dx}\right)_c \tag{7.43}$$

i.e. the condition is satisfied in the plane of the body. In Eqs. (7.42) and (7.43), the elevation above the x-axis is neglected.

Bodies of Revolution

For bodies of revolution, the term $\frac{1}{r}\frac{\partial}{\partial r}(rv_r)$ is present in the continuity equation (7.29); because of this term the perturbations near the body are not small. So a power series for velocity components is not possible. However, we can apply the following approximation to express the perturbation velocity as a power series. For axi-symmetric bodies,

$$\frac{1}{r}\frac{\partial}{\partial r}(rv_r) \sim \frac{\partial u}{\partial x}, \qquad \frac{\partial}{\partial r}(rv_r) \sim r\frac{\partial u}{\partial x}$$

when $r \to 0$; $\frac{\partial}{\partial r}(rv_r) \approx 0$ or $rv_r = a_0(x)$. Thus, though the velocity v_r on the axis of a body of revolution is of the order of $1/r$, it can be estimated near the

Scanned by CamScanner

axis similar to the potential vortex. For a potential vortex,

$$v_r \propto \frac{1}{r}$$

Now, v_r can be expressed in terms of a power series as

$$rv_r = a_0 + a_1 r + a_2 r^2 + \ldots$$

For the axi-symmetric body with its surface profile contour given by the function $R(x)$, we have

$$\frac{v_r}{V_\infty + u} = \left(\frac{dR(x)}{dx}\right)_c$$

The simplified kinematic flow condition for the body in Fig. 7.5 is

$$\frac{(rv_r)_0}{V_\infty} = R(x)\frac{dR(x)}{dx} \tag{7.44}$$

where the subscript 0 refers to the axis of the body.

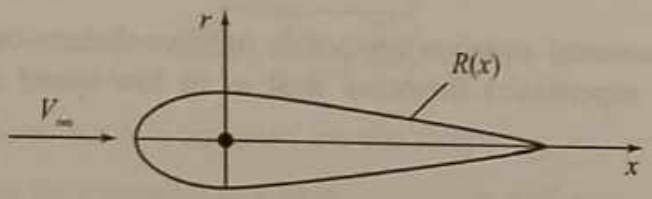


Fig. 7.5 Axi-symmetric body in a flow.

This is called the simplified kinematic flow condition in the sense that the kinematic flow condition is fulfilled on the axis, rather than on the contour.

Equation (7.44) gives

$$\lim_{r \to 0} (rv_r) = V_\infty R(x)\frac{dR(x)}{dx} \tag{7.45}$$

From the above discussions, it may be summarized that the boundary conditions are as follows:

$$\left(\frac{w}{V_\infty + u}\right)_c \approx \frac{(w)_0}{V_\infty} = \left(\frac{\partial z}{\partial x}\right)_c \quad \text{for two-dimensional (planar) bodies} \tag{7.46}$$

$$R(x)\left(\frac{v_r}{V_\infty + u}\right)_c \approx \frac{(rv_r)_0}{V_\infty} = R(x)\frac{dR(x)}{dx} \quad \text{for bodies of revolution (elongated bodies} \tag{7.47}$$

7.7 PRESSURE COEFFICIENT

The idea of finding the velocity distribution is to find the pressure distribution

Scanned by CamScanner

and then integrate it to get lift, moment, and pressure drag. For three-dimensional flows, the C_p is given by (Eq. 4.48) as

$$C_p = \frac{2}{\gamma M_\infty^2}\left\{\left[\frac{\gamma-1}{2}M_\infty^2\left(1-\frac{(V_\infty+u)^2+v^2+w^2}{V_\infty^2}\right)+1\right]^{\gamma/(\gamma-1)}-1\right\}$$

or

$$C_p = \frac{2}{\gamma M_\infty^2}\left\{\left[1-\frac{\gamma-1}{2}M_\infty^2\left(\frac{2u}{V_\infty}+\frac{u^2+v^2+w^2}{V_\infty^2}\right)\right]^{\gamma/(\gamma-1)}-1\right\}$$

Expanding the RHS of this equation binomially, and neglecting the cubes and higher-order terms of the perturbation velocity components, we get

$$C_p = -\left(2\frac{u}{V_\infty}+(1-M_\infty^2)\frac{u^2}{V_\infty^2}+\frac{v^2+w^2}{V_\infty^2}\right)$$

For two-dimensional or planar bodies, the C_p simplifies further, resulting in

$$\boxed{C_p = -2\frac{u}{V_\infty}} \tag{7.48}$$

This is a fundamental equation applicable to three-dimensional compressible (subsonic and supersonic) flows, as well as to low-speed two-dimensional flows.

Bodies of Revolution

For bodies of revolution, by small perturbation assumption, we have $u \ll V_\infty$, but v and w are not negligible. Therefore,

$$C_p = -2\frac{u}{V_\infty} - \frac{v^2+w^2}{V_\infty^2} \tag{7.49}$$

The above equation, which is in Cartesian coordinates, may also be expressed as

$$C_p = -2\frac{u}{V_\infty} - \left(\frac{v_r}{V_\infty}\right)^2 \tag{7.50}$$

Combining Eqs. (7.47) and (7.50), we get

$$C_p = -2\frac{u}{V_\infty} - \left[\frac{dR(x)}{dx}\right]^2 \tag{7.51}$$

7.8 SUMMARY

In this chapter we have presented some of the aspects of the linearized compressible flow. It is important to recognize the fundamental nature of the approximations introduced to linearize the basic potential equation for

Scanned by CamScanner

compressible flow. Although modern numerical techniques are capable of yielding accurate solutions for flows with complex geometries, linearized solutions still play a vital role in the field of compressible flows.

By *Crocco's theorem*, we have, for two-dimensional flows, the equation

$$T\frac{\partial s}{\partial n} = \frac{dh_0}{dn} + V\zeta \tag{7.6}$$

where s is entropy, h_0 is stagnation enthalpy, and ζ is vorticity. Equation (7.6) relates the vorticity of a flow field to the entropy of the fluid. Also, it stipulates the conditions under which a frictionless flow will have the same entropy on different streamlines, that is, it will be isentropic. The conditions are

h_0 = constant throughout the flow

$\zeta = 0$ throughout the flow

That is, isentropic flows are irrotational and irrotational flows are isentropic. This result is true, in general, only for steady flows of inviscid fluids in which there are no body forces and in which the stagnation enthalpy is constant. For irrotational flows, by *Laplace's equation*, we have

$$\frac{\partial^2\phi}{\partial x^2} + \frac{\partial^2\phi}{\partial y^2} + \frac{\partial^2\phi}{\partial z^2} = 0$$

The basic solutions for this equation are the following:

1. Uniform flow parallel to x-axis $\quad \phi = V_\infty x$
2. Source $\quad \phi = \dfrac{Q}{2\pi}\ln r$
   where Q is the strength of the source.
3. Doublet (issuing in the x-direction) $\quad \phi = \dfrac{\mu\cos\theta}{r}$
   where μ is moment of the doublet.
4. Potential vortex (counterclockwise) $\quad \phi = \dfrac{\Gamma}{2\pi}\theta$
   where Γ is circulation.

The governing equations for three-dimensional potential flow in Cartesian coordinates are:

The continuity equation is

$$\frac{\partial(\rho V_x)}{\partial x} + \frac{\partial(\rho V_y)}{\partial y} + \frac{\partial(\rho V_z)}{\partial z} = 0 \tag{7.12}$$

The Euler's equations of motion (neglecting body forces) or the momentum equations are

$$\rho\left(V_x\frac{\partial V_x}{\partial x} + V_y\frac{\partial V_x}{\partial y} + V_z\frac{\partial V_x}{\partial z}\right) = -\frac{\partial p}{\partial x} \tag{7.13a}$$

Scanned by CamScanner

$$\rho\left(V_x\frac{\partial V_y}{\partial x}+V_y\frac{\partial V_y}{\partial y}+V_z\frac{\partial V_y}{\partial z}\right)=-\frac{\partial p}{\partial y} \tag{7.13b}$$

$$\rho\left(V_x\frac{\partial V_z}{\partial x}+V_y\frac{\partial V_z}{\partial y}+V_z\frac{\partial V_z}{\partial z}\right)=-\frac{\partial p}{\partial z} \tag{7.13c}$$

and the isentropic relation is

$$\frac{p}{p_0}=\left(\frac{\rho}{\rho_0}\right)^{\gamma}$$

Instead of the energy equation, we have the isentropic relation. The isentropic relation given above is for a perfect gas. The more general form of the isentropic relation is, simply, s = constant.

In terms of velocity potential, the momentum equation becomes

$$\left(1-\frac{\phi_x^2}{a^2}\right)\phi_{xx}+\left(1-\frac{\phi_y^2}{a^2}\right)\phi_{yy}+\left(1-\frac{\phi_z^2}{a^2}\right)\phi_{zz}$$

$$-2\left(\frac{\phi_x\phi_y}{a^2}\phi_{xy}+\frac{\phi_y\phi_z}{a^2}\phi_{yz}+\frac{\phi_z\phi_x}{a^2}\phi_{zx}\right)=0 \tag{7.15}$$

This is the *basic potential equation for compressible flow* and it is nonlinear. Because of the nonlinearity of Eq. (7.15), the superposition of solutions is not valid. Further, the local speed of sound a in Eq. (7.15) is also a variable.

With small perturbation theory, Eq. (7.15) reduces to

$$(1-M_\infty^2)\phi_{xx}+\phi_{yy}+\phi_{zz}=0 \tag{7.19}$$

Equation (7.19) is an approximate equation; it no longer represents the exact physics of the flow. However, the original nonlinear equation (7.15) has been reduced to a linear equation (7.19). It is also called the *linearized perturbation velocity potential equation*. It is important to note that Eq. (7.19) *is valid for subsonic and supersonic flows* only. It is not valid for transonic flows.

The linearized potential flow equation valid for subsonic, supersonic, and transonic flows is

$$(1-M_\infty^2)\phi_{xx}+\phi_{yy}+\phi_{zz}=\frac{2}{V_\infty}M_\infty^2\,\phi_x\,\phi_{xx}\left(1+\frac{\gamma-1}{2}M_\infty^2\right) \tag{7.24}$$

Equation (7.24) is nonlinear unlike Eq. (7.19) which is linear.

From the above governing equations it is evident that subsonic and supersonic flows lend themselves to approximate, linearized theory for the case of irrotational, isentropic flow with small perturbations. But transonic and hypersonic flows cannot be linearized, even with small perturbations.

The potential equations for bodies of resolution in cylindrical polar coordinates are the following: The continuity equation

$$\frac{\partial(\rho V_x)}{\partial x}+\frac{1}{r}\frac{\partial(\rho r V_r)}{\partial r}+\frac{1}{r}\frac{\partial(\rho V_\theta)}{\partial\theta}=0 \tag{7.29}$$

Scanned by CamScanner

The momentum equation

$$\left(1-\frac{\phi_x^2}{a^2}\right)\phi_{xx}+\left(1-\frac{\phi_r^2}{a^2}\right)\phi_{rr}+\left(1-\frac{1}{r^2}\frac{\phi_\theta^2}{a^2}\right)\frac{1}{r^2}\phi_{\theta\theta}$$

$$-2\left(\frac{\phi_x\phi_r}{a^2}\phi_{xr}+\frac{\phi_x\phi_\theta}{a^2r^2}\phi_{x\theta}+\frac{\phi_r\phi_\theta}{a^2r^2}\phi_{r\theta}\right)+\left(1+\frac{1}{r^2}\frac{\phi_\theta^2}{a^2}\right)\frac{1}{r}\phi_r=0$$

With small perturbation assumption, this equation reduces to (7.31)

$$(1-M_\infty^2)\phi_{xx}+\phi_{rr}+\frac{1}{r}\phi_r+\frac{1}{r^2}\phi_{\theta\theta}=0 \tag{7.35}$$

This equation is valid for subsonic and supersonic flows in cylindrical coordinates. For transonic flows the governing equation is

$$-\frac{\gamma+1}{V_\infty}\phi_x\,\phi_{xx}+\phi_{rr}+\frac{1}{r}\phi_r+\frac{1}{r^2}\phi_{\theta\theta}=0 \tag{7.36}$$

For axially symmetric flows, $\phi_{\theta\theta}=0$; therefore, Eqs. (7.35) and (7.36) reduce to

$$(1-M_\infty^2)\phi_{xx}+\phi_{rr}+\frac{1}{r}\phi_r=0 \tag{7.37}$$

$$-\frac{\gamma+1}{V}\phi_x\,\phi_{xx}+\phi_{rr}+\frac{1}{r}\phi_r=0 \tag{7.38}$$

All these equations are valid only for small perturbations, that is, for small values of angle of attack and yaw (< 15°). The pressure coefficient C_p given by small perturbation theory is

$$C_p=-\left(2\frac{u}{V_\infty}+(1-M_\infty^2)\frac{u^2}{V_\infty^2}+\frac{v^2+w^2}{V_\infty^2}\right)$$

For bodies of revolution, the C_p becomes

$$C_p=-2\frac{u}{V_\infty}-\left(\frac{dR(x)}{dx}\right)^2 \tag{7.51}$$

where $R(x)$ is the expression for body contour.

In the light of the discussions of this chapter it may be summarized that:

- The small perturbation equations for subsonic and supersonic flows are linear, but for transonic flows the equation is nonlinear.
- Subsonic and supersonic equations do not contain γ, but the transonic flow equation contains γ. This implies that the results obtained for subsonic and supersonic flows with small perturbation equations can be applied to any gas, but this cannot be done for transonic flows.

Scanned by CamScanner

PROBLEMS

1. Show that for compressible flow of a perfect gas, the variation of total pressure across a streamline is given by

$$-\frac{1}{\rho_0}\frac{dp_0}{dn} = \left(1+\frac{\gamma-1}{2}M^2\right)u\zeta + \frac{\gamma-1}{2}c_p M^2\frac{dT_0}{dn}$$

where n is the direction normal to the streamline.

2. The nose of a cylindrical body has the profile $R = \varepsilon x^{3/2}$, $0 \le x \le 1$. Show that the pressure distribution on the body is given by

$$\frac{C_p}{\varepsilon^2} = 6x \ln\frac{2}{\varepsilon\sqrt{M^2-1}} - 3x \ln(x) - \frac{33}{4}x$$

Estimate the drag coefficient for $M = \sqrt{2}$ and $\varepsilon = 0.1$.

(**Hint:** For obtaining C_D, use $C_D S(L) = \int_0^L C_p(x)\, S'(x)dx$, where $S(x)$ is the cross-sectional area of the body at x and L is the length of the body.)

[**Ans.** $C_D = 0.0786$]

Scanned by CamScanner

8 Similarity Rule

8.1 INTRODUCTION

From Section 7.4, it is seen that the governing equation for compressible flow is elliptic for subsonic flows and becomes hyperbolic for supersonic flows. This change in the nature of the partial differential equation, upon going from subsonic to supersonic flow, indicates the possibility of deriving similarity relationships between subsonic compressible flow and the corresponding incompressible flow, and the importance of Mach wave in a supersonic solution. In this chapter we shall derive an expression which relates the subsonic compressible flow past a certain profile to the incompressible flow past a second profile derived from the first through an *affine transformation*. Such an expression is called a *similarity law*.

If the governing equations of motion could be solved easily, the solutions themselves would indicate quite clearly the nature of any similarities which might exist among members of a family of flow patterns. Then there is no need for a separate derivation of similarity laws.

But in the majority of situations, we are unable to solve the equations of motion. However, even though solutions are lacking, we may use our knowledge of the forms of the differential equations and the related boundary conditions to derive the similarity laws.

8.2 TWO-DIMENSIONAL FLOW: THE PRANDTL-GLAUERT RULE FOR SUBSONIC FLOW

The Prandtl-Glauert Transformations

Prandtl and Glauert have shown that it is possible to relate the solution of compressible flow about a body to the incompressible flow solution.

Scanned by CamScanner

The transformation from one to another is achieved in the following manner: Laplace's equations for two-dimensional compressible and incompressible flows, respectively, are

$$(1 - M_\infty^2)\phi_{xx} + \phi_{zz} = 0 \tag{8.1}$$

$$(\phi_{xx})_{inc} + (\phi_{zz})_{inc} = 0 \tag{8.2}$$

where x is along the flow direction and z is normal to the flow. These equations, however, are not the complete description of the problem, since it is necessary to specify the boundary conditions too.

Equations (8.1) and (8.2) can be transformed into one another by the following transformation:

$$x_{inc} = x, \quad z_{inc} = K_1 z$$
$$\phi(x, z) = K_2\, \phi_{inc}(x_{inc}, z_{inc}) \tag{8.3}$$

In Eq. (8.3), the variables with subscript "inc" are for incompressible flow and the variables without subscript are for compressible flow. Combining Eqs. (8.1) and (8.3), we get

$$(1 - M_\infty^2)\, K_2 \frac{\partial^2 \phi_{inc}}{\partial x_{inc}^2} + K_1^2 K_2 \frac{\partial^2 \phi_{inc}}{\partial z_{inc}^2} = 0$$

i.e.

$$K_2 \left((1 - M_\infty^2) \frac{\partial^2 \phi_{inc}}{\partial x_{inc}^2} + K_1^2 \frac{\partial^2 \phi_{inc}}{\partial z_{inc}^2} \right) = 0$$

This is identical to the incompressible potential equation (8.2) if

$$K_1 = \sqrt{1 - M_\infty^2} \tag{8.4}$$

Now, K_2 is to be determined from the boundary conditions.

For slender bodies, by small perturbation theory (see Section 7.6), we have

$$\frac{w}{V_\infty + u} \approx \frac{w}{V_\infty} = \frac{dz}{dx} \tag{8.5}$$

since $u/V_\infty \ll 1$. Equation (8.5) can be expressed in terms of the potential function as

$$w = \left(\frac{\partial \phi}{\partial z} \right)_{z=0} = V_\infty \frac{dz}{dx} \tag{8.6a}$$

$$w_{inc} = \left(\frac{\partial \phi_{inc}}{\partial z_{inc}} \right)_{z_{inc}=0} = V_\infty \frac{dz_{inc}}{dx_{inc}} \tag{8.6b}$$

Also, by Eq. (8.3),

$$\left(\frac{\partial \phi}{\partial z} \right)_{z=0} = K_1 K_2 \left(\frac{\partial \phi_{inc}}{\partial z_{inc}} \right)_{z_{inc}=0}$$

Scanned by CamScanner

With this relation and Eqs. (8.6), we get

$$\frac{dz}{dx} = K_1 K_2 \left(\frac{dz_{\text{inc}}}{dx_{\text{inc}}} \right) \tag{8.7a}$$

$$\frac{dz}{dx} = K_2 \sqrt{1 - M_\infty^2} \left(\frac{dz_{\text{inc}}}{dx_{\text{inc}}} \right) \tag{8.7b}$$

From Eq. (8.7b), it is seen that K_2 can be determined from the boundary conditions.

Equation (8.7b) simply means that the slope of the profile in the compressible flow pattern is $(K_2\sqrt{1 - M_\infty^2})$ times the slope of the corresponding profile in the related incompressible flow pattern.

For further treatment of similarity law, let us consider the three specific versions of the problems, namely, the direct problem (Version I), in which the body profile is treated as invariant, the indirect problem (Version II), which is the case of equal potentials (the pressure distribution around the body in incompressible flow and compressible flow are taken as the same), and the streamline analogy (Version III), which is also called *Gothert's rule.*

The Direct Problem—Version I

Consider an invariant profile. In this case, there is no transformation of geometry at all. For the profile to be invariant, from Eq. (8.7b), we have the condition

$$K_2 = \frac{1}{\sqrt{1 - M_\infty^2}} \tag{8.8}$$

Therefore, Eq. (8.7b) reduces to

$$\frac{dz}{dx} = \frac{dz_{\text{inc}}}{dx_{\text{inc}}} \tag{8.9}$$

Equation (8.9) contradicts the original transformation equations (8.3). However, the error involved in this contradiction is not large since the Prandtl–Glauert transformation is valid only for small perturbations.

By Eq. (8.3), we have

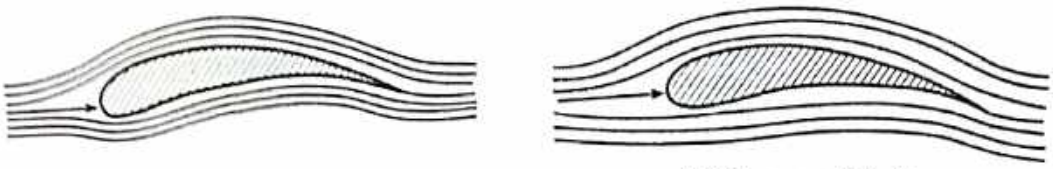
$$\boxed{z = \frac{z_{\text{inc}}}{\sqrt{1 - M_\infty^2}}} \tag{8.10}$$

Equation (8.3) is valid only for streamlines away from the body. Since the Prandtl–Glauert transformation is based on small perturbation theory, the error increases with increasing thickness of the body. In addition to this, some error is introduced by the above contradiction (see Eq. (8.9)).

Equation (8.10) shows that the streamlines around a body in a compressible flow are more separated than those around the body in incompressible flow by

Scanned by CamScanner

an amount given by $1/\sqrt{1-M_\infty^2}$. In other words, by the existence of body in the flow field, the streamlines are more displaced in a compressible flow than in an incompressible flow, as shown in Fig. 8.1, i.e. the disturbances introduced by an object are larger in compressible flow than in incompressible flow and they increase with the rise in Mach number. This is so because in compressible flow there is density decrease as the flow passes over the body due to acceleration, whereas in incompressible flow there is no change in density at all. That is to say, across the body there is a drop in density, and hence by streamtube area-velocity relationships (Section 4.4), the streamtube area increases as the density decreases. At $M_\infty = 1$, this disturbance becomes infinitely large and this treatment is no longer valid.



(a) Incompressible flow (b) Compressible flow

Fig. 8.1 Aerofoil in uniform flow.

The potential function for compressible flow given by Eq. (8.3) is

$$\phi = \frac{\phi_{\text{inc}}}{\sqrt{1-M_\infty^2}} \tag{8.11a}$$

By Eqs. (7.20) and (7.48), we have

$$u = \frac{\partial \phi}{\partial x}, \quad C_p = -2\frac{u}{V_\infty}$$

Using Eq. (8.11a), the perturbation velocity and the pressure coefficient may be expressed as follows:

$$\frac{\partial \phi}{\partial x} = \frac{1}{\sqrt{1-M_\infty^2}} \frac{\partial \phi_{\text{inc}}}{\partial x_{\text{inc}}}$$

Therefore,

$$u = \frac{u_{\text{inc}}}{\sqrt{1-M_\infty^2}}$$

$$\boxed{C_p = \frac{C_{p_{\text{inc}}}}{\sqrt{1-M_\infty^2}}} \tag{8.11b}$$

Since the lift coefficient C_L and the pitching moment coefficient C_M are integrals of C_p, they can be expressed following Eq. (8.11b) as

$$\boxed{C_L = \frac{C_{L_{\text{inc}}}}{\sqrt{1-M_\infty^2}}} \tag{8.11c}$$

Scanned by CamScanner

$$\frac{dC_L}{d\alpha} = \frac{(dC_L/d\alpha)_{inc}}{\sqrt{1-M_\infty^2}} \tag{8.11d}$$

For a flat plate in compressible flow,

$$\frac{dC_L}{d\alpha} = \frac{2\pi}{\sqrt{1-M_\infty^2}} \tag{8.11e}$$

$$\boxed{C_M = \frac{C_{M_{inc}}}{\sqrt{1-M_\infty^2}}} \tag{8.11f}$$

Similarly, we can express the circulation in compressible flow in terms of circulation in incompressible flow as

$$\Gamma = \frac{\Gamma_{inc}}{\sqrt{1-M_\infty^2}} \tag{8.11g}$$

From the discussions on version I of the Prandtl–Glauert transformation, the following two statements can be made:

1. Streamlines for compressible flow are farther apart from each other by $1/\sqrt{1-M_\infty^2}$ than in incompressible flow.
2. The ratio between aerodynamic characteristics in compressible and incompressible flows is also $1/\sqrt{1-M_\infty^2}$.

From Eqs. (8.11c) and (8.11f), we infer that the locations of aerodynamic centre and centre of pressure do not change with M_∞, as they are ratios between C_M and C_L.

The theoretical lift-curve slope and the drag coefficient from the Prandtl–Glauert rule and the measured C_L and C_D versus Mach number for symmetrical NACA-profiles of different thickness are shown in Fig. 8.2. From this figure it is seen that the thinner the aerofoil, the better is the accuracy of the P–G rule. For 6% aerofoil, there is good agreement up to $M_\infty = 0.8$; for 12% aerofoil also the agreement is good up to $M_\infty = 0.8$; thus 12% may be taken as the limit of applicability of the P–G rule. For 15% aerofoil, there is a good agreement up to $M_\infty = 0.6$. But above this, there is no more any agreement. However, for supersonic aircraft, the profiles used are very thin; so from a practical point of view, the P–G rule is very good even with the contradicting assumptions involved.

After some Mach number, there is decrease in lift. This can be explained by Fig. 8.2. There is a sudden increase in drag when the local speed increases beyond the sonic speed. This is because at sonic point on the profile, there is a λ-shock which gives rise to separation of boundary layer, as shown in Fig. 8.3. The freestream Mach number which gives sonic velocity somewhere on the boundary is called the critical Mach number M_∞^*. M_∞^* decreases with increasing thickness ratio of profile. The P–G rule is valid only up to about M_∞^*.

Scanned by CamScanner

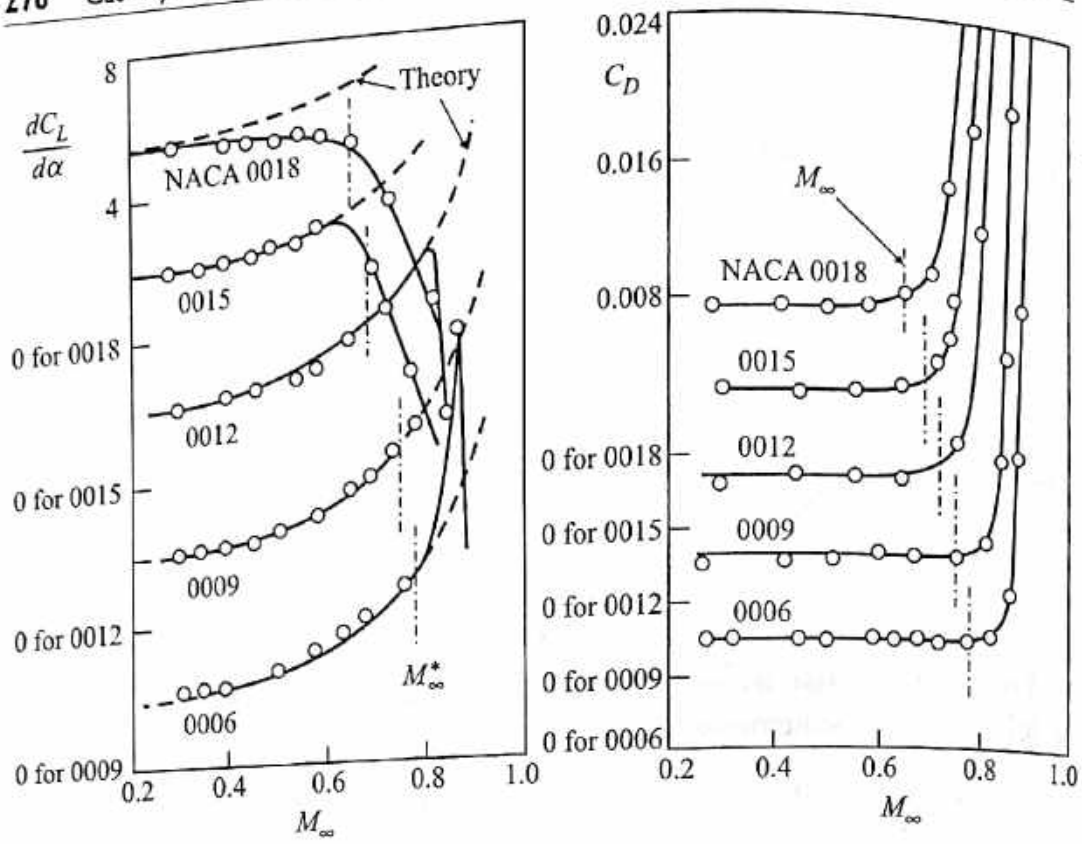


Fig. 8.2 Variation of lift-curve slope and drag coefficient with Mach number (o-measured).

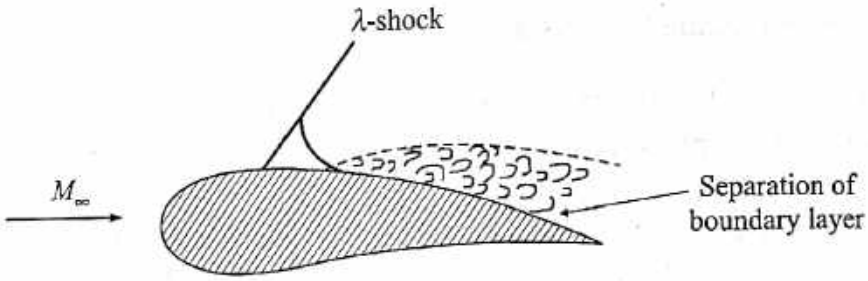


Fig. 8.3 Flow separation because of λ-shock.

The Indirect Problem (case of equal potentials): P–G transformation—Version II In the indirect problem, the requirement is to find a transformation, for the profile, by which we can obtain a body in incompressible flow with exactly the same pressure distribution, as in the compressible flow.

For two-dimensional or planar bodies, the pressure coefficient C_p is given by Eq. (7.48) as

$$C_p = -2\frac{u}{V_\infty}$$

and the perturbation velocity component, u, is

$$u = \frac{\partial \phi}{\partial x}$$

Scanned by CamScanner

But in this case, $C_p = C_{p_{inc}}$; therefore, from the above expressions for C_p and u, we have

$$C_p = C_{p_{inc}}, \quad u = u_{inc}, \quad \phi = \phi_{inc}$$

For this situation the transformation Eq. (8.3) gives

$$K_2 = 1 \tag{8.12}$$

From Eq. (8.7b) with $K_2 = 1$, we get

$$\boxed{\frac{dz}{dx} = \sqrt{1 - M_\infty^2}\,\frac{dz_{inc}}{dx_{inc}}} \tag{8.13}$$

Equation (8.13) is the relation between the geometries of the actual profile in compressible flow and the transformed profile in the incompressible flow, resulting in same pressure distribution around them.

From Eq. (8.13), we see that in a compressible flow, the body must be thinner by the factor $\sqrt{1 - M_\infty^2}$ than the body in incompressible flow as shown in Fig. 8.4. Also, the angle of attack in compressible flow must be smaller by the same factor than in incompressible flow.



Incompressible flow Compressible flow

Fig. 8.4 Aerofoils in compressible and incompressible flows.

From the above relation for C_p, we have

$$\frac{C_p}{C_{p_{inc}}} = \frac{C_L}{C_{L_{inc}}} = \frac{C_M}{C_{M_{inc}}} = 1 \tag{8.14}$$

That is, the lift coefficient and pitching moment coefficient are also the same in both the incompressible and compressible flows. But, because of decreased α in compressible flow,

$$\frac{dC_L}{d\alpha} = \frac{1}{\sqrt{1 - M_\infty^2}}\left(\frac{dC_L}{d\alpha}\right)_{inc}$$

This is so because of the fact that the disturbances introduced in a compressible flow are larger than those in an incompressible flow and, therefore, we must reduce α and the geometry by that amount (the difference in the magnitude of disturbance in a compressible and an incompressible flow). In other words, because of Eq. (8.3) ($z = K_1 z_{inc}$), every dimension in the z-direction must be reduced and so the angle of attack α also should be transformed.

Scanned by CamScanner

The Streamline Analogy (Version III)

Gothert's rule states (Shapiro, 1953) that the slope of a profile in a compressible flow pattern is larger by the factor $1/\sqrt{1-M_\infty^2}$ than the slope of the corresponding profile in the related incompressible flow pattern. But if the slope of the profile at each point is greater by the factor $1/\sqrt{1-M_\infty^2}$, it is also true that the camber (f) ratio, the angle of attack (α) ratio, and the thickness (t) ratio, must all be greater for the compressible aerofoil by the factor $1/\sqrt{1-M_\infty^2}$.

Thus, by Gothert's rule we have

$$\frac{\alpha_{inc}}{\alpha} = \frac{f_{inc}}{f} = \frac{t_{inc}}{t} = \sqrt{1-M_\infty^2}$$

Compute the aerodynamic coefficients for this transformed body for incompressible flow. The aerodynamic coefficients of the given body at the given Mach number flow are given by

$$\boxed{\frac{C_p}{C_{p_{inc}}} = \frac{C_L}{C_{L_{inc}}} = \frac{C_M}{C_{M_{inc}}} = \frac{1}{1-M_\infty^2}} \qquad (8.15)$$

The application of Gothert rule is much more complicated than the application of version I of the P–G rule. This is because, for finding the behaviour of a body with respect to M_∞, we have to calculate for each M_∞ at a time, whereas by the P–G rule (version I) the complete variation is obtained at a time. However, only the Gothert rule is exact with the framework of linearised theory and the P–G rule is only approximate because of the contradicting assumptions involved.

Now, we can see some aspects about the practical significance of these results. A fairly good amount of theoretical and experimental information on the properties of classes of affinely related profiles in incompressible flow, with variations in camber, thickness ratio, and angle of attack is available. If it is necessary to find the C_L of one of these profiles at a finite Mach number M_∞, either theoretically or experimentally, we first find the lift coefficient in incompressible flow of an affinely related profile. The camber, the thickness ratio, and the angle of attack are all smaller than the corresponding values for the original profile by the factor $\sqrt{1-M_\infty^2}$. Then, by multiplying this C_L for incompressible flow profile by $1/(1-M_\infty^2)$, we find the desired lift coefficient for the compressible flow.

This method of collecting data for incompressible flow is cumbersome, since the data is required for a large number of thickness ratios. It would be more convenient in many respects to know how Mach number affects the performance of a profile of fixed shape. The direct problem, discussed in Section 8.2, yields information of this type.

Scanned by CamScanner

8.3 PRANDTL-GLAUERT RULE FOR SUPERSONIC FLOW: VERSIONS I AND II

In Section 8.2, we have seen the similarity rules for subsonic flows. Now let us examine the similarity rules for supersonic flows. We can visualize from our previous discussions on similarity rule for subsonic compressible flows that the factor K_1 in the transformation Eq. (8.3) should have the following relations depending on the flow regime:

$$K_1 = \sqrt{1 - M_\infty^2} \quad \text{for subsonic flow}$$

$$K_1 = \sqrt{M_\infty^2 - 1} \quad \text{for supersonic flow}$$

Therefore, in general, we can write

$$K_1 = \sqrt{\left|1 - M_\infty^2\right|} \tag{8.16}$$

However, there is one important difference between the treatment of supersonic flow and subsonic flow, i.e. we cannot find any incompressible flow in the supersonic flow regime.

Subsonic Flow

We know that for subsonic flow the transformation relations are given by Eq. (8.3) as

$$x_{\text{inc}} = x, \quad z_{\text{inc}} = K_1 z, \quad \phi = K_2 \phi_{\text{inc}}$$

The transformed equation is

$$K_2[(1 - M_\infty^2)\,(\phi_{xx})_{\text{inc}} + K_1^2(\phi_{zz})_{\text{inc}}] = 0$$

and the condition to be satisfied by this equation in order to be identical to Eq. (8.2) is

$$K_1 = \sqrt{1 - M_\infty^2}$$

For this case the above transformed equation becomes Laplace's equation.

Supersonic Flow

The transformation relations for supersonic flow are

$$x' = x, \quad z' = K_1 z, \quad \phi = K_2 \phi'$$

where the variables with "prime" are the transformed variables. The aim in writing these transformations is to make the Mach number M_∞ in the governing equation (8.1) to vanish.

With the above transformation relations, the governing equation becomes

$$K_2[(1 - M_\infty^2)\phi'_{xx} + K_1^2 \phi'_{zz}] = 0$$

Scanned by CamScanner

For supersonic flow, $M_\infty > 1$, and so the above equation becomes

$$K_2[(M_\infty^2 - 1)\phi'_{xx} - K_1^2\phi'_{zz}] = 0$$

By inspection of this equation, we can see that the Mach number M_∞ can be eliminated from the above equation with

$$K_1 = \sqrt{M_\infty^2 - 1}$$

The equation becomes

$$\phi'_{xx} - \phi'_{zz} = 0 \tag{8.17a}$$

Now we must find out as to which supersonic Mach number this flow belongs.

The original form of the governing differential equation for this kind of flow, given by Eq. (8.1), is

$$(M_\infty^2 - 1)\phi_{xx} - \phi_{zz} = 0 \tag{8.17b}$$

For Eqs. (8.17a) and (8.17b) to be identical, it is necessary that

$$M_\infty = \sqrt{2}$$

By following the arguments of P–G rule for subsonic compressible flow, we can show the following results for versions I and II of the Prandtl–Glauert rule for supersonic flow.

Analogy version I For this case of invariant profile in supersonic flow,

$$K_2 = \frac{1}{\sqrt{M_\infty^2 - 1}}$$

Compute the flow about the given body at $M_\infty = \sqrt{2}$. For any other supersonic Mach number, the aerodynamic coefficients are given by

$$\frac{C_p}{C'_p} = \frac{C_L}{C'_L} = \frac{C_M}{C'_M} = \frac{1}{\sqrt{M_\infty^2 - 1}} \tag{8.18a}$$

Analogy version II Here the requirement is to find a transformation for the profile, by which we can obtain a body, for which the governing equation is Eq. (8.17a) with exactly the same pressure distribution as the actual body for which the governing equation is Eq. (8.17b). For this,

$$K_2 = 1$$

The derivation of the above two results are left to the reader as an exercise. From the above results, we see that in supersonic flow $M_\infty = \sqrt{2}$ plays the same role as $M_\infty = 0$ in subsonic flow.

For version II, we can write

$$\frac{C_p}{C'_p} = \frac{C_L}{C'_L} = \frac{C_M}{C'_M} = 1 \tag{8.18b}$$

Scanned by CamScanner

Analogy version III: Gothert rule For any given body, at given Mach number M_∞, find the transformed shape by using the rule

$$\frac{\alpha'}{\alpha} = \frac{f'}{f} = \frac{t'}{t} = \sqrt{M_\infty^2 - 1} \tag{8.19}$$

where α is the angle of attack, f and t are the camber and thickness of the given body, respectively. The primed quantities are for the transformed body and the unprimed ones are for the actual body.

Compute the aerodynamic characteristics of the transformed body for $M_\infty = \sqrt{2}$. The aerodynamic characteristics of the given body at the given Mach number M_∞ follow from

$$\frac{C_p}{C_p'} = \frac{C_L}{C_L'} = \frac{C_M}{C_M'} = \frac{1}{M_\infty^2 - 1} \tag{8.20}$$

We can state the Gothert rule for subsonic and supersonic flows by using a modulus: $\left|1 - M_\infty^2\right|$.

From the discussions on similarity rules for compressible subsonic and supersonic flows, it is clear that in subsonic flow there is a ready-made linearized solution for $M_\infty = 0$. Hence for such cases we can use the Prandtl–Glauert rule. But for supersonic flow the linear theory equations are very simple and, therefore, we can conveniently use the Gothert rule.

EXAMPLE 8.1 A given profile has at $M_\infty = 0.29$ the following lift coefficients:

$$C_L = 0.2 \quad \text{at} \quad \alpha = 3°$$
$$C_L = -0.1 \quad \text{at} \quad \alpha = -2°$$

where α is the angle of attack. Plot the relation showing $dC_L/d\alpha$ vs. M_∞ for the profile for values of M_∞ up to 1.0.

Solution At $M_\infty = 0.29$,

$$\frac{dC_L}{d\alpha} = \frac{0.2 + 0.1}{3 + 2} = 0.06/\text{degree}$$
$$= 3.438/\text{rad}$$
$$= 1.094\pi/\text{rad}$$

By the Prandtl–Glauert rule,

$$\left(\frac{dC_L}{d\alpha}\right)_{M=M_\infty} = \frac{\left(\frac{dC_L}{d\alpha}\right)_{\text{inc}}}{\sqrt{1 - M_\infty^2}}$$

Therefore,

$$\left(\frac{dC_L}{d\alpha}\right)_{\text{inc}} = 1.047\pi/\text{rad}$$

Scanned by CamScanner

For any other subsonic Mach number, by the Prandtl–Glauert rule,

$$\frac{dC_L}{d\alpha} = \frac{\left(\frac{dC_L}{d\alpha}\right)_{\text{inc}}}{\sqrt{1-M_\infty^2}} = \frac{1.047\pi}{\sqrt{1-M_\infty^2}}$$

Therefore, we have the following variation:

M	0.1	0.2	0.3	0.4	0.5	0.6	0.7	0.8	0.9	1.0
$\frac{dC_L}{d\alpha}$	1.05π	1.07π	1.10π	1.14π	1.21π	1.31π	1.47π	1.74π	2.40π	∞

8.4 THE VON KARMAN RULE FOR TRANSONIC FLOW

The potential equation (7.24), for the present case of two-dimensional transonic flow, reduces to

$$(1-M_\infty^2)\phi_{xx} + \phi_{zz} = \frac{2}{V_\infty}\left(1+\frac{\gamma-1}{2}M_\infty^2\right)M_\infty^2\phi_x\phi_{xx} \tag{8.21}$$

Equation (8.21) results in a form due to Sprieter (see also Liepmann and Roshko (1963)) for $M_\infty \approx 1$, as

$$C_p = \frac{\left(\frac{t}{c}\right)^{2/3}}{[(\gamma+1)M_\infty^2]^{1/3}}\tilde{C}_p(\chi) \tag{8.21a}$$

where

$$\chi = \frac{1-M_\infty^2}{\left[\left(\frac{t}{c}\right)(\gamma+1)M_\infty^2\right]^{2/3}} \tag{8.21b}$$

and $\tilde{C}_p$ is the similarity pressure coefficient. It follows from Eq. (8.21a) that the lift and drag coefficients are given by

$$C_L = \frac{\left(\frac{t}{c}\right)^{2/3}}{[(\gamma+1)M_\infty^2]^{1/3}}\tilde{C}_L(\chi) \tag{8.21c}$$

$$C_D = \frac{\left(\frac{t}{c}\right)^{5/3}}{[(\gamma+1)M_\infty^2]^{1/3}}\tilde{C}_D(\chi) \tag{8.21d}$$

Equations (8.21a) and (8.21c) and (8.21d) are valid for local as well as for total values. Sometimes, instead of the thickness-to-chord ratio t/c, the "fineness ratio" defined as in Fig. 8.5 is used.

Scanned by CamScanner



Fig. 8.5 Wedge at an angle of attack.

For the wedge shown in Fig. 8.5,

$$\frac{1}{2}\frac{t}{c} = \tan\theta_0, \quad \frac{t}{c} = 2\tan\theta_0$$

The ratio t/c is called the fineness ratio (at angle of attack = 0).

$$\tan(\theta_0 \pm \alpha) = \tan\left(\frac{1}{2}\frac{t}{c}\left(1 \pm \frac{2\alpha}{t/c}\right)\right) \tag{8.22}$$

where the "plus" sign is for the upper surface and the "minus" sign is for the lower surface. For finding the local values of C_p, C_L and C_D, we must use the fineness ratio defined by these equations.

Use of Karman Rule

If we know the solution for one profile, we can find solutions for other affinely related profiles. For example, the NACA profiles designated by 8405, 8410, 8415 all have the same distribution, same nose radius etc.; only the absolute magnitude of t/c is different. This rule can be extended to transonic flow range as well. From Fig. 8.6, it is seen that in the transonic range, the aerodynamic characters change very quickly with Mach number, so that the proper values to be considered are not M_∞, C_L, C_D and C_p; instead they are χ, $\tilde{C}_L$, $\tilde{C}_D$ and $\tilde{C}_p$.

From the discussions made so far, we can make the following remarks:

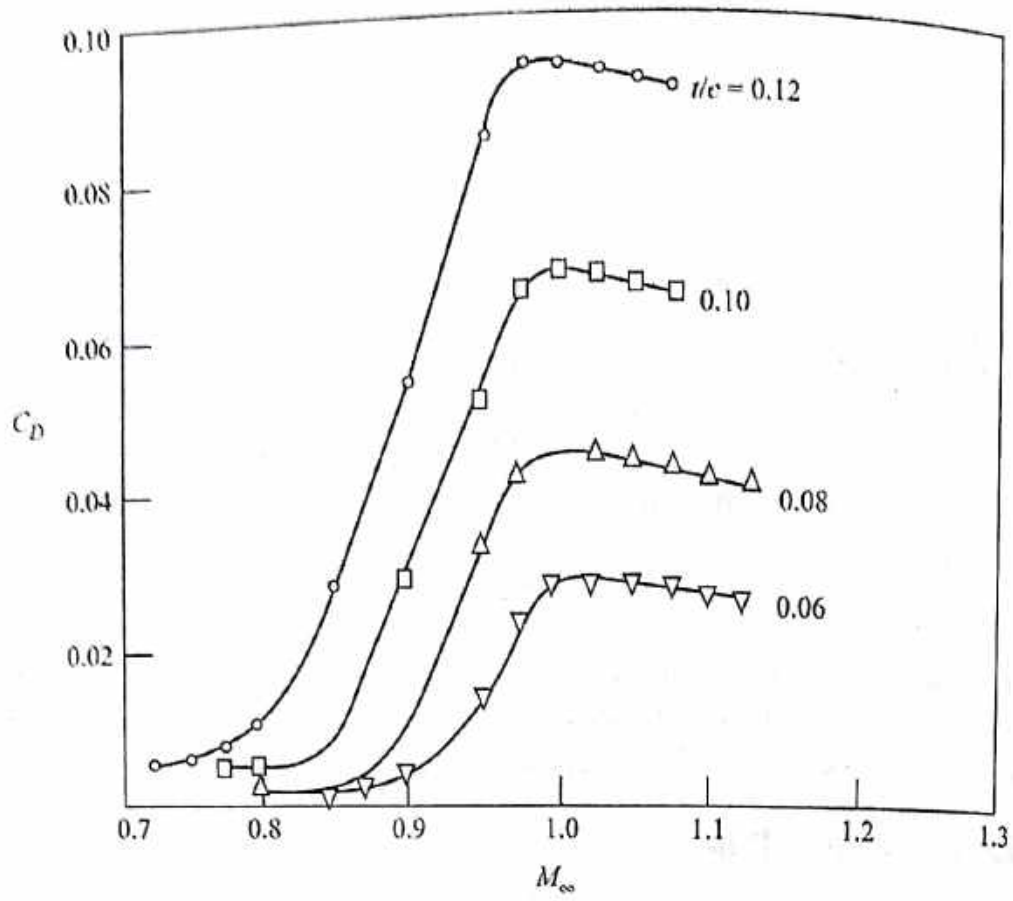
1. For subsonic and supersonic flows, the governing equation $\left(\left|1 - M_\infty^2\right|\right)\phi_{xx} + \phi_{zz} = 0$ is independent of γ, so that the results from similarity rules can be applied to any gas; but for transonic flow, the potential equations are not independent of γ. Therefore, the results have to be properly applied to different gases, with suitable correction for γ, e.g. a probe used for air in transonic range can be calibrated for steam.
2. For transonic flow,

$$C_p \sim C_L \sim \left(\frac{t}{c}\right)^{2/3}$$

For subsonic flow,

$$C_p \sim C_L \sim \left(\frac{t}{c}\right)$$

Scanned by CamScanner



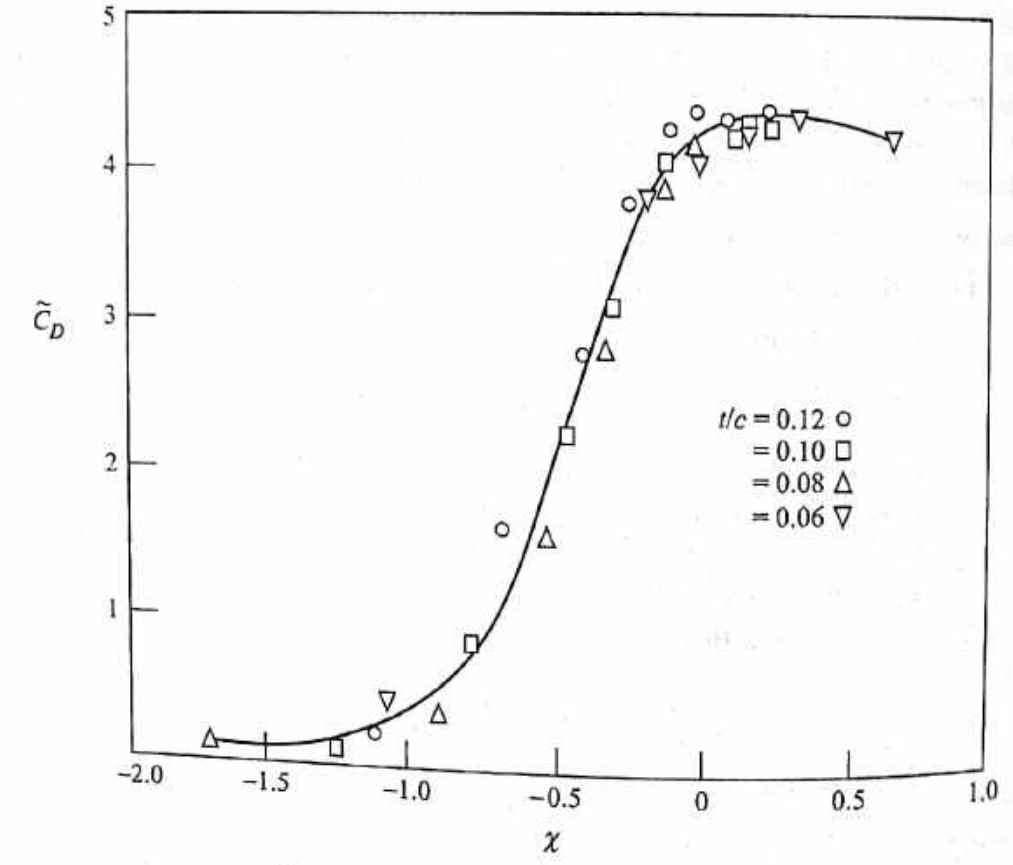


Fig. 8.6 The transonic similarity rule.

Scanned by CamScanner

For supersonic flow,

$$C_p \sim C_L \sim \left(\frac{t}{c}\right)$$

Transonic flow is characterized by the occurrence of shock and boundary layer separation. This explains the steep increase in C_D at transonic range. We should also recall that the shock should be sufficiently weak for small perturbations. For circular cylinders this theory cannot be applied, because the perturbations are not small.

8.5 HYPERSONIC SIMILARITY

The linear theory is not valid at high supersonic Mach numbers, since

$\frac{u}{V_\infty} \ll 1$ is true only for supersonic flow, and

$\frac{u}{V_\infty} \approx 1$ for hypersonic flow.

Even slender bodies (such as that shown in Fig. 8.7) produce large disturbances in hypersonic flow. The original nonlinear equations have to be used for such flows. So, mathematically hypersonic flow is similar to transonic flow. In supersonic flow, slender bodies produce weak shocks and so these can be considered as Mach lines. But in hypersonic flow, even slender bodies produce strong shocks and, therefore, in hypersonic flow we can no more deal with Mach lines and must deal with the actual shock waves. At high Mach numbers, the Mach angle μ may be of the same order or less than the maximum deflection angle θ of the body.

From these considerations, the similarity rule can be obtained for hypersonic flow. The Mach angle μ is given by the relation

$$\sin \mu = \frac{1}{M_\infty}$$

For the present case of flow shown in Fig. 8.7,

$$\sin \mu \approx \mu = \frac{1}{M_\infty} \leq \theta$$

where θ is the half-angle of the wedge in the figure, i.e. for hypersonic flow,

$$M_\infty \theta \geq 1 \tag{8.23}$$

But in hypersonic flows even for small disturbances, there are shock lines, and the angle of shock is always less than the angle of Mach line. Therefore, in reality the inequality in Eq. (8.23), obtained with the approximation that μ is of the same order or less than θ, has to be modified since the shock angle is always less than μ. In other words, it can be stated that $M_\infty \theta$ is greater than some quantity K, whose numerical value can be less than unity too.

Scanned by CamScanner

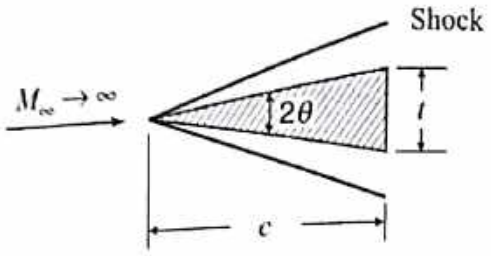


Fig. 8.7 Slender body in hypersonic flow.

It is a common practice to express

$$K = M_\infty \theta \geq 0.5 \tag{8.24}$$

$$\boxed{K = M\theta} \tag{8.25}$$

where K is called the *Hypersonic similarity parameter*.

EXAMPLE 8.2 For $\theta = 10°$ (≈ 0.174 radian), $M_\infty = 4$; the hypersonic similarity parameter $K = M_\infty \theta = 0.7$. For $\theta = 20°$ and $M_\infty = 2$,

$$K = M_\infty \theta \approx 0.7$$

That is, for a wedge with half-angle 20°, $M_\infty = 2$ should be considered hypersonic. This implies that $M \geq 5$ for hypersonic flow is only a crude limit. For $\theta = 5°$ and $M_\infty = 8$,

$$K = M_\infty \theta \approx 0.7$$

Thus, a wedge with half-angle 5° in a flow with $M_\infty = 8$ produces shocks as strong as a wedge with half-angle 20° in a flow with $M_\infty = 2$. Also, by Eq. (8.22),

$$\theta = \theta_0 \pm \alpha = \frac{1}{2}\frac{t}{c}\left(1 \pm \frac{2\alpha}{t/c}\right) \tag{8.26}$$

Whenever $M_\infty \theta$ is the same for a number of bodies, the flow about them will be dynamically similar, i.e. to investigate the hypersonic flow about a wedge with half-angle 5°, $M_\infty = 8$, we can use a supersonic tunnel with $M_\infty = 2$ and $\theta = 20°$. This is of paramount importance in testing; of course the two bodies should be affinely related (geometrically similar). Consider two models, 1 and 2:

$$\frac{K_1}{K_2} = \frac{M_{\infty 1}\left(\frac{t}{c}\right)_1\left(1 \pm 2\frac{\alpha}{(t/c)_1}\right)}{M_{\infty 2}\left(\frac{t}{c}\right)_2\left(1 \pm 2\frac{\alpha}{(t/c)_2}\right)}$$

$$\frac{K_1}{K_2} = 1 \quad \text{for dynamic similarity}$$

Scanned by CamScanner

This condition for dynamic similarity will be satisfied only when

$$M_{\infty 1}\left(\frac{t}{c}\right)_1 = M_{\infty 2}\left(\frac{t}{c}\right)_2$$

$$\left(\frac{\alpha}{(t/c)_1}\right) = \left(\frac{\alpha}{(t/c)_2}\right)$$

That is, these two conditions should be satisfied for dynamic similarity, when there is geometric similarity

$$C_p \approx C_L = \left(\frac{t}{c}\right)^2 F_1\left(\frac{x}{c}, M_\infty\left(\frac{t}{c}\right), \frac{\alpha}{t/c}\right) \tag{8.27}$$

The total lift and drag coefficients are given by

$$C_L = \left(\frac{t}{c}\right)^2 F_2\left(M_\infty\left(\frac{t}{c}\right), \frac{\alpha}{t/c}\right) \tag{8.28}$$

$$C_D = \left(\frac{t}{c}\right)^3 F_3\left(M_\infty\left(\frac{t}{c}\right), \frac{\alpha}{t/c}\right) \tag{8.29}$$

Equations (8.27)–(8.29) give the functional dependence of various aerodynamic characteristics for hypersonic flow.

A plot like the one shown in Fig. 8.8 gives the correct representation of the different parameters. This similarity rule is also valid for axially symmetric bodies like rockets and missiles.

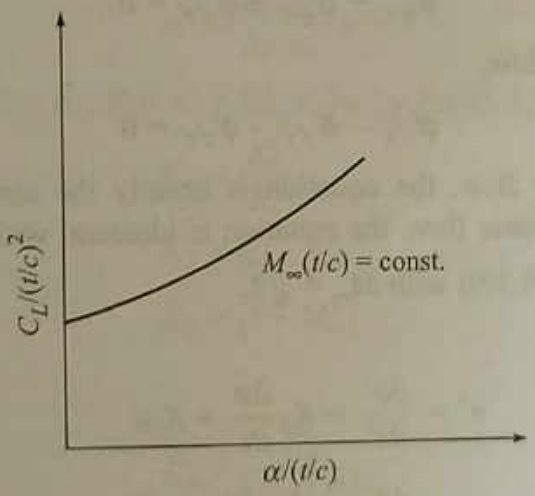


Fig. 8.8 A plot of $C_L/(t/c)^2$ against $\alpha/(t/c)$.

Detailed analysis of transonic and hypersonic flows is beyond the scope of this book. The transonic and hypersonic similarity rules discussed here are just a few glimpses, highlighting some of the vital features associated with them. Those who are looking for a deeper understanding of these problems should consult standard books on these topics.

Scanned by CamScanner

8.6 THREE-DIMENSIONAL FLOW: THE GOTHERT RULE

The General Similarity Rule

The Prandtl–Glauert rule is approximate because it satisfies the boundary conditions only on the axis, and not on the contour. But Gothert rule is exact and valid for both two-dimensional and three-dimensional bodies. The potential equation is (for $M_\infty <$ or > 1)

$$(1 - M_\infty^2)\phi_{xx} + \phi_{yy} + \phi_{zz} = 0 \tag{8.30}$$

For $M_\infty < 1$, the equation is elliptic in nature and for $M_\infty > 1$, it is hyperbolic. Here also, we make transformation by which the transformed equation does not contain M_∞ explicitly any more. Let

$$x' = x, \quad y' = K_1 y, \quad z' = K_1 z, \quad \phi' = K_2 \phi$$

With the above new variables, Eq. (8.30) transforms into

$$(1 - M_\infty^2)\phi'_{x'x'} + K_1^2(\phi'_{y'y'} + \phi'_{z'z'}) = 0$$

M_∞ vanishes from the above equation for

$$K_1 = \sqrt{\left|1 - M_\infty^2\right|} \tag{8.31}$$

With Eq. (8.31), the resulting potential flow equation for subsonic flow is

$$\phi'_{x'x'} + \phi'_{y'y'} + \phi'_{z'z'} = 0$$

and for supersonic flow,

$$\phi'_{x'x'} - \phi'_{y'y'} - \phi'_{z'z'} = 0$$

Again, for subsonic flow, the equation is exactly the same as the Laplace equation. For supersonic flow, the equation is identical with the compressible flow equation (Eq. (8.30)) with $M_\infty = \sqrt{2}$.

Now,

$$u' = \frac{\partial \phi'}{\partial x'} = K_2 \frac{\partial \phi}{\partial x} = K_2 u \tag{8.32a}$$

$$v' = \frac{\partial \phi'}{\partial y'} = \frac{K_2}{K_1}\frac{\partial \phi}{\partial y} = \frac{K_2}{K_1} v \tag{8.32b}$$

$$w' = \frac{\partial \phi'}{\partial z'} = \frac{K_2}{K_1}\frac{\partial \phi}{\partial z} = \frac{K_2}{K_1} w \tag{8.32c}$$

$$C_p = \frac{p - p_\infty}{\frac{1}{2}\rho V_\infty^2} = -2\frac{u}{V_\infty} = -\frac{2}{V_\infty}\frac{\partial \phi}{\partial x} \tag{8.33}$$

Scanned by CamScanner

and

$$C_p' = -2\frac{u'}{V_\infty} \tag{8.34}$$

with the assumption that $V_\infty = V_\infty'$. This assumption really does not impose any restriction on the rule, because in supersonic flow, the velocity itself is not important (i.e. V/a is more relevant than V). Introduction of Eq. (8.32a) into Eq. (8.34) results in

$$C_p' = -2K_2\frac{u}{V_\infty}$$

i.e.

$$C_p' = K_2 C_p \tag{8.35}$$

The kinematic flow condition (Eq. (8.6)) states that

$$\frac{w}{V_\infty} = \frac{\partial z}{\partial x}$$

$$w = V_\infty \frac{\partial z}{\partial x} \tag{8.36a}$$

$$w' = V_\infty \frac{\partial z'}{\partial x'} \tag{8.36b}$$

Combining Eqs. (8.36a) and (8.36b), we get

$$w' = \frac{\partial x}{\partial z}\frac{\partial z'}{\partial x'} w = K_1 w$$

since $x' = x$, and $z'/z = K_1$. But $w' = (K_2/K_1)w$ by Eq. (8.32c); therefore,

$$K_1 = \frac{K_2}{K_1}$$

i.e.

$$K_2 = K_1^2$$

$$K_2 = \left|1 - M_\infty^2\right| \tag{8.37}$$

Therefore,

$$C_p = \frac{C_p'}{\left|1 - M_\infty^2\right|} \tag{8.38}$$

Equation (8.38) is valid (exactly) at any point on the boundary of the body, as well as in the flow field. Therefore,

$$\boxed{\frac{C_p}{C_p'} = \frac{C_L}{C_L'} = \frac{C_M}{C_M'} = \frac{1}{\left|1 - M_\infty^2\right|}} \tag{8.39}$$

Equation (8.39) is an important equation, relating the aerodynamic characteristics for the actual and transformed bodies.

Scanned by CamScanner

Gothert Rule

The aerodynamic characteristics of a body in three-dimensional compressible flow are obtained as follows:

The geometry of the given body is transformed in such away that its lateral and normal dimensions (both in y and z directions) are multiplied by $\sqrt{|1-M_\infty^2|}$. If the flow is subsonic, compute the incompressible flow about the transformed body; if the flow is supersonic, compute the field with $M_\infty = \sqrt{2}$ about the transformed body. The aerodynamic coefficients of the given body in given flow, follow from transformed flow with Eq. (8.39).

Gothert rule can be applied to two-dimensional flow also (stated as version III of the Prandtl–Glauert rule).

It is exact in the framework of linear theory, whereas the Prandtl–Glauert rule is only approximate. For thicker bodies, when there is doubt about the accuracy with P–G rule, Gothrt rule should be used even though it is tedious.

The coefficient of pressure $C_p = -2\dfrac{u}{V_\infty}$

the error involved in $\dfrac{C_p}{C_p'} = O\left(\left(\dfrac{u}{V_\infty}\right)^2\right)$

That is why, the P–G rule, though approximate, can be used quite satisfactorily up to $t/c = 15\%$ (because the error is less). Gothert rule is still superior and is applicable not only to flow past bodies but also to flow through ducts where the diameter is small.

Application to wings of finite span Consider a wing planform transformation described now.

Planform

$$\text{Taper ratio: } \lambda' = \lambda$$

$$\text{Aspect ratio: } A' = A\sqrt{|1-M_\infty^2|} \tag{8.40}$$

$$\text{Sweep angle: } \cot\phi' = \cot\phi\sqrt{|1-M_\infty^2|}$$

$$A'\tan\phi' = A\tan\phi \tag{8.41}$$

For subsonic flow, the transformation decreases A and for supersonic flow, the transformation increases A. Note that ϕ is the sweep angle here.

Profile The profile is given by the relations

$$\frac{\alpha'}{\alpha} = \frac{f'}{f} = \frac{t'}{t} = \sqrt{|1-M_\infty^2|} \tag{8.42}$$

Scanned by CamScanner

Thus, for wings (three-dimensional bodies), the Gothert rule is still more complicated; we have to transform not only the profile but also the planform, for each M_∞. But this is the only reasonable method for wing analysis. In subsonic flow, these similarity rules are of great importance; but in supersonic flow, they are not that much important because even in two-dimensional subsonic flow, the elliptical equation is very difficult to solve, but in supersonic flow, the hyperbolic equation can be easily solved.

After making the transformations with Eqs. (8.40) and (8.42), find C_L, C_M, etc. for the incompressible case, and then the corresponding coefficients for the compressible case will be determined by the relations

$$\frac{C_p}{C'_p} = \frac{C_L}{C'_L} = \frac{C_M}{C'_M} = \frac{1}{\left|1 - M_\infty^2\right|} \tag{8.39}$$

But it is tedious to find the variation of C_p, C_L, C_M with M_∞ because for each M_∞ we have to make the above transformations.

Application to bodies of revolution and fuselage The general, three-dimensional equations can be applied to these shapes. But it is more convenient to use polar coordinates for bodies of revolution and fuselage.

The potential equation in cylindrical polar coordinates, for incompressible flow is

$$\frac{\partial^2\phi}{\partial x^2} + \frac{\partial^2\phi}{\partial r^2} + \frac{1}{r}\frac{\partial\phi}{\partial r} + \frac{1}{r^2}\frac{\partial^2\phi}{\partial \theta^2} = 0 \tag{8.43}$$

where x, r, and θ are the axial, radial and angular (circumferential) coordinates respectively. For compressible flow, the equation is

$$(1 - M_\infty^2)\frac{\partial^2\phi}{\partial x^2} + \frac{\partial^2\phi}{\partial r^2} + \frac{1}{r}\frac{\partial\phi}{\partial r} + \frac{1}{r^2}\frac{\partial^2\phi}{\partial \theta^2} = 0 \tag{8.44}$$

The transformation is

$$x' = x, \qquad r' = K_1 r, \qquad \theta' = \theta, \quad \phi = K_2\phi' \tag{8.45}$$

Equation (8.44) is independent of M_∞ for

$$K_1 = \sqrt{\left|1 - M_\infty^2\right|}$$

From the streamline analogy,

$$K_2 = \frac{1}{\left|1 - M_\infty^2\right|}$$

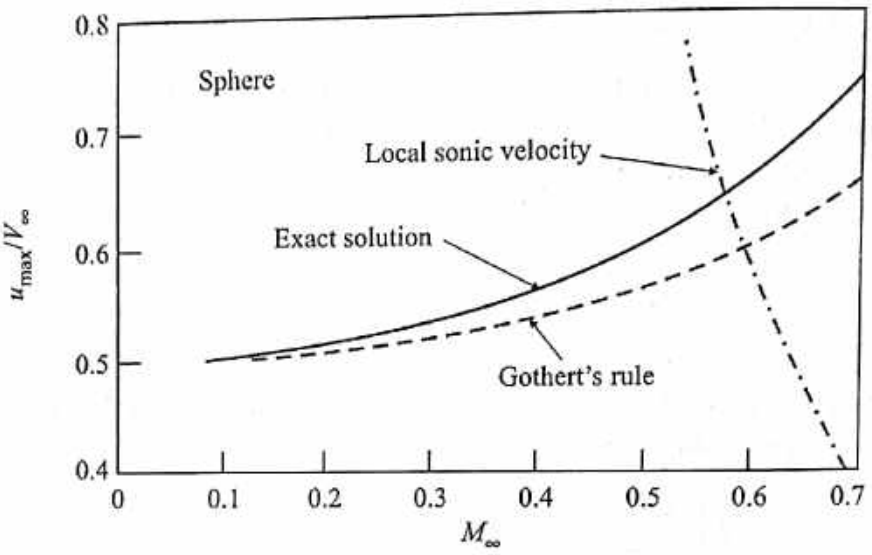
Here again, as in Cartesian coordinates, *transform the geometry* and then calculate the aerodynamic coefficients for the incompressible case, and then the values for the compressible case are given by Eq. (8.39). If $f = 0$, the only transformation required will be $t'/t = \sqrt{\left|1 - M_\infty^2\right|}$. The variations of $\frac{u_{\max}}{V_\infty}$, $\left(\frac{dC_L}{d\alpha}\right)_{C_L=0}$ and $\frac{u_{\max}}{V_\infty}\Big/\left(\frac{u_{\max}}{V_\infty}\right)_{\text{inc}}$ with M_∞ are shown in Figs. 8.9(a)–8.9(c), respectively.

Scanned by CamScanner

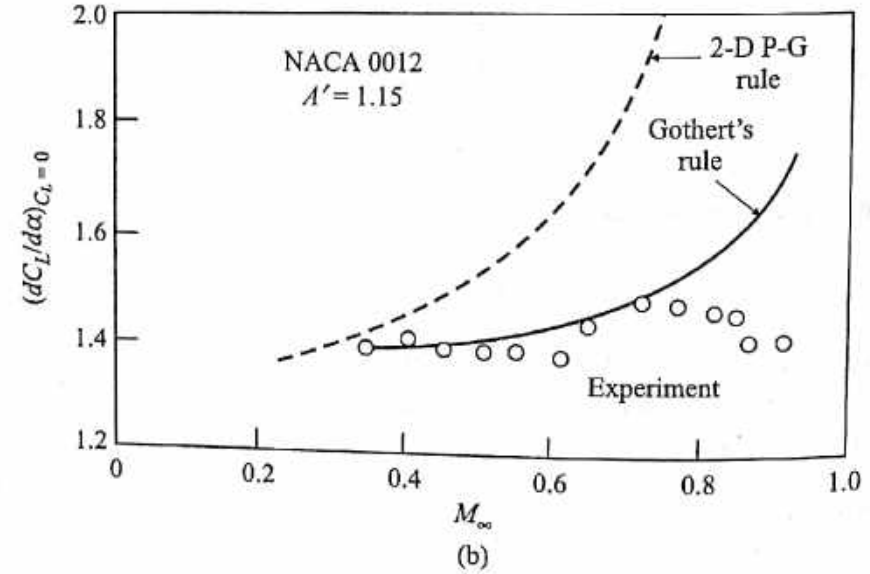
In Fig. 8.9(a), it is seen that beyond the chain line the results cannot be applied because once the speed of sound is reached locally, there will be shock somewhere and this is certainly a nonlinear effect. Though the plot is for a sphere, which is not a slender body, the results of Gothert rule are quite good (at $M_\infty = 0.5$, the error is only ~ 5%). For slender bodies, Gothert's rule applies very well.

In Fig. 8.9(b), the results for NACA 0012 profile with Aspect Ratio ($A' = 1.15$) are shown. For those Mach numbers for which locally speed of sound is not reached anywhere on the profile, Gothert's rule checks very well with experimental values. The Prandtl–Glauert rule for $A' = \infty$ shows that for large A', the $dC_L/d\alpha$ obtained is much higher.

The three-dimensional relief effect is seen in Fig. 8.9(c). For an infinitely long circular cylinder in a stream of velocity V_∞, $u_{max} = V_\infty$, but for a sphere



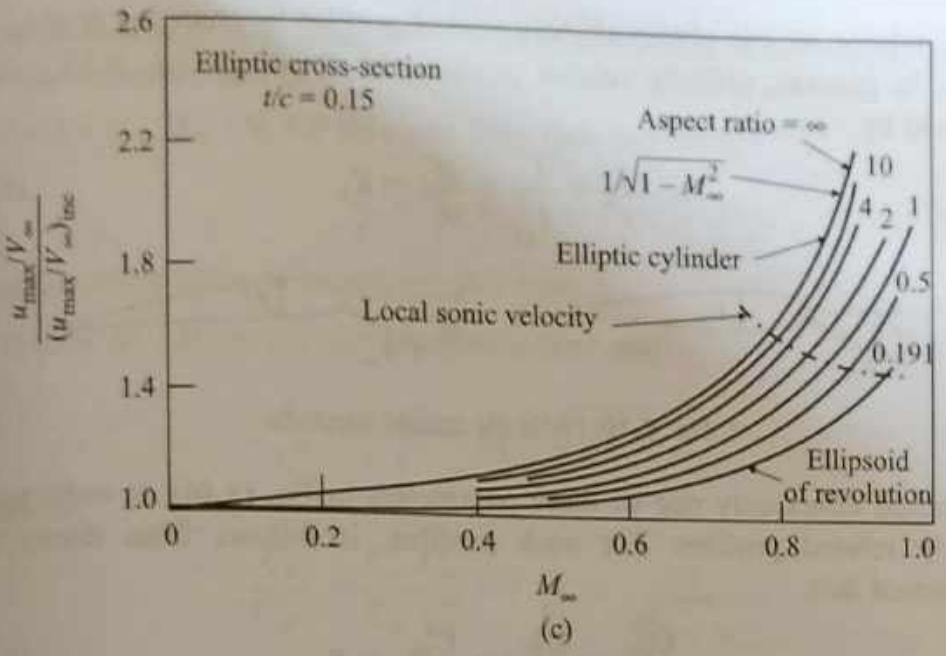
(a)



(b)

Fig. 8.9 *(Contd.)*

Scanned by CamScanner



(c)

Fig. 8.9 Results of Gothert's rule for three-dimensional subsonic flow.

$u_{max} = 0.5V_\infty$. From the plot, the three-dimensional relief effect increases with increase in M_∞. A slender body (small A') introduces smaller perturbations, i.e. the disturbances produced by wings are much more compared to those produced by fuselage. This difference in disturbances of wings and fuselage is greater at larger M_∞. So, locally speed of sound is reached first on wings and not on fuselage. That is, we should find out the critical Mach number for wings and not for the fuselage, since only the former is significant. The M_{cr} for the fuselage will be much higher than the M_{cr} for the wing.

Comparison of two-dimensional symmetric body and axially symmetric body For an axi-symmetric body, in any cross-section the flow will be same. But this will not be so for a two-dimensional body. Also, at any cross-section, the disturbances produced by an axi-symmetric body will be much smaller, i.e. the acceleration of flow will be much less, and hence the drop in C_p is much smaller compared to that produced by a two-dimensional body.

The Prandtl–Glauert Rule

This is only an approximation and a greater simplification compared to Gothert's rule. Here we need not effect any transformation in the z-direction at all. It means that Eq. (8.42) is no more necessary. Only Eq. (8.40) which gives transformation to planform is necessary.

General considerations The P–G rule introduces the concept of affinely related profiles in incompressible flow. Affinely related profiles are those for which, e.g. the t/c ratio alone is different and α and f are the same, i.e. all the ordinates of the two profiles are related simply by a constant.

Scanned by CamScanner

Similarly, we can obtain affinely related profiles by changing α alone or f alone. In general, affinely related profiles, as shown in Fig. 8.10, can be obtained by

$$\frac{t'}{t''} = \frac{f'}{f''} = \frac{\alpha'}{\alpha''} = K_1 \tag{8.46}$$

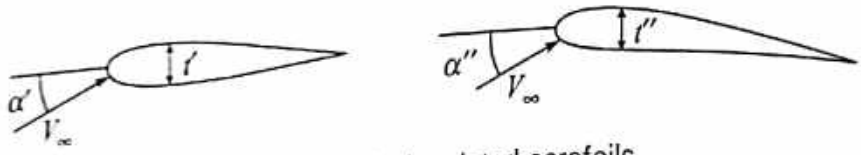


Fig. 8.10 Affinely related aerofoils.

We should effect only one of these parameters in Eq. (8.46), in order to get affinely related profiles. For such profiles, it follows from theory and experiment that,

$$\frac{C'_p}{C''_p} = \frac{C'_L}{C''_L} = \frac{C'_M}{C''_M} = K_1 \tag{8.47}$$

This can be thought as: if α for one wing is K times α for the second wing, then the C_L, C_p, C_M for the first wing should be correspondingly K times larger than those for the second wing. This is so because of the linearity of lift curve, shown in Fig. 8.11.

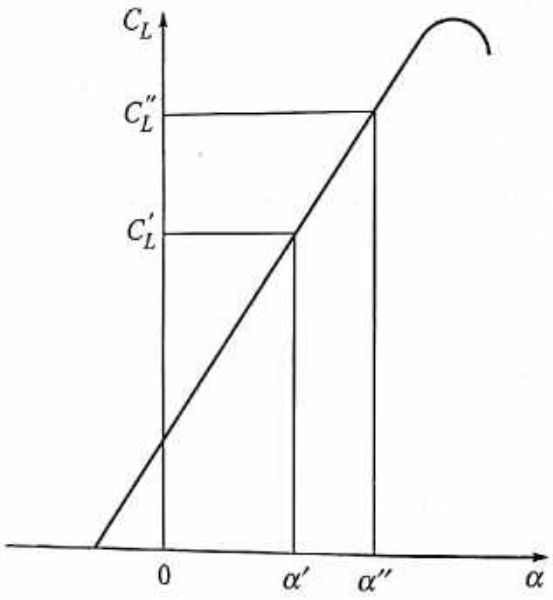


Fig. 8.11 C_L against α.

These relationships hold only for the linear portion, because of the linearity involved in the theory.

P–G rule for two-dimensional flow, using Eqs. (8.46) and (8.47) We have to use Eq. (8.46) with (8.42), and (8.47) with (8.39), and set $K_1 = \sqrt{|1 - M_\infty^2|}$

Scanned by CamScanner

in Eqs. (8.46) and (8.47). What we have to prescribe now is our postulation for P–G rule versions I and II:

Version I: $M_\infty = 0$, for subsonic flow and, therefore,

$$\frac{t}{t'} = \frac{f}{f'} = \frac{\alpha}{\alpha'} = 1 \tag{8.48}$$

where the prime refers to incompressible case.

Version II: $M_\infty = \sqrt{2}$ for supersonic flow and

$$\frac{t}{t''} = \frac{t}{t'}\frac{t'}{t''} = K_1 = \sqrt{\left|1 - M_\infty^2\right|}$$

Therefore,

$$\frac{C_p}{C_p''} = \frac{C_p}{C_p'}\frac{C_p'}{C_p''} = 1\,\frac{1}{K_1} = \frac{1}{\sqrt{\left|1 - M_\infty^2\right|}} \tag{8.49}$$

where the double prime refers to transformed profile.

Application to wings The general relation between the pressure coefficients of closely related wing profiles (Eq. (8.39)) is

$$\frac{(C_p)_{A,\alpha,t/c,f/c,x/c,y/s,z/t}}{(C_p')_{K_1A,K_1\alpha,K_1(t/c),K_1(f/c),x/c,y/s,z/t}} = \frac{1}{\left|1 - M_\infty^2\right|}$$

where "s" is the semi-span of wing. This transformed pressure coefficient ratio corresponds to $M_\infty = 0$ (Version I of P–G rule), for subsonic flow.

For $M_\infty = \sqrt{2}$ (supersonic flow), by Eq. (8.49) of Version II, we get

$$\frac{(C_p)_{A,\alpha,t/c,f/c,x/c,y/s,z/t}}{(C_p')_{K_1A,\alpha,t/c,f/c,x/c,y/s,z/t}} = \frac{1}{\sqrt{\left|1 - M_\infty^2\right|}} \tag{8.50}$$

$$\frac{(C_L)_{A,t/c,\alpha}}{(C_L')_{K_1A,t/c,\alpha}} = \frac{(C_M)_{A,t/c,\alpha}}{(C_M')_{K_1A,t/c,\alpha}} = \frac{1}{\sqrt{\left|1 - M_\infty^2\right|}} \tag{8.51}$$

By Gothert rule, we have

$$\frac{C_p}{C_p'} = \frac{C_L}{C_L'} = \frac{C_M}{C_M'} = \frac{1}{\left|1 - M_\infty^2\right|} \tag{8.39}$$

$$\frac{\alpha'}{\alpha} = \frac{f'}{f} = \frac{t'}{t} = \sqrt{\left|1 - M_\infty^2\right|} \tag{8.42}$$

By similarity rule for affinely related profiles in incompressible flow, if

$$\frac{t'}{t''} = \frac{f'}{f''} = \frac{\alpha'}{\alpha''} = K_1 \tag{8.46}$$

then

$$\frac{C_p'}{C_p''} = \frac{C_L'}{C_L''} = \frac{C_M'}{C_M''} = K_1 \tag{8.47}$$

Scanned by CamScanner

This is an empirical rule. For low speed flows, this can be explained with respect to α. But these equations are only approximate. Actually, for supersonic flow, C_L, does not depend on t at all. It depends only on f and α. We relate the given profile in compressible flow (unprimed) to the transformed profile (double primed) by

$$\frac{t}{t''} = \frac{f}{f''} = \frac{\alpha}{\alpha''} = 1 \tag{8.48a}$$

With Eqs. (8.48a) and (8.42), we find that

$$\frac{t'}{t''} = \frac{t'}{t}\frac{t}{t''} = 1\sqrt{\left|1 - M_\infty^2\right|} \quad \text{or} \quad K_1 = \sqrt{\left|1 - M_\infty^2\right|}$$

Then the aerodynamic coefficients of the given profile in compressible flow are related to those of the transformed profile (which has the same geometry) in incompressible flow or at $M_\infty = \sqrt{2}$ by

$$\frac{C_p}{C_p''} = \frac{C_L}{C_L''} = \frac{C_M}{C_M''} = \frac{1}{\sqrt{\left|1 - M_\infty^2\right|}} \tag{8.49a}$$

because

$$\frac{C_p}{C_p''} = \frac{C_p}{C_p'}\frac{C_p'}{C_p''} = \frac{1}{\left|1 - M_\infty^2\right|}\sqrt{\left|1 - M_\infty^2\right|} \text{ by Eqs. (8.39) and (8.47).}$$

Application to wings of finite span The Gothert's rule (Eq. (8.39)) states that

$$\frac{(C_p)_{A,\,\alpha,\,t/c,\,f/c,\,x/c,\,y/s,\,z/t}}{(C_p')_{K_1A,\,K_1\alpha,\,K_1(t/c),\,K_1(f/c),\,x/c,\,y/s,\,z/t}} = \frac{1}{\left|1 - M_\infty^2\right|}$$

and by P–G rule, we have

$$\frac{(C_p)_{A,\,\alpha,\,t/c,\,f/c,\,x/c,\,y/s,\,z/t}}{(C_p'')_{K_1A,\,\alpha,\,t/c,\,f/c,\,x/c,\,y/s,\,z/t}} = \frac{1}{\sqrt{\left|1 - M_\infty^2\right|}} \tag{8.50a}$$

Equation (8.50a) is only an approximate relation. Further,

$$\frac{(C_L)_{A,\,\alpha,\,t/c,\,f/c}}{(C_L'')_{K_1A,\,\alpha,\,t/c,\,f/c}} = \frac{(C_M)_{A,\,\alpha,\,t/c,\,f/c}}{(C_M'')_{K_1A,\,\alpha,\,t/c,\,f/c}} = \frac{1}{\sqrt{\left|1 - M_\infty^2\right|}} \tag{8.51a}$$

The P–G rule is only approximate, but the Gothert's rule, though exact, is very tedious, especially in three-dimensions, because here we have to transform profile as well. For P–G rule, only the planform has to be transformed.

From the P–G rule, for three-dimensional wings we obtain a similarity rule in the following way: If the relation

$$C_p' = \theta' F_1\left(\lambda', A', \cot\phi', \frac{x'}{c}, \frac{y'}{s}\right) \tag{8.52}$$

Scanned by CamScanner

for a wing is known at $M_\infty = 0$ and $M_\infty = \sqrt{2}$ then it follows for an arbitrary Mach number from Eqs. (8.40), (8.41) and (8.50), that

$$C_p = \frac{\theta}{\sqrt{|1-M_\infty^2|}} F_2\left(\lambda, A\tan\phi, A\sqrt{|1-M_\infty^2|}, \frac{x}{c}, \frac{y}{s}\right) \quad (8.53a)$$

$$C_L = \frac{\theta}{\sqrt{|1-M_\infty^2|}} F_3\left(\lambda, A\tan\phi, A\sqrt{|1-M_\infty^2|}\right) \quad (8.53b)$$

$$C_{D_0} = \frac{\theta}{\sqrt{|1-M_\infty^2|}} F_4\left(\lambda, A\tan\phi, A\sqrt{|1-M_\infty^2|}\right) \quad (8.53c)$$

where λ is the taper ratio.

In Eq. (8.53a), θ means α or f/c or t/c.

In Eq. (8.53b), θ means α or f/c or t/c, but t/c only in subsonic flow.

In Eq. (8.53c), θ means either t/c or f/c.

In Eqs. (8.52) and (8.53), ϕ is the angle of sweep for the wing.

Application to bodies of revolution The application of P–G rule to bodies of revolution is similar to that for aerofoils (2-D), i.e. no transformation of the body is necessary. The aerodynamic coefficients in compressible flow are the same as in incompressible flow or at $M_\infty = \sqrt{2}$. Hence, there is no Mach number effect at all and the results are the same as those for slender body theory.

This contradicts the more exact Gothert rule. A closer examination shows that the P–G rule for bodies of revolution is valid only for very slender and extremely pointed bodies. This theory is applied to rockets, very small aspect ratio wings, etc. Of course, wave drag is influenced by M even for slender bodies. We can use the results of incompressible flow for the calculation of pressure distribution, etc.

From Fig. 8.9(c), it is seen that for very small aspect ratio, the effect of Mach number is very small and at $A = 0$, the Mach number effect vanishes.

The von Karman Rule for Transonic Flow

Application to wings For $M_\infty = 1$,

$$C_p = \theta^{2/3} F_5(\lambda, A\tan\phi, A\theta^{1/3}, x/c, y/s) \quad (8.54a)$$

$$C_L = \theta^{2/3} F_6(\lambda, A\tan\phi, A\theta^{1/3}) \quad (8.54b)$$

$$C_D = \theta^{5/3} F_7(\lambda, A\tan\phi, A\theta^{1/3}) \quad (8.54c)$$

Mathematically, these can be derived from the nonlinear differential equation (7.24). These laws are also approximately valid in the vicinity of $M_\infty = 1$. The main advantage of these similarity rules is that we have to investigate the influence of λ, $A\tan\phi$, $A\theta^{1/3}$ only, and not the influence of λ, A, ϕ and θ separately, which is very tedious. Thus, the rules are very important for experimental investigations.

Scanned by CamScanner

Applications to bodies of revolution The pressure distribution of a body (unprimed) is related to the pressure distribution of an affinely related body (primed) at $M_\infty = 1$, by the relation

$$C_p = C'_p \left(\frac{\theta_f}{\theta'_f} \right)^2 \tag{8.55}$$

where the subscript f stands for fuselage. This rule was derived by von Karman, but later on it was shown that a correction factor should be applied.

8.7 CRITICAL MACH NUMBER

In Section 8.2, we saw that the freestream subsonic Mach number which gives the sonic Mach number somewhere on the boundary of the body is called the critical Mach number M^*_∞, and this decreases with the increasing thickness to chord ratio of the profile, without going into the details about the calculation of this important parameter. The calculation of M^*_∞ for a given wing is extremely important because a local transonic flow zone over the profile will influence the aerodynamic efficiency of the wing considerably. Let us have a closer look at this vital parameter, influencing the performance of flying objects.

We are familiar with the definition of critical Reynolds number. The critical Reynolds number is the Reynolds number, at which the nature of the flow field changes from laminar to turbulent. Also, we know that, any transition is gradual and hence, over a range around the critical Reynolds number, the flow field consists of both laminar and turbulent pockets. This leads to the definition of lower and upper critical Reynolds numbers. The lower critical Reynolds number is that below which the entire flow field is laminar, and the upper critical Reynolds number is that above which the entire field is turbulent. The laminar and turbulent flows dictated by the lower and upper critical Reynolds numbers can be precisely encountered in practice. In an analogous manner, one may define that the critical Mach number is that at which both the subsonic and supersonic zones exist in the flow field. The lower critical Mach number is that below which the entire flow field is subsonic, and the upper critical Mach number is that above which the entire flow field is supersonic. But these definitions of lower and upper critical Mach numbers are only of mathematical interest. It is because the upper critical Mach number cannot be encountered in any physical flow process. This is essentially due to the waves present in the supersonic field. Therefore, it will be of great value, from design point of view, to have a thorough understanding about the critical Mach number.

The Mach number (M) refers to the method of measuring airspeed that was developed by the Austrian physicist Ernst Mach. It is used to indicate flight velocities in high-speed flight and is related to the speed of sound. The actual speed of sound varies depending on the altitude above sea level because sound travels at slightly different speeds at different temperatures, and the temperature

Scanned by CamScanner

varies according to the altitude. At sea level, the speed of sound is about 1225 km/h ($a = \sqrt{\gamma RT} = \sqrt{1.4 \times 287 \times 288.15} = 340.26$ m/s or $340.26 \times 3.6 \approx$ 1225 km/h). At 20,000 ft (6096 m), the speed of sound is 1062 km/h.

If an aircraft is travelling at one half of the speed of sound, it is said to be travelling at Mach 0.5. A speed of Mach 2 is twice the speed of sound. Because the speed of sound varies, a particular speed at sea level expressed as a Mach number would be faster than the same speed at 30,000 ft (9144 m), which would be faster than the same speed at 40,000 ft (12,192 m). In other words, Mach 2 at sea level is a greater number of kilometres per hour than Mach 2 at 30,000 ft, which is a greater number of kilometres per hour than Mach 2 at 40,000 ft. When an aircraft reaches Mach 1, it is said to "break the sound barrier".

The following breakdowns have been generally accepted to classify speeds: M less than 0.8 subsonic, $M = 0.8$ to 1.2 transonic, M from 1.2 to 5.0 supersonic and M greater than 5.0 hypersonic.

A "critical Mach number" is the speed of an aircraft (below Mach 1) when the air flowing over some area of the airfoil has reached the speed of sound. For instance, if the air flowing over a wing reaches Mach 1 when the wing is only moving at Mach 0.8, then the wing's critical Mach number is 0.8.

Examine the subsonic flow past an aerofoil, illustrated in Fig. 8.12. The flow accelerates from the leading edge to a maximum value at the maximum thickness location and then decelerates towards the trailing edge, as shown in Fig. 8.12(a). The corresponding variations of temperature and Mach number, from the leading edge to the trailing edge of the aerofoil, are shown in Fig. 8.12(b).

This flow process can be treated as adiabatic, with the stagnation temperature T_0 = constant. Therefore, by energy equation, we have

$$h + \frac{u^2}{2} = h_0$$

where h and h_0 are the static and total enthalpies, respectively, and u is the local velocity. Assuming air to be a perfect gas, we can express, $h = c_p T$ and $h_0 = c_p T_0$. Thus,

$$h = h_0 - \frac{u^2}{2}$$

$$c_p T = c_p T_0 - \frac{u^2}{2}$$

$$T = T_0 - \frac{u^2}{2c_p}$$

$$= T_0 - \frac{u^2}{2\frac{\gamma}{\gamma - 1}R}$$

Scanned by CamScanner

$$= T_0 - \frac{(\gamma-1)}{2}\frac{u^2}{\gamma R}$$

$$= T_0 - \frac{(\gamma-1)}{2}\frac{u^2 T}{\gamma R T}$$

$$= T_0 - \frac{(\gamma-1)}{2} M^2 T$$

since $c_p = \gamma(\gamma-1)R$, $a = \sqrt{\gamma RT}$.

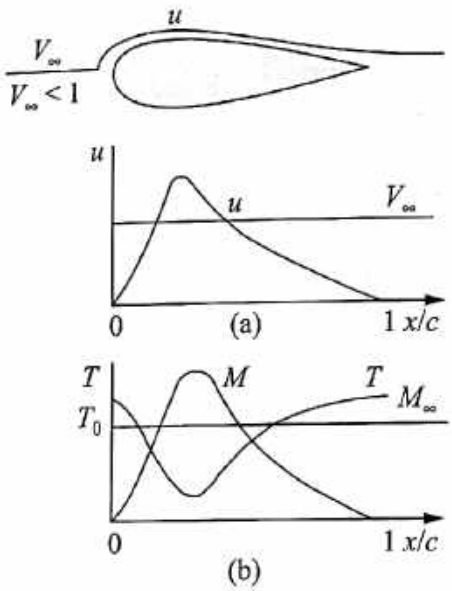


Fig. 8.12 (a) Variation of flow velocity, (b) variation of Mach number and temperature.

This shows that the temperature is maximum at the leading edge, which is a stagnation point, assumes a minimum at the maximum thickness location and then increases towards the trailing edge, as shown in Fig. 8.12(b). The Mach number of the flow increases from zero at the leading edge to the maximum level at the maximum thickness location and then decreases towards the trailing edge. The Mach number variation over the profile depends on the airfoil shape and the angle of attack. Thus, it is evident that as the freestream Mach number M_∞ is increased, the highest local M on the surface may exceed 1 long before M_∞ reaches 1. The value of the freestream Mach number M_∞ at which the highest M on the airfoil first reaches 1 is called the critical Mach number, and is represented as M_∞^*. Note that M_∞^* is a value of the freestream Mach number. M_∞^* is less than 1 for any object with finite thickness.

Calculation of M_∞^*

If the pressure coefficient C_p is known at a lower freestream Mach number M_∞, the critical Mach number can be calculated as follows:

Scanned by CamScanner

We know that the isentropic pressure–Mach number relation is,

$$\frac{p_0}{p} = \left(1 + \frac{\gamma - 1}{2} M^2\right)^{\gamma/(\gamma-1)}$$

where p and p_0 are the local static and stagnation pressures, respectively. If p_∞ and M_∞ are the freestream static pressure and Mach number, respectively, then we can express the local pressure as

$$\frac{p}{p_\infty} = \left[\frac{1 + \frac{\gamma - 1}{2} M_\infty^2}{1 + \frac{\gamma - 1}{2} M^2}\right]^{\gamma/(\gamma-1)}$$

since $p_0 = p_{0_\infty}$ for isentropic flows. The pressure coefficient is defined as

$$C_p = \frac{p - p_\infty}{\frac{1}{2}\rho_\infty V_\infty^2}$$

where ρ_∞ and V_∞^2 are the freestream density and velocity, respectively. The C_p can be expressed, in terms of M_∞, as

$$\begin{aligned} C_p &= \frac{2}{\rho_\infty V_\infty^2} p_\infty \left(\frac{p}{p_\infty} - 1\right) \\ &= \frac{2}{\rho_\infty V_\infty^2} \rho_\infty R T_\infty \left(\frac{p}{p_\infty} - 1\right) \\ &= \frac{2}{\gamma V_\infty^2} \gamma R T_\infty \left(\frac{p}{p_\infty} - 1\right) \\ &= \frac{2}{\gamma M_\infty^2} \left(\frac{p}{p_\infty} - 1\right) \end{aligned}$$

Substituting for p/p_∞, we get the pressure coefficient as

$$C_p = \frac{2}{\gamma M_\infty^2} \left\{ \left(\frac{2 + (\gamma - 1) M_\infty^2}{2 + (\gamma - 1) M^2} \right)^{\gamma/(\gamma-1)} - 1 \right\} \tag{8.56}$$

At the point where the local Mach number $M = 1$, the local pressure coefficient becomes

$$C_p\big|_{M=1} = \frac{2}{\gamma M_\infty^2} \left\{ \left(\frac{2 + (\gamma - 1) M_\infty^2}{\gamma + 1} \right)^{\gamma/(\gamma-1)} - 1 \right\} \tag{8.57}$$

Scanned by CamScanner

This equation can be used to find the critical Mach number, once C_p at the minimum pressure point is known.

At $M_\infty = M_\infty^*$, the local Mach number M reaches 1 somewhere over the aerofoil. The value of C_p at this point can be found by setting $M = 1$.

For any given airfoil, the value of M_∞^* can be found from the value of the minimum C_p on the airfoil.

If the incompressible pressure distribution is known, the $C_{p_{inc}}$ data on the airfoil can be used to get the C_p values at the desired higher freestream Mach number using the Prandtl–Glauert relation, Eq. (8.11b),

$$C_p = \frac{C_{p_{inc}}}{\sqrt{1 - M_\infty^2}}$$

A plot of C_p variation with freestream Mach number is shown in Fig. 8.13.

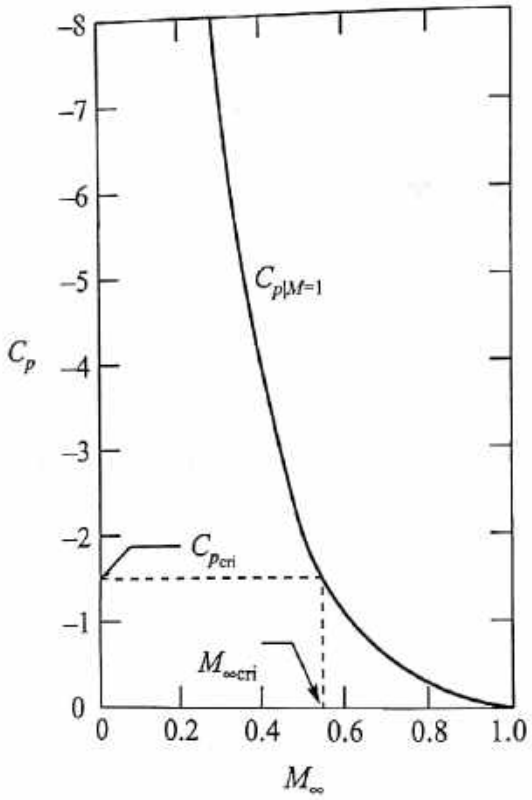


Fig. 8.13 Pressure coefficient variation with freestream Mach number.

EXAMPLE 8.3 If the value of the pressure coefficient at the maximum velocity location on a profile is –2.13, determine the critical Mach number.

Solution Given, $C_{p_{min}} = -2.13$. If this is taken as the pressure coefficient corresponding to $M = 1$, then the freestream Mach number becomes the critical Mach number. Therefore, from Eq. (8.57), we have

$$C_p\big|_{M=1} = \frac{2}{\gamma M_\infty^2}\left\{\left(\frac{2 + (\gamma - 1)M_\infty^2}{\gamma + 1}\right)^{\gamma/(\gamma-1)} - 1\right\}$$

Scanned by CamScanner

$$-2.13 = \frac{2}{1.4M_\infty^2}\left\{\left(\frac{2+0.4M_\infty^2}{2.4}\right)^{3.5} - 1\right\}$$

$$-M_\infty^2 = \frac{2}{1.4\times 2.13}\left\{\left(\frac{2+0.4M_\infty^2}{2.4}\right)^{3.5} - 1\right\}$$

$$= 0.67\left\{\left(\frac{2+0.4M_\infty^2}{2.4}\right)^{3.5} - 1\right\}$$

Solving, we get

$$M_\infty = \boxed{0.5}$$

8.8 SUMMARY

In this chapter, the basic facts about similarity rule for *affinely transformed* shapes are outlined. In a geometrical transformation, if all coordinates in a given direction are changed by a uniform ratio, then the transformation involved is termed *affine*. We have demonstrated in this chapter that it is possible to derive an expression which relates the subsonic compressible flow past a certain profile to the incompressible flow past a second profile derived from the first through an affine transformation. Such an expression is called a *similarity law*.

In many practical applications the similarity laws may be useful. For instance, the Gothert's rule for subsonic flow allows us to predict the details of the compressible subsonic flow past a body at subsonic speeds if we know the details of an incompressible flow past an affinely related body. In the same manner, the supersonic similarity rule shows how experimental data for a certain body at a certain M_∞ can be made applicable to a related body at a different M_∞.

The derivation of similarity laws is a form of dimensional analysis involving *distorted models* rather than geometrically similar models. However, there are a number of differences between these two methods. Dimensional analysis simply lists the dimensionless parameters that are involved, whereas similarity analysis goes much further, showing how to group these dimensionless quantities in such a way as to reduce the number of independent variables. For dimensional analysis we need to know or guess only the variables involved in a problem. But for similarity analysis, we need to know more, for instance, the differential equations and the boundary conditions. Sometimes similarity rules come from a set of experiments.

The Laplace's equations for two-dimensional compressible and incompressible flows, respectively, are

$$(1 - M_\infty^2)\phi_{xx} + \phi_{zz} = 0 \qquad (8.1)$$

$$(\phi_{xx})_{inc} + (\phi_{zz})_{inc} = 0 \qquad (8.2)$$

Scanned by CamScanner

The generalized transformation which transforms Eqs. (8.1) and (8.2) into one another is

$$\left.\begin{aligned} x_{\text{inc}} &= x \\ z_{\text{inc}} &= K_1 z \\ \phi(x, z) &= K_2 \phi_{\text{inc}}(x_{\text{inc}}, z_{\text{inc}}) \end{aligned}\right\} \tag{8.3}$$

where $K_1 = \sqrt{1 - M_\infty^2}$ and K_2 has to be determined from the boundary conditions.

The relation between the geometries of the corresponding profiles is

$$\frac{dz}{dx} = K_2 \sqrt{1 - M_\infty^2} \left(\frac{dz_{\text{inc}}}{dx_{\text{inc}}}\right) \tag{8.7b}$$

which means that the shape of the profile in the compressible flow pattern is $(K_2\sqrt{1 - M_\infty^2})$ times the slope of the corresponding profile in the related incompressible flow pattern.

In the similarity analysis three types of problems, namely,

- the direct problem (version I of P–G. rule), in which the body profile is treated as invariant,
- the indirect problem (version II of P–G rule), which is the case of equal potential (the pressure distributions around the body in incompressible flow and compressible flow are taken to be the same), and
- the streamline analogy (version III), which is also called Gothert's rule,

are considered.

In the direct problem, there is no transformation of geometry at all. Therefore,

$$\frac{dz}{dx} = \frac{dz_{\text{inc}}}{dx_{\text{inc}}} \tag{8.9}$$

In other words, the ratio of angle of attack α, the thickness t and the camber f is

$$\frac{\alpha}{\alpha_{\text{inc}}} = \frac{t}{t_{\text{inc}}} = \frac{f}{f_{\text{inc}}} = 1$$

Then the forces acting in the two flows are related through

$$\frac{C_p}{C_{p_{\text{inc}}}} = \frac{C_L}{C_{L_{\text{inc}}}} = \frac{C_M}{C_{M_{\text{inc}}}} = \frac{1}{\sqrt{1 - M_\infty^2}} \tag{8.11}$$

These equations mean that for the same profile at the same angle of attack the pressure coefficient, lift coefficient, and moment coefficient are all affected by Mach number in proportion to the factor $1/\sqrt{1 - M^2}$.

Scanned by CamScanner

The Prandtl–Glauert rule I also implies that the streamlines around a given profile in compressible flow are farther apart from each other by $1/\sqrt{1-M_\infty^2}$ than in incompressible flow.

The freestream Mach number which gives sonic velocity somewhere on the boundary of an object placed in the fluid stream is called critical Mach number M_∞^*. The critical Mach number M_∞^* decreases with increasing thickness of the body. The freestream Mach number for which the entire flow around the body is subsonic is called the *lower critical Mach number*. The freestream Mach number for which the entire flow around the body is supersonic, is called the *upper critical Mach number*.

In the *indirect problem*, the requirement is to find a transformation, for the profile, by which we can obtain a body in incompressible flow with exactly the same pressure distribution as in the compressible flow. The compressible profile is affinely related to the incompressible profile in such a way that

$$\frac{dz}{dx} = \sqrt{1-M_\infty^2}\,\frac{dz_{\text{inc}}}{dx_{\text{inc}}} \tag{8.13}$$

$$\frac{\alpha}{\alpha_{\text{inc}}} = \frac{t}{t_{\text{inc}}} = \frac{f}{f_{\text{inc}}} = \sqrt{1-M_\infty^2}$$

Then

$$\frac{C_p}{C_{p_{\text{inc}}}} = \frac{C_L}{C_{L_{\text{inc}}}} = \frac{C_M}{C_{M_{\text{inc}}}} = 1 \tag{8.14}$$

These equations mean that the dimensionless pressure distribution, lift coefficient, and moment coefficient will be the same for compressible and incompressible flow if the profiles are affinely related in such a way that the compressible profile is smaller in camber ratio, thickness ratio, and angle of attack by the factor $\sqrt{1-M_\infty^2}$.

By Gothert's rule, we have

$$\frac{\alpha}{\alpha_{\text{inc}}} = \frac{t}{t_{\text{inc}}} = \frac{f}{f_{\text{inc}}} = \frac{1}{\sqrt{1-M_\infty^2}}$$

The aerodynamic coefficients of the given body at the given Mach number M_∞ are given by

$$\frac{C_p}{C_{p_{\text{inc}}}} = \frac{C_L}{C_{L_{\text{inc}}}} = \frac{C_M}{C_{M_{\text{inc}}}} = \frac{1}{1-M_\infty^2} \tag{8.15}$$

This means that if the two profiles are related affinely, the pressure, lift, and moment coefficients for the compressible flow pattern will be greater than those for the related incompressible flow pattern by the factor $1/(1-M_\infty^2)$. In this method, if the lift coefficient of one of these profiles at a finite Mach number M_∞ is required, we have to find, either theoretically or experimentally, the lift

Scanned by CamScanner

coefficient in incompressible flow of an affinely related profile whose camber, thickness ratio, and angle of attack are all smaller than the corresponding values for the original profile by the ratio $\sqrt{1-M_\infty^2}$. Then, by multiplying this lift coefficient by $1/(1-M_\infty^2)$, we find the desired lift coefficient for the compressible flow.

This method of projecting experimental data for incompressible flow is sometimes tedious, since it requires incompressible data for a large range of the thickness ratio. It would be more convenient in many cases to know how the Mach number affects the performance of a profile of fixed slope. The Prandtl–Glauert rule version I yields information of this type.

The similarity rules for supersonic flow are the following:

For Version I:

$$\frac{C_p}{C_p'} = \frac{C_L}{C_L'} = \frac{C_M}{C_M'} = \frac{1}{\sqrt{M_\infty^2-1}} \tag{8.18a}$$

For Version II:

$$\frac{C_p}{C_p'} = \frac{C_L}{C_L'} = \frac{C_M}{C_M'} = 1 \tag{8.18b}$$

For Version III:

$$\frac{C_p}{C_p'} = \frac{C_L}{C_L'} = \frac{C_M}{C_M'} = \frac{1}{M_\infty^2-1} \tag{8.20}$$

In the above relations, the *primed* quantities are for the transformed body and the unprimed ones are for the actual body. Compute the flow about the given body at $M_\infty = \sqrt{2}$. For any other supersonic Mach number, the aerodynamic coefficients are given by Eq. (8.18). In supersonic flow, $M_\infty = \sqrt{2}$ plays the same role as $M_\infty = 0$ in subsonic flow. In version II, the ratios of the aerodynamic forces are equal to unity. In version III, compute the aerodynamic characteristics of the transformed body for $M_\infty = \sqrt{2}$. The aerodynamic characteristics of the given body at the given Mach number M_∞ follow from Eq. (8.20).

For transonic flows, by von Karman rule, we have

$$C_p = \frac{\left(\frac{t}{c}\right)^{2/3}}{[(\gamma+1)\,M_\infty^2]^{1/3}}\,\tilde{C}_p(\chi) \tag{8.21a}$$

$$C_L = \frac{\left(\frac{t}{c}\right)^{2/3}}{[(\gamma+1)\,M_\infty^2]^{1/3}}\,\tilde{C}_L(\chi) \tag{8.21b}$$

Scanned by CamScanner

$$C_D = \frac{\left(\frac{t}{c}\right)^{5/3}}{[(\gamma+1)M_\infty^2]^{1/3}} \tilde{C}_D(\chi) \qquad (8.21c)$$

where

$$\chi = \frac{1 - M_\infty^2}{\left[\left(\frac{t}{c}\right)((\gamma+1)M_\infty^2)\right]^{2/3}}$$

By hypersonic similarity, we have

$$K = M\theta \qquad (8.25)$$

where K is the *hypersonic similarity parameter*.

It is evident from the discussions of this chapter that, if the equations of motion could be solved, the solutions themselves would indicate quite clearly the nature of any similarities which might exist among members of a family of flow patterns. A separate derivation of similarity laws would, therefore, be superfluous. But, in many flow situations of practical interest, we are unable to solve the equations of motion. However, even though solutions are lacking, we may use our knowledge of the forms of the differential equations, along with the associated boundary conditions, and thus derive the similarity laws.

PROBLEMS

1. An aerofoil has the following lift-curve slopes at the Mach numbers given (measurements):

M	0.2	0.3	0.4	0.5	0.6	0.7	0.75
$\frac{dC_L}{d\alpha}$/deg.	0.108	0.113	0.115	0.124	0.130	0.127	0.100

Plot $\frac{dC_L}{d\alpha}$ against M-curve.

2. A slender model with semi-vertex angle $\theta = 3°$ has to operate at $M_\infty = 10$ with angle of attack $\alpha = 3°$. What are the respective angles of attack required to simulate the conditions if a wind tunnel test has to be carried out at (a) $M_\infty = 3.0$, $\theta = 12°$ and (b) $M_\infty = 3.0$, $\theta = 3°$?

[**Ans.** (a) 7.3°; (b) 16.3°]

3. A missile has a conical nose with a semi-vertex angle of 4°, and is subjected to a Mach number of 12 under actual conditions. A model of the missile has to be tested in a supersonic wind tunnel at a test-section Mach number of 2.5. Calculate the semi-vertex angle of the conical nose of the model.

[**Ans.** 19.2°]

Scanned by CamScanner

4. Show that the results of the linearized supersonic theory for flow past a wedge of semi-wedge angle θ may be put into the following similarity form

$$C_p \frac{((\gamma+1)M_\infty^2)^{1/3}}{\theta^{2/3}} = \frac{2}{\chi^{1/2}}$$

where

$$\chi = \frac{M_\infty^2 - 1}{(\theta(\gamma+1)M_\infty^2)^{2/3}}$$

5. Determine the minimum C_p for a wing if the critical Mach number is (a) 0.3 and (b) 0.4.

[**Ans.** (a) –7.22, (b) –3.94]

Scanned by CamScanner

9 Two-Dimensional Compressible Flows

9.1 INTRODUCTION

The equations of motion in terms of velocity potential for steady, irrotational isentropic motion, as derived in Chapter 7, turn out to be nonlinear partial differential equations. Although the equations were derived somewhat easily, exact solutions of these equations for particular flow problems often involve tedious mathematical procedures; in many cases, solutions are not possible. To solve this problem, two courses of action seem to be open:

1. Find exact solutions for a simplified problem in the hope of obtaining a qualitative understanding of the nature of other flow patterns for which solutions are not available.
2. Find simple, though approximate, solutions suitable for practical applications. Both methods of approach yield useful information and in a sense complement each other, as the few exact solutions serve as a check to the validity and reliability of the approximate methods. In this chapter we shall see how the second method may be applied to some important problems of two-dimensional flow.

The assumptions of two-dimensionality itself serves as a first approximation to the flow past the wings of aeroplanes, the flow through the blade system of propellers and of axial-flow in compressors and turbines. In many such applications the perturbation velocities produced by the body immersed in the flow are small, because the bodies are very thin. In this fact lies the essence of the linearized method where the flow pattern may be thought of as the combination of a uniform, parallel velocity with the superposed small perturbation velocities.

The advantage of making such an assumption, as seen in Chapter 7, lies in the fact that the governing equation of motion is greatly simplified and also becomes linear. Further, it is shown in Chapter 7 that from this linearized theory

Scanned by CamScanner

or small perturbation theory, we can draw useful approximate information as to the effect of Mach number for subsonic flow. The linearized theory also makes evident, an approximate similarity law for different flow fields, as seen in Chapter 8.

9.2 GENERAL LINEAR SOLUTION FOR SUPERSONIC FLOW

The fundamental equation governing most of the compressible flow regime, within the frame of small perturbations is [Eq. (7.27)]

$$(1 - M_\infty^2)\phi_{xx} + \phi_{zz} = 0 \tag{9.1}$$

Equation (9.1) is elliptic for $M_\infty < 1$ and hyperbolic for $M_\infty > 1$. There is hardly any method available for analytical solution to the above equation for $M_\infty < 1$. But for $M_\infty > 1$, analytical solutions are available for Eq. (9.1).

Solution of Eq. (9.1) for $M_\infty > 1$ For $M_\infty > 1$, Eq. (9.1) is of the hyperbolic type, with the form being similar to that of the wave equation. The general solution to this equation can be written as the sum of two arbitrary functions f and g such that

$$\phi(x, z) = f(z - x \tan \mu) + g(z + x \tan \mu) \tag{9.2}$$

where μ is the Mach angle and

$$\tan \mu = \frac{1}{\sqrt{M_\infty^2 - 1}} \tag{9.3}$$

The arbitrary functions f and g are to be determined from the boundary conditions for the specific problems.

Proof To show that Eq. (9.2) is the solution to Eq. (9.1) when $M_\infty > 1$, rewrite Eq. (9.2) as

$$\phi = f(\xi) + g(\eta)$$

where ξ and η are the new variables, defined as

$$\xi = z - x \tan \mu, \quad \eta = z + x \tan \mu$$

Therefore,

$$\phi_x = \frac{\partial f}{\partial \xi}\frac{\partial \xi}{\partial x} + \frac{\partial g}{\partial \eta}\frac{\partial \eta}{\partial x} = -f' \tan \mu + g' \tan \mu$$

$$\phi_x = \tan \mu (g' - f')$$

$$\phi_{xx} = \frac{\partial \phi_x}{\partial x} = \tan \mu \left(\frac{\partial g'}{\partial \eta}\frac{\partial \eta}{\partial x} - \frac{\partial f'}{\partial \xi}\frac{\partial \xi}{\partial x} \right)$$

On simplification this yields

$$\phi_{xx} = \tan^2 \mu (f'' + g'') \tag{9.4a}$$

Scanned by CamScanner

$$\phi_z = \frac{\partial f}{\partial \xi}\frac{\partial \xi}{\partial z} + \frac{\partial g}{\partial \eta}\frac{\partial \eta}{\partial z}$$

$$\phi_z = f' + g'$$

Differentiation of the above expression for ϕ_z, with respect to z gives

$$\phi_{zz} = f'' + g'' \tag{9.4b}$$

Substituting Eqs. (9.4) into (9.1), we get

$$(1 - M_\infty^2)\tan^2\mu\,(f'' + g'') + (f'' + g'') = 0$$

This equation is satisfied for $\tan\mu$ from Eq. (9.3). That is, Eq. (9.2) is the general solution of Eq. (9.1). However, the functions f and g differ from problem to problem. Instead of Eq. (9.2), solution to Eq. (9.1) can also be written as

$$\phi(x, z) = f(x - \beta z) + g(x + \beta z) \tag{9.5}$$

where

$$\beta = \cot\mu = \sqrt{M_\infty^2 - 1} \tag{9.6}$$

On inspection of the solution equation (9.2) or (9.5), it is seen that ϕ, and hence, all the flow properties are constant along the straight lines given by the equation

$$z = \pm x\tan\mu + \text{constant}$$

This equation gives two families of straight lines as shown in Fig. 9.1, one family running to the left of the object and the other family running to the right, when viewed in the flow direction.

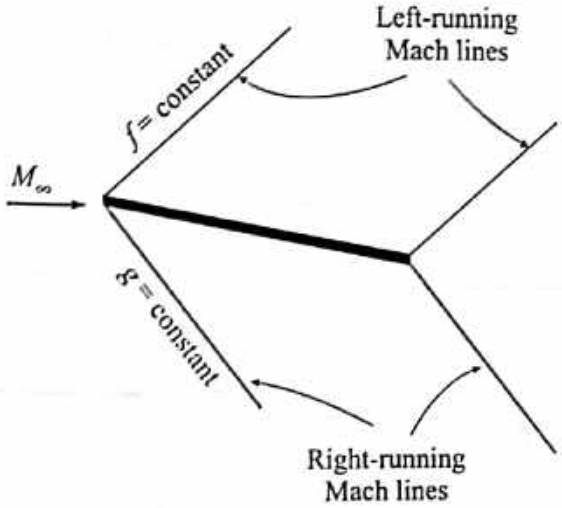


Fig. 9.1 Flat plate in supersonic stream.

These are called Mach lines or characteristics. The lines of constant f that make a positive angle with the flow direction and run to the left of the

Scanned by CamScanner

disturbance (object) are called left-running characteristics and the lines of constant g, making a negative angle with the flow direction and running to the right of object are called right-running characteristics. Depending on the geometry of the object, there will only be left-running or right-running or both the characteristics present in the field as shown in Fig. 9.2.

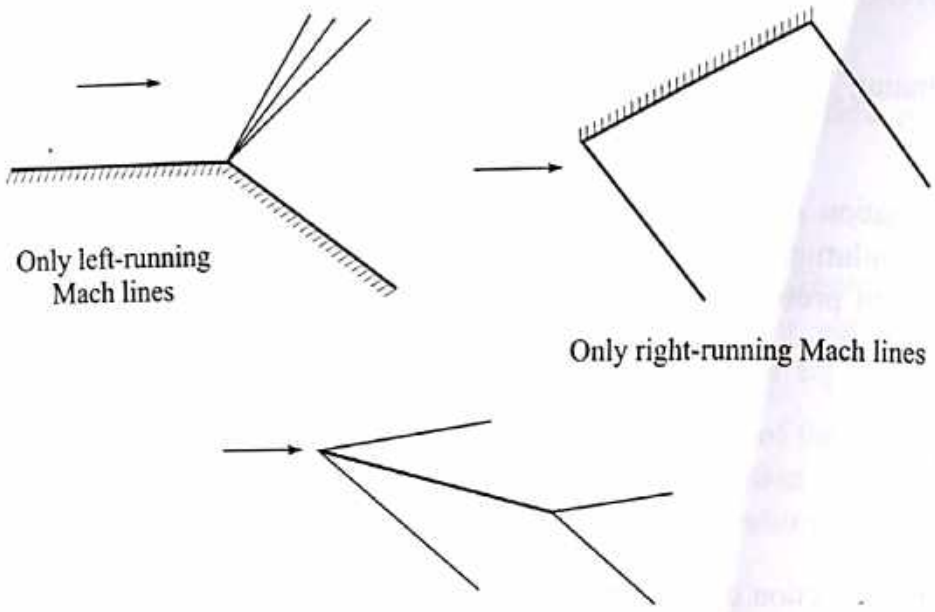
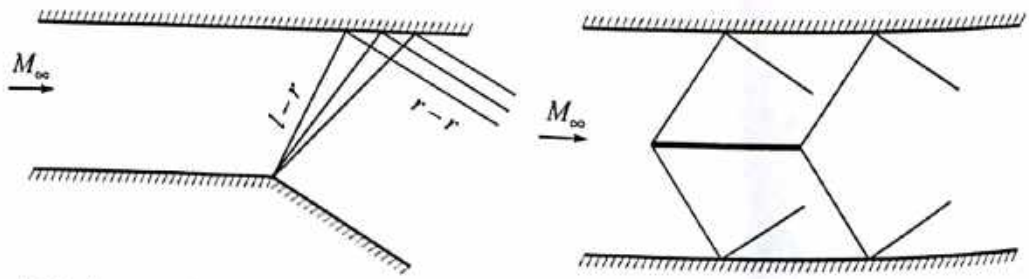


Fig. 9.2 Characteristics on different objects.

Existence of characteristics in a physical problem From the above discussions it is observed that:

1. Disturbances and Mach lines can be produced only by boundaries.
2. Disturbances can travel only in downstream direction.

In Fig. 9.2, we have shown that the characteristics of two families are independent of each other. This is because the geometries chosen are such that on one side of the boundary there is only one family of Mach lines. This is not the case always. In fact, in many situations of practical importance, the opposite characteristics will intersect each other as shown in Figs. 9.3(a) and (b).



(a) Existence of both left- and right-running Mach lines due to reflection

(b) Thin aerofoil in a wind tunnel

Fig. 9.3 Coexistence of left-running ($l-r$) and right-runing ($r-r$) characteristics.

Scanned by CamScanner

By knowing the type of Mach lines present in the problems, the equations can be suitably taken.

From Eq. (9.5), we have the potential function as

$$\phi(x, z) = f(x - \beta z) + g(x + \beta z)$$

where f represents the left-running Mach lines, on which $g = 0$ and g represents the right-running Mach lines, on which $f = 0$. The perturbation velocities are

$$u = \frac{\partial \phi}{\partial x} = \phi_x = f' + g' \tag{9.7}$$

$$w = \frac{\partial \phi}{\partial z} = \phi_z = \beta(g' - f')$$

Then the pressure coefficient is given by Eq. (7.48) as

$$C_p = -2\frac{u}{V_\infty} = -\frac{2}{V_\infty}(f' + g') \tag{9.8}$$

That is, to compute the pressure distribution, we need to know only the derivatives of f and g. There is no need to know the functions f and g themselves.

Equation for the streamlines from kinematic flow condition From Section 7.6, by kinematic flow condition we know that

$$\frac{dz}{dx} = \frac{w}{V_\infty + u} = \frac{w/V_\infty}{1 + u/V_\infty}$$

To make the integration of this equation easier, we write the equation as follows:

$$\frac{dz}{dx} = \frac{w/V_\infty}{1 + \frac{u}{V_\infty} - M_\infty^2 \frac{u}{V_\infty}} = \frac{w/V_\infty}{1 - \beta^2 \frac{u}{V_\infty}}$$

where the denominator $(1 + u/V_\infty)$ has been written as $\left(1 + \frac{u}{V_\infty} - M_\infty^2 \frac{u}{V_\infty}\right)$. This is possible because $u/V_\infty \ll 1$, and so $\left(M_\infty^2 \frac{u}{V_\infty}\right) < 1$. Hence, the error introduced by this change is not significant. Rearranging the above equation, we get

$$V_\infty\, dz\left(1 - \beta^2 \frac{u}{V_\infty}\right) = w\, dx$$

Substituting for u and w from Eq. (9.7), we obtain

$$V_\infty\, dz\left(1 - \frac{\beta^2}{V_\infty}(f' + g')\right) = \beta(g' - f')dx$$

$$V_\infty\, dz = \beta(g'\, dx - f'\, dx) + \beta^2(f'dz + g'dz)$$

Scanned by CamScanner

$$V_\infty dz = \beta[(g'dx + \beta g'dz) - (f'dx - \beta f'dz)]$$
$$= \beta(dg - df)$$

since

$$df = \frac{\partial f}{\partial x}dx + \frac{\partial f}{\partial z}dz = f'dx - \beta f'dz$$

$$dg = \frac{\partial g}{\partial x}dx + \frac{\partial g}{\partial z}dz = g'dx + \beta g'dz$$

Hence,

$$dz = \frac{\beta}{V_\infty}(dg - df)$$

Integrating, we get the result

$$\boxed{z = \frac{\beta}{V_\infty}(g - f) + \text{constant}} \tag{9.9}$$

This is the general solution of supersonic flow. Once the geometry is known, Eq. (9.9) gives g and f and then from Eq. (9.8) C_p, and hence the lift and drag can be calculated. Therefore, in any problem if we are not interested in the geometry of the body present, then it is not necessary to find f and g. It is sufficient if f' and g' are found, to get the C_p, which is very much simpler.

EXAMPLE 9.1 The upper and lower surfaces of a symmetrical two-dimensional aerofoil are given by $z = \pm\varepsilon x(1 - x/c)^2$, where c is the chord and $\varepsilon \ll 1$. The aerofoil is at zero incidence in a steady supersonic stream of Mach number M_∞ in positive x-direction. (a) Find the velocity components according to the linear theory in the upper region of disturbance. (b) Show that the drag coefficient of the aerofoil is given by

$$C_D = \frac{8}{15}\frac{\varepsilon^2}{(M_\infty^2 - 1)^{1/2}}$$

Solution (a) $z = \pm\varepsilon x(1 - x/c)^2$ (i)

The governing equation is

$$\beta^2 \frac{\partial^2 \phi}{\partial x^2} - \frac{\partial^2 \phi}{\partial z^2} = 0$$

$$\phi(x, z) = f(x - \beta z) \quad \text{for } z > 0 \text{ (i.e. above the aerofoil)}$$

where $\beta = \sqrt{M_\infty^2 - 1}$. On the upper surface, the boundary condition is

$$\left(\frac{\partial \phi}{\partial z}\right)_{z=0} = -\beta f'(x) \equiv U\left(\frac{dz}{dx}\right)_{z=0}$$

Scanned by CamScanner

With Eq. (i) the boundary condition becomes

$$\left(\frac{\partial \phi}{\partial z}\right)_{z=0} = U\varepsilon\left(1 - 4\frac{x}{c} + 3\left(\frac{x}{c}\right)^2\right)$$

Therefore,

$$f'(x) = -\frac{U}{\beta}\varepsilon\left(1 - 4\frac{x}{c} + 3\left(\frac{x}{c}\right)^2\right)$$

$$\phi_x = f'(x - \beta z) = -\frac{U}{\beta}\varepsilon\left(1 - \frac{4}{c}(x - \beta z) + \frac{3}{c^2}(x - \beta z)^2\right)$$

$$\phi_z = -\beta f'(x - \beta z) = U\varepsilon\left(1 - \frac{4}{c}(x - \beta z) + \frac{3}{c^2}(x - \beta z)^2\right)$$

(b) $$C_D = \frac{2}{\beta c}\int_0^c (\lambda_u^2 + \lambda_L^2)\,dx = \frac{4}{\beta c}\int_0^c \lambda_t^2\,dx$$

$$\lambda_t = \frac{dz}{dx} = \varepsilon\left(1 - 4\frac{x}{c} + 3\left(\frac{x}{c}\right)^2\right)$$

Substituting λ_t^2 in the equation for C_D and simplifying, we get

$$C_D = \frac{8}{15}\frac{\varepsilon^2}{(M_\infty^2 - 1)^{1/2}}$$

9.3 FLOW ALONG A WAVE-SHAPED WALL

Consider the incompressible flow [Fig. 9.4(a)], compressible subsonic flow [Fig. 9.4(b)] and supersonic flow [Fig. 9.4(c)] of velocity V_∞ over a two-dimensional wave-shaped wall, with wavelength L and amplitude h.

Let the wall be defined by the equation

$$z_w = h\sin(\lambda x) \tag{9.10}$$

In Eq. (9.10), the subscript w stands for wall and $\lambda = 2\pi/L$. Let us assume $h \ll L$, so that linear theory can be applied. By kinematic flow condition [Eq. (7.43)], for $z \to 0$, we have

$$\frac{w}{V_\infty} = \frac{dz_w}{dx} = h\lambda\cos(\lambda x) \tag{9.11}$$

Now, with this background, let us try to solve the governing equation for incompressible flow, compressible subsonic flow, and supersonic flow.

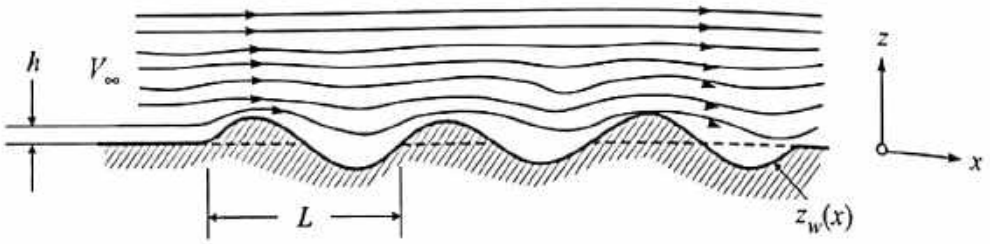
Incompressible flow The governing equation for incompressible flow is the Laplace equation

$$\phi_{xx} + \phi_{zz} = 0$$

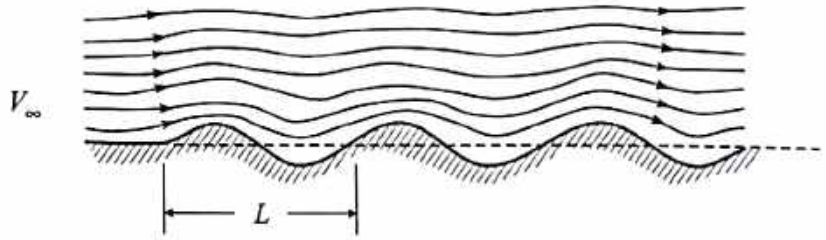
Scanned by CamScanner

This can be solved by expressing the potential function as

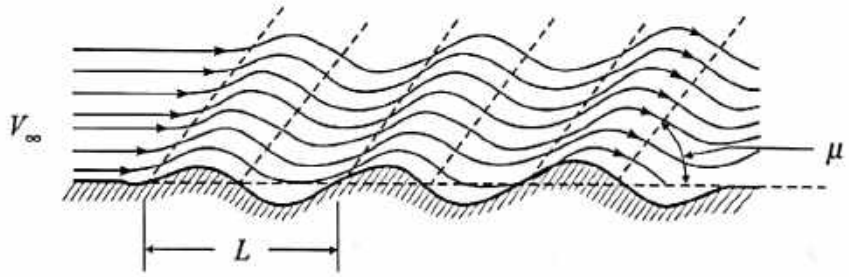
$$\phi(x, z) = F(x)\,G(z)$$



(a) Incompressible flow, $V_\infty << a_\infty$



(b) Subsonic flow, $V_\infty = 0.9a_\infty$



(c) Supersonic flow, $V_\infty = 1.3a_\infty$

Fig. 9.4 Flow past a wave-shaped wall.

Solving by separation of variables, we get

$$\phi(x, z) = -V_\infty h e^{-\lambda z} \cos(\lambda x) \tag{9.12}$$

where this is only the perturbation potential. Obtaining the expression for ϕ, given by Eq. (9.12), is left as an exercise to the reader.

Using Eq. (9.12), we can easily get the resultant velocity U and the perturbation velocity w as

$$U = V_\infty + u = V_\infty[1 + h\lambda e^{-\lambda z} \sin(\lambda x)]$$

$$w = V_\infty h\lambda e^{-\lambda z} \cos(\lambda x) \tag{9.13}$$

Compressible subsonic flow The governing equation for this flow is

$$(1 - M_\infty^2)\phi_{xx} + \phi_{zz} = 0$$

Scanned by CamScanner

Solving as before, we get the result

$$\phi(x, z) = -\frac{V_\infty h}{\sqrt{1 - M_\infty^2}} \exp\left(-\lambda z \sqrt{1 - M_\infty^2}\right) \cos(\lambda x) \qquad (9.14)$$

Hence, we have

$$U = V_\infty + u = V_\infty\left(1 + \frac{h\lambda}{\sqrt{1 - M_\infty^2}} \exp\left(-\lambda z \sqrt{1 - M_\infty^2}\right) \sin(\lambda x)\right)$$

$$w = V_\infty h\lambda \exp\left(-\lambda z \sqrt{1 - M_\infty^2}\right) \cos(\lambda x) \qquad (9.15)$$

Supersonic flow For supersonic flow the governing potential equation is

$$(M_\infty^2 - 1)\phi_{xx} - \phi_{zz} = 0 \qquad (9.16)$$

For this equation, by Eq. (9.5), we have the solution as

$$\phi(x, z) = f(x - \beta z) + g(x + \beta z)$$

where $\beta = \cot \mu = \sqrt{M_\infty^2 - 1}$.

From the geometry of the problem under consideration, since the disturbances can move only in the direction of flow, there can be only left-running Mach lines, as shown in Fig. 9.4(c). Therefore,

$$\phi(x, z) = f(x - \beta z), \quad g = 0$$

Hence, the perturbation velocity w on the wall is

$$w_w = \left(\frac{\partial \phi}{\partial z}\right)_{z=0} = -\beta(f'(x - \beta z))_{z=0} = -\beta f'(x)$$

Equating this to w given by Eq. (9.11), we get

$$f'(x) = -\frac{V_\infty}{\beta} \lambda h \cos(\lambda x)$$

$$f(x) = -\frac{V_\infty h \sin(\lambda x)}{\beta}$$

This is only on the wall. In general,

$$\phi(x, z) = f(x - \beta z)$$

$$\phi(x, z) = -\frac{V_\infty}{\beta} h \sin(\lambda(x - \beta z)) \qquad (9.17)$$

i.e.

$$\phi(x, z) = -\frac{V_\infty h}{\sqrt{M_\infty^2 - 1}} \sin(\lambda(x - \sqrt{M_\infty^2 - 1}\, z)) \qquad (9.18)$$

Scanned by CamScanner

Therefore,

$$U = V_\infty + u = V_\infty \left(1 - \frac{h\lambda}{\sqrt{M_\infty^2 - 1}}\right) \cos\left(\lambda\left(x - \sqrt{M_\infty^2 - 1}\ z\right)\right)$$

$$w = V_\infty h\lambda \cos\left(\lambda\left(x - \sqrt{M_\infty^2 - 1}\ z\right)\right) \tag{9.19}$$

The ϕ here is only the disturbance potential, and if the total potential is required, add $(V_\infty x)$ to ϕ.

Pressure coefficient The fundamental form of expression for the coefficient of pressure applicable to two-dimensional compressible flow, with the frame of small perturbations, given by Eq. (7.48), is

$$C_p = -2\frac{u}{V_\infty}$$

Therefore, in the present problem:

1. $C_p = -2h\lambda e^{-\lambda z} \sin(\lambda x)$ for incompressible flow

2. $C_p = -\dfrac{2h\lambda}{\sqrt{1 - M_\infty^2}} \exp\left(-\lambda z\sqrt{1 - M_\infty^2}\right) \sin(\lambda x)$

for subsonic compressible flow

3. $C_p = \dfrac{2h\lambda}{\sqrt{M_\infty^2 - 1}} \cos\left[\lambda\left(x - \sqrt{M_\infty^2 - 1}\ z\right)\right]$ for supersonic flow

On the surface of the wall ($z = 0$), the above results reduce to

$$C_p = -2h\lambda \sin(\lambda x) \quad \text{for incompressible flow} \tag{9.20}$$

$$C_p = -\frac{2h\lambda}{\sqrt{1 - M_\infty^2}} \sin(\lambda x) \quad \text{for subsonic flow} \tag{9.21}$$

$$C_p = \frac{2h\lambda}{\sqrt{M_\infty^2 - 1}} \cos(\lambda x) \quad \text{for supersonic flow} \tag{9.22}$$

In the above solution we did not get f directly. The results are obtained from f'. If only C_p on the wall is needed, it is not necessary to find f, since the C_p on the wall is given by Eq. (9.8).

$$C_p = -\frac{2}{V_\infty}(f' + g')$$

Usually, for aerodynamic applications, only C_p on the wall is necessary.

From the plots of incompressible, compressible subsonic, and supersonic flow over the wave-shaped wall, shown in Fig. 9.4, the following observations can be made:

Scanned by CamScanner

1. For $M_\infty = 0$, the disturbances die down rapidly because of the $e^{-\lambda z}$ term in C_p expression.
2. For $M_\infty < 1$, the larger the M_∞, the slower is the dying down of disturbances in the transverse direction to the wall.
3. For $M_\infty = 1$, the disturbances do not die down at all (of course the equations derived in this chapter cannot be used for transonic flows).
4. For $M_\infty > 1$, the disturbances do not die down at all. The disturbance can be felt even at ∞ (far away from the wall) if the flow is inviscid.

Further, for equal perturbations, we have

$$x - z\sqrt{M_\infty^2 - 1} = \text{constant}$$

As $z \to \infty$,

for $M_\infty < 1$, the disturbances vanish

for $M_\infty > 1$, the disturbances are finite and they do not die down at all

Equation (9.21) is symmetric with respect to wall geometry and Eq. (9.22) is asymmetric with respect to wall geometry. Therefore, when C_p is integrated along x, for $M_\infty < 1$, the integral goes to zero and for $M_\infty > 1$, the integral > 0. In other words, in subsonic flow, the pressure coefficient is in phase with the wall shape so that there is no drag force on the wall, but in supersonic flow, the pressure coefficient is out of phase with the wall shape, and hence there is drag force acting on the wall.

9.4 SUMMARY

In this chapter, the governing equation for compressible flow, derived with small perturbation assumption, has been solved for the specific flow situation of flow past a wave-shaped wall, highlighting the importance of Mach number in compressible flow analysis.

The governing equation for compressible flow, within the frame of small perturbation, is

$$(1 - M_\infty^2)\phi_{xx} + \phi_{zz} = 0 \tag{9.1}$$

This equation is elliptic for $M_\infty < 1$ and hyperbolic for $M_\infty > 1$.

For $M_\infty > 1$, Eq. (9.1) is similar to the wave equation. The general solution can be written as

$$\phi(x, z) = f(z - x \tan \mu) + g(z + x \tan \mu) \tag{9.2}$$

where f and g are arbitrary functions and μ is the Mach angle.

It can be inferred from Eq. (9.2) that the velocity potential ϕ, and hence all the flow properties, are constant along the straight lines given by the equation

$$z = \pm x \tan \mu + \text{constant}$$

This equation gives the left-running and the right-running characteristics.

Scanned by CamScanner

The general solution for supersonic flow is given by

$$z = \frac{\beta}{V_\infty}(g - f) + \text{constant} \tag{9.9}$$

Once the geometry is known, Eq. (9.9) gives g and f and then from Eq. (9.8), C_p, and hence the lift and drag can be calculated.

For flow along a wave-shaped wall, the solutions are:

- for incompressible flow the perturbation potential is

$$\phi(x, z) = -V_\infty h e^{-\lambda z} \cos(\lambda x) \tag{9.12}$$

- for compressible subsonic flow,

$$\phi(x, z) = -\frac{V_\infty h}{\sqrt{1 - M_\infty^2}} \exp(-\lambda z \sqrt{1 - M_\infty^2}) \cos(\lambda x) \tag{9.14}$$

- for supersonic flow,

$$\phi(x, z) = -\frac{V_\infty h}{\sqrt{M_\infty^2 - 1}} \sin(\lambda (x - \sqrt{M_\infty^2 - 1}\ z)) \tag{9.18}$$

In subsonic flow, the pressure coefficient is in phase with the wall shape, and so there is no drag force on the wall. But in supersonic flow, the pressure coefficient is out of phase with the wall and, therefore, there is drag force acting on the wall.

PROBLEMS

1. A shallow irregularity of length l, in a plane wall, shown in Fig. P9.1, is given by the expression $y = kx(1 - x/l)$, where $0 < x < l$ and $k \ll 1$. A uniform supersonic stream with freestream Mach number M_∞ is flowing over it. Using linearized theory, show that the velocity potential due to disturbance in the flow is

$$\phi(x, y) = -\frac{U_\infty}{\beta} k(x - \beta y)\left(1 - \frac{x - \beta y}{l}\right)$$

where $\beta = \sqrt{M_\infty^2 - 1}$.

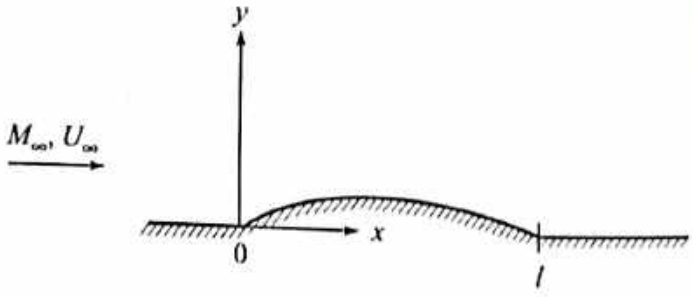


Fig. P9.1

Scanned by CamScanner

2. A two-dimensional wing profile shown in Fig. P9.2 is placed in stream of Mach number 2.5 at an incidence of 2°. Using linearized theory, calculate C_L and C_D.

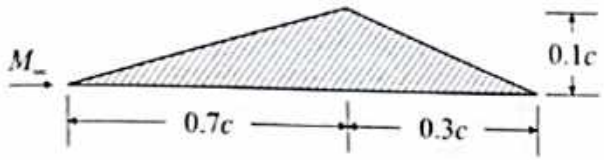


Fig. P9.2

[**Ans.** 0.06096 and 0.04372]

3. A two-dimensional thin aerofoil shown in Fig. P9.3 is placed in a stream with Mach number 3.0 and is at an angle of attack of 2°. Using linearized theory, estimate C_{p_u} and C_{p_l}.

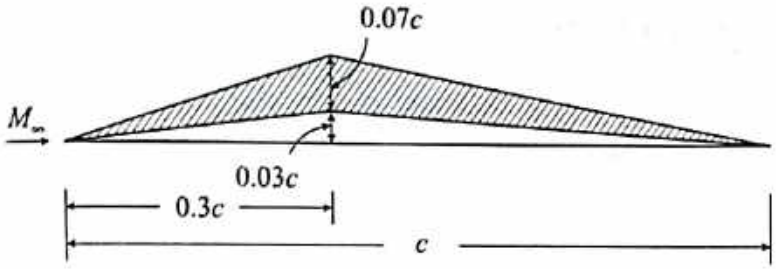


Fig. P9.3

[**Ans.** $C_{p_u} = 0.211$, $C_{p_l} = 0.046 (0 \le x \le 0.3c)$
$C_{p_u} = -0.1258$, $C_{p_l} = -0.0551 (0.3c \le x \le c)$]

Scanned by CamScanner

10 Prandtl–Meyer Flow

10.1 INTRODUCTION

When a supersonic flow is turned into itself as discussed in Section 6.1, an oblique shock is formed as illustrated in Fig. 6.1(a). This is directly opposite to the situation when the flow is turned away from itself, with the consequent expansion fan as sketched in Fig. 6.1(b).

The expansion fan emanating from a sharp convex corner such as that sketched in Figs. 6.1(b) and 10.1 is called a centred expansion fan. A theory for this was first worked out by Prandtl in 1907, followed by Meyer in 1908 and therefore, it is referred to as *Prandtl–Meyer expansion wave* and the flow through these waves is called *Prandtl–Meyer flow*.

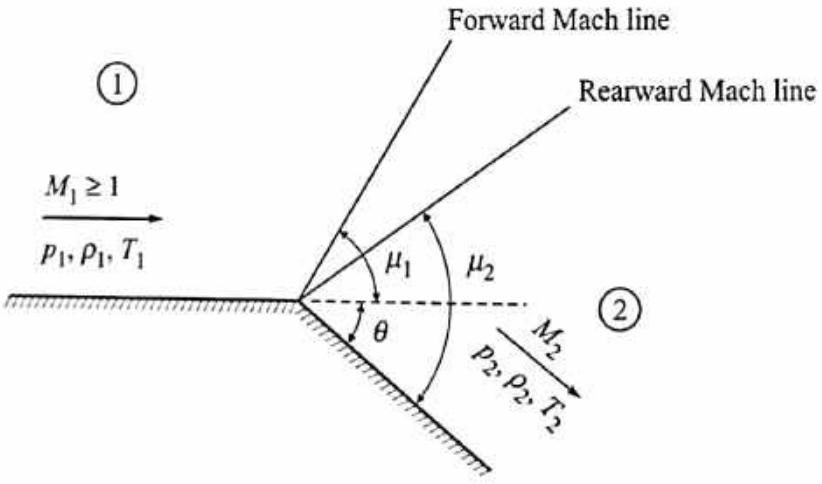


Fig. 10.1 Prandtl–Meyer expansion.

The Prandtl–Meyer flow plays a vital role in supersonic flow analysis, since, in many practical situations like supersonic flow over a convex corner, flow at the exit of an underexpanded supersonic nozzle and so on, the flow expands

Scanned by CamScanner

through the Prandtl–Meyer fan. Further, this flow forms the basis for the development of "method of characteristics" (discussed in Chapter 12).

10.2 THERMODYNAMIC CONSIDERATIONS

Consider a two-dimensional, supersonic flow over a convex corner as shown in Fig. 10.1. The mechanism of this flow, turning through a finite angle, is discussed in detail in Sections 6.7 and 6.8. From that discussion, it is clear that the expansion at a convex corner occurs through a centred expansion wave, defined by a "fan" of straight Mach lines. We may notice the following qualitative aspects of flow through an expansion fan:

1. $M_2 > M_1$, i.e. an expansion corner is a means to increase the flow Mach number.
2. $p_2/p_1 < 1$, $\rho_2/\rho_1 < 1$, and $T_2/T_1 < 1$, i.e. the pressure, density and temperature of the flow decrease through an expansion wave.
3. The expansion fan is a continuous expansion region, composed of an infinite number of Mach lines, bounded upstream and downstream by μ_1 and μ_2 respectively (Ref. Fig. 10.1), where $\mu_1 = \arcsin(1/M_1)$ and $\mu_2 = \arcsin(1/M_2)$.
4. Streamlines through an expansion wave are smooth curved lines.
5. Since the expansion takes place through a large number of Mach lines in continuous succession, and $ds = 0$ for each Mach line, the expansion is isentropic.

The above observations are based on the results of Chapter 6, where it has been shown that an expansion of flow can take place only gradually through an infinite number of Mach lines. Further, it is emphasized that there is no possibility of an oblique shock occurring at an expansion or convex corner (Section 6.8).

10.3 PRANDTL–MEYER EXPANSION FAN

From the discussions on oblique shock and expansion waves (Chapter 6), it is well known that supersonic expansion flow around a convex corner involves a smooth, gradual change in the flow properties. The Prandtl–Meyer fan consists of a series of Mach lines, centred at the convex corner. The initial line is inclined to the approach flow at an angle $\mu_1 = \arcsin(1/M_1)$; the final line is inclined to the downstream flow at an angle $\mu_2 = \arcsin(1/M_2)$, as illustrated in Fig. 10.2.

By Eq. (6.36), it is also known that the component of flow velocity normal to the wave at each point in the flow is equal to the local velocity of sound. Therefore, flow conditions along each Mach line are uniform; the variation of pressure, density, temperature, and velocity, through the expansion fan is only a function of angular position.

Scanned by CamScanner

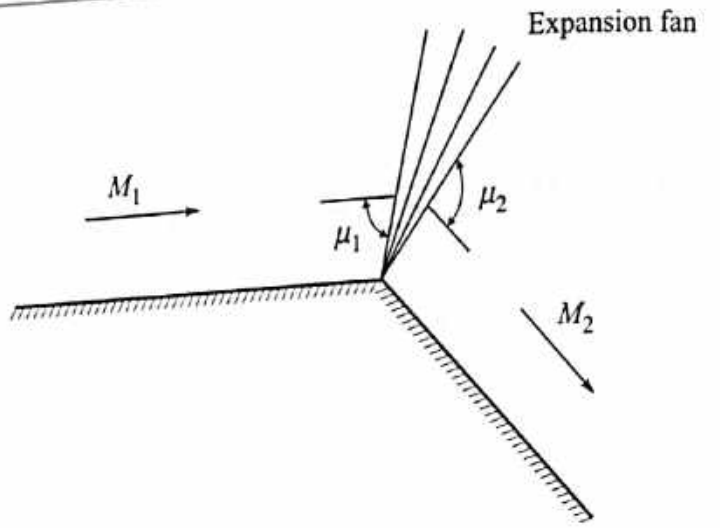


Fig. 10.2 Prandtl–Meyer expansion fan.

We are familiar with the fact that from the discussions of Chapter 6, the Prandtl–Meyer expansion is a self-similar motion and the Prandtl–Meyer function, ν, is a similarity variable. By Eq. (6.47), we have the expression for Prandtl–Meyer function as

$$\boxed{\nu = \sqrt{\frac{\gamma+1}{\gamma-1}} \arctan \sqrt{\frac{\gamma-1}{\gamma+1}(M^2-1)} - \arctan\sqrt{M^2-1}}$$

The Prandtl–Meyer function represents the angle through which a flow, initially at $M = 1$, must be expanded to reach a supersonic Mach number M. The values of ν as a function of Mach number, for $\gamma = 1.4$, have been tabulated in isentropic flow tables (Table A1 of Appendix A).

To calculate the angle through which a flow would have to be turned to expand from M_1 to M_2, with M_1 not equal to 1, it is necessary only to subtract the value of ν_1 at M_1 from the value of ν_2 at M_2.

The variation of pressure, temperature, and density of the flow through the expansion can be found from the thermodynamic relations for isentropic flow (Chapter 2). For isentropic process, with no pressure loss,

$$\frac{p_2}{p_1} = \left(\frac{1 + \frac{\gamma-1}{2} M_1^2}{1 + \frac{\gamma-1}{2} M_2^2} \right)^{\gamma/(\gamma-1)}$$

$$\frac{T_2}{T_1} = \frac{1 + \frac{\gamma-1}{2} M_1^2}{1 + \frac{\gamma-1}{2} M_2^2}$$

Scanned by CamScanner

$$\frac{\rho_2}{\rho_1} = \left(\frac{1 + \frac{\gamma - 1}{2} M_1^2}{1 + \frac{\gamma - 1}{2} M_2^2} \right)^{1/(\gamma - 1)}$$

EXAMPLE 10.1 A uniform supersonic stream at Mach 2.2 expands around two convex corners of 10° each, as shown in Fig. 10.3. Determine the Mach number downstream of the second corner and the angle of the second fan.

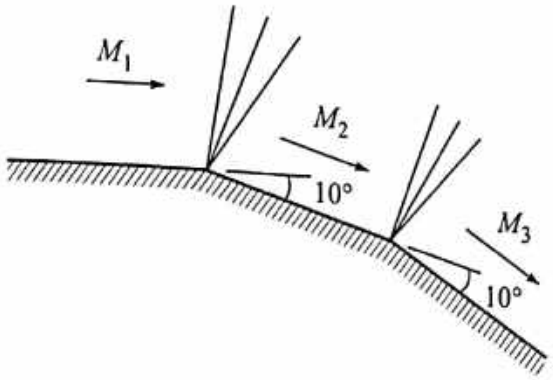


Fig. 10.3 Example 10.1.

Solution After expanding through the first and second fans, the flow must be parallel to the second and third segments of the wall respectively. That is, the initial wave of the second fan is parallel to the final wave of the first fan. Also, the distance between the fans can have no effect on the resultant flow, since the flow between the fans is uniform. Therefore, the flow acceleration is the same whether it is expanded through two 10° turns or one 20° turn.

From isentropic tables (Table A1 of Appendix A), for $M_1 = 2.2$, $\nu_1 = 31.732°$. Thus,

$$\nu_2 = \nu_1 + \theta_1 = 31.732° + 10° = 41.732°$$
$$\nu_3 = \nu_2 + \theta_2 = 41.732° + 10° = 51.732°$$

Alternatively,

$$\nu_3 = \nu_1 + 20° = 51.732°$$

For $\nu_3 = 51.732°$ (from Table A1 of the Appendix A)

$$M_3 = \boxed{3.106}$$

For $\nu_2 = 41.732°$, from the same table,

$$M_2 = 2.615$$

Now,

$$\mu_2 - \mu_3 = 22.483° - 18.781° = 3.702°$$

The angle of the second fan $= \nu_3 - \nu_2 + \mu_2 - \mu_3 = 10° + 3.702° = \boxed{13.702°}$

Scanned by CamScanner

EXAMPLE 10.2 The underexpanded, two-dimensional nozzle shown in Fig. 10.4, exhausts into an atmosphere with $p = 10^5$ N/m^2. For uniform flow at the nozzle exit, with $p = 2 \times 10^5$ N/m^2 and $M = 2.2$, determine the Mach number and flow direction after the initial expansion.

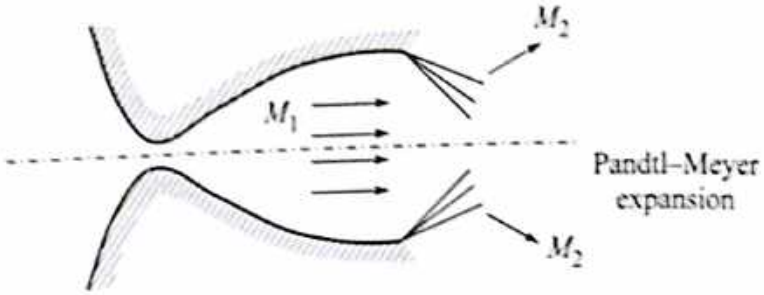


Fig. 10.4 Example 10.2.

Solution The flow at the exit expands through the Prandtl–Meyer expansion fan. From Table A1 in Appendix A, for $M_1 = 2.2$, $\nu_1 = 31.732°$, $p_1/p_{t1} = 0.0935$,

$$p_{t1} = \frac{p_1}{0.0935} = \frac{2 \times 10^5}{0.0935} = 21.39 \times 10^5 \text{ N/m}^2$$

The flow through the Prandtl–Meyer expansion is isentropic and, therefore, we have

$$p_{t1} = p_{t2}$$

Thus,

$$\frac{p_2}{p_{t2}} = \frac{10^5}{21.39 \times 10^5} = 0.0467$$

From the same table, for $\dfrac{p_2}{p_{t2}} = 0.0467$,

$$M_2 = \boxed{2.645}, \quad \nu_2 = 42.419°$$

The flow direction after the initial expansion is

$$\nu_2 - \nu_1 = 42.419° - 31.732° = \boxed{10.687°}$$

10.4 REFLECTIONS

Examine the impingement of a Prandtl–Meyer expansion fan on a plane wall, as illustrated in Fig. 10.5.

Now, sufficient waves must be generated to maintain the boundary condition at the wall; that is, at the wall boundary the flow must be parallel to the wall. Each Mach line of the incident Prandtl–Meyer fan must reflect as an expansion Mach line. This is in agreement with the fact that the reflection of an incident wave from a solid boundary is like, i.e. a shock wave will reflect as a shock and an expansion wave will reflect as an expansion wave (Section 6.11). The resultant wave interactions result in a nonsimple region that

Scanned by CamScanner

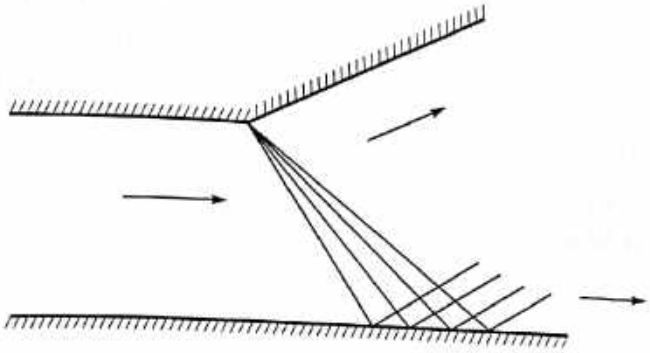


Fig. 10.5 Expansion fan impingement on a plane wall.

render an exact analysis of the flow extremely difficult; however, the general nature of the flow can be recognized. The expansion that occurs at the exit of an underexpanded, two-dimensional nozzle, sketched in Fig. 10.6 is a typical example of the flow with simple and nonsimple regions.

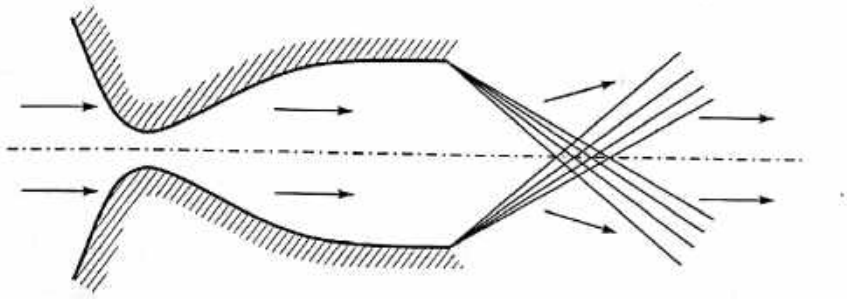


Fig. 10.6 Flow through an underexpanded nozzle.

The flow is symmetrical about the centre line, and therefore, there can be no flow across the central streamline. Also, this central streamline can be replaced by a slid wall. By doing so, we get a flow situation equivalent to that sketched in Fig. 10.3.

10.5 SUMMARY

In the strict sense, we have only consolidated some of the salient features of expansion flow under the heading Prandtl–Meyer flow in this chapter. The usefulness of this will be felt while dealing with the flow process involving acceleration of supersonic flow. Further, this type of flow plays an important role in designing nozzles to generate supersonic flow. The designing technique and procedure for supersonic nozzle will be discussed in Chapter 12.

PROBLEMS

1. A reservoir containing air at 33.5×10^5 N/m^2 is connected to ambient air at atmospheric pressure through a Laval nozzle with design Mach

Scanned by CamScanner

number 2.0, with axial flow at the nozzle exit plane. Under these conditions, the nozzle is underexpanded, with a Prandtl–Meyer fan at the exit. Find the flow direction after the initial expansion.
[**Ans.** After initial expansion, the flow is at 22° with respect to nozzle axis]

2. For flow at Mach 2.3 over the protrusion shown in Fig. P10.2, find M_2, M_3, M_4, T_2, T_3 and T_4.

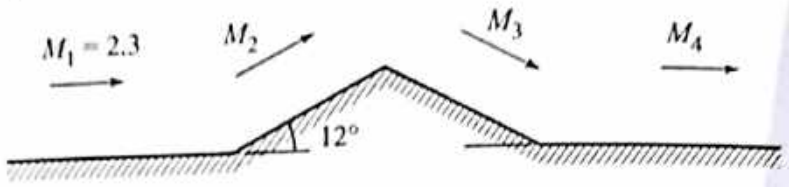


Fig. P10.2

[**Ans.** $M_2 = 1.815$, $M_3 = 2.764$, $M_4 = 2.09$, $T_2 = 617.5$ K, $T_3 = 405.7$ K, $T_4 = 524.9$ K]

3. An underexpanded, two-dimensional supersonic nozzle exhausts into a region, where $p = 240$ mm of mercury (suction). Flow at nozzle exit plane is uniform, with $p = 275$ mm of mercury and $M = 2.0$. Determine the flow direction and Mach number after the initial expansion.

[**Ans.** Mach number = 2.44 and flow direction is 11.33° away from the nozzle axis] *Note*: Compare this problem with Problem 6.5.

Scanned by CamScanner

11 Flow with Friction and Heat Transfer

11.1 INTRODUCTION

So far, we have discussed compressible flow of gases in ducts, where changes in flow properties were brought about solely by area change, i.e. where effects of viscosity are neglected. But, in a real flow situation like stationary power plants, aircraft propulsion engines, high-vacuum technology, transport of natural gas in long pipe lines, transport of fluids in chemical process plants, and various types of flow systems, the high-speed flow travels through passages of sufficient length, the effects of viscosity (friction) cannot be neglected. In many practical flow situations, friction may even have a decisive effect on the resultant flow characteristics. The inclusion of friction terms in the equations of motion makes the analysis of the problem far more complex. In this chapter, we intend to discuss such flows from a simple one-dimensional point of view.

11.2 FLOW IN CONSTANT-AREA DUCT WITH FRICTION

Consider one-dimensional steady flow of a perfect gas, with constant specific heats, through a constant-area duct. Also, let there be neither external heat exchange nor external shaft work and let differences in elevation produce negligible changes compared to frictional effects. The flow with the above-mentioned conditions, namely, *adiabatic flow with no external work*, is called *Fanno line flow*.

Let the wall friction (due to viscosity) be the chief factor bringing about changes in fluid properties, for the adiabatic compressible flow through ducts of constant-area under consideration.

Scanned by CamScanner

The energy equation of steady flow under the above assumptions may be written [Eq. (2.15)] as

$$h + \frac{V^2}{2} = h_0 \tag{11.1}$$

where h and V are respectively the corresponding values of the enthalpy and velocity at an arbitrary section of the duct, and h_0 (the stagnation enthalpy) has a constant value for all sections of the duct.

By equation of continuity,

$$\frac{\dot{m}}{A} = \rho V = G \tag{11.2}$$

where ρ is the density at the section where V and h are measured, and G is called the *mass velocity*, which has a constant value for all sections of the duct.

Combining Eqs. (11.1) and (11.2), we get the equation of the Fanno line in terms of the enthalpy and density as

$$h = h_0 - \frac{G^2}{2\rho^2} \tag{11.3}$$

Since h_0 and G are constants for a given flow, Eq. (11.3) defines a relation between the local density and the local enthalpy. This relation defines families of curves (the particular curve depending on the choice of the parameters G and h_0) in the plane of any two thermodynamic variables; in Fig. 11.1, this relation is shown graphically in the h–v plane, for a single value of h_0 and for several values of G. Such curves are, in general, called *Fanno lines*.

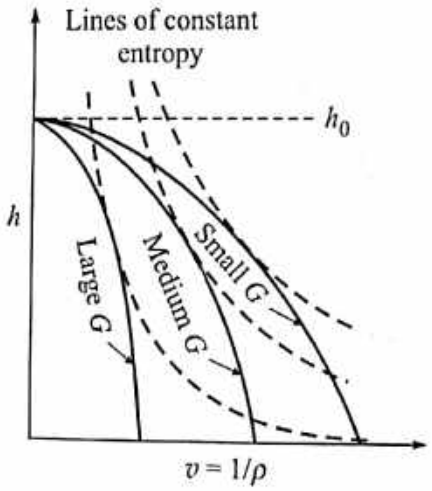


Fig. 11.1 Fanno lines on $h-v$ plane.

The Fanno Line

For a pure substance,

$$s = s(h, \rho)$$

That is, the entropy is determined by the enthalpy and density. The curves of Fig. 11.1 may thus be transferred to the enthalpy–entropy diagram, giving the

Scanned by CamScanner

familiar *Fanno curves* of Fig. 11.2. For all substances so far investigated, the Fanno curves have the general shape shown in Fig. 11.2. The three curves shown in Fig. 11.2 have the same stagnation enthalpy but different mass flow rates per unit area.

We know by the Second Law of Thermodynamics that for an adiabatic flow, the entropy may increase but cannot decrease. Thus, in Fig. 11.2, the path of states along any one of the Fanno curves must be towards the right. Therefore, if the flow at some point in the duct is subsonic (point "a" of Fig. 11.2), the effect of friction will be to increase the velocity and Mach number and to decrease the enthalpy and pressure of the stream. On the other hand, if the flow is initially supersonic (point "b" of Fig. 11.2), the effect of friction will be to decrease the velocity and Mach number and to increase the enthalpy and pressure of the stream. A subsonic flow may therefore never become supersonic, and a supersonic flow may never become subsonic, unless a discontinuity is present. Thus we observe that, as in the case of isentropic flow, the qualitative character of the flow is markedly influenced by the flow speed, i.e. whether it is subsonic or supersonic.

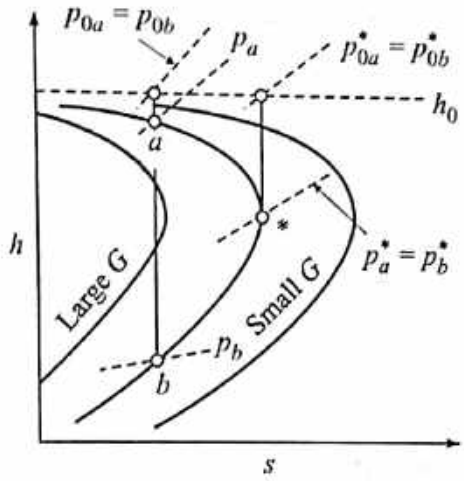


Fig. 11.2 Fanno lines on $h-s$ diagram.

The limiting pressure, beyond which the entropy would decrease, occurs at Mach number unity and is denoted by p^*. The "asterisk" here denotes the state where $M = 1$, for the particular case of adiabatic flow through ducts of constant area.

From Fig. 11.2 it is seen that the isentropic stagnation pressure is reduced as a result of friction, irrespective of whether the flow is subsonic or supersonic.

11.3 ADIABATIC, CONSTANT-AREA FLOW OF A PERFECT GAS

In this section, the fluid is assumed to be perfect so as to make the analytical treatment of the problem simpler. Further, with this assumption, it becomes

Scanned by CamScanner

possible to draw broad conclusions which would not be otherwise apparent. The aim here is to express in analytical form the variations in flow characteristics along the length of a duct of constant area. This requires the introduction of momentum equation, with a term accounting for the frictional forces acting on the control volume, since the rate of change of flow properties depends on the amount of friction. In Chapter 2, the isentropic relations were derived by writing the various physical relations for two sections a finite distance apart. To demonstrate another method of approach, let us carry out the present analysis in differential form.

Select an infinitesimal control volume as shown in Fig. 11.3. In the figure, τ_w is the shear stress due to friction, acting on the wall of the duct. For a perfect gas,

$$p = \rho RT$$

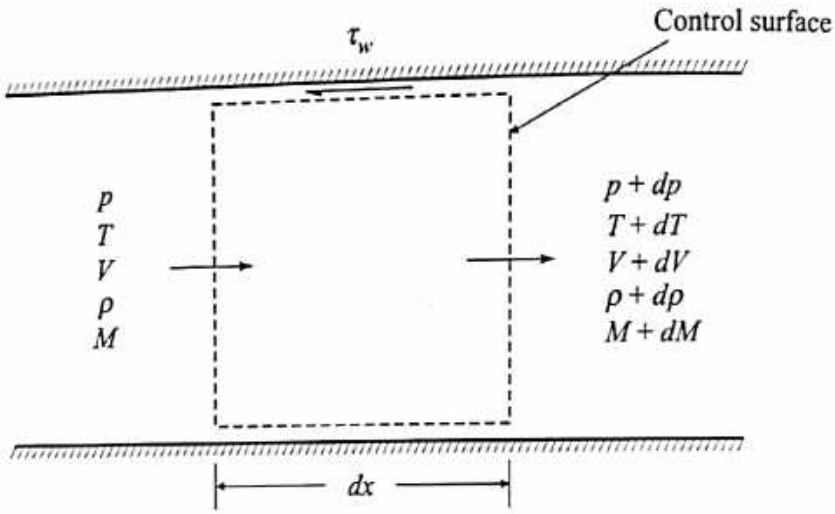


Fig. 11.3 Control surface for the analysis of adiabatic, constant-area flow.

This relation may also be expressed as

$$\frac{dp}{p} = \frac{d\rho}{\rho} + \frac{dT}{T} \tag{11.4}$$

By definition of the Mach number,

$$M^2 = \frac{V^2}{\gamma RT}$$

This gives

$$\frac{dM^2}{M^2} = \frac{dV^2}{V^2} - \frac{dT}{T} \tag{11.5}$$

The energy equation for a perfect gas gives

$$c_p dT + d\left(\frac{V^2}{2}\right) = 0$$

Scanned by CamScanner

Dividing throughout by $c_p T$, and using the definition of Mach number, we get

$$\frac{dT}{T} + \frac{\gamma - 1}{2} M^2 \frac{dV^2}{V^2} = 0 \tag{11.6}$$

The continuity equation (relation (11.2)) is

$$G = \frac{\dot{m}}{A} = \rho V$$

Noting that G is a constant, this equation can be expressed as

$$\frac{d\rho}{\rho} + \frac{1}{2}\frac{dV^2}{V^2} = 0 \tag{11.7}$$

Referring to Fig. 11.3, the momentum balance gives

$$-A\,dp - \tau_w dA_w = \dot{m}\,dV$$

where A is the cross-sectional area of duct and dA_w is the wetted wall area of the duct over which τ_w acts.

Definition of Friction Coefficient

The coefficient of drag, or the coefficient of friction, as it is generally referred to for flow in ducts, is defined as

$$f = \frac{\text{wall shearing stress}}{\text{dynamic head of the stream}}$$

$$f = \frac{\tau_w}{\frac{1}{2}\rho V^2}$$

It is a common practice in such analysis to use a parameter called hydraulic diameter D, defined as

$$D = \frac{4(\text{cross-sectional area})}{\text{wetted perimeter}}$$

$$D = \frac{4A}{\frac{dA_w}{dx}} = 4\frac{A}{dA_w}dx$$

The advantage of using hydraulic diameter is that the equations in terms of hydraulic diameter are valid even for ducts with noncircular cross-section.

Introducing the above f and D along with continuity equation into the momentum equation, we get

$$-dp - 4f\frac{\rho V^2}{2}\frac{dx}{D} = \frac{\dot{m}}{A}dV = \rho V^2\frac{dV}{V}$$

Dividing throughout by p and expressing $\rho V^2 = \gamma p M^2$, we obtain

$$\frac{dp}{p} + \frac{\gamma M^2}{2} 4f\frac{dx}{D} + \frac{\gamma M^2}{2}\frac{dV^2}{V^2} = 0 \tag{11.8}$$

Scanned by CamScanner

The isentropic stagnation pressure p_0 is given by Eq. (2.49) as

$$p_0 = p\left(1+\frac{\gamma-1}{2}M^2\right)^{\gamma/(\gamma-1)}$$

i.e.

$$\frac{dp_0}{p_0} = \frac{dp}{p} + \frac{\gamma M^2/2}{1+\frac{\gamma-1}{2}M^2}\frac{dM^2}{M^2} \tag{11.9}$$

Now, we may define a new parameter called *impulse function* F as

$$\boxed{F \equiv pA + \rho AV^2 = pA(1+\gamma M^2)}$$

After noting that A is a constant, this may be expressed in differential form in terms of p and M, as

$$\frac{dF}{F} = \frac{dp}{p} + \frac{\gamma M^2}{1+\gamma M^2}\frac{dM^2}{M^2} \tag{11.10}$$

Effects of Wall Friction on Fluid Properties

Now we see that the simultaneous algebraic Eqs. (11.4)–(11.10) relate eight differential variables:

$$\frac{dp}{p},\quad \frac{d\rho}{\rho},\quad \frac{dT}{T},\quad \frac{dM^2}{M^2}$$

$$\frac{dV^2}{V^2},\quad \frac{dp_0}{p_0},\quad \frac{dF}{F},\quad \frac{4fdx}{D}$$

The physical phenomenon causing changes in flow properties is the viscous friction. Hence, we choose the variable $4fdx/D$ as independent. Now, solving the seven equations as simultaneous equations for the remaining seven variables, we can obtain

$$\frac{dM^2}{M^2} = \frac{\gamma M^2\left(1+\frac{\gamma-1}{2}M^2\right)}{1-M^2}4f\frac{dx}{D} \tag{11.11}$$

$$\frac{dp}{p} = -\frac{\gamma M^2(1+(\gamma-1)M^2)}{2(1-M^2)}4f\frac{dx}{D} \tag{11.12}$$

$$\frac{dV}{V} = \frac{\gamma M^2}{2(1-M^2)}4f\frac{dx}{D} \tag{11.13}$$

$$\frac{dT}{T} = \frac{1}{2}\frac{da}{a} = -\frac{\gamma(\gamma-1)M^4}{2(1-M^2)}4f\frac{dx}{D} \tag{11.14}$$

Scanned by CamScanner

$$\frac{d\rho}{\rho} = -\frac{\gamma M^2}{2(1-M^2)} 4f\frac{dx}{D} \tag{11.15}$$

$$\frac{dp_0}{p_0} = -\frac{\gamma M^2}{2} 4f\frac{dx}{D} \tag{11.16}$$

$$\frac{dF}{F} = -\frac{\gamma M^2}{2(1+\gamma M^2)} 4f\frac{dx}{D} \tag{11.17}$$

Second Law of Thermodynamics

For an adiabatic flow, the stagnation temperature is invariant. Therefore, from Eq. (2.33), the entropy change can be expressed as

$$\frac{ds}{c_p} = -\frac{\gamma-1}{\gamma}\frac{dp_0}{p_0} \tag{11.18}$$

Substituting for dp_0/p_0, from Eq. (11.16), we have

$$\frac{ds}{c_p} = \frac{(\gamma-1)M^2}{2} 4f\frac{dx}{D} \tag{11.19}$$

The Second Law of Thermodynamics states that entropy should not decrease in an adiabatic flow process. Therefore, from Eq. (11.19), it follows that the friction coefficient f must always be a positive quantity, since by convention dx in Eq. (11.9) is positive in the direction of flow.

In Fig. 11.3 we have marked the shear stress in a direction opposite to that of the flow. Since f must always be positive, we conclude that the shear stress must always act in a direction opposite to the flow, as marked in the figure.

From Eqs. (11.11) to (11.17), for flow parameters in terms of f, it may be summarized that

1. For subsonic inlet flow, the effect of friction on the downstream flow is such that:
   (a) Pressure p decreases
   (b) Mach number M increases
   (c) Velocity V increases
   (d) Temperature T decreases
   (e) Density ρ decreases
   (f) Stagnation pressure p_0 decreases
   (g) Impulse function F decreases.
2. For supersonic inlet flow, the effect of friction on the downstream flow is such that:
   (a) Pressure p increases
   (b) Mach number M decreases
   (c) Velocity V decreases

Scanned by CamScanner

(d) Temperature T increases
(e) Density ρ increases
(f) Stagnation pressure p_0 decreases
(g) Impulse function F decreases.

From the above summary we may observe that the friction has the net effect of accelerating a subsonic stream, and causes a rise in static pressure at supersonic speeds.

Working Relations

Equations (11.11)–(11.19) can be integrated to result in formulae suitable for practical calculations. Let the Mach number be the independent variable for this purpose. Then Eq. (11.11) may be rearranged to give

$$\int_0^{L_{max}} 4f\frac{dx}{D} = \int_{M^2}^{1} \frac{1-M^2}{\gamma M^4\left(1+\frac{\gamma-1}{2}M^2\right)}\,dM^2$$

where the integration limits are taken as the section where the Mach number is M, and where x is arbitrarily set equal to zero, and as the section where Mach number is unity, and x is the maximum possible length of duct, L_{max}.

On integration, the above equation yields

$$\boxed{4\bar{f}\frac{L_{max}}{D} = \frac{1-M^2}{\gamma M^2} + \frac{\gamma+1}{2\gamma}\ln\left[\frac{(\gamma+1)M^2}{2\left(1+\frac{\gamma-1}{2}M^2\right)}\right]} \qquad (11.20)$$

where $\bar{f}$ is the mean friction coefficient with respect to duct length defined by

$$\bar{f} = \frac{1}{L_{max}}\int_0^{L_{max}} f\,dx$$

Equation (11.20) gives the maximum value of $4f(L/D)$ corresponding to any initial Mach number M.

Since $4\bar{f}(L_{max}/D)$ is a function only of M, the duct length required for the flow to pass from a given initial Mach number M_1 to a given final Mach number M_2 is obtained from the expression

$$4\bar{f}\frac{L}{D} = \left(4\bar{f}\frac{L_{max}}{D}\right)_{M_1} - \left(4\bar{f}\frac{L_{max}}{D}\right)_{M_2} \qquad (11.21)$$

Similarly, the local flow properties can be found in terms of local Mach number. Indicating the properties at $M = 1$ as superscripted with "asterisk", and integrating between the duct sections with Mach number M and 1, we obtain [from Eqs. (11.12)–(11.17) and (11.19)]

$$\frac{p}{p^*} = \frac{1}{M}\left[\frac{\gamma+1}{2\left(1+\frac{\gamma-1}{2}M^2\right)}\right]^{1/2} \qquad (11.22)$$

Scanned by CamScanner

$$\frac{V}{V^*} = M\left[\frac{\gamma+1}{2\left(1+\frac{\gamma-1}{2}M^2\right)}\right]^{1/2} \tag{11.23}$$

$$\frac{T}{T^*} = \frac{a^2}{a^{*2}} = \frac{\gamma+1}{2\left(1+\frac{\gamma-1}{2}M^2\right)} \tag{11.24}$$

$$\frac{\rho}{\rho^*} = \frac{V^*}{V} = \frac{1}{M}\left[\frac{2\left(1+\frac{\gamma-1}{2}M^2\right)}{\gamma+1}\right]^{1/2} \tag{11.25}$$

$$\frac{p_0}{p_0^*} = \frac{1}{M}\left[\frac{2\left(1+\frac{\gamma-1}{2}M^2\right)}{\gamma+1}\right]^{(\gamma+1)/2(\gamma-1)} \tag{11.26}$$

$$\frac{F}{F^*} = \frac{1+\gamma M^2}{M\left[2(\gamma+1)\left(1+\frac{\gamma-1}{2}M^2\right)\right]^{1/2}} \tag{11.27}$$

$$\frac{s-s^*}{c_p} = \ln M^2\left[\frac{(\gamma+1)}{2M^2\left(1+\frac{\gamma-1}{2}M^2\right)}\right]^{(\gamma+1)/2\gamma} \tag{11.28}$$

We know that the quantities marked with asterisk in these equations are constants for a given adiabatic constant-area flow. Therefore, they may be regarded as convenient reference values for normalizing the equations. To find the change in a flow property, say the density, between sections of the duct where the Mach numbers are M_1 and M_2, we set

$$\frac{\rho_2}{\rho_1} = \frac{\left(\frac{\rho}{\rho^*}\right)_{M_2}}{\left(\frac{\rho}{\rho^*}\right)_{M_1}}$$

where $\left(\frac{\rho}{\rho^*}\right)_{M_1}$ is the value on the right-hand side of Eq. (11.25) corresponding to M_1, and so on.

The variation of dimensionless ratios given by Eqs. (11.20) and (11.22)–(11.27) with Mach number is tabulated in Table A4 of Appendix A.

EXAMPLE 11.1 Atmospheric air at pressure 1.0135×10^5 N/m^2 and temperature 300 K is drawn through a frictionless bell-mouth entrance into a 3 m long tube having a 0.05 m diameter. The average friction coefficient $\overline{f} = 0.005$, for the tube. The system is perfectly insulated.

Scanned by CamScanner

(a) Find the maximum mass flow rate and the range of backpressure that will produce this flow.

(b) What is the exit pressure required to produce 90% of the maximum mass flow rate, and what will be the stagnation pressure and the velocity at the exit for that mass flow rate?

Solution (a) The mass flow rate will be maximum for choked flow conditions. For choked flow,

$$4\bar{f}\frac{L_{max}}{D} = \frac{4 \times 0.005 \times 3}{0.05} = 1.2$$

For $4\bar{f}\frac{L_{max}}{D} = 1.2$, from Fanno flow table (Table A4 of Appendix A),

$$M_1 = 0.485, \quad \frac{p_1}{p^*} = 2.2076, \quad \frac{T_1}{T^*} = 1.146$$

From isentropic table (Table A1 of Appendix A) for $M_1 = 0.485$,

$$\frac{p_1}{p_0} = 0.851, \quad \frac{T_1}{T_0} = 0.955$$

Therefore,

$$p_1 = (0.851)(1.0135 \times 10^5) = 8.62 \times 10^4 \text{ N/m}^2$$

$$T_1 = (0.955)(300) = 286.5 \text{ K}$$

$$p^* = \frac{p_1}{2.2076} = 3.90 \times 10^4 \text{ N/m}^2$$

$$T^* = \frac{T_1}{1.146} = 250 \text{ K}$$

$$\rho^* = \frac{p^*}{RT^*} = 0.543 \text{ kg/m}^3$$

$$a^* = \sqrt{\gamma RT^*} = \sqrt{1.4 \times 287 \times 250} = 316.94 \text{ m/s}$$

The maximum mass flow rate is

$$\dot{m}^* = \rho^* a^* A = 0.544 \times 316.94 \times \frac{\pi}{4}(0.05)^2$$

$$\dot{m}^* = \boxed{0.3385 \text{ kg/s}}$$

The range of backpressure (p_b) that would produce this flow is

$$\boxed{p_b \le p^* = 3.90 \times 10^4 \text{ N/m}^2}$$

(b) 90% of $\dot{m}^*$ is

$$\dot{m}^* = 0.9 \times 0.3385 = 0.3047 \text{ kg/s}$$

$$G = \frac{\dot{m}}{A} = 155.16 \text{ kg/s-m}^2$$

Scanned by CamScanner

$$\rho_1 V_1 = G = \frac{\dot{m}}{A}, \quad p_1 M_1 \sqrt{\frac{\gamma}{RT_1}} = G$$

$$\frac{p_1}{p_0}\sqrt{\frac{T_0}{T_1}}\, M_1 = \sqrt{\frac{R}{\gamma}}\frac{\sqrt{T_0}}{p_0} G = \frac{\sqrt{\gamma R T_0}}{\gamma}\frac{G}{p_0}$$

$$= \frac{\sqrt{1.4 \times 287 \times 300}}{1.4}\frac{155.16}{1.0135 \times 10^5}$$

$$= 0.3797$$

Solving this for M_1, by trial and error method, we get

$$M_1 = 0.42$$

From isentropic table, for $M_1 = 0.42$,

$$\frac{p_1}{p_0} = 0.886, \quad p_1 = 8.98 \times 10^4 \text{ N/m}^2$$

$$\frac{T_1}{T_0} = 0.966, \quad T_1 = 289.8 \text{ K}$$

By Eq. (11.21),

$$4\bar{f}\frac{L}{D} = 1.2 = \left(4\bar{f}\frac{L_{\max}}{D}\right)_{M_1} - \left(4\bar{f}\frac{L_{\max}}{D}\right)_{M_2}$$

Using Eq. (11.20) or the Fanno flow table, for $M_1 = 0.42$,

$$\left(4\bar{f}\frac{L_{\max}}{D}\right)_{M_1} = 1.9744$$

Hence,

$$1.2 = 1.9744 - \left(4\bar{f}\frac{L_{\max}}{D}\right)_{M_2}$$

i.e.

$$\left(4\bar{f}\frac{L_{\max}}{D}\right)_{M_2} = 0.7744$$

For this value of $4\bar{f}\,(L_{\max}/D)$ from Fanno flow table,

$$M_2 = 0.541$$

Now, using Fanno table, for $M_1 = 0.42$,

$$\frac{p_1}{p^*} = 2.563, \quad \frac{T_1}{T^*} = 1.159, \quad \frac{p_{01}}{p_0^*} = 1.529$$

and for $M_2 = 0.541$

$$\frac{p_2}{p^*} = 1.96, \quad \frac{T_2}{T^*} = 1.134, \quad \frac{p_{02}}{p_0^*} = 1.264$$

Scanned by CamScanner

Therefore,

$$p_2 = \frac{p_2}{p^*}\frac{p^*}{p_1}p_1 = \boxed{6.867\times10^4\ \text{N/m}^2}$$

$$T_2 = \frac{T_2}{T^*}\frac{T^*}{T_1}T_1 = 283.5\ \text{K}$$

$$p_{02} = \frac{p_{02}}{p_0^*}\frac{p_0^*}{p_{01}}p_{01} = \boxed{8.378\times10^4\ \text{N/m}^2}$$

$$a_2 = \sqrt{\gamma RT_2} = 337.5\ \text{m/s}$$

The exit velocity

$$V_2 = M_2a_2 = 0.541 \times 337.5$$
$$= \boxed{182.59\ \text{m/s}}$$

EXAMPLE 11.2 A straight pipe of 0.05 m diameter is attached to a large air reservoir at pressure 13.8×10^5 N/m^2 and temperature 310 K. The exit of the pipe is open to atmosphere. Assuming adiabatic flow with an average friction coefficient of 0.005, calculate the pipe length necessary to obtain a mass flow rate of 2.25 kg/s.

Solution Let the subscripts 1 and 2 refer to conditions at entry and exit of the pipe, respectively. Given

$$\dot{m} = 2.25\ \text{kg/s}$$

By Eq. (11.2), the mass velocity is

$$G = \frac{\dot{m}}{A} = \frac{2.25}{(\pi/4)(0.05)^2} = 0.1146 \times 10^4\ \text{kg/s-m}^2$$

Also,

$$G = p_1M_1\left(\frac{\gamma}{RT_1}\right)^{1/2} = p_2M_2\left(\frac{\gamma}{RT_2}\right)^{1/2} = \text{constant}$$

Now, $$p_1M_1\left(\frac{\gamma}{RT_1}\right)^{1/2} = G$$

can be rewritten as

$$\frac{p_1}{p_0}\left(\frac{T_0}{T_1}\right)^{1/2}M_1 = \left(\frac{R}{\gamma}\right)^{1/2}G\frac{T_0^{1/2}}{p_0} = \frac{\sqrt{\gamma RT_0}}{\gamma}\frac{G}{p_0} \qquad \text{(i)}$$

$$= \frac{352.9}{1.4} \times \frac{0.1146\times10^4}{13.8\times10^5}$$

$$= 0.209$$

Scanned by CamScanner

The L.H.S. of Eq. (i) has three parameters and out of them the pressure ratio and temperature ratio are uniquely related to Mach number. By trials, we can solve this equation as follows: Let $M_1 = 0.21$. Then

$$\text{L.H.S.} = \frac{0.21 \times 0.9697}{\sqrt{0.9913}} = 0.2045$$

$$\text{L.H.S.} < \text{R.H.S.}$$

Let $M_1 = 0.22$. Then

$$\text{L.H.S.} = \frac{0.22 \times 0.9668}{\sqrt{0.9904}} = 0.2137$$

$$\text{L.H.S.} > \text{R.H.S.}$$

Hence, M_1 lies between 0.21 and 0.22. For $M_1 = 0.213$, L.H.S. is nearly equal to R.H.S. Therefore, $M_1 = 0.213$ can be taken as the correct solution. For this value of M_1,

$$\frac{p_1}{p_0} = 0.969, \quad \frac{p_1}{p^*} = 5.12$$

Thus,

$$p_1 = 13.37 \times 10^5 \text{ N/m}^2$$
$$p^* = 2.611 \times 10^5 \text{ N/m}^2$$

For $M_1 = 0.213$, from Eq. (11.20),

$$4f \frac{L_{max}}{D} = 12.11$$

Therefore,

$$L_{max} = \frac{12.11 \times 0.05}{4 \times 0.005} \text{m}$$

$$L_{max} = \boxed{30.275 \text{ m}}$$

11.4 FLOW WITH HEATING OR COOLING IN DUCTS

So far we have considered only the effects of area change and friction on gas flow process. From one-dimensional aspect, there is yet another effect producing continuous changes in the state of flowing stream and this third factor is called *energy effect*. External heat exchange, combustion, or moisture condensations are examples of energy effects. In the discussion on the effects of area change on flow state, we considered the process to be isentropic with frictional and energy effects absent. In Section 11.2 we dealt with the effects of wall friction in the absence of area change and energy effects; the corresponding process is described by the Fanno curve and may aptly be termed *simple friction*.

Scanned by CamScanner

In this section, we discuss processes involving change in the stagnation temperature or the stagnation enthalpy of a gas stream which flows at constant area and without frictional effects. Though a process involving a simple T_0 change is difficult to achieve in practice, many useful conclusions of practical significance may be drawn by analyzing the process of simple T_0 change. These conclusions can be expected to have a higher degree of validity when the departures from the assumptions of the model are small.

Governing Equations

For the flow of gas through a constant-area duct without friction, the momentum equation may be written as

$$p + \rho V^2 = \frac{F}{A} = \text{constant} \tag{11.29}$$

By continuity,

$$\rho V = \frac{\dot{m}}{A} = G = \text{constant} \tag{11.30}$$

Combining Eqs. (11.29) and (11.30), we get

$$p + \frac{G^2}{\rho} = \frac{F}{A} \tag{11.31}$$

For constant values of G and F/A, Eq. (11.31) defines a unique relation between pressure and density, called Rayleigh line. Since both the enthalpy h and entropy s are functions of p and ρ, Eq. (11.31) may be used for representing Rayleigh line on the h–s diagram, as illustrated in Fig. 11.4. In general, most of the fluids in practical use have Rayleigh curves of the general form shown in Fig. 11.4.

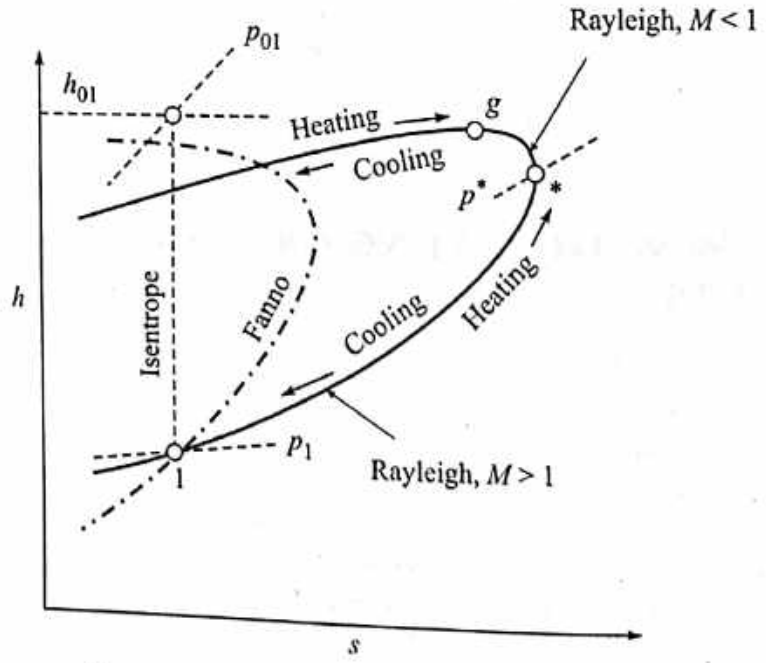


Fig. 11.4 Rayleigh curve for simple T_0-change.

Scanned by CamScanner

The portion of the Rayleigh curve above the point of maximum entropy usually corresponds to subsonic flow and the portion below the maximum entropy point corresponds to supersonic flow. The process of simple heating is thermodynamically reversible; therefore, heat addition should correspond to an entropy increase and heat rejection must correspond to an entropy decrease. Therefore, the Mach number is increased by heating and decreased by cooling, at subsonic speeds. On the other hand, the Mach number is decreased by heating and increased by cooling, at supersonic speeds. Thus, like friction, the heat addition also always tends to make the Mach number in the duct approach unity. Cooling causes the Mach number to change always in the direction away from unity.

For heat addition at either subsonic or supersonic speeds, the amount of heat input cannot be greater than that for which the leaving Mach number is unity. If the heat addition is too large, the flow will be choked, i.e. the initial Mach number will be reduced to a magnitude which is consistent with the specified amount of heat input.

Simple-Heating Relations for a Perfect Gas

As in Section 11.3, we shall describe the flow of a perfect gas through a constant-area duct. Let there be no friction. Consider the control volume shown in Fig. 11.5.

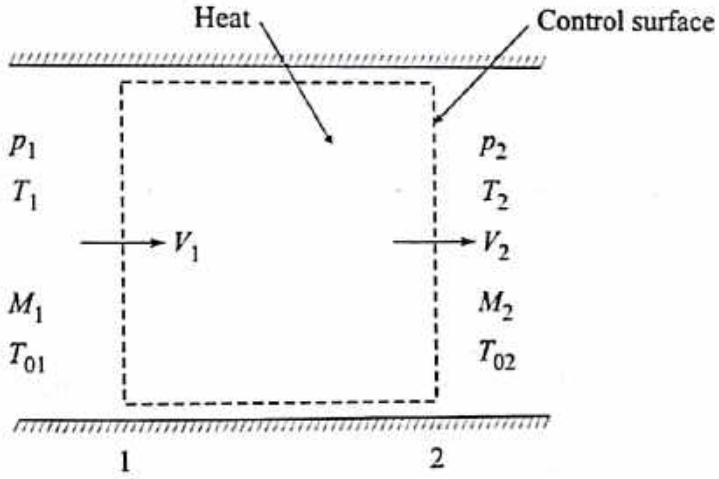


Fig. 11.5 Control volume for Rayleigh flow.

For the flow through the constant-area duct, by continuity,

$$\frac{\rho_2}{\rho_1} = \frac{V_1}{V_2} \tag{11.32}$$

The momentum balance in the absence of friction gives

$$p_1 - p_2 = \frac{\dot{m}}{A}(V_2 - V_1)$$

Scanned by CamScanner

But $\dot{m}/A = \rho V$ and $\rho V^2 = \gamma p M^2$ (for perfect gas). Using these relations, the above momentum equation may be rewritten as

$$\frac{p_2}{p_1} = \frac{1+\gamma M_1^2}{1+\gamma M_2^2} \tag{11.33}$$

By the state equation,

$$\frac{p_2}{p_1} = \frac{\rho_2 T_2}{\rho_1 T_1} \tag{11.34}$$

The Mach number ratio between states 1 and 2 can be expressed as

$$\frac{M_2}{M_1} = \frac{V_2 a_1}{V_1 a_2} = \frac{V_2}{V_1}\sqrt{\frac{T_1}{T_2}} \tag{11.35}$$

Similarly, for impulse function,

$$\frac{F_2}{F_1} = \frac{p_2(1+\gamma M_2^2)}{p_1(1+\gamma M_1^2)}$$

Using Eq. (11.33), we get

$$\frac{F_2}{F_1} = 1 \tag{11.36}$$

The isentropic stagnation pressure ratio is given by Eq. (2.49) as

$$\frac{p_{02}}{p_{01}} = \frac{p_2}{p_1}\frac{\left(1+\dfrac{\gamma-1}{2}M_2^2\right)^{\gamma/(\gamma-1)}}{\left(1+\dfrac{\gamma-1}{2}M_1^2\right)^{\gamma/(\gamma-1)}} \tag{11.37}$$

The entropy change may be found from Eq. (2.35) as

$$\frac{s_2 - s_1}{c_p} = \ln\frac{T_2/T_1}{(p_2/p_1)^{(\gamma-1)/\gamma}} \tag{11.38}$$

So far, we have seen the relation between the parameters at two different states of the process. All these changes are brought about due to changes in stagnation temperature. That is, the rate of change of stream properties along Rayleigh lines is a function of the rate of change of stagnation temperature. From the energy relation, the stagnation temperature T_0 is

$$T_0 = T + \frac{V^2}{2c_p} = T\left(1+\frac{V^2}{2c_pT}\right) = T\left(1+\frac{\gamma-1}{2}M^2\right)$$

Therefore,

$$\frac{T_{02}}{T_{01}} = \frac{T_2}{T_1}\frac{1+\dfrac{\gamma-1}{2}M_2^2}{1+\dfrac{\gamma-1}{2}M_1^2} \tag{11.39}$$

Scanned by CamScanner

For the process involving only heat exchange, the change in stagnation temperature is a direct measure of the amount of heat transfer. If Q is the heat added to the control volume, then by the energy equation,

$$Q = c_p(T_2 - T_1) + \frac{V_2^2 - V_1^2}{2} = c_p(T_{02} - T_{01}) \tag{11.40}$$

Equations (11.32)–(11.34) may be combined to result in

$$\frac{T_2}{T_1} = \frac{M_2^2}{M_1^2}\frac{(1+\gamma M_1^2)^2}{(1+\gamma M_2^2)^2} \tag{11.41}$$

Using Eq. (11.41) in Eq. (11.39), we get

$$\frac{T_{02}}{T_{01}} = \frac{M_2^2}{M_1^2}\frac{(1+\gamma M_1^2)^2}{(1+\gamma M_2^2)^2}\frac{\left(1+\frac{\gamma-1}{2}M_2^2\right)}{\left(1+\frac{\gamma-1}{2}M_1^2\right)} \tag{11.42}$$

Equations (11.41) and (11.42) express the static and stagnation temperature ratios between states 1 and 2 in terms of Mach numbers at these states.

Following the same procedure as that in Section 11.3, we can get the following normalized expressions (working formulae) for the present flow process involving only heat transfer:

$$\frac{T}{T^*} = \frac{(\gamma+1)^2 M^2}{(1+\gamma M^2)^2} \tag{11.43}$$

$$\frac{T_0}{T_0^*} = \frac{2(\gamma+1)M^2\left(1+\frac{\gamma-1}{2}M^2\right)}{(1+\gamma M^2)^2} \tag{11.44}$$

$$\frac{V}{V^*} = \frac{\rho^*}{\rho} = \frac{(\gamma+1)M^2}{1+\gamma M^2} \tag{11.45}$$

$$\frac{p}{p^*} = \frac{\gamma+1}{1+\gamma M^2} \tag{11.46}$$

$$\frac{p_0}{p_0^*} = \frac{\gamma+1}{1+\gamma M^2}\left[\frac{2\left(1+\frac{\gamma-1}{2}M^2\right)}{1+\gamma}\right]^{\gamma/(\gamma-1)} \tag{11.47}$$

$$\frac{s-s^*}{c_p} = \ln M^2\left(\frac{\gamma+1}{1+\gamma M^2}\right)^{(\gamma+1)/\gamma} \tag{11.48}$$

Also,

$$\frac{T_{02}}{T_{01}} = \frac{(T_0/T_0^*)_{M_2}}{(T_0/T_0^*)_{M_1}} \tag{11.49}$$

where $(T_0/T_0^*)_{M_2}$ is given by Eq. (11.44), and so on. The variation of the dimensionless ratios given by Eqs. (11.43)–(11.47) with Mach number is tabulated in Table A5 of Appendix A.

Scanned by CamScanner

From our discussions on Reyleigh flow and the properties relations the physical trends associated with flow with simple T_0-change may be summarized as follows:

1. For *subsonic flow* ($M_1 < 1$), when heat is added:
   (a) Pressure decreases, $p_2 < p_1$
   (b) Mach number increases, $M_2 > M_1$
   (c) Velocity increases, $V_2 > V_1$
   (d) Temperature increases for $M_1 < \gamma^{-1/2}$ and Temperature decreases for $M_1 > \gamma^{-1/2}$
   (e) Total temperature increases, $T_{02} > T_{01}$
   (f) Total pressure decreases, $p_{02} < p_{01}$.
2. For *supersonic flow* ($M_1 > 1$), when heat is added:
   (a) Pressure increases, $p_2 > p_1$
   (b) Mach number decreases, $M_2 < M_1$
   (c) Velocity decreases, $V_2 < V_1$
   (d) Temperature increases, $T_2 > T_1$
   (e) Total temperature increases, $T_{02} > T_{01}$
   (f) Total pressure decreases, $p_{02} < p_{01}$.

Note that for subsonic flow when heat is added, the temperature increases for $M_1 < \gamma^{-1/2}$ and decreases for $M_1 > \gamma^{-1/2}$. This is due to the fact that the value of T/T^* goes through a maximum at $M = 1/\sqrt{\gamma}$, corresponding to point g on Fig. 11.4. In the case of air, therefore, for values of M between 0.85 and 1, heat addition results in decrease in stream temperature, and heat rejection results in increase in stream temperature.

EXAMPLE 11.3 Air at standard sea level conditions enters the tube shown in Fig. 11.6, at Mach 0.68 and reaches a value of Mach 0.25 at the exit of the diffuser (station B). The entrance area is 1 m^2.

(a) Assuming no dissipative losses in the diffuser, show that the area at station B is 2.16 m^2. Will the area be larger or smaller if losses are present?

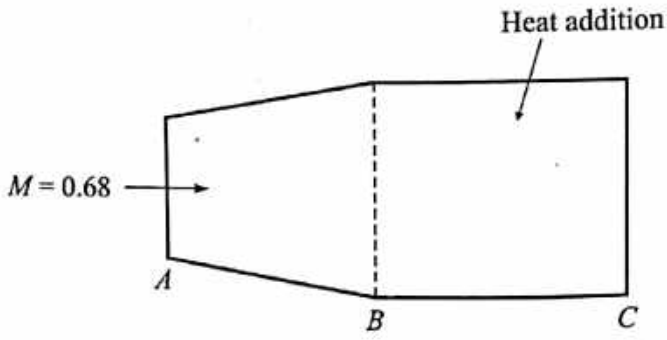


Fig. 11.6 Example 11.3.

Scanned by CamScanner

(b) Show that, assuming no losses, the static pressure at B is 1.322×10^5 N/m^2 and the density is 1.48 kg/m^3. If losses are present, will the stagnation pressure rise or fall from station A to station B? Will the stagnation density rise or fall? Give reasons for your answer.

(c) Heat is added at Mach 0.25 between stations B and C until thermal choking occurs. Show that the heat added is 9.15×10^5 N-m/kg and the stagnation temperature at station C is 1225 K.

Solution Given

$$p_A = 1.0133 \times 10^5 \text{ N/m}^2, \quad M_A = 0.68$$
$$T_A = 288 \text{ K}, \quad M_B = 0.25$$
$$\rho_A = 1.225 \text{ kg/m}^3, \quad A_A = 1 \text{ m}^2$$

(a) From isentropic flow table,

$$\frac{A_A}{A^*} = 1.110 \quad \text{for } M_A = 0.68$$

$$\frac{A_B}{A^*} = 2.403 \quad \text{for } M_B = 0.25$$

Therefore,

$$A_B = \frac{A_B}{A^*}\frac{A^*}{A_A}A_A = \frac{2.403}{1.11} \times 1 = \boxed{2.165 \text{ m}^2}$$

If losses were present, the area would have been larger since

$$\dot{m} = \frac{\Gamma}{\sqrt{\gamma R T_0}} p_0 f(M) A$$

where

$$\Gamma = \gamma\left(\frac{2}{\gamma+1}\right)^{(\gamma+1)/2(\gamma-1)}$$

$\dot{m}$, T_0, M being constants, p_0 decreases with losses; hence A_B has to increase.

(b) From isentropic table,

$$\frac{p_A}{p_0} = 0.7338, \quad \frac{\rho_A}{\rho_0} = 0.8016 \quad \text{for } M_A = 0.68$$

$$\frac{p_B}{p_0} = 0.9575, \quad \frac{\rho_B}{\rho_0} = 0.9694 \quad \text{for } M_B = 0.25$$

Therefore,

$$p_B = \frac{p_B}{p_0}\frac{p_0}{p_A}p_A = \boxed{1.322 \times 10^5 \text{ N/m}^2}$$

$$\rho_B = \frac{\rho_B}{\rho_0}\frac{\rho_0}{\rho_A}\rho_A = \boxed{1.48 \text{ kg/m}^3}$$

Scanned by CamScanner

$$\Delta s = R \ln \frac{p_{0A}}{p_{0B}} \quad \text{for } \Delta s > 0,\ p_{0A} > p_{0B}$$

Hence, if losses were present, the stagnation pressure would have decreased from A to B:

$$\frac{p_{0A}}{\rho_{0A}} = RT_{0A}, \quad \frac{p_{0B}}{\rho_{0B}} = RT_{0B}$$

$$\frac{\rho_{0B}}{\rho_{0A}} \frac{p_{0A}}{p_{0B}} = 1 \quad \text{since } T_{0A} = T_{0B}$$

$$\frac{\rho_{0B}}{\rho_{0A}} = \frac{p_{0B}}{p_{0A}} < 1$$

Therefore, the stagnation density falls from A to B.

(c) For $M_A = 0.68$, from isentropic table, we have

$$\frac{T_A}{T_{0A}} = 0.9153$$

Hence,

$$T_{0A} = 314.7 \text{ K} = T_{0B}$$

For thermal choking, from Table A5 of Appendix A,

$$\frac{T_{0B}}{T_0^*} = 0.25684 \quad \text{at } M_B = 0.25$$

Therefore,

$$T_0^* = \boxed{1225.3 \text{ K}} = T_{0C}$$

Heat added is given by Eq. (11.40) as

$$Q = c_p(T_{0C} - T_{0B})$$

Also,

$$c_p = \frac{\gamma}{\gamma - 1} R = 1004.5 \text{ m}^2/\text{s}^2\text{-K}$$

Thus,

$$Q = 1004.5(1225.3 - 314.7)$$
$$= \boxed{9.147 \times 10^5 \text{ N-m/kg}}$$

EXAMPLE 11.4 Air enters a gas turbine engine at 288 K and 150 m/s. The specific enthalpy drop across the engine is 6 kJ/kg and the velocity at the exit is 300 m/s. If the work delivered by the engine is 22.25 kW/kg, determine the heat added by combustion. Assume the mass flow rate at the exit is almost the

Scanned by CamScanner

same as the inlet mass flow rate and the air and combustion products are perfect gases with specific heat ratio 1.4.

Solution Let subscripts 1 and 2, respectively, refer to the inlet and exit states of the engine. Given, $T_1 = 288$ K, $V_1 = 150$ m/s, $h_1 - h_2 = 6$ kJ/kg, $\dot{w} = 22.25$ kW/kg, $V_2 = 300$ m/s.

By energy equation, we have

$$\dot{m}_2\left(h_2 + \frac{V_2^2}{2}\right) - \dot{m}_1\left(h_1 + \frac{V_1^2}{2}\right) = \dot{Q} - \dot{W}$$

But $\dot{m}_1 = \dot{m}_2$, therefore,

$$(h_2 - h_1) + \left(\frac{V_2^2}{2} - \frac{V_1^2}{2}\right) = \frac{\dot{Q}}{\dot{m}_1} - \frac{\dot{W}}{\dot{m}_1}$$

or

$$-6000 + \frac{(300)^2}{2} - \frac{(150)^2}{2} = q - w$$

$$27{,}750 = q - 22{,}250$$

$$q = \boxed{5500 \text{ J/kg}}$$

EXAMPLE 11.5 For the Rayleigh flow of a perfect gas, show that

$$\frac{T}{T^*} = \frac{(1+\gamma)^2 M^2}{(1+\gamma M^2)^2}$$

Solution Flow of a perfect gas through a constant-area duct, involving only heat transfer, by continuity,

$$\frac{\rho_2}{\rho_1} = \frac{V_1}{V_2}$$

where subscripts 1 and 2, respectively, refer to the state of flow before and after heat addition.

From momentum equation,

$$\frac{p_2}{p_1} = \frac{1+\gamma M_1^2}{1+\gamma M_2^2}$$

By state equation,

$$\frac{p_2}{p_1} = \frac{\rho_2}{\rho_1}\frac{T_2}{T_1}$$

This gives,

$$\frac{p_2}{p_1} = \frac{V_1}{V_2}\frac{T_2}{T_1}$$

$$\frac{T_2}{T_1} = \frac{p_2}{p_1}\frac{V_2}{V_1}$$

Scanned by CamScanner

The velocity ratio can be expressed as

$$\frac{V_2}{V_1} = \frac{M_2 a_2}{M_1 a_1}$$

$$= \frac{M_2}{M_1}\sqrt{\frac{T_2}{T_1}}$$

Therefore,

$$\frac{T_2}{T_1} = \frac{p_2}{p_1}\frac{M_2}{M_1}\sqrt{\frac{T_2}{T_1}}$$

$$\frac{T_2}{T_1} = \left(\frac{p_2}{p_1}\frac{M_2}{M_1}\right)^2$$

$$= \left(\frac{1+\gamma M_1^2}{1+\gamma M_2^2}\right)^2 \left(\frac{M_2}{M_1}\right)^2$$

If state 2 is sonic state, and state 1 in a general state, we have $M_2 = 1$ and $M_1 = M$. Thus

$$\frac{T^*}{T} = \frac{(1+\gamma M^2)^2}{(1+\gamma)^2}\frac{1}{M^2}$$

This simplifies to

$$\frac{T}{T^*} = \boxed{\frac{(1+\gamma)^2 M^2}{(1+\gamma M^2)^2}}$$

11.5 SUMMARY

From our discussions in Chapters 1–11, it is clear that the change of state in flow properties is achieved by three means: (a) with area change, treating the fluid to be inviscid and passage to be frictionless, (b) with friction, considering the heat transfer between the surrounding and system to be negligible, and (c) with heat transfer, assuming the fluid to be inviscid and passage to be frictionless. These three types of flows are called *isentropic flow*, *frictional* or *Fanno type flow*, and *Rayleigh type flow*, respectively.

All gas dynamic problems encountered in practice can be classified under these three flow processes, of course with the assumptions mentioned. Although it is impossible to have a flow process which is purely isentropic or Fanno type or Rayleigh type, in practice it is justified in assuming so, since the results obtained from these processes prove to be accurate enough for most of the practical situations in gas dynamics.

Scanned by CamScanner

Flows in which wall friction is the chief factor bringing about changes in fluid properties, assuming that no heat is transferred to or from the fluid stream are termed Fanno type flow. When the ducts are short, the flow is approximately adiabatic. However, when the ducts are extremely long, as in the case of natural-gas pipe lines, there is sufficient area for heat transfer to make the flow nonadiabatic and approximately isothermal.

Considering one-dimensional steady flow of a perfect gas through a constant area duct, with the assumption that there is no external heat exchange and external shaft work and differences in elevation produce negligible changes compared to frictional effects, we can write

$$h = h_0 - \frac{G^2}{2\rho^2} \tag{11.3}$$

where h and h_0 are the static and stagnation enthalpy, ρ is density and G is mass velocity. This equation shows that for a given initial condition, the relation between the local density ρ and local enthalpy h is fixed. This implies that the relation between any two properties of the flowing gas is also fixed. Thus all the states that satisfy Eq. (11.3) can be plotted on an h–s diagram. The locus of these states on such a diagram is called the Fanno line. Figure 11.2 shows such lines for a certain value of h_0.

The friction coefficient f is defined as

$$f = \frac{\text{wall shearing stress}}{\text{dynamic head of the stream}}$$

The hydraulic diameter D is defined as

$$D = \frac{4\,(\text{cross-sectional area})}{\text{wetted perimeter}}$$

The advantage of using hydraulic diameter is that the equations, in terms of hydraulic diameter, are valid even for ducts with non-circular cross-section.

The maximum length of the duct required for the flow to choke for a given initial Mach number is given by

$$4\bar{f}\frac{L_{\max}}{D} = \frac{1-M^2}{\gamma M^2} + \frac{\gamma+1}{2\gamma}\ln\left(\frac{(\gamma+1)M^2}{2\left(1+\frac{\gamma-1}{2}M^2\right)}\right) \tag{11.20}$$

where $\bar{f}$ is the mean friction coefficient with respect to duct length, defined by

$$\bar{f} = \frac{1}{L_{\max}}\int_0^{L_{\max}} f\,dx$$

The duct length required for the flow to pass from a given initial Mach number M_1 to a given final Mach number M_2 can be obtained from the expression

$$4\bar{f}\frac{L}{D} = \left(4\bar{f}\frac{L_{\max}}{D}\right)_{M_1} - \left(4\bar{f}\frac{L_{\max}}{D}\right)_{M_2} \tag{11.21}$$

Scanned by CamScanner

At the maximum entropy point of the Fanno curve the velocity is sonic velocity. For subsonic flow, the enthalpy decreases as the velocity increases in the direction of flow. For supersonic flow, the enthalpy increases as the velocity decreases in the direction of flow. Thus the upper part of the Fanno line represents the states of subsonic flow, while the lower part of the line represents the states of supersonic flow.

The physical significance of the point of maximum entropy may be illustrated by considering the flow in a pipe with friction. If in such a case both the initial pressure and the discharge pressure are maintained constant, there is a maximum pipe length that we can use for a given mass flow rate. However, the variation in pressure, velocity, entropy, etc. of the fluid as a function of pipe length can be predicted if the friction coefficient for the pipe is known.

From the discussion on Fanno flow it is clear that friction always drives the Mach number towards unity, decelerating a supersonic flow and accelerating a subsonic flow. In Fig. 11.2, which is a Mollier diagram of one-dimensional flow with friction, the above-mentioned effect of friction on Mach number is emphasized. For any given initial Mach number, for a certain value of L the flow becomes sonic. For this condition the flow is said to be *choked*, since any further increase in L is not possible without causing a drastic change of the inlet conditions. For instance, if the inlet conditions were achieved by expansion through a supersonic nozzle, and if L were larger than that allowed for attaining Mach 1 at the exit, then a normal shock would form inside the supersonic nozzle and the duct inlet conditions would suddenly become subsonic.

It is important to note that friction always causes the total pressure to decrease whether the inlet flow is subsonic or supersonic. Further, unlike the Rayleigh curve for flow with heating or cooling, the upper and lower portions of the Fanno curve cannot be traversed by the same one-dimensional flow. In other words, it is not possible to first decelerate a supersonic flow to sonic condition by friction, and then further retard it to subsonic speeds also by friction, since such a subsonic deceleration violates the second law of thermodynamics.

A process involving changes in the stagnation enthalpy or stagnation temperature of a gas stream which flows at constant area and without frictional effects is called a process with *Simple T_0-change*. In this process, energy effects such as external heat exchange, combustion, or moisture condensation are the prime parameters causing changes in the state of a flowing gas.

For fixed values of the flow per unit area and the impulse function per unit area, a unique relation between the pressure and the density is defined as

$$p + \frac{G^2}{\rho} = \frac{F}{A} \tag{11.31}$$

This equation is called the *Rayleigh line relation*. Since both the enthalpy and entropy are functions of pressure and density, it follows that Eq. (11.31) may be used for representing the Rayleigh line on the enthalpy–entropy diagram, as shown in Fig. 11.4.

Scanned by CamScanner

From a physical point of view the changes in stream properties are due primarily to changes in stagnation temperature. That is, the rate of change of stream properties along a Rayleigh line is a function of the rate of change of stagnation temperature.

The stagnation temperature corresponding to a given state is that temperature which the stream would assume if it were adiabatically decelerated to zero velocity. The ratio of stagnation temperatures at sections 1 and 2 in terms of Mach numbers at these sections, for a Rayleigh flow, can be expressed as

$$\frac{T_{02}}{T_{01}} = \frac{M_2^2}{M_1^2}\frac{(1+\gamma M_1^2)^2}{(1+\gamma M_2^2)^2}\frac{\left(1+\frac{\gamma-1}{2}M_2^2\right)}{\left(1+\frac{\gamma-1}{2}M_1^2\right)} \tag{11.42}$$

It is important to note that heat addition always drives the Mach numbers towards 1, accelerating a subsonic flow and decelerating a supersonic flow. This is emphasized on the Rayleigh curve in Fig. 11.4. Heating always acts to reduce the stagnation pressure, irrespective of whether the speed is subsonic or supersonic. Increase in stagnation pressure, on the other hand, may be obtained at either subsonic or supersonic speeds by a cooling process which reduces to stagnation temperature; in practice this is difficult because other effects are always present which tend to reduce the stagnation pressure.

Finally, it is extremely important to realize that we have considered only simple types of flow to study the flow processes in which only a simple independent parameter was allowed to change, e.g. isentropic flow in Chapter 4 where the effects of area change alone was considered; Fanno and Rayleigh flows in this chapter where the effects of friction alone and the effects of changes in stagnation temperature alone, respectively, have been considered. But in many practical problems of interest these effects occur simultaneously, and, in addition, there may be present such other phenomena as chemical reaction, change of phase, injection or withdrawal of gases, and changes in molecular weight and specific heat. Rocket nozzles, ram jets, combustion chambers of gas turbine engines, moving flame fronts, moisture condensation shocks, injectors and ejectors, detonation waves, and heat exchangers are typical examples of flow passages in which simultaneous effects are present. For solving such flows, all the effects associated with such processes must be taken into account simultaneously; readers are encouraged to consult books specializing on such topics, see, for instance Shapiro (1953).

PROBLEMS

1. The stagnation chamber of a wind tunnel is connected to a high-pressure air reservoir by a long pipe of 100 mm diameter. If the static pressure ratio between the reservoir and the stagnation chamber is 10, and the reservoir static pressure is 1.0135×10^7 N/m^2, how long can

Scanned by CamScanner

the pipe be without choking? Assume adiabatic, subsonic, one-dimensional flow with a friction coefficient of 0.005.

[**Ans.** $L_{max} = 1034.4$ m]

2. Air at a pressure of 3.5×10^5 N/m^2 and a temperature of 300 K is to be transported at the rate of 0.090 kg/s over a distance of 600 m through a pipe. The final pressure is to be at least 1.40×10^5 N/m^2. Assuming isothermal flow and $\bar{f} = 0.004$, determine the minimum pipe diameter.

[**Ans.** 0.0402 m]

3. With an experimental rig comprising a convergent-divergent nozzle attached to a smooth round tube, the following data were measured with the aim of measuring friction coefficients for the supersonic flow of air: Stagnation pressure and temperature upstream of the nozzle: $p_0 = 67.3 \times 10^5$ N/m^2, and $T_0 = 312$ K; throat diameter = 0.0061 m; diameter of nozzle exit and tube $D = 0.0127$ m; pressure of stream at stations $x_1/D = 1.75$ and $x_2/D = 29.60$ from the tube inlet: $p_1 = 2.38 \times 10^5$ N/m^2 and $p_2 = 4.85 \times 10^5$ N/m^2. Calculate the average friction coefficient between stations x_1 and x_2. Assume that the flow to the throat of the nozzle is isentropic, and that the flow in the entire system is adiabatic.

[**Ans.** 0.002577]

4. An isentropic nozzle having an area ratio of 2, discharges air into an insulated pipe of length L and diameter D. The nozzle is supplied at 7×10^5 N/m^2 and 300 K, and the duct discharges into a space where the pressure is 2.8×10^5 N/m^2. Calculate the $4\bar{f}L/D$ of the pipe and mass flow rate per unit area in the pipe for the cases where a normal shock stands: (a) in the nozzle throat, (b) in the nozzle exit plane, and (c) in the duct exit plane.

[**Ans.** (a) 4.8576, 816.5 kg/m^2-s; (b) 0.5251, 815.9 kg/m^2-s; (c) 0.21312, 815.6 kg/m^2-s]

5. A gaseous mixture of air and fuel enters a ramjet combustion chamber with a velocity of 73.15 m/s, at a static temperature and pressure of 333.3 K and 0.5516×10^5 N/m^2. The heat of reaction ΔH of the fuel-air mixture is 1395.5 kJ/kg. Assuming that the working fluid has the same thermodynamic properties as air before and after combustion, that the friction is negligible, and that the cross-sectional area of the combustion chamber is constant, calculate: (a) the stagnation temperature after combustion, (b) the Mach number after combustion, (c) the final static temperature, (d) the loss in stagnation pressure due to heat addition, (e) the entropy change, (f) the final velocity of

Scanned by CamScanner

combustion mixture, and (g) the maximum heat of reaction for which the flow with the specified initial conditions can be maintained.

[Hint: $\Delta H = c_p(T_{02} - T_{01})$]

[**Ans.** (a) 1725.2 K; (b) 0.68; (c) 1583.2 K; (d) 8.53 kPa; (e) 1690.1 J/kg-K; (f) 542.1 m/s; (g) 1607.2 kJ/kg]

6. Air flows adiabatically through a duct of diameter 20 mm. At a station 1 in the duct, $M_1 = 0.2$, $p_1 = 5$ atm, and $T_1 = 300$ K. Compute p_2, T_2, V_2, and p_{02} at a station 2 where $M_2 = 0.5$.

[**Ans.** 198.558 kPa, 288 K, 170 m/s, 235.52 kPa]

7. Air flows through a perfectly insulated square tube of cross-section 0.1 m by 0.1 m. At a section 1 inside the tube, $M_1 = 0.2$, $T_1 = 72°C$, and $p_1 = 2$ atm. At a downstream section 2, $M_2 = 0.76$. Determine the mass flow rate through the tube and the drag force acting on the duct between sections 1 and 2.

[**Ans.** 1.524 kg/s, 1223.43 N]

8. Carbon dioxide gas enters an insulated circular tube of length-to-diameter ratio 50. At the entrance, the flow velocity is 195 m/s and the temperature is 310 K. If the flow at the tube exit is choked, determine the average friction factor of the tube.

[**Ans.** 0.00105]

9. Air flows through a pipe of 25 mm diameter and 51 m length. The conditions at the pipe exit are $M_2 = 0.8$, $p_2 = 1$ atm and $T_2 = 270$ K. Assuming adiabatic one-dimensional flow, calculate M_1, p_1 and T_1 at the pipe entrance. Take the local friction coefficient to be 0.005.

[**Ans.** 0.13, 6.56 atm, 303.52 K]

10. Air enters a perfectly insulated tube of 5 cm diameter with a stagnation state at $p_0 = 135$ kPa and $T_0 = 359$ K. The velocity at the entrance is $V_1 = 135$ m/s. If the average friction factor $f = 0.02$, determine (a) the minimum length of the duct required for the flow to choke and (b) the mass flow rate and the stagnation pressure at the exit if the tube length is 0.6 m.

[**Ans.** (a) 1.99 m; (b) 0.326 kg/s; 121.23 kPa]

11. Hydrogen gas enters an insulated tube of 25 mm diameter with $V_1 = 200$ m/s, $p_1 = 250$ kPa and $T_1 = 303$ K. What is the length of the tube required for this flow to choke? Determine the exit pressure. The average friction factor of the tube is $\bar{f} = 0.03$.

[**Ans.** 5.82 m, 34.31 kPa]

12. An air stream flowing out of a convergent nozzle at 200 m/s and 30°C is made to enter an insulated pipe of diameter 20 mm. Determine the length of the pipe at which the flow will become sonic if the average friction factor is 0.02.

[**Ans.** 15.6 cm]

Scanned by CamScanner

13. Methane gas flows in a commercial steel pipe of 25 mm diameter. At the inlet, $p_1 = 1.0$ MPa, $T_1 = 320$ K and $V_1 = 25$ m/s. Determine the velocity and pressure at the pipe length at which the flow just chokes. Treat the flow to be adiabatic. For Methane $R = 518.4$ J/kg-K and $\mu = 0.011 \times 10^{-3}$ kg/m-s at the given inlet conditions. Take the average friction factor to be $\bar{f} = 0.004$.

[**Ans.** 432.87 m/s, 50.18 kPa]

14. Argon gas enters an insulated, constant area duct with a Mach number of 0.6, static pressure 90 kPa, and static temperature 300 K. The diameter is 30 cm and length is 1.9 m. If the average friction factor for the duct is 0.02, determine the Mach number, the pressure, and the temperature at the duct exit.

[**Ans.** 0.73, 72.81 kPa, 290.62 K]

15. Air flows through a pipe of 50 mm diameter with a friction factor of 0.006. At a certain point along the pipe the Mach number is 0.2. Find the maximum distance from the point to the exit of the pipe if choking is to be avoided.

[**Ans.** 30.277 m]

16. Air flows adiabatically at the rate of 2.7 kg/s through a 100 mm diameter pipe with mean friction coefficient of 0.006. If the initial pressure and temperature are 1.8 bar and 50°C, what is the maximum length of the pipe up to which choking will not occur. Determine T and p (a) at the exit end and (b) half way along the pipe.

[**Ans.** 4.8 m; (a) 82.4 kPa, 9.08°C; (b) 150.6 kPa, 44.19°C]

17. Air flows adiabatically through a long pipe of 50 mm diameter. If the entrance Mach number is 0.2, calculate the distance from the entrance at which the Mach number will be (a) 1.0 and (b) 0.6. Assume the friction coefficient to be 0.00375.

[**Ans.** (a) 48.44 m, (b) 46.8 m]

18. Air at a stagnation temperature of 380 K is to be transported through a duct of 55 m length. What is the minimum diameter of the duct for the flow to remain unchoked for velocity at the duct entrance of (a) 30 m/s, (b) 90 m/s, and (c) 425 m/s. The average friction factor for the duct is 0.02. Assume the flow to be adiabatic.

[**Ans.** (a) 4.12 cm; (b) 0.422 m; (c) 96.77 m]

19. Air enters a square duct of side 3 cm with velocity 1000 m/s and temperature 350 K. The friction factor for the duct is 0.0025. Determine the duct length required for the flow to decelerate to Mach 1.0.

[**Ans.** 1.40 m]

20. A constant area duct of 25 mm diameter and 250 mm length is connected to a reservoir through a convergent nozzle, as shown in Fig. P11.20. The reservoir is at 50 atm and 320 K. Determine the maximum air flow rate through the system. Also determine the range

Scanned by CamScanner

of backpressure over which the mass flow rate will remain maximum. Assume the average friction factor for the duct to be 0.023.

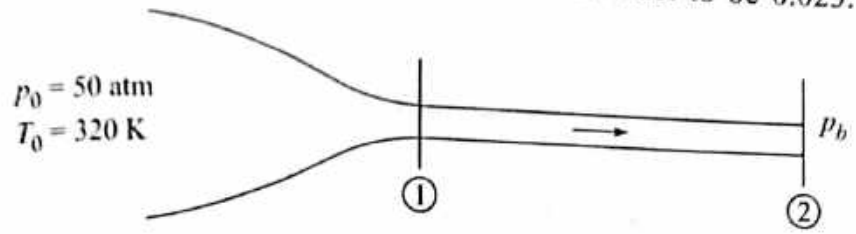


Fig. P11.20

[**Ans.** 4.3 kg/s, $0 < p_b < 2.05$ MPa]

21. Air flows through an insulated duct of diameter 30 mm. Determine the duct length required to accelerate the flow from (a) 0.2 to 0.5 and (b) 0.2 to 1.0. The average friction factor for the duct is 0.025. The specific heat ratio for air is 1.4.

[**Ans.** (a) 16.157 m, (b) 17.44 m]

22. A compressor delivers air into a pipe of 5 cm diameter and 18 m length at a rate of 0.3 kg/s. The average friction factor for the pipe is 0.02. If the air leaves the pipe with $p_e = 1$ atm and $T_e = 195°C$, compute the mass flow rate through the pipe.

[**Ans.** 0.096 kg/s]

23. Argon gas from a large tank at 5 atm (gauge) and 300 K is discharging through an insulated tube of 30 cm diameter into an ambient atmosphere at nearly zero pressure. What will be the mass flow rate through the tube if its length (a) is 0 m, (b) 2.22 m. Assume the average friction factor for the tube to be 0.005.

[**Ans.** (a) 125 kg/s, (b) 115.68 kg/s]

24. The settling chamber of a wind tunnel and a high-pressure air storage are connected by a long pipe of 100 mm diameter. If the static pressure ratio between the storage tank and the settling chamber is 15, and the settling chamber static pressure is 150 atm, how long can the pipe be without choking? Assume one-dimensional flow in the pipe and a friction coefficient of 0.005. [**Ans.** 703.3 m]

25. Air at a stagnation state of 600 kPa and 390 K is expanded through a piping system, shown in Fig. P11.25, to a pressure of 45 kPa. Estimate the mass flow rate through the system if the average friction factor for pipe A is 0.015 and that for pipe B is 0.013.

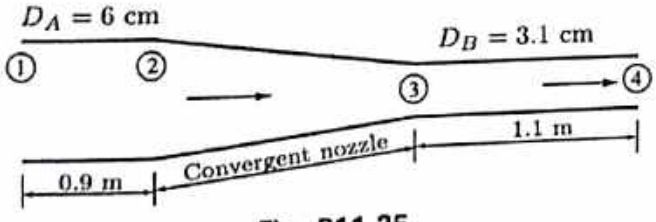


Fig. P11.25

[**Ans.** 0.596 kg/s]

Scanned by CamScanner

26. Air flows through a 45 m long tube of diameter 75 mm. The flow process is isothermal at 15°C and the pressures at the inlet and outlet of the tube are 600 kPa and 240 kPa, respectively. If the average friction coefficient for the tube is 0.008, calculate the rate at which heat is transferred to the surroundings.

[Ans. 12.677 kW]

27. Air from a storage tank at 410 kPa (gauge) and 294 K flows through a 20 mm diameter tube. At the tube entrance, the pressure is 400 kPa (gauge), and at a downstream location 12 m from the entrance, the pressure is 180 kPa (gauge). Determine (a) the average friction coefficient for the tube, (b) the total length of the tube, if the pressure at the exit is 1 atm, and (c) the mass flow rate through the tube. Assume atmospheric pressure to be 101 kPa.

[Ans. (a) 0.0067, (b) 15.923 m, (c) 0.109 kg/s]

Scanned by CamScanner

12 Method of Characteristics

12.1 INTRODUCTION

Method of characteristics is a numerical method for solving the full nonlinear equations of motion for inviscid, irrotational flow. As we have already discussed, except the Prandtl–Meyer expansion, all other problems have been solved with the linear theory. If we are looking for better accuracy of results than that obtained by using the approximate linearized equations, it is necessary to work out improved solutions, by including higher-order terms in the approximate equations or by considering the exact equations. However, in the latter case, it is rarely possible to get solutions in analytical form because of the nonlinear nature of the equations. We must then resort to numerical techniques; the method of characteristics being one such technique.

12.2 THE CONCEPTS OF CHARACTERISTICS

In Sections 3.4 and 6.5, Mach lines were identified as characteristic lines, and they have been labelled as "left-running" and "right-running", depending upon whether they run to the left or right with respect to an observer looking in the flow direction. Now, let us see some of the important features of the characteristics. From the earlier discussions on the properties of Mach lines and expansion flows, we may observe the following *general features of characteristics*:

1. They exist only in supersonic flow field.
2. Characteristics are coincident with Mach lines. (Mach lines are lines along which very weak disturbances propagate.)
3. While the derivatives of flow properties are discontinuous, the flow properties themselves are continuous on the characteristics.

Scanned by CamScanner

4. Given the characteristics or Mach lines, the dependent variables satisfy a relation known as the compatibility relation. This provides the key to the method of computation.

Because the characteristics are lines across which there is a jump in flow properties, the downstream flow does not affect the upstream flow. Therefore, it is sufficient to calculate the flow for different regions of the flow field and then they can be patched up. But in subsonic flow, any downstream flow affects the upstream flow. So the entire flow has to be solved simultaneously.

12.3 THE COMPATIBILITY RELATION

Consider a steady, adiabatic, two-dimensional, irrotational supersonic flow. The governing equations for this flow are

$$(V_x^2 - a^2)\frac{\partial V_x}{\partial x} + V_x V_z\left(\frac{\partial V_x}{\partial z} + \frac{\partial V_z}{\partial x}\right) + (V_z^2 - a^2)\frac{\partial V_z}{\partial z} = 0 \quad (12.1)$$

$$\frac{\partial V_z}{\partial x} - \frac{\partial V_x}{\partial z} = 0 \quad (12.2)$$

If $(V_x^2 + V_z^2)/a^2 < 1$, the equations are of *elliptic type*, and the *relaxation method* of solution is appropriate. If $(V_x^2 + V_z^2)/a^2 > 1$, the equations are of *hyperbolic type*. The numerical solution may be obtained by the *method of characteristics*.

Using the natural coordinate system, in which the velocity is expressed in terms of its magnitude and direction (V, θ), and the independent variables are the streamline coordinates (l, n), with l varying along the streamline and n varying normal to streamline, Eqs. (12.1) and (12.2) can be written as

$$\left(\frac{V^2}{a^2} - 1\right)\frac{1}{V}\frac{\partial V}{\partial l} - \frac{\partial \theta}{\partial n} = 0 \quad (12.3)$$

$$\frac{\partial V}{\partial n} - V\frac{\partial \theta}{\partial l} = 0 \quad (12.4)$$

where Eqs. (12.3) and (12.4) are respectively the momentum and irrotationality equations.

With the introduction of Mach angle μ, we can write Eqs. (12.3) and (12.4) as

$$\frac{\cot^2\mu}{V}\frac{\partial V}{\partial l} - \frac{\partial \theta}{\partial n} = 0 \quad (12.5)$$

$$\frac{1}{V}\frac{\partial V}{\partial n} - \frac{\partial \theta}{\partial l} = 0 \quad (12.6)$$

where

$$\cot^2\mu = M^2 - 1 \quad (12.7)$$

Scanned by CamScanner

In Section 6.6, it was shown that for a finite deflection angle θ, the direction of a weak oblique shock wave differs from the Mach wave direction μ by an amount ε, which is of the same order as θ. The change in flow speed across such a wave may be found as follows: From Fig. 6.2, we have

$$\frac{V_2^2}{V_1^2} = \frac{V_{x2}^2 + V_y^2}{V_{x1}^2 + V_y^2} = \frac{(V_{x2}/V_y)^2 + 1}{(V_{x1}/V_y)^2 + 1} = \frac{\tan^2(\beta - \theta) + 1}{\tan^2\beta + 1} = \frac{\cos^2\beta}{\cos^2(\beta - \theta)}$$

From Eq. (6.27), we have

$$\cos^2\beta = 1 - \sin^2\beta = \frac{M_1^2 - 1}{M_1^2}\left(1 - \frac{2\varepsilon}{\sqrt{M_1^2 - 1}}\right)$$

A similar expression for $\cos^2(\beta - \theta)$ can be obtained by replacing ε by $(\varepsilon - \theta)$ in the above expression. Substituting the expressions for $\cos^2\beta$ and $\cos^2(\beta - \theta)$ in terms of ε and θ in the above expression for velocity ratio and dropping all terms of order θ^2 and higher, we obtain

$$\frac{V_2}{V_1} \approx 1 - \frac{\theta}{\sqrt{M_1^2 - 1}}$$

$$\frac{\Delta V}{V_1} \approx -\frac{\theta}{\sqrt{M_1^2 - 1}} \tag{12.8}$$

In Section 6.9, it was defined that the Prandtl–Meyer function $\nu = \pm\theta$, where the plus sign holds across a right-running characteristic and the minus sign holds across a left-running characteristic.

Now, the Prandtl–Meyer function ν, which is a dimensionless measure of the speed may be defined, using Eq. (12.8), as

$$\nu = \int \frac{\cot\mu}{V}\, dV \tag{12.9}$$

where $\cot\mu = \sqrt{M^2 - 1}$. In differential form, Eq. (12.9) becomes

$$d\nu = \cot\mu\, \frac{dV}{V} \tag{12.10}$$

Now it will be seen that for the method of characteristics the Prandtl–Meyer function ν is the most appropriate one of the many functions that are related to the velocity V (or the Mach number M).

Substitution of Eq. (12.10) into Eqs. (12.5) and (12.6) results in

$$\frac{\partial\nu}{\partial l} - \tan\mu\, \frac{\partial\theta}{\partial n} = 0 \tag{12.11}$$

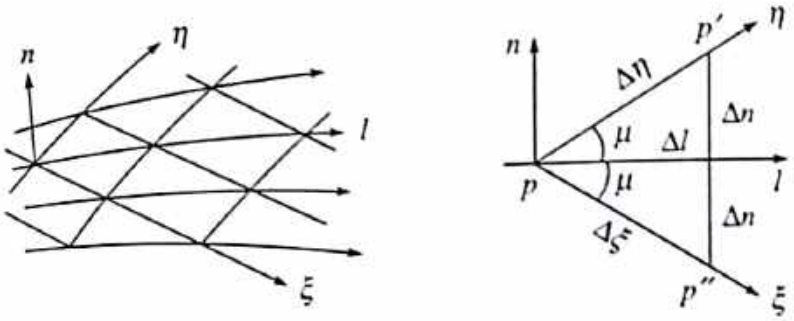
$$\tan\mu\, \frac{\partial\nu}{\partial n} - \frac{\partial\theta}{\partial l} = 0 \tag{12.12}$$

Scanned by CamScanner

The objective here is to find the *compatibility relation* between ν and θ which, according to the theory of hyperbolic equations, must exist on the characteristics, or Mach lines. Though the theory gives rules for finding the compatibility condition, here we shall obtain it only by *inspection*, since our interest is only from the application point of view.

We are familiar with the fact that the Mach lines are inclined to the streamlines at an angle $\pm\mu$. Therefore, we may expect to get the compatibility relations by rewriting Eqs. (12.11) and (12.12) in a coordinate system (ξ, η) consisting of the network of Mach lines, as shown in Fig. 12.1(a). The change in any function f, in going from point p to point p' [Fig. 12.1(b)] along the η coordinate may be written as

$$\Delta f = \frac{\partial f}{\partial \eta}\Delta\eta$$



(a) Characteristic coordinates (b) Natural coordinates

Fig. 12.1 Characteristic and natural coordinate systems.

Δf may also be calculated by going along the streamline coordinate system (Fig. 12.1(b)) as

$$\Delta f = \frac{\partial f}{\partial l}\Delta l + \frac{\partial f}{\partial n}\Delta n = \left(\frac{\partial f}{\partial l} + \frac{\partial f}{\partial n}\frac{\Delta n}{\Delta l}\right)\Delta l$$

From the above two equations,

$$\frac{\partial f}{\partial \eta}\frac{\Delta\eta}{\Delta l} = \frac{\partial f}{\partial l} + \frac{\partial f}{\partial n}\frac{\Delta n}{\Delta l}$$

From the geometry of Fig. 12.1(b), this may be expressed as

$$\sec\mu\,\frac{\partial f}{\partial \eta} = \frac{\partial f}{\partial l} + \tan\mu\,\frac{\partial f}{\partial n} \tag{12.13}$$

Similarly, we can write

$$\sec\mu\,\frac{\partial f}{\partial \xi} = \frac{\partial f}{\partial l} - \tan\mu\,\frac{\partial f}{\partial n} \tag{12.14}$$

Equations (12.13) and (12.14) give the rules that relate the derivatives of any function f, in the two coordinate systems. Adding and subtracting Eqs. (12.11) and (12.12), we get

$$\frac{\partial}{\partial l}(\nu - \theta) + \tan\mu\,\frac{\partial}{\partial n}(\nu - \theta) = 0$$

Scanned by CamScanner

$$\frac{\partial}{\partial l}(\nu + \theta) - \tan \mu \frac{\partial}{\partial n}(\nu + \theta) = 0$$

Comparing the above equations with Eqs. (12.13) and (12.14) respectively, we obtain

$$\frac{\partial}{\partial \eta}(\nu - \theta) = 0, \quad \frac{\partial}{\partial \xi}(\nu + \theta) = 0$$

That is,

$$\boxed{\begin{aligned} &\nu - \theta = R \text{ (constant) along the } \eta\text{-characteristic} \\ &\nu + \theta = Q \text{ (constant) along the } \xi\text{-characteristic} \end{aligned}} \tag{12.15}$$

These are the compatibility relations between ν and θ. They simply mean that the functions $Q = \nu + \theta$ and $R = \nu - \theta$ are invariants on the ξ and η characteristics, respectively.

Note: At this juncture we should note that the compatibility relations are not always obtained in such convenient form as Eq. (12.15). Generally, they are obtained in differential form, and cannot always be integrated in this way, independently of the specific flow field to be solved.

12.4 THE NUMERICAL COMPUTATIONAL METHOD

Consider the element from a characteristic network, illustrated in Fig. 12.2. Flow properties along AB are given. To find the flow properties at point P, consider the right-running characteristic AP, with Q = constant, and the left-running characteristic BP, with R = constant. For the above element we can write

$$Q_P = Q_A, \quad R_P = R_B$$

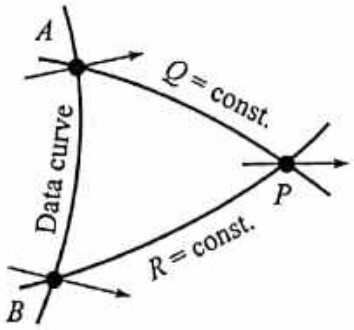


Fig. 12.2 Characteristic network element.

But by Eq. (12.15),

$$Q = \nu + \theta, \quad R = \nu - \theta$$

Hence,

$$\nu = \frac{1}{2}(Q + R), \quad \theta = \frac{1}{2}(Q - R)$$

Scanned by CamScanner

Therefore,

$$\nu_P = \frac{1}{2}(Q_P + R_P), \quad \theta_P = \frac{1}{2}(Q_P - R_P)$$

Now, the problem is solved since, once ν is known, M, μ, p/p_0 are all known from the isentropic table. Also, once θ is known, the flow inclination with respect to the data line is known. The location of the point P, which is an unknown, is found by a numerical technique. In this technique, the space is divided into parts to result in a characteristic network, as illustrated in Fig. 12.3. As a first approximation, the characteristics are replaced by straight line segments. Because of this linear approximation, we arrive at point 3′ instead of 3, as shown in Fig. 12.3. The error adds up and finally we get a point P' instead of P. To minimize the error, the dimensions of the meshes should be of smaller size. Applying a step-by-step procedure, starting from the data curve, giving the data, or boundary conditions, we can identify the flow field at point P. For instance, point 3 is located by using the known Mach angles and flow directions at points 1 and A to draw the characteristic segments. Flow conditions at point 3 are determined from the data at points A and 1. Similarly, point 4 is found, and then point 6 is found from points 3 and 4. Thus, starting from the data curve the computation proceeds outwards.

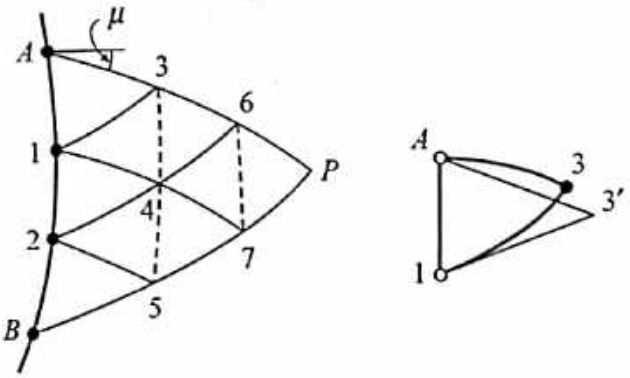


Fig. 12.3 Characteristic network.

The "working outward" computation from the data curve indicates that the nature of the boundary condition is such that it influences the flow only in the downstream direction. This is in contrast to the Laplacian or elliptic type of field, in which the region of computation must be completely bounded, and in which each point is influenced by all other points in the region.

Solid and Free Boundary Points

From the characteristic network shown in Fig. 12.3, it is seen that for computing ν and θ at point 3, the invariants Q and R at points A and 1 must be known. These points A and 1 may lie on a solid wall or free boundary, like the edge of a jet, i.e. the boundary conditions fit into the computation quite readily. Consider the characteristic network element shown in Fig. 12.4.

Scanned by CamScanner

In Fig. 12.4, the properties on the data curve arc 1–2 are known, i.e. ν_1, θ_1, ν_2, θ_2 are known. In other words, the invariants Q on the arc 1–3 and R on the arc 2–3 are known. Therefore, the flow properties (ν_3, θ_3) at point 3 can easily be obtained from the relations of Eq. (12.15) as follows:

$$Q_1 = \nu_1 + \theta_1, \quad R_2 = \nu_2 - \theta_2 \tag{12.16a}$$

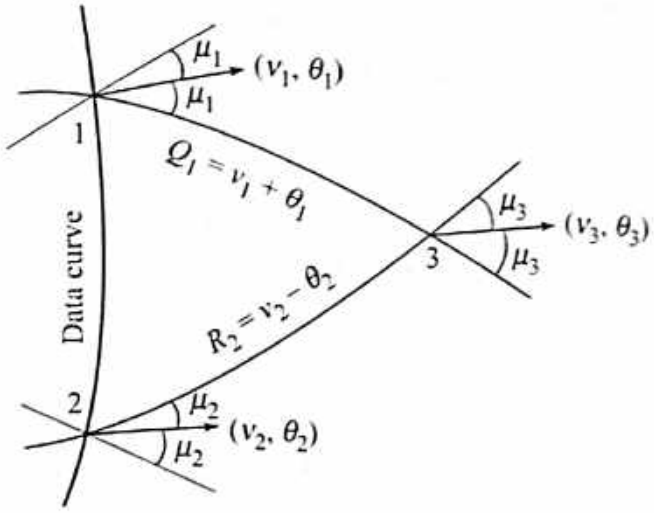


Fig. 12.4 Characteristic network element.

Hence,

$$\nu_3 = \frac{1}{2}(Q_1 + R_2), \quad \theta_3 = \frac{1}{2}(Q_1 - R_2) \tag{12.16b}$$

With Eqs. (12.16), we can form the data given in Fig. 12.5, which should be known for computing data for point 3, depending on whether 3 is an interior point or a point on a solid wall, or a point on a free boundary.

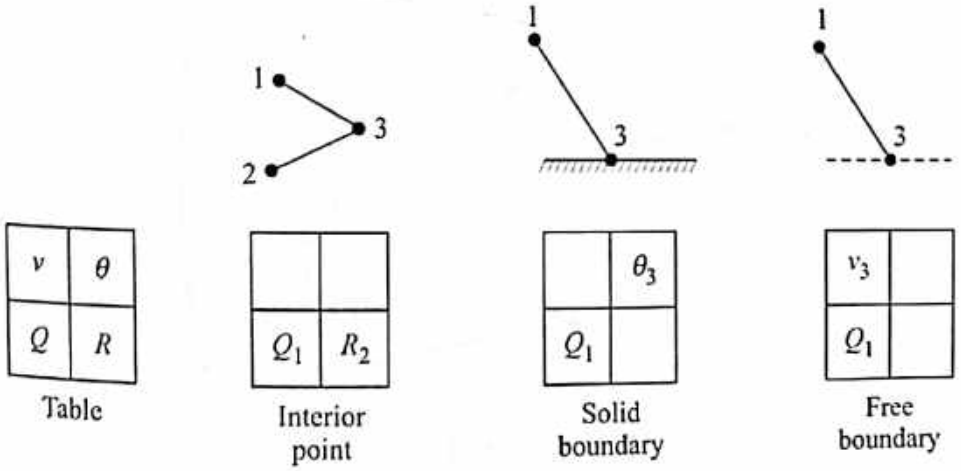


Fig. 12.5 Known data for computing flow at point 3.

From Fig. 12.5, it is seen that if any two of the quantities in the table are known, the other two may be calculated with the relations in Eqs. (12.16).

Sometimes it may be necessary to compute flows in which shocks appear. On such occasions, the method illustrated in Fig. 12.6 may be employed. As

Scanned by CamScanner

seen from the figure, point 3 is just behind the shock. One invariant R is obtained from point 1, since arc 1–3 is a left-running characteristic. The other is determined by the shock equations (see Section 6.3); it is not given explicitly, but as a relation between ν_3 and θ_3. Thus the flow at point 3 may be solved. These then determine the shock angle β, which is used to draw the next shock segment. If the shock is strongly curved, the flow downstream of it will have vorticity and the isentropic equations are not valid in this region, and they must be replaced by appropriate equations accounting for vorticity effects.

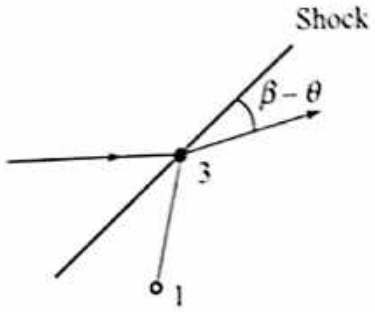


Fig. 12.6 Shock in a flow.

EXAMPLE 12.1 Computation of flow in a diverging channel is shown in Fig. 12.7 with walls diverging by 15° and $M_{data} = 1.348$. Divide the data curve into three equal segments, i.e. $\Delta\theta = 5°$. The values of ν and θ are known at points 1 to 4 (data curve). Therefore, the invariants Q and R on all left- and right-running characteristics originating from the above points may be calculated with the relations

$$Q = \nu + \theta, \quad R = \nu - \theta$$

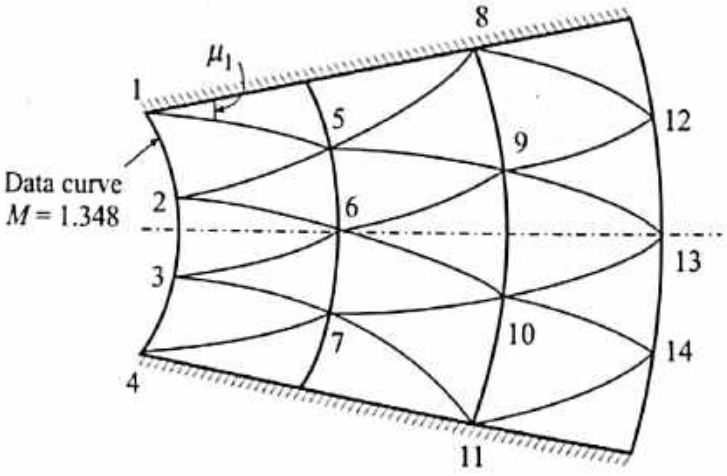


Fig. 12.7 Example 12.1.

Hence, with the Prandtl–Meyer function ν and turning angle θ at points 5 to 14 may be obtained from the corresponding values of Q and R for each point using the relations

$$\nu = \frac{1}{2}(Q + R), \quad \theta = \frac{1}{2}(Q - R)$$

Scanned by CamScanner

Table 12.1 gives the computed values of ν, θ, μ and M at points 5 to 14 following the above procedure.

Remarks

1. The compatibility conditions $Q = \nu + \theta$ and $R = \nu - \theta$ make the whole procedure simple. These conditions are simple only for two-dimensional irrotational flows.
2. A drawing should always be made along with the computation, to locate the points.

Source of Error

1. In actual flow, there will be a boundary layer. This introduces error to the results obtained, since it is not correct to assume the characteristics to be straight near the wall. The error may be corrected by calculating the displacement thickness at different stations and by adding it to the contour already calculated.
2. The values obtained with $\Delta\theta = 1°$ and $\Delta\theta = 0.5°$ are almost the same. Therefore, there is no necessity to take $\Delta\theta$ less than 1°.

Axi-symmetric Flow

The important features of the method of characteristics have been already been described in our discussion of plane flow. The computations for two-dimensional flow were seen to be very easy because of the simple nature of the compatibility relations (12.15). But the theory of characteristics for general three-dimensional flow is quite involved and the computations are cumbersome. However, for axi-symmetric flow, the method is easily extended from two-dimensional flow case.

Consider the fluid element shown in Fig. 12.8. The governing equation for this motion may be shown as

$$\frac{\cot^2\mu}{V}\frac{\partial V}{\partial l} - \frac{\partial \theta}{\partial n} = \frac{\sin\theta}{r} \tag{12.17}$$

$$\frac{1}{V}\frac{\partial V}{\partial n} - \frac{\partial \theta}{\partial l} = 0 \tag{12.18}$$

where (V, θ) define the velocity in the natural coordinates plane. Equation (12.17) differs from Eq. (12.5) only in the last term. The irrotationality equation [Eq. (12.18)] is the same as Eq. (12.6). Multiplication of Eq. (12.17) by tan μ and Eq. (12.18) by tan μ cot μ yields

$$\frac{\cot\mu}{V}\frac{\partial V}{\partial l} - \tan\mu\frac{\partial \theta}{\partial n} = \tan\mu\frac{\sin\theta}{r} \tag{12.17a}$$

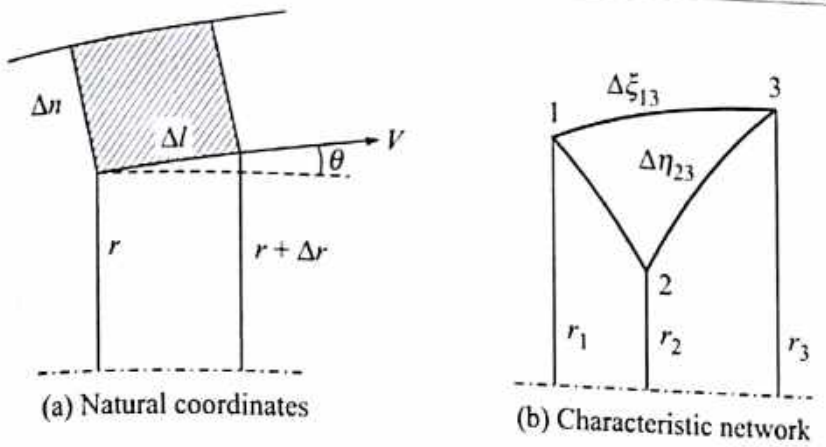
$$\tan\mu\frac{\cot\mu}{V}\frac{\partial V}{\partial n} - \frac{\partial \theta}{\partial l} = 0 \tag{12.18a}$$

Scanned by CamScanner

TABLE 12.1 Example 12.1

Boundary conditions						*Point*	*Q*	*R*	$\nu°$	$\theta°$	$\mu°$	*M*
Given				Derived		5	15	5	10	5	44.2	1.434
Point	$\mu°$	$\nu°$	$\theta°$	*Q*	*R*	6	10	10	10	0	44.2	1.434
1	47.9	7.5	7.5	15	0	7	5	15	10	−5	44.2	1.434
2	47.9	7.5	2.5	10	5	8	20	5	12.5	7.5	41.1	1.520
3	47.9	7.5	−2.5	5	10	9	15	10	12.5	2.5	41.1	1.520
4	47.9	7.5	−7.5	0	15	10	10	15	12.5	−2.5	41.1	1.520
						11	5	20	12.5	−7.5	41.1	1.520
						12	20	10	15	5	38.5	1.606
						13	15	15	15	0	38.5	1.606
						14	10	20	15	−5	38.5	1.606

Scanned by CamScanner



(a) Natural coordinates (b) Characteristic network

Fig. 12.8 Axi-symmetric flow coordinates.

With the help of relations (12.9) and (12.10), Eqs. (12.17a) and (12.18a) become

$$\frac{\partial v}{\partial t} - \tan \mu \frac{\partial \theta}{\partial n} = \tan \mu \frac{\sin \theta}{r}$$

$$\tan \mu \frac{\partial v}{\partial n} - \frac{\partial \theta}{\partial t} = 0$$

The above two relations correspond to Eqs. (12.11) and (12.12) for the two-dimensional case. Following the same procedure as that adopted for two-dimensional flow, we can obtain the following equations:

$$\frac{\partial}{\partial \eta}(v - \theta) = \sin \mu \frac{\sin \theta}{r} \tag{12.19}$$

$$\frac{\partial}{\partial \xi}(v + \theta) = \sin \mu \frac{\sin \theta}{r} \tag{12.20}$$

Now the integration has to be done numerically, step by step, simultaneously with the construction of the characteristic network.

Consider the characteristic mesh element shown in Fig. 12.8(b). Point 3 is to be solved from the known data at points 2 and 1. From Eqs. (12.19) and (12.20), we may write

$$\int_2^3 d(v - \theta) = \int_2^3 \left(\sin \mu \frac{\sin \theta}{r}\right) d\eta$$

$$\int_1^3 d(v + \theta) = \int_1^3 \left(\sin \mu \frac{\sin \theta}{r}\right) d\xi$$

Now assume that for a small size mesh, the quantities in parentheses on the RHS to be approximately constant, over the interval of integration, and to have the known values at 1 and 2, respectively. The integrations yield:

Scanned by CamScanner

$$(\nu_3 - \theta_3) - (\nu_2 - \theta_2) = \sin \mu_2 \frac{\sin \theta_2}{r_2} \Delta\eta_{23}$$

$$(\nu_3 + \theta_3) - (\nu_1 + \theta_1) = \sin \mu_1 \frac{\sin \theta_1}{r_1} \Delta\xi_{13}$$

From the above two equations, we get

$$\nu_3 = \frac{1}{2}(\nu_1 + \nu_2) + \frac{1}{2}(\theta_1 - \theta_2) + \frac{1}{2}\left(\sin \mu_1 \frac{\sin \theta_1}{r_1} \Delta\xi_{13} + \sin \mu_2 \frac{\sin \theta_2}{r_2} \Delta\eta_{23}\right) \tag{12.21}$$

$$\theta_3 = \frac{1}{2}(\nu_1 - \nu_2) + \frac{1}{2}(\theta_1 + \theta_2) + \frac{1}{2}\left(\sin \mu_1 \frac{\sin \theta_1}{r_1} \Delta\xi_{13} - \sin \mu_2 \frac{\sin \theta_2}{r_2} \Delta\eta_{23}\right) \tag{12.22}$$

Equations (12.21) and (12.22) differ from the two-dimensional equations (12.15) only in the additional terms which depend on the geometry of the particular problem. In these terms, the radial distances r_1 and r_2 of the points in consideration, and the lengths of the mesh sides, $\Delta\eta_{23}$ and $\Delta\xi_{13}$, must be obtained from the flow field by measurement on a drawing or by computation.

Nonisentropic Flow

For a nonisentropic flow, the governing equation of motion becomes

$$\frac{\cot^2 \mu}{V} \frac{\partial V}{\partial t} - \frac{\partial \theta}{\partial n} = \frac{\sin \theta}{r} \tag{12.23}$$

and the velocity equation follows from relation (7.6) as

$$\frac{1}{V} \frac{\partial V}{\partial n} - \frac{\partial \theta}{\partial t} = -\frac{T}{V^2} \frac{ds}{dn} + \frac{1}{V^2} \frac{dh_0}{dn} \tag{12.24}$$

Transforming Eqs. (12.23) and (12.24) into characteristic coordinates, we get

$$\frac{\partial}{\partial \eta}(\nu - \theta) = \sin \mu \frac{\sin \theta}{r} - \frac{\cos \mu}{V^2}\left(T \frac{ds}{dn} - \frac{dh_0}{dn}\right)$$

$$\frac{\partial}{\partial \xi}(\nu + \theta) = \sin \mu \frac{\sin \theta}{r} + \frac{\cos \mu}{V^2}\left(T \frac{ds}{dn} - \frac{dh_0}{dn}\right)$$

The last terms in each equation may be written as derivatives along the characteristics with the geometry shown in Fig. 12.1(b), i.e.

$$\frac{\partial \eta}{\partial n} = \text{cosec } \mu, \quad \frac{\partial \xi}{\partial n} = -\text{cosec } \mu$$

Integration of the above governing equations over a small-mesh element yields

$$\nu_3 - \theta_3 = \nu_2 - \theta_2 + \sin \mu_2 \frac{\sin \theta_2}{r_2} \Delta\eta_{23} - \frac{\cos \mu_2}{V_2^2}[T_2(s_3 - s_2) - (h_{03} - h_{02})] \tag{12.25}$$

Scanned by CamScanner

$$\nu_3 + \theta_3 = \nu_1 + \theta_1 + \sin \mu_1 \frac{\sin \theta_1}{r_1} \Delta\xi_{13} - \frac{\cot \mu_1}{V_1^2} [T_1(s_3 - s_1) - (h_{03} - h_{01})] \tag{12.26}$$

where ν_3 and θ_3 may be obtained from Eqs. (12.25) and (12.26). From the above relations, it is seen that the values of s_3 and h_{03} at point 3 are needed for computation. These may be determined as follows: In Fig. 12.9, once the point 3 is located, the streamline through it may be approximately located by drawing a line with slope $\theta_{3'} = (1/2)(\theta_1 + \theta_2)$, intersecting the data curve at 3′. Since s and h_0 are invariant along streamlines, their values at point 3 are the same as at 3′ on the data curve, where they are known.

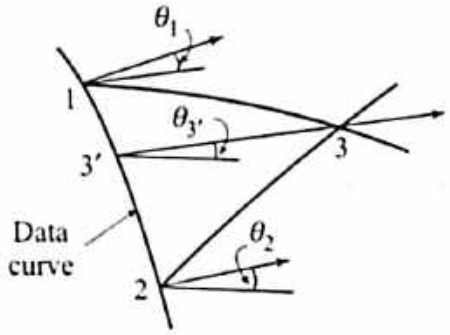


Fig. 12.9 Characteristic mesh and a streamline.

12.5 THEOREMS FOR TWO-DIMENSIONAL FLOW

For two-dimensional (plane) supersonic flow, from the compatibility relations (12.15), we have

$$\nu - \theta = R \quad \text{(along } \eta\text{-characteristics)}$$
$$\nu + \theta = Q \quad \text{(along } \xi\text{-characteristics)}$$

These two relations, which are *independent of the specific flow geometry*, lead to three useful theorems which we now give under three types of flow:

1. *General or nonsimple region* Characteristics of both the families are curved and are physically significant.
2. *Simple region* (*simple wave*) One family of characteristics is straight. The other family (curved) is physically insignificant and not shown (by convention).
3. *Uniform flow* Both families are straight and physically insignificant and not shown (by convention).

Consider the *general region* shown in Fig. 12.10. The values of ν and θ at the intersection of any two characteristics are found from the solution of the above equations, as

$$\nu = \frac{1}{2}(Q + R), \quad \theta = \frac{1}{2}(Q - R)$$

Scanned by CamScanner

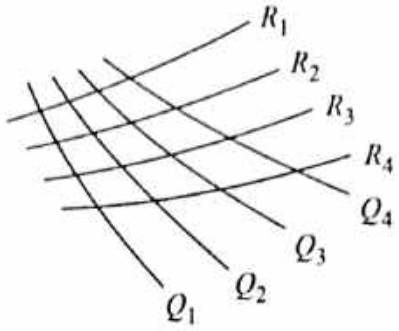


Fig. 12.10 Characteristics of a general region.

Along any η-characteristic, R is constant and so the changes in ν and θ depend only on the changes in Q. Thus,

$$\Delta\nu = \frac{1}{2}\Delta Q = \Delta\theta \tag{12.27a}$$

Similarly, along ξ-characteristics,

$$\Delta\nu = \frac{1}{2}\Delta R = -\Delta\theta \tag{12.27b}$$

Thus, the entire flow field is known if the values of R and Q on the characteristics are known.

Consider next the *simple region* shown in Fig. 12.11. In a simple region, by definition, either Q or R is constant throughout the region. In the figure, all the η-characteristics have the same value of R ($= R_0$). Then, by Eq. (12.27b), ν and θ are individually constant along a ξ-characteristic, which must be straight. Thus, in a simple region, one set of characteristics is straight lines, with uniform conditions on each one. The flow changes encountered in crossing the straight characteristics are given by

$$\boxed{\Delta\nu = \pm\Delta\theta} \tag{12.28}$$

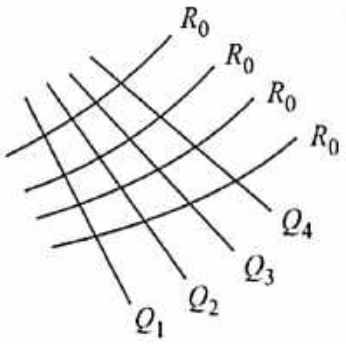


Fig. 12.11 Characteristics of a simple region.

In Eq. (12.28), the plus sign is for ξ-characteristics and the minus sign for η-characteristics. The relation given by Eq. (12.28) is different from that given

Scanned by CamScanner

by Eq. (12.27) in the sense that Eq. (12.28) is valid on any line that crosses the straight characteristics, and in particular on a streamline.

Consider now the *uniform flow* shown in Fig. 12.12. By definition, a uniform flow is that for which $R = R_0$ and $Q = Q_0$ throughout. That is, ν and θ are uniform, and both ξ-type and η-type characteristics are straight lines constituting a parallel network, as illustrated in Fig. 12.11.

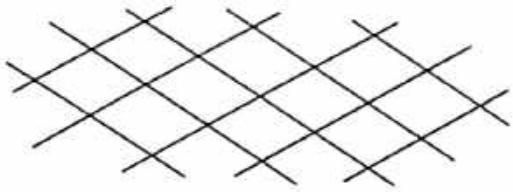


Fig. 12.12 Characteristics in a uniform flow region.

A flow field in which all three regions coexist is given in Fig. 6.20. As shown in the figure, the usual convention is to omit the Mach lines in the uniform region, to show only the straight lines in a simple wave, and both sets in the nonsimple region.

It is seen that *the uniform region does not adjoin the nonsimple region* (except at one point). This is a general theorem, which may be easily proved by trying to construct the contrary case, if we remember the definitions given above.

12.6 NUMERICAL COMPUTATION WITH WEAK FINITE WAVES

The method of constructing two-dimensional, supersonic flows by using waves was outlined in Chapter 6. If the waves are weak, we can set up a computing procedure which is equivalent to the characteristic method (see Section 6.6). In computation with weak waves, it is assumed that the entire gradual change in flow is assumed to occur discontinuously along a single line given by Mach angle $\bar{\mu}$, as shown in Fig. 12.13.

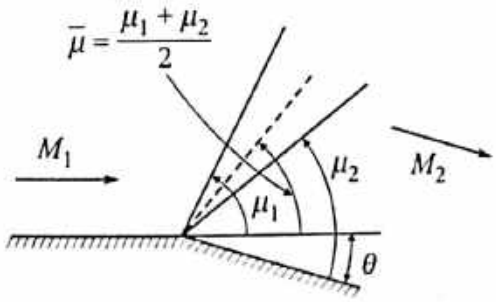


Fig. 12.13 Isentropic expansion.

It is further assumed that the strength of weak finite waves ($\Delta\theta$) does not change in intersections. This assumption is valid only for two-dimensional flow.

Scanned by CamScanner

Reflection of Waves

(a) On rigid walls a wave is reflected as a wave of the same sense (of opposite family), as illustrated in Fig. 12.14 (see also Section 6.11).

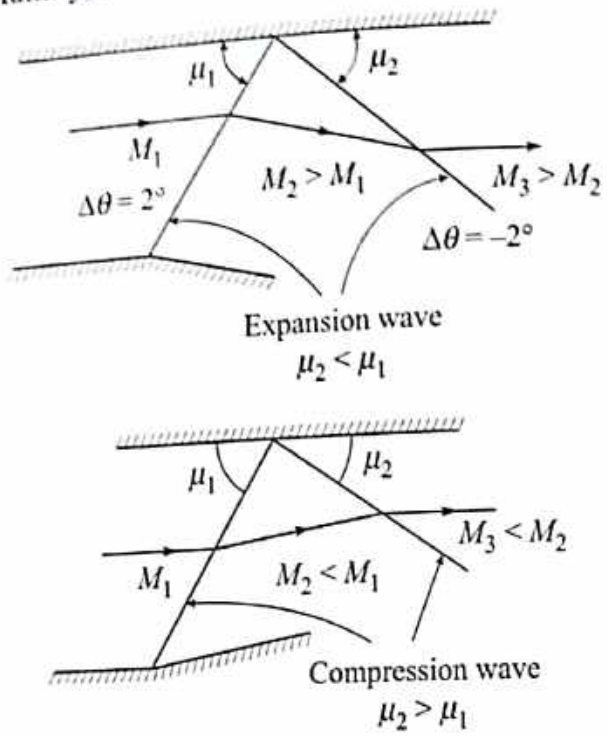


Fig. 12.14 Reflection of waves from solid wall.

(b) On an open or free boundary (jet), a wave is reflected as a wave of opposite sense, as illustrated in Fig. 12.15.

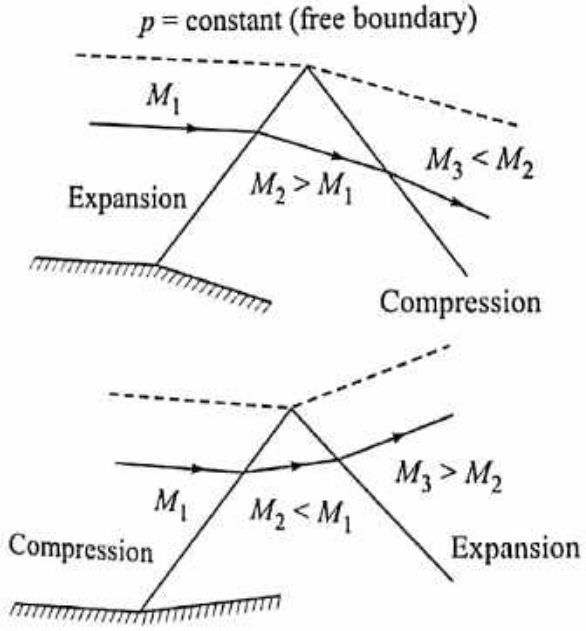


Fig. 12.15 Reflection of waves from free boundary.

Scanned by CamScanner

It is seen from Fig. 12.15 that the boundary itself is deflected. *The deflection of the free boundary is downwards if an expansion wave hits it and the deflection is upwards when a compression wave hits it.*

From the above reflection, it is seen that on reflection from a wall, a wave of ξ-type is changed to a wave of η-type. The turning strength of the reflected wave is the same as that of the incident wave, since the flow must return to the original direction, parallel to the wall. From this process we can visualize that the wave reflection may be 'cancelled' by suitable accommodation of the portion of the wall after the incident wave, i.e. there will not be reflection of wave if the wall is accommodated to the flow direction after incident wave, as shown in Fig. 12.16. The wall deflection is equal to the strength of the wave. We can summarize the above reflection patterns as follows (Fig. 12.17):

In Fig. 12.17, if $\Delta\theta_2 = \Delta\theta_1$, then there will not be any reflection. If $\Delta\theta_2 < \Delta\theta_1$, then the reflected wave will be an expansion wave and when $\Delta\theta_2 > \Delta\theta_1$, the reflected wave will be a compression wave.

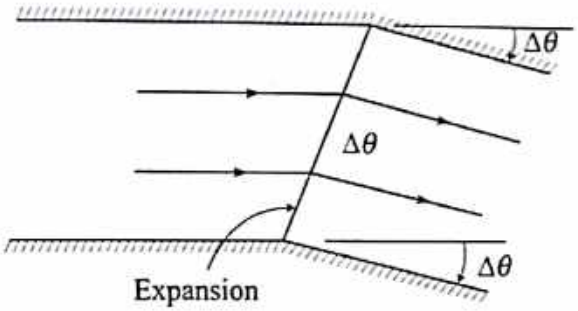


Fig. 12.16 Cancellation of reflection.

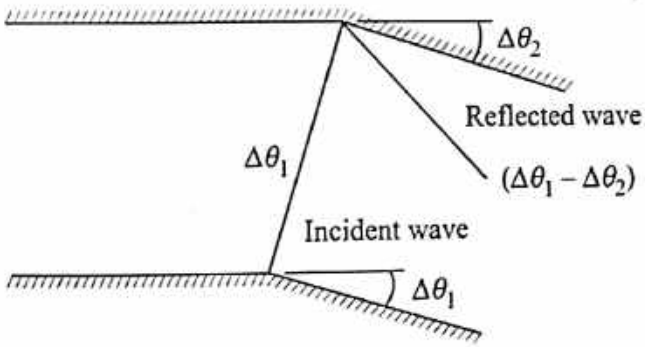


Fig. 12.17 Wave reflection.

In a process involving a large number of reflections of expansion waves, the flow condition at any point in the flow field is given by

$$\theta - \theta_1 = m - n, \quad \nu - \nu_1 = m + n \tag{12.29}$$

where m is the number of expansion waves of equal strength, say 1°, i.e. one family (ξ-type) crossed by the flow, and n is the number of expansion waves of equal strength, say 1°, the other family (η-type) crossed by the flow. The initial flow field is given by (ν_1, θ_1).

Scanned by CamScanner

More generally, the flow field condition (M, p, ρ, T) at any point in a flow involving multiple reflections of expansion and compression waves of both ξ-type and η-type is given by

$$\begin{aligned} \theta - \theta_1 &= m - n - k + l \\ \nu - \nu_1 &= m + n - k - l \end{aligned} \tag{12.30}$$

where k is the number of compression waves of one family (ξ-type) crossed by the flow, l is the number of compression waves of the other family (η-type) crossed by the flow.

EXAMPLE 12.2 Solve the flow field at the exit of an underexpanded two-dimensional nozzle with air flow, shown in Fig. 12.18. At the nozzle exit, $M_A = 1.435$ and $\theta_A = 0°$.

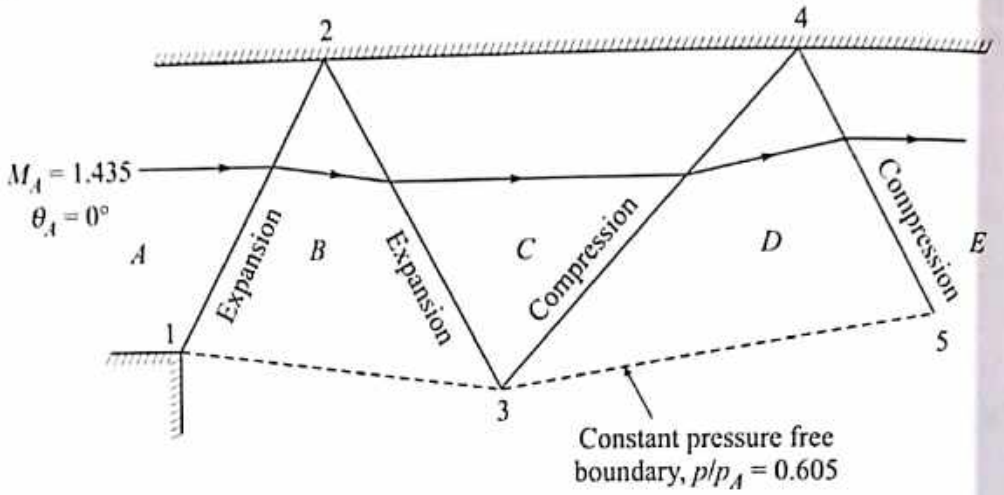


Fig. 12.18 Example 12.2.

Solution Because of symmetry, the streamline along the axis of the nozzle must be straight, and may be replaced by a solid wall, as shown in the figure. Given $M_A = 1.435$ and $\theta_A = 0$, from Table A1, we get $\nu_A = 10°$ and $p_A/p_0 = 0.299$ at $M_A = 1.435$. In this example, it is assumed that the entire expansion is taking place through a single expansion wave.

From our discussions on the Prandtl–Meyer function (Section 6.9), we know that ν and θ are connected by the relation $\nu = \pm\theta$, where the plus sign holds across a right-running characteristic and the minus sign holds across a left-running characteristic.

Now, the entire expansion from region A to region B is taking place across a left-running characteristic and, therefore, $\theta_B = -\nu_A = -10°$.

Also, by Eq. (6.49a), for the expansion

$$\nu_B = \nu_A + |\theta_B - \theta_A| = 10 + 10 = 20°$$

with the value of the Prandtl–Meyer function, we can get the flow properties. For $\nu_B = 20°$, from Table A1 of Appendix A,

$$M_B = 1.775, \quad p_B/p_0 = 0.181$$

Scanned by CamScanner

After the expansion, the pressure ratio in region B is 0.181. At the free boundary, the pressure outside the boundary must be equal to p_B. Therefore, the pressure ratio at the free boundary for the given exit pressure p_A is

$$\frac{p}{p_A} = \frac{p_B/p_0}{p_A/p_0} = \frac{0.181}{0.299} = 0.605$$

Following the above procedure, we can get the flow field as given in Table 12.2.

TABLE 12.2 Example 12.2

Field	ν	M	μ	p/p_0	θ
A	10°	1.435	44.2°	0.299	0°
B	20°	1.775	34.3°	0.181	−10°
C	30°	2.134	27.9°	0.104	0°
D	20°	1.775	34.3°	0.181	10°
E	10°	1.435	44.2°	0.299	0°

The above solution can yield the wave and deflection angles as well. The mean Mach angle $\bar{\mu}$ for an expansion fan with μ_1 and μ_2 as the Mach angles at the beginning and end of the fan is given by

$$\bar{\mu} = \frac{\mu_1 + \mu_2}{2}$$

Similarly, the mean deflection angle $\bar{\theta}$ is given by

$$\bar{\theta} = \frac{\theta_1 + \theta_2}{2}$$

With the above relations, for the present flow field, we have

Wave	$\bar{\mu}$	$\bar{\theta}$
1–2	39.25°	−5
2–3	31.1°	5°
3–4	31.1°	5°
4–5	39.25°	−5°

Note In the above problem, all the regions are assumed to be simple regions. There is a 10° deflection of the jet boundary as it leaves the nozzle.

12.7 DESIGN OF SUPERSONIC NOZZLE

In this design, we are looking for a proper geometry of the nozzle to accelerate the flow to result in uniform, parallel, and wave-free supersonic flow. In Sections 4.4 and 4.6, it has been highlighted that only a shape like the one shown in Fig. 12.19 can produce such a flow.

That is, in order to accelerate a flow from subsonic to supersonic speed, the duct has to be convergent-divergent in shape, as shown in Fig. 12.19.

Scanned by CamScanner

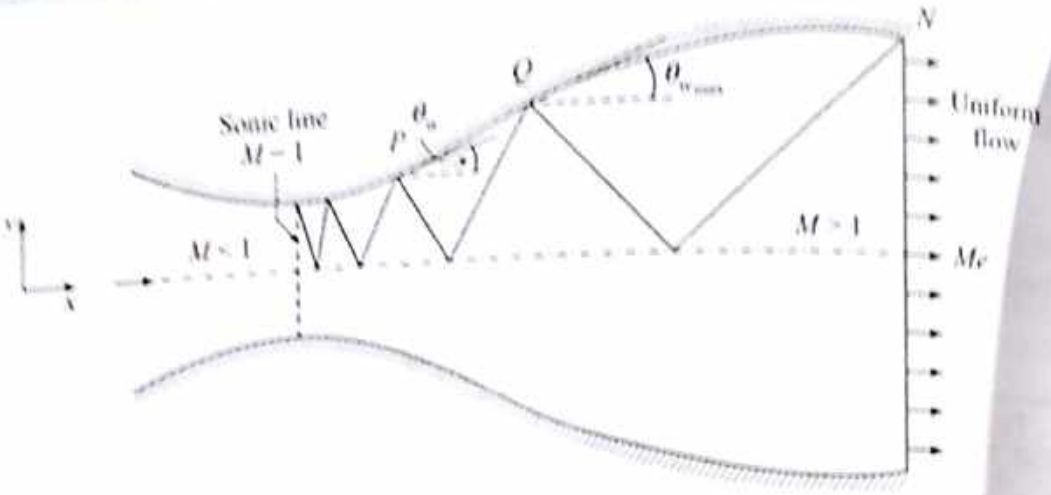


Fig. 12.19 Supersonic nozzle.

Further, for a supersonic convergent-divergent nozzle, it is essential to have wave-free and parallel flow in the test-section at the desired Mach number. An improper contour will result in the presence of weak waves, which may coalesce to form a finite shock and prevent the establishment of uniform flow in the test-section. Therefore, it is imperative to have a proper design of nozzle contours for generation of uniform supersonic flows.

The method of characteristics provides a technique for properly designing the contour of supersonic nozzle for shock-free, isentropic flow, taking into account the multidimensional flow inside the duct. The purpose here is to illustrate the design of a supersonic nozzle by the method of computation with weak waves (characteristics).

Consider the supersonic nozzle shown in Fig. 12.19. The subsonic flow in the convergent portion of the nozzle is accelerated to sonic speed at the throat. Generally, because of the multidimensionality of the converging subsonic flow, the sonic line is gently curved. However, in most applications, we assume the sonic line to be straight, as shown in Fig. 12.19. In the divergent portion downstream of the throat, let θ_w be the angle at any point P on the duct wall. The portion of the nozzle with increasing θ_w is called the *expansion* section, where expansion waves are generated and propagate in the downstream direction, reflecting from the opposite wall. In Fig. 12.19, because of symmetry, waves above the centre-line only are shown. At point Q, there is an inflection of the duct wall contour and θ_w is maximum. Downstream of Q, θ_w decreases until the wall becomes parallel to the x-direction at point N.

Supersonic nozzles with gradual expansions as illustrated in Fig. 12.19 are characteristic of the wind tunnel nozzle where high-quality, uniform flow is required in the test-section. Hence, wind tunnel nozzles are long, with very smooth gradual expansion. But in applications like rocket motors, nozzles are comparatively short in order to minimize weight. Also, in applications where rapid expansions are the requirements, such as the non-equilibrium flow in gas dynamic lasers, the nozzle length should be as short as possible. In such cases,

Scanned by CamScanner

the expansion portion of the nozzle is shrunk to a point, and the expansion takes place through a centred Prandtl–Meyer wave emanating from a sharp-corner throat with an angle $\theta_{w_{max}}$, as shown in Fig. 12.20. The length L shown in Fig. 12.20 is the minimum length possible for shock-free, isentropic flow. If the contour is made within a length shorter than L, shocks will develop inside the nozzle.

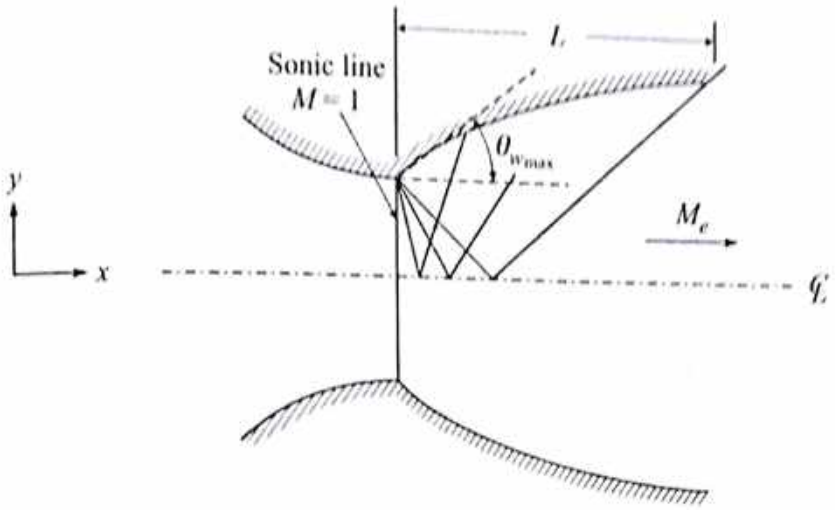


Fig. 12.20 Minimum-length nozzle.

Contour Design Details

To illustrate the application of the method of characteristics for supersonic nozzle design, let us consider the specific problem of designing a minimum length nozzle to expand the flow from $M = 1$ at the throat to $M = 2.0$ in the test-section where the flow is to be uniform and parallel to the flow direction at the throat.

Let us employ the region-to-region Method of Characteristics for designing the contour. Since minimum length nozzle is to be designed, sharp-cornered nozzle assumption will be made.

For characteristics it can be proved that

1. along left-running characteristic or across right-running characteristic, $\nu - \theta$ = constant;
2. along right-running characteristic or across left-running characteristic, $\nu + \theta$ = constant;

where ν is the Prandtl–Meyer function and θ is the flow turning angle.

In the region-to-region method, the flow is divided into various regions by the incident and reflected characteristics (from the centreline). Now, with the help of ν and θ, Mach numbers in the regions can be calculated using the above mentioned relations between ν and θ.

The sonic line at the throat is assumed to be straight and the design is done for one-half of the nozzle, as the other half is only a mirror image of the first, because of symmetry.

Scanned by CamScanner

The characteristic lines and contour points for the proposed nozzle are shown in Fig. 12.21. For a sharp-cornered nozzle,

$$\boxed{\theta_{\text{fan}} = \frac{\nu_{\text{TS}}}{2}}$$

where the subscript "TS" refers to the test-section.

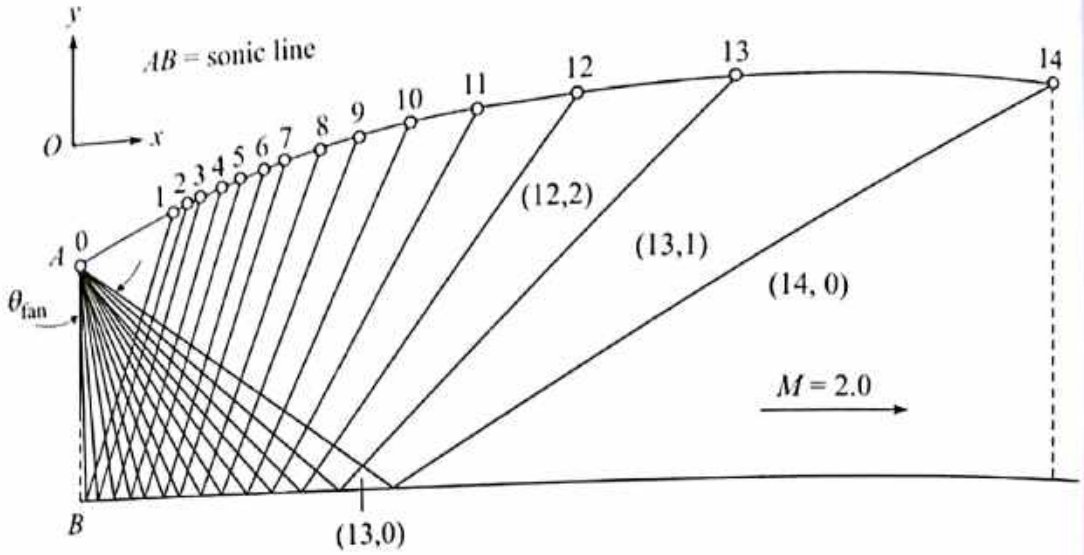


Fig. 12.21 Characteristic lines and contour points.

From Table A1 in Appendix A, for $M_{\text{TS}} = 2.0$, $\nu_{\text{TS}} = 26.38°$. Hence,

$$\theta_{\text{fan}} = 13.19°$$

A total of 14 characteristics are considered in the fan, with the first being at an angle of 0.19° with the sonic line and the rest being at a difference of 1° to each other, as illustrated in Fig. 12.21, i.e. all the waves (except the first) are of strength 1°. The reflections from the centreline form the regions. For example, characteristic 1 gives rise to 15 regions from (0, 0) to (0, 14), as shown in the figure.

The values of ν and θ at every region can be calculated as follows. For the regions formed by the first wave, we have

$\theta = 0°$, $\nu = 0°$ [region (0, 0)]
$\theta = 0.19°$, $\nu = 0.19°$ [region (0, 1)]
$\theta = 1.19°$, $\nu = 1.19°$ [region (0, 2)]

For the regions formed by the second wave,

$\theta = 0°$, $\nu = 0.38$ [region (1, 0)]
$\theta = 1°$, $\nu = 1.38$ [region (1, 1)]

etc.

Similarly, we can go up to region (14, 0).

Scanned by CamScanner

A computer program is written for the calculation of θ and ν in every region. The program takes the input of a number n and divides the θ_{fan} into $(13/n + 1)$ characteristics. In the present calculation, n is taken as unity. The program listing for calculating the values of ν and θ in the regions considered are given in Appendix B. Once ν is known, the Mach number can be obtained from Table A1 in Appendix A. The values of ν and θ at different regions shown in Fig. 12.21 and the corresponding Mach numbers are listed in the program output given in Appendix B. Note that in the present nozzle design for Mach 2, the computed area ratio is $A_e/A^* = 1.6875$ (see the output on page 437). This is within 0.03 per cent of the value $A_e/A^* = 1.688$ from isentropic table.

TABLE 12.3 Coordinates of contour points

Contour point	*Throat*	1	2	3	4	5	6	7
x mm	0.0	7.76	7.95	9.01	10.25	11.69	13.38	15.40
y mm	8.8	10.62	10.66	10.89	11.13	11.38	11.65	11.93
		8	9	10	11	12	13	14
		17.84	20.85	24.66	29.69	36.78	48.00	71.70
		12.23	12.55	12.88	13.24	13.61	14.00	14.41

For calculating the x-location of a contour point i, the following formula may be used:

$$x_i = \frac{(A/A^*)_i - (A/A^*)_{i-1}}{2 \tan(\theta_{i-1})} y^* + x_{i-1}$$

$$y_i = (A/A^*)_i \, y^*$$

where $i = 1, 2, \ldots, 14$. In these equations,

θ_{i-1} = turning angle in region $i - 1$
$(A/A^*)_i$ = area ratio at point i
$(A/A^*)_{i-1}$ = area ratio at point $i - 1$
A^* = area at throat
y^* = y-coordinate at the throat

Also,

$(A/A^*)_0$ = area ratio at throat = 1
$\theta_0 = 13.19°$ (in the present case)

The area ratio at a particular point may be calculated from Eq. (4.32) or Table 1 in the Appendix as the Mach number at that point is known. The area ratio also gives the y-location of the point. Table 12.3 shows the x and y coordinates of contour points. These contour points along with characteristic lines are shown in Fig. 12.21.

Scanned by CamScanner

The resulting nozzle contour given by the calculated points is shown in Fig. 12.22. A nozzle fabricated as per the contour in this figure generated a uniform parallel supersonic stream with Mach number 1.97 at the gas dynamics laboratory at the Indian Institute of Technology Kanpur.

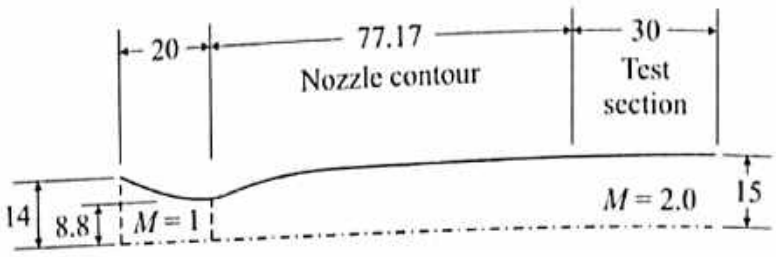


Fig. 12.22 Supersonic nozzle.

In the above calculations, viscosity has been neglected. But in actual flow, the boundary layer on the nozzle and side walls will have a displacing effect which will reduce the effective height and width of the nozzle. Allowance for this should be made by adding a correction for boundary-layer growth to the designed contour. Finally, we should note that in the present example, calculation procedure has been very much simplified by assuming the flow in the nozzle to be two-dimensional. For axi-symmetric and three-dimensional flow, the strength of a wave, generally, varies continuously in space and, therefore, the simple relations between ν and θ used in the present case are no longer valid.

12.8 SUMMARY

The method of Characteristics is basically a numerical technique. Characteristics are weak waves across which there is a jump in the gradients of flow properties. The general features of the characteristics are:

- They exist only in supersonic flows.
- They are coincident with Mach lines.
- On the characteristics the derivatives of flow properties are discontinuous, while the flow properties themselves are continuous.
- On the characteristics the dependent variables satisfy a certain relation known as the compatibility relation.

The compatibility relations are

$$\begin{aligned} \nu - \theta &= R \text{ (constant) along } \eta\text{-characteristics} \\ \nu + \theta &= Q \text{ (constant) along } \xi\text{-characteristics} \end{aligned} \qquad (12.15)$$

These relations provide the key to the method of computation. The compatibility relations, which are independent of the specific flow geometry, lead to the result that the flow changes encountered in crossing characteristics which are straight are given by

$$\Delta\nu = \pm\Delta\theta \qquad (12.28)$$

Scanned by CamScanner

where the plus sign is for ξ-characteristics and minus sign is for η-characteristics.

On a rigid boundary a wave is reflected as a wave of the same sense (of opposite family) and on an open or free boundary a wave is reflected as a wave of opposite sense.

The deflection of a free boundary is downwards if an expansion wave hits it and the deflection is upwards when a compression wave hits it.

The wave reflection may be *cancelled* by a suitable accommodation of portion of the wall after the incident wave.

The method of characteristics provides a technique for the proper design of supersonic nozzle for shockfree, isentropic flow. Centred expansion of the flow at the throat results in a short length nozzle and continuous expansion at the throat results in a long nozzle.

For calculating the x and y coordinates of a contour point i, the following formula may be used:

$$x_i = \frac{(A/A^*)_i - (A/A^*)_{i-1}}{2 \tan(\theta_{i-1})} y^* + x_{i-1}$$

$$y_i = (A/A^*)_i \; y^*$$

where

θ_{i-1} = flow turning angle in region $i - 1$

$(A/A^*)_i$ = area ratio at point i

$(A/A^*)_{i-1}$ = area ratio at point $i - 1$

A^* = throat area

y^* = y coordinate at the throat

$(A/A^*)_0$ = area ratio at throat = 1

$\theta_0 = \theta_{\text{fan}}$

The close agreement between the design and measured Mach numbers experienced by experimental researchers highlights the validity of this method for the design of supersonic nozzles for practical applications such as supersonic wind tunnels.

Scanned by CamScanner

13 Measurements in Compressible Flow

13.1 INTRODUCTION

For calibration and use of flow devices like wind tunnel, we have to do many measurements to define the properties of the flow in the device. Once the calibration of the device is over, to compute the forces and their distribution on the models which are to be tested by placing them in the known flow field generated by wind tunnel, etc. we again require instruments and techniques for making these measurements. In this chapter we shall study some of the popular techniques and devices used for measuring the properties of a compressible flow. From our basic studies on fluid flows, we know that the important variables that need measurement are pressure, temperature, density, flow velocity and its direction. We shall discuss the methods available for the measurement of these properties for compressible flows.

13.2 PRESSURE MEASUREMENTS

The pressure measuring devices used for fluid flow pressure measurements may generally be grouped into manometers and pressure transducers. Various types of liquid manometers are employed, depending on the range of pressures to be measured and the degree of precision required. The U-type manometers, multitube manometers, micro manometers, and Betz type manometers are some of the popular liquid manometers. The pressure transducers used may be classified as electrical type transducers, mechanical type transducers, and optical type transducers.

Liquid Manometers

In a liquid manometer the pressure is balanced by the weight of the liquid column. The sensitivity of the instrument depends on the density of the fluid

Scanned by CamScanner

used. Water, alcohol, and mercury are the commonly used fluids. For compressible flows with high subsonic and supersonic Mach numbers, mercury is suitable since fluids like water and alcohol will show unmanageable variations in manometer columns for pressures associated with such speeds.

In addition to these manometers, an accurate *barometer* is essential for pressure measurements, since pressures are invariably measured in terms of a difference in pressure from some known reference. The most common reference is the local atmospheric pressure. For pressures measured with reference to atmospheric pressure, conversion to absolute pressures requires that atmospheric pressure be known. The common mercury barometer, shown in Fig. 13.1, is quite satisfactory for this purpose. When equipped with a suitable device for viewing the meniscus of the mercury column and reading the mercury column height scale, a good barometer will allow measurement of atmospheric pressure with an accuracy of a small fraction of millimetre of mercury. This is usually quite adequate for purposes of compressible flow measurements.

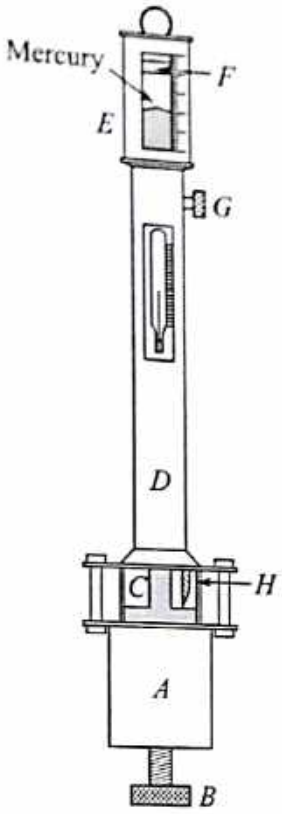


Fig.13.1 A mercury barometer.

Measuring Principle of Manometers

The manometers measure the difference between a known and an unknown pressure by observing the difference in heights of two fluid columns. Two common types of manometers are illustrated in Fig. 13.2.

Figure 13.2(a) consists of two vertical glass tubes joined together with a U-type connection at the bottom. Each tube has a linear scale attached to it which is usually marked off in millimetres. The tubes are filled with a fluid until the fluid level in the tube is at the centre of the adjacent scales. A reference pressure is applied to the top of one of the tubes and the pressure to be measured is applied to the top of the second tube. The heights of the two columns of fluid will change until the difference between the two heights, h, is equal to the pressure to be measured in terms of fluid column height. The commonly employed reference pressure for this type of manometer is atmospheric pressure. However, in many cases the difference between atmospheric and measured pressure will represent a much longer column of the manometer fluid

Scanned by CamScanner

than can be accommodated by the tubes. In such cases, the only way to use the manometer (other than changing the fluid) is to adjust the reference so that a smaller fluid height will be reached. This has the disadvantage of adding an intermediate pressure to measure.

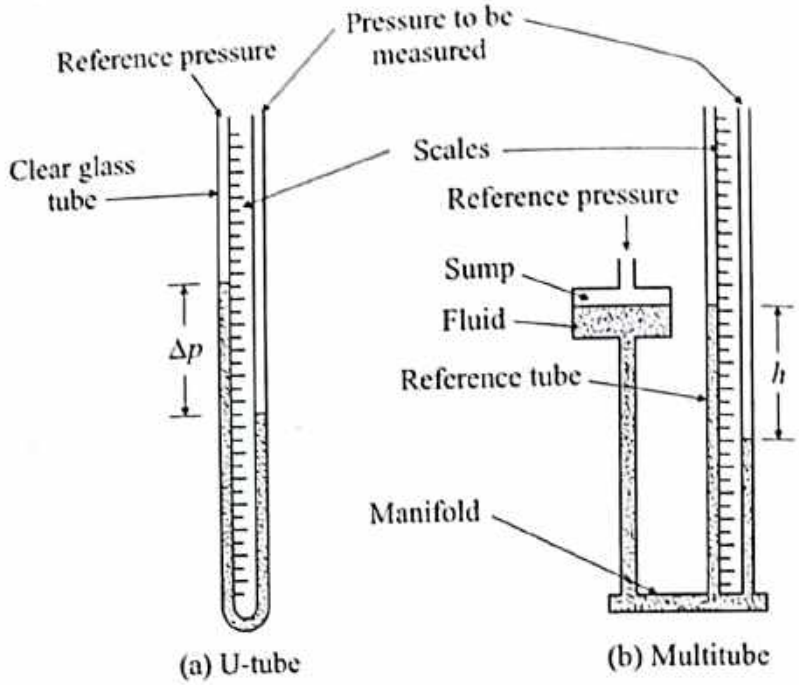


Fig. 13.2 Manometers.

The sump and tube manometer, illustrated in Fig. 13.2(b), operates on the same principle as the U-tube manometer. However, in this manometer a large cross-sectional area sump takes the place of the tube to which the reference pressure is applied. The sump level is used as reference and, frequently, a number of tubes are employed to form a multitube manometer. The sump and tube manometer has the following advantages over the U-tube manometer:

1. It can be used for the measurement of more than one differential pressure at a time.
2. The reference level can be adjusted so that only one scale has to be read instead of two, to determine the fluid column height. Photographs of a U-type and sump and multitube manometers are depicted in Figs. 13.3 and 13.4, respectively.

Either of the two types of manometer may be constructed with tubes and scale that can be tilted. In this way, an improvement in reading accuracy is obtained, since a given distance along the scale will represent a smaller vertical height and consequently a smaller pressure.

The ordinary liquid manometers are not suitable for very high or very low pressure measurements. In addition, they have a very poor frequency response. Further, a little dirt in a tube, a bubble in a line, or condensate changing the fluid specific gravities can all produce anomalous readings. If the user could take

Scanned by CamScanner

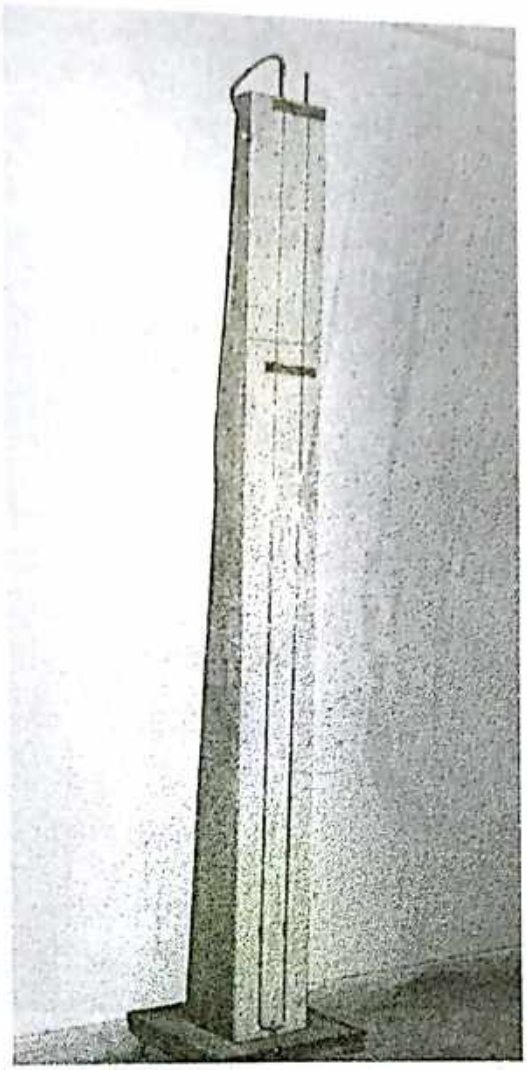


Fig.13.3 U-tube manometer.

care of the above-mentioned problems, the liquid manometers will prove to be an excellent device for pressure measurement in most of the practical situations barring a few flow situations like flow in intermittent tunnels where accurate measurement of pressures with liquid manometers is very difficult because of the availability of the short durations for measurements. However, these problems can be sorted out if one could arrange to connect an effective pinching mechanism, which could close all the columns of the manometer at an appropriate time, thereby making the liquids in different tubes to stay wherever they are. After noting down the readings, the tubes can be opened again for the next measurement.

Dial-Type Pressure Gauges

The dial-type pressure gauge, shown in Fig. 13.5, usually operates on the principle of a bellows or a Bourdon tube deflecting as a result of a pressure change and driving the needle on a dial through a mechanical linkage. Although gauges of this type may be obtained with accuracies suitable for quantitative

Scanned by CamScanner

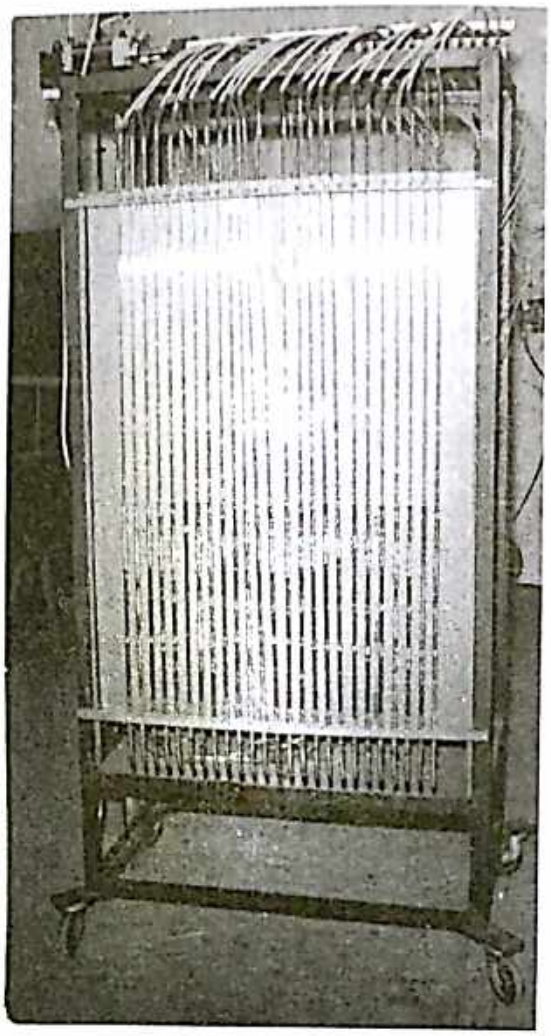


Fig. 13.4 Sump and multitube manometer.

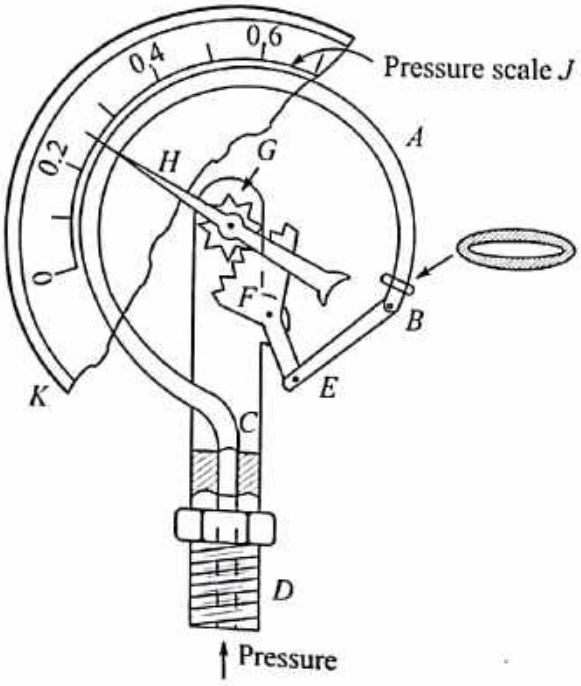


Fig. 13.5 Dial-type pressure gauge.

Scanned by CamScanner

pressure measurements, they are not extensively used for this purpose. The are primarily used for visual monitoring of pressure in many plumbing circuits.

As compared to manometers, the dial-type gauges have the advantage of being easier to read. Also, they can be obtained in pressure ranges well beyond those of the manometers. However, they do have the following disadvantages:

1. They must be calibrated periodically to ensure that they continue to read correctly.
2. The manometers are less expensive when there is a large number of pressures to be read.
3. Like manometers, they cannot be easily read electronically.

Pressure Transducers

Pressure transducers can be designed and built for almost any pressure generally encountered in fluid flow measurement. These can also be used for remote indication. Pressure transducers are electromechanical devices that convert pressures to electrical signals which can be recorded with a data system such as that used for recording strain gauge signals. These transducers are generally classified into mechanical, electrical or optical type.

The commonly used transducers employ an elastic diaphragm (various shapes) which is subjected to a displacement whenever pressure is applied. This movement is generally small and kept within linear range, and is amplified using mechanical, electrical, electronic, or optical system. A typical diaphragm pressure capsule is illustrated in Fig. 13.6.

The local strain produced on the diaphragm is proportional to the pressure applied. For a circular diaphragm, the deflection δ at the centre is given by

$$\delta = \frac{3p}{16Et^2} a^4(1 - \mu_r^2)$$

where

a = the radius of diaphragm
t = the thickness of diaphragm
μ_r = Poisson's ratio
E = Young's modulus
p = pressure.

This holds good for small deflections only.

For large deflections, corrugated diaphragms have to be used. Usually, the diaphragms are made using beryllium copper or phosphor brozone sheets. Heat-treated stainless steel diaphragms are also often employed. Photographs of some transducers are shown in Fig. 13.7.

The following are the advantages of pressure transducers over manometers and other pressure gauges:

1. They provide a signal proportional to pressure which can be automatically recorded by any data system.

Scanned by CamScanner

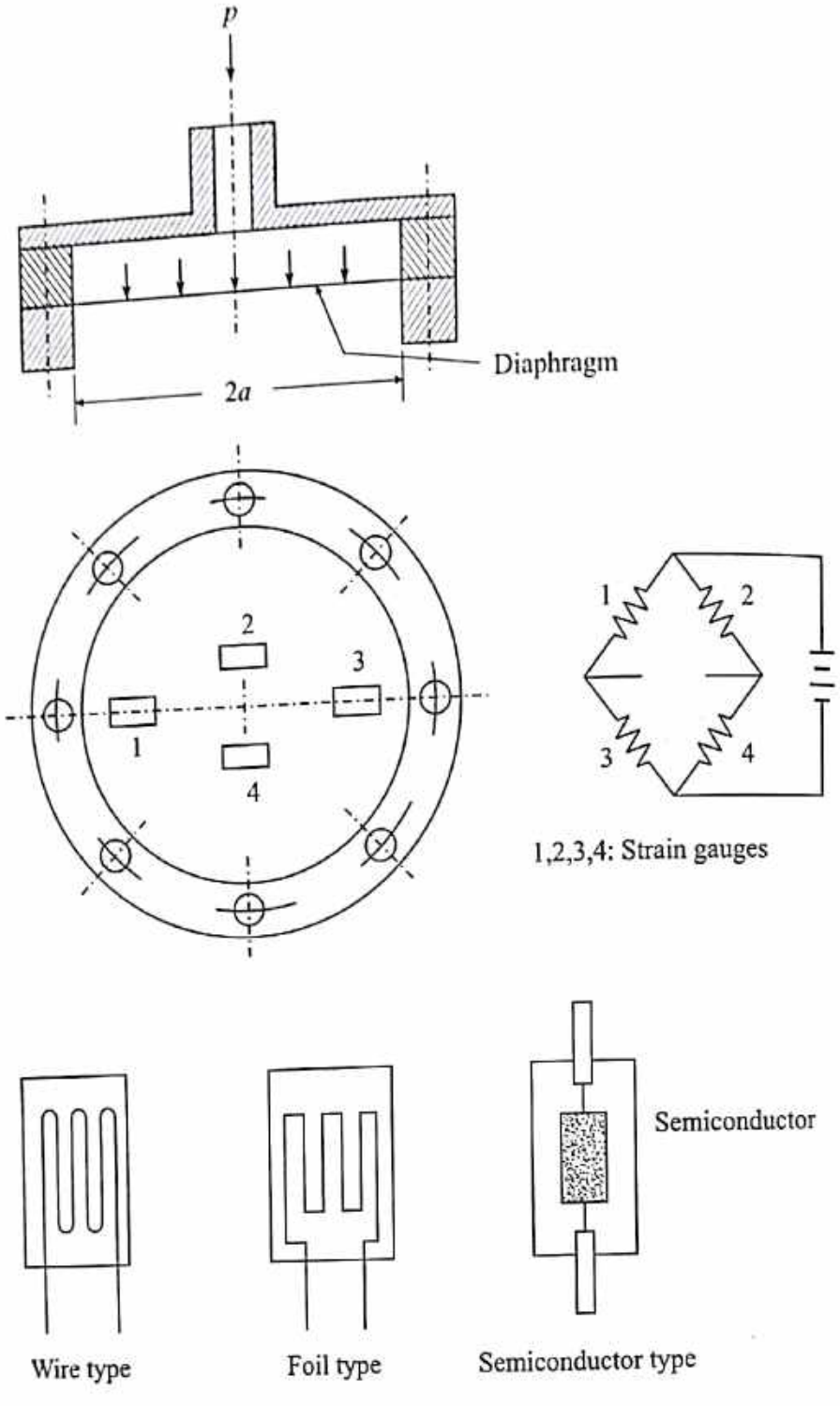


Fig. 13.6 Pressure transducer (strain gauge type).

2. They are relatively low volume devices and consequently respond more rapidly to pressure changes.
3. They are small enough to be mounted inside the wind tunnel models.

Their major disadvantage relative to a good manometer is that they must be calibrated, whereas the manometer with a known fluid can be considered as the pressure standard.

Scanned by CamScanner

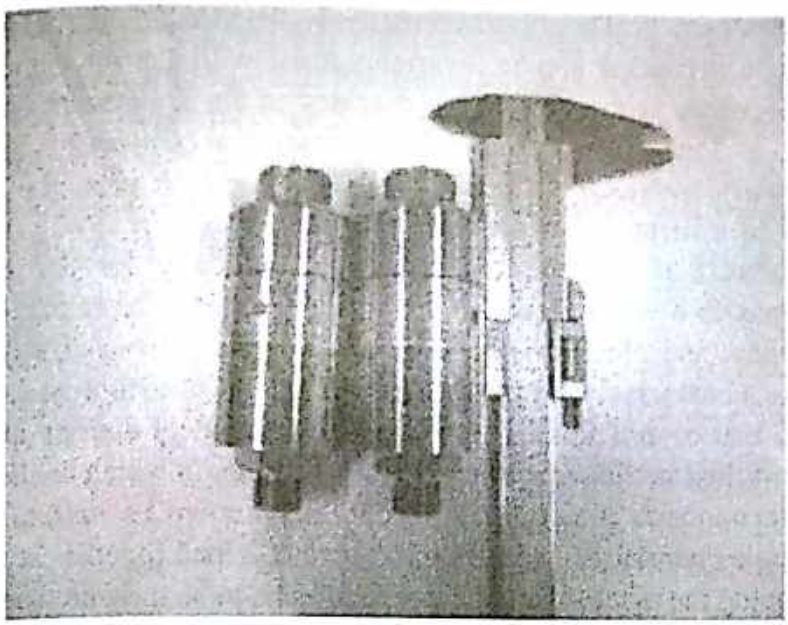


Fig. 13.7 Pressure transducers.

Because of the relatively high cost of pressure transducers in quantity, a scheme has been devised for using one transducer to measure a number of pressures—up to 48 or more. This scheme is the commutation of pressures using a device known as a *pressure scanner valve*.

In using the scanner valve, model pressures are allowed to stabilize in the lines leading from the model through the stator of the scanner valve. The rotor is then turned through one revolution, connecting each model pressure in turn to the pressure transducer through a slot.

EXAMPLE 13.1 The U-type manometer measures total and static pressures of a high-speed flow as 535 mm Hg (suction) and 610 mm of mercury (suction), respectively. Determine the flow Mach number.

Solution Let the atmospheric pressure be 760 mm Hg (standard sea level pressure). Then the total and static pressures of the stream in absolute scale are

$$p_{t_{abs}} = p_{t_{meas}} + p_{atm} = -535 + 760 = 225 \text{ mm Hg}$$
$$p_{abs} = p_{meas} + p_{atm} = -610 + 760 = 150 \text{ mm Hg}$$
$$\frac{p}{p_t} = \frac{150}{225} = 0.667$$

For this pressure ratio, from Table A1 in Appendix A,

$$M = \boxed{0.783}$$

13.3 TEMPERATURE MEASUREMENTS

For direct measurement of the static temperature the device which measures the temperature should travel at the velocity of the flow without disturbing the flow.

Scanned by CamScanner

But this is impractical. Therefore, alternatively, the measurement of temperature of high-speed streams is almost invariably made with thermocouples.

Thermocouple is a device which operates on the *Seebeck principle*, which states that, *a flow of heat in a metal is always accompanied by a flow of electromotive force (emf)*. In other words, the Seebeck principle states that, "heat flow in a metal is always accompanied by an emf flow". This is also referred to as Seebeck effect. This forms the basis for the working of thermocouple. In a vast number of metals like, copper, platinum, chromal and iron, both heat and emf flow in the same direction. But in another group of metals, like constantan, alumal, and rhodium, the direction of heat flow is opposite to that of emf flow. These two groups, namely the one in which the heat and emf flow in the same direction and the other in which the heat and emf flow in the opposite directions are popularly known as *dissimilar metals*. Thermocouples consist of two dissimilar metals joined together at two points, one point being the place where the temperature is to be measured and the other point being a place where the temperature is known (called the reference junction).

First, let us consider the measurement of temperature by locating a thermocouple or other thermometric device at the wall surface, as shown in Fig. 13.8.

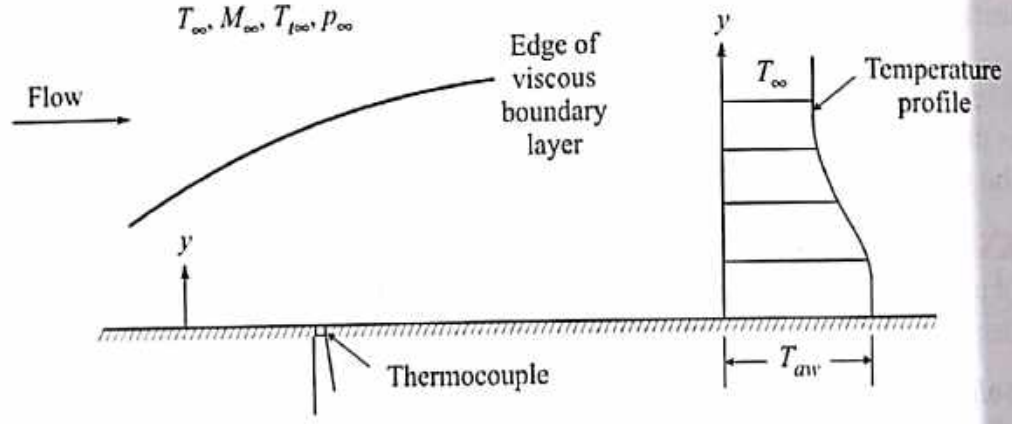


Fig. 13.8 Thermocouple located at the wall surface.

The thermocouple at the wall surface lies inside the viscous boundary layer, at a fixed wall, where the flow velocity is zero, and we should expect the measured wall temperature to be closer to the freestream total temperature $T_{t\infty}$ than the freestream static temperature T_∞. A temperature distribution in a compressible-flow boundary layer is as shown in Fig. 13.8. Let the wall be an insulated surface. Therefore,

$$\frac{\partial T}{\partial y} = 0 \quad \text{at } y = 0$$

and the temperature at the wall is called *adiabatic wall temperature* T_{aw}. There is heat flow in the y-direction due to conduction. Because of the flow of a high velocity gas stream near a surface, there can be an appreciable frictional heating

Scanned by CamScanner

of the fluid. In other words, the fast moving layers in the boundary layer do work on the slowly moving layers. If the heat loss due to conduction and energy gain from viscous heating cancel each other, then the flow can be considered to be brought to rest adiabatically in the boundary layer, and $T_{aw} = T_{t\infty}$. A measure of the relative importance of heating is given by the *Prandtl number*, defined as

$$\boxed{\mathrm{Pr} = \frac{\mu c_p}{K}}$$

For a fluid with Pr = 1, the adiabatic wall temperature is equal to the freestream stagnation temperature. If Pr < 1, then $T_{aw} < T_{t\infty}$. This can be summarized by defining a *recovery factor* $\mathbb{R}$, where

$$\boxed{\mathbb{R} = \frac{T_{aw} - T_\infty}{T_{t\infty} - T_\infty}}$$

Since $T_{t\infty} = T_\infty\left(1 + \dfrac{\gamma - 1}{2} M_\infty^2\right)$, from Eqs. (2.48), it follows that

$$T_{aw} = T_\infty\left(1 + \mathbb{R}\frac{\gamma - 1}{2} M_\infty^2\right)$$

It can be shown that for laminar compressible boundary layer,

$$\mathbb{R} = (\mathrm{Pr})^{1/2}$$

whereas for a turbulent boundary layer,

$$\mathbb{R} \approx (\mathrm{Pr})^{1/3}$$

For air, up to moderately high temperatures, Pr = 0.72, so that $\mathbb{R} \approx 1$, for a turbulent boundary layer.

From the foregoing discussion, it is clear that a direct measurement of freestream static temperature is not possible; a measurement of the adiabatic wall temperature can be used to determine $T_{t\infty}$; then by measuring $p_{t\infty}$ and p_∞, M_∞ and T_∞ can be calculated.

For measurement of temperature in the absence of a wall, a stagnation temperature probe, as illustrated in Fig. 13.9, can be used to determine $T_{t\infty}$. The flow is brought to rest inside the tube. Vent holes are provided in the sides of the probe to allow for proper ventilation of space inside the probe. If the air is

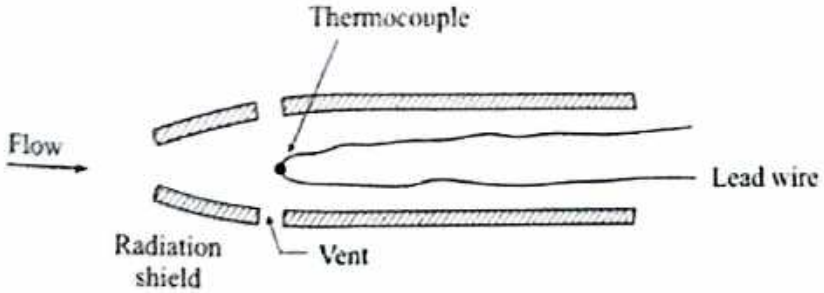


Fig. 13.9 Stagnation temperature probe.

Scanned by CamScanner

allowed to be stagnant inside, it may get cooled and yield a false reading. It is necessary that the flow be slowed down to zero velocity at the thermocouple with no gain or loss of heat.

Shields have been provided to prevent radiation heat loss from the thermocouple; also, the thermocouple lead wires must be made as thin as possible so as to minimize heat flow by conduction back along the wires.

When the flow is of supersonic Mach number, there will be a detached shock standing in front of the probe. However, the measurement of $T_{t\infty}$ is unaffected by the presence of the shock, since the flow across the shock is adiabatic. In such streams, the probes usually measure temperatures from slightly below to considerably below the true stagnation temperatures. The performance of such a probe is usually defined by a *recovery factor* k as follows:

$$\boxed{k = \frac{T_{ti} - T_\infty}{T_t - T_\infty}}$$

where

k = recovery factor
T_{ti} = indicated or measured temperature, K
T_t = total temperature, K
T_∞ = static temperature, K.

By suitable design, k can be made very close to unity for air. In any case, such a probe must be calibrated to define k as a function of Re, Pr and M.

The above-mentioned techniques for measuring temperature of a compressible flow stream are only selective representations of the various techniques available for such measurements. For a deeper understanding of these measurement procedures, the reader should refer to books on Experimental Techniques, like Rathakrishnan (2016).

EXAMPLE 13.2 A total temperature probe measures the temperature of a supersonic flow with Mach number 1.5 as 520 K. If the probe has a recovery factor of 0.97, determine the stream static temperature.

Solution From Table A1 of Appendix A, for $M_\infty = 1.5$, $T_\infty/T_{t\infty} = 0.6897$

$$\text{Recovery factor, } k = \frac{T_{ti} - T_\infty}{T_{t\infty} - T_\infty} = 0.970$$

$$= \frac{520 - T_\infty}{\left(\frac{1}{0.6897} - 1\right) T_\infty} = 0.97$$

This gives the stream static temperature T_∞ as

$$T_\infty = \boxed{362 \text{ K}}$$

Scanned by CamScanner

13.4 VELOCITY AND DIRECTION

The velocity or Mach number and flow angularity are essential for calibrating flow devices like wind tunnels. With the measured pressure and temperature, the magnitude of velocity can be calculated with the relation

$$V = M\sqrt{\gamma RT}$$

In order to decide on the quality of the flow device, it is also necessary to know the direction of the velocity vector or flow angularity. At supersonic speeds, this can be found with a symmetric wedge or cone as shown in Fig. 13.10. For a uniform flow passing over a symmetrical wedge, the angle of attack of the wedge can be determined from a measurement of the pressure difference $(p_u - p_l)$. For a flow without angularity, a symmetrical wedge with its centreline aligned with the flow must read the pressure difference $(p_u - p_l)$ as zero. A typical symmetrical wedge for measuring flow angularity is depicted in Fig. 13.11.

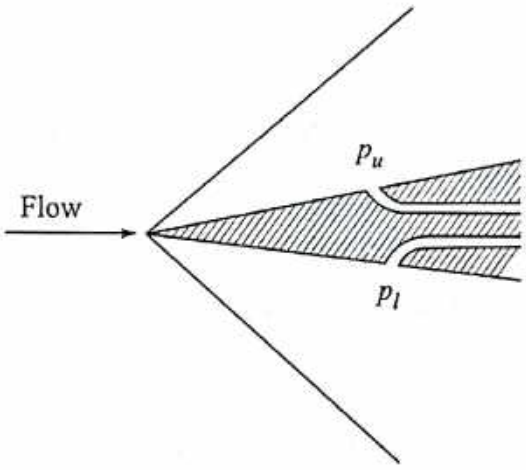


Fig. 13.10 Symmetrical wedge.

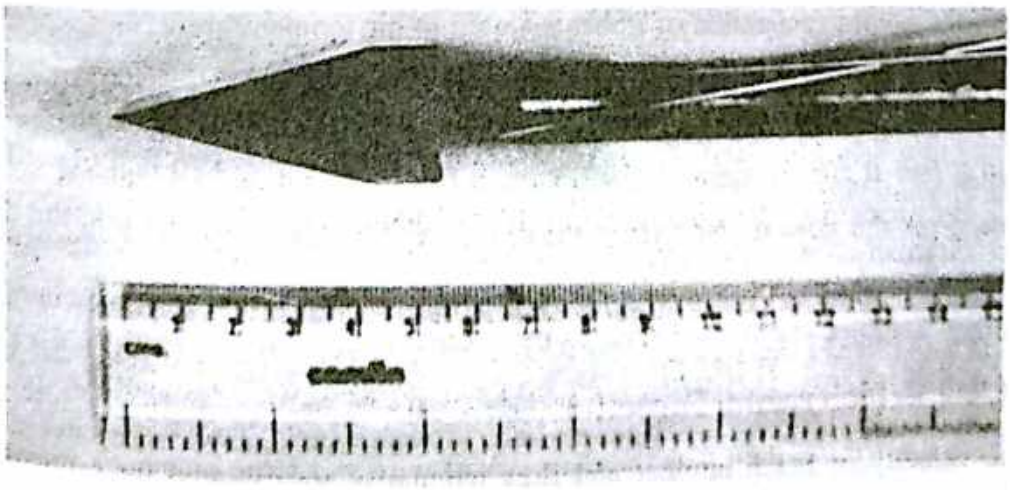


Fig. 13.11 Symmetrical wedge.

Scanned by CamScanner

Instead of obtaining the velocity from the pressure and temperature measurements, we can measure it directly by using a hot wire probe. The probe consists of a short length of a thin wire kept in the flow stream, with the wire heated by passing electric current through it. An equilibrium of the convective cooling of the wire with electrical energy input is maintained. Therefore,

$$I^2R_w = hA(T_w - T_\infty)$$

where

I = electric current
R_w = electrical resistance of wire
A = surface area of wire exposed to flow
h = convective heat transfer coefficient
T_w = wire surface temperature
T_∞ = freestream temperature.

Thus, measuring R_w, I, and T_∞, and knowing wire temperature as a function of resistance, h can he calculated from the above relation.

The flow velocity and the convective heat transfer are related in a unique fashion, generally known as *King's law*:

$$\boxed{\text{Nu} = A_1\text{Pr} + B_1\text{Pr}(\text{Re})^{1/2}}$$

where the Nusselt number Nu gives the heat transfer rate and the Prandtl number Pr is constant for air at room temperature. Therefore,

$$\text{Heat transfer rate} = A_2 + B_2(\text{Re})^{1/2}$$

Using electrical units, we obtain, for a given wire in air flow, the equation

$$\boxed{\frac{I^2R_w}{R_w - R_g} = A + B(V)^{1/2}}$$

where

R_g = cold resistance of unheated wire at air temperature
R_w = wire resistance when exposed to the flow
V = flow velocity

and A and B are constants to be obtained from calibration experiments.

By measuring the quantities on the left-hand side of King's law, the flow velocity can be determined.

The above heat transfer-velocity relation is valid in the Reynolds number range

$$0.1 < \text{Re} < 10^5$$

where $\text{Re} = Vd/\nu$, with d as the diameter of wire and ν the kinematic viscosity of the fluid.

Scanned by CamScanner

In reality it is difficult to measure I and R_w simultaneously, especially at high velocities. Hence, one of the quantities is kept constant and the other allowed to vary. A system where I is kept constant is called *constant current hot wire anemometer system*; the other one with R_w constant is called *constant resistance system*. Since the resistance and temperature are uniquely related for a given wire material, the latter is also known as *constant temperature hot wire anemometer*. For more details about the Hot Wire Anemometry, the reader may refer Hinze (1975) and Rathakrishnan (2016).

13.5 DENSITY PROBLEMS

The density of the flow can be calculated by measuring or determining the pressure and temperature. However, apart from the above discussed methods of experimentally investigating flow patterns by means of pressure and velocity surveys, compressible flows lend themselves particularly well to optical methods of investigation These optical methods (considered here) depend on the variation of density or its derivatives in the flow field.

The commonly used optical methods for compressible flow analysis, the interferometer, the Schlieren, and the shadowgraph, depend on anyone of the two physical phenomena:

1. The speed of light depends on the index of refraction of a gas and, this in turn, depends on its density.
2. Light passing through a density gradient in a gas is deflected in the same manner as though it were passing through a prism. (This is a consequence of the first phenomenon.)

In a high-speed flow, the density changes are adequate to make these phenomena sufficient for optical observation. The interferometer measures directly the changes in density, and is primarily suited for quantitative determination of density field.

The Schlieren method measures the density gradients. Though theoretically it is possible to adapt it for quantitative use, it is inferior to the interferometer in this respect.

The shadowgraph method measures the second derivative of the density. Therefore, it makes visible only those parts of the flow field where the density gradients change very rapidly and is therefore suitable for the study of shock waves.

13.6 COMPRESSIBLE FLOW VISUALIZATION

In supersonic flows, the air density changes are sufficiently large to allow the air to be photographed directly, using optical systems which are sensitive to density

Scanned by CamScanner

changes. In this chapter we will study some of the widely used popular techniques which are often employed for fluid flow analysis. The general principle for flow visualization is to render the "fluid elements" visible either by observing the motion of suitable selected foreign materials added to the flowing fluid or by using an optical pattern resulting from the variation in the optical properties of the fluid, such as refractive index, due to the variation in the properties of the flowing fluid itself. Each of these groups of techniques is generally used for incompressible and compressible flow, respectively. Some of popularly used visualization techniques to study supersonic flow problems of practical interest are the following:

- *Interferometer* is an optical technique to visualize high-speed flows in the ranges of transonic and supersonic Mach numbers. This gives a qualitative estimate of flow *density* in the field.
- *Schlieren* technique is used to study high-speed flows in the transonic and supersonic Mach number ranges. This again gives only a qualitative estimate of the density gradient of the field. This is used to visualize faint shock waves, expansion waves, etc.
- *Shadowgraph* method is yet another flow visualization technique meant for high-speed flows with transonic and supersonic Mach numbers. This is employed for fields with strong shock waves.

Supersonic Flows

For visualizing compressible flows, optical flow visualization techniques are commonly used. *Interferometer*, *Schlieren* and *shadowgraph* are the three popularly employed optical visualization techniques for visualizing shock and expansion waves in supersonic flows. They are based upon the variation in the refractive index, which is related to the fluid density by the Gladstone–Dale formula and consequently to the pressure and velocity of the flow. For making these variations visible, three different classes of methods mentioned above are generally used. With respect to a reference ray, that is, a ray which has passed through a homogeneous field with refractive index n, the

- *Interferometer* makes visible the *optical phase changes* resulting from the relative retardation of the disturbed rays.
- *Schlieren* system gives the *deflection angles of the incident rays*.
- *Shadowgraph* visualizes the *displacement experienced by an incident* ray which has crossed the high-speed flowing gas.

These optical visualization techniques have the advantage of being nonintrusive and thereby in the supersonic regime of flow, avoiding the formation of unwanted shock or expansion waves. They also avoid problems associated with the introduction of foreign particles which may not exactly follow the fluid motion at high-speeds, because of inertia effects. However, none of the these techniques give information directly on the velocity field. The

Scanned by CamScanner

optical patterns given by interferometer, Schlieren and shadowgraph, respectively are sensitive to the *flow density*, *its first derivative*, and *its second derivative*. For quantitative evaluation, the interferometry is generally chosen because this evaluation is based upon the precise measurement of fringe pattern distortion instead of the not so precise measurement of change in photographic contrast, as in Schlieren and shadowgraph. However, Schlieren and shadowgraph visualisations being useful and less expensive are often used to visualize flow patterns, especially at supercritical Reynolds numbers. In particular, they clearly show shock waves and, when associated with ultrashort duration recordings, they also show the flow structure. Although these optical techniques are simple in principle, they are rather difficult to implement. High precision and high optical quality of the setup components, including the wind tunnel test-section windows, are required for a proper visualization with these techniques.

Interferometer

Interferometer is an optical method most suited for qualitative determination of the density field of high-speed flows. Several types of interferometer are used for the measurement of the refractive index, but the instrument most widely used for density measurements in gas streams (wind tunnels) is that attributed to Mach and Zhender.

The fundamental principle of the interferometer is the following. From the wave theory of light, we have

$$c = f\lambda \tag{13.1}$$

where c is the velocity of propagation of light, f is its frequency, and λ is its wavelength.

From corpuscular properties of light, we know that when light travels through a gas the velocity of propagation is affected by the physical properties of the gas. The velocity of light in a given medium is related to the velocity of light in vacuum through the index of refraction n, defined as

$$\frac{c_{\text{vac}}}{c_{\text{gas}}} = n \tag{13.2}$$

The value of refractive index n is 1.303 for air and 1.5 for glass.

The Gladstone–Dale empirical equation relates the refractive index n with the density of the medium as

$$\frac{n-1}{\rho} = K \tag{13.3}$$

where K is the Gladstone–Dale constant and is constant for a given gas, and ρ is the gas density.

Scanned by CamScanner

Formation of Interference Patterns

Figure 13.12 shows the essential features of the Mach–Zhender interferometer, schematically.

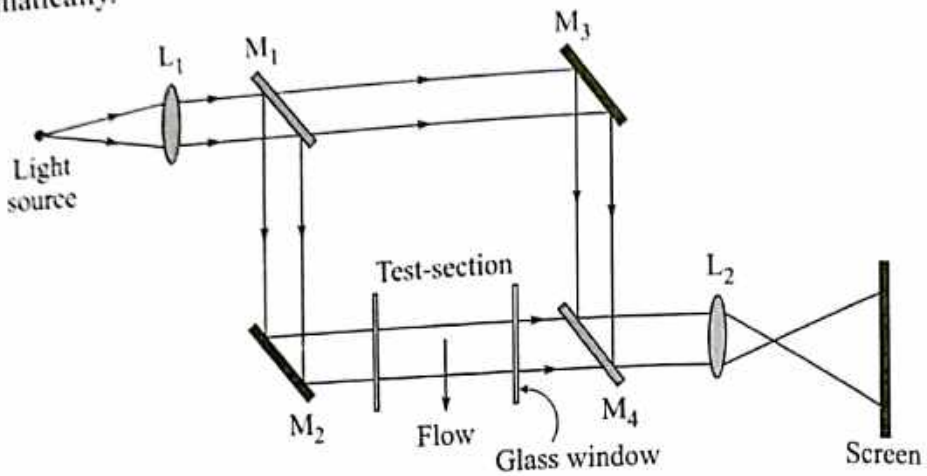


Fig. 13.12 Mach–Zhender interferometer.

Light from the source is made to pass through lens L_1 which renders the light parallel. The parallel beam of light leaving the lens passes through a monochromatic filter. The light wave passes through two paths: 1–2–4 and 1–3–4, before falling on the screen, as shown in the figure. The light rays from the source are divided into two beams by the half-silvered mirror M_1. The two beams, after passing through two different paths (the lengths of paths being the same) recombine at lens L_2 and get projected on the screen. The difference between the two rays is that one (1–3–4) has travelled through room air while the other (1–2–4) has travelled through the test-section. When there is no flow through the test-section, the two rays having passed through identical paths are in phase with each other and recombine into a single ray. Thus, a uniform patch of light will be seen on the screen. Now, *if the density of the medium of one of the paths is changed (say increased) then the light beam passing through will be retarded and there will be a phase difference between the two beams*. When the magnitude of the phase difference is equal to $\lambda/2$, the two rays interfere with each other giving rise to a dark spot on the screen. Hence, if there is an appreciable difference in the density the picture on the screen will consist of dark and white bands, the phase difference between the consecutive dark bands being equal to unity. An interferogram of a two-dimensional supersonic jet is shown in Fig. 13.13.

It is seen that, far away from the jet axis, the fringes (dark and white bands) are parallel, indicting that the flow field is with uniform density (in this case, the zone is without flow). The mild kinks in the fringes are the location of density change. Those who are familiar with free jet structure can easily observe the barrel shock, the Mach disk, and the reflection of the barrel shock from the Mach disk.

Scanned by CamScanner

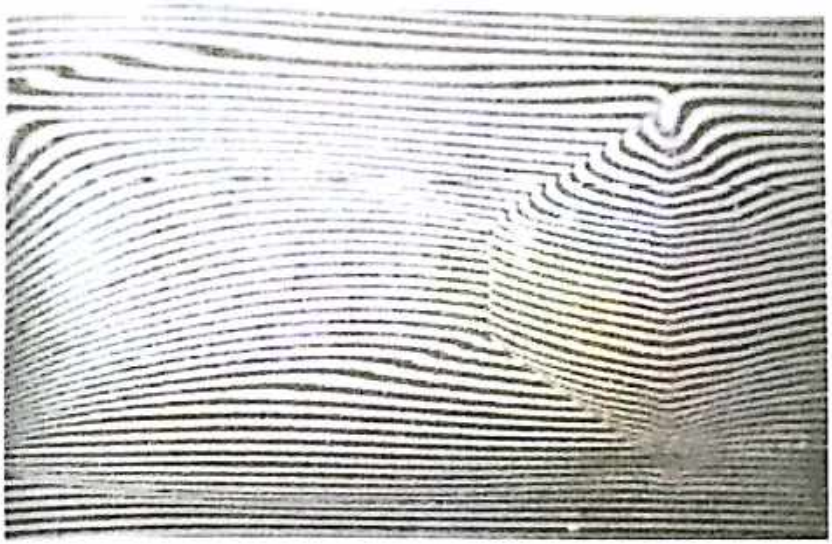


Fig. 13.13 Interferogram of a two-dimensional supersonic jet at $M = 1.62$.

Quantitative Evaluation

Before attempting any quantitative evaluation of an interferogram, it is imperative to understand the "bands" on the picture. If the optical path of each ray in one leg of the interferometer is equal to the optical path of the corresponding ray in the other leg, the split beams coming together at M_4 in Fig. 13.12 will reinforce each other so as to render the screen uniformly bright. This also will occur if the optical path lengths are different by an integer number of wavelengths. Let us assume that this is the condition of the interferometer when there is no flow in the test-section. When there is flow in the test-section, the optical path lengths of each ray through the test-section may change depending on the density change encountered by the ray traversing the flow. If a ray going through the test-section has an optical path length which is an integer plus one-half of wavelength difference from the corresponding ray through the other leg of the interferometer, there will be complete destructive interference of the two rays as they emerge from the mirror M_4. This will give rise to a "black band" on the screen. Similarly, a complete constructive interference will result in a "white band" on the screen. Therefore, there is a possibility of a range of partially constructive and partially destructive interference, giving rise to a "gray zone" on the screen. The picture then will be a series of black and white fringes with a variation in hue between the fringes.

At this stage, we must note that a slight rotation of the mirrors M_1 and M_4 about their vertical axes will result in a series of equally spaced vertical fringes. In practice, this is the initial setting usually taken, since the use of such an initial setting makes it easier to ascertain the amount of retardation associated with each fringe when there is a flow present and in this way permits an easier means of determining the density field of the flow.

With this background we can now attempt to evaluate the interferogram quantitatively. We know that, on the dark bands of Fig. 13.13 the light waves

Scanned by CamScanner

passing through the test-section are out of phase with those which pass through the room air in the compensating chamber by 1/2, 3/2, 5/2, ... of the wavelength λ_{room} of light in the room atmosphere. Therefore, the light beams passing through the adjacent dark bands of the test-section are out of phase by one wave length ($1 \times \lambda_{room}$). Hence, if a represents the fluid lying in one dark band, and b the fluid in an adjacent dark band, the difference in time for a light beam to pass through a compared to that passing through b is given by

$$t_b - t_a = \frac{\lambda_{room}}{c_{room}} \tag{13.4}$$

where t_a is the time for the light to pass through the region of density a and t_b is the time required for the light to pass through the region of density b. Let c_a and c_b be the velocities of propagation of light through regions a and b and L to be the length of the test-section along the light direction.

We know that, the frequency f of a given monochromatic light is constant. Therefore,

$$f = \frac{V}{\lambda} = \frac{c_{room}}{\lambda_{room}} = \frac{c_a}{\lambda_a} = \frac{c_b}{\lambda_b} = \frac{c_{vac}}{\lambda_{vac}} \tag{13.5}$$

The difference in travel time given by Eq. (13.4) may also be expressed in terms of difference in speed of light in the test-section, using Eq. (13.5), as

$$t_b - t_a = \frac{1}{f} = \frac{\lambda_{vac}}{c_{vac}} \tag{13.6}$$

Also,

$$t_b - t_a = \frac{L}{c_b} - \frac{L}{c_a} = \frac{\lambda_{vac}}{c_{vac}}$$

where L is the test-section width.

The velocity of light in a given medium is related to the velocity of light in vacuum through the index of refraction n, defined as

$$n \equiv \frac{c_{vac}}{c}, \quad n_a \equiv \frac{c_{vac}}{c_a}, \quad n_b \equiv \frac{c_{vac}}{c_b} \tag{13.7}$$

i.e.

$$n_b - n_a = c_{vac}\left(\frac{L}{c_a} - \frac{L}{c_b}\right) = \frac{c_{vac}}{L}\frac{\lambda_{vac}}{c_{vac}}$$

That is,

$$n_b - n_a = \frac{\lambda_{vac}}{L} \tag{13.8}$$

Now, the index of refraction may be connected to the gas density through the empirical Gladstone–Dale equation (Eq. 13.3) to result in

$$\boxed{\rho_b - \rho_a = \frac{\lambda_{vac}}{LK}} \tag{13.9}$$

Scanned by CamScanner

The right-hand side of this equation can easily be computed from the dimension of the test-section, the colour of the monochromatic light used, and the value of K for air. The density in the low-speed flow upstream of the nozzle throat may be found by measuring the temperature and pressure in that region. With that region as a reference, the density on each dark band in the nozzle may be computed from Eq. (13.9). This kind of interferogram is also termed "infinite-fringe", which signifies that the light field is uniform in the absence of flow through the test-section. Although, in principle it is possible to compute the density field quantitatively, as discussed above, using interferograms, the accuracy of this procedure using the infinite-fringe interferogram will not be high unless the optical components are extraordinarily accurate. In fact, this is one of the major hurdles in the use of this technique for the quantitative evaluation of compressible flow fields.

Fringe-Displacement Method

This method is used when more accurate quantitative estimate is required. This is just a modified version of the infinite-fringe technique described above. Let us consider the interferometer arrangement shown in Figure 13.12. Let the mirror M_3 be rotated through a small angle with respect to mirror M_1. The two rays of light which were in phase at M_1 will now be out of phase at the screen. Thus, the image on the screen (with no flow in the test-section) will consist of alternate white and dark bands, uniformly spaced, with each fringe lying parallel to the axis of rotation. The spacing of successive dark fringes may be shown to be equal to $\lambda/2\delta$, where δ is the difference in the angles of rotation between the two splitters (i.e. mirrors M_1 and M_3).

Now, assume that the air density in the test-section is increased uniformly. This will result in a uniform displacement of all the wave fronts passing through the test-section. This displacement in turn will cause the interference bands on the screen to shift in a direction normal to the bands, even though the bands will remain parallel and uniformly spaced. The fringe shift is a measure of density change in the test-section. It can be shown that,

$$\boxed{\rho_2 - \rho_1 = \frac{\lambda_{vac}}{LK}\frac{l}{d}} \tag{13.10}$$

where ρ_1 and ρ_2 are the density at the initial reference condition and the density in the test-section, respectively, d is the distance between the dark fringes in the reference condition, and l is the distance shifted by a dark fringe in passing from condition 1 to condition 2.

When there is flow in the test-section, non-uniform fringe shift will occur corresponding to the density field, the resultant fringes will be curved. Equation (13.10) may then be applied at each point in the flow. If both a flow and no-flow photographs are taken, Eq. (13.10) may be used to determine the density change at each point, with respect to the no-flow density.

Scanned by CamScanner

Schlieren System

The Schlieren method is a technique for visualizing the density gradients in a transparent medium. Figure 13.14 shows a typical Schlieren arrangement, usually employed for supersonic flow visualization.

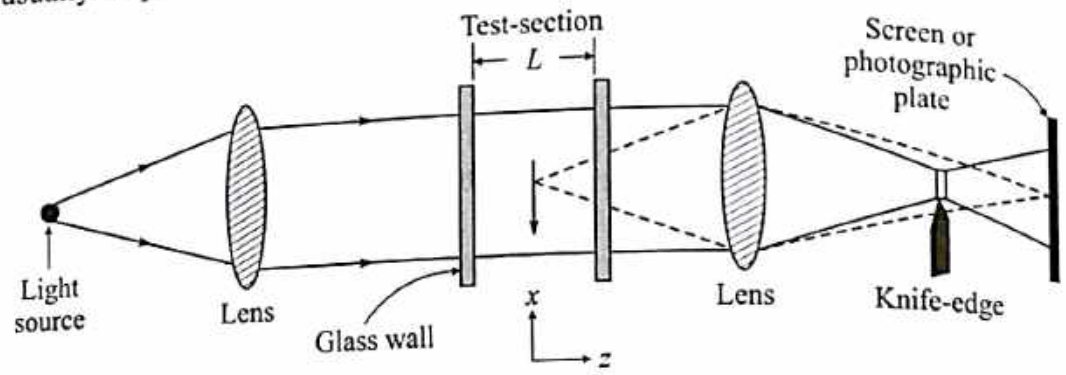


Fig. 13.14 Schlieren system.

Light from a source is collimated by the first lens and then passed through the test-section. It is then brought to a focus by the second lens and projected on the screen. At the focal point of the second lens, where the image of the source is formed, a knife-edge (which is an opaque object) is introduced to cut-off part of the light. The screen is made to be uniformly illuminated by the portion of the light escaping the knife-edge, by suitably adjusting it to intercept about half the light, when there is no flow in the test-section. For the sake of simplicity, for instance, let us assume the test-section to be two-dimensional, with each light ray passing through a path of constant air density. When flow is taking place through the test-section, the light rays will get deflected, since any light ray passing through a region in which there is a density gradient normal to the light direction will be deflected as though it had passed through a prism. In other words, if the medium in the test-section is homogeneous (constant density) the rays from the source will continue in their straight line path. If there is density gradient in the medium, the rays will follow a curved path, *bending towards the region of higher density and away from the region of lower density*. Therefore, depending on the orientation of the knife-edge with respect to the density gradient, and on the sign of the density gradient, more or less of the light passing through each part of the test-section will escape the knife-edge and illuminate the screen. Thus, *the Schlieren system makes density gradients visible in terms of intensity of illumination*. A photographic plate at the viewing screen records density gradients in the test-section as different shades of gray.

Let us assume that the flow through the test-section is parallel and in the xy-plane. Let the light be passing through the test-section in the z-direction. From theory of light it is known that, *the speed of a wavefront of light varies inversely with the index of refraction of the medium through which the light travels*. Therefore, a given wavefront will rotate as it passes through a gradient in the refractive index n. Hence, the normal to the wavefront will follow a curved path.

Scanned by CamScanner

This effect is stated earlier in other words as "the ray will follow a curved path bending towards the region of higher density and away from the region of lower density". In such a case, the radius of curvature R of the light ray is proportional to $1/n$. It can be shown that,

$$\frac{1}{R} = \text{gradient } n$$

The total angular defection ε of the ray in passing through the test-section of width L is therefore given by

$$\varepsilon = \frac{L}{R} = L \text{ grad } n$$

Resolving this into Cartesian components, we have

$$\varepsilon_x = L\frac{\partial n}{\partial x} \qquad \varepsilon_y = L\frac{\partial n}{\partial y}$$

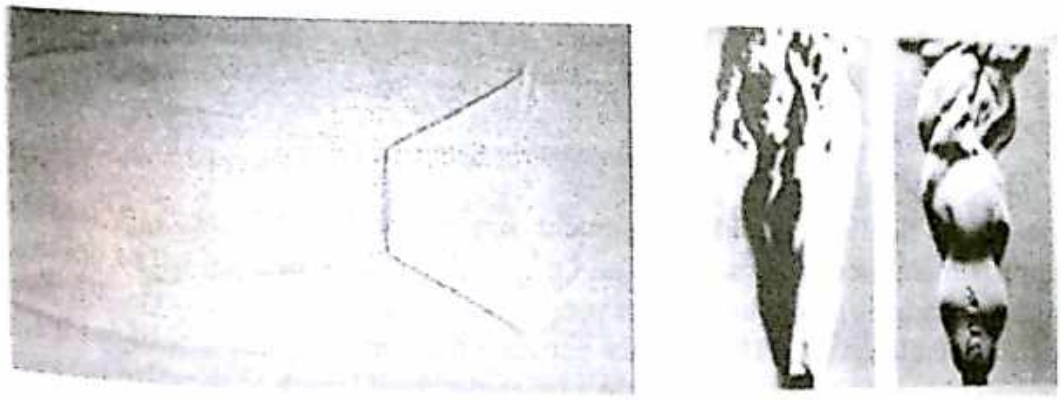
Using Eq. (13.3), these equations can be expressed as

$$\boxed{\varepsilon_x = LK\frac{\partial \rho}{\partial x}} \tag{13.11}$$

$$\boxed{\varepsilon_y = LK\frac{\partial \rho}{\partial y}} \tag{13.11a}$$

From Eqs. (13.11) and (13.11a) it is seen that the Schlieren is sensitive to the first derivative of the density.

Referring to Fig. 13.14 it can be visualized that, if the knife-edge is aligned normal to the flow, i.e. in the y-direction, only the defection ε_x will influence the light passing the knife-edge. Therefore, only density gradients in the x-direction will be made visible, and the gradients in the y-direction will not be visible. Similarly, if the knife-edge is aligned parallel to x-direction, only the gradients in the y-direction will be visible. A typical Schlieren picture of a free jet is shown in Fig. 13.15(a). Pictures of Bunsen flame with knife-edge vertical and horizontal are shown in Fig. 13.15(b).



(a) (b)

Fig. 13.15 Schlieren picture: (a) picture of a supersonic free jet, (b) pictures of Bunsen flame with knife-edge vertical (left) and knife-edge horizontal (right).

Scanned by CamScanner

At this stage, we should note that the Schlieren lenses must not only be of high optical quality but also must have large diameters and long focal lengths. The large diameter is necessary to cover the required portion of the flow field, which is often large in size (say 200 mm in diameter). The long focal length is necessary in order to get the "required" precision and image size. Further, the Schlieren lens should be free of chromatic and spherical aberrations. Also, the astigmatism must be as small as possible.

In experiments where the region under study has a large cross-section as in the case of many modern wind tunnels, it is difficult to obtain lenses of sufficient diameter and focal lengths, and at the same time with the required optical properties, even if such lenses are made specially for such use they will prove to be extremely expensive. As a result concave mirrors have been widely used. They are comparatively free from chromatic aberration and mirrors of large diameters and long focal lengths are much easier to grind and correct than lenses. A twin-mirror Schlieren system that gives good resolving power is shown in Fig. 13.16. The mirrors C and E are a carefully matched pair. Usually they are made of glass and their front surfaces are a parabolized to better than one tenth of a wavelength of light. The excellence of their optical quality bears a direct relation with the image quality produced. Also, due to their size (often more than 300 mm in diameter) and weight they must be carefully mounted to avoid distortions.

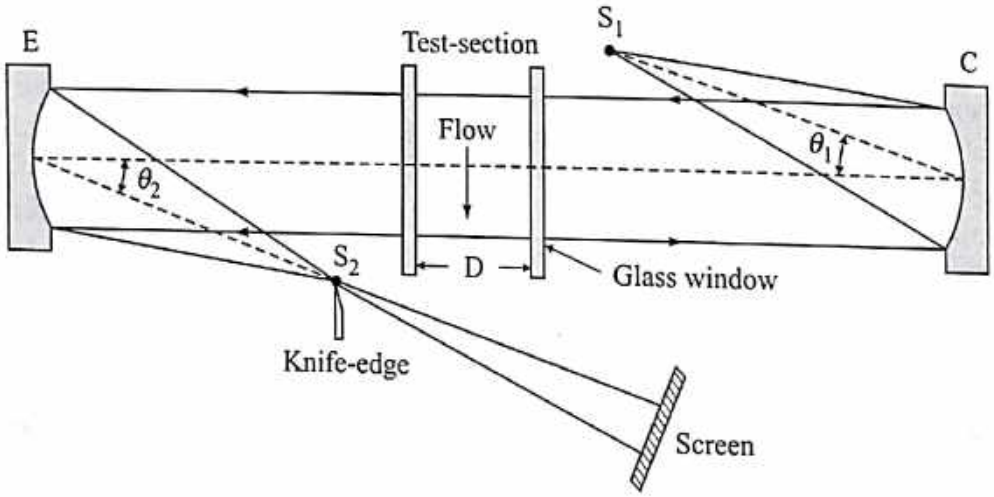


Fig. 13.16 Twin-mirror Schlieren system.

In the Schlieren setup arrangement, it is essential that the angle θ_1 must be approximately equal to angle θ_2 and their value should be as small as possible although angles up to about 7° are used successfully to obtain flow visualization of acceptable quality. The distance between the mirrors is not critical but it is a good practice to make it greater than twice the focal length of the mirrors. Also, the optical system beyond S_2 is simplified if the distance from the disturbance to be observed at test-section D to the mirror E is greater than the focal length of E. The parallel rays entering the region D are bent by the refractive index

Scanned by CamScanner

gradient and are no longer parallel to the beam from C and hence, cannot be focused by the second mirror unless the distance from D to the second mirror E is greater than the focal length of E.

The image of the test-section flow field (with the model) focused at the focal point at S_2 will diverge and proceed further. This image can be made to fall on a flat screen. The clarity of the image can be modified by adjusting the knife-edge. Proper adjustment of the knife-edge can result in sharp images of the shock (or compression) and expansion waves prevailing in the flow to fall on the screen. A still or video camera can record the image on the screen. When a video camera is used, the image can be made to fall on the camera lens. This will avoid the parallax error associated with capturing the image from the screen with a still camera kept at an angle from the screen, without cutting the light rays from S_2.

Range and Sensitivity of the Schlieren System

Let us assume that the contrast on the screen is increased by reducing the size of the image. That is, the knife-edge is made to cut-off most of the light, any ray deflecting beyond a certain limit will be completely cut-off by the knife-edge and further defection will have no effect on the contrast. This means that the range gets limited. Increase in sensitivity affects the range of density gradient for which the system could be used. The contrast or sensitivity requirement depends on the problem to be studied. Hence, to adjust the contrast the knife-edge is generally mounted on a vertical movement so that its position could be altered with respect to the image.

Optical Components—Quality Requirements

The quality of the optical equipment to be used in the Schlieren setup depends on the type of the investigation carried out. The cost increases rapidly with the quality of the optical components. The vital components are the mirrors and the light source. Now, optical quality mirrors are easily available. The following specifications are sufficient to meet the visualization requirements of a 200 mm diameter flow field.

Schlieren Mirrors

- Two parabolic mirrors of 200 mm diameter.
- Focal length of the mirrors about 1.75 m.
- Thickness of the mirror glass about 25 mm.

The reflecting surface of the mirrors is ground to an accuracy of 1/4 wavelength of sodium light and aluminized. Parabolic mirrors are the most suitable even though they are more expensive than spherical mirrors which also will serve the purpose. It is important to note here that, though optical finish of $\lambda/4$ is good

Scanned by CamScanner

enough for visualization of shock waves, if it is the aim to study the structure of the flow field (e.g. shear layers in a free jet, etc.) with ultra short Schlieren photography, mirror surface finish of the order of $\lambda/20$ is essential.

Light Source

- Small intense halogen lamp of 30 watts is commonly used.
- Mercury vapour lamp of suitable intensity (say 200 watts) may also be employed.
- Provision to vary the intensity of light will prove to be useful.

Condenser Lens

Any condenser lens pair generally used for projection systems will be sufficient. This need not be of very high quality.

Focusing Lens

This lens is positioned in the Schlieren system in such a way that a flow field is focused on the screen. An ordinary double convex lens can be used.

Knife-Edge

Any straight sharp-edged opaque object mounted on an adjustable stand will be sufficient to serve as knife-edge. Schlieren technique is generally used only for qualitative work, even though in principle it can be used for quantitative work. If quantitative measurements are to be done the density of the image has to be measured and this can be done with a photo densitometer. This instrument contains a photo cell and it is scanned over the photographic film of the Schlieren image. By properly adjusting the exposure time the brightness of the pattern on the photographic print can be made proportional to the brightness of the Schlieren system. The effect of knife-edge on the image obtained with Schlieren is evident from Fig. 13.15(b).

Colour Schlieren

If the knife-edge which is kept at the focal point of the second mirror is replaced by a coloured filter containing different colours, the image formed on the screen will have different colours depending on which way the beam bends. The contrast in the ordinary black and white Schlieren will now be represented by colours. Usually the colours red, yellow, and green are used. These filters are of 1 or 2 mm in width and placed side by side. When there is no flow the image of the source is allowed to fall on the yellow portion of the filter. Now the image on the viewing screen will be completely yellow. When the density gradient is introduced the image gets displaced and falls partly on the neighbouring filter,

Scanned by CamScanner

thus altering the colour on the screen. In the three filter colour Schlieren screen the colour indicates the size of the density gradient too. The colour effect described can also be achieved with a dispersion prism placed at the knife-edge location.

Short Duration Light Source

To study unsteady phenomena such as flow over a moving object or turbulent fluctuations in the wake of a body or the mixing shear layer in a jet flow field, it is often necessary to take short duration exposures of the Schlieren image to arrest (record) the unsteadiness in the photograph. For this the duration of exposure required is of the order of one or two microseconds or even less. An ordinary shutter in conjunction with a continuous light source is limited to an exposure time of not more than 1/1000 second. Therefore, to obtain shorter exposures the light sources capable of emitting light of very short duration should be employed. A condenser discharge type electric spark unit is commonly used for this purpose. Sparks of durations of the order of microseconds could be obtained by condenser discharge.

A spark light source of short duration can be made in the laboratory. A low inductance conductor and a high voltage DC source are the vital components of this unit. The simplest form of spark unit consists of two electrodes separated by an air gap and the electrodes are connected to the terminals of the capacitor. The discharge time depends on the value of the time constant of the system, that is, on the CR value, where C is the capacitance and R is the resistance which includes the effect of the inductance of the circuit. The total energy of the discharge is $\frac{1}{2}CV^2$, where V is the voltage. The energy discharge during the sparking gets partly dissipated into heat and the rest goes into electromagnetic radiation including the visible range. To obtain a discharge of very short duration it is necessary to use a high voltage with a small capacitor having negligible inductance. In addition, the resistance of the overall circuit should be kept minimum by mounting the spark gap assembly directly on the condenser electrodes. A DC voltage of 10 kV and a capacitor of 0.1 microfarad is sufficient to make a good spark source. If carefully designed, a discharge time of 1 microsecond could easily be achieved.

A spark source should be capable of being triggered whenever needed. This is generally done by using a hydrogen thyratron capable of conducting high current as well as high voltage. Sometimes a simple third ionizing electrode is employed since the hydrogen thyratrons are expensive and have a short lifetime. The electric circuit for the above system is shown in Fig. 13.17. The electrode is used to reduce the resistance in the path between the two main electrodes by ionization. For the Schlieren system a line source is needed and this could be achieved by placing two electrodes between two glass plates, as shown in Fig. 13.17. The glass plates confine the spark instead of allowing it to wander

Scanned by CamScanner

around. The material of the electrodes can be steel, nickel, aluminium or even tungsten. Aluminium electrodes produce high intensity light and increase the duration due to after glow. The after glow is in the low frequency of the visible spectrum and can be filtered out to some extent by using special optical filters.

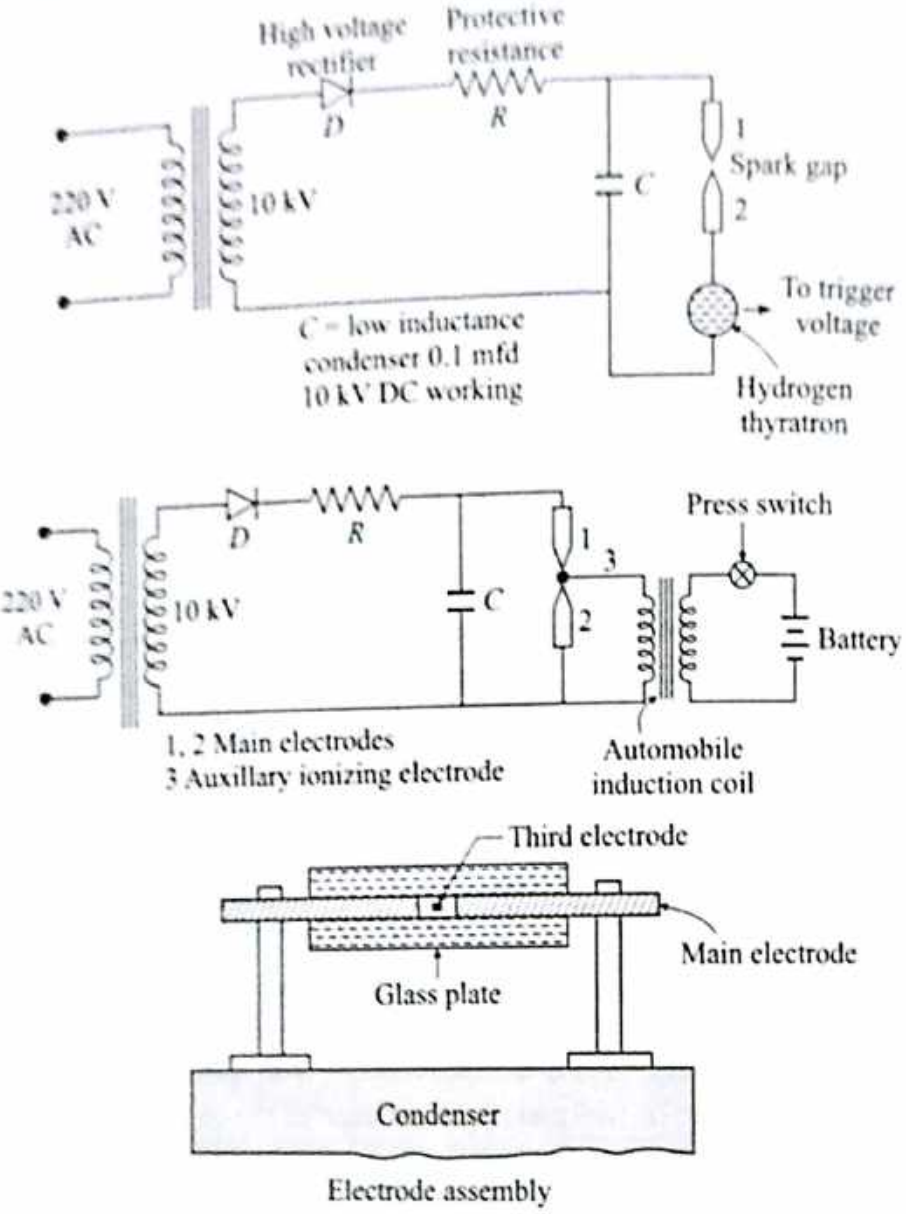


Fig. 13.17 Schlieren spark source circuit.

In general, the Schlieren method is used either for the detection of small refractive index gradients or for the quantitative measurement of these gradients. For the detection of small gradients the apparatus described in Fig. 13.16 in which the deviation of the light ray ε gives rise to the relative light intensity change $\Delta I/I$ on the photographic plate, is almost universally used for studying phenomena in gas dynamics. The method may also be made quantitative, but careful attention must be paid to the several variables in the experimental arrangement. If the disturbance is to be photographed, the

Scanned by CamScanner

arrangement must give a maximum contrast between the images of the undisturbed and disturbed regions and at the same time the photograph must be dense enough to be measurable by photometric means. In most cases high contrast photographic plates are preferable even though they are somewhat slower. In order to calibrate the system, a known refractive index gradient such as a small glass prism may be inserted in some corner of the median plane of the test-field zone which allows a check on the formulae used for the optical system. The sensitivity, i.e. $\Delta I/I$ depends directly upon the brightness of the image of S_1 and S_2 and upon its uniformity of illumination. This of course requires as bright and uniform a source as possible to start with and an optical system which sacrifices no more light than that is necessary. Rectangular sources are usually superior. For proper adjustment, the knife-edges or slits should be of high quality and should be mounted in such a manner that they can be raised and lowered, rotated or moved forward or backward by micrometer adjustments. Also, the mirrors should be accurately adjustable. The mounting of all components should be rigid. The sensitivity also increases directly with the focal length of the Schlieren mirror or lens.

When the Schlieren method is applied to the study of disturbances such as density gradients in a supersonic wind tunnel in which the flow is two-dimensional, with the flow in the x-direction and the light beam in the z-direction, the component of the gradient of the refractive index in the z-direction vanishes. The index of refraction in air for sodium light can be expressed in terms of density, by the relation

$$n = 1 + 0.000293\frac{\rho}{\rho_{NTP}}$$

where ρ_{NTP} is the density at 1 atm and 0°C. The components of the angular deflection ε_x and ε_y in the x- and y-directions, respectively, are given by

$$\varepsilon_x = \int C\frac{\partial \rho}{\partial x}\,dz, \qquad \varepsilon_y = \int C\frac{\partial \rho}{\partial y}\,dz \tag{13.12}$$

where C is a constant.

When the component of the density gradient in the direction of the light beam does not vanish (as in the case of a three-dimensional flow field), the interpretation of the pictures becomes more complicated.

Sensitivity of the Schlieren Method for Shock and Expansion Studies

So far we have discussed the various aspects of the technical and application details of Schlieren method. The emphasis was laid mainly on the qualitative aspects of the flows with density gradients, such as the supersonic flow over an object. Now we can ask a question, whether the Schlieren method is capable of detecting every density gradient irrespective of the intensity of the gradient or is there any threshold below which it is not possible to detect the disturbance with

Scanned by CamScanner

the Schlieren method? Let us try to get an answer for this question. Let us assume that our interest now is to know that *under what condition will an oblique shock become visible?* Assume the knife-edge to be parallel to the front of the oblique shock and, as a typical value, the angle between the shock and the optic axis $\theta = 1^\circ = 0.0175$ radians. For the present arrangement, it can be shown that all the light incident upon the shock is refracted and the amount of light reflected is negligible. Let subscripts 0, 1 and 2 refer to the stagnation state at 20°C, and states upstream and downstream of the shock, respectively. For this flow field, Snell's law of refraction leads to the relation (Ladenburg, R.W. (Ed), *Physical Measurement in Gas Dynamics and Combustion*—Part I, Princeton University Series, Princeton, NJ, 1954)

$$1 + 0.000293\left(\frac{273}{293}\right) p_0 \left(\frac{\rho_1}{\rho_0} - \frac{\rho_2}{\rho_0}\right) = 1 - \varepsilon \tan\theta \tag{13.13}$$

where ε is the angular deflection of the light ray due to the presence of the shock. Let ε be 10^{-5} radians (which is a typical value). Equation (13.13) becomes

$$\rho_2 - \rho_1 = \rho_0 \frac{\tan\theta}{27.3 p_0} \tag{13.14}$$

The relation between the shock angle β and the Mach angle μ can be written as

$$\sin\beta = \frac{M_n}{M_1} = M_n \sin\mu \tag{13.15}$$

where M_n is the component of upstream Mach number M_1, normal to the oblique shock. The ratio of the static-to-stagnation densities upstream of the shock is

$$\frac{\rho_1}{\rho_0} = \left(1 + \frac{\gamma - 1}{2} M_1^2\right)^{-1/(\gamma-1)}$$

With $\gamma = 1.4$, the density ratio becomes

$$\frac{\rho_1}{\rho_0} = \left(1 + \frac{M_1^2}{5}\right)^{-5/2}$$

The ratio of the downstream-to-upstream densities of the shock wave is

$$\frac{\rho_2}{\rho_1} = \frac{6 M_n^2}{M_n^2 + 5}$$

$$\frac{\rho_2 - \rho_1}{\rho_0} = \frac{\rho_2 - \rho_1}{\rho_1}\frac{\rho_1}{\rho_0} = \frac{5(M_n^2 - 1)}{M_n^2 + 5}\frac{\rho_1}{\rho_0} = \frac{\tan\theta}{27.3\, p_0} \tag{13.16}$$

provided the knife-edge is parallel to the shock front. Therefore, for the given values of θ, p_0 and M_1, the minimum difference $(\beta - \theta)$, which will give a visible Schlieren effect can be determined.

If the density change across the oblique shock is small, then $\beta - \theta$ becomes small. Further, $M_n^2 = 1 + \delta$, with $\delta << 1$. For this case, we can show that,

$$\beta - \mu = \frac{3}{5}\frac{\rho_0}{\rho_1}\frac{\tan\theta}{27.3\, p_0 \sqrt{M_1^2 - 1}} \tag{13.17}$$

Scanned by CamScanner

If $\varepsilon = 10^{-5}$, the knife-edge is parallel to the front of the shock wave, and $\theta = \beta - \mu = 1°$, the minimum stagnation pressure (for some given Mach numbers) at which shock can be visualized with Schlieren (at the above assumed rather favourable condition) is given in Table 13.1.

TABLE 13.1 Limiting stagnation pressure to visualize waves with Schlieren

M	1.5	2.0	2.5	3.0	3.5	4.0	4.5	5.0	6.0	7.0	8.0	9.0	10.0
$p_{0\,min}$, atm	0.050	0.055	0.073	0.102	0.145	0.205	0.287	0.396	0.715	1.216	1.959	3.015	4.465

Shadowgraph

In our discussion on Schlieren system we have seen that the positions of the image points on the viewing screen are not affected by deflections of light rays in the test-section. This is because the deflected rays are also brought to focus in the focal plane, and that the screen is uniformly illuminated when the knife-edge is not inserted into the light beam. On the other hand, if the screen is placed at a position close to the test-section, the effect of ray deflection will be visible. This effect, termed *shadow effect*, is illustrated in Fig. 13.18.

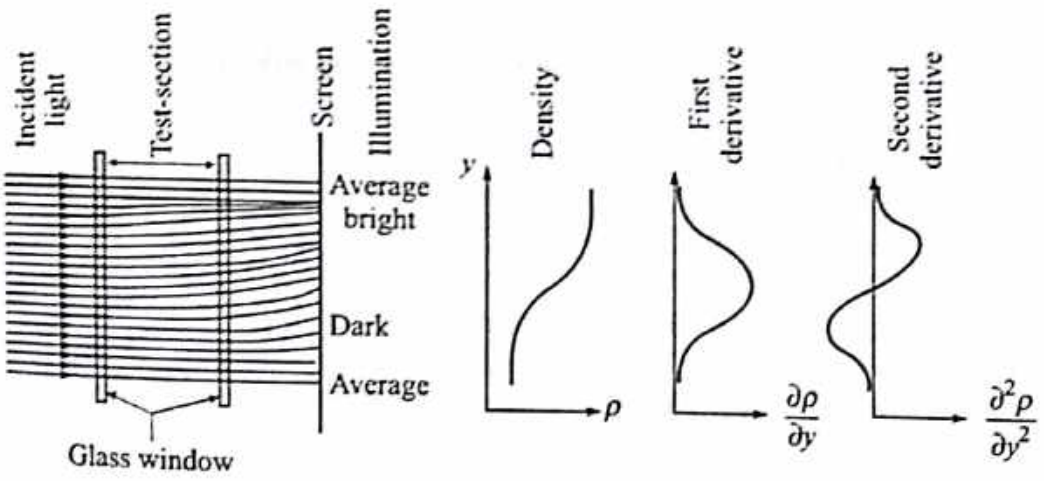


Fig. 13.18 The shadow effect.

On the screen there are bright zones where the rays crowd closer and dark zones where the rays diverge away. At places where the spacing between the rays is unchanged, the illumination is normal even though there has been refraction. Thus, the shadow effect depends not on the absolute deflection but on the relative deflection of the light rays, that is, on the rate at which they converge or diverge on coming out of the test-section.

A shadowgraph consists of a light source, a collimating lens, and a viewing screen, as shown in Fig. 13.19.

Let us assume that the test-section has stagnant air in it and that the illumination on the screen is of uniform intensity. When flow takes place through the test-section the light beam will be refracted wherever there is a density gradient. However, if the density gradient everywhere in the test-section

Scanned by CamScanner

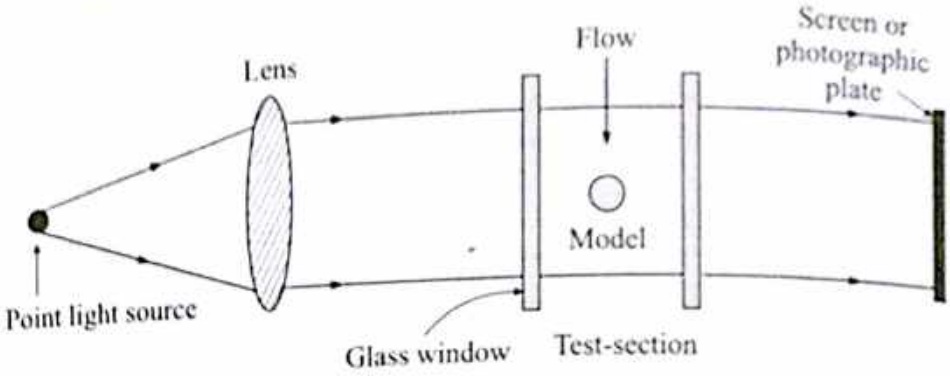


Fig. 13.19 Shadowgraph system

is constant, all light rays would deflect by the same amount, and there would be no change in the illumination of the picture on the screen. Only when there is a gradient in density gradient there will be tendency for light rays to converge or diverge. In other words, the variations in illumination of the picture on the screen are proportional to the second derivative of the density. For a two-dimensional flow the increase in light intensity can be expressed as

$$\boxed{\Delta I = k\left(\frac{\partial^2 \rho}{\partial x^2} + \frac{\partial^2 \rho}{\partial y^2}\right)} \tag{13.18}$$

where k is a constant and x and y are the coordinates in a plane normal to the light path.

Therefore, the shadowgraph is best suited only for flow fields with rapidly varying density gradients. A typical shadowgraph of a highly underexpanded circular sonic jet is shown in Fig. 13.20. Since the jet is underexpanded, the waves present in the field would be strong enough to result in a large density gradient across them. One such wave termed *Mach disk*, normal to the jet axis, is seen in the field. The Mach disk is essentially a normal shock and hence, the shock has positive and negative rate of change of density gradient across it. Therefore, the shock is made up of a dark line followed by a bright line in the shadow picture, in accordance with the *shadow effect*.

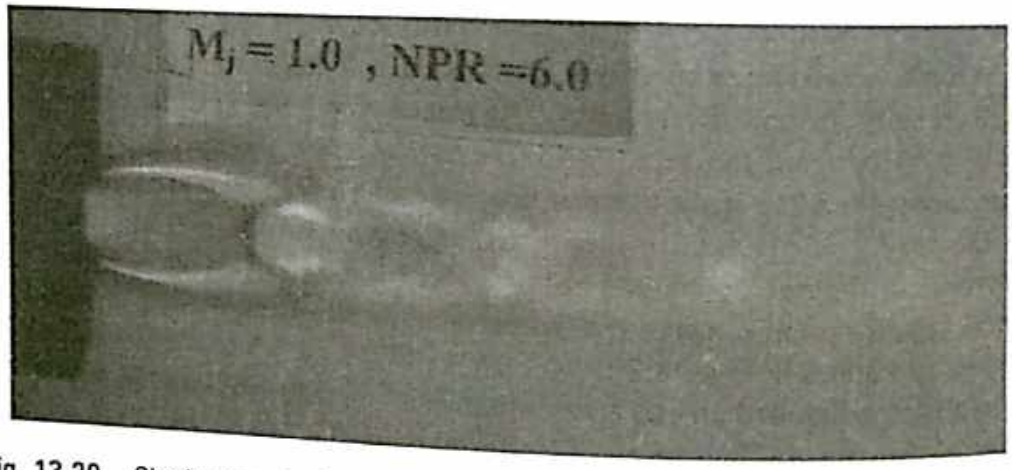


Fig. 13.20 Shadowgraph of an underexpanded sonic jet operating at nozzle pressure ratio 6.

Scanned by CamScanner

Comparison of Schlieren and Shadowgraph Methods

As we saw in Section 13.6.3, the theory shows that the Schlieren technique depends upon the first derivative of the refractive index (flow density) while the shadowgraph method depends upon its second derivative. Consequently, in phenomena where the refractive index varies relatively slowly, the Schlieren method is to be preferred to the shadowgraph method, other things being equal. On the other hand, the shadow method beautifully brings out the rapid changes in the index of refraction. The shadow method also has the advantage of greater simplicity and somewhat wider possible application. The two methods therefore supplement each other and both should be used wherever possible. Fortunately, in many cases the same apparatus or optical parts can be used for both the methods by simple rearrangement and without too much effort on the part of the experimenter. In addition to the first and second derivatives, the refractive index can also be obtained by integration. However, whenever possible, it is preferable to measure the density directly rather than obtaining it from its derivative. For this reason it is clear that the Schlieren and shadow methods should be supplemented by the interference method, which gives the refractive index directly.

13.7 HIGH-SPEED WIND TUNNELS

Tunnels with test-section speed more than 650 kmph are called high-speed tunnels. The predominant aspect in high-speed tunnel operation is that the influence of compressibility is significant. This means that, in high-speed flows it is essential to consider *Mach number* as a more appropriate parameter than velocity. A lower limit of *high-speed* might be considered to be the flow with Mach number approximately 0.5 (about 650 kmph) at standard sea level conditions.

Based on the range of test-section Mach number M, the high-speed tunnels are classified as follows:

- $0.8 < M < 1.2$ Transonic tunnel
- $1.2 < M < 5$ Supersonic tunnel
- $M > 5$ Hypersonic tunnel

High-speed tunnels are classified as *intermittent* or *open-circuit tunnels* and *continuous return circuit tunnels*, based on the type of operation. The power to drive a low-speed wind tunnel varies as the cube of the test-section velocity. Although this rule does not hold in the high-speed regime, the implication of rapidly increasing power requirements with increasing test-section speed holds for high-speed tunnels too. Because of the power requirements, high-speed wind tunnels are often of the *intermittent type*, in which energy is stored in the form of pressure or vacuum or both and is allowed to drive the tunnel only a few seconds out of each pumping hour.

Scanned by CamScanner

The intermittent blowdown and induction tunnels are normally used for Mach numbers from 0.5 to about 5.0, and the intermittent pressure-vacuum tunnels are normally used for higher Mach numbers. The continuous tunnel is used throughout the speed range. Both intermittent and continuous tunnels have their own advantages and disadvantages.

Blowdown Type Wind Tunnels

The essential features of the intermittent blowdown wind tunnels are schematically shown in Fig. 13.21.

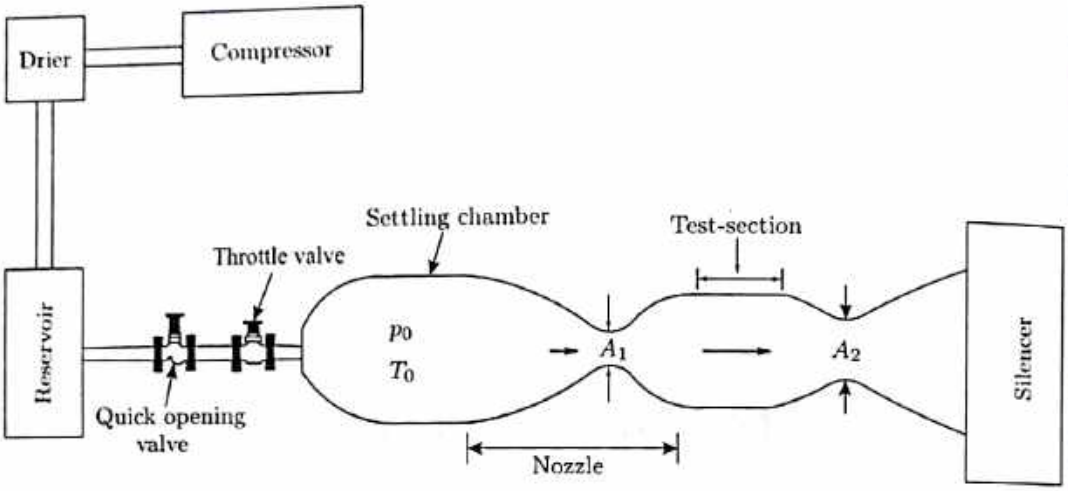


Fig. 13.21 Schematic layout of intermittent blowdown tunnel.

Advantages

The main advantages of blowdown type wind tunnels are the following:

- They are the simplest among the high-speed tunnel types and most economical to build.
- Large size test-sections and high Mach numbers (up to $M = 4$) can be obtained.
- Constant blowing pressure can be maintained and running time of considerable duration can be achieved.

These are the primary advantages of intermittent blowdown tunnels. In addition to these, there are many more advantages of this type of tunnel such as, a single drive may easily run several tunnels of different capabilities, failure of a model usually will not result in tunnel damage. Extra power is available to start the tunnel and so on.

Disadvantages

The major disadvantages of blowdown tunnels are the following:

- Charging time to running time ratio will be very high for large size tunnels.

Scanned by CamScanner

- Stagnation temperature in the reservoir drops during tunnel run, thus changing the Reynolds number of the flow in the test-section.
- Adjustable (automatic) throttling valve between the reservoir and the settling chamber is necessary for constant stagnation pressure (temperature varying) operation.
- Starting load is high (no control possible).
- Reynolds number of flow is low due to low static pressure in the test-section.

The commonly employed reservoir pressure range is from 600 kPa to 2 MPa for blowdown tunnel operations. As large as 15 MPa psi is also used where space limitations necessitate the same.

Induction Type Tunnels

In this type of tunnel, a vacuum created at the downstream end of the tunnel is used to establish the flow in the test-section. A typical induction tunnel circuit is shown schematically in Fig. 13.22.

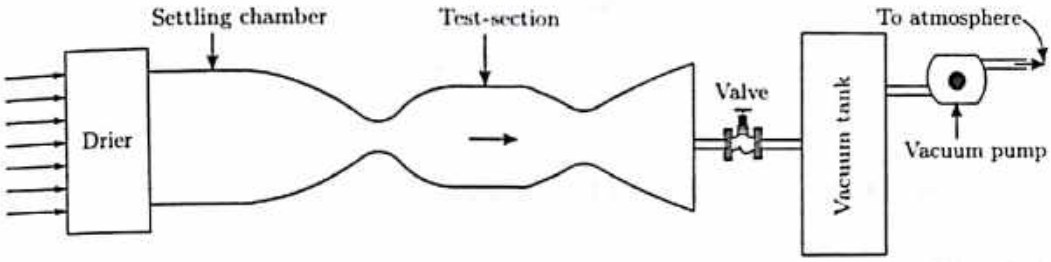


Fig. 13.22 Schematic layout of induction tunnel.

Advantages

The advantages of induction tunnels are the following:

- Both stagnation pressure and stagnation temperature are constant.
- No oil contamination in air, since the pump is at the downstream end.
- Starting and shutdown operations are simple.

Disadvantages

The disadvantages of induction type supersonic tunnels are the following:

- Size of the air drier required is very large, since it has to handle a large mass flow in a short duration.
- Vacuum tank size required is also very large.
- High Mach numbers ($M > 2$) are not possible because of large suction requirements for such Mach numbers.
- Reynolds number is very low, since the stagnation pressure is atmospheric.

The blowdown and induction tunnels can also be employed together for supersonic tunnel operation in order to derive the benefits of both the types.

Scanned by CamScanner

Continuous Supersonic Wind Tunnels

The essential features of a continuous flow supersonic wind tunnel are shown in Fig. 13.23.

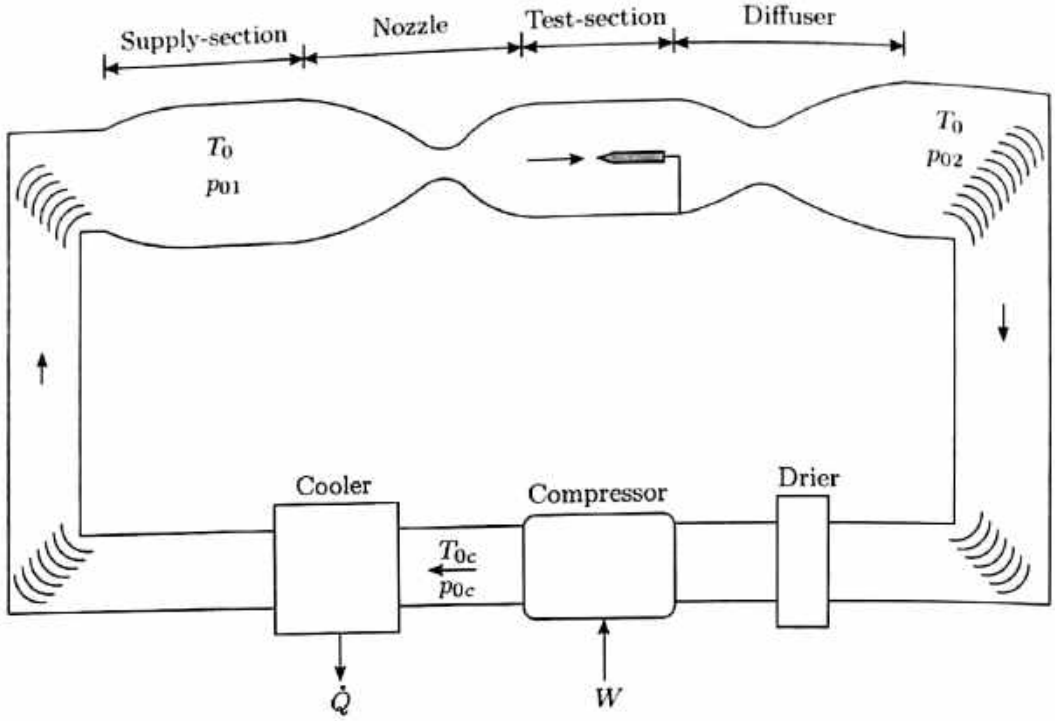


Fig. 13.23 Schematic layout of closed-circuit supersonic wind tunnel.

Like intermittent tunnels, the continuous tunnels also have some advantages and disadvantages. The main advantages of continuous supersonic wind tunnels are the following:

- Better control over the Reynolds number is possible, since the shell is pressurized.
- Only a small capacity drier is required.
- Testing conditions can be held the same over a long period of time.
- The test-section can be designed for high Mach numbers ($M > 4$) and large size models.
- Starting load can be reduced by starting at low pressure in the tunnel shell.

The major disadvantages of continuous supersonic tunnels are the following:

- Power required is very high.
- Temperature stabilization requires a large size cooler.
- Compressor drive has to be designed to match the tunnel characteristics.
- Tunnel design and operation are more complicated.

It is seen from the foregoing discussion that both intermittent and continuous tunnels have certain specific advantages and disadvantages. Before going into the specific details about supersonic tunnel operation, it will be useful to note the following details about supersonic tunnels.

Scanned by CamScanner

- Axial flow compressor is better suited for large pressure ratios and mass flow rates.
- Diffuser design is critical since increasing diffuser efficiency will lower the power requirement considerably. Supersonic diffuser portion (geometry) must be carefully designed to make the Mach number of the flow to be as small as possible, before shock formation. Subsonic portion of the diffuser must have an optimum angle, to minimize the frictional and separation losses.
- Proper nozzle geometry is very important to obtain good distribution of Mach number and freedom from flow angularity in the test-section. Theoretical calculations to high accuracy and boundary layer compensation, etc. have to be carefully worked out for large test-sections. Fixed geometry nozzle blocks for different Mach numbers is simple but expensive and laborious for change over in the case of large size test-sections. Flexible wall type nozzle is complicated and expensive from design point of view and Mach number range is limited (usually $1.5 < M < 3.0$).
- Model size is determined from the test-rhombus, shown in Fig. 13.24.

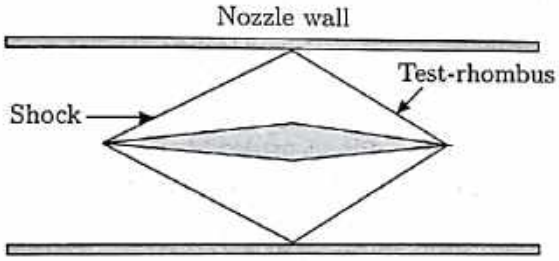


Fig. 13.24 Test-rhombus.

The model must be accommodated inside the rhombus formed by the incident and reflected shocks, for proper measurements.

Losses in Supersonic Tunnels

The total power loss in a continuous supersonic wind tunnel may be split into the following components:

1. Frictional losses (in the return circuit)
2. Expansion losses (in the diffuser)
3. Losses in contraction cone and test-section
4. Losses in guide vanes
5. Losses in the cooling system
6. Losses due to shock wave (in the diffuser supersonic part)
7. Losses due to model and support system drag.

The first five components of losses represent the usual low-speed tunnel losses. All the five components together constitute only about 10 per cent of the total loss. Components 6 and 7 are additional losses in a supersonic wind tunnel and usually amount to approximately 90 per cent of the total loss, with shock wave

Scanned by CamScanner

losses alone accounting to nearly 80 per cent and model and support system drag constituting nearly 10 per cent of the total loss. Therefore, it is customary in estimating the power requirements to determine the pressure ratio required for supersonic tunnel operation, that is, the pressure ratio across the diffuser alone is considered and a correction factor is applied to take care of the remaining losses.

The pressure ratio across the diffuser multiplied by the correction factor must therefore be equal to the pressure ratio required across the compressor to run the tunnel continuously. The relationship between these two vital pressure ratios, namely the diffuser pressure ratio, p_{01}/p_{02}, and the compressor pressure ratio, p_{0c}/p_{03}, may be related as follows:

$$\text{Compressor pressure ratio } \frac{p_{0c}}{p_{03}} = \frac{p_{01}}{p_{02}} \frac{1}{\eta} \tag{13.19}$$

where

p_{0c} = stagnation pressure at compressor exit
p_{03} = stagnation pressure at compressor inlet
p_{01} = stagnation pressure at diffuser inlet
p_{02} = stagnation pressure at diffuser exit.

and

$$\eta = \frac{\text{diffuser losses}}{\text{total loss}}$$

is the correction factor.

The value of η varies from 0.6 to 0.85, depending on the kind of shock pattern through which the pressure recovery is achieved in the diffuser. The variation of compressor pressure ratio, p_{0c}/p_{03}, with the test-section Mach number, M, is shown in Fig. 13.25.

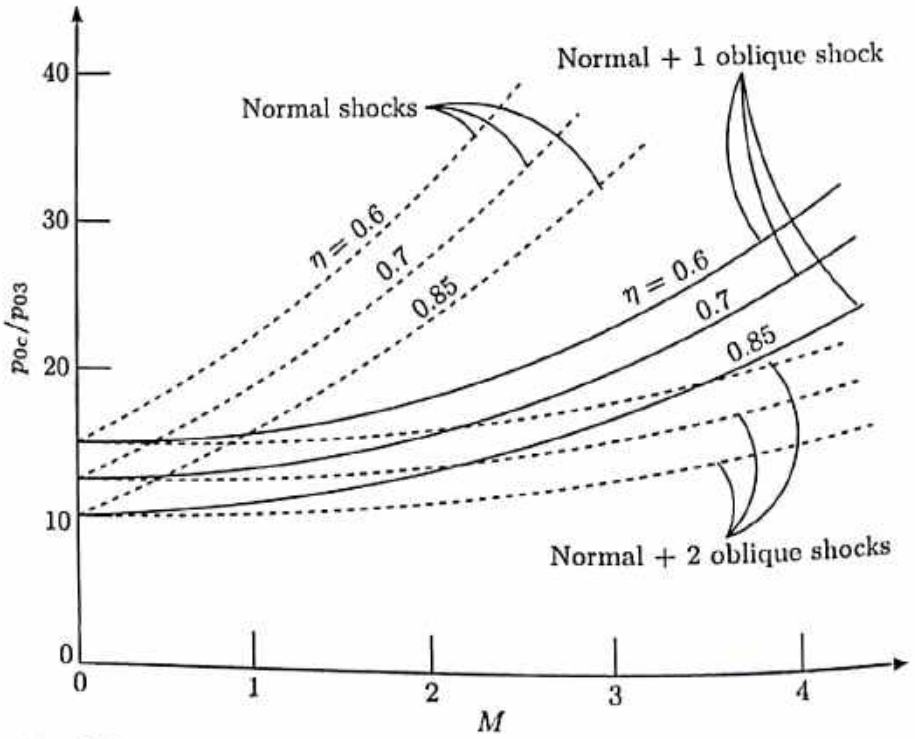


Fig. 13.25 Compressor pressure ratio variation with Mach number.

Scanned by CamScanner

Supersonic Wind Tunnel Diffusers

Basically the diffuser is a device to convert the kinetic energy of a flow to pressure energy. The diffuser efficiency may be defined in the following two ways.

1. Polytropic efficiency, η_d.
2. Isentropic efficiency, η_σ.

Polytropic Efficiency

It is known that, at any point in a diffuser a small change in kinetic energy of unit mass of fluid results in an increase in pressure energy as per the equation

$$\Delta p = \eta_d d\left(\frac{V^2}{2}\right) \tag{13.20}$$

and the pressure ratio is given by

$$\frac{p_{02}}{p_1} = \left(\frac{T_{02}}{T_1}\right)^{(\gamma/(\gamma-1))\,\eta_d} = \left(1+\frac{\gamma-1}{2}M_1^2\right)^{(\gamma/(\gamma-1))\,\eta_d} \tag{13.21}$$

where p_1 and p_{02} are the static and stagnation pressures upstream and downstream of the point under consideration, respectively, and η_d is the polytropic efficiency. M_1, T_1, and T_{02}, respectively, are the Mach number, static temperature and stagnation temperature at the appropriate locations.

Isentropic Efficiency

The isentropic efficiency of a diffuser may be defined as

$$\eta_\sigma = \frac{\text{ideal KE required for observed power}}{\text{actual KE transferred}}$$

and

ideal KE from p_1 to p_{02} (without loss)

$$= \int_{p_1}^{p_{02}} \frac{dp}{\rho} = \frac{\gamma}{\gamma-1}\frac{p_1}{\rho_1}\left(\left(\frac{p_{02}}{p_1}\right)^{(\gamma-1)/\gamma} - 1\right) \tag{13.22}$$

Note that, in Eqs. (13.21) and (13.22) the velocity at the diffuser outlet is assumed to be negligible, that is why the pressure at location 2 is taken as p_{02}, the stagnation pressure. With Eq. (13.22) the isentropic efficiency, η_σ, becomes

$$\eta_\sigma = \frac{\frac{\gamma}{\gamma-1}\frac{p_1}{\rho_1}\left(\left(\frac{p_{02}}{p_1}\right)^{(\gamma-1)/\gamma} - 1\right)}{\frac{1}{2}V_1^2} = \frac{2}{\gamma-1}\frac{1}{M_1^2}\left(\left(\frac{p_{02}}{p_1}\right)^{(\gamma-1)/\gamma} - 1\right)$$

Scanned by CamScanner

From the above equation, the pressure ratio p_{02}/p_1 becomes

$$\frac{p_{02}}{p_1} = \left(1 + \frac{\gamma - 1}{2} M_1^2 \eta_\sigma\right)^{\gamma/(\gamma-1)} \tag{13.23}$$

From Eqs. (13.21) and (13.23), we get

$$\left(1 + \frac{\gamma - 1}{2} M_1^2\right)^{\eta_d} = \left(1 + \frac{\gamma - 1}{2} M_1^2 \eta_\sigma\right) \tag{13.24}$$

Let H be the total pressure (total head) upstream of the test-section, and p_1 be the static pressure there, then we have by isentropic relation,

$$\frac{H}{p_1} = \left(1 + \frac{\gamma - 1}{2} M^2\right)^{\gamma/(\gamma-1)} \tag{13.25}$$

Therefore, the overall pressure ratio, H/p_{02}, for the tunnel becomes

$$\frac{H}{p_{02}} = \frac{H}{p_1}\frac{p_1}{p_{02}}$$

But this is also *the compressor pressure ratio required to run the tunnel*. Hence, using Eqs. (13.21) and (13.23), the compressor pressure ratio, p_σ, can be expressed as

$$p_\sigma = \frac{H}{p_{02}} = \left(\frac{1 + \frac{\gamma - 1}{2} M_1^2}{1 + \frac{\gamma - 1}{2} M_1^2 \eta_\sigma}\right)^{\gamma/(\gamma-1)} \tag{13.26}$$

For continuous and intermittent supersonic wind tunnels, the energy ratio, ER, may be defined as follows:

1. *For continuous tunnel*

$$ER = \frac{KE \text{ at the test-section}}{\text{work done in isentropic compression per unit time}}$$

Using Eq. (13.24), ER may be expressed as

$$ER = \frac{1}{(p_\sigma^{(\gamma-1)/\gamma} - 1)\left(\frac{2}{(\gamma - 1)M_1^2} + 1\right)} \tag{13.27}$$

2. *For intermittent tunnel*

$$ER = \frac{(KE \text{ in test-section})(\text{time of tunnel run})}{\text{energy required for charging the reservoir}} \tag{13.28}$$

Scanned by CamScanner

From the above discussions, we can infer that

- For $M < 1.7$, induced flow tunnels are more efficient than the blowdown tunnels.
- In spite of this advantage, most of the supersonic tunnels even over this Mach number range are operated as blowdown tunnels and not as induced flow tunnels. This is because vacuum tanks are more expensive than compressed air storage tanks.

Effects of Second Throat

A typical supersonic tunnel with second throat is shown schematically in Fig. 13.26.

The second throat, shown in Fig. 13.26, provides isentropic deceleration and highly efficient pressure recovery after the test-section. Neglecting frictional and boundary layer effects, a wind tunnel can be run at design conditions indefinitely, with no pressure difference requirement to maintain the flow, once started. But this is an ideal situation which is not encountered in practice. Even under the assumptions of this ideal situation, during start-up a pressure difference must be maintained across the entire system, shown in Fig. 13.26, to establish the flow. For the supersonic tunnel sketched in Fig. 13.26, the following observations may be made.

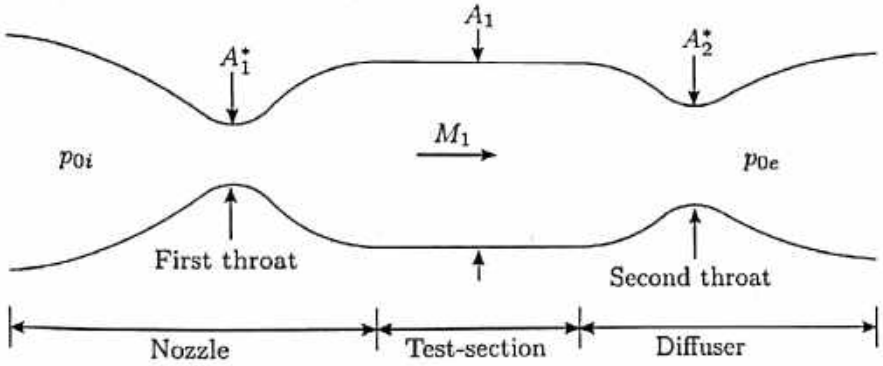


Fig. 13.26 Schematic of supersonic wind tunnel with second throat.

- As the pressure ratio p_{0e}/p_{0i} is decreased below 1.0, the flow situation is the same as that in a convergent–divergent nozzle, where p_{0i} and p_{0e} represent the stagnation pressure at the nozzle inlet and the diffuser exit, respectively.
- Now, any further decrease in p_{0e}/p_{0i} would cause a shock to appear downstream of nozzle throat.
- Further decrease in p_{0e}/p_{0i} moves the shock downstream, towards the nozzle exit.
- With a shock in the diverging portion of the nozzle, there is a severe stagnation pressure loss in the system.
- To pass the flow after the shock, the second throat must be at least of an area A_2^*.

Scanned by CamScanner

- The worst case causing maximum loss of stagnation pressure is that with a normal shock in the test-section. For this case, the second throat area must be at least A_2^*.
- If the second throat area is less than this, it cannot pass the required flow and the shock can never reach the test-section, and will remain in the divergent part of the nozzle.
- Under these conditions, supersonic flow can never be established in the test-section.
- As p_{0e}/p_{0i} is further lowered, the shock jumps to an area in the divergent portion of the diffuser which is greater than the test-section area, i.e. the shock is swallowed by the diffuser.
- To maximize the pressure recovery in the diffuser, p_{0e}/p_{0i} can now be increased, which makes the shock to move upstream to the diffuser throat, and the shock can be positioned at the location where the shock strength is the minimum.

From the above observations, it is evident that the second throat area must be large enough to accommodate the mass flow, when a normal shock is present in the test-section. Assuming the flow to be one-dimensional in the tunnel sketched in Fig. 13.26, it can be shown from continuity equation that

$$\rho_1^* a_1^* A_1^* = \rho_2^* a_2^* A_2^*$$

The flow process across a normal shock is adiabatic and therefore,

$$T_1^* = T_2^*$$

and

$$\frac{\rho_1^*}{\rho_2^*} = \frac{p_1^*}{p_2^*} = \frac{p_{01}}{p_{02}}$$

Also,

$$a_2^* = a_1^*$$

since $T_1^* = T_2^*$. Therefore, the minimum area of the second throat required for starting the tunnel becomes

$$\boxed{\frac{A_2^*}{A_1^*} = \frac{p_{01}}{p_{02}}} \qquad (13.29)$$

where p_{01} and p_{02} represent the stagnation pressures upstream and downstream, respectively, of the normal shock just ahead of the second throat. The pressures p_{01} and p_{02} are identically equal to p_{0i} and p_{0e}, respectively. Instead of the ratio of the throats area, it is convenient to deal with the ratio of the test-section area A_1 to diffuser throat area A_2^*. This is called the *diffuser contraction ratio*, ψ. Thus, the maximum permissible contraction ratio for starting the tunnel is given by

Scanned by CamScanner

$$\psi_{\max} = \frac{A_1}{A_2^*} = \frac{A_1}{A_1^*} \times \frac{A_1^*}{A_2^*} = \frac{A_1}{A_1^*} \times \frac{p_{02}}{p_{01}} = f(M_1) \qquad (13.30)$$

when the second throat area is larger than the minimum required for any given condition, the shock wave is able to "jump" from the test-section to the downstream side of diffuser throat. This is termed *shock swallowing*. The complete test-section has supersonic flow, which is the required state for a supersonic wind tunnel test-section. However, the second throat and part of the diffuser as well have supersonic flow. Apparently we have only shifted the shock from the test-section to the diffuser. This again will result in considerable loss. In principle, it is possible to bring down the loss to a very low level by reducing the area of the second throat, after starting the tunnel. As A_2^* is reduced, the shock becomes weaker (as seen from Eq. (13.29)) and moves upstream towards the second throat. When $A_2^* = A_1^*$, the shock just reaches the second throat, and its strength becomes vanishingly small. This is the ideal situation, resulting in supersonic flow in the test-section and isentropic flow in the diffuser.

At this stage, we should realize that the above model is based on the assumption that the flow is one-dimensional and inviscid, with a normal shock in the test-section. A more realistic model might have to take into account the non-stationary effects of the shock, the possibility of oblique shocks, and the role of boundary layer development. Further reduction of A_2^* to A_1^*, which is the ideal value, is not possible in practice. However, some contraction after starting is possible, up to a limiting value at which the boundary layer effects prevent the maintenance of sufficient mass flow for maintaining a supersonic test-section, and beyond that the flow *breaks down*.

Experimental studies confirm, in a general way, the theoretical considerations outlined above, although there are modifications owing to viscous effects.

The skin friction at the wall, of course, causes some additional loss of stagnation pressure. Some of the diffuser problems outlined here may be avoided to a large extent by

- Using a variable-geometry diffuser
- Using a variable-geometry diffuser in conjunction with a variable-geometry nozzle
- Driving the shock through the diffuser throat by means of a large-amplitude pressure pulse
- Taking advantage of effects which are not one-dimensional.

Compressor Tunnel Matching

Usually the design of a continuous supersonic wind tunnel has either of the following two objectives:

Scanned by CamScanner

1. Choose a compressor for the specified test-section size, Mach number, and pressure level.
2. Determine the best utilization of an already available compressor.

In the first case, wind tunnel characteristics govern the selection of compressor and in the second case it is the other way about. In either case the characteristics to be matched are the *overall pressure ratio* and *mass flow*.

The compressor characteristics are usually given in terms of the volumetric flow $\mathbb{V}$ rather than mass flow. Therefore, it is also convenient to give the wind tunnel characteristics in terms of $\mathbb{V}$. We know that, the volume can be expressed as

$$\mathbb{V} = \frac{m}{\rho}$$

Since the density ρ varies in the tunnel circuit, the volumetric flow also varies for a given constant mass flow m. For the compressor, we specify the intake flow as

$$\mathbb{V}_i = \frac{m}{\rho_i} \tag{13.31}$$

which is essentially the same as the volume flow at the diffuser exit.

On the other hand, the volume flow at the supply section (wind tunnel settling chamber) is

$$\mathbb{V}_0 = \frac{m}{\rho_0} \tag{13.32}$$

Using the throat as the reference section, the mass flow can be expressed as

$$m = \rho^* a^* A^* = \left(\frac{2}{\gamma+1}\right)^{(\gamma+1)/2(\gamma-1)} \rho_0 a_0 A^* \tag{13.33}$$

where a^* and a_0 represent the sonic speeds at the throat and stagnation state, respectively.

With Eq. (13.33), Eq. (13.32) can be rewritten as

$$\mathbb{V}_0 = \left(\frac{2}{\gamma+1}\right)^{(\gamma+1)/2(\gamma-1)} a_0 A^*$$

$$= \left(\frac{2}{\gamma+1}\right)^{(\gamma+1)/2(\gamma-1)} \sqrt{\gamma R T_0}\, \frac{A^*}{A} A$$

$$= \text{constant}\ \sqrt{T_0}\, A \left(\frac{A^*}{A}\right)$$

Scanned by CamScanner

From this equation it is seen that the volume flow rate $\mathbb{V}_0$ depends on the stagnation temperature, test-section area, and test-section Mach number (since A/A^* is a function of M).

The compressor intake flow and the supply section (settling chamber) flow may easily be related, using Eqs. (13.31) and (13.32), to result in

$$\frac{\mathbb{V}_i}{\mathbb{V}_0} = \frac{\rho_0}{\rho_i} = \frac{p_0}{p_i} \times \frac{T_i}{T_0} = \Lambda \tag{13.34}$$

since $T_i = T_0$, Λ is simply the pressure ratio at which the tunnel is actually operating. This pressure ratio Λ must always be more than the minimum pressure ratio required for supersonic operation at any desired Mach number.

Equation (13.34) gives the relation between the operating pressure ratio, Λ, and the compressor intake volume, $\mathbb{V}_0$, as

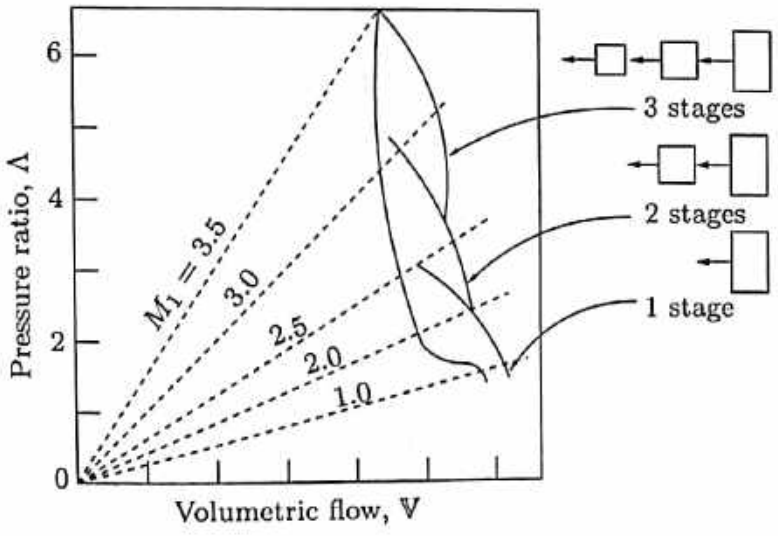
$$\Lambda = \left(\frac{1}{\mathbb{V}_0}\right)\mathbb{V}_i$$

The plot of Λ verses $\mathbb{V}_i$ is a straight line, through the origin, with slope $1/\mathbb{V}_0$, as shown in Fig. 13.27 (Liepmann and Roshko, 1957).

The power requirement for a multistage compressor is given by

$$\text{HP} = \left(\frac{1}{746}\right)\left(\frac{N\gamma}{\gamma - 1}\right)\dot{m}RT_s\left(\left(\frac{p_{0c}}{p_{03}}\right)^{(\gamma-1)/\gamma N} - 1\right) \tag{13.35}$$

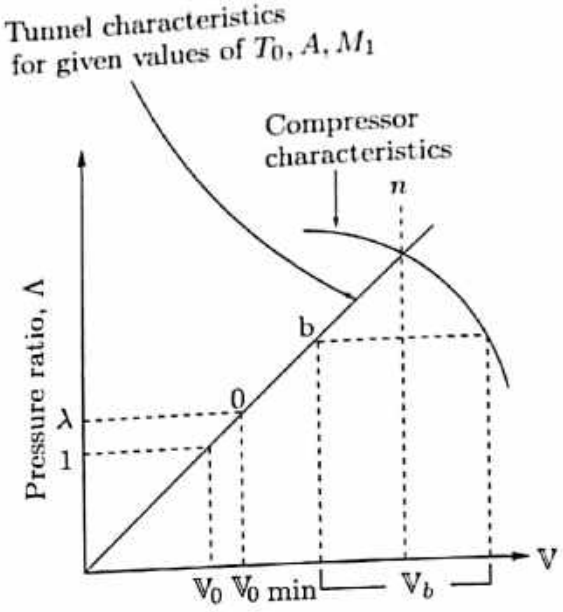
where $\dot{m}$ is the mass flow rate of air in kg/s, p_{03} and p_{0c} are the total pressures at the inlet and outlet of the compressor, respectively, N is the number of stages, and T_s is the stagnation temperature.



(a)

Fig. 13.27 *(Contd.)*

Scanned by CamScanner



(b)

Fig. 13.27 Wind tunnel and compressor characteristics (a) Operation over a range of M, using multistage compressor; (b) matching of wind tunnel compressor characteristics (one test-section condition): n, matching point; b, matching point with by-pass; 0, match point at minimum operating pressure ratio.

EXAMPLE 13.3 Determine the minimum possible diffuser contraction ratio and the power required for a two-stage compressor to run a close circuit supersonic tunnel at $M = 2.2$. The efficiency of the compressor is 85 per cent, $p_{01} = 4$ atm, $T_0 = 330$ K and $A_{TS} = 0.04$ m^2.

Solution Compressor pressure ratio is

$$\frac{p_{0c}}{p_{03}} = \frac{p_{01}}{p_{02}} \frac{1}{\eta}$$

Given, $M = 2.2$, $\eta = 0.85$, $N = 2$, $T_0 = 330$ K, $p_{01} = 4$ atm, $A_{TS} = 0.04$ m^2.

For $M_1 = 2.2$, $\dfrac{p_{02}}{p_{01}} = 0.6281$, from normal shock table, and $\dfrac{A_1}{A_1^*} = 2.005$, from isentropic table. Therefore, the maximum possible contraction ratio becomes

$$\begin{aligned} \psi_{max} &= \frac{A_1}{A_1^*} \times \frac{p_{02}}{p_{01}} \\ &= 2.005 \times 0.6281 \\ &= \boxed{1.26} \end{aligned}$$

Scanned by CamScanner

The mass flow rate is given by

$$\dot{m} = \frac{0.6847}{\sqrt{RT_0}} p_0 A^*$$

$$= \frac{0.6847 \times 4 \times 101325}{\sqrt{287 \times 330}} \times \frac{0.04}{2.005}$$

$$= 17.99 \text{ kg/s}$$

The power required to run the tunnel is

$$\text{Power} = \frac{1}{746} \times \frac{2 \times 1.4}{0.4} \times 17.99 \times 287 \times 330 \left[\left(\frac{1}{0.6281/0.85} \right)^{0.2857/2} - 1 \right]$$

$$= \boxed{1499.57 \text{ hp}}$$

Basic Formulae for Supersonic Wind Tunnel Calculations

From our discussion so far, it is easy to identify that the following are the important relations required for supersonic tunnel calculations.

$$\frac{p_1}{p_2} = \left(\frac{\rho_1}{\rho_2} \right)^{\gamma} = \left(\frac{T_1}{T_2} \right)^{\gamma/(\gamma-1)}$$

$$a = \sqrt{\gamma RT} = 20.04\sqrt{T} \text{ m/s}$$

$$\frac{\gamma}{\gamma - 1} \frac{p}{\rho} + \frac{V^2}{2} = \text{constant} = \frac{\gamma}{\gamma - 1} \frac{p_t}{\rho_t}$$

where p_t and ρ_t are the stagnation pressure and density, respectively.

$$\frac{p_2}{p_1} = \left(\frac{1 + \frac{\gamma - 1}{2} M_1^2}{1 + \frac{\gamma - 1}{2} M_2^2} \right)^{\gamma/(\gamma-1)}$$

$$\frac{p_t}{p} = \left(1 + \frac{\gamma - 1}{2} M^2 \right)^{\gamma/(\gamma-1)}$$

$$\frac{\rho_t}{\rho} = \left(1 + \frac{\gamma - 1}{2} M^2 \right)^{1/(\gamma-1)}$$

$$\frac{T_t}{T} = \left(1 + \frac{\gamma - 1}{2} M^2 \right)$$

where p, ρ and T are the local pressure, density, and temperature, respectively, and p_1 and p_2 are the pressures upstream and downstream of a normal shock.

Scanned by CamScanner

The Mass Flow

The mass flow rate is one of the primary considerations in sizing a wind tunnel test-section and the associated equipment, such as compressor and diffuser. The mass flow rate is given by

$$\dot{m} = \rho A V$$

From isentropic relations, for air with γ=1.4, we have

$$\rho = \rho_t (1 + 0.2\, M^2)^{-5/2}$$

where ρ_t is the total or stagnation density. By perfect gas state equation, we have

$$\rho_t = \frac{p_t}{RT_t}$$

Therefore,

$$\rho = \left(\frac{p_t}{RT_t}\right)(1 + 0.2M^2)^{-5/2}$$

where, R = 287 m^2/(s^2-K) is the gas constant for air, p_t is the total pressure in pascal, and T_t is the total temperature in kelvin.

Also, the local temperature and velocity are given by

$$T = T_t(1 + 0.2M^2)^{-1}$$

$$V = M(1.4RT)^{1/2}$$

Substituting the above expression for T into the expression for V, we get

$$V = M\left(\frac{1.4RT_t}{1 + 0.2M^2}\right)^{1/2}$$

Using the above expressions for V and ρ in the equation for $\dot{m}$, we get the mass flow rate as

$$\boxed{\dot{m} = \left[\frac{1.4}{RT_t}\right]^{1/2}\left[\frac{M\, p_t A}{(1 + 0.2M^2)^3}\right]} \qquad (13.36)$$

This equation is valid for both subsonic and supersonic flows. When the mass flow rate being calculated is for subsonic Mach number, Eq. (13.36) is evaluated using the test-section Mach number in conjunction with the total temperature and pressure. For supersonic flows, it is usually convenient to make the calculations at the nozzle throat, where the Mach number is 1.0. Further, it should be noted that blowdown tunnels are usually operated at a constant pressure during run. The main objective of constant pressure run is to obtain a steady flow while data is being recorded. Thus, the total pressures to be used in the evaluation of Eq. (13.36) are the minimum allowable (or required) operating pressures.

Scanned by CamScanner

EXAMPLE 13.4 A continuous wind tunnel operates at Mach 2.5 at test-section, with static conditions corresponding to 10,000 m altitude. The test-section is 150 mm × 150 mm in cross-section, with a supersonic diffuser downstream of the test-section. Determine the power requirements of the compressor during start-up and during steady-state operation. Assume the compressor inlet temperature to be the same as the test-section stagnation temperature.

Solution At the test-section, $M = 2.5$. At 10,000 m altitude, from atmospheric table, we have

$$p = 26.452 \text{ kPa}, \quad T = 223.15 \text{ K}$$

These are the pressure and temperature at the test-section.

From isentropic table, for $M = 2.5$, we have

$$\frac{p}{p_0} = 0.058528; \quad \frac{T}{T_0} = 0.4444$$

Therefore, the stagnation pressure and temperature at the test-section are

$$p_0 = \frac{26.452}{0.058528} = 451.95 \text{ kPa}$$

$$T_0 = \frac{223.15}{0.44444} = 502.1 \text{ K}$$

During steady-state operation, the mass flow rate through the test-section is

$$\dot{m} = \rho AV$$

$$= \frac{p}{RT} AM\sqrt{\gamma RT}$$

$$= \frac{26452}{287 \times 223.15}(0.15 \times 0.15)(2.5)\sqrt{1.4 \times 287 \times 223.15}$$

$$= 6.96 \text{ kg/s}$$

From isentropic table, for $M = 2.5$, we have

$$\frac{A}{A^*} = 2.63671$$

Therefore,

$$A^* = \frac{0.15 \times 0.15}{2.63671}$$

$$= 0.00853 \text{ m}^2$$

This is the area of the first throat.

During start-up, a shock wave is formed when the flow becomes supersonic. The pressure loss due to this shock is maximum when it is at the test-section.

Scanned by CamScanner

For $M = 2.5$, from normal-shock table, we have

$$\frac{p_{02}}{p_{01}} = 0.499$$

Also, we know that

$$\frac{p_{02}}{p_{01}} = \frac{A_1^*}{A_2^*}$$

Therefore,

$$\frac{A_1^*}{A_2^*} = 0.499$$

$$A_2^* = \frac{A_1^*}{0.499} = \frac{0.00853}{0.499}$$

Thus,

$$\frac{A}{A_2^*} = \frac{0.15 \times 0.15}{0.00853} \times 0.499$$

$$= 1.316$$

For this area ratio, from isentropic table, we get $M = 1.68$. This is the Mach number ahead of the shock when the shock is at the second throat.

For $M = 1.68$, from normal shock table, we have

$$\frac{p_{02}}{p_{01}} = 0.86394$$

This pressure loss must be compensated by the compressor. The power input required for the compressor to compensate for this loss is

$$\text{Power} = h_0 - h_i = c_p(T_0 - T_i)$$

where the subscripts 0 and i, respectively, refer to compressor outlet and inlet conditions. For an isentropic compressor,

$$\frac{T_0}{T_i} = \left(\frac{p_0}{p_i}\right)^{(\gamma-1)/\gamma}$$

$$T_0 - T_i = T_i\left(\left(\frac{p_0}{p_i}\right)^{(\gamma-1)/\gamma} - 1\right)$$

$$= 502.1\left[\left(\frac{1}{0.86394}\right)^{0.286} - 1\right]$$

$$= 21.44 \text{ K}$$

Thus, the power input required becomes

$$\text{Power} = 1004.5(21.44) = 21543.8 \text{ J/kg}$$

Scanned by CamScanner

The horsepower required for the compressor is

$$\text{Power} = \frac{\dot{m}W}{746}$$

$$= \frac{6.96 \times 21543.8}{746}$$

$$= \boxed{201 \text{ hp}}$$

This is the running horsepower required for the compressor.

During start-up, $M_1 = 2.5$, the corresponding $p_{02}/p_{01} = 0.499$, from normal shock table. The isentropic work required for the compressor during start-up is

$$W = \left[\left(\frac{1}{0.499}\right)^{0.286} - 1\right] 502.1\, c_p$$

$$= 110.4\, c_p$$

$$= 1004.5 \times 110.4$$

$$= 110896.8 \text{ J/kg}$$

Thus, the power required is

$$\text{Power} = \frac{6.96 \times 110896.8}{746}$$

$$= \boxed{1034.7 \text{ hp}}$$

EXAMPLE 13.5 Estimate the settling chamber pressure and temperature and the area ratio required to operate a Mach 2 tunnel under standard sea-level conditions. Assume the flow to be one-dimensional and the tunnel to be operating with correct expansion.

Solution The tunnel is operating with correct expansion. Therefore, the sea-level pressure and temperature become the pressure and temperature in the test-section (i.e. at the nozzle exit). Thus, $p_e = 101.325$ kPa and $T_e = 15°C$.

This problem can be solved by using the appropriate equations or by using the gas tables. Let us solve the problem by both the methods.

Solution Using Equations

Let the subscripts e and 0 refer to nozzle exit and stagnation states, respectively.

From isentropic relations, we have the temperature and pressure ratio as

$$\frac{T_0}{T_e} = 1 + \frac{\gamma - 1}{2} M_e^2$$

$$= 1 + \frac{1.4 - 1}{2} \times 2^2 = 1.8$$

$$T_0 = 1.8\, T_e = 1.8 \times 288.15$$

$$= \boxed{518.67 \text{ K}}$$

Scanned by CamScanner

$$\frac{p_0}{p_e} = \left(1 + \frac{\gamma - 1}{2} M_e^2\right)^{\gamma/(\gamma-1)}$$

$$= 1.8^{3.5} = 7.824$$

$$p_0 = 7.824 p_e$$

$$= \boxed{792.77 \text{ Pa}}$$

From isentropic relations, we have the area ratio as

$$\left(\frac{A_e}{A_{th}}\right)^2 = \frac{1}{M_e^2}\left[\frac{2}{\gamma+1}\left(1 + \frac{\gamma-1}{2} M_e^2\right)\right]^{(\gamma+1)/(\gamma-1)}$$

$$= \frac{1}{2^2}\left[\frac{2}{2.4} \times 1.8\right]^6 = 2.8476$$

$$\frac{A_e}{A_{th}} = \boxed{1.687}$$

Solution Using Gas Tables

From isentropic table, for $M_e = 2$, we have

$$\frac{p_e}{p_0} = 0.1278, \quad \frac{T_e}{T_0} = 0.55556, \quad \frac{A_e}{A_{th}} = \boxed{1.6875}$$

Thus,

$$p_0 = \frac{p_e}{0.1278}$$

$$= \frac{101325}{0.1278} = \boxed{792.84 \text{ kPa}}$$

$$T_0 = \frac{T_e}{0.55556}$$

$$= \frac{288.15}{0.55556} = \boxed{518.67 \text{ K}}$$

Blowdown Tunnel Operation

In a blowdown tunnel circuit, the pressure and temperature of air in the compressed air reservoir (also called storage tank) change during operation. This change of reservoir pressure causes the following effects:

- The tunnel stagnation and settling chamber pressures fall correspondingly.
- The tunnel is subjected to dynamic condition.

Scanned by CamScanner

- Dynamic pressure in the test-section falls and hence, the forces acting on the model change during the test.
- Reynolds number of the flow changes during the tunnel run.

Usually three methods of operation are adopted for blowdown tunnel operation. They are:

- Constant Reynolds number operation
- Constant pressure operation
- Constant throttle operation.

The ratio between the settling chamber initial pressure p_{bi} and the reservoir initial pressure p_{0i} is an important parameter influencing the test-section Reynolds number. Let

$$\frac{p_{bi}}{p_{0i}} = \frac{\text{settling chamber initial pressure}}{\text{reservoir initial pressure}} = \alpha$$

The variation of Reynolds number with tunnel running time t, as a function of α is as shown in Fig. 13.28.

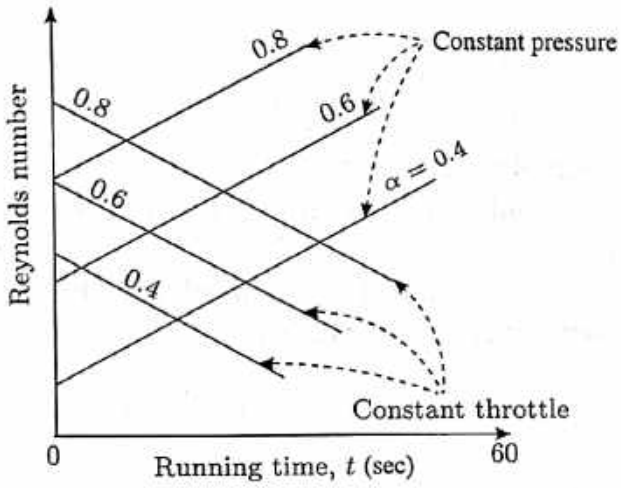


Fig. 13.28 Reynolds number variation with tunnel running time.

As seen from Fig. 13.28, the Reynolds number increases with running time for constant pressure operation, and decreases with running time for constant throttle operation. The change in Reynolds number results in the change of boundary layer thickness, and which in turn causes area and Mach number change in the test-section. Usually, Mach number variation due to the above causes is small.

Reynolds Number Control

By definition, Reynolds number is the ratio between the inertia and viscous forces.

$$\text{Re} = \frac{\text{inertia force}}{\text{viscous force}}$$

Scanned by CamScanner

It can be shown that

$$\mathrm{Re} = \frac{\rho V L}{\mu}$$

where ρ, V, and μ are the density, velocity, and viscosity, respectively, and L is a characteristic dimension of the model being tested. The above equation may be expressed as

$$\frac{\mathrm{Re}}{L} = \frac{\rho V}{\mu} \tag{13.37}$$

Also, the viscosity coefficient may be expressed as

$$\mu = cT^m V = cT^m M\sqrt{\gamma RT} = c_1 f(M)\sqrt{T}$$

In the above expression, c_1 and c are constants, m is the viscosity index, γ is the isentropic index, and R is the gas constant.

Let p_b and p_{bi} be the instantaneous and initial pressures in the settling chamber, respectively, and T_b and T_{bi} be the corresponding temperatures. With the above relations for μ, Eq. (13.37) can be expressed as

$$\frac{\mathrm{Re}}{L} = g_1 f(M,m)\left[\frac{p_b/p_{bi}}{(T_b/T_{bi})^{(m+(1/2))}}\right] \tag{13.38}$$

where g_1 is a function of initial (starting) conditions (p_{bi}, p_{ti}). From Eq. (13.38) it is seen that the Reynolds number during tunnel run is influenced only by the quantities within the square brackets. These quantities can easily be held constant by a suitable manipulation of a throttling valve located between the reservoir and the settling chamber, as shown in Fig. 13.29.

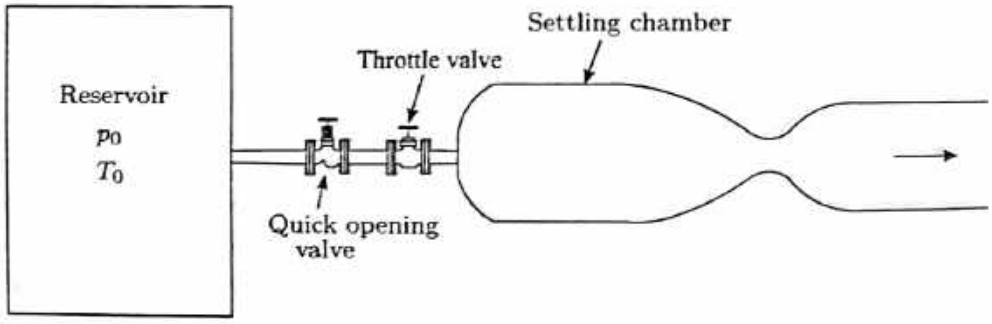


Fig. 13.29 Blowdown tunnel layout.

The throttling process may be expressed by the following equation,

$$p_{bi} = \alpha p_0^{\beta} \tag{13.39}$$

where p_{bi} and p_0 are the total pressures after (stagnation pressure in the settling chamber) and before (stagnation pressure in the reservoir) throttling, respectively, and α and β are constants.

Scanned by CamScanner

The function g in Eq. (13.38), at settling chamber conditions, is

$$g_i = \frac{\gamma p_{bi}}{a_{bo}\mu_{bo}}$$

where a_{bo} is the proportionality constant and μ_{bo} is the viscosity coefficient of air in the settling chamber.

The function $f(M, m)$, from isentropic relations, is

$$f(M, m) = \frac{M}{\left(1 + \frac{\gamma - 1}{2} M^2\right)^{[(\gamma+1)/2(\gamma-1)]-m}}$$

Now, applying the polytropic law for the expansion of gas in the storage tank, we can write

$$\frac{p_0}{p_{0i}} = \left(\frac{T_0}{T_{0i}}\right)^{n/(n-1)}$$

where the subscripts 0 and $0i$ refer to instantaneous and initial conditions in the reservoir and n is the polytropic index.

Also, from Eq. (13.39), we have

$$\frac{p_b}{p_{bi}} = \left(\frac{p_0}{p_{0i}}\right)^{\beta}$$

Therefore, with the above relations, Eq. (13.38) can be expressed as

$$\boxed{\frac{\mathrm{Re}}{L} = g_1 f(M, m)\left(\frac{p_0}{p_{0i}}\right)^{\beta-[(2m+1)(n-1)/2n]}} \tag{13.40}$$

This is the general relation between the test-section Reynolds number and the reservoir pressure. From this equation, the following observations can be made.

- For Re = constant; $\beta = \dfrac{(2m+1)(n-1)}{2n}$
- For constant "p_b" operation, $p_b = \alpha p_0{}^{\beta}$ = constant, and $\beta = 0$. Thus, Eq. (13.40) simplifies to

$$\frac{\mathrm{Re}}{L} = K_3\left(\frac{p_{0i}}{p_0}\right)^{(2m+1)(n-1)/2n}$$

  where K_3 is a constant. This implies that Re increases with time t because p_0 decreases with t.
- For constant throttle operation, $\beta = 1$ and

$$p_b = \alpha p_0{}^{\beta} = \alpha p_0$$

Scanned by CamScanner

Therefore,

$$\frac{\mathrm{Re}}{L} = K_3 \left(\frac{p_0}{p_{0i}} \right)^{\left[1 - \frac{(2m+1)(n-1)}{2n}\right]} \qquad 0 < \frac{(2m+1)(n-1)}{2n} < 1$$

This implies that, Re decreases with t for constant throttle operation.

From the above observations it can be inferred that, for a given settling chamber pressure and temperature, the running time is:

- The shortest for constant throttle operation.
- The longest for constant Reynolds number operation.
- In between the above two for constant pressure operation.

Optimum Conditions

For optimum performance of a tunnel in terms of running time t, the drop in reservoir pressure should be as slow as possible. To achieve this slow rate of fall in reservoir pressure, the pressure regulating valve should be adjusted after the tunnel has been started, in such a manner that the pressure in the settling chamber is the minimum pressure $p_{b\min}$ required for the run.

The performance of the tunnel, i.e. the test-section Mach number M versus the tunnel run time t, for different methods of control mentioned above should be evaluated for the entire range of operation. These performance data can be recorded in the form of graphs for convenient reference. From such graphs, the best suited method of operation for any particular test and the required settings of the throttle valve (α, β, etc.) can be chosen. A typical performance chart will look like the one shown in Fig. 13.30.

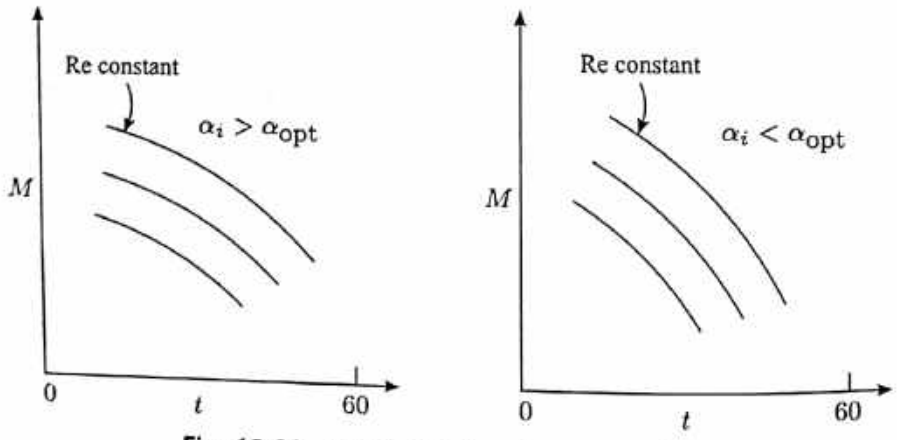


Fig. 13.30 Wind tunnel performance chart.

For a given test-section Mach number M there is a p_b minimum in the settling chamber, given by the pressure ratio relation. The Reynolds number in the test-section depends on this p_b value and constant Reynolds number operation is possible only if

Scanned by CamScanner

- the p_{bi} value is so chosen that as t proceeds (increases) both p_0 and p_b reach $p_{b\,\min}$ value simultaneously (to result in an optimum constant Reynolds number).
- $p_{bi} > p_{b\,\text{opt}}$. The reservoir pressure will become equal to p_b at some instant and then onwards constant Reynolds number operation is not possible.
- $p_{bi} < p_{b\,\text{opt}}$. The $p_b = p_{b\,\min}$ state will be reached at time t when $p_0 > p_b$ and supersonic operation will not be further possible.

Running Time of Blowdown Wind Tunnels

Blowdown supersonic wind tunnels are usually operated with either constant dynamic pressure (q) or constant mass flow rate ($\dot{m}$).

For constant q operation, the only control necessary is a pressure regulating valve (PRV) that holds the stagnation pressure in the settling chamber at a constant value. The stagnation pressure in the storage tank falls according to the polytropic process—with the polytropic index $n = 1.4$ for short duration runs, with high mass flow, approaching $n = 1.0$ for long duration runs with thermal mass[1] in the tank.

For constant mass flow run, the stagnation temperature and pressure in the settling chamber must be held constant. For this, either a heater or a thermal mass external to the storage tank is essential. The addition of heat energy to the pressure energy in the storage tank results in a longer running time of the tunnel. Another important consequence of this heat addition is that the constant settling chamber temperature of the constant mass run keeps the test-section Reynolds number at a constant value.

For calculating the running time of a tunnel, let us make the following assumptions.

- Expansion of the gas in the storage tank is polytropic.
- Gas temperature in the storage tank is held constant with a heater.
- Gas pressure in the settling chamber is kept constant with a pressure regulating valve.
- No heat is lost in the pipelines from the storage tank to the test-section.
- Expansion of the gas from the settling chamber to the test-section is isentropic.
- Test-section speed is supersonic.

The mass flow rate $\dot{m}$ through the tunnel, as given by Eq. (4.36), is

$$\dot{m} = \left(\frac{1.4}{RT_t}\right)^{1/2} \frac{M\, p_t\, A}{(1+0.2M^2)^3}$$

where M is the test-section Mach number, p_t and T_t, respectively, are the pressure and temperature in the settling chamber.

[1] Thermal mass is a material which has high value of thermal capacity.

Scanned by CamScanner

We know that for supersonic flows it is convenient to calculate the mass flow rate with nozzle throat conditions. At the throat, $M = 1.0$ and then Eq. (13.36) becomes

$$\dot{m} = 0.0404 \frac{p_t A^*}{\sqrt{T_t}} \tag{13.41}$$

The value of gas constant used in the above equation is $R = 287\ \text{m}^2/(\text{s}^2\ \text{K})$, which is the gas constant for air.

The product of mass flow rate and run time gives the change of mass in the storage tank. Therefore,

$$\dot{m}t = (\rho_i - \rho_f)\mathbb{V}_t \tag{13.42}$$

where $\mathbb{V}_t$ is the tank volume and ρ_i and ρ_f are the initial and final densities in the tank, respectively.

From Eq. (13.42), the running time t is obtained as

$$t = \frac{\rho_i - \rho_f}{\dot{m}} \mathbb{V}_t$$

Substituting for $\dot{m}$ from Eq. (13.41) and arranging the above equation, we get

$$\boxed{t = 24.728 \frac{\sqrt{T_t}}{p_t} \frac{\mathbb{V}_t}{A^*} \rho_i \left(1 - \frac{\rho_f}{\rho_i}\right)} \tag{13.43}$$

For polytropic expansion of air in the storage tank, we can write

$$\frac{\rho_f}{\rho_i} = \left(\frac{p_f}{p_i}\right)^{1/n} ; \quad \rho_i = \frac{p_i}{RT_i}$$

where the subscripts i and f denote the initial and final conditions in the tank, respectively.

Substitution of the above relations into Eq. (13.43) results in

$$\boxed{t = 0.086 \frac{\mathbb{V}_t}{A^*} \frac{\sqrt{T_t}}{T_i} \frac{p_i}{p_t} \left[1 - \left(\frac{p_f}{p_i}\right)^{1/n}\right]} \tag{13.44}$$

with $\mathbb{V}_t$ in m^3, this equation gives the run time in seconds for the general case of blowdown tunnel operation with constant mass flow rate condition.

From Eq. (13.44) it is obvious that for $t_{\max}$ the condition required is p_t minimum. At this stage we should realize that the above equation for running time has to be approached from the practical point of view and not from purely from the mathematical point of view. Realizing this, it can be seen that the tunnel run does not continue until the tank pressure drops to the settling chamber stagnation pressure p_t, but stops when the storage pressure reaches a value which is appreciably higher than p_t, i.e. when $p_f = p_t + \Delta p$. This Δp is required to overcome the frictional and other losses in the piping system

Scanned by CamScanner

between the storage tank and the settling chamber. The value of Δp varies from about $0.1p_t$ for very-small-mass flow runs to somewhere around $1.0p_t$ for high-mass flow runs.

The proper value of the polytropic index n in Eq. (13.44) depends on the rate at which the stored high-pressure air is used, the total amount of air used, and the shape of the storage tank. The value of n tends towards 1.4 as the storage tank shape approaches spherical shape. With heat storage material in the tank (i.e. for the isothermal condition), the index n approaches unity. Equation (13.44) may also be used with reasonable accuracy for constant-pressure runs in which the change in total temperature is small, since these runs approach the constant-mass flow rate situation.

EXAMPLE 13.6 Determine the running time for a Mach 2 blowdown wind tunnel with test-section cross-section of 300 mm × 300 mm. The storage tank volume is 20 m^3 and the pressure and temperature of air in the tank are 20 atm and 25°C, respectively. The inside of the tank is provided with a heat-sink material. Take the starting pressure ratio required for Mach 2.0 to be 3.0, the loss in pressure regulating valve (PRV) to be 50 per cent and the polytropic index $n = 1.0$.

Solution Given that the settling chamber pressure required to start the tunnel is $p_t = 3.0 \times 101.3$ kPa. The pressure loss in the PRV is 50 per cent, therefore,

$$p_f = 1.5 \times 303.9 = 455.85 \text{ kPa}$$

From isentropic tables, for $M = 2.0$, we have $A^*/A = 0.593$. Therefore,

$$A^* = 0.593 \times 0.09 = 0.0534 \text{ m}^2$$

Using Eq. (13.42), the running time, t, is given by

$$t = 0.086\left(\frac{20}{0.0534}\right)\left(\frac{\sqrt{298}}{298}\right)\left(\frac{2026}{303.9}\right)\left[1-\left(\frac{455.85}{2026}\right)\right]$$

$$= \boxed{9.64 \text{ s}}$$

13.8 INSTRUMENTATION AND CALIBRATION OF WIND TUNNELS

Calibration of wind tunnel test-section to ensure uniform flow characteristics everywhere in the test-section is an essential requirement in wind tunnel operation.

Calibration of Supersonic Wind Tunnels

Supersonic tunnels operate in the Mach number range of about 1.4 to 5.0. They usually have operating total pressures from about atmospheric to 2 MPa (≈ 300 psi) and operating total temperatures of about ambient to 100°C.

Scanned by CamScanner

Maximum model cross-section area (projected area of the model, normal to the test-section axis) of the order of 4 per cent of the test-section area is quite common for supersonic tunnels. *Model size is limited by tunnel choking and wave reflection considerations*. When proper consideration is given to choking and wave reflection while deciding the size of a model, there will be no effects of the wall on the flow over the models (unlike low-speed tunnels), since the reflected disturbances will propagate only downstream of the model. However, there will be a buoyancy effect if there is a pressure gradient in the tunnel. Luckily, typical pressure gradients associated with properly designed tunnels are small, and the buoyancy effects in such tunnels are usually negligible. The Mach number in a supersonic tunnel with solid walls cannot be adjusted, because it is set by the geometry of the nozzle. Small increases in Mach number usually accompany large increases in operating pressure (the stagnation pressure in the settling chamber in the case of constant backpressure or the nozzle pressure ratio in the case of blowdown indraft combination), in that the boundary layer thickness is reduced and consequently the effective area ratio is increased.

During calibration as well as testing, the condensation of moisture in the test gas must be avoided. To ensure that condensation will not be present in significant amounts, the air dewpoint in the tunnel should be continuously monitored during tunnel operation. The amount of moisture that can be held by a cubic metre of air increases with increasing temperature, but is independent of the pressure. The moist atmospheric air cools as it expands isentropically through a wind tunnel. The air may become supercooled (cooled to a temperature below the dew-point temperature) and the moisture will then condense out. If the moisture content is sufficiently high, it will appear as a dense fog in the tunnel. Detailed information about the effect of condensation on the flow quality in the test-section of a tunnel can be found in the book *Instrumentation, Measurements, and Experiments in Fluids* by E. Rathakrishnan.

Calibration

The calibration of a supersonic wind tunnel includes determining the test-section flow Mach number throughout the range of operating pressure of each nozzle, determining flow angularity, and determining an indication of the turbulence level effects.

Mach Number Determination

The following methods may be employed for determining the test-section Mach number of supersonic wind tunnels.

- Mach numbers from close to the speed of sound to 1.6 are usually obtained by measuring the static pressure (p) in the test-section and the total pressure (p_{01}) in the settling chamber and using the isentropic relation

Scanned by CamScanner

$$\boxed{\frac{p_{01}}{p} = \left(1 + \frac{\gamma - 1}{2} M^2\right)^{\gamma/(\gamma-1)}}$$

- For Mach numbers above 1.6, it is more accurate to use the pitot pressure in the test-section (p_{02}) with the total head in the settling chamber (p_{01}) and the normal shock relation.

$$\boxed{\frac{p_{02}}{p_{01}} = \left[1 + \frac{2\gamma}{\gamma+1}(M_1^2 - 1)\right]^{-1/(\gamma-1)} \left[\frac{(\gamma+1)M_1^2}{(\gamma-1)M_1^2 + 2}\right]^{\gamma/(\gamma-1)}}$$

- Measurement of static pressure p_1 using a wall pressure tap in the test-section and measurement of pitot pressure p_{02} at the test-section axis, above the static tap, can be used through the Rayleigh pitot formula,

$$\boxed{\frac{p_1}{p_{02}} = \frac{\left(\frac{2\gamma}{\gamma+1} M_1^2 - \frac{\gamma-1}{\gamma+1}\right)^{1/(\gamma-1)}}{\left(\frac{\gamma+1}{2} M_1^2\right)^{\gamma/(\gamma-1)}}}$$

for accurate determination of the Mach number.

- Measurement of shock wave angle β from Schlieren and shadowgraph photograph of flow past a wedge or cone of angle θ can be used to obtain the Mach number through the $(\theta - \beta - M)$ relation,

$$\boxed{\tan\theta = 2\cot\beta \left[\frac{M_1^2 \sin^2\beta - 1}{M_1^2(\gamma + \cos 2\beta) + 2}\right]}$$

- The Mach angle μ measured from a Schlieren photograph of a clean test-section can also be used for determining the Mach number with the relation

$$\boxed{\sin\mu = \frac{1}{M_1}}$$

For this the Schlieren system used must be powerful enough to capture the Mach waves in the test-section.

- Mach number can also be obtained by measuring pressures on the surface of cones or twodimensional wedges, although this is rarely done in calibration.

Pitot Pressure Measurement

Pitot pressures are measured by using a *pitot probe*. The pitot probe is simply a tube with a blunt end facing into the air stream. The tube will normally have an

Scanned by CamScanner

inside-to-outside diameter ratio of 0.5 to 0.75, and a length aligned with the air stream of 15 to 20 times the tube diameter. The inside diameter of the tube forms the pressure orifice. For test-section calibration, a rake consisting of a number of pitot probes is usually employed. The pitot tube is simple to construct and accurate to use. It should always have a squared-off entry and the largest practical ratio of hole (inside) diameter to outside diameter.

At this stage, it is important to note that an open-ended tube facing into the air stream always measures the stagnation pressure (a term identical in meaning to the "total head") it sees. For flows with Mach number greater than 1, a bow shock wave will be formed ahead of the pitot tube nose. Therefore, the flow reaching the probe nose is not the actual freestream flow, but the flow traversed by the bow shock at the nose. Thus, what the pitot probe measures is not the actual static pressure but the total pressure behind a normal shock (the portion of the bow shock at the nose hole can be approximated to a normal shock). This new value is called pitot pressure and in modern terminology refers to the pressure measured by a pitot probe in a supersonic stream.

Static Pressure Measurement

Supersonic flow static pressure measurements are much more difficult than the measurement of pitot and static pressures in a subsonic flow. The primary problem in the use of static pressure probes at supersonic speeds is that the probe will have a shock wave (either attached or detached shock) at its nose, causing a rise in static pressure. The flow passing through the oblique shock at the nose will be decelerated. However, the flow will continue to be supersonic because all naturally occurring oblique shocks are weak shocks with supersonic flow on either side of them. The supersonic flow of reduced Mach number will get decelerated further, while passing over the nose-cone of the probe because a decrease in streamtube area would decelerate a supersonic stream. This progressively decelerating flow over the nose-cone would be expanded by the expansion fan at the nose-cone shoulder junction of the probe. Therefore, the distance over the shoulder should be sufficient for the flow to get accelerated to the level of the undisturbed freestream static pressure, in order to measure the correct static pressure of the flow. The static pressure hole should be located at the point where the flow comes to the level of freestream Mach number. Here, it is essential to note that, the flow deceleration process through the oblique shock at the probe nose, and over the nose-cone portion can be made to be approximately isentropic, if the flow turning angles through these compression waves are kept less than 5°.

Static pressures on the walls of supersonic tunnels are often used for rough estimation of the test-section Mach numbers. However, it should be noted that the wall pressures will not correspond to the pressures on the tunnel centre line if compression or expansion waves are present between the wall and the centre line. When Mach number is to be determined from static pressure

Scanned by CamScanner

measurements, the total pressure of the stream is measured in the settling chamber simultaneously with the test-section static pressure. Mach number is then calculated using the isentropic relation.

Determination of Flow Angularity

The flow angularity in a supersonic tunnel is usually determined by using either the cone or the wedge yaw meters. Sensitivities of these yaw meters are maximum when the wedge or cone angles are maximum. They work below Mach numbers for which wave detachment occurs, and are so used. The cone yaw meter is more extensively used than the wedge yaw meter, since it is easier to fabricate.

Determination of Turbulence Level

Measurements with a hot-wire anemometer demonstrate that there are high-frequency fluctuations in the air stream of supersonic tunnels that do not occur in free air. These fluctuations, broadly grouped under the heading of "turbulence", consists of small oscillations in velocity, stream temperature (entropy), and static pressure (sound). Some typical values of these fluctuations are given in Table 13.2.

TABLE 13.2 Turbulence levels in the settling chamber and test-section of a supersonic tunnel

Parameter	*Settling chamber*	*Test-section*	
M	all	2.2	4.5
Sound, $\Delta p/p$	< 0.1%	0.2%	1%
Entropy, $\Delta T/T$	< 0.1%	< 0.1%	1%
Velocity, $\Delta V/V$	0.5–1%	< 0.1%	1%

The pressure regulating valve, the drive system, the after cooler, and the test-section boundary layer are the major causes for the fluctuations. Velocity fluctuations due to upstream causes may be reduced at low and moderate Mach numbers by the addition of screens in the settling chambers. At high Mach numbers, the upstream pressure and velocity effects are usually less, since the large nozzle contraction ratios damp them out. Temperature fluctuations are unaffected by the contraction ratio.

Determination of Test-Section Noise

The test-section noise is defined as pressure fluctuations. Noise may result from unsteady settling chamber pressure fluctuations due to upstream flow conditions. It may also be due to weak unsteady shocks originating in a turbulent boundary layer on the tunnel wall. Noise in the testsection is very

Scanned by CamScanner

likely to influence the point of boundary layer transition on a model. Also, it is probable that the noise will influence the other test results as well.

Test-section noise can be detected by either hot-wire anemometry measurements or by high-response pitot pressure measurements. It is a usual practice to make measurements in both the test-section and the settling chamber of the tunnel to determine whether the noise is coming from the test-section boundary layer. It is then possible to determine whether the fluctuations in the two places are related. The *test-section noise usually increases with increasing tunnel operating pressure, and the test-section noise originating in the settling chamber usually decreases as tunnel Mach number increases.*

The Use of Calibration Results

The Mach number in the vicinity of a model during a test is assumed to be equal to an average of those obtained in the same portion of the test-section during calibrations. With this Mach number and the total pressure (p_{01}) measured in the settling chamber, it is possible to define the dynamic pressure q as

$$\frac{q}{p_{01}} = \frac{\gamma}{2} M^2 \left(1 + \frac{\gamma - 1}{2} M^2\right)^{-\gamma/(\gamma-1)}$$

for use in data reduction. If the total temperature is also measured in the settling chamber, all properties of the flow in the test-section can be obtained using isentropic relations. The flow angularities measured during calibration are used to adjust model angles set with respect to the tunnel axis to a mean flow direction reference. The transition point and noise measurements made during the calibration may be used to decrease the tunnel turbulence and noise level.

Starting of Supersonic Tunnels

Supersonic tunnels are usually started by operating a quick-operating valve, which causes air to flow through the tunnel. In continuous-operation tunnels, the compressors are normally brought up to the desired operating speed with air passing through a by-pass line. When the operating speed is reached, a valve in the bypass line is closed, which forces the air through the tunnel. In blowdown tunnels a valve between the pressure storage tanks and the tunnel is opened.

Quick starting is desirable for supersonic tunnels, since the model is subjected to high loads during the starting process. Also, the quick start of the blowdown tunnel conserves air. To determine when the tunnel is started, the pressure at an orifice in the test-section wall near the model nose is usually observed. When this pressure suddenly drops to a value close to the static pressure for the design Mach number, the tunnel is started. If the model is blocking the tunnel, the pressure will not drop. We can easily identify the starting of the tunnel from the sound it makes.

Some tunnels are provided with variable second-throat diffusers, designed to decrease the pressure ratio required for tunnel operation. These diffusers are

Scanned by CamScanner

designed to allow the setting of a cross-sectional area large enough for starting the tunnel and to allow the setting of a less crosssectional area for more efficient tunnel operation. When used as designed, the variable diffuser throat area is reduced to a predetermined area as soon as the tunnel starts.

Starting Loads

Whenever a supersonic tunnel is being started or stopped, a normal shock passes through the testsection and large forces are imposed on the model. The model oscillates violently at the natural frequency of the model support system, and normal force loads of about 5 times those which the model would experience during steady flow in the same tunnel at an angle of attack of 10 degrees are not uncommon. The magnitudes of starting loads on a given model in a given tunnel are quite random and exactly what causes the large loads is not yet understood.

Starting loads pose a serious problem in the design of balances for wind tunnel models. If the balances are designed to be strong enough to withstand these severe starting loads, it is difficult to obtain sensitivities adequate for resolving the much smaller aerodynamic loads during tests. Several methods have been used for alleviating this problem. Among them the more commonly used methods are:

- Starting at a reduced total pressure in continuous tunnels.
- Shielding the model with retractable protective shoes at start.
- Injecting the model into the air stream after the tunnel is started.

Reynolds Number Effects

The primary effects of Reynolds number in supersonic wind tunnel testing are on drag measurements. The aerodynamic drag of a model is usually made up of the following four parts:

1. The skin friction drag, which is equal to the momentum loss of air in the boundary layer.
2. The pressure drag, which is equal to the integration of pressure loads in the axial direction, over all surfaces of the model ahead of the base.
3. The base drag, which is equal to the product of base pressure differential and base area.
4. The drag due to lift, which is equal to the component of normal force in the flight direction.

The pressure drag and drag due to lift are essentially independent of model scale or Reynolds number, and can be evaluated from wind tunnel tests of small models. But the skin friction and base drags are influenced by Reynolds number. In the supersonic regime, the skin friction is only a small portion of the total drag due to the increased pressure drag over the fore body of the model. However, it is still quite significant and needs to be accounted for. Although the

Scanned by CamScanner

probability of downstream disturbances affecting the base pressure and hence the base drag is reduced because of the inability of downstream disturbances to move upstream in supersonic flow, enough changes make their way through the subsonic wake to cause significant base interference effects.

Model Mounting-Sting Effects

Any sting extending downstream from the base of a model will have an effect on the flow and, therefore, likely to affect the model base pressure. For actual tests the sting must be considerably larger than that required to withstand the tunnel starting loads and to allow testing to the maximum steady load condition, with a reasonable model deflection. Sting diameters of 1/4 to 3/4 model base diameters are typical in the wind tunnel tests. The effects on the base pressure of typical sting diameters are significant, but represent less than 1 per cent of the dynamic pressure and therefore, a small amount of the total drag of most of the models.

13.9 SUMMARY

In this chapter we have outlined some of the major measurement techniques which are commonly employed for compressible flow analysis. In any flow field the prime quantities of interest are the pressure, temperature, density, velocity and its direction.

The devices used for pressure measurements in fluid flows may broadly be grouped as manometers and pressure transducers. Some of the popular manometers are the U-type manometer, multitube manometer, micro manometers, and Betz manometer. The pressure transducers used are of electrical type, mechanical type, and optical type.

Thermocouple is the commonly used device for temperature measurements in fluid flow. It operates on the principle that a flow of current in a metal accompanies a flow of heat. In some metals, heat and current flow in the same direction. In some other metals, heat flow and current flow are in opposite directions. These are called dissimilar metals. Thermocouples are made with dissimilar metals like copper–constantan, iron–constantan, etc.

The flow velocity can be calculated from the measured pressure and temperature through the relation

$$V = M\sqrt{\gamma RT}$$

The flow direction may be obtained using a symmetric wedge or cone with pressure taps at directly opposite locations, as shown in Fig. 13.10.

The velocity may also be measured using a hot-wire manometer. By Kings law,

$$\frac{I^2 R_w}{R_w - R_g} = A + B(V)^{1/2}$$

Scanned by CamScanner

By measuring the resistances R_w and R_g, keeping the current constant or measuring I, and by keeping the resistances constant, the flow velocity can be determined. The hot-wire system with I constant is called the *constant current hot-wire anemometer*, and the system with R_w constant is called the *constant temperature hot-wire anemometer*.

The density of a flow can be calculated by measuring the pressure and temperature. Supersonic flows with significant density changes can be visualized with optical systems such as interferometer, Schlieren, and shadowgraph. These techniques may be used to get a considerable insight into the qualitative aspects of the flow field. Event though these optical techniques have been thought of as qualitative visualization methods for supersonic flows in classical literature, today they are being used for quantitative analysis too, with suitable transformation and image processing techniques. The present understanding is that out of these, interferometer is very much amenable for quantitative studies. When proper methods are developed for quantitative studies of the field with this kind of optical techniques, which are nonintrusive and since they do not require any seeding like laser Doppler Anemometer, they will stay as the most reliable hightech experimental methods for supersonic flow studies.

For visualizing compressible flows, *interferometer*, *Schlieren* and *shadowgraph* are the three popularly employed optical flow visualization techniques. Interferometer makes visible the optical phase changes resulting from the relative retardation of the disturbed rays. Schlieren system gives the deflection angles of the incident rays. Shadowgraph visualizes the displacement experienced by an incident ray which has crossed the high-speed gas flow.

The quality of the optical equipment to be used in the Schlieren setup depends on the type of the investigation carried out. The cost increases rapidly with the quality of the optical components. The vital components are the mirrors, and the light source.

Interferometer is an optical method most suited for qualitative determination of the density field of high-speed flows. In general, the Schlieren method is used either for the detection of small refractive index gradients or for the quantitative measurement of these gradients.

The shadowgraph is best suited only for flow fields with rapidly varying density gradients.

The theory shows that the Schlieren technique depends upon the first derivative of the refractive index (flow density) while the shadowgraph method depends upon its second derivative. Consequently, in phenomena where the refractive index varies relatively slowly, the Schlieren method is to be preferred to the shadowgraph method, other things being equal. On the other hand, the shadow method beautifully brings out the rapid changes in the index of refraction. The shadow method also has the advantage of greater simplicity and somewhat wider possible application. The two methods therefore supplement each other and both should be used wherever possible.

Scanned by CamScanner

Tunnels with test-section speed more than 650 kmph are called high-speed tunnels.

Based on the range of test-section Mach number M, the high-speed tunnels are classified as follows:

- $0.8 < M < 1.2$ Transonic tunnel
- $1.2 < M < 5$ Supersonic tunnel
- $M > 5$ Hypersonic tunnel

High-speed tunnels are classified as intermittent or *open-circuit tunnels* and *continuous return circuit tunnels*, based on the type of operation.

The commonly employed reservoir pressure range is from 600 kPa to 2 MPa for blowdown tunnel operations. As large as 15 MPa psi is also used where space limitations necessitates the same.

In induction type tunnels, a vacuum created at the downstream end of the tunnel is used to establish the flow in the test-section.

The main advantages of continuous supersonic wind tunnels are the following:

- Better control over the Reynolds number is possible, since the shell is pressurized.
- Only a small capacity drier is required.
- Testing conditions can be held the same over a long period of time.
- The test-section can be designed for high Mach numbers ($M > 4$) and large size models.
- Starting load can be reduced by starting at low pressure in the tunnel shell.

The major disadvantages of continuous supersonic tunnels are the following:

- Power required is very high.
- Temperature stabilization requires a large size cooler.
- Compressor drive has to be designed to match the tunnel characteristics.
- Tunnel design and operation are more complicated.
- Axial flow compressor is better suited for large pressure ratios and mass flow rates.
- Diffuser design is critical since increasing diffuser efficiency will lower the power requirement considerably. Supersonic diffuser portion (geometry) must be carefully designed to make the Mach number of the flow to be as small as possible, before shock formation. Subsonic portion of the diffuser must have an optimum angle, to minimize the frictional and separation losses.
- Proper nozzle geometry is very important to obtain good distribution of Mach number and freedom from flow angularity in the test-section. Theoretical calculations to high accuracy and boundary layer compensation, etc., have to be carefully worked out for large test-sections. Fixing nozzle blocks for different Mach numbers is simple but expensive and laborious for change over in the case of large

Scanned by CamScanner

size test-sections. Flexible wall type nozzle is complicated and expensive from design point of view and Mach number range is limited (usually $1.5 < M < 3.0$).

- Model size is determined from the test-rhombus. The model must be accommodated inside the rhombus formed by the incident and reflected shocks, for proper measurements.

The total power loss in a continuous supersonic wind tunnel may be split into the following components:

1. Frictional losses (in the return circuit).
2. Expansion losses (in the diffuser).
3. Losses in contraction cone and test-section.
4. Losses in guide vanes.
5. Losses in the cooling system.
6. Losses due to shock wave (in the diffuser supersonic part).
7. Losses due to model and support system drag.

The first five components of losses represent the usual low-speed tunnel losses. All the five components together constitute only about 10 per cent of the total loss. Components 6 and 7 are additional losses in a supersonic wind tunnel and usually amount to approximately 90 per cent of the total loss, with shock wave losses alone accounting to nearly 80 per cent and model and support system drag constituting nearly 10 per cent of the total loss.

For continuous and intermittent supersonic wind tunnels, the energy ratio, ER, may be defined as follows:

1. *For continuous tunnel*

$$ER = \frac{KE \text{ at the test-section}}{\text{work done in isentropic compression per unit time}}$$

Using Eq. (13.24), ER may be expressed as

$$ER = \frac{1}{(p_\sigma^{(\gamma-1)/\gamma} - 1)\left(\dfrac{2}{(\gamma-1)M_1^2} + 1\right)} \tag{13.27}$$

2. *For intermittent tunnel*

$$ER = \frac{(KE \text{ in test-section})(\text{time of tunnel run})}{\text{energy required for charging the reservoir}} \tag{13.28}$$

- For $M < 1.7$, induced flow tunnels are more efficient than the blowdown tunnels.
- In spite of this advantage, most of the supersonic tunnels even over this Mach number range are operated as blowdown tunnels and not as induced flow tunnels. This is because vacuum tanks are more expensive than compressed air storage tanks.

The second throat, provides isentropic deceleration and highly efficient pressure recovery after the test-section. Neglecting frictional and boundary

Scanned by CamScanner

layer effects, a wind tunnel can be run at design conditions indefinitely, with no pressure difference requirement to maintain the flow, once started. But this is an ideal situation which is not encountered in practice.

The second throat area must be large enough to accommodate the mass flow, when a normal shock is present in the test-section.

$$\boxed{\frac{A_2^*}{A_1^*} = \frac{p_{01}}{p_{02}}}$$

Usually the design of a continuous supersonic wind tunnel has either of the following two objectives:

1. Choose a compressor for specified test-section size, Mach number, and pressure level.
2. Determine the best utilization of an already available compressor.

The power requirement for a multistage compressor is given by

$$\text{HP} = \left(\frac{1}{746}\right)\left(\frac{N\gamma}{\gamma - 1}\right)\dot{m}RT_s\left(\left(\frac{p_{0c}}{p_{03}}\right)^{(\gamma-1)/\gamma N} - 1\right)$$

where $\dot{m}$ is the mass flow rate of air in kg/s, p_{03} and p_{0c} are the total pressures at the inlet and outlet of the compressor, respectively, N is the number of stages, and T_s is the stagnation temperature.

Mass flow rate is one of the primary considerations in sizing a wind tunnel test-section and the associated equipment, such as compressor and diffuser.

In a blowdown tunnel circuit, the pressure and temperature of air in the compressed air reservoir (also called storage tank) change during operation. This change of reservoir pressure causes the following effects.

- The tunnel stagnation and settling chamber pressures fall correspondingly.
- The tunnel is subjected to dynamic condition.
- Dynamic pressure in the test-section falls and hence, the forces acting on the model change during the test.
- Reynolds number of the flow changes during the tunnel run.

Usually three methods of operation are adopted for blowdown tunnel operation. They are:

- Constant Reynolds number operation
- Constant pressure operation
- Constant throttle operation

For a given settling chamber pressure and temperature, the running time is:

- The shortest for constant throttle operation.
- The longest for constant Reynolds number operation.
- In between the above two for constant pressure operation.

Scanned by CamScanner

Blowdown supersonic wind tunnels are usually operated with either constant dynamic pressure (q) or constant mass flow rate ($\dot{m}$).

For constant q operation, the only control necessary is a pressure regulating valve (PRV) that holds the stagnation pressure in the settling chamber at a constant value. For constant mass flow run, the stagnation temperature and pressure in the settling chamber must be held constant. For this, either a heater or a thermal mass external to the storage tank is essential. The addition of heat energy to the pressure energy in the storage tank results in a longer running time of the tunnel.

Calibration of wind tunnel test-section to ensure uniform flow characteristics everywhere in the test-section is an essential requirement in wind tunnel operation.

Supersonic tunnels operate in the Mach number range of about 1.4 to 5.0. They usually have operating total pressures from about atmospheric to 2 MPa ($\approx$ 300 psi) and operating total temperatures of about ambient to 100°C. Maximum model cross-section area (projected area of the model, normal to the test-section axis) of the order of 4 per cent of the test-section area is quite common for supersonic tunnels.

During calibration as well as testing, the condensation of moisture in the test gas must be avoided.

The calibration of a supersonic wind tunnel includes determining the test-section flow Mach number throughout the range of operating pressure of each nozzle, determining flow angularity, and determining an indication of the turbulence level effects.

The following methods may be employed for determining the test-section Mach number of supersonic wind tunnels.

- Mach numbers from close to the speed of sound to 1.6 are usually obtained by measuring the static pressure (p) in the test-section and the total pressure (p_{01}) in the settling chamber and using the isentropic relation

$$\boxed{\frac{p_{01}}{p} = \left(1 + \frac{\gamma - 1}{2} M^2\right)^{\gamma/(\gamma-1)}}$$

- For Mach numbers above 1.6, it is more accurate to use the pitot pressure in the test-section (p_{02}) with the total head in the settling chamber (p_{01}) and the normal shock relation.

$$\boxed{\frac{p_{02}}{p_{01}} = \left[1 + \frac{2\gamma}{\gamma + 1}(M_1^2 - 1)\right]^{-1/(\gamma-1)} \left[\frac{(\gamma + 1)M_1^2}{(\gamma - 1)M_1^2 + 2}\right]^{\gamma/(\gamma-1)}}$$

Scanned by CamScanner

- Measurement of static pressure p_1 using a wall pressure tap in the test-section and measurement of pitot pressure p_{02} at the test-section axis, above the static tap can be used through the Rayleigh pitot formula,

$$\boxed{\frac{p_1}{p_{02}} = \frac{\left(\frac{2\gamma}{\gamma+1}M_1^2 - \frac{\gamma-1}{\gamma+1}\right)^{1/(\gamma-1)}}{\left(\frac{\gamma+1}{2}M_1^2\right)^{\gamma/(\gamma-1)}}}$$

for accurate determination of the Mach number.

- Measurement of shock wave angle β from Schlieren and shadowgraph photograph of flow past a wedge or cone of angle θ can be used to obtain the Mach number through the $(\theta - \beta - M)$ relation,

$$\boxed{\tan\theta = 2\cot\beta\left[\frac{M_1^2\sin^2\beta - 1}{M_1^2(\gamma + \cos 2\beta) + 2}\right]}$$

- The Mach angle μ measured from a Schlieren photograph of a clean test-section can also be used for determining the Mach number with the relation

$$\boxed{\sin\mu = \frac{1}{M_1}}$$

For this the Schlieren system used must be powerful enough to capture the Mach waves in the test-section.

- Mach number can also be obtained by measuring pressures on the surface of cones or twodimensional wedges, although this is rarely done in calibration.

Pitot pressures are measured by using a *pitot probe*. The pitot probe is simply a tube with a blunt end facing into the air stream. The tube will normally have an inside-to-outside diameter ratio of 0.5 to 0.75, and a length aligned with the air stream of 15 to 20 times the tube diameter. The inside diameter of the tube forms the pressure orifice. For test-section calibration, a rack consisting of a number of pitot probes is usually employed. The pitot tube is simple to construct and accurate to use. It should always have a squared-off entry and the largest practical ratio of hole (inside) diameter to outside diameter.

Supersonic flow static pressure measurements are much more difficult than the measurement of pitot and static pressures in a subsonic flow. The flow deceleration process through the oblique shock at the probe nose, and over the nose-cone portion can be made to be approximately isentropic, if the flow turning angles through these compression waves are kept less than 5°.

Scanned by CamScanner

Static pressures on the walls of supersonic tunnels are often used for rough estimation of the test-section Mach numbers.

The flow angularity in a supersonic tunnel is usually determined by using either the cone or the wedge yaw meters.

Measurements with a hot-wire anemometer demonstrate that there are high-frequency fluctuations in the air stream of supersonic tunnels that do not occur in free air. These fluctuations, broadly grouped under the heading of "turbulence", consists of small oscillations in velocity, stream temperature (entropy), and static pressure (sound).

The test-section noise, defined as pressure fluctuations, may result from unsteady settling chamber pressure fluctuations due to upstream flow conditions. It may also be due to weak unsteady shocks originating in a turbulent boundary layer on the tunnel wall. Noise in the test-section is very likely to influence the point of boundary layer transition on a model. Test-section noise can be detected by either hot-wire anemometry measurements or by high-response pitot pressure measurements.

Quick starting is desirable for supersonic tunnels, since the model is subjected to high loads during the starting process. Also, the quick start of the blowdown tunnel conserves air.

Some tunnels are provided with variable second-throat diffusers, designed to decrease the pressure ratio required for tunnel operation.

Whenever a supersonic tunnel is being started or stopped, a normal shock passes through the test-section and large forces are imposed on the model. The model oscillates violently at the natural frequency of the model support system and normal force loads of about 5 times those which the model would experience during steady flow in the same tunnel at an angle of attack of 10 degrees are not uncommon.

Starting loads pose a serious problem in the design of balances for wind tunnel models.

The primary effects of Reynolds number in supersonic wind tunnel testing are on drag measurements. The pressure drag and drag due to lift are essentially independent of model scale or Reynolds number, and can be evaluated from wind tunnel tests of small models. But the skin friction and base drags are influenced by Reynolds number. In the supersonic regime, the skin friction is only a small portion of the total drag due to the increased pressure drag over the fore body of the model. However, it is still quite significant and need to be accounted for.

Any sting extending downstream from the base of a model will have an effect on the flow and therefore, is likely to affect the model base pressure. For actual tests the sting must be considerably larger than that required to withstand the tunnel starting loads and to allow testing to the maximum steady load condition, with a reasonable model deflection.

Scanned by CamScanner

PROBLEMS

1. The Mach number of a compressible flow is to be determined from static probe and pitot tube measurements. If the static probe indicates 500 mm Hg suction and the pitot tube 350 mm Hg suction, (a) determine the flow Mach number, and (b) repeat the calculation for a pitot pressure of 275 mm Hg compression.

[**Ans.** (a) 0.835; (b) 1.56]

2. A pitot-static tube in an air stream records a dynamic pressure of 50 cm of mercury. The static pressure and stagnation temperature of the air stream are 3.6×10^4 N/m^2 (gauge) and 27°C, respectively. The barometer reads 75.6 cm of mercury. Compute the air velocity, assuming the air as (a) compressible, and (b) incompressible.

[**Ans.** (a) 256.06 m/s; (b) 237.55 m/s]

3. Air flows through an adiabatic frictionless passage. At station 1, the Mach number is 0.9, and the static pressure is 4.15×10^5 N/m^2. At station 2, the Mach number is 0.2. Calculate the change in static pressure between stations 1 and 2.

[**Ans.** 2.676×10^5 N/m^2]

4. Air flows at a speed of 400 m/s and a static pressure of 1 atmosphere. The air is isentropically brought to rest in a steady flow process. Find the Mach number and stagnation pressure if the static temperature is (a) 500°C, (b) −50°C.

[**Ans.** (a) 0.718, 1.428×10^5 N/m^2; (b) 1.336, 2.949×10^5 N/m^2]

5. An aeroplane flies at a constant speed of 900 kmph at 10,000 m altitude. A pressure traverse shows that the air is brought to rest at a particular location on the fuselage. Calculate (a) the temperature of air in stagnation region, and (b) the temperature rise caused by impact. Assume air as a perfect gas and $\gamma = 1.4$.

[**Ans.** (a) 254.17 K; (b) 31.02 K]

6. An intermittent wind tunnel is designed for a Mach number of 4 at the test-section. The tunnel operates by sucking air from the atmosphere through a duct into a vacuum tank. The tunnel is located at an altitude of 1650 m, where $\rho = 1.044$ kg/m^3. If the flow is isentropic, show that the density at the test-section is 0.029 kg/m^3.

7. A stationary temperature probe inserted into a duct reads 100°C where the air is flowing at 250 m/s. What is the actual temperature of the air?

[**Ans.** 68.9°C]

8. The test-section area of a Mach 2.5 tunnel is half of the nozzle inlet area. If the test-section pressure is 100 kPa, determine the pressure and Mach number at the nozzle inlet.

[**Ans.** 1.696 MPa, 0.11]

Scanned by CamScanner

14 Rarefied Gas Dynamics

14.1 INTRODUCTION

Classical hydrodynamics formed the beginning of fluid flow studies. At that stage, fluids were assumed to be inviscid, incompressible, continuous and chemically invariant, and attention was mainly focussed on the lift force on bodies placed in fluid flows. The subject of aerodynamics emerged by removing the restriction on fluid as inviscid and treating it as viscous, which provided a better understanding of the drag force experienced by bodies in motion. The steady improvement in increasing the speed of the bodies in motion (e.g. aircraft, missiles) soon made it necessary to remove the limitation imposed by the assumption of incompressibility, and the subject of Gas Dynamics was born. The need for placing emphasis on the study of major compressibility effects such as shock waves has already been discussed in some detail. The stage has now been reached when the assumption of continuity (namely, the number of molecules per unit volume is large enough so that, in general, the fluid properties could be assumed to vary continuously from point to point throughout a flow field) must be carefully examined. It is well known that flight through the earth's atmosphere involves rarefaction and high temperature effects, which can only be explained on the basis of the molecular properties of gases. The advent of very high temperatures indicates that even chemical invariance may no longer be valid.

In continuum treatment the gas flow is modelled on a macroscopic level. This treatment is justified, since at 1 atmosphere and 20°C there are approximately 2×10^{19} molecules in 1 cm^3 of air, with the mean free path (distance travelled by a molecule between two successive collisions) being only 6.35×10^{-6} cm. Under these conditions, the smallest volume we are considering will contain enough number of molecules so that we can effectively average over the molecules present and use a macroscopic approach. That is, the macroscopic model regards the gas as a continuum and the description is in

Scanned by CamScanner

terms of the variations of the macroscopic velocity, density, pressure, and temperature with distance and time. The second treatment of gas flow is based on microscopic or molecular model. This model recognizes the particulate structure of a gas as a myriad of discrete molecules and ideally provides information on the position and velocity of every molecule at all times.

The macroscopic quantities at any location in a flow field may be identified with average values of appropriate molecular quantities, the average being taken over the molecules in the vicinity of the location. The continuum description is valid as long as the smallest significant volume in the flow field contains sufficient number of molecules to establish meaningful averages. The existence of a formal link between the macroscopic and microscopic quantities means that the equations which express the conservations of mass, momentum, and energy in the flow may be derived from either approach. At this stage, we may recall that the conservation equations do not form a determinate set unless the shear stresses and heat flux can be expressed in terms of the other macroscopic quantities. It is the failure to meet this requirement rather than the breakdown of the continuum equations. Specifically, the Navier–Stokes equations of continuum gas dynamics fail when gradients of the macroscopic variables become so steep that their scale length is of the same order as the *mean free path*. For such flows the assumption of continuum is no longer valid, and the flow is referred to as *rarefied gas flow*.

In this chapter we discuss some preliminary aspects about the rarefied gas flows.

14.2 KNUDSEN NUMBER

A rarefied gas flow is a flow in which the length of the molecular mean free path λ is comparable to some characteristic dimension L of the flow field. The gas then does not behave entirely as a continuous fluid but rather exhibits some characteristics of its coarse molecular structure. For rarefied flows, a less precise but more convenient parameter is obtained if the scale length of the gradients is replaced by a characteristic dimension of the flow. The ratio of the mean free path λ to the characteristic dimension L defines the *Knudsen number* (Kn), i.e.

$$\boxed{\text{Kn} = \lambda / L}$$

The necessary condition for the validity of the continuum approach is, therefore, that the Knudsen number be small compared to unity. In other words, a rarefied gas flow is one for which the Knudsen number is not negligibly small.

The Knudsen number is related to the familiar parameters of fluid dynamics, the Mach number M, and the Reynolds number Re. From kinetic theory, we can define λ by the relation

$$\nu = \frac{1}{2}\lambda V_m \qquad (14.1)$$

Scanned by CamScanner

where ν is the kinematic viscosity and V_m the mean molecular speed. V_m is related to the speed of sound as

$$a = V_m \sqrt{\frac{\pi\gamma}{8}} \tag{14.2}$$

where λ is the ratio of specific heats. From Eqs. (14.1) and (14.2),

$$\lambda = 1.2533 \sqrt{\gamma}\, \frac{\nu}{a} \tag{14.3}$$

Equation (14.3) can also be written as

$$\frac{\lambda}{L} = 1.2533 \sqrt{\gamma}\, \frac{\nu}{L} \frac{1}{a}$$

Now, dividing and multiplying the RHS of the above equation by velocity V, we get

$$\text{Kn} = 1.2533 \sqrt{\gamma}\, \frac{M}{\text{Re}} \tag{14.4}$$

where both Kn and Re are based on the same characteristic length L.

Flow Regimes

Like Mach number and Reynolds number, the Knudsen number can also be used to divide the flow into various regimes. In fact, once the mean free path becomes comparable to any characteristic dimension in a flow field, only the Knudsen number will prove to be the appropriate parameter for the division of gas dynamics into various regimes. Based on characteristic ranges of values of an appropriate Knudsen number, Gas Dynamics is broadly classified into *continuum flow, slip flow, transition flow, and free molecule flow*. Physically, the above regimes correspond to flows in which, roughly speaking, the density levels are respectively, ordinary, slightly rarefied, moderately rarefied, and highly rarefied.

The widely accepted classification of flow regimes based on the Knudsen number is as follows:

(i) $\text{Kn} < 0.01$ (continuum flow)
(ii) $0.01 < \text{Kn} < 0.1$ (slip flow)
(iii) $0.1 < \text{Kn} < 1.0$ (transition flow)
(iv) $\text{Kn} > 1.0$ (free molecule flow)

Since the Knudsen number is related to Mach number and Reynolds number, the above classification of flow regimes can also be expressed in terms of M and Re. We know from our basic studies on fluid flows that for high Reynolds number flows, i.e. Re>> 1, the significant characteristic dimension of the flow field, which is important in determining viscous effects, is the boundary layer thickness δ rather than a dimension L of the body itself.

$$\frac{\delta}{L} \sim \frac{1}{\sqrt{\text{Re}}} \tag{14.5}$$

Scanned by CamScanner

Since the corresponding Knudsen number is given by

$$\boxed{\text{Kn} \sim \frac{M}{\sqrt{\text{Re}}}} \tag{14.6}$$

the continuum gas dynamics prevails for $M/\sqrt{\text{Re}} << 1$ and $\sqrt{\text{Re}} >> 1$. On the other hand, for very small Re, the Stokes type 'slow flow' occurs and the characteristic dimension itself is the significant parameter. Also, for internal flows, only the diameter of the duct is of significance. Hence the appropriate Knudsen number is simply Kn based on the body dimension, and ordinary low speed continuum flow prevails for $M/\sqrt{\text{Re}} << 1$. For flows in which the value of the appropriate Kn is small but not negligible, some departure from continuum gas dynamics phenomena may be expected to occur. As discussed in Section 14.3, one of the more striking of these effects is the phenomenon of "slip", i.e. the layer of gas at the solid face is no longer at rest but has a finite tangential velocity, in other words, the slip condition is not valid. The change from continuum gas dynamics to this slip regime takes place gradually. The slip regime on the basis of experimental evidence is defined as follows:

$$0.01 < \frac{M}{\sqrt{\text{Re}}} < 0.1 \ (\text{Re} > 1)$$
$$0.02 < \frac{M}{\text{Re}} < 0.1 \ (\text{Re} < 1) \tag{14.7}$$

In the slip regime, the mean free path is of the order of 1–10 per cent of the boundary layer thickness or other characteristic dimensions of the flow field. Slip effects may thus be expected to be approximately of this order. True rarefaction effects such as slip occur only in conjunction with either strong viscous or compressibility effects (see Schaaf and Chambre, 1961). In slip regime, these phenomena quite often dominate rarefaction effects associated with the coarse molecular structure of the gas, and even large-scale deviations from continuum behaviour are not apparent until the "transition" regime is reached.

For highly rarefied flows, the mean free path λ is very large compared to a characteristic body dimension L. Under these circumstances no boundary layer is formed. In fact, the probability of intermolecular collisions becomes rare compared to the collision of the molecules with the body surface; hence the former can be neglected. Therefore, the flow phenomena are mostly governed by the molecule-surface interaction. This regime of fluid mechanics is called *free molecule flow* and may be defined on the basis of experimental evidence by

$$\frac{M}{\text{Re}} > 3 \tag{14.8}$$

In the transition regime between slip flow and free molecule flow, the mean free path is of the same order as any characteristic body dimension. Both the intermolecular collisions and surface collisions are significant. With the present knowledge, the analysis of transition flow is very difficult.

Scanned by CamScanner

14.3 SLIP FLOW

The slip flow regime is the flow regime of slight rarefaction. The density of gas is slightly lower than that of a completely continuum flow. From Eq. (14.6) it parameters: the Mach number M, the Reynolds number Re, and the appropriate Knudsen number Kn. These parameters serve to indicate the importance of compressibility, viscosity, and rarefaction effects, respectively. For the Knudsen number to be in the range from 0.01 to 0.1, from Eq. (14.7), it is clear that either M must be large, or Re must be small, or both. Hence the rarefaction effects in the slip flow re:gime are associated with, and are in fact often dominated by, very strong compressibility or viscosity effects. In general, in this flow regime, it is expected that the boundary layers will be laminar; mostly they will be very thick and in fact the Reynolds number may be so low that the boundary layer theory is not strictly applicable. Also, it is expected that effects due to the interaction between these thick viscous layer and supersonic inviscid flow field will be significant. Because of the complexity associated with this interaction, there are only a few situations in the slip flow regime which can be solved, with proper accounting, for viscosity, compressibility, and rarefaction effects. However, the use of Navier–Stokes equations with slip boundary conditions is permissible for solving problems in this regime. The results obtained by this procedure agree fairly close to experimental results.

14.4 TRANSITION AND FREE MOLECULE FLOW

The transition flow regime lies between the slip and the free molecule flow regimes. Also, we know that the slip flow and free molecule flow may be analysed with some simplification assumptions based on the facts that the slip flow is only a moderately rarefied flow and the Navier–Stokes equations of continuum flow regime can still be used with slip boundary conditions; and in free molecule flow, the intermolecular collisions can be neglected in comparison with the collisions of the gas molecules with the surface of the object present in the flow field. But no such simplifying assumption can be made for transition flow regime, since in this regime, extremely complex transfer processes occur and hence intermolecular collisions and collisions between gas molecules and a wall are of equal importance. As yet no satisfactory theory exists for the analysis of flow in this regime.

As we discussed in the beginning of this chapter, the free molecule flow regime is the regime of extreme rarefaction. The molecular mean free path λ is, by definition, many times the characteristic dimension of the body which is assumed to be located in the flow. The molecules which hit the surface of the body are then re-emitted and travel very far before colliding with other molecules. It becomes necessary therefore to neglect the effect of the re-emitted molecules on the incident stream. In other words, the incident flow

Scanned by CamScanner

is assumed to be totally undisturbed by the presence of the body. This is the basic assumption of tree molecule flow theory .It is a consequence of this basic assumption that no shock waves are expected to form in the vicinity of the object. The boundary layer will be very diffuse and has no effect on the flow incident on the body.

Theoretical analysis of the external heat transfer and aerodynamic characteristics of bodies submerged in a free molecule flow field may be carried out by treating the flows of incident and reflected molecules separately. In calculating the flow of momentum or energy incident on the surface, it is assumed that the approaching gas is in local Maxwellian equilibrium. The results should therefore be applied to very high altitude considerations with some care.

EXAMPLE 14.1 Determine the resultant mass passing through area A of the aperture in unit time, for the motion of free molecules through a small aperture in a diaphragm which separates two large compartments filled with gas as shown in Fig. 14.1.

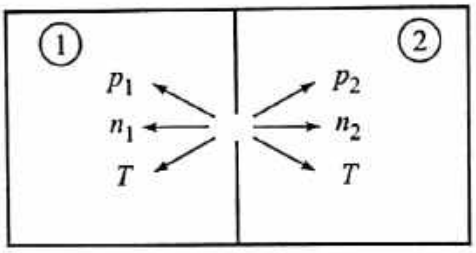


Fig. 14.1 Example 14.1.

[Hint: The average number of molecules striking a unit area of surface per unit time is given by

$$\frac{N}{A} = \frac{1}{4} n\bar{c}$$

where

n = number of molecules per unit volume

$\bar{c}$ = average molecular speed, $\sqrt{8RT/\pi}$ with R as the gas constant].

Solution The mean free path in either compartment is much greater than the diameter of the hole, but very small compared to tile dimensions of the compartments. Therefore, the molecules of each gas will pass through the aperture, unhindered by collisions as if the other gas were absent. On the other hand, there will be sufficient molecules in each compartment to permit the determination of the macroscopic properties like pressure and temperature of the gas.

Let the loss of a molecule from either gas through the hole produce no appreciable effect on the motion of the molecules in the body of the gas. Thus, neither gas develops a mass motion towards the opening. Therefore, we may assume that the molecular velocities are distributed throughout the motion according to Maxwell's law for a gas at rest.

Scanned by CamScanner

The flow of mass through unit area leaving compartment 1 in unit time is

$$mN_1 = \frac{1}{4} m_1 n_1 \bar{c}$$

where m is the mass of a molecule. Therefore,

$$mN_1 = \frac{1}{4} \rho_1 \bar{c}$$

since $mn = \rho$, the density. Thus,

$$mN_1 = \frac{1}{4} \rho_1 \sqrt{\frac{8RT}{\pi}} = \rho_1 RT \sqrt{\frac{8RT}{16\pi R^2 T^2}} = \frac{p_1}{\sqrt{2\pi RT}}$$

as $p_1 = \rho_1 RT$, by the state equation. Similarly, the corresponding flow of mass leaving compartment 2 is

$$mN_2 = \frac{p_2}{\sqrt{2\pi RT}}$$

Hence, the resultant mass flow through area A in unit time is

$$Q_m = m(N_2 - N_1)A$$

$$Q_m = \frac{A(p_2 - p_1)}{\sqrt{2\pi RT}}$$

14.5 SUMMARY

The continuum approach to gas dynamics is valid as long as the smallest significant volume in the flow field contains sufficient number of molecules to establish meaningful averages of flow properties, like pressure and temperature. When the number of molecules per unit volume becomes insufficient for a meaningful averaging of flow properties, the field is termed rarefied gas dynamics. The Navier–Stokes equations of continuum gas dynamics fail when gradients of the macroscopic variables become so steep that their length scale is of the same order as the mean free path. For such flows the assumption of continuum is no longer valid, and the flow is referred to as rarefied gas flow.

The Knudsen number Kn is defined as

$$\text{Kn} = \frac{\lambda}{L}$$

where λ is the mean free path and L is characteristic dimension. The Knudsen number is related to Mach number and Reynolds number by the relation

$$\text{Kn} = 1.2533\sqrt{\gamma}\,\frac{M}{\text{Re}} \tag{14.4}$$

The classification of flow regimes based on Knudsen number is the following:

(i) $\text{Kn} < 0.01$ (continuum flow)
(ii) $0.01 < \text{Kn} < 0.1$ (slip flow)
(iii) $0.1 < \text{Kn} < 1.0$ (transition flow)
(iv) $\text{Kn} > 1.0$ (free molecule flow)

Scanned by CamScanner

The slip flow is a flow of slight rarefaction. In this regime, M, Re, and Kn serve to indicate the importance of compressibility, viscosity, and rarefaction effects, respectively. The boundary layers in slip regime will be very thick and laminar.

The transition flow regime lies between the slip and the free molecule flow regimes. In this regime extremely complex transfer processes occur and hence intermolecular collisions and collisions between gas molecules and a wall are of equal importance.

The free molecule flow regime is the regime of extreme rarefaction. The molecular mean free path λ is much longer than the characteristic length L. The intermolecular collisions can be completely neglected in free molecule flows.

The discussions presented in this chapter are meant to give an exposure to a rapidly growing branch of gas dynamics, associated with higher altitude (low-density) space missions. What is presented in this chapter is just an introduction to rarefied gas dynamics giving some vital glimpses about the field. For a deeper understanding of the subject the readers are encouraged to consult books specializing on this topic (like Patterson, 1956; Schaaf and Chambre, 1961; and Bird, 1976).

Scanned by CamScanner

15 High Temperature Gas Dynamics

15.1 INTRODUCTION

In Section 2.5, it was mentioned that a gas can be treated as perfect, with the specific heats independent of temperature, only when the temperature is below a specified limit. For example, air can be treated as both thermally and calorically perfect for temperatures below 800 K, and for temperatures from 800 K to 2000 K, it is only thermally perfect but calorically imperfect. For temperatures above 2000 K, the air is thermally as well as calorically imperfect. For such processes, none of the gas dynamic relations which are obtained with perfect gas assumptions are valid.

In many engineering problems of practical interest, the temperature of the flow is appreciably above the limiting value for which the gas can be treated as perfect. For example, the flow through rocket engines, arc-driven hypersonic wind tunnels, flow in shock tubes, high-energy gas dynamic and chemical lasers, and internal combustion engines are some of the engineering devices with operating temperatures well above the perfect gas limiting temperature. Therefore, there is a need for including some discussion on high-temperature effects in the study of Gas Dynamics. Our aim in this chapter is to study some of the fundamental aspects of the high-temperature effects on compressible flows.

15.2 THE IMPORTANCE OF HIGH-TEMPERATURE FLOWS

Consider the re-entry of spacecraft into earth's atmosphere. Let its velocity at 50 km altitude be 11 km/s (equal to escape velocity from the earth). Let the nose shape of the vehicle be as shown in Fig. 15.1. There is a very strong detached shock standing ahead of the nose. The portion of the shock near the nose can be treated as a normal shock. The vehicle Mach number at that altitude with

Scanned by CamScanner

temperature $T_\infty = 270$ K is 33.4. From Section 5.3 we know that when $M \to \infty$, the temperature behind the shock tends to infinity. These theoretical limits indicate that for the present shock with $M_1 = 33.4$, T_2 will be very high. That is, the massive amount of flow kinetic energy in the hypersonic freestream is converted to internal energy of the gas across the shock, thereby creating very high temperatures in the shock layer near the nose. Downstream of the nose region, where the shock layer gas has expanded and cooled around the body, there is a boundary layer with high Mach number at its outer edge; hence, the intense frictional dissipation within the hypersonic boundary layer creates high temperatures, and can cause the boundary layer to become chemically reacting. Another problem associated with re-entry body occurs when ionization is present in the shock layer, thereby resulting in production of a large number of free electrons throughout the shock layer. Because of the above complications associated with high-temperature gas streams, the results of gas dynamics based on perfect gas assumptions become invalid for the analysis of high-temperature gas dynamic problems. However, the analysis of such problems becomes essential since, in many flow processes of engineering importance, we come across high-temperature effects.

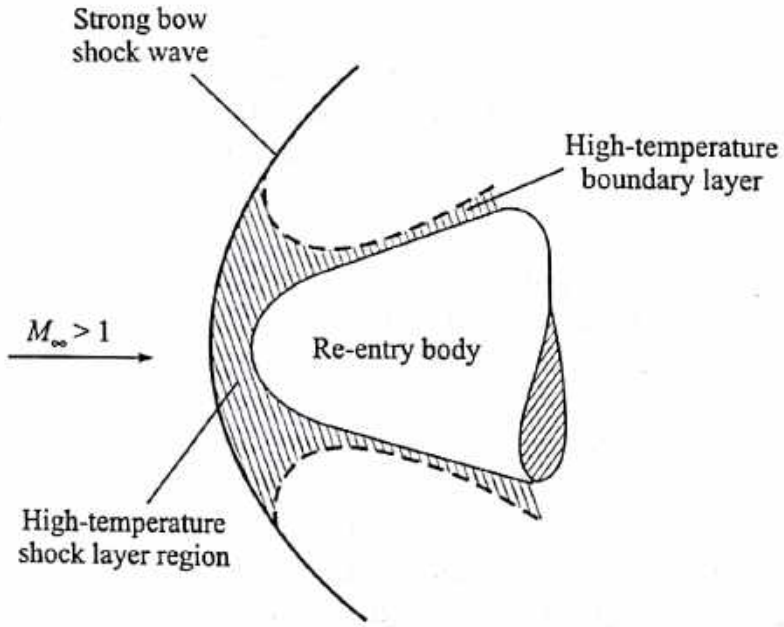


Fig. 15.1 Flow field around a body at re-entry.

15.3 THE NATURE OF HIGH-TEMPERATURE FLOWS

There are two major physical characteristics which cause a high-temperature gas to deviate from calorically perfect gas behaviour. These are:

1. At high-temperatures, the vibrational motion of the gas molecules becomes important, absorbing some of the energy which, at normal temperatures, would go into the translational and rotational motion. The

Scanned by CamScanner

excitation of vibrational energy causes the specific heats to become a function of temperature, causing the gas to become calorically imperfect.

2. With further increase in temperature, the molecules begin to dissociate and even ionize. Under these conditions, the gas becomes chemically reacting, and the specific heats become functions of both temperature and pressure.

Because of the above effects, the high temperature gas flows have the following differences compared to flow of gas with constant specific heats (perfect gas):

- The specific heats ratio, $\gamma = c_p/c_v$, is a variable.
- The thermodynamic properties are totally different.
- Usually some numerical procedure, rather than analytical approach, is required for high-temperature problems.

For these reasons, a study of high-temperature flow is different from that of Gas Dynamics with perfect gas assumption.

15.4 SUMMARY

This chapter has given some glimpses about the high temperature gas dynamics. After the advent of hypersonic vehicles the urge for learning more about high-temperature gas flows has gained momentum, since the temperature experienced in such streams is too high to treat the air as perfect. Besides hypersonic flow, high temperature gas dynamic plays a dominant role in combustion, high-energy lasers, plasmas, and so on. For detailed information about high temperature flow, the reader may consult books that deal specially with this topic, e.g. Anderson (1989) and Rathakrishnan (2015).

Scanned by CamScanner

Appendix A

TABLE A1 Isentropic Flow of Perfect Gas ($\gamma = 1.4$)

M	p/p_0	T/T_0	ρ/ρ_0	A/A^*	a/a_0	M^*	μ	ν
0.00	1.0000	1.0000	1.0000	∞	1.0000	0.0000		
0.01	0.9999	1.0000	1.0000	57.874	1.0000	0.0110		
0.02	0.9997	0.9999	0.9998	28.942	1.0000	0.0219		
0.03	0.9994	0.9998	0.9996	19.301	0.9999	0.0329		
0.04	0.9989	0.9997	0.9992	14.481	0.9998	0.0438		
0.05	0.9983	0.9995	0.9988	11.591	0.9998	0.0548		
0.06	0.9975	0.9993	0.9982	9.666	0.9996	0.0657		
0.07	0.9966	0.9990	0.9976	8.292	0.9995	0.0766		
0.08	0.9955	0.9987	0.9968	7.262	0.9994	0.0876		
0.09	0.9944	0.9984	0.9960	6.461	0.9992	0.0985		
0.10	0.9930	0.9980	0.9950	5.822	0.9990	0.1094		
0.11	0.9916	0.9976	0.9940	5.299	0.9988	0.1204		
0.12	0.9900	0.9971	0.9928	4.864	0.9986	0.1313		
0.13	0.9883	0.9966	0.9916	4.497	0.9983	0.1422		
0.14	0.9864	0.9961	0.9903	4.182	0.9980	0.1531		
0.15	0.9844	0.9955	0.9888	3.910	0.9978	0.1639		
0.16	0.9823	0.9949	0.9873	3.673	0.9974	0.1748		
0.17	0.9800	0.9943	0.9857	3.464	0.9971	0.1857		
0.18	0.9776	0.9936	0.9840	3.278	0.9968	0.1965		
0.19	0.9751	0.9928	0.9822	3.112	0.9964	0.2074		
0.20	0.9725	0.9921	0.9803	2.964	0.9960	0.2182		
0.21	0.9697	0.9913	0.9783	2.829	0.9956	0.2290		
0.22	0.9668	0.9904	0.9762	2.708	0.9952	0.2398		
0.23	0.9638	0.9895	0.9740	2.597	0.9948	0.2506		
0.24	0.9607	0.9886	0.9718	2.496	0.9943	0.2614		
0.25	0.9575	0.9877	0.9694	2.403	0.9938	0.2722		
0.26	0.9541	0.9867	0.9670	2.317	0.9933	0.2829		

(*Contd.*)

Scanned by CamScanner

TABLE A1 Isentropic Flow of Perfect Gas ($\gamma = 1.4$) (*contd.*)

M	p/p_0	T/T_0	ρ/ρ_0	A/A^*	a/a_0	M^*	$\bar{u}$	$\bar{v}$
0.27	0.9506	0.9856	0.9645	2.238	0.9928	0.2936		
0.28	0.9470	0.9846	0.9619	2.166	0.9923	0.3043		
0.29	0.9433	0.9835	0.9592	2.098	0.9917	0.3150		
0.30	0.9395	0.9823	0.9564	2.035	0.9911	0.3257		
0.31	0.9355	0.9811	0.9535	1.977	0.9905	0.3364		
0.32	0.9315	0.9799	0.9506	1.922	0.9899	0.3470		
0.33	0.9274	0.9787	0.9476	1.871	0.9893	0.3576		
0.34	0.9231	0.9774	0.9445	1.823	0.9886	0.3682		
0.35	0.9188	0.9761	0.9413	1.778	0.9880	0.3788		
0.36	0.9143	0.9747	0.9380	1.736	0.9873	0.3893		
0.37	0.9098	0.9733	0.9347	1.696	0.9866	0.3999		
0.38	0.9052	0.9719	0.9313	1.659	0.9859	0.4104		
0.39	0.9004	0.9705	0.9278	1.623	0.9851	0.4209		
0.40	0.8956	0.9690	0.9243	1.590	0.9844	0.4313		
0.41	0.8907	0.9675	0.9207	1.559	0.9836	0.4418		
0.42	0.8857	0.9659	0.9170	1.529	0.9828	0.4522		
0.43	0.8807	0.9643	0.9132	1.501	0.9820	0.4626		
0.44	0.8755	0.9627	0.9094	1.474	0.9812	0.4729		
0.45	0.8703	0.9611	0.9055	1.449	0.9803	0.4833		
0.46	0.8650	0.9594	0.9016	1.425	0.9795	0.4936		
0.47	0.8596	0.9577	0.8976	1.402	0.9786	0.5038		
0.48	0.8541	0.9559	0.8935	1.380	0.9777	0.5141		
0.49	0.8486	0.9542	0.8894	1.359	0.9768	0.5243		
0.50	0.8430	0.9524	0.8852	1.340	0.9759	0.5345		
0.51	0.8374	0.9506	0.8809	1.321	0.9750	0.5447		
0.52	0.8317	0.9487	0.8766	1.303	0.9740	0.5548		
0.53	0.8259	0.9468	0.8723	1.286	0.9730	0.5649		
0.54	0.8201	0.9449	0.8679	1.270	0.9721	0.5750		
0.55	0.8142	0.9430	0.8634	1.255	0.9711	0.5851		
0.56	0.8082	0.9410	0.8589	1.240	0.9700	0.5951		
0.57	0.8022	0.9390	0.8544	1.226	0.9690	0.6051		
0.58	0.7962	0.9370	0.8498	1.213	0.9680	0.6150		
0.59	0.7901	0.9349	0.8451	1.200	0.9669	0.6249		
0.60	0.7840	0.9328	0.8405	1.188	0.9658	0.6348		
0.61	0.7778	0.9307	0.8357	1.177	0.9647	0.6447		
0.62	0.7716	0.9286	0.8310	1.166	0.9636	0.6545		
0.63	0.7654	0.9265	0.8262	1.155	0.9625	0.6643		
0.64	0.7591	0.9243	0.8213	1.145	0.9614	0.6740		
0.65	0.7528	0.9221	0.8164	1.136	0.9603	0.6837		
0.66	0.7465	0.9199	0.8115	1.127	0.9591	0.6934		
0.67	0.7401	0.9176	0.8066	1.118	0.9579	0.7031		

(*Contd.*)

Scanned by CamScanner

TABLE A1 Isentropic Flow of Perfect Gas ($\gamma = 1.4$) (*contd.*)

M	p/p_0	T/T_0	ρ/ρ_0	A/A^*	a/a_0	M^*	μ	ν
0.68	0.7338	0.9153	0.8016	1.110	0.9567	0.7127		
0.69	0.7274	0.9131	0.7966	1.102	0.9555	0.7223		
0.70	0.7209	0.9107	0.7916	1.094	0.9543	0.7318		
0.71	0.7145	0.9084	0.7865	1.087	0.9531	0.7413		
0.72	0.7080	0.9061	0.7814	1.081	0.9519	0.7508		
0.73	0.7016	0.9037	0.7763	1.074	0.9506	0.7602		
0.74	0.6951	0.9013	0.7712	1.068	0.9494	0.7696		
0.75	0.6886	0.8989	0.7660	1.062	0.9481	0.7789		
0.76	0.6821	0.8964	0.7609	1.057	0.9468	0.7883		
0.77	0.6756	0.8940	0.7557	1.052	0.9455	0.7975		
0.78	0.6691	0.8915	0.7505	1.047	0.9442	0.8068		
0.79	0.6625	0.8890	0.7452	1.043	0.9429	0.8160		
0.80	0.6560	0.8865	0.7400	1.038	0.9416	0.8251		
0.81	0.6495	0.8840	0.7347	1.034	0.9402	0.8343		
0.82	0.6430	0.8815	0.7295	1.030	0.9389	0.8433		
0.83	0.6365	0.8789	0.7242	1.027	0.9375	0.8524		
0.84	0.6300	0.8763	0.7189	1.024	0.9361	0.8614		
0.85	0.6235	0.8737	0.7136	1.021	0.9347	0.8704		
0.86	0.6170	0.8711	0.7083	1.018	0.9333	0.8793		
0.87	0.6106	0.8685	0.7030	1.015	0.9319	0.8882		
0.88	0.6041	0.8659	0.6977	1.013	0.9305	0.8970		
0.89	0.5977	0.8632	0.6924	1.011	0.9291	0.9058		
0.90	0.5913	0.8606	0.6870	1.009	0.9277	0.9146		
0.91	0.5849	0.8579	0.6817	1.007	0.9262	0.9233		
0.92	0.5785	0.8552	0.6764	1.006	0.9248	0.9320		
0.93	0.5721	0.8525	0.6711	1.004	0.9233	0.9407		
0.94	0.5658	0.8498	0.6658	1.003	0.9219	0.9493		
0.95	0.5595	0.8471	0.6604	1.002	0.9204	0.9578		
0.96	0.5532	0.8444	0.6551	1.001	0.9189	0.9663		
0.97	0.5469	0.8416	0.6498	1.001	0.9174	0.9748		
0.98	0.5407	0.8389	0.6445	1.000	0.9159	0.9833		
0.99	0.5345	0.8361	0.6392	1.000	0.9144	0.9916		
1.00	0.5283	0.8333	0.6339	1.000	0.9129	1.0000	90.000	0.000
1.01	0.5221	0.8306	0.6287	1.000	0.9113	1.0083	81.931	0.045
1.02	0.5160	0.8278	0.6234	1.000	0.9098	1.0166	78.635	0.126
1.03	0.5099	0.8250	0.6181	1.001	0.9083	1.0248	76.138	0.229
1.04	0.5039	0.8222	0.6129	1.001	0.9067	1.0330	74.058	0.351
1.05	0.4979	0.8193	0.6077	1.002	0.9052	1.0411	72.247	0.487
1.06	0.4919	0.8165	0.6024	1.003	0.9036	1.0492	70.630	0.637
1.07	0.4860	0.8137	0.5972	1.004	0.9020	1.0573	69.160	0.797
1.08	0.4800	0.8108	0.5920	1.005	0.9005	1.0653	67.808	0.968

(*Contd.*)

Scanned by CamScanner

TABLE A1 Isentropic Flow of Perfect Gas ($\gamma = 1.4$) (*contd.*)

M	p/p_0	T/T_0	ρ/ρ_0	A/A^*	a/a_0	M^*	μ	ν
1.09	0.4742	0.8080	0.5869	1.006	0.8989	1.0733	66.553	1.148
1.10	0.4684	0.8052	0.5817	1.008	0.8973	1.0812	65.380	1.336
1.11	0.4626	0.8023	0.5766	1.010	0.8957	1.0891	64.277	1.532
1.12	0.4568	0.7994	0.5714	1.011	0.8941	1.0970	63.234	1.735
1.13	0.4511	0.7966	0.5663	1.013	0.8925	1.1048	62.246	1.944
1.14	0.4455	0.7937	0.5612	1.015	0.8909	1.1126	61.306	2.160
1.15	0.4398	0.7908	0.5562	1.017	0.8893	1.1203	60.408	2.381
1.16	0.4343	0.7879	0.5511	1.020	0.8877	1.1280	59.550	2.607
1.17	0.4287	0.7851	0.5461	1.022	0.8860	1.1356	58.727	2.839
1.18	0.4232	0.7822	0.5411	1.025	0.8844	1.1432	57.936	3.074
1.19	0.4178	0.7793	0.5361	1.028	0.8828	1.1508	57.176	3.314
1.20	0.4124	0.7764	0.5311	1.030	0.8811	1.1583	56.443	3.558
1.21	0.4070	0.7735	0.5262	1.033	0.8795	1.1658	55.735	3.806
1.22	0.4017	0.7706	0.5213	1.037	0.8778	1.1732	55.052	4.057
1.23	0.3964	0.7677	0.5164	1.040	0.8762	1.1806	54.391	4.312
1.24	0.3912	0.7648	0.5115	1.043	0.8745	1.1879	53.751	4.569
1.25	0.3861	0.7619	0.5067	1.047	0.8729	1.1952	53.130	4.830
1.26	0.3809	0.7590	0.5019	1.050	0.8712	1.2025	52.528	5.093
1.27	0.3759	0.7561	0.4971	1.054	0.8695	1.2097	51.943	5.359
1.28	0.3708	0.7532	0.4923	1.058	0.8679	1.2169	51.375	5.627
1.29	0.3658	0.7503	0.4876	1.062	0.8662	1.2240	50.823	5.898
1.30	0.3609	0.7474	0.4829	1.066	0.8645	1.2311	50.285	6.170
1.31	0.3560	0.7445	0.4782	1.071	0.8628	1.2382	49.761	6.445
1.32	0.3512	0.7416	0.4736	1.075	0.8611	1.2452	49.251	6.721
1.33	0.3464	0.7387	0.4690	1.080	0.8595	1.2522	48.753	7.000
1.34	0.3417	0.7358	0.4644	1.084	0.8578	1.2591	48.268	7.279
1.35	0.3370	0.7329	0.4598	1.089	0.8561	1.2660	47.795	7.561
1.36	0.3323	0.7300	0.4553	1.094	0.8544	1.2729	47.332	7.844
1.37	0.3277	0.7271	0.4508	1.099	0.8527	1.2797	46.880	8.128
1.38	0.3232	0.7242	0.4463	1.104	0.8510	1.2864	46.439	8.413
1.39	0.3187	0.7213	0.4418	1.109	0.8493	1.2932	46.007	8.699
1.40	0.3142	0.7184	0.4374	1.115	0.8476	1.2999	45.585	8.987
1.41	0.3098	0.7155	0.4330	1.120	0.8459	1.3065	45.171	9.276
1.42	0.3055	0.7126	0.4287	1.126	0.8442	1.3131	44.767	9.565
1.43	0.3012	0.7097	0.4244	1.132	0.8425	1.3197	44.371	9.855
1.44	0.2969	0.7069	0.4201	1.138	0.8407	1.3262	43.983	10.146
1.45	0.2927	0.7040	0.4158	1.144	0.8390	1.3327	43.603	10.438
1.46	0.2886	0.7011	0.4116	1.150	0.8373	1.3392	43.230	10.731
1.47	0.2845	0.6982	0.4074	1.156	0.8356	1.3456	42.865	11.023
1.48	0.2804	0.6954	0.4032	1.163	0.8339	1.3520	42.507	11.317
1.49	0.2764	0.6925	0.3991	1.169	0.8322	1.3583	42.155	11.611
1.50	0.2724	0.6897	0.3950	1.176	0.8305	1.3646	41.810	11.905

(*Contd.*)

Scanned by CamScanner

TABLE A1 Isentropic Flow of Perfect Gas ($\gamma = 1.4$) *(contd.)*

M	p/p_0	T/T_0	ρ/ρ_0	A/A^*	a/a_0	M^*	μ	ν
1.51	0.2685	0.6868	0.3909	1.183	0.8287	1.3708	41.472	12.200
1.52	0.2646	0.6840	0.3869	1.190	0.8270	1.3770	41.140	12.495
1.53	0.2608	0.6811	0.3829	1.197	0.8253	1.3832	40.813	12.790
1.54	0.2570	0.6783	0.3789	1.204	0.8236	1.3894	40.493	13.086
1.55	0.2533	0.6754	0.3750	1.212	0.8219	1.3955	40.178	13.381
1.56	0.2496	0.6726	0.3710	1.219	0.8201	1.4015	39.868	13.677
1.57	0.2459	0.6698	0.3672	1.227	0.8184	1.4075	39.564	13.973
1.58	0.2423	0.6670	0.3633	1.234	0.8167	1.4135	39.265	14.269
1.59	0.2388	0.6642	0.3595	1.242	0.8150	1.4195	38.971	14.565
1.60	0.2353	0.6614	0.3557	1.250	0.8133	1.4254	38.682	14.860
1.61	0.2318	0.6586	0.3520	1.258	0.8115	1.4313	38.398	15.156
1.62	0.2284	0.6558	0.3483	1.267	0.8098	1.4371	38.118	15.452
1.63	0.2250	0.6530	0.3446	1.275	0.8081	1.4429	37.843	15.747
1.64	0.2217	0.6502	0.3409	1.284	0.8064	1.4487	37.572	16.043
1.65	0.2184	0.6475	0.3373	1.292	0.8046	1.4544	37.305	16.338
1.66	0.2151	0.6447	0.3337	1.301	0.8029	1.4601	37.043	16.633
1.67	0.2119	0.6419	0.3302	1.310	0.8012	1.4657	36.784	16.928
1.68	0.2088	0.6392	0.3266	1.319	0.7995	1.4713	36.530	17.222
1.69	0.2057	0.6364	0.3232	1.328	0.7978	1.4769	36.279	17.516
1.70	0.2026	0.6337	0.3197	1.338	0.7961	1.4825	36.032	17.810
1.71	0.1996	0.6310	0.3163	1.347	0.7943	1.4880	35.789	18.103
1.72	0.1966	0.6283	0.3129	1.357	0.7926	1.4935	35.549	18.396
1.73	0.1936	0.6256	0.3095	1.367	0.7909	1.4989	35.312	18.689
1.74	0.1907	0.6229	0.3062	1.376	0.7892	1.5043	35.080	18.981
1.75	0.1878	0.6202	0.3029	1.386	0.7875	1.5097	34.850	19.273
1.76	0.1850	0.6175	0.2996	1.397	0.7858	1.5150	34.624	19.565
1.77	0.1822	0.6148	0.2964	1.407	0.7841	1.5203	34.400	19.855
1.78	0.1794	0.6121	0.2931	1.418	0.7824	1.5256	34.180	20.146
1.79	0.1767	0.6095	0.2900	1.428	0.7807	1.5308	33.963	20.436
1.80	0.1740	0.6068	0.2868	1.439	0.7790	1.5360	33.749	20.725
1.81	0.1714	0.6041	0.2837	1.450	0.7773	1.5411	33.538	21.014
1.82	0.1688	0.6015	0.2806	1.461	0.7756	1.5463	33.329	21.302
1.83	0.1662	0.5989	0.2776	1.472	0.7739	1.5514	33.124	21.590
1.84	0.1637	0.5963	0.2745	1.484	0.7722	1.5564	32.921	21.877
1.85	0.1612	0.5936	0.2715	1.495	0.7705	1.5614	32.720	22.163
1.86	0.1587	0.5910	0.2686	1.507	0.7688	1.5664	32.523	22.449
1.87	0.1563	0.5884	0.2656	1.519	0.7671	1.5714	32.328	22.734
1.88	0.1539	0.5859	0.2627	1.531	0.7654	1.5763	32.135	23.019
1.89	0.1516	0.5833	0.2598	1.543	0.7637	1.5812	31.945	23.303
1.90	0.1492	0.5807	0.2570	1.555	0.7620	1.5861	31.757	23.586
1.91	0.1470	0.5782	0.2542	1.568	0.7604	1.5909	31.571	23.869
1.92	0.1447	0.5756	0.2514	1.580	0.7587	1.5957	31.388	24.151

(Contd.)

Scanned by CamScanner

TABLE A1 Isentropic Flow of Perfect Gas ($\gamma = 1.4$) (*contd.*)

M	p/p_0	T/T_0	ρ/ρ_0	A/A^*	a/a_0	M^*	μ	ν
1.93	0.1425	0.5731	0.2486	1.593	0.7570	1.6005	31.207	24.432
1.94	0.1403	0.5705	0.2459	1.606	0.7553	1.6052	31.028	24.712
1.95	0.1381	0.5680	0.2432	1.619	0.7537	1.6099	30.852	24.992
1.96	0.1360	0.5655	0.2405	1.633	0.7520	1.6146	30.677	25.271
1.97	0.1339	0.5630	0.2378	1.646	0.7503	1.6192	30.505	25.549
1.98	0.1318	0.5605	0.2352	1.660	0.7487	1.6239	30.335	25.827
1.99	0.1298	0.5580	0.2326	1.674	0.7470	1.6284	30.166	26.104
2.00	0.1278	0.5556	0.2300	1.688	0.7454	1.6330	30.000	26.380
2.01	0.1258	0.5531	0.2275	1.702	0.7437	1.6375	29.836	26.655
2.02	0.1239	0.5506	0.2250	1.716	0.7420	1.6420	29.673	26.930
2.03	0.1220	0.5482	0.2225	1.730	0.7404	1.6465	29.512	27.203
2.04	0.1201	0.5458	0.2200	1.745	0.7388	1.6509	29.353	27.476
2.05	0.1182	0.5433	0.2176	1.760	0.7371	1.6553	29.196	27.748
2.06	0.1164	0.5409	0.2152	1.775	0.7355	1.6597	29.041	28.020
2.07	0.1146	0.5385	0.2128	1.790	0.7338	1.6640	28.888	28.290
2.08	0.1128	0.5361	0.2104	1.806	0.7322	1.6683	28.736	28.560
2.09	0.1111	0.5337	0.2081	1.821	0.7306	1.6726	28.585	28.829
2.10	0.1094	0.5313	0.2058	1.837	0.7289	1.6769	28.437	29.097
2.11	0.1077	0.5290	0.2035	1.853	0.7273	1.6811	28.290	29.364
2.12	0.1060	0.5266	0.2013	1.869	0.7257	1.6853	28.145	29.631
2.13	0.1043	0.5243	0.1990	1.885	0.7241	1.6895	28.001	29.896
2.14	0.1027	0.5219	0.1968	1.902	0.7225	1.6936	27.859	30.161
2.15	0.1011	0.5196	0.1946	1.919	0.7208	1.6977	27.718	30.425
2.16	0.0996	0.5173	0.1925	1.935	0.7192	1.7018	27.578	30.688
2.17	0.0980	0.5150	0.1903	1.953	0.7176	1.7059	27.441	30.951
2.18	0.0965	0.5127	0.1882	1.970	0.7160	1.7099	27.304	31.212
2.19	0.0950	0.5104	0.1861	1.987	0.7144	1.7139	27.169	31.473
2.20	0.0935	0.5081	0.1841	2.005	0.7128	1.7179	27.036	31.732
2.21	0.0921	0.5059	0.1820	2.023	0.7112	1.7219	26.903	31.991
2.22	0.0906	0.5036	0.1800	2.041	0.7097	1.7258	26.773	32.249
2.23	0.0892	0.5014	0.1780	2.059	0.7081	1.7297	26.643	32.507
2.24	0.0878	0.4991	0.1760	2.078	0.7065	1.7336	26.515	32.763
2.25	0.0865	0.4969	0.1740	2.096	0.7049	1.7374	26.388	33.018
2.26	0.0851	0.4947	0.1721	2.115	0.7033	1.7412	26.262	33.273
2.27	0.0838	0.4925	0.1702	2.134	0.7018	1.7450	26.138	33.527
2.28	0.0825	0.4903	0.1683	2.154	0.7002	1.7488	26.014	33.780
2.29	0.0812	0.4881	0.1664	2.173	0.6986	1.7526	25.892	34.032
2.30	0.0800	0.4859	0.1646	2.193	0.6971	1.7563	25.771	34.283
2.31	0.0787	0.4837	0.1628	2.213	0.6955	1.7600	25.652	34.533
2.32	0.0775	0.4816	0.1609	2.233	0.6940	1.7637	25.533	34.782
2.33	0.0763	0.4794	0.1592	2.254	0.6924	1.7673	25.416	35.031
2.34	0.0751	0.4773	0.1574	2.274	0.6909	1.7709	25.300	35.279

(*Contd.*)

Scanned by CamScanner

TABLE A1 Isentropic Flow of Perfect Gas ($\gamma = 1.4$) (*contd.*)

M	p/p_0	T/T_0	ρ/ρ_0	A/A^*	a/a_0	M^*	μ	ν
2.35	0.0740	0.4752	0.1556	2.295	0.6893	1.7745	25.184	35.526
2.36	0.0728	0.4731	0.1539	2.316	0.6878	1.7781	25.070	35.771
2.37	0.0717	0.4709	0.1522	2.338	0.6863	1.7817	24.957	36.017
2.38	0.0706	0.4688	0.1505	2.359	0.6847	1.7852	24.845	36.261
2.39	0.0695	0.4668	0.1488	2.381	0.6832	1.7887	24.734	36.504
2.40	0.0684	0.4647	0.1472	2.403	0.6817	1.7922	24.624	36.747
2.41	0.0673	0.4626	0.1456	2.425	0.6802	1.7956	24.515	36.988
2.42	0.0663	0.4606	0.1439	2.448	0.6786	1.7991	24.407	37.229
2.43	0.0653	0.4585	0.1424	2.471	0.6771	1.8025	24.301	37.469
2.44	0.0643	0.4565	0.1408	2.494	0.6756	1.8059	24.195	37.708
2.45	0.0633	0.4544	0.1392	2.517	0.6741	1.8092	24.090	37.946
2.46	0.0623	0.4524	0.1377	2.540	0.6726	1.8126	23.985	38.183
2.47	0.0613	0.4504	0.1362	2.564	0.6711	1.8159	23.882	38.420
2.48	0.0604	0.4484	0.1346	2.588	0.6696	1.8192	23.780	38.655
2.49	0.0594	0.4464	0.1332	2.612	0.6682	1.8225	23.679	38.890
2.50	0.0585	0.4444	0.1317	2.637	0.6667	1.8257	23.578	39.124
2.51	0.0576	0.4425	0.1302	2.661	0.6652	1.8290	23.479	39.357
2.52	0.0567	0.4405	0.1288	2.686	0.6637	1.8322	23.380	39.589
2.53	0.0559	0.4386	0.1274	2.712	0.6622	1.8354	23.282	39.820
2.54	0.0550	0.4366	0.1260	2.737	0.6608	1.8386	23.185	40.050
2.55	0.0542	0.4347	0.1246	2.763	0.6593	1.8417	23.089	40.280
2.56	0.0533	0.4328	0.1232	2.789	0.6578	1.8448	22.993	40.508
2.57	0.0525	0.4309	0.1218	2.815	0.6564	1.8479	22.899	40.736
2.58	0.0517	0.4289	0.1205	2.842	0.6549	1.8510	22.805	40.963
2.59	0.0509	0.4271	0.1192	2.869	0.6535	1.8541	22.712	41.189
2.60	0.0501	0.4252	0.1179	2.896	0.6521	1.8571	22.620	41.415
2.61	0.0493	0.4233	0.1166	2.923	0.6506	1.8602	22.528	41.639
2.62	0.0486	0.4214	0.1153	2.951	0.6492	1.8632	22.438	41.863
2.63	0.0478	0.4196	0.1140	2.979	0.6477	1.8662	22.348	42.086
2.64	0.0471	0.4177	0.1128	3.007	0.6463	1.8691	22.259	42.307
2.65	0.0464	0.4159	0.1115	3.036	0.6449	1.8721	22.170	42.529
2.66	0.0457	0.4141	0.1103	3.065	0.6435	1.8750	22.082	42.749
2.67	0.0450	0.4122	0.1091	3.094	0.6421	1.8779	21.995	42.968
2.68	0.0443	0.4104	0.1079	3.123	0.6406	1.8808	21.909	43.187
2.69	0.0436	0.4086	0.1067	3.153	0.6392	1.8837	21.823	43.405
2.70	0.0430	0.4068	0.1056	3.183	0.6378	1.8865	21.738	43.621
2.71	0.0423	0.4051	0.1044	3.213	0.6364	1.8894	21.654	43.838
2.72	0.0417	0.4033	0.1033	3.244	0.6350	1.8922	21.571	44.053
2.73	0.0410	0.4015	0.1022	3.275	0.6337	1.8950	21.488	44.267
2.74	0.0404	0.3998	0.1010	3.306	0.6323	1.8978	21.405	44.481
2.75	0.0398	0.3980	0.0999	3.338	0.6309	1.9005	21.324	44.694
2.76	0.0392	0.3963	0.0989	3.370	0.6295	1.9033	21.243	44.906

(*Contd.*)

Scanned by CamScanner

TABLE A1 Isentropic Flow of Perfect Gas ($\gamma = 1.4$) (*contd.*)

M	p/p_0	T/T_0	ρ/ρ_0	A/A^*	a/a_0	M^*	μ	ν
2.77	0.0386	0.3945	0.0978	3.402	0.6281	1.9060	21.162	45.117
2.78	0.0380	0.3928	0.0967	3.434	0.6267	1.9087	21.083	45.327
2.79	0.0374	0.3911	0.0957	3.467	0.6254	1.9114	21.003	45.537
2.80	0.0368	0.3894	0.0946	3.500	0.6240	1.9140	20.925	45.746
2.81	0.0363	0.3877	0.0936	3.534	0.6227	1.9167	20.847	45.954
2.82	0.0357	0.3860	0.0926	3.567	0.6213	1.9193	20.770	46.161
2.83	0.0352	0.3844	0.0916	3.601	0.6200	1.9219	20.693	46.368
2.84	0.0347	0.3827	0.0906	3.636	0.6186	1.9246	20.617	46.573
2.85	0.0341	0.3810	0.0896	3.671	0.6173	1.9271	20.541	46.778
2.86	0.0336	0.3794	0.0886	3.706	0.6159	1.9297	20.466	46.982
2.87	0.0331	0.3777	0.0877	3.741	0.6146	1.9323	20.391	47.185
2.88	0.0326	0.3761	0.0867	3.777	0.6133	1.9348	20.318	47.388
2.89	0.0321	0.3745	0.0858	3.813	0.6119	1.9373	20.244	47.589
2.90	0.0317	0.3729	0.0849	3.850	0.6106	1.9398	20.171	47.790
2.91	0.0312	0.3712	0.0840	3.887	0.6093	1.9423	20.099	47.990
2.92	0.0307	0.3696	0.0831	3.924	0.6080	1.9448	20.027	48.190
2.93	0.0302	0.3681	0.0822	3.961	0.6067	1.9472	19.956	48.388
2.94	0.0298	0.3665	0.0813	3.999	0.6054	1.9497	19.885	48.586
2.95	0.0293	0.3649	0.0804	4.038	0.6041	1.9521	19.815	48.783
2.96	0.0289	0.3633	0.0796	4.076	0.6028	1.9545	19.745	48.980
2.97	0.0285	0.3618	0.0787	4.115	0.6015	1.9569	19.676	49.175
2.98	0.0281	0.3602	0.0779	4.155	0.6002	1.9593	19.607	49.370
2.99	0.0276	0.3587	0.0770	4.194	0.5989	1.9616	19.539	49.564
3.00	0.0272	0.3571	0.0762	4.235	0.5976	1.9640	19.471	49.757
3.01	0.0268	0.3556	0.0754	4.275	0.5963	1.9663	19.404	49.950
3.02	0.0264	0.3541	0.0746	4.316	0.5951	1.9686	19.337	50.142
3.03	0.0260	0.3526	0.0738	4.357	0.5938	1.9709	19.271	50.333
3.04	0.0256	0.3511	0.0730	4.399	0.5925	1.9732	19.205	50.523
3.05	0.0253	0.3496	0.0723	4.441	0.5913	1.9755	19.139	50.713
3.06	0.0249	0.3481	0.0715	4.483	0.5900	1.9777	19.075	50.902
3.07	0.0245	0.3466	0.0707	4.526	0.5887	1.9800	19.010	51.090
3.08	0.0242	0.3452	0.0700	4.570	0.5875	1.9822	18.946	51.277
3.09	0.0238	0.3437	0.0692	4.613	0.5862	1.9844	18.882	51.464
3.10	0.0234	0.3422	0.0685	4.657	0.5850	1.9866	18.819	51.650
3.11	0.0231	0.3408	0.0678	4.702	0.5838	1.9888	18.756	51.835
3.12	0.0228	0.3393	0.0671	4.747	0.5825	1.9910	18.694	52.020
3.13	0.0224	0.3379	0.0664	4.792	0.5813	1.9931	18.632	52.203
3.14	0.0221	0.3365	0.0657	4.838	0.5801	1.9953	18.571	52.386
3.15	0.0218	0.3351	0.0650	4.884	0.5788	1.9974	18.509	52.569
3.16	0.0215	0.3337	0.0643	4.930	0.5776	1.9995	18.449	52.751
3.17	0.0211	0.3323	0.0636	4.977	0.5764	2.0016	18.388	52.932
3.18	0.0208	0.3309	0.0630	5.025	0.5752	2.0037	18.329	53.112

(*Contd.*)

Scanned by CamScanner

TABLE A1 Isentropic Flow of Perfect Gas ($\gamma = 1.4$) (*contd.*)

M	p/p_0	T/T_0	ρ/ρ_0	A/A^*	a/a_0	M^*	μ	ν
3.19	0.0205	0.3295	0.0623	5.073	0.5740	2.0058	18.269	53.291
3.20	0.0202	0.3281	0.0617	5.121	0.5728	2.0079	18.210	53.470
3.21	0.0199	0.3267	0.0610	5.170	0.5716	2.0099	18.151	53.649
3.22	0.0196	0.3253	0.0604	5.219	0.5704	2.0119	18.093	53.826
3.23	0.0194	0.3240	0.0597	5.268	0.5692	2.0140	18.035	54.003
3.24	0.0191	0.3226	0.0591	5.319	0.5680	2.0160	17.977	54.179
3.25	0.0188	0.3213	0.0585	5.369	0.5668	2.0180	17.920	54.355
3.26	0.0185	0.3199	0.0579	5.420	0.5656	2.0200	17.863	54.529
3.27	0.0183	0.3186	0.0573	5.472	0.5645	2.0220	17.807	54.704
3.28	0.0180	0.3173	0.0567	5.523	0.5633	2.0239	17.751	54.877
3.29	0.0177	0.3160	0.0561	5.576	0.5621	2.0259	17.695	55.050
3.30	0.0175	0.3147	0.0555	5.629	0.5609	2.0278	17.640	55.222
3.31	0.0172	0.3134	0.0550	5.682	0.5598	2.0297	17.585	55.393
3.32	0.0170	0.3121	0.0544	5.736	0.5586	2.0317	17.530	55.564
3.33	0.0167	0.3108	0.0538	5.790	0.5575	2.0336	17.476	55.734
3.34	0.0165	0.3095	0.0533	5.845	0.5563	2.0355	17.422	55.904
3.35	0.0163	0.3082	0.0527	5.900	0.5552	2.0373	17.368	56.073
3.36	0.0160	0.3069	0.0522	5.956	0.5540	2.0392	17.315	56.241
3.37	0.0158	0.3057	0.0517	6.012	0.5529	2.0411	17.262	56.409
3.38	0.0156	0.3044	0.0511	6.069	0.5517	2.0429	17.209	56.576
3.39	0.0153	0.3032	0.0506	6.126	0.5506	2.0447	17.157	56.742
3.40	0.0151	0.3019	0.0501	6.184	0.5495	2.0466	17.105	56.908
3.41	0.0149	0.3007	0.0496	6.242	0.5484	2.0484	17.053	57.073
3.42	0.0147	0.2995	0.0491	6.301	0.5472	2.0502	17.002	57.237
3.43	0.0145	0.2982	0.0486	6.360	0.5461	2.0520	16.950	57.401
3.44	0.0143	0.2970	0.0481	6.420	0.5450	2.0537	16.900	57.564
3.45	0.0141	0.2958	0.0476	6.480	0.5439	2.0555	16.849	57.726
3.46	0.0139	0.2946	0.0471	6.541	0.5428	2.0573	16.799	57.888
3.47	0.0137	0.2934	0.0466	6.602	0.5417	2.0590	16.749	58.050
3.48	0.0135	0.2922	0.0462	6.664	0.5406	2.0607	16.700	58.210
3.49	0.0133	0.2910	0.0457	6.727	0.5395	2.0625	16.651	58.370
3.50	0.0131	0.2899	0.0452	6.790	0.5384	2.0642	16.602	58.530
3.51	0.0129	0.2887	0.0448	6.853	0.5373	2.0659	16.553	58.689
3.52	0.0127	0.2875	0.0443	6.917	0.5362	2.0676	16.505	58.847
3.53	0.0126	0.2864	0.0439	6.982	0.5351	2.0693	16.456	59.005
3.54	0.0124	0.2852	0.0434	7.047	0.5340	2.0709	16.409	59.162
3.55	0.0122	0.2841	0.0430	7.113	0.5330	2.0726	16.361	59.318
3.56	0.0120	0.2829	0.0426	7.179	0.5319	2.0743	16.314	59.474
3.57	0.0119	0.2818	0.0421	7.246	0.5308	2.0759	16.267	59.629
3.58	0.0117	0.2806	0.0417	7.313	0.5298	2.0775	16.220	59.784
3.59	0.0115	0.2795	0.0413	7.381	0.5287	2.0792	16.174	59.938
3.60	0.0114	0.2784	0.0409	7.450	0.5276	2.0808	16.128	60.091

(*Contd.*)

Scanned by CamScanner

TABLE A1 Isentropic Flow of Perfect Gas ($\gamma = 1.4$) (*contd.*)

M	p/p_0	T/T_0	ρ/ρ_0	A/A^*	a/a_0	M^*	μ	ν
3.61	0.0112	0.2773	0.0405	7.519	0.5266	2.0824	16.082	60.244
3.62	0.0111	0.2762	0.0401	7.589	0.5255	2.0840	16.036	60.397
3.63	0.0109	0.2751	0.0397	7.659	0.5245	2.0856	15.991	60.549
3.64	0.0108	0.2740	0.0393	7.730	0.5234	2.0871	15.946	60.700
3.65	0.0106	0.2729	0.0389	7.802	0.5224	2.0887	15.901	60.850
3.66	0.0105	0.2718	0.0385	7.874	0.5213	2.0903	15.856	61.001
3.67	0.0103	0.2707	0.0381	7.947	0.5203	2.0918	15.812	61.150
3.68	0.0102	0.2697	0.0378	8.020	0.5193	2.0933	15.768	61.299
3.69	0.0100	0.2686	0.0374	8.094	0.5183	2.0949	15.724	61.447
3.70	0.0099	0.2675	0.0370	8.169	0.5172	2.0964	15.680	61.595
3.71	0.0098	0.2665	0.0367	8.244	0.5162	2.0979	15.637	61.743
3.72	0.0096	t).2654	0.0363	8.320	0.5152	2.0994	15.594	61.889
3.73	0.0095	0.2644	0.0359	8.397	0.5142	2.1009	15.551	62.036
3.74	0.0094	0.2633	0.0356	8.474	0.5132	2.1024	15.508	62.181
3.75	0.0092	0.2623	0.0352	8.552	0.5121	2.1039	15.466	62.326
3.76	0.0091	0.2613	0.0349	8.630	0.5111	2.1053	15.424	62.471
3.77	0.0090	0.2602	0.0345	8.709	0.5101	2.1068	15.382	62.615
3.78	0.0089	0.2592	0.0342	8.789	0.5091	2.1082	15.340	62.758
3.79	0.0087	0.2582	0.0339	8.869	0.5081	2.1097	15.299	62.901
3.80	0.0086	0.2572	0.0335	8.951	0.5072	2.1111	15.258	63.044
3.81	0.0085	0.2562	0.0332	9.032	0.5062	2.1125	15.217	63.186
3.82	0.0084	0.2552	0.0329	9.115	0.5052	2.1140	15.176	63.327
3.83	0.0083	0.2542	0.0326	9.198	0.5042	2.1154	15.135	63.468
3.84	0.0082	0.2532	0.0323	9.282	0.5032	2.1168	15.095	63.608
3.85	0.0081	0.2522	0.0320	9.366	0.5022	2.1182	15.055	63.748
3.86	0.0080	0.2513	0.0316	9.451	0.5013	2.1195	15.015	63.887
3.87	0.0078	0.2503	0.0313	9.537	0.5003	2.1209	14.975	64.026
3.88	0.0077	0.2493	0.0310	9.624	0.4993	2.1223	14.936	64.164
3.89	0.0076	0.2484	0.0307	9.711	0.4984	2.1236	14.896	64.302
3.90	0.0075	0.2474	0.0304	9.799	0.4974	2.1250	14.857	64.440
3.91	0.0074	0.2464	0.0302	9.888	0.4964	2.1263	14.818	64.576
3.92	0.0073	0.2455	0.0299	9.977	0.4955	2.1277	14.780	64.713
3.93	0.0072	0.2446	0.0296	10.067	0.4945	2.1290	14.741	64.848
3.94	0.0071	0.2436	0.0293	10.158	0.4936	2.1303	14.703	64.984
3.95	0.0070	0.2427	0.0290	10.250	0.4926	2.1316	14.665	65.118
3.96	0.0069	0.2418	0.0287	10.342	0.4917	2.1329	14.627	65.253
3.97	0.0069	0.2408	0.0285	10.435	0.4908	2.1342	14.589	65.386
3.98	0.0068	0.2399	0.0282	10.529	0.4898	2.1355	14.552	65.520
3.99	0.0067	0.2390	0.0279	10.623	0.4889	2.1368	14.515	65.652
4.00	0.0066	0.2381	0.0277	10.719	0.4880	2.1381	14.478	65.785
4.01	0.0065	0.2372	0.0274	10.815	0.4870	2.1394	14.441	65.917
4.02	0.0064	0.2363	0.0271	10.912	0.4861	2.1406	14.404	66.048

(*Contd.*)

Scanned by CamScanner

TABLE A1 Isentropic Flow of Perfect Gas ($\gamma = 1.4$) (*contd.*)

M	p/p_0	T/T_0	ρ/ρ_0	A/A^*	a/a_0	M^*	μ	ν
4.03	0.0063	0.2354	0.0269	11.009	0.4852	2.1419	14.367	66.179
4.04	0.0062	0.2345	0.0266	11.108	0.4843	2.1431	14.331	66.309
4.05	0.0062	0.2336	0.0264	11.207	0.4833	2.1444	14.295	66.439
4.06	0.0061	0.2327	0.0261	11.307	0.4824	2.1456	14.259	66.569
4.07	0.0060	0.2319	0.0259	11.408	0.4815	2.1468	14.223	66.698
4.08	0.0059	0.2310	0.0256	11.509	0.4806	2.1480	14.188	66.826
4.09	0.0058	0.2301	0.0254	11.611	0.4797	2.1493	14.152	66.954
4.10	0.9058	0.2293	0.0252	11.715	0.4788	2.1505	14.117	67.082
4.11	0.0057	0.2284	0.0249	11.819	0.4779	2.1517	14.082	67.209
4.12	0.0056	0.2275	0.0247	11.923	0.4770	2.1529	14.047	67.336
4.13	0.0055	0.2267	0.0245	12.029	0.4761	2.1540	14.012	67.462
4.14	0.0055	0.2258	0.0242	12.135	0.4752	2.1552	13.978	67.588
4.15	0.0054	0.2250	0.0240	12.243	0.4743	2.1564	13.943	67.713
4.16	0.0053	0.2242	0.0238	12.351	0.4735	2.1576	13.909	67.838
4.17	0.0053	0.2233	0.0236	12.460	0.4726	2.1587	13.875	67.963
4.18	0.0052	0.2225	0.0234	12.570	0.4717	2.1599	13.841	68.087
4.19	0.0051	0.2217	0.0231	12.680	0.4708	2.1610	13.808	68.210
4.20	0.0051	0.2208	0.0229	12.792	0.4699	2.1622	13.774	68.333
4.21	0.0050	0.2200	0.0227	12.904	0.4691	2.1633	13.741	68.456
4.22	0.0049	0.2192	0.0225	13.017	0.4682	2.1644	13.708	68.578
4.23	0.0049	0.2184	0.0223	13.131	0.4673	2.1655	13.675	68.700
4.24	0.0048	0.2176	0.0221	13.246	0.4665	2.1667	13.642	68.821
4.25	0.0047	0.2168	0.0219	13.362	0.4656	2.1678	13.609	68.942
4.26	0.0047	0.2160	0.0217	13.479	0.4648	2.1689	13.576	69.063
4.27	0.0046	0.2152	0.0215	13.597	0.4639	2.1700	13.544	69.183
4.28	0.0046	0.2144	0.0213	13.715	0.4631	2.1711	13.512	69.303
4.29	0.0045	0.2136	0.0211	13.835	0.4622	2.1721	13.480	69.422
4.30	0.0044	0.2129	0.0209	13.955	0.4614	2.1732	13.448	69.541
4.31	0.0044	0.2121	0.0207	14.076	0.4605	2.1743	13.416	69.659
4.32	0.0043	0.2113	0.0205	14.198	0.4597	2.1754	13.384	69.777
4.33	0.0043	0.2105	0.0203	14.322	0.4588	2.1764	13.353	69.895
4.34	0.0042	0.2098	0.0202	14.446	0.4580	2.1775	13.321	70.012
4.35	0.0042	0.2090	0.0200	14.571	0.4572	2.1785	13.290	70.129
4.36	0.0041	0.2083	0.0198	14.697	0.4563	2.1796	13.259	70.245
4.37	0.0041	0.2075	0.0196	14.823	0.4555	2.1806	13.228	70.361
4.38	0.0040	0.2067	0.0194	14.951	0.4547	2.1816	13.198	70.476
4.39	0.0040	0.2060	0.0193	15.080	0.4539	2.1827	13.167	70.591
4.40	0.0039	0.2053	0.0191	15.210	0.4531	2.1837	13.137	70.706
4.41	0.0039	0.2045	0.0189	15.341	0.4522	2.1847	13.106	70.820
4.42	0.0038	0.2038	0.0187	15.472	0.4514	2.1857	13.076	70.934
4.43	0.0038	0.2030	0.0186	15.605	0.4506	2.1867	13.046	71.048
4.44	0.0037	0.2023	0.0184	15.739	0.4498	2.1877	13.016	71.161

(*Contd.*)

Scanned by CamScanner

TABLE A1 Isentropic Flow of Perfect Gas ($\gamma = 1.4$) (*contd.*)

M	p/p_0	T/T_0	ρ/ρ_0	A/A^*	a/a_0	M^*	μ	ν
4.45	0.0037	0.2016	0.0182	15.873	0.4490	2.1887	12.986	71.274
4.46	0.0036	0.2009	0.0181	16.009	0.4482	2.1897	12.957	71.386
4.47	0.0036	0.2002	0.0179	16.146	0.4474	2.1907	12.927	71.498
4.48	0.0035	0.1994	0.0178	16.284	0.4466	2.1917	12.898	71.610
4.49	0.0035	0.1987	0.0176	16.422	0.4458	2.1926	12.869	71.721
4.50	0.0035	0.1980	0.0174	16.562	0.4450	2.1936	12.840	71.832
4.51	0.0034	0.1973	0.0173	16.703	0.4442	2.1946	12.811	71.942
4.52	0.0034	0.1966	0.0171	16.845	0.4434	2.1955	12.782	72.052
4.53	0.0033	0.1959	0.0170	16.988	0.4426	2.1965	12.753	72.162
4.54	0.0033	0.1952	0.0168	17.132	0.4418	2.1974	12.725	72.271
4.55	0.0032	0.1945	0.0167	17.277	0.4411	2.1984	12.696	72.380
4.56	0.0032	0.1938	0.0165	17.423	0.4403	2.1993	12.668	72.489
4.57	0.0032	0.1932	0.0164	17.570	0.4395	2.2002	12.640	72.597
4.58	0.0031	0.1925	0.0163	17.718	0.4387	2.2012	12.612	72.705
4.59	0.0031	0.1918	0.0161	17.867	0.4380	2.2021	12.584	72.812
4.60	0.0031	0.1911	0.0160	18.018	0.4372	2.2030	12.556	72.919
4.61	0.0030	0.1905	0.0158	18.169	0.4364	2.2039	12.528	73.026
4.62	0.0030	0.1898	0.0157	18.322	0.4357	2.2048	12.501	73.132
4.63	0.0029	0.1891	0.0156	18.476	0.4349	2.2057	12.473	73.238
4.64	0.0029	0.1885	0.0154	18.630	0.4341	2.2066	12.446	73.344
4.65	0.0029	0.1878	0.0153	18.786	0.4334	2.2075	12.419	73.449
4.66	0.0028	0.1872	0.0152	18.943	0.4326	2.2084	12.392	73.554
4.67	0.0028	0.1865	0.0150	19.101	0.4319	2.2093	12.365	73.659
4.68	0.0028	0.1859	0.0149	19.261	0.4311	2.2102	12.338	73.763
4.69	0.0027	0.1852	0.0148	19.421	0.4304	2.2110	12.311	73.867
4.70	0.0027	0.1846	0.0146	19.583	0.4296	2.2119	12.284	73.970
4.71	0.0027	0.1839	0.0145	19.746	0.4289	2.2128	12.258	74.073
4.72	0.0026	0.1833	0.0144	19.910	0.4281	2.2136	12.232	74.176
4.73	0.0026	0.1827	0.0143	20.075	0.4274	2.2145	12.205	74.279
4.74	0.0026	0.1820	0.0141	20.241	0.4267	2.2154	12.179	74.381
4.75	0.0025	0.1814	0.0140	20.408	0.4259	2.2162	12.153	74.482
4.76	0.0025	0.1808	0.0139	20.577	0.4252	2.2170	12.127	74.584
4.77	0.0025	0.1802	0.0138	20.747	0.4245	2.2179	12.101	74.685
4.78	0.0025	0.1795	0.0137	20.918	0.4237	2.2187	12.076	74.786
4.79	0.0024	0.1789	0.0135	21.090	0.4230	2.2196	12.050	74.886
4.80	0.0024	0.1783	0.0134	21.264	0.4223	2.2204	12.025	74.986
4.81	0.0024	0.1777	0.0133	21.438	0.4216	2.2212	11.999	75.086
4.82	0.0023	0.1771	0.0132	21.614	0.4208	2.2220	11.974	75.185
4.83	0.0023	0.1765	0.0131	21.792	0.4201	2.2228	11.949	75.285
4.84	0.0023	0.1759	0.0130	21.970	0.4194	2.2236	11.924	75.383
4.85	0.0023	0.1753	0.0129	22.150	0.4187	2.2245	11.899	75.482

(*Contd.*)

Scanned by CamScanner

TABLE A1 Isentropic Flow of Perfect Gas ($\gamma = 1.4$) (*contd.*)

M	p/p_0	T/T_0	ρ/ρ_0	A/A^*	a/a_0	M^*	μ	ν
4.86	0.0022	0.1747	0.0128	22.331	0.4180	2.2253	11.874	75.580
4.87	0.0022	0.1741	0.0126	22.513	0.4173	2.2261	11.849	75.678
4.88	0.0022	0.1735	0.0125	22.696	0.4166	2.2268	11.825	75.775
4.89	0.0022	0.1729	0.0124	22.881	0.4159	2.2276	11.800	75.872
4.90	0.0021	0.1724	0.0123	23.067	0.4152	2.2284	11.776	75.969
4.91	0.0021	0.1718	0.0122	23.254	0.4145	2.2292	11.751	76.066
4.92	0.0021	0.1712	0.0121	23.443	0.4138	2.2300	11.727	76.162
4.93	0.0021	0.1706	0.0120	23.633	0.4131	2.2308	11.703	76.258
4.94	0.0020	0.1700	0.0119	23.824	0.4124	2.2315	11.679	76.353
4.95	0.0020	0.1695	0.0118	24.017	0.4117	2.2323	11.655	76.449
4.96	0.0020	0.1689	0.0117	24.211	0.4110	2.2331	11.631	76.544
4.97	0.0020	0.1683	0.0116	24.406	0.4103	2.2338	11.608	76.638
4.98	0.0019	0.1678	0.0115	24.603	0.4096	2.2346	11.584	76.732
4.99	0.0019	0.1672	0.0114	24.801	0.4089	2.2353	11.560	76.826
5.00	0.0019	0.1667	0.0113	25.000	0.4082	2.2361	11.537	76.920

[Note: In Table A1 μ and ν values are in degrees]

Scanned by CamScanner

TABLE A2 Normal Shock in Perfect Gas ($\gamma = 1.4$)

M_1	M_2	p_2/p_1	ρ_2/ρ_1	T_2/T_1	a_2/a_1	p_{02}/p_{01}
1.01	0.9901	1.0234	1.0167	1.0066	1.0033	1.0000
1.02	0.9805	1.0471	1.0334	1.0132	1.0066	1.0000
1.03	0.9712	1.0710	1.0502	1.0198	1.0099	1.0000
1.04	0.9620	1.0952	1.0671	1.0263	1.0131	0.9999
1.05	0.9531	1.1196	1.0840	1.0328	1.0163	0.9999
1.06	0.9444	1.1442	1.1009	1.0393	1.0195	0.9998
1.07	0.9360	1.1690	1.1179	1.0458	1.0226	0.9996
1.08	0.9277	1.1941	1.1349	1.0522	1.0258	0.9994
1.09	0.9196	1.2194	1.1520	1.0586	1.0289	0.9992
1.10	0.9118	1.2450	1.1691	1.0649	1.0320	0.9989
1.11	0.9041	1.2708	1.1862	1.0713	1.0350	0.9986
1.12	0.8966	1.2968	1.2034	1.0776	1.0381	0.9982
1.13	0.8892	1.3230	1.2206	1.0840	1.0411	0.9978
1.14	0.8820	1.3495	1.2378	1.0903	1.0442	0.9973
1.15	0.8750	1.3762	1.2550	1.0966	1.0472	0.9967
1.16	0.8682	1.4032	1.2723	1.1029	1.0502	0.9961
1.17	0.8615	1.4304	1.2896	1.1092	1.0532	0.9953
1.18	0.8549	1.4578	1.3069	1.1154	1.0561	0.9946
1.19	0.8485	1.4854	1.3243	1.1217	1.0591	0.9937
1.20	0.8422	1.5133	1.3416	1.1280	1.0621	0.9928
1.21	0.8360	1.5414	1.3590	1.1343	1.0650	0.9918
1.22	0.8300	1.5698	1.3764	1.1405	1.0680	0.9907
1.23	0.8241	1.5984	1.3938	1.1468	1.0709	0.9896
1.24	0.8183	1.6272	1.4112	1.1531	1.0738	0.9884
1.25	0.8126	1.6562	1.4286	1.1594	1.0767	0.9871
1.26	0.8071	1.6855	1.4460	1.1657	1.0797	0.9857
1.27	0.8016	1.7150	1.4634	1.1720	1.0826	0.9842
1.28	0.7963	1.7448	1.4808	1.1783	1.0855	0.9827
1.29	0.7911	1.7748	1.4983	1.1846	1.0884	0.9811
1.30	0.7860	1.8050	1.5157	1.1909	1.0913	0.9794
1.31	0.7809	1.8354	1.5331	1.1972	1.0942	0.9776
1.32	0.7760	1.8661	1.5505	1.2035	1.0971	0.9758
1.33	0.7712	1.8970	1.5680	1.2099	1.0999	0.9738
1.34	0.7664	1.9282	1.5854	1.2162	1.1028	0.9718
1.35	0.7618	1.9596	1.6028	1.2226	1.1057	0.9697
1.36	0.7572	1.9912	1.6202	1.2290	1.1086	0.9676
1.37	0.7527	2.0230	1.6376	1.2354	1.1115	0.9653
1.38	0.7483	2.0551	1.6549	1.2418	1.1144	0.9630
1.39	0.7440	2.0874	1.6723	1.2482	1.1172	0.9607
1.40	0.7397	2.1200	1.6897	1.2547	1.1201	0.9582
1.41	0.7355	2.1528	1.7070	1.2612	1.1230	0.9557
1.42	0.7314	2.1858	1.7243	1.2676	1.1259	0.9531

(*Contd.*)

Scanned by CamScanner

TABLE A2 Normal Shock in Perfect Gas ($\gamma = 1.4$) (*contd.*)

M_1	M_2	p_2/p_1	ρ_2/ρ_1	T_2/T_1	a_2/a_1	p_{02}/p_{01}
1.43	0.7274	2.2190	1.7416	1.2741	1.1288	0.9504
1.44	0.7235	2.2525	1.7589	1.2807	1.1317	0.9476
1.45	0.7196	2.2862	1.7761	1.2872	1.1346	0.9448
1.46	0.7157	2.3202	1.7934	1.2938	1.1374	0.9420
1.47	0.7120	2.3544	1.8106	1.3003	1.1403	0.9390
1.48	0.7083	2.3888	1.8278	1.3069	1.1432	0.9360
1.49	0.7047	2.4234	1.8449	1.3136	1.1461	0.9329
1.50	0.7011	2.4583	1.8621	1.3202	1.1490	0.9298
1.51	0.6976	2.4934	1.8792	1.3269	1.1519	0.9266
1.52	0.6941	2.5288	1.8963	1.3336	1.1548	0.9233
1.53	0.6907	2.5644	1.9133	1.3403	1.1577	0.9200
1.54	0.6874	2.6002	1.9303	1.3470	1.1606	0.9166
1.55	0.6841	2.6362	1.9473	1.3538	1.1635	0.9132
1.56	0.6809	2.6725	1.9643	1.3606	1.1664	0.9097
1.57	0.6777	2.7090	1.9812	1.3674	1.1694	0.9062
1.58	0.6746	2.7458	1.9981	1.3742	1.1723	0.9026
1.59	0.6715	2.7828	2.0149	1.3811	1.1752	0.8989
1.60	0.6684	2.8200	2.0317	1.3880	1.1781	0.8952
1.61	0.6655	2.8574	2.0485	1.3949	1.1811	0.8915
1.62	0.6625	2.8951	2.0653	1.4018	1.1840	0.8877
1.63	0.6596	2.9330	2.0820	1.4088	1.1869	0.8838
1.64	0.6568	2.9712	2.0986	1.4158	1.1899	0.8799
1.65	0.6540	3.0096	2.1152	1.4228	1.1928	0.8760
1.66	0.6512	3.0482	2.1318	1.4299	1.1958	0.8720
1.67	0.6485	3.0870	2.1484	1.4369	1.1987	0.8680
1.68	0.6458	3.1261	2.1649	1.4440	1.2017	0.8639
1.69	0.6431	3.1654	2.1813	1.4512	1.2046	0.8599
1.70	0.6405	3.2050	2.1977	1.4583	1.2076	0.8557
1.71	0.6380	3.2448	2.2141	1.4655	1.2106	0.8516
1.72	0.6355	3.2848	2.2304	1.4727	1.2136	0.8474
1.73	0.6330	3.3250	2.2467	1.4800	1.2165	0.8431
1.74	0.6305	3.3655	2.2629	1.4873	1.2195	0.8389
1.75	0.6281	3.4062	2.2791	1.4946	1.2225	0.8346
1.76	0.6257	3.4472	2.2952	1.5019	1.2255	0.8302
1.77	0.6234	3.4884	2.3113	1.5093	1.2285	0.8259
1.78	0.6210	3.5298	2.3273	1.5167	1.2315	0.8215
1.79	0.6188	3.5714	2.3433	1.5241	1.2346	0.8171
1.80	0.6165	3.6133	2.3592	1.5316	1.2376	0.8127
1.81	0.6143	3.6554	2.3751	1.5391	1.2406	0.8082
1.82	0.6121	3.6978	2.3909	1.5466	1.2436	0.8038
1.83	0.6099	3.7404	2.4067	1.5541	1.2467	0.7993
1.84	0.6078	3.7832	2.4224	1.5617	1.2497	0.7948

(*Contd.*)

Scanned by CamScanner

TABLE A2 Normal Shock in Perfect Gas ($\gamma = 1.4$) (*contd.*)

M_1	M_2	p_2/p_1	ρ_2/ρ_1	T_2/T_1	a_2/a_1	p_{02}/p_{01}
1.85	0.6057	3.8262	2.4381	1.5693	1.2527	0.7902
1.86	0.6036	3.8695	2.4537	1.5770	1.2558	0.7857
1.87	0.6016	3.9130	2.4693	1.5847	1.2588	0.7811
1.88	0.5996	3.9568	2.4848	1.5924	1.2619	0.7765
1.89	0.5976	4.0008	2.5003	1.6001	1.2650	0.7720
1.90	0.5956	4.0450	2.5157	1.6079	1.2680	0.7674
1.91	0.5937	4.0894	2.5310	1.6157	1.2711	0.7627
1.92	0.5918	4.1341	2.5463	1.6236	1.2742	0.7581
1.93	0.5899	4.1790	2.5616	1.6314	1.2773	0.7535
1.94	0.5880	4.2242	2.5767	1.6394	1.2804	0.7488
1.95	0.5862	4.2696	2.5919	1.6473	1.2835	0.7442
1.96	0.5844	4.3152	2.6069	1.6553	1.2866	0.7395
1.97	0.5826	4.3610	2.6220	1.6633	1.2897	0.7349
1.98	0.5808	4.4071	2.6369	1.6713	1.2928	0.7302
1.99	0.5791	4.4534	2.6518	1.6794	1.2959	0.7255
2.00	0.5774	4.5000	2.6667	1.6875	1.2990	0.7209
2.01	0.5757	4.5468	2.6815	1.6956	1.3022	0.7162
2.02	0.5740	4.5938	2.6962	1.7038	1.3053	0.7115
2.03	0.5723	4.6410	2.7108	1.7120	1.3084	0.7069
2.04	0.5707	4.6885	2.7255	1.7203	1.3116	0.7022
2.05	0.5691	4.7362	2.7400	1.7285	1.3147	0.6975
2.06	0.5675	4.7842	2.7545	1.7369	1.3179	0.6928
2.07	0.5659	4.8324	2.7689	1.7452	1.3211	0.6882
2.08	0.5643	4.8808	2.7833	1.7536	1.3242	0.6835
2.09	0.5628	4.9294	2.7976	1.7620	1.3274	0.6789
2.10	0.5613	4.9783	2.8119	1.7704	1.3306	0.6742
2.11	0.5598	5.0274	2.8261	1.7789	1.3338	0.6696
2.12	0.5583	5.0768	2.8402	1.7875	1.3370	0.6649
2.13	0.5568	5.1264	2.8543	1.7960	1.3402	0.6603
2.14	0.5554	5.1762	2.8683	1.8046	1.3434	0.6557
2.15	0.5540	5.2262	2.8823	1.8132	1.3466	0.6511
2.16	0.5525	5.2765	2.8962	1.8219	1.3498	0.6464
2.17	0.5511	5.3270	2.9100	1.8306	1.3530	0.6419
2.18	0.5498	5.3778	2.9238	1.8393	1.3562	0.6373
2.19	0.5484	5.4288	2.9376	1.8481	1.3594	0.6327
2.20	0.5471	5.4800	2.9512	1.8569	1.3627	0.6281
2.21	0.5457	5.5314	2.9648	1.8657	1.3659	0.6236
2.22	0.5444	5.5831	2.9784	1.8746	1.3691	0.6191
2.23	0.5431	5.6350	2.9918	1.8835	1.3724	0.6145
2.24	0.5418	5.6872	3.0053	1.8924	1.3756	0.6100
2.25	0.5406	5.7396	3.0186	1.9014	1.3789	0.6055
2.26	0.5393	5.7922	3.0319	1.9104	1.3822	0.6011

(*Contd.*)

Scanned by CamScanner

TABLE A2 Normal Shock in Perfect Gas ($\gamma = 1.4$) (*contd.*)

M_1	M_2	p_2/p_1	ρ_2/ρ_1	T_2/T_1	a_2/a_1	p_{02}/p_{01}
2.27	0.5381	5.8450	3.0452	1.9194	1.3854	0.5966
2.28	0.5368	5.8981	3.0584	1.9285	1.3887	0.5921
2.29	0.5356	5.9514	3.0715	1.9376	1.3920	0.5877
2.30	0.5344	6.0050	3.0845	1.9468	1.3953	0.5833
2.31	0.5332	6.0588	3.0975	1.9560	1.3986	0.5789
2.32	0.5321	6.1128	3.1105	1.9652	1.4019	0.5745
2.33	0.5309	6.1670	3.1234	1.9745	1.4052	0.5702
2.34	0.5297	6.2215	3.1362	1.9838	1.4085	0.5658
2.35	0.5286	6.2762	3.1490	1.9931	1.4118	0.5615
2.36	0.5275	6.3312	3.1617	2.0025	1.4151	0.5572
2.37	0.5264	6.3864	3.1743	2.0119	1.4184	0.5529
2.38	0.5253	6.4418	3.1869	2.0213	1.4217	0.5486
2.39	0.5242	6.4974	3.1994	2.0308	1.4251	0.5444
2.40	0.5231	6.5533	3.2119	2.0403	1.4284	0.5401
2.41	0.5221	6.6094	3.2243	2.0499	1.4317	0.5359
2.42	0.5210	6.6658	3.2367	2.0595	1.4351	0.5317
2.43	0.5200	6.7224	3.2489	2.0691	1.4384	0.5276
2.44	0.5189	6.7792	3.2612	2.0788	1.4418	0.5234
2.45	0.5179	6.8362	3.2733	2.0885	1.4451	0.5193
2.46	0.5169	6.8935	3.2855	2.0982	1.4485	0.5152
2.47	0.5159	6.9510	3.2975	2.1080	1.4519	0.5111
2.48	0.5149	7.0088	3.3095	2.1178	1.4553	0.5071
2.49	0.5140	7.0668	3.3215	2.1276	1.4586	0.5030
2.50	0.5130	7.1250	3.3333	2.1375	1.4620	0.4990
2.51	0.5120	7.1834	3.3452	2.1474	1.4654	0.4950
2.52	0.5111	7.2421	3.3569	2.1574	1.4688	0.4911
2.53	0.5102	7.3010	3.3686	2.1674	1.4722	0.4871
2.54	0.5092	7.3602	3.3803	2.1774	1.4756	0.4832
2.55	0.5083	7.4196	3.3919	2.1875	1.4790	0.4793
2.56	0.5074	7.4792	3.4034	2.1976	1.4824	0.4754
2.57	0.5065	7.5390	3.4149	2.2077	1.4858	0.4715
2.58	0.5056	7.5991	3.4263	2.2179	1.4893	0.4677
2.59	0.5047	7.6594	3.4377	2.2281	1.4927	0.4639
2.60	0.5039	7.7200	3.4490	2.2383	1.4961	0.4601
2.61	0.5030	7.7808	3.4602	2.2486	1.4995	0.4564
2.62	0.5022	7.8418	3.4714	2.2590	1.5030	0.4526
2.63	0.5013	7.9030	3.4826	2.2693	1.5064	0.4489
2.64	0.5005	7.9645	3.4936	2.2797	1.5099	0.4452
2.65	0.4996	8.0262	3.5047	2.2902	1.5133	0.4416
2.66	0.4988	8.0882	3.5156	2.3006	1.5168	0.4379
2.67	0.4980	8.1504	3.5266	2.3111	1.5202	0.4343
2.68	0.4972	8.2128	3.5374	2.3217	1.5237	0.4307

(*Contd.*)

Scanned by CamScanner

TABLE A2 Normal Shock in Perfect Gas ($\gamma = 1.4$) (*contd.*)

M_1	M_2	p_2/p_1	ρ_2/ρ_1	T_2/T_1	a_2/a_1	p_{02}/p_{01}
2.69	0.4964	8.2754	3.5482	2.3323	1.5272	0.4271
2.70	0.4956	8.3383	3.5590	2.3429	1.5307	0.4236
2.71	0.4949	8.4014	3.5697	2.3536	1.5341	0.4201
2.72	0.4941	8.4648	3.5803	2.3642	1.5376	0.4166
2.73	0.4933	8.5284	3.5909	2.3750	1.5411	0.4131
2.74	0.4926	8.5922	3.6015	2.3858	1.5446	0.4097
2.75	0.4918	8.6562	3.6119	2.3966	1.5481	0.4062
2.76	0.4911	8.7205	3.6224	2.4074	1.5516	0.4028
2.77	0.4903	8.7850	3.6327	2.4183	1.5551	0.3994
2.78	0.4896	8.8498	3.6431	2.4292	1.5586	0.3961
2.79	0.4889	8.9148	3.6533	2.4402	1.5621	0.3928
2.80	0.4882	8.9800	3.6635	2.4512	1.5656	0.3895
2.81	0.4875	9.0454	3.6737	2.4622	1.5691	0.3862
2.82	0.4868	9.1111	3.6838	2.4733	1.5727	0.3829
2.83	0.4861	9.1770	3.6939	2.4844	1.5762	0.3797
2.84	0.4854	9.2432	3.7039	2.4955	1.5797	0.3765
2.85	0.4847	9.3096	3.7138	2.5067	1.5833	0.3733
2.86	0.4840	9.3762	3.7238	2.5179	1.5868	0.3701
2.87	0.4833	9.4430	3.7336	2.5292	1.5903	0.3670
2.88	0.4827	9.5101	3.7434	2.5405	1.5939	0.3639
2.89	0.4820	9.5774	3.7532	2.5518	1.5974	0.3608
2.90	0.4814	9.6450	3.7629	2.5632	1.6010	0.3577
2.91	0.4807	9.7128	3.7725	2.5746	1.6046	0.3547
2.92	0.4801	9.7808	3.7821	2.5861	1.6081	0.3517
2.93	0.4795	9.8490	3.7917	2.5975	1.6117	0.3487
2.94	0.4788	9.9175	3.8012	2.6091	1.6153	0.3457
2.95	0.4782	9.9862	3.8106	2.6206	1.6188	0.3428
2.96	0.4776	10.0552	3.8200	2.6322	1.6224	0.3398
2.97	0.4770	10.1244	3.8294	2.6439	1.6260	0.3369
2.98	0.4764	10.1938	3.8387	2.6555	1.6296	0.3340
2.99	0.4758	10.2634	3.8479	2.6673	1.6332	0.3312
3.00	0.4752	10.3333	3.8571	2.6790	1.6368	0.3283
3.01	0.4746	10.4034	3.8663	2.6908	1.6404	0.3255
3.02	0.4740	10.4738	3.8754	2.7026	1.6440	0.3227
3.03	0.4734	10.5444	3.8845	2.7145	1.6476	0.3200
3.04	0.4729	10.6152	3.8935	2.7264	1.6512	0.3172
3.05	0.4723	10.6862	3.9025	2.7383	1.6548	0.3145
3.06	0.4717	10.7575	3.9114	2.7503	1.6584	0.3118
3.07	0.4712	10.8290	3.9203	2.7623	1.6620	0.3091
3.08	0.4706	10.9008	3.9291	2.7744	1.6656	0.3065
3.09	0.4701	10.9728	3.9379	2.7865	1.6693	0.3038
3.10	0.4695	11.0450	3.9466	2.7986	1.6729	0.3012

(*Contd.*)

Scanned by CamScanner

TABLE A2 Normal Shock in Perfect Gas ($\gamma = 1.4$) (*contd.*)

M_1	M_2	p_2/p_1	ρ_2/ρ_1	T_2/T_1	a_2/a_1	p_{02}/p_{01}
3.11	0.4690	11.1174	3.9553	2.8108	1.6765	0.2986
3.12	0.4685	11.1901	3.9639	2.8230	1.6802	0.2960
3.13	0.4679	11.2630	3.9725	2.8352	1.6838	0.2935
3.14	0.4674	11.3362	3.9811	2.8475	1.6875	0.2910
3.15	0.4669	11.4096	3.9896	2.8598	1.6911	0.2885
3.16	0.4664	11.4832	3.9981	2.8722	1.6947	0.2860
3.17	0.4659	11.5570	4.0065	2.8846	1.6984	0.2835
3.18	0.4654	11.6311	4.0149	2.8970	1.7021	0.2811
3.19	0.4648	11.7054	4.0232	2.9095	1.7057	0.2786
3.20	0.4643	11.7800	4.0315	2.9220	1.7094	0.2762
3.21	0.4639	11.8548	4.0397	2.9345	1.7130	0.2738
3.22	0.4634	11.9298	4.0479	2.9471	1.7167	0.2715
3.23	0.4629	12.0050	4.0561	2.9597	1.7204	0.2691
3.24	0.4624	12.0805	4.0642	2.9724	1.7241	0.2668
3.25	0.4619	12.1562	4.0723	2.9851	1.7277	0.2645
3.26	0.4614	12.2322	4.0803	2.9979	1.7314	0.2622
3.27	0.4610	12.3084	4.0883	3.0106	1.7351	0.2600
3.28	0.4605	12.3848	4.0963	3.0234	1.7388	0.2577
3.29	0.4600	12.4614	4.1042	3.0363	1.7425	0.2555
3.30	0.4596	12.5383	4.1120	3.0492	1.7462	0.2533
3.31	0.4591	12.6154	4.1198	3.0621	1.7499	0.2511
3.32	0.4587	12.6928	4.1276	3.0751	1.7536	0.2489
3.33	0.4582	12.7704	4.1354	3.0881	1.7513	0.2468
3.34	0.4578	12.8482	4.1431	3.1011	1.7610	0.2446
3.35	0.4573	12.9262	4.1507	3.1142	1.7647	0.2425
3.36	0.4569	13.0045	4.1583	3.1273	1.7684	0.2404
3.37	0.4565	13.0830	4.1659	3.1405	1.7721	0.2383
3.38	0.4560	13.1618	4.1734	3.1537	1.7759	0.2363
3.39	0.4556	13.2408	4.1809	3.1669	1.7796	0.2342
3.40	0.4552	13.3200	4.1884	3.1802	1.7833	0.2322
3.41	0.4548	13.3994	4.1958	3.1935	1.7870	0.2302
3.42	0.4544	13.4791	4.2032	3.2069	1.7908	0.2282
3.43	0.4540	13.5590	4.2105	3.2203	1.7945	0.2263
3.44	0.4535	13.6392	4.2178	3.2337	1.7982	0.2243
3.45	0.4531	13.7196	4.2251	3.2471	1.8020	0.2224
3.46	0.4527	13.8002	4.2323	3.2607	1.8057	0.2205
3.47	0.4523	13.8810	4.2395	3.2742	1.8095	0.2186
3.48	0.4519	13.9621	4.2467	3.2878	1.8132	0.2167
3.49	0.4515	14.0434	4.2538	3.3014	1.8170	0.2148
3.50	0.4512	14.1250	4.2609	3.3150	1.8207	0.2129
3.51	0.4508	14.2068	4.2679	3.3287	1.8245	0.2111
3.52	0.4504	14.2888	4.2749	3.3425	1.8282	0.2093

(*Contd.*)

Scanned by CamScanner

TABLE A2 Normal Shock in Perfect Gas ($\gamma = 1.4$) (*contd.*)

M_1	M_2	p_2/p_1	ρ_2/ρ_1	T_2/T_1	a_2/a_1	p_{02}/p_{01}
3.53	0.4500	14.3710	4.2819	3.3562	1.8320	0.2075
3.54	0.4496	14.4535	4.2888	3.3701	1.8358	0.2057
3.55	0.4492	14.5362	4.2957	3.3839	1.8395	0.2039
3.56	0.4489	14.6192	4.3026	3.3978	1.8433	0.2022
3.57	0.4485	14.7024	4.3094	3.4117	1.8471	0.2004
3.58	0.4481	14.7858	4.3162	3.4257	1.8509	0.1987
3.59	0.4478	14.8694	4.3229	3.4397	1.8546	0.1970
3.60	0.4474	14.9533	4.3296	3.4537	1.8584	0.1953
3.61	0.4471	15.0374	4.3363	3.4678	1.8622	0.1936
3.62	0.4467	15.1218	4.3429	3.4819	1.8660	0.1920
3.63	0.4463	15.2064	4.3496	3.4961	1.8698	0.1903
3.64	0.4460	15.2912	4.3561	3.5103	1.8736	0.1887
3.65	0.4456	15.3762	4.3627	3.5245	1.8774	0.1871
3.66	0.4453	15.4615	4.3692	3.5388	1.8812	0.1855
3.67	0.4450	15.5470	4.3756	3.5531	1.8850	0.1839
3.68	0.4446	15.6328	4.3821	3.5674	1.8888	0.1823
3.69	0.4443	15.7188	4.3885	3.5818	1.8926	0.1807
3.70	0.4439	15.8050	4.3949	3.5962	1.8964	0.1792
3.71	0.4436	15.8914	4.4012	3.6107	1.9002	0.1777
3.72	0.4433	15.9781	4.4075	3.6252	1.9040	0.1761
3.73	0.4430	16.0650	4.4138	3.6397	1.9078	0.1746
3.74	0.4426	16.1522	4.4200	3.6549	1.9116	0.1731
3.75	0.4423	16.2396	4.4262	3.6689	1.9154	0.1717
3.76	0.4420	16.3272	4.4324	3.6836	1.9193	0.1702
3.77	0.4417	16.4150	4.4385	3.6983	1.9231	0.1687
3.78	0.4414	16.5031	4.4447	3.7130	1.9269	0.1673
3.79	0.4410	16.5914	4.4507	3.7278	1.9307	0.1659
3.80	0.4407	16.6800	4.4568	3.7426	1.9346	0.1645
3.81	0.4404	16.7688	4.4628	3.7574	1.9384	0.1631
3.82	0.4401	16.8578	4.4688	3.7723	1.9422	0.1617
3.83	0.4398	16.9470	4.4747	3.7873	1.9461	0.1603
3.84	0.4395	17.0365	4.4807	3.8022	1.9499	0.1589
3.85	0.4392	17.1262	4.4866	3.8172	1.9538	0.1576
3.86	0.4389	17.2162	4.4924	3.8323	1.9576	0.1563
3.87	0.4386	17.3063	4.4983	3.8473	1.9615	0.1549
3.88	0.4383	17.3968	4.5041	3.8625	1.9653	0.1536
3.89	0.4380	17.4874	4.5098	3.8776	1.9692	0.1523
3.90	0.4377	17.5783	4.5156	3.8928	1.9730	0.1510
3.91	0.4375	17.6694	4.5213	3.9080	1.9769	0.1497
3.92	0.4372	17.7608	4.5270	3.9233	1.9807	0.1485
3.93	0.4369	17.8524	4.5326	3.9386	1.9846	0.1472
3.94	0.4366	17.9442	4.5383	3.9540	1.9885	0.1460

(*Contd.*)

Scanned by CamScanner

TABLE A2 Normal Shock in Perfect Gas ($\gamma = 1.4$) (*contd.*)

M_1	M_2	p_2/p_1	ρ_2/ρ_1	T_2/T_1	a_2/a_1	p_{02}/p_{01}
3.95	0.4363	18.0362	4.5439	3.9694	1.9923	0.1448
3.96	0.4360	18.1285	4.5494	3.9848	1.9962	0.1435
3.97	0.4358	18.2210	4.5550	4.0002	2.0001	0.1423
3.98	0.4355	18.3138	4.5605	4.0157	2.0039	0.1411
3.99	0.4352	18.4068	4.5660	4.0313	2.0078	0.1399
4.00	0.4350	18.5000	4.5714	4.0469	2.0117	0.1388
4.01	0.4347	18.5934	4.5769	4.0625	2.0156	0.1376
4.02	0.4344	18.6871	4.5823	4.0781	2.0194	0.1364
4.03	0.4342	18.7810	4.5876	4.0938	2.0233	0.1353
4.04	0.4339	18.8752	4.5930	4.1096	2.0272	0.1342
4.05	0.4336	18.9696	4.5983	4.1253	2.0311	0.1330
4.06	0.4334	19.0642	4.6036	4.1412	2.0350	0.1319
4.07	0.4331	19.1590	4.6089	4.1570	2.0389	0.1308
4.08	0.4329	19.2541	4.6141	4.1729	2.0428	0.1297
4.09	0.4326	19.3494	4.6193	4.1888	2.0467	0.1286
4.10	0.4324	19.4450	4.6245	4.2048	2.0506	0.1276
4.11	0.4321	19.5408	4.6296	4.2208	2.0545	0.1265
4.12	0.4319	19.6368	4.6348	4.2368	2.0584	0.1254
4.13	0.4316	19.7331	4.6399	4.2529	2.0623	0.1244
4.14	0.4314	19.8295	4.6450	4.2690	2.0662	0.1234
4.15	0.4311	19.9262	4.6500	4.2852	2.0701	0.1223
4.16	0.4309	20.0232	4.6550	4.3014	2.0740	0.1213
4.17	0.4306	20.1204	4.6601	4.3176	2.0779	0.1203
4.18	0.4304	20.2178	4.6650	4.3339	2.0818	0.1193
4.19	0.4302	20.3155	4.6700	4.3502	2.0857	0.1183
4.20	0.4299	20.4133	4.6749	4.3666	2.0896	0.1173
4.21	0.4297	20.5115	4.6798	4.3830	2.0936	0.1164
4.22	0.4295	20.6098	4.6847	4.3994	2.0975	0.1154
4.23	0.4292	20.7084	4.6896	4.4159	2.1014	0.1144
4.24	0.4290	20.8072	4.6944	4.4324	2.1053	0.1135
4.25	0.4288	20.9063	4.6992	4.4489	2.1092	0.1126
4.26	0.4286	21.0056	4.7040	4.4655	2.1132	0.1116
4.27	0.4283	21.1051	4.7087	4.4821	2.1171	0.1107
4.28	0.4281	21.2048	4.7135	4.4988	2.1210	0.1098
4.29	0.4279	21.3048	4.7182	4.5155	2.1250	0.1089
4.30	0.4277	21.4050	4.7229	4.5322	2.1289	0.1080
4.31	0.4275	21.5055	4.7275	4.5490	2.1328	0.1071
4.32	0.4272	21.6062	4.7322	4.5658	2.1368	0.1062
4.33	0.4270	21.7071	4.7368	4.5827	2.1407	0.1054
4.34	0.4268	21.8083	4.7414	4.5996	2.1447	0.1045
4.35	0.4266	21.9096	4.7460	4.6165	2.1486	0.1036
4.36	0.4264	22.0113	4.7505	4.6335	2.1525	0.1028

(*Contd.*)

Scanned by CamScanner

TABLE A.2 Normal Shock in Perfect Gas ($\gamma = 1.4$) (*contd.*)

M_1	M_2	p_2/p_1	ρ_2/ρ_1	T_2/T_1	a_2/a_1	p_{02}/p_{01}
4.37	0.4262	22.1131	4.7550	4.6505	2.1565	0.1020
4.38	0.4260	22.2152	4.7595	4.6675	2.1604	0.1011
4.39	0.4258	22.3175	4.7640	4.6846	2.1644	0.1003
4.40	0.4255	22.4201	4.7685	4.7017	2.1683	0.0995
4.41	0.4253	22.5229	4.7729	4.7189	2.1723	0.0987
4.42	0.4251	22.6259	4.7773	4.7361	2.1763	0.0979
4.43	0.4249	22.7291	4.7817	4.7533	2.1802	0.0971
4.44	0.4247	22.8326	4.7861	4.7706	2.1842	0.0963
4.45	0.4245	22.9363	4.7904	4.7879	2.1881	0.0955
4.46	0.4243	23.0403	4.7948	4.8053	2.1921	0.0947
4.47	0.4241	23.1445	4.7991	4.8227	2.1961	0.0940
4.48	0.4239	23.2489	4.8034	4.8401	2.2000	0.0932
4.49	0.4237	23.3535	4.8076	4.8576	2.2040	0.0924
4.50	0.4236	23.4584	4.8119	4.8751	2.2080	0.0917
4.51	0.4234	23.5635	4.8161	4.8926	2.2119	0.0910
4.52	0.4232	23.6689	4.8203	4.9102	2.2159	0.0902
4.53	0.4230	23.7745	4.8245	4.9279	2.2199	0.0895
4.54	0.4228	23.8803	4.8287	4.9455	2.2239	0.0888
4.55	0.4226	23.9864	4.8328	4.9632	2.2278	0.0881
4.56	0.4224	24.0926	4.8369	4.9810	2.2318	0.0874
4.57	0.4222	24.1992	4.8410	4.9988	2.2358	0.0867
4.58	0.4220	24.3059	4.8451	5.0166	2.2398	0.0860
4.59	0.4219	24.4129	4.8492	5.0344	2.2438	0.0853
4.60	0.4217	24.5201	4.8532	5.0523	2.2477	0.0846
4.61	0.4215	24.6276	4.8572	5.0703	2.2517	0.0839
4.62	0.4213	24.7353	4.8612	5.0883	2.2557	0.0832
4.63	0.4211	24.8432	4.8652	5.1063	2.2597	0.0826
4.64	0.4210	24.9513	4.8692	5.1243	2.2637	0.0819
4.65	0.4208	25.0597	4.8731	5.1424	2.2677	0.0813
4.66	0.4206	25.1683	4.8771	5.1605	2.2717	0.0806
4.67	0.4204	25.2772	4.8810	5.1787	2.2757	0.0800
4.68	0.4203	25.3863	4.8849	5.1969	2.2797	0.0793
4.69	0.4201	25.4956	4.8887	5.2152	2.2837	0.0787
4.70	0.4199	25.6051	4.8926	5.2335	2.2877	0.0781
4.71	0.4197	25.7149	4.8964	5.2518	2.2917	0.0775
4.72	0.4196	25.8249	4.9002	5.2701	2.2957	0.0769
4.73	0.4194	25.9352	4.9040	5.2885	2.2997	0.0762
4.74	0.4192	26.0457	4.9078	5.3070	2.3037	0.0756
4.75	0.4191	26.1564	4.9116	5.3255	2.3077	0.0750
4.76	0.4189	26.2673	4.9153	5.3440	2.3117	0.0745
4.77	0.4187	26.3785	4.9190	5.3625	2.3157	0.0739
4.78	0.4186	26.4900	4.9227	5.3811	2.3197	0.0733

(*Contd.*)

Scanned by CamScanner

TABLE A2 Normal Shock in Perfect Gas ($\gamma = 1.4$) (*contd.*)

M_1	M_2	p_2/p_1	ρ_2/ρ_1	T_2/T_1	a_2/a_1	p_{02}/p_{01}
4.79	0.4184	26.6016	4.9264	5.3998	2.3237	0.0727
4.80	0.4183	26.7135	4.9301	5.4184	2.3278	0.0721
4.81	0.4181	26.8256	4.9338	5.4372	2.3318	0.0716
4.82	0.4179	26.9380	4.9374	5.4559	2.3358	0.0710
4.83	0.4178	27.0505	4.9410	5.4747	2.3398	0.0705
4.84	0.4176	27.1634	4.9446	5.4935	2.3438	0.0699
4.85	0.4175	27.2764	4.9482	5.5124	2.3478	0.0694
4.86	0.4173	27.3897	4.9518	5.5313	2.3519	0.0688
4.87	0.4172	27.5032	4.9553	5.5502	2.3559	0.0683
4.88	0.4170	27.6170	4.9589	5.5692	2.3599	0.0677
4.89	0.4169	27.7310	4.9624	5.5882	2.3639	0.0672
4.90	0.4167	27.8452	4.9659	5.6073	2.3680	0.0667
4.91	0.4165	27.9596	4.9694	5.6264	2.3720	0.0662
4.92	0.4164	28.0743	4.9728	5.6455	2.3760	0.0657
4.93	0.4162	28.1893	4.9763	5.6647	2.3801	0.0652
4.94	0.4161	28.3044	4.9797	5.6839	2.3841	0.0647
4.95	0.4160	28.4198	4.9831	5.7032	2.3881	0.0642
4.96	0.4158	28.5354	4.9865	5.7225	2.3922	0.0637
4.97	0.4157	28.6513	4.9899	5.7418	2.3962	0.0632
4.98	0.4155	28.7673	4.9933	5.7612	2.4002	0.0627
4.99	0.4154	28.8837	4.9967	5.7806	2.4043	0.0622
5.00	0.4152	29.0002	5.0000	5.8000	2.4083	0.0617

Scanned by CamScanner

TABLE A3 Oblique Shock in Perfect Gas ($\gamma = 1.4$)*

		Weak solution			Strong solution		
M_1	θ	β	p_2/p_1	M_2	β	p_2/p_1	M_2
1.05	0	72.07	0.998	1.052	89.66	1.120	0.953
1.10	0	65.28	0.998	1.101	89.83	1.245	0.912
1.10	1	69.80	1.077	1.039	83.57	1.227	0.925
1.15	0	60.34	0.998	1.151	89.89	1.376	0.875
1.15	1	63.16	1.062	1.102	85.98	1.369	0.880
1.15	2	67.00	1.141	1.043	81.17	1.340	0.901
1.20	0	56.39	0.998	1.201	89.92	1.513	0.842
1.20	1	58.55	1.056	1.158	87.04	1.509	0.845
1.20	2	61.05	1.120	1.111	83.86	1.494	0.855
1.20	3	64.34	1.198	1.056	80.03	1.463	0.876
1.25	0	53.08	0.999	1.251	89.94	1.656	0.813
1.25	1	54.88	1.053	1.211	87.65	1.653	0.815
1.25	2	56.85	1.111	1.170	85.21	1.644	0.821
1.25	3	59.13	1.176	1.124	82.55	1.626	0.832
1.25	4	61.99	1.254	1.072	79.39	1.594	0.852
1.25	5	66.50	1.366	0.999	74.63	1.528	0.895
1.30	0	50.24	0.999	1.301	89.95	1.805	0.786
1.30	1	51.81	1.051	1.263	88.05	1.803	0.787
1.30	2	53.47	1.106	1.224	86.06	1.796	0.792
1.30	3	55.32	1.167	1.184	83.95	1.783	0.800
1.30	4	57.42	1.233	1.140	81.65	1.763	0.812
1.30	5	59.96	1.311	1.090	78.97	1.733	0.831
1.30	6	63.46	1.411	1.027	75.37	1.679	0.864
1.35	0	47.76	0.999	1.351	89.96	1.960	0.762
1.35	1	49.17	1.050	1.314	88.34	1.958	0.763
1.35	2	50.63	1.104	1.277	86.65	1.952	0.766
1.35	3	52.22	1.162	1.239	84.89	1.943	0.772
1.35	4	53.97	1.224	1.199	83.03	1.928	0.781
1.35	5	55.93	1.292	1.157	80.99	1.907	0.793
1.35	6	58.23	1.370	1.109	78.66	1.877	0.811
1.35	7	61.18	1.465	1.052	75.72	1.830	0.839
1.35	8	66.91	1.632	0.954	70.02	1.711	0.909
1.40	0	45.55	0.999	1.401	89.96	2.120	0.740
1.40	1	46.84	1.050	1.365	88.55	2.119	0.741
1.40	2	48.17	1.103	1.329	87.08	2.114	0.743
1.40	3	49.59	1.159	1.293	85.57	2.106	0.748
1.40	4	51.12	1.219	1.255	83.99	2.095	0.754
1.40	5	52.78	1.283	1.216	82.31	2.079	0.764
1.40	6	54.63	1.354	1.174	80.49	2.057	0.776
1.40	7	56.76	1.433	1.128	78.41	2.028	0.793

*In this table, the θ and β values are in degrees.

(Contd.)

Scanned by CamScanner

TABLE A3 Oblique Shock in Perfect Gas ($\gamma = 1.4$) (*contd.*)

		Weak solution			*Strong solution*		
M_1	θ	β	p_2/p_1	M_2	β	p_2/p_1	M_2
1.40	8	59.37	1.526	1.074	75.89	1.984	0.818
1.40	9	63.18	1.655	1.003	72.19	1.906	0.863
1.45	0	43.57	0.999	1.451	89.97	2.286	0.720
1.45	1	44.77	1.050	1.416	88.71	2.285	0.720
1.45	2	46.00	1.103	1.381	87.41	2.281	0.722
1.45	3	47.30	1.158	1.345	86.08	2.275	0.726
1.45	4	48.68	1.217	1.309	84.70	2.265	0.732
1.45	5	50.16	1.279	1.272	83.27	2.252	0.739
1.45	6	51.76	1.346	1.232	81.73	2.236	0.749
1.45	7	53.52	1.419	1.191	80.07	2.213	0.761
1.45	8	55.52	1.500	1.146	78.20	2.184	0.778
1.45	9	57.89	1.593	1.095	75.98	2.142	0.801
1.45	10	61.05	1.711	1.032	72.99	2.076	0.837
1.50	0	41.78	0.999	1.501	89.97	2.458	0.701
1.50	1	42.91	1.050	1.466	88.84	2.457	0.702
1.50	2	44.07	1.103	1.432	87.67	2.454	0.704
1.50	3	45.27	1.158	1.397	86.48	2.448	0.707
1.50	4	46.54	1.216	1.362	85.26	2.440	0.711
1.50	5	47.89	1.278	1.325	83.99	2.430	0.717
1.50	6	49.33	1.343	1.288	82.66	2.415	0.725
1.50	7	50.88	1.413	1.249	81.25	2.398	0.735
1.50	8	52.57	1.489	1.208	79.71	2.375	0.748
1.50	9	54.47	1.572	1.164	78.00	2.345	0.764
1.50	10	56.68	1.666	1.114	76.00	2.305	0.785
1.50	11	59.46	1.781	1.055	73.44	2.245	0.817
1.50	12	64.35	1.967	0.961	68.79	2.115	0.885
1.55	0	40.15	0.999	1.551	89.97	2.636	0.684
1.55	1	41.23	1.051	1.516	88.95	2.635	0.685
1.55	2	42.32	1.104	1.482	87.88	2.632	0.686
1.55	3	43.45	1.159	1.448	86.80	2.628	0.689
1.55	4	44.64	1.217	1.413	85.70	2.620	0.693
1.55	5	45.89	1.278	1.378	84.57	2.611	0.698
1.55	6	47.21	1.343	1.341	83.39	2.599	0.705
1.55	7	48.62	1.411	1.304	82.15	2.584	0.713
1.55	8	50.13	1.484	1.265	80.83	2.565	0.723
1.55	9	51.77	1.563	1.224	79.40	2.541	0.736
1.55	10	53.60	1.649	1.180	77.81	2.511	0.752
1.55	11	55.69	1.746	1.132	75.97	2.471	0.772
1.55	12	58.24	1.860	1.076	73.69	2.415	0.801
1.55	13	61.98	2.018	0.999	70.24	2.316	0.852

(*Contd.*)

Scanned by CamScanner

TABLE A3 Oblique Shock in Perfect Gas ($\gamma = 1.4$) (*contd.*)

		Weak solution			*Strong solution*		
M_1	θ	β	p_2/p_1	M_2	β	p_2/p_1	M_2
1.60	0	38.66	0.999	1.601	89.97	2.820	0.668
1.60	1	39.69	1.051	1.566	89.03	2.819	0.669
1.60	2	40.72	1.105	1.532	88.06	2.817	0.670
1.60	3	41.81	1.160	1.498	87.07	2.812	0.673
1.60	4	42.93	1.219	1.464	86.06	2.806	0.676
1.60	5	44.11	1.280	1.429	85.03	2.798	0.681
1.60	6	45.34	1.345	1.393	83.97	2.787	0.686
1.60	7	46.65	1.412	1.357	82.86	2.774	0.693
1.60	8	48.03	1.484	1.320	81.69	2.758	0.702
1.60	9	49.51	1.561	1.281	80.45	2.738	0.712
1.60	10	51.12	1.643	1.240	79.10	2.713	0.725
1.60	11	52.88	1.732	1.196	77.61	2.682	0.741
1.60	12	54.89	1.832	1.148	75.90	2.643	0.761
1.60	13	57.28	1.947	1.094	73.82	2.588	0.789
1.60	14	60.54	2.097	1.023	70.90	2.500	0.832
1.65	0	37.28	0.999	1.651	89.98	3.010	0.654
1.65	1	38.27	1.052	1.616	89.10	3.009	0.654
1.65	2	39.27	1.106	1.582	88.20	3.006	0.656
1.65	3	40.30	1.162	1.548	87.29	3.002	0.658
1.65	4	41.38	1.221	1.514	86.37	2.997	0.661
1.65	5	42.50	1.283	1.479	85.42	2.989	0.665
1.65	6	43.67	1.347	1.444	84.45	2.980	0.670
1.65	7	44.89	1.415	1.409	83.44	2.968	0.676
1.65	8	46.18	1.487	1.372	82.39	2.954	0.683
1.65	9	47.55	1.562	1.334	81.28	2.937	0.692
1.65	10	49.01	1.643	1.295	80.10	2.916	0.703
1.65	11	50.58	1.729	1.254	78.83	2.890	0.716
1.65	12	52.31	1.822	1.210	77.41	2.859	0.732
1.65	13	54.26	1.926	1.163	75.80	2.818	0.752
1.65	14	56.54	2.044	1.109	73.86	2.764	0.778
1.65	15	59.52	2.192	1.042	71.25	2.681	0.818
1.70	0	36.01	0.999	1.701	89.98	3.205	0.641
1.70	1	36.96	1.052	1.666	89.17	3.204	0.641
1.70	2	37.93	1.107	1.632	88.33	3.202	0.642
1.70	3	38.92	1.164	1.598	87.48	3.198	0.644
1.70	4	39.96	1.224	1.564	86.62	3.193	0.647
1.70	5	41.03	1.286	1.529	85.75	3.186	0.650
1.70	6	42.15	1.351	1.495	84.85	3.178	0.655
1.70	7	43.31	1.420	1.459	83.93	3.167	0.660
1.70	8	44.53	1.491	1.423	82.97	3.154	0.667

(*Contd.*)

Scanned by CamScanner

TABLE A3 Oblique Shock in Perfect Gas ($\gamma = 1.4$) (*contd.*)

		Weak solution			*Strong solution*		
M_1	θ	β	p_2/p_1	M_2	β	p_2/p_1	M_2
1.70	9	45.81	1.567	1.386	81.97	3.139	0.675
1.70	10	47.17	1.647	1.348	80.91	3.121	0.684
1.70	11	48.61	1.731	1.309	79.78	3.099	0.695
1.70	12	50.17	1.822	1.267	78.56	3.072	0.708
1.70	13	51.87	1.919	1.223	77.21	3.040	0.724
1.70	14	53.77	2.027	1.176	75.67	2.998	0.744
1.70	15	55.98	2.150	1.122	73.84	2.944	0.770
1.70	16	58.79	2.300	1.057	71.43	2.863	0.808
1.70	17	64.61	2.585	0.933	65.99	2.647	0.905
1.75	0	34.83	0.999	1.751	89.98	3.406	0.628
1.75	1	35.76	1.053	1.716	89.22	3.406	0.628
1.75	2	36.69	1.109	1.682	88.43	3.404	0.629
1.75	3	37.65	1.167	1.648	87.64	3.400	0.631
1.75	4	38.65	1.227	1.613	86.84	3.395	0.634
1.75	5	39.68	1.290	1.579	86.03	3.389	0.637
1.75	6	40.76	1.356	1.544	85.19	3.381	0.641
1.75	7	41.87	1.425	1.509	84.34	3.371	0.646
1.75	8	43.04	1.497	1.473	83.45	3.360	0.652
1.75	9	44.25	1.573	1.437	82.53	3.346	0.659
1.75	10	45.53	1.653	1.400	81.57	3.329	0.667
1.75	11	46.88	1.737	1.361	80.55	3.310	0.677
1.75	12	48.32	1.826	1.321	79.47	3.287	0.688
1.75	13	49.86	1.922	1.279	78.29	3.259	0.701
1.75	14	51.55	2.024	1.235	76.99	3.225	0.718
1.75	15	53.42	2.137	1.187	75.51	3.183	0.738
1.75	16	55.59	2.265	1.133	73.76	3.127	0.763
1.75	17	58.30	2.419	1.068	71.48	3.046	0.800
1.75	18	62.94	2.667	0.965	67.27	2.873	0.877
1.80	0	33.73	0.998	1.801	89.98	3.613	0.617
1.80	1	34.63	1.054	1.766	89.27	3.613	0.617
1.80	2	35.54	1.110	1.731	88.53	3.611	0.618
1.80	3	36.48	1.169	1.697	87.78	3.608	0.619
1.80	4	37.44	1.231	1.662	87.03	3.603	0.622
1.80	5	38.44	1.295	1.628	86.27	3.597	0.625
1.80	6	39.48	1.361	1.593	85.49	3.590	0.628
1.80	7	40.56	1.431	1.558	84.69	3.581	0.633
1.80	8	41.67	1.504	1.523	83.87	3.570	0.638
1.80	9	42.84	1.581	1.486	83.02	3.557	0.644
1.80	10	44.06	1.661	1.449	82.13	3.542	0.652
1.80	11	45.34	1.745	1.412	81.20	3.525	0.660

(*Contd.*)

Scanned by CamScanner

TABLE A3 Oblique Shock in Perfect Gas ($\gamma = 1.4$) (*contd.*)

		Weak solution			Strong solution		
M_1	θ	β	p_2/p_1	M_2	β	p_2/p_1	M_2
1.80	12	46.69	1.834	1.373	80.22	3.504	0.670
1.80	13	48.12	1.929	1.332	79.16	3.480	0.682
1.80	14	49.66	2.029	1.290	78.02	3.450	0.696
1.80	15	51.34	2.138	1.245	76.76	3.415	0.712
1.80	16	53.20	2.257	1.196	75.33	3.371	0.733
1.80	17	55.34	2.391	1.142	73.62	3.313	0.759
1.80	18	57.99	2.551	1.077	71.42	3.230	0.796
1.80	19	62.30	2.797	0.977	67.58	3.063	0.867
1.85	0	32.70	0.998	1.851	89.98	3.826	0.606
1.85	1	33.58	1.055	1.815	89.31	3.826	0.606
1.85	2	34.47	1.112	1.781	88.61	3.824	0.607
1.85	3	35.38	1.172	1.746	87.91	3.821	0.608
1.85	4	36.32	1.234	1.711	87.20	3.817	0.610
1.85	5	37.30	1.299	1.677	86.48	3.811	0.613
1.85	6	38.30	1.367	1.642	85.74	3.804	0.617
1.85	7	39.34	1.438	1.607	84.99	3.796	0.621
1.85	8	40.42	1.512	1.571	84.22	3.786	0.626
1.85	9	41.55	1.590	1.535	83.43	3.774	0.631
1.85	10	42.72	1.671	1.498	82.61	3.760	0.638
1.85	11	43.94	1.756	1.461	81.75	3.744	0.646
1.85	12	45.22	1.845	1.422	80.85	3.725	0.655
1.85	13	46.58	1.940	1.383	79.89	3.703	0.665
1.85	14	48.01	2.039	1.341	78.86	3.677	0.677
1.85	15	49.56	2.146	1.298	77.75	3.646	0.692
1.85	16	51.23	2.261	1.252	76.51	3.609	0.709
1.85	17	53.09	2.386	1.203	75.11	3.562	0.729
1.85	18	55.23	2.527	1.148	73.44	3.502	0.756
1.85	19	57.87	2.696	1.082	71.28	3.415	0.793
1.85	20	62.10	2.952	0.982	67.54	3.244	0.865
1.90	0	31.73	0.998	1.901	89.98	4.045	0.596
1.90	1	32.60	1.056	1.865	89.34	4.044	0.596
1.90	2	33.47	1.114	1.830	88.68	4.043	0.597
1.90	3	34.36	1.175	1.795	88.01	4.040	0.598
1.90	4	35.28	1.238	1.760	87.34	4.036	0.600
1.90	5	36.23	1.304	1.725	86.66	4.031	0.603
1.90	6	37.21	1.373	1.690	85.97	4.024	0.606
1.90	7	38.22	1.446	1.655	85.26	4.016	0.610
1.90	8	39.27	1.521	1.619	84.54	4.007	0.614
1.90	9	40.36	1.600	1.583	83.79	3.996	0.620
1.90	10	41.49	1.682	1.546	83.02	3.983	0.626

(*Contd.*)

Scanned by CamScanner

TABLE A3 Oblique Shock in Perfect Gas ($\gamma = 1.4$) (*contd.*)

		Weak solution			*Strong solution*		
M_1	θ	β	p_2/p_1	M_2	β	p_2/p_1	M_2
1.90	11	42.67	1.768	1.509	82.22	3.968	0.633
1.90	12	43.90	1.858	1.471	81.38	3.950	0.641
1.90	13	45.19	1.953	1.432	80.50	3.930	0.650
1.90	14	46.55	2.053	1.391	79.57	3.907	0.661
1.90	15	48.00	2.159	1.349	78.56	3.879	0.674
1.90	16	49.54	2.272	1.305	77.47	3.847	0.688
1.90	17	51.23	2.393	1.258	76.25	3.807	0.706
1.90	18	53.10	2.526	1.208	74.86	3.758	0.727
1.90	19	55.24	2.676	1.151	73.21	3.693	0.755
1.90	20	57.90	2.856	1.084	71.06	3.601	0.794
1.90	21	62.25	3.132	0.979	67.22	3.414	0.869
1.95	0	30.83	0.998	1.951	89.98	4.270	0.586
1.95	1	31.68	1.057	1.914	89.37	4.269	0.586
1.95	2	32.53	1.116	1.879	88.74	4.267	0.587
1.95	3	33.40	1.178	1.844	88.11	4.265	0.589
1.95	4	34.30	1.242	1.809	87.47	4.261	0.590
1.95	5	35.23	1.310	1.773	86.82	4.256	0.593
1.95	6	36.19	1.380	1.738	86.17	4.250	0.596
1.95	7	37.18	1.454	1.702	85.50	4.242	0.599
1.95	8	38.20	1.530	1.667	84.81	4.233	0.604
1.95	9	39.26	1.610	1.630	84.11	4.223	0.609
1.95	10	40.36	1.694	1.594	83.38	4.211	0.614
1.95	11	41.50	1.781	1.557	82.63	4.197	0.621
1.95	12	42.69	1.873	1.519	81.85	4.180	0.628
1.95	13	43.93	1.968	1.480	81.03	4.162	0.637
1.95	14	45.23	2.069	1.440	80.17	4.140	0.647
1.95	15	46.60	2.175	1.398	79.25	4.115	0.658
1.95	16	48.06	2.288	1.355	78.25	4.086	0.671
1.95	17	49.62	2.408	1.310	77.17	4.051	0.686
1.95	18	51.32	2.537	1.262	75.97	4.009	0.705
1.95	19	53.21	2.678	1.210	74.58	3.956	0.727
1.95	20	55.38	2.838	1.152	72.93	3.887	0.756
1.95	21	58.10	3.030	1.082	70.74	3.787	0.796
1.95	22	62.85	3.346	0.966	66.52	3.565	0.883
2.00	0	29.98	0.998	2.001	89.99	4.500	0.577
2.00	1	30.81	1.058	1.964	89.40	4.499	0.578
2.00	2	31.65	1.118	1.928	88.80	4.498	0.578
2.00	3	32.51	1.181	1.892	88.19	4.495	0.580
2.00	4	33.39	1.247	1.857	87.58	4.492	0.581
2.00	5	34.30	1.315	1.821	86.97	4.487	0.584

(*Contd.*)

Scanned by CamScanner

TABLE A3 Oblique Shock in Perfect Gas ($\gamma = 1.4$) (*contd.*)

		Weak solution			*Strong solution*		
M_1	θ	β	p_2/p_1	M_2	β	p_2/p_1	M_2
2.00	6	35.24	1.387	1.786	86.34	4.481	0.586
2.00	7	36.21	1.462	1.750	85.70	4.474	0.590
2.00	8	37.21	1.540	1.714	85.05	4.465	0.594
2.00	9	38.24	1.621	1.677	84.39	4.455	0.598
2.00	10	39.31	1.707	1.641	83.70	4.444	0.604
2.00	11	40.42	1.795	1.603	82.99	4.431	0.610
2.00	12	41.58	1.888	1.565	82.26	4.415	0.617
2.00	13	42.78	1.986	1.526	81.49	4.398	0.625
2.00	14	44.03	2.087	1.487	80.69	4.378	0.634
2.00	15	45.34	2.195	1.446	79.83	4.355	0.644
2.00	16	46.73	2.307	1.403	78.92	4.328	0.656
2.00	17	48.20	2.427	1.359	77.94	4.296	0.669
2.00	18	49.79	2.554	1.313	76.86	4.259	0.685
2.00	19	51.51	2.692	1.264	75.66	4.214	0.704
2.00	20	53.42	2.843	1.210	74.27	4.157	0.728
2.00	21	55.64	3.014	1.150	72.59	4.082	0.758
2.00	22	58.46	3.223	1.076	70.33	3.971	0.802
2.10	0	28.42	0.998	2.101	89.99	4.978	0.561
2.10	1	29.22	1.060	2.063	89.45	4.978	0.561
2.10	2	30.03	1.122	2.026	88.90	4.976	0.562
2.10	3	30.87	1.187	1.989	88.34	4.974	0.563
2.10	4	31.72	1.256	1.953	87.78	4.971	0.565
2.10	5	32.61	1.327	1.917	87.21	4.966	0.567
2.10	6	33.51	1.402	1.880	86.64	4.961	0.569
2.10	7	34.45	1.480	1.844	86.06	4.954	0.572
2.10	8	35.41	1.561	1.807	85.47	4.946	0.576
2.10	9	36.41	1.646	1.770	84.86	4.937	0.580
2.10	10	37.43	1.734	1.733	84.24	4.926	0.585
2.10	11	38.49	1.827	1.695	83.60	4.914	0.590
2.10	12	39.59	1.923	1.656	82.94	4.901	0.596
2.10	13	40.73	2.024	1.617	82.26	4.885	0.603
2.10	14	41.91	2.129	1.578	81.54	4.867	0.611
2.10	15	43.14	2.239	1.537	80.79	4.847	0.620
2.10	16	44.43	2.355	1.495	80.00	4.823	0.630
2.10	17	45.78	2.476	1.452	79.16	4.796	0.641
2.10	18	47.21	2.604	1.408	78.26	4.765	0.654
2.10	19	48.73	2.740	1.361	77.28	4.729	0.669
2.10	20	50.36	2.885	1.312	76.19	4.685	0.687
2.10	21	52.16	3.042	1.260	74.96	4.632	0.708
2.10	22	54.17	3.215	1.202	73.52	4.564	0.735

(*Contd.*)

Scanned by CamScanner

TABLE A3 Oblique Shock in Perfect Gas ($\gamma = 1.4$) *(contd.)*

		Weak solution			*Strong solution*		
M_1	θ	β	p_2/p_1	M_2	β	p_2/p_1	M_2
2.10	23	56.55	3.415	1.136	71.72	4.472	0.770
2.10	24	59.77	3.674	1.049	69.10	4.324	0.824
2.20	0	27.01	0.998	2.201	89.99	5.480	0.547
2.20	1	27.80	1.062	2.162	88.49	5.480	0.547
2.20	2	28.59	1.127	2.124	88.98	5.478	0.548
2.20	3	29.40	1.194	2.086	87.46	5.476	0.549
2.20	4	30.24	1.265	2.049	87.94	5.473	0.550
2.20	5	31.10	1.340	2.011	87.42	5.468	0.552
2.20	6	31.98	1.417	1.974	86.89	5.463	0.554
2.20	7	32.89	1.498	1.936	86.35	5.457	0.557
2.20	8	33.83	1.583	1.899	85.80	5.450	0.561
2.20	9	34.79	1.672	1.861	85.24	5.441	0.564
2.20	10	35.79	1.764	1.823	84.67	5.431	0.569
2.20	11	36.81	1.860	1.784	84.09	5.420	0.573
2.20	12	37.87	1.961	1.745	83.48	5.407	0.579
2.20	13	38.96	2.066	1.706	82.86	5.393	0.585
2.20	14	40.10	2.176	1.666	82.22	5.376	0.592
2.20	15	41.27	2.290	1.625	81.55	5.358	0.600
2.20	16	42.29	2.409	1.583	80.84	5.337	0.609
2.20	17	43.76	2.535	1.540	80.10	5.313	0.618
2.20	18	45.09	2.666	1.496	79.31	5.286	0.630
2.20	19	46.49	2.804	1.451	78.47	5.254	0.642
2.20	20	47.98	2.949	1.404	77.55	5.217	0.657
2.20	21	49.56	3.104	1.354	76.55	5.174	0.674
2.20	22	51.28	3.270	1.301	75.42	5.122	0.694
2.20	23	53.18	3.451	1.244	74.13	5.057	0.718
2.20	24	55.36	3.655	1.181	72.56	4.973	0.749
2.20	25	58.05	3.899	1.104	70.49	4.850	0.793
2.20	26	62.69	4.291	0.980	66.48	4.581	0.885
2.30	0	25.75	0.998	2.301	89.99	6.005	0.534
2.30	1	26.52	1.064	2.260	89.52	6.005	0.535
2.30	2	27.29	1.131	2.221	89.04	6.003	0.535
2.30	3	28.09	1.201	2.182	88.56	6.001	0.536
2.30	4	28.91	1.275	2.144	88.07	5.998	0.537
2.30	5	29.75	1.353	2.105	87.58	5.994	0.539
2.30	6	30.61	1.434	2.067	87.09	5.989	0.541
2.30	7	31.50	1.518	2.028	86.59	5.983	0.544
2.30	8	32.42	1.607	1.990	86.08	5.976	0.547
2.30	9	33.36	1.699	1.951	85.56	5.968	0.550
2.30	10	34.33	1.796	1.912	85.03	5.959	0.554

(Contd.)

Scanned by CamScanner

TABLE A3 Oblique Shock in Perfect Gas ($\gamma = 1.4$) (*contd.*)

		Weak solution			*Strong solution*		
M_1	θ	β	p_2/p_1	M_2	β	p_2/p_1	M_2
2.30	11	35.33	1.897	1.872	84.49	5.948	0.559
2.30	12	36.35	2.002	1.833	83.93	5.936	0.564
2.30	13	37.42	2.112	1.792	83.36	5.922	0.569
2.30	14	38.51	2.226	1.751	82.77	5.907	0.576
2.30	15	39.64	2.345	1.710	82.15	5.890	0.583
2.30	16	40.82	2.470	1.668	81.51	5.870	0.591
2.30	17	42.03	2.600	1.625	80.84	5.849	0.599
2.30	18	43.30	2.736	1.580	80.14	5.824	0.609
2.30	19	44.62	2.878	1.535	79.39	5.796	0.620
2.30	20	46.01	3.028	1.488	78.58	5.763	0.633
2.30	21	47.47	3.185	1.440	77.72	5.726	0.647
2.30	22	49.03	3.351	1.389	76.77	5.682	0.663
2.30	23	50.70	3.529	1.336	75.72	5.629	0.683
2.30	24	52.54	3.721	1.279	74.51	5.565	0.706
2.30	25	54.61	3.934	1.216	73.09	5.482	0.735
2.30	26	57.08	4.182	1.143	71.27	5.368	0.774
2.30	27	60.55	4.513	1.044	68.46	5.173	0.839
2.40	0	24.60	0.998	2.401	89.99	6.553	0.523
2.40	1	25.36	1.066	2.359	89.55	6.553	0.523
2.40	2	26.12	1.136	2.318	89.10	6.552	0.524
2.40	3	26.90	1.209	2.278	88.64	6.550	0.525
2.40	4	27.70	1.286	2.238	88.18	6.547	0.526
2.40	5	28.53	1.366	2.199	87.72	6.543	0.528
2.40	6	29.38	1.450	2.159	87.26	6.538	0.530
2.40	7	30.25	1.539	2.119	86.79	6.532	0.532
2.40	8	31.15	1.631	2.079	86.31	6.525	0.535
2.40	9	32.07	1.728	2.040	85.82	6.518	0.538
2.40	10	33.02	1.829	1.999	85.33	6.509	0.542
2.40	11	34.00	1.935	1.959	84.82	6.499	0.546
2.40	12	35.01	2.045	1.918	84.30	6.487	0.550
2.40	13	36.04	2.160	1.877	83.77	6.474	0.556
2.40	14	37.11	2.280	1.835	83.22	6.460	0.561
2.40	15	38.21	2.405	1.793	82.65	6.443	0.568
2.40	16	39.35	2.535	1.750	82.06	6.425	0.575
2.40	17	40.53	2.671	1.706	81.45	6.405	0.583
2.40	18	41.75	2.813	1.661	80.80	6.382	0.592
2.40	19	43.02	2.961	1.616	80.12	6.356	0.602
2.40	20	44.34	3.115	1.569	79.40	6.326	0.613
2.40	21	45.72	3.277	1.521	78.63	6.292	0.625
2.40	22	47.17	3.448	1.471	77.80	6.253	0.640

(*Contd.*)

Scanned by CamScanner

TABLE A3 Oblique Shock in Perfect Gas ($\gamma = 1.4$) (*contd.*)

		Weak solution			*Strong solution*		
M_1	θ	β	p_2/p_1	M_2	β	p_2/p_1	M_2
2.40	23	48.72	3.628	1.419	76.90	6.208	0.656
2.40	24	50.37	3.819	1.364	75.89	6.154	0.675
2.40	25	52.17	4.026	1.306	74.75	6.088	0.698
2.40	26	54.18	4.252	1.243	73.40	6.005	0.726
2.40	27	56.54	4.511	1.170	71.72	5.892	0.763
2.40	28	59.65	4.838	1.078	69.29	5.713	0.820
2.50	0	23.56	0.998	2.501	89.99	7.125	0.513
2.50	1	24.30	1.068	2.457	89.57	7.125	0.513
2.50	2	25.05	1.140	2.415	89.14	7.123	0.514
2.50	3	25.82	1.216	2.374	88.71	7.121	0.514
2.50	4	26.61	1.296	2.333	88.28	7.118	0.516
2.50	5	27.42	1.380	2.292	87.84	7.115	0.517
2.50	6	28.26	1.468	2.251	87.40	7.110	0.519
2.50	7	29.12	1.560	2.210	86.96	7.104	0.521
2.50	8	30.01	1.657	2.169	86.50	7.098	0.524
2.50	9	30.92	1.758	2.127	86.05	7.090	0.527
2.50	10	31.85	1.864	2.086	85.58	7.082	0.530
2.50	11	32.81	1.974	2.044	85.10	7.072	0.534
2.50	12	33.80	2.090	2.002	84.61	7.061	0.539
2.50	13	34.82	2.211	1.960	84.11	7.048	0.544
2.50	14	35.87	2.336	1.917	83.60	7.034	0.549
2.50	15	36.95	2.467	1.874	83.07	7.019	0.555
2.50	16	38.06	2.604	1.830	82.52	7.001	0.562
2.50	17	39.20	2.746	1.785	81.95	6.982	0.569
2.50	18	40.39	2.895	1.739	81.35	6.960	0.577
2.50	19	41.62	3.049	1.693	80.73	6.936	0.586
2.50	20	42.89	3.211	1.646	80.07	6.908	0.596
2.50	21	44.22	3.379	1.597	79.37	6.877	0.607
2.50	22	45.60	3.556	1.548	78.63	6.841	0.620
2.50	23	47.06	3.741	1.496	77.82	6.800	0.634
2.50	24	48.60	3.936	1.443	76.94	6.753	0.651
2.50	25	50.25	4.143	1.387	75.96	6.696	0.670
2.50	26	52.04	4.365	1.327	74.86	6.627	0.693
2.50	27	54.02	4.609	1.262	73.56	6.541	0.721
2.50	28	56.33	4.884	1.189	71.95	6.425	0.757
2.50	29	59.31	5.225	1.098	69.68	6.246	0.812
2.60	0	22.60	0.998	2.601	89.99	7.720	0.504
2.60	1	23.34	1.071	2.556	89.59	7.720	0.504
2.60	2	24.07	1.145	2.512	89.18	7.718	0.505
2.60	3	24.83	1.224	2.469	88.77	7.716	0.505

(*Contd.*)

Scanned by CamScanner

TABLE A3 Oblique Shock in Perfect Gas ($\gamma = 1.4$) (*contd.*)

		Weak solution			*Strong solution*		
M_1	θ	β	p_2/p_1	M_2	β	p_2/p_1	M_2
2.60	4	25.61	1.307	2.427	88.36	7.714	0.506
2.60	5	26.42	1.394	2.384	87.95	7.710	0.508
2.60	6	27.24	1.486	2.342	87.53	7.705	0.510
2.60	7	28.09	1.582	2.299	87.10	7.700	0.512
2.60	8	28.97	1.683	2.257	86.67	7.693	0.514
2.60	9	29.87	1.789	2.214	86.24	7.686	0.517
2.60	10	30.79	1.900	2.172	85.79	7.678	0.520
2.60	11	31.74	2.016	2.129	85.34	7.668	0.524
2.60	12	32.71	2.137	2.085	84.88	7.657	0.528
2.60	13	33.72	2.263	2.041	84.41	7.645	0.533
2.60	14	34.75	2.395	1.997	83.92	7.632	0.538
2.60	15	35.81	2.533	1.953	83.42	7.616	0.543
2.60	16	36.90	2.677	1.908	82.91	7.600	0.550
2.60	17	38.03	2.826	1.862	82.37	7.581	0.557
2.60	18	39.19	2.982	1.815	81.82	7.560	0.564
2.60	19	40.38	3.144	1.768	81.24	7.537	0.572
2.60	20	41.62	3.313	1.720	80.63	7.511	0.582
2.60	21	42.91	3.489	1.671	79.98	7.481	0.592
2.60	22	44.24	3.672	1.621	79.30	7.448	0.604
2.60	23	45.64	3.864	1.569	78.57	7.410	0.616
2.60	24	47.10	4.066	1.516	77.78	7.367	0.631
2.60	25	48.65	4.278	1.460	76.92	7.316	0.648
2.60	26	50.31	4.503	1.403	75.96	7.255	0.667
2.60	27	52.10	4.744	1.341	74.87	7.182	0.690
2.60	28	54.09	5.007	1.274	73.59	7.091	0.719
2.60	29	56.39	5.304	1.199	72.01	6.967	0.756
2.60	30	59.35	5.670	1.106	69.78	6.778	0.811
2.70	0	21.72	0.998	2.701	89.99	8.338	0.496
2.70	1	22.44	1.073	2.654	89.61	8.338	0.496
2.70	2	23.17	1.150	2.609	89.22	8.337	0.496
2.70	3	23.92	1.232	2.564	88.83	8.335	0.497
2.70	4	24.70	1.318	2.520	88.43	8.332	0.498
2.70	5	25.49	1.409	2.476	88.03	8.328	0.499
2.70	6	26.31	1.504	2.432	87.63	8.324	0.501
2.70	7	27.15	1.605	2.388	87.23	8.318	0.503
2.70	8	28.02	1.710	2.344	86.82	8.312	0.506
2.70	9	28.91	1.821	2.300	86.40	8.305	0.508
2.70	10	29.82	1.937	2.256	85.98	8.296	0.511
2.70	11	30.76	2.058	2.212	85.55	8.287	0.515
2.70	12	31.73	2.185	2.167	85.11	8.276	0.519

(*Contd.*)

Scanned by CamScanner

TABLE A3 Oblique Shock in Perfect Gas ($\gamma = 1.4$) (*contd.*)

		Weak solution			*Strong solution*		
M_1	θ	β	p_2/p_1	M_2	β	p_2/p_1	M_2
2.70	13	32.72	2.318	2.122	84.66	8.265	0.523
2.70	14	33.74	2.457	2.076	84.20	8.251	0.528
2.70	15	34.79	2.601	2.030	83.73	8.237	0.533
2.70	16	35.86	2.752	1.984	83.24	8.220	0.539
2.70	17	36.97	2.909	1.937	82.74	8.202	0.546
2.70	18	38.11	3.073	1.889	82.21	8.182	0.553
2.70	19	39.28	3.243	1.841	81.67	8.160	0.560
2.70	20	40.50	3.420	1.792	81.10	8.135	0.569
2.70	21	41.75	3.604	1.742	80.50	8.106	0.579
2.70	22	43.05	3.796	1.691	79.86	8.075	0.589
2.70	23	44.40	3.997	1.638	79.19	8.039	0.601
2.70	24	45.81	4.206	1.585	78.47	7.998	0.614
2.70	25	47.29	4.425	1.530	77.69	7.951	0.630
2.70	26	48.85	4.656	1.472	76.83	7.897	0.647
2.70	27	50.52	4.900	1.412	75.88	7.832	0.667
2.70	28	52.33	5.162	1.349	74.79	7.753	0.691
2.70	29	54.35	5.449	1.280	73.51	7.653	0.720
2.70	30	56.69	5.773	1.202	71.92	7.519	0.759
2.70	31	59.72	6.176	1.104	69.63	7.307	0.817
2.80	0	20.91	0.998	2.801	89.99	8.980	0.488
2.80	1	21.62	1.075	2.752	89.63	8.980	0.488
2.80	2	22.34	1.155	2.706	89.25	8.978	0.489
2.80	3	23.09	1.240	2.659	88.87	8.976	0.489
2.80	4	23.85	1.329	2.613	88.49	8.974	0.491
2.80	5	24.64	1.423	2.568	88.11	8.970	0.492
2.80	6	25.46	1.523	2.522	87.73	8.966	0.493
2.80	7	26.29	1.628	2.477	87.34	8.960	0.495
2.80	8	27.15	1.738	2.431	86.95	8.954	0.498
2.80	9	28.03	1.854	2.386	86.55	8.947	0.500
2.80	10	28.94	1.975	2.340	86.14	8.939	0.503
2.80	11	29.87	2.102	2.294	85.73	8.929	0.507
2.80	12	30.83	2.236	2.248	85.31	8.919	0.510
2.80	13	31.81	2.375	2.201	84.88	8.907	0.514
2.80	14	32.82	2.520	2.154	84.44	8.894	0.519
2.80	15	33.86	2.672	2.107	83.99	8.880	0.524
2.80	16	34.92	2.831	2.059	83.53	8.864	0.530
2.80	17	36.02	2.996	2.010	83.05	8.846	0.536
2.80	18	37.14	3.168	1.961	82.55	8.826	0.543
2.80	19	38.30	3.346	1.911	82.04	8.804	0.550
2.80	20	39.49	3.532	1.861	81.50	8.780	0.558

(*Contd.*)

Scanned by CamScanner

TABLE A3 Oblique Shock in Perfect Gas ($\gamma = 1.4$) (*contd.*)

		Weak solution			*Strong solution*		
M_1	θ	β	p_2/p_1	M_2	β	p_2/p_1	M_2
2.80	21	40.72	3.726	1.810	80.93	8.753	0.567
2.80	22	41.99	3.927	1.758	80.34	8.722	0.577
2.80	23	43.31	4.136	1.705	79.71	8.688	0.588
2.80	24	44.68	4.355	1.651	79.04	8.649	0.600
2.80	25	46.10	4.583	1.595	78.33	8.605	0.614
2.80	26	47.60	4.822	1.538	77.55	8.554	0.630
2.80	27	49.19	5.073	1.479	76.69	8.495	0.648
2.80	28	50.89	5.340	1.416	75.73	8.424	0.668
2.80	29	52.73	5.625	1.350	74.63	8.337	0.693
2.80	30	54.79	5.938	1.278	73.33	8.227	0.724
2.80	31	57.20	6.295	1.197	71.68	8.076	0.766
2.80	32	60.43	6.752	1.091	69.21	7.828	0.831
2.90	0	20.15	0.998	2.901	89.99	9.645	0.481
2.90	1	20.86	1.078	2.851	89.64	9.645	0.482
2.90	2	21.58	1.160	2.802	89.28	9.643	0.482
2.90	3	22.32	1.248	2.754	88.91	9.641	0.483
2.90	4	23.08	1.341	2.706	88.55	9.639	0.484
2.90	5	23.86	1.439	2.659	88.18	9.635	0.485
2.90	6	24.67	1.542	2.612	87.81	9.631	0.486
2.90	7	25.50	1.651	2.565	87.44	9.625	0.488
2.90	8	26.35	1.766	2.518	87.06	9.619	0.491
2.90	9	27.23	1.887	2.470	86.67	9.612	0.493
2.90	10	28.13	2.014	2.423	86.28	9.604	0.496
2.90	11	29.06	2.148	2.375	85.89	9.595	0.499
2.90	12	30.01	2.287	2.327	85.49	9.584	0.503
2.90	13	30.98	2.433	2.279	85.07	9.573	0.507
2.90	14	31.99	2.586	2.230	84.65	9.560	0.511
2.90	15	33.01	2.746	2.181	84.22	9.545	0.516
2.90	16	34.07	2.912	2.132	83.78	9.530	0.521
2.90	17	35.15	3.086	2.082	83.32	9.512	0.527
2.90	18	36.26	3.266	2.031	82.85	9.493	0.533
2.90	19	37.41	3.454	1.980	82.36	9.471	0.540
2.90	20	38.58	3.649	1.928	81.85	9.447	0.548
2.90	21	39.80	3.853	1.876	81.31	9.421	0.557
2.90	22	41.04	4.064	1.823	80.75	9.391	0.566
2.90	23	42.34	4.283	1.769	80.16	9.358	0.576
2.90	24	43.67	4.512	1.714	79.54	9.321	0.588
2.90	25	45.06	4.750	1.658	78.87	9.279	0.601
2.90	26	46.51	4.998	1.600	78.14	9.231	0.615
2.90	27	48.04	5.258	1.540	77.36	9.175	0.631

(*Contd.*)

Scanned by CamScanner

TABLE A3 Oblique Shock in Perfect Gas ($\gamma = 1.4$) (*contd.*)

		Weak solution			*Strong solution*		
M_1	θ	β	p_2/p_1	M_2	β	p_2/p_1	M_2
2.90	28	49.65	5.533	1.479	76.49	9.109	0.650
2.90	29	51.39	5.823	1.414	75.52	9.031	0.672
2.90	30	53.27	6.136	1.345	74.39	8.935	0.699
2.90	31	55.40	6.480	1.270	73.04	8.810	0.732
2.90	32	57.93	6.879	1.183	71.29	8.635	0.777
2.90	33	61.57	7.420	1.063	68.44	8.319	0.855
3.00	0	19.45	0.998	3.001	89.99	10.333	0.475
3.00	1	20.16	1.080	2.949	89.65	10.333	0.475
3.00	2	20.87	1.165	2.898	89.30	10.332	0.476
3.00	3	21.60	1.256	2.848	88.95	10.330	0.476
3.00	4	22.35	1.352	2.799	88.60	10.327	0.477
3.00	5	23.13	1.454	2.750	88.24	10.323	0.479
3.00	6	23.94	1.562	2.701	87.88	10.319	0.480
3.00	7	24.76	1.675	2.652	87.52	10.314	0.482
3.00	8	25.61	1.795	2.603	87.16	10.307	0.484
3.00	9	26.49	1.922	2.554	86.79	10.300	0.486
3.00	10	27.38	2.054	2.505	86.41	10.292	0.489
3.00	11	28.30	2.194	2.456	86.03	10.283	0.492
3.00	12	29.25	2.340	2.406	85.64	10.273	0.496
3.00	13	30.22	2.494	2.356	85.24	10.261	0.500
3.00	14	31.22	2.654	2.306	84.84	10.248	0.504
3.00	15	32.24	2.821	2.255	84.42	10.234	0.508
3.00	16	33.29	2.996	2.204	84.00	10.218	0.514
3.00	17	34.36	3.179	2.152	83.56	10.201	0.519
3.00	18	35.47	3.368	2.100	83.11	10.182	0.525
3.00	19	36.60	3.566	2.047	82.64	10.161	0.532
3.00	20	37.76	3.771	1.994	82.15	10.137	0.539
3.00	21	38.96	3.984	1.940	81.64	10.111	0.547
3.00	22	40.19	4.206	1.886	81.11	10.082	0.556
3.00	23	41.46	4.436	1.831	80.55	10.050	0.566
3.00	24	42.78	4.676	1.774	79.96	10.014	0.577
3.00	25	44.14	4.925	1.717	79.33	9.973	0.589
3.00	26	45.55	5.184	1.659	78.65	9.927	0.602
3.00	27	47.03	5.455	1.599	77.92	9.874	0.617
3.00	28	48.59	5.739	1.537	77.13	9.812	0.635
3.00	29	50.24	6.038	1.473	76.24	9.739	0.654
3.00	30	52.01	6.356	1.406	75.24	9.652	0.678
3.00	31	53.96	6.699	1.334	74.07	9.542	0.706
3.00	32	56.18	7.081	1.254	72.64	9.399	0.743
3.00	33	58.91	7.533	1.160	70.71	9.188	0.794

(*Contd.*)

Scanned by CamScanner

TABLE A3 Oblique Shock in Perfect Gas ($\gamma = 1.4$) (*contd.*)

		Weak solution			*Strong solution*		
M_1	θ	β	p_2/p_1	M_2	β	p_2/p_1	M_2
3.00	34	63.67	8.267	1.003	66.75	8.697	0.908
3.10	0	18.80	0.998	3.102	89.99	11.045	0.470
3.10	1	19.50	1.083	3.047	89.66	11.045	0.470
3.10	2	20.20	1.171	2.994	89.32	11.043	0.470
3.10	3	20.93	1.264	2.942	88.98	11.041	0.471
3.10	4	21.68	1.364	2.891	88.64	11.039	0.472
3.10	5	22.46	1.470	2.840	88.30	11.035	0.473
3.10	6	23.26	1.581	2.789	87.95	11.031	0.474
3.10	7	24.08	1.700	2.739	87.60	11.025	0.476
3.10	8	24.93	1.825	2.688	87.24	11.019	0.478
3.10	9	25.80	1.957	2.637	86.89	11.012	0.480
3.10	10	26.69	2.096	2.586	86.52	11.004	0.483
3.10	11	27.61	2.241	2.535	86.15	10.994	0.486
3.10	12	28.55	2.395	2.484	85.78	10.984	0.489
3.10	13	29.52	2.555	2.432	85.39	10.973	0.493
3.10	14	30.51	2.724	2.380	85.00	10.960	0.497
3.10	15	31.53	2.899	2.327	84.60	10.946	0.502
3.10	16	32.57	3.083	2.274	84.19	10.930	0.507
3.10	17	33.64	3.274	2.221	83.77	10.913	0.512
3.10	18	34.74	3.474	2.167	83.33	10.894	0.518
3.10	19	35.86	3.681	2.113	82.88	10.873	0.524
3.10	20	37.02	3.897	2.058	82.42	10.850	0.531
3.10	21	38.20	4.121	2.003	81.93	10.824	0.539
3.10	22	39.42	4.354	1.947	81.42	10.795	0.548
3.10	23	40.67	4.596	1.890	80.89	10.764	0.557
3.10	24	41.97	4.847	1.833	80.33	10.728	0.567
3.10	25	43.31	5.108	1.775	79.73	10.688	0.578
3.10	26	44.69	5.379	1.715	79.09	10.643	0.591
3.10	27	46.14	5.661	1.655	78.41	10.592	0.605
3.10	28	47.65	5.956	1.593	77.67	10.533	0.621
3.10	29	49.24	6.265	1.529	76.85	10.465	0.639
3.10	30	50.93	6.592	1.462	75.94	10.383	0.661
3.10	31	52.77	6.940	1.392	74.90	10.284	0.686
3.10	32	54.80	7.319	1.316	73.66	10.158	0.717
3.10	33	57.15	7.747	1.230	72.11	9.987	0.758
3.10	34	60.20	8.276	1.124	69.87	9.717	0.820
3.20	0	18.19	0.998	3.202	89.99	11.780	0.464
3.20	1	18.89	1.085	3.145	89.67	11.780	0.464
3.20	2	19.59	1.176	3.090	89.34	11.778	0.465
3.20	3	20.31	1.273	3.036	89.01	11.776	0.466

(*Contd.*)

Scanned by CamScanner

TABLE A3 Oblique Shock in Perfect Gas ($\gamma = 1.4$) (*contd.*)

		Weak solution			*Strong solution*		
M_1	θ	β	p_2/p_1	M_2	β	p_2/p_1	M_2
3.20	4	21.06	1.376	2.983	88.68	11.774	0.466
3.20	5	21.83	1.485	2.930	88.34	11.770	0.468
3.20	6	22.63	1.602	2.878	88.01	11.765	0.469
3.20	7	23.45	1.725	2.825	87.67	11.760	0.471
3.20	8	24.29	1.855	2.773	87.32	11.754	0.473
3.20	9	25.16	1.993	2.720	86.97	11.747	0.475
3.20	10	26.05	2.138	2.667	86.62	11.738	0.478
3.20	11	26.97	2.290	2.614	86.26	11.729	0.480
3.20	12	27.91	2.451	2.561	85.90	11.719	0.484
3.20	13	28.87	2.619	2.507	85.53	11.707	0.487
3.20	14	29.86	2.795	2.453	85.15	11.694	0.491
3.20	15	30.88	2.980	2.398	84.76	11.680	0.496
3.20	16	31.92	3.172	2.344	84.36	11.665	0.500
3.20	17	32.98	3.373	2.289	83.96	11.647	0.506
3.20	18	34.07	3.583	2.233	83.54	11.628	0.511
3.20	19	35.19	3.801	2.177	83.10	11.608	0.517
3.20	20	36.34	4.027	2.121	82.65	11.584	0.524
3.20	21	37.51	4.263	2.064	82.18	11.559	0.532
3.20	22	38.72	4.507	2.006	81.70	11.531	0.540
3.20	23	39.96	4.761	1.948	81.19	11.499	0.549
3.20	24	41.24	5.024	1.889	80.65	11.464	0.558
3.20	25	42.56	5.297	1.830	80.08	11.425	0.569
3.20	26	43.92	5.581	1.770	79.48	11.381	0.581
3.20	27	45.34	5.876	1.708	78.83	11.332	0.595
3.20	28	46.81	6.184	1.645	78.13	11.275	0.610
3.20	29	48.36	6.505	1.581	77.37	11.209	0.627
3.20	30	49.99	6.842	1.514	76.53	11.131	0.646
3.20	31	51.74	7.200	1.445	75.58	11.039	0.669
3.20	32	53.65	7.583	1.371	74.48	10.924	0.697
3.20	33	55.79	8.004	1.291	73.15	10.776	0.731
3.20	34	58.35	8.490	1.198	71.41	10.566	0.779
3.20	35	62.06	9.157	1.069	68.52	10.178	0.863
3.30	0	17.62	0.998	3.302	89.99	12.538	0.460
3.30	1	18.31	1.088	3.242	89.68	12.538	0.460
3.30	2	19.01	1.181	3.186	89.36	12.537	0.460
3.30	3	19.73	1.281	3.130	89.04	12.535	0.461
3.30	4	20.48	1.388	3.075	88.71	12.532	0.462
3.30	5	21.25	1.501	3.020	88.39	12.528	0.463
3.30	6	22.04	1.622	2.965	88.06	12.524	0.464
3.30	7	22.86	1.750	2.911	87.73	12.518	0.466

(*Contd.*)

Scanned by CamScanner

TABLE A3 Oblique Shock in Perfect Gas ($\gamma = 1.4$) (*contd.*)

		Weak solution			*Strong solution*		
M_1	θ	β	p_2/p_1	M_2	β	p_2/p_1	M_2
3.30	8	23.70	1.886	2.856	87.39	12.512	0.468
3.30	9	24.57	2.029	2.802	87.05	12.505	0.470
3.30	10	25.46	2.181	2.747	86.71	12.496	0.472
3.30	11	26.37	2.340	2.692	86.36	12.487	0.475
3.30	12	27.31	2.508	2.636	86.01	12.477	0.478
3.30	13	28.27	2.684	2.581	85.65	12.465	0.482
3.30	14	29.26	2.869	2.525	85.28	12.452	0.486
3.30	15	30.27	3.062	2.469	84.90	12.438	0.490
3.30	16	31.31	3.264	2.412	84.52	12.422	0.495
3.30	17	32.37	3.475	2.355	84.12	12.405	0.500
3.30	18	33.46	3.695	2.297	83.72	12.386	0.505
3.30	19	34.57	3.923	2.240	83.30	12.365	0.511
3.30	20	35.71	4.161	2.181	82.86	12.342	0.518
3.30	21	36.88	4.409	2.123	82.41	12.317	0.525
3.30	22	38.08	4.665	2.064	81.94	12.288	0.533
3.30	23	39.31	4.932	2.004	81.45	12.257	0.541
3.30	24	40.57	5.208	1.944	80.93	12.223	0.551
3.30	25	41.88	5.494	1.883	80.39	12.184	0.561
3.30	26	43.22	5.792	1.822	79.81	12.141	0.572
3.30	27	44.61	6.100	1.759	79.20	12.092	0.585
3.30	28	46.06	6.421	1.696	78.54	12.036	0.599
3.30	29	47.57	6.755	1.631	77.82	11.973	0.615
3.30	30	49.16	7.105	1.564	77.03	11.898	0.634
3.30	31	50.85	7.474	1.495	76.15	11.810	0.655
3.30	32	52.67	7.865	1.422	75.15	11.704	0.680
3.30	33	54.67	8.289	1.344	73.97	11.569	0.710
3.30	34	56.96	8.762	1.258	72.50	11.390	0.750
3.30	35	59.85	9.333	1.153	70.45	11.115	0.809
3.40	0	17.09	0.998	3.402	89.99	13.320	0.455
3.40	1	17.77	1.090	3.340	89.69	13.320	0.455
3.40	2	18.47	1.187	3.281	89.37	13.318	0.456
3.40	3	19.19	1.290	3.224	89.06	13.316	0.456
3.40	4	19.93	1.400	3.166	88.74	13.313	0.457
3.40	5	20.70	1.518	3.109	88.43	13.310	0.458
3.40	6	21.49	1.643	3.053	88.10	13.305	0.460
3.40	7	22.31	1.776	2.996	87.78	13.300	0.461
3.40	8	23.15	1.917	2.940	87.46	13.293	0.463
3.40	9	24.01	2.067	2.883	87.13	13.286	0.465
3.40	10	24.90	2.224	2.826	86.79	13.278	0.468
3.40	11	25.82	2.391	2.769	86.45	13.268	0.471

(*Contd.*)

Scanned by CamScanner

TABLE A3 Oblique Shock in Perfect Gas ($\gamma = 1.4$) (*contd.*)

		Weak solution			*Strong solution*		
M_1	θ	β	p_2/p_1	M_2	β	p_2/p_1	M_2
3.40	12	26.75	2.566	2.712	86.11	13.258	0.474
3.40	13	27.72	2.751	2.654	85.76	13.246	0.477
3.40	14	28.70	2.944	2.596	85.40	13.233	0.481
3.40	15	29.71	3.146	2.537	85.03	13.219	0.485
3.40	16	30.75	3.358	2.479	84.66	13.203	0.489
3.40	17	31.81	3.579	2.420	84.27	13.186	0.494
3.40	18	32.89	3.810	2.360	83.88	13.166	0.500
3.40	19	34.00	4.050	2.301	83.47	13.145	0.506
3.40	20	35.13	4.300	2.241	83.05	13.122	0.512
3.40	21	36.30	4.559	2.180	82.61	13.097	0.519
3.40	22	37.49	4.829	2.120	82.16	13.069	0.526
3.40	23	38.71	5.108	2.058	81.68	13.038	0.535
3.40	24	39.97	5.398	1.997	81.19	13.003	0.544
3.40	25	41.26	5.698	1.934	80.66	12.965	0.554
3.40	26	42.59	6.009	1.872	80.11	12.922	0.565
3.40	27	43.96	6.332	1.808	79.52	12.874	0.577
3.40	28	45.39	6.667	1.744	78.89	12.819	0.590
3.40	29	46.87	7.016	1.678	78.21	12.757	0.605
3.40	30	48.42	7.380	1.611	77.47	12.685	0.623
3.40	31	50.06	7.761	1.541	76.65	12.600	0.642
3.40	32	51.81	8.164	1.469	75.72	12.499	0.665
3.40	33	53.71	8.595	1.393	74.65	12.374	0.693
3.40	34	55.84	9.067	1.310	73.35	12.213	0.728
3.40	35	58.36	9.608	1.215	71.67	11.986	0.775
3.40	36	61.91	10.330	1.088	68.96	11.582	0.856
3.50	0	16.58	0.997	3.502	89.99	14.125	0.451
3.50	1	17.27	1.092	3.438	89.70	14.125	0.451
3.50	2	17.96	1.192	3.377	89.39	14.123	0.452
3.50	3	18.67	1.298	3.317	89.08	14.121	0.452
3.50	4	19.42	1.412	3.257	88.77	14.118	0.453
3.50	5	20.18	1.534	3.198	88.46	14.115	0.454
3.50	6	20.97	1.664	3.140	88.15	14.110	0.456
3.50	7	21.79	1.802	3.081	87.83	14.104	0.457
3.50	8	22.63	1.949	3.022	87.51	14.098	0.459
3.50	9	23.49	2.105	2.963	87.19	14.091	0.461
3.50	10	24.38	2.269	2.904	86.86	14.082	0.463
3.50	11	25.30	2.443	2.845	86.53	14.073	0.466
3.50	12	26.24	2.626	2.786	86.20	14.062	0.469
3.50	13	27.20	2.819	2.726	85.85	14.050	0.473
3.50	14	28.18	3.021	2.666	85.50	14.037	0.476

(*Contd.*)

Scanned by CamScanner

TABLE A3 Oblique Shock in Perfect Gas ($\gamma = 1.4$) (*contd.*)

		Weak solution			Strong solution		
M_1	θ	β	p_2/p_1	M_2	β	p_2/p_1	M_2
3.50	15	29.19	3.233	2.605	85.15	14.023	0.480
3.50	16	30.22	3.455	2.545	84.78	14.007	0.485
3.50	17	31.28	3.686	2.484	84.41	13.989	0.489
3.50	18	32.36	3.928	2.422	84.02	13.970	0.495
3.50	19	33.47	4.180	2.361	83.63	13.949	0.500
3.50	20	34.60	4.442	2.299	83.22	13.926	0.506
3.50	21	35.76	4.714	2.236	82.79	13.900	0.513
3.50	22	36.95	4.997	2.174	82.35	13.872	0.521
3.50	23	38.16	5.290	2.111	81.90	13.841	0.529
3.50	24	39.41	5.593	2.048	81.41	13.806	0.537
3.50	25	40.69	5.908	1.984	80.91	13.768	0.547
3.50	26	42.01	6.234	1.920	80.38	13.725	0.557
3.50	27	43.37	6.572	1.855	79.81	13.678	0.569
3.50	28	44.77	6.922	1.789	79.21	13.624	0.582
3.50	29	46.23	7.286	1.723	78.56	13.562	0.596
3.50	30	47.76	7.665	1.655	77.85	13.492	0.613
3.50	31	49.36	8.061	1.585	77.08	13.410	0.631
3.50	32	51.05	8.477	1.513	76.21	13.313	0.653
3.50	33	52.88	8.919	1.438	75.22	13.194	0.678
3.50	34	54.89	9.396	1.357	74.05	13.046	0.710
3.50	35	57.19	9.928	1.268	72.59	12.846	0.750
3.50	36	60.09	10.571	1.159	70.55	12.539	0.810
3.60	0	16.11	0.997	3.602	89.99	14.953	0.447
3.60	1	16.79	1.095	3.536	89.70	14.953	0.448
3.60	2	17.48	1.197	3.472	89.40	14.952	0.448
3.60	3	18.19	1.307	3.410	89.10	14.950	0.448
3.66	4	18.93	1.425	3.348	88.80	14.947	0.449
3.60	5	19.70	1.551	3.287	88.49	14.943	0.450
3.60	6	20.49	1.686	3.226	88.19	14.938	0.452
3.60	7	21.30	1.829	3.165	87.88	14.933	0.453
3.60	8	22.14	1.981	3.104	87.56	14.926	0.455
3.60	9	23.01	2.143	3.043	87.25	14.918	0.457
3.60	10	23.90	2.315	2.982	86.93	14.910	0.460
3.60	11	24.81	2.496	2.921	86.61	14.900	0.462
3.60	12	25.75	2.687	2.859	86.28	14.889	0.465
3.60	13	26.71	2.888	2.797	85.94	14.878	0.468
3.60	14	27.70	3.100	2.735	85.60	14.864	0.472
3.60	15	28.71	3.322	2.672	85.25	14.850	0.476
3.60	16	29.74	3.554	2.609	84.90	14.834	0.480
3.60	17	30.80	3.796	2.546	84.53	14.816	0.485

(*Contd.*)

Scanned by CamScanner

TABLE A3 Oblique Shock in Perfect Gas ($\gamma = 1.4$) (*contd.*)

		Weak solution			*Strong solution*		
M_1	θ	β	p_2/p_1	M_2	β	p_2/p_1	M_2
3.60	18	31.88	4.050	2.483	84.16	14.796	0.490
3.60	19	32.98	4.314	2.419	83.77	14.775	0.495
3.60	20	34.11	4.588	2.355	83.37	14.752	0.501
3.60	21	35.27	4.873	2.291	82.96	14.726	0.508
3.60	22	36.45	5.170	2.227	82.53	14.698	0.515
3.60	23	37.66	5.477	2.162	82.08	14.666	0.523
3.60	24	38.90	5.795	2.097	81.62	14.632	0.531
3.60	25	40.17	6.125	2.032	81.13	14.594	0.541
3.60	26	41.48	6.466	1.966	80.62	14.551	0.551
3.60	27	42.83	6.820	1.900	80.07	14.504	0.562
3.60	28	44.22	7.186	1.834	79.49	14.450	0.575
3.60	29	45.65	7.566	1.766	78.87	14.389	0.588
3.60	30	47.15	7.961	1.697	78.19	14.320	0.604
3.60	31	48.72	8.372	1.627	77.45	14.240	0.622
3.60	32	50.38	8.803	1.555	76.64	14.145	0.642
3.60	33	52.14	9.259	1.480	75.71	14.032	0.666
3.60	34	54.07	9.746	1.400	74.64	13.892	0.695
3.60	35	56.22	10.279	1.314	73.33	13.709	0.731
3.60	36	58.79	10.894	1.215	71.62	13.450	0.780
3.60	37	62.54	11.738	1.078	68.73	12.963	0.869
3.70	0	15.66	0.997	3.702	89.99	15.805	0.444
3.70	1	16.34	1.098	3.633	89.71	15.805	0.444
3.70	2	17.03	1.203	3.567	89.41	15.803	0.444
3.70	3	17.74	1.316	3.503	89.12	15.801	0.445
3.70	4	18.48	1.438	3.439	88.82	15.798	0.446
3.70	5	19.24	1.568	3.375	88.52	15.794	0.447
3.70	6	20.03	1.707	3.312	88.22	15.790	0.448
3.70	7	20.85	1.856	3.249	87.92	15.784	0.450
3.70	8	21.69	2.014	3.186	87.61	15.777	0.451
3.70	9	22.55	2.183	3.123	87.30	15.770	0.454
3.70	10	23.44	2.361	3.059	86.99	15.761	0.456
3.70	11	24.36	2.550	2.995	86.67	15.751	0.458
3.70	12	25.30	2.750	2.931	86.35	15.740	0.461
3.70	13	26.26	2.960	2.867	86.02	15.728	0.464
3.70	14	27.25	3.181	2.803	85.69	15.715	0.468
3.70	15	28.25	3.412	2.738	85.35	15.700	0.472
3.70	16	29.29	3.655	2.673	85.00	15.684	0.476
3.70	17	30.34	3.909	2.608	84.64	15.666	0.481
3.70	18	31.42	4.174	2.542	84.28	15.646	0.486
3.70	19	32.53	4.451	2.476	83.90	15.624	0.491

(*Contd.*)

Scanned by CamScanner

TABLE A3 Oblique Shock in Perfect Gas ($\gamma = 1.4$) (*contd.*)

		Weak solution			*Strong solution*		
M_1	θ	β	p_2/p_1	M_2	β	p_2/p_1	M_2
3.70	20	33.65	4.738	2.411	83.51	15.601	0.497
3.70	21	34.81	5.037	2.344	83.11	15.575	0.503
3.70	22	35.99	5.347	2.278	82.69	15.546	0.510
3.70	23	37.19	5.669	2.212	82.26	15.515	0.518
3.70	24	38.43	6.002	2.145	81.80	15.480	0.526
3.70	25	39.69	6.348	2.079	81.33	15.442	0.535
3.70	26	40.99	6.705	2.011	80.83	15.399	0.545
3.70	27	42.33	7.075	1.944	80.30	15.352	0.556
3.70	28	43.70	7.458	1.876	79.74	15.298	0.568
3.70	29	45.13	7.854	1.807	79.14	15.238	0.581
3.70	30	46.61	8.266	1.738	78.49	15.169	0.596
3.70	31	48.15	8.694	1.667	77.79	15.090	0.613
3.70	32	49.77	9.142	1.594	77.01	14.998	0.632
3.70	33	51.49	9.612	1.519	76.14	14.888	0.655
3.70	34	53.34	10.112	1.440	75.14	14.754	0.681
3.70	35	55.39	10.653	1.356	73.95	14.584	0.714
3.70	36	57.76	11.259	1.262	72.44	14.352	0.758
3.70	37	60.82	12.007	1.146	70.25	13.982	0.824
3.80	0	15.24	0.997	3.802	89.99	16.680	0.441
3.80	1	15.92	1.100	3.731	89.71	16.680	0.441
3.80	2	16.60	1.208	3.662	89.42	16.678	0.441
3.80	3	17.31	1.325	3.595	89.13	16.676	0.442
3.80	4	18.05	1.450	3.529	88.84	16.673	0.443
3.80	5	18.81	1.585	3.463	88.55	16.669	0.444
3.80	6	19.60	1.729	3.398	88.25	16.664	0.445
3.80	7	20.42	1.883	3.332	87.96	16.658	0.446
3.80	8	21.26	2.048	3.267	87.66	16.652	0.448
3.80	9	22.13	2.223	3.201	87.35	16.644	0.450
3.80	10	23.02	2.409	3.135	87.05	16.635	0.452
3.80	11	23.93	2.605	3.069	86.73	16.625	0.455
3.80	12	24.87	2.813	3.003	86.42	16.614	0.458
3.80	13	25.83	3.032	2.937	86.10	16.602	0.461
3.80	14	26.82	3.263	2.870	85.77	16.588	0.464
3.80	15	27.83	3.505	2.803	85.44	16.573	0.468
3.80	16	28.86	3.759	2.735	85.09	16.557	0.472
3.80	17	29.92	4.025	2.668	84.74	16.538	0.477
3.80	18	31.00	4.302	2.600	84.39	16.519	0.482
3.80	19	32.10	4.591	2.532	84.02	16.497	0.487
3.80	20	33.23	4.892	2.464	83.64	16.473	0.493
3.80	21	34.38	5.205	2.396	83.24	16.447	0.499

(*Contd.*)

Scanned by CamScanner

TABLE A3 Oblique Shock in Perfect Gas ($\gamma = 1.4$) (*contd.*)

		Weak solution			*Strong solution*		
M_1	θ	β	p_2/p_1	M_2	β	p_2/p_1	M_2
3.80	22	35.56	5.530	2.328	82.84	16.418	0.506
3.80	23	36.76	5.867	2.260	82.41	16.386	0.513
3.80	24	37.99	6.216	2.192	81.97	16.351	0.521
3.80	25	39.25	6.577	2.123	81.51	16.313	0.530
3.80	26	40.54	6.951	2.055	81.02	16.270	0.540
3.80	27	41.87	7.337	1.986	80.51	16.222	0.550
3.80	28	43.23	7.737	1.917	79.97	16.169	0.562
3.80	29	44.64	8.152	1.847	79.39	16.108	0.575
3.80	30	46.10	8.581	1.776	78.76	16.040	0.589
3.80	31	47.63	9.027	1.704	78.09	15.962	0.605
3.80	32	49.22	9.492	1.631	77.34	15.871	0.624
3.80	33	50.90	9.979	1.556	76.52	15.764	0.645
3.80	34	52.70	10.494	1.478	75.57	15.634	0.670
3.80	35	54.67	11.045	1.395	74.47	15.472	0.700
3.80	36	56.89	11.654	1.304	73.12	15.259	0.739
3.80	37	59.60	12.367	1.198	71.28	14.944	0.795
3.80	38	64.18	13.485	1.030	67.57	14.227	0.913
3.90	0	14.84	0.997	3.902	89.99	17.578	0.438
3.90	1	15.51	1.103	3.828	89.72	17.578	0.438
3.90	2	16.20	1.214	3.757	89.43	17.577	0.438
3.90	3	16.91	1.334	3.688	89.15	17.574	0.439
3.90	4	17.64	1.463	3.619	88.86	17.571	0.440
3.90	5	18.41	1.602	3.551	88.57	17.567	0.441
3.90	6	19.20	1.752	3.483	88.28	17.562	0.442
3.90	7	20.01	1.911	3.415	87.99	17.556	0.443
3.90	8	20.85	2.082	3.347	87.70	17.550	0.445
3.90	9	21.72	2.264	3.279	87.40	17.542	0.447
3.90	10	22.61	2.457	3.211	87.10	17.533	0.449
3.90	11	23.53	2.662	3.143	86.79	17.523	0.452
3.90	12	24.47	2.878	3.074	86.48	17.511	0.455
3.90	13	25.44	3.107	3.005	86.16	17.499	0.458
3.90	14	26.42	3.347	2.936	85.84	17.485	0.461
3.90	15	27.43	3.600	2.866	85.51	17.470	0.465
3.90	16	28.47	3.865	2.797	85.18	17.453	0.469
3.90	17	29.53	4.143	2.727	84.84	17.434	0.473
3.90	18	30.61	4.433	2.657	84.49	17.414	0.478
3.90	19	31.71	4.735	2.587	84.12	17.392	0.483
3.90	20	32.83	5.050	2.517	83.75	17.368	0.489
3.90	21	33.98	5.377	2.447	83.37	17.341	0.495
3.90	22	35.16	5.717	2.377	82.97	17.312	0.502

(*Contd.*)

Scanned by CamScanner

TABLE A3 Oblique Shock in Perfect Gas ($\gamma = 1.4$) (*contd.*)

		Weak solution			Strong solution		
M_1	θ	β	p_2/p_1	M_2	β	p_2/p_1	M_2
3.90	23	36.36	6.069	2.307	82.55	17.280	0.509
3.90	24	37.58	6.434	2.237	82.12	17.245	0.517
3.90	25	38.84	6.812	2.167	81.67	17.206	0.525
3.90	26	40.13	7.203	2.097	81.20	17.163	0.535
3.90	27	41.45	7.607	2.026	80.70	17.115	0.545
3.90	28	42.80	8.025	1.956	80.17	17.061	0.556
3.90	29	44.20	8.458	1.885	79.61	17.001	0.569
3.90	30	45.65	8.906	1.813	79.01	16.933	0.583
3.90	31	47.15	9.370	1.741	78.36	16.855	0.598
3.90	32	48.72	9.853	1.667	77.64	16.765	0.616
3.90	33	50.37	10.358	1.591	76.85	16.660	0.636
3.90	34	52.13	10.890	1.513	75.96	16.533	0.660
3.90	35	54.03	11.456	1.431	74.92	16.378	0.688
3.90	36	56.15	12.072	1.343	73.68	16.177	0.724
3.90	37	58.64	12.773	1.242	72.06	15.895	0.772
3.90	38	62.08	13.689	1.111	69.50	15.402	0.853
4.00	0	14.46	0.997	4.002	89.99	18.500	0.435
4.00	1	15.13	1.105	3.925	89.72	18.500	0.435
4.00	2	15.81	1.219	3.852	89.44	18.498	0.435
4.00	3	16.52	1.343	3.780	89.16	18.496	0.436
4.00	4	17.26	1.476	3.709	88.88	18.493	0.437
4.00	5	18.02	1.620	3.638	88.60	18.489	0.438
4.00	6	18.81	1.774	3.568	88.31	18.484	0.439
4.00	7	19.63	1.940	3.498	88.02	18.478	0.440
4.00	8	20.47	2.117	3.427	87.73	18.471	0.442
4.00	9	21.34	2.305	3.357	87.44	18.463	0.444
4.00	10	22.23	2.506	3.286	87.14	18.453	0.446
4.00	11	23.15	2.719	3.215	86.84	18.443	0.449
4.00	12	24.10	2.944	3.144	86.54	18.432	0.452
4.00	13	25.06	3.182	3.073	86.23	18.419	0.455
4.00	14	26.05	3.433	3.001	85.91	18.405	0.458
4.00	15	27.06	3.697	2.929	85.59	18.389	0.462
4.00	16	28.10	3.974	2.857	85.26	18.372	0.466
4.00	17	29.16	4.264	2.785	84.92	18.354	0.470
4.00	18	30.24	4.566	2.713	84.58	18.333	0.475
4.00	19	31.34	4.882	2.641	84.22	18.311	0.480
4.00	20	32.46	5.211	2.569	83.86	18.286	0.485
4.00	21	33.61	5.553	2.497	83.48	18.259	0.491
4.00	22	34.79	5.909	2.425	83.09	18.230	0.498
4.00	23	35.98	6.277	2.353	82.68	18.197	0.505

(*Contd.*)

Scanned by CamScanner

TABLE A3 Oblique Shock in Perfect Gas ($\gamma = 1.4$) (*contd.*)

		Weak solution			*Strong solution*		
M_1	θ	β	p_2/p_1	M_2	β	p_2/p_1	M_2
4.00	24	37.21	6.659	2.281	82.26	18.161	0.513
4.00	25	38.46	7.054	2.209	81.82	18.122	0.521
4.00	26	39.74	7.462	2.137	81.36	18.079	0.530
4.00	27	41.05	7.885	2.066	80.88	18.030	0.540
4.00	28	42.40	8.321	1.994	80.36	17.976	0.551
4.00	29	43.79	8.772	1.921	79.81	17.916	0.563
4.00	30	45.22	9.239	1.849	79.23	17.848	0.577
4.00	31	46.71	9.723	1.775	78.60	17.770	0.592
4.00	32	48.26	10.226	1.701	77.91	17.681	0.609
4.00	33	49.88	10.749	1.625	77.15	17.576	0.628
4.00	34	51.61	11.299	1.546	76.30	17.452	0.651
4.00	35	53.46	11.881	1.465	75.32	17.301	0.678
4.00	36	55.50	12.509	1.378	74.16	17.109	0.711
4.00	37	57.84	13.210	1.281	72.70	16.849	0.754
4.00	38	60.83	14.064	1.164	70.60	16.441	0.820
4.10	0	14.10	0.997	4.102	89.99	19.445	0.432
4.10	1	14.77	1.108	4.023	89.73	19.445	0.432
4.10	2	15.45	1.225	3.947	89.45	19.443	0.433
4.10	3	16.16	1.352	3.872	89.17	19.441	0.433
4.10	4	16.89	1.489	3.798	88.90	19.438	0.434
4.10	5	17.66	1.638	3.725	88.62	19.433	0.435
4.10	6	18.45	1.797	3.652	88.33	19.428	0.436
4.10	7	19.27	1.968	3.580	88.05	19.422	0.438
4.10	8	20.11	2.152	3.507	87.77	19.415	0.439
4.10	9	20.98	2.347	3.434	87.48	19.407	0.441
4.10	10	21.88	2.556	3.360	87.18	19.398	0.444
4.10	11	22.80	2.777	3.287	86.89	19.387	0.446
4.10	12	23.74	3.012	3.213	86.59	19.375	0.449
4.10	13	24.71	3.260	3.139	86.28	19.362	0.452
4.10	14	25.70	3.521	3.065	85.97	19.348	0.455
4.10	15	26.71	3.796	2.991	85.65	19.332	0.459
4.10	16	27.75	4.085	2.916	85.33	19.315	0.462
4.10	17	28.81	4.387	2.842	85.00	19.296	0.467
4.10	18	29.89	4.703	2.768	84.66	19.275	0.471
4.10	19	30.99	5.033	2.693	84.31	19.252	0.476
4.10	20	32.12	5.377	2.619	83.95	19.227	0.482
4.10	21	33.27	5.734	2.545	83.58	19.200	0.488
4.10	22	34.44	6.105	2.471	83.20	19.170	0.494
4.10	23	35.64	6.490	2.397	82.80	19.137	0.501
4.10	24	36.86	6.889	2.323	82.39	19.101	0.509

(*Contd.*)

Scanned by CamScanner

TABLE A3 Oblique Shock in Perfect Gas ($\gamma = 1.4$) (*contd.*)

		Weak solution			Strong solution		
M_1	θ	β	p_2/p_1	M_2	β	p_2/p_1	M_2
4.10	25	38.10	7.301	2.250	81.96	19.061	0.517
4.10	26	39.38	7.728	2.177	81.51	19.017	0.526
4.10	27	40.69	8.169	2.103	81.03	18.968	0.536
4.10	28	42.03	8.625	2.030	80.53	18.914	0.547
4.10	29	43.41	9.095	1.956	80.00	18.853	0.558
4.10	30	44.83	9.582	1.883	79.43	18.785	0.572
4.10	31	46.31	10.086	1.808	78.82	18.707	0.586
4.10	32	47.84	10.609	1.733	78.15	18.618	0.603
4.10	33	49.44	11.152	1.656	77.42	18.514	0.621
4.10	34	51.13	11.722	1.578	76.60	18.392	0.643
4.10	35	52.94	12.322	1.496	75.67	18.244	0.669
4.10	36	54.91	12.965	1.410	74.58	18.059	0.700
4.10	37	57.15	13.672	1.316	73.24	17.814	0.739
4.10	38	59.86	14.501	1.207	71.42	17.452	0.796
4.10	39	64.50	15.811	1.031	67.66	16.611	0.919
4.20	0	13.76	0.997	4.202	89.99	20.413	0.430
4.20	1	14.42	1.110	4.120	89.73	20.413	0.430
4.20	2	15.10	1.231	4.041	89.46	20.411	0.430
4.20	3	15.81	1.361	3.964	89.18	20.409	0.431
4.20	4	16.55	1.503	3.888	88.91	20.406	0.432
4.20	5	17.31	1.655	3.812	88.63	20.402	0.433
4.20	6	18.10	1.820	3.736	88.36	20.396	0.434
4.20	7	18.92	1.997	3.661	88.08	20.390	0.435
4.20	8	19.77	2.187	3.586	87.80	20.383	0.437
4.20	9	20.64	2.390	3.510	87.51	20.374	0.439
4.20	10	21.54	2.607	3.434	87.22	20.365	0.441
4.20	11	22.46	2.837	3.358	86.93	20.354	0.443
4.20	12	23.41	3.081	3.282	86.64	20.342	0.446
4.20	13	24.38	3.339	3.205	86.33	20.329	0.449
4.20	14	25.37	3.611	3.128	86.03	20.314	0.452
4.20	15	26.38	3.897	3.052	85.72	20.298	0.456
4.20	16	27.42	4.198	2.975	85.40	20.281	0.460
4.20	17	28.48	4.513	2.898	85.07	20.261	0.464
4.20	18	29.56	4.843	2.821	84.74	20.240	0.468
4.20	19	30.67	5.187	2.745	84.40	20.217	0.473
4.20	20	31.79	5.546	2.668	84.04	20.191	0.479
4.20	21	32.94	5.919	2.592	83.68	20.164	0.485
4.20	22	34.11	6.306	2.516	83.30	20.133	0.491
4.20	23	35.31	6.708	2.440	82.91	20.100	0.498
4.20	24	36.53	7.124	2.365	82.51	20.063	0.505

(*Contd.*)

Scanned by CamScanner

TABLE A3 Oblique Shock in Perfect Gas ($\gamma = 1.4$) (*contd.*)

		Weak solution			*Strong solution*		
M_1	θ	β	p_2/p_1	M_2	β	p_2/p_1	M_2
4.20	25	37.77	7.555	2.290	82.09	20.023	0.513
4.20	26	39.05	8.000	2.215	81.64	19.978	0.522
4.20	27	40.35	8.461	2.140	81.18	19.929	0.532
4.20	28	41.69	8.936	2.065	80.69	19.874	0.542
4.20	29	43.06	9.427	1.990	80.17	19.813	0.554
4.20	30	44.47	9.934	1.915	79.61	19.744	0.567
4.20	31	45.93	10.459	1.840	79.02	19.666	0.581
4.20	32	47.45	11.002	1.764	78.37	19.577	0.597
4.20	33	49.03	11.567	1.686	77.66	19.474	0.615
4.20	34	50.70	12.157	1.608	76.88	19.352	0.636
4.20	35	52.47	12.777	1.526	75.99	19.207	0.660
4.20	36	54.39	13.437	1.441	74.96	19.026	0.690
4.20	37	56.54	14.156	1.349	73.70	18.793	0.726
4.20	38	59.07	14.977	1.244	72.07	18.461	0.777
4.20	39	62.66	16.072	1.104	69.37	17.859	0.864
4.30	0	13.43	0.997	4.302	89.99	21.405	0.428
4.30	1	14.10	1.113	4.217	89.73	21.405	0.428
4.30	2	14.77	1.236	4.136	89.46	21.403	0.428
4.30	3	15.48	1.370	4.056	89.20	21.401	0.428
4.30	4	16.22	1.516	3.977	88.92	21.397	0.429
4.30	5	16.98	1.674	3.898	88.65	21.393	0.430
4.30	6	17.78	1.844	3.820	88.38	21.388	0.432
4.30	7	18.60	2.027	3.742	88.10	21.381	0.433
4.30	8	19.44	2.223	3.664	87.82	21.374	0.435
4.30	9	20.32	2.434	3.586	87.54	21.365	0.436
4.30	10	21.22	2.658	3.507	87.26	21.356	0.439
4.30	11	22.14	2.897	3.428	86.97	21.345	0.441
4.30	12	23.09	3.151	3.349	86.68	21.333	0.444
4.30	13	24.06	3.419	3.270	86.38	21.319	0.447
4.30	14	25.06	3.702	3.191	86.08	21.304	0.450
4.30	15	26.07	4.000	3.111	85.77	21.288	0.453
4.30	16	27.11	4.314	3.032	85.46	21.270	0.457
4.30	17	28.18	4.642	2.953	85.14	21.250	0.461
4.30	18	29.26	4.986	2.874	84.81	21.228	0.466
4.30	19	30.36	5.345	2.795	84.47	21.205	0.471
4.30	20	31.49	5.719	2.716	84.12	21.179	0.476
4.30	21	32.64	6.108	2.638	83.77	21.150	0.482
4.30	22	33.81	6.512	2.560	83.40	21.120	0.488
4.30	23	35.00	6.931	2.482	83.01	21.086	0.495
4.30	24	36.22	7.366	2.405	82.62	21.048	0.502

(*Contd.*)

Scanned by CamScanner

TABLE A3 Oblique Shock in Perfect Gas ($\gamma = 1.4$) (*contd.*)

		Weak solution			Strong solution		
M_1	θ	β	p_2/p_1	M_2	β	p_2/p_1	M_2
4.30	25	37.47	7.815	2.328	82.20	21.007	0.510
4.30	26	38.74	8.280	2.251	81.77	20.962	0.518
4.30	27	40.04	8.759	2.175	81.31	20.912	0.528
4.30	28	41.37	9.255	2.099	80.83	20.857	0.538
4.30	29	42.73	9.766	2.023	80.32	20.795	0.550
4.30	30	44.14	10.295	1.947	79.78	20.726	0.562
4.30	31	45.59	10.841	1.870	79.20	20.647	0.576
4.30	32	47.09	11.406	1.793	78.57	20.558	0.592
4.30	33	48.66	11.993	1.715	77.89	20.455	0.609
4.30	34	50.30	12.604	1.636	77.13	20.334	0.629
4.30	35	52.05	13.245	1.554	76.27	20.190	0.653
4.30	36	53.92	13.924	1.469	75.29	20.013	0.681
4.30	37	56.00	14.658	1.378	74.11	19.787	0.715
4.30	38	58.40	15.481	1.277	72.61	19.477	0.761
4.30	39	61.54	16.506	1.151	70.37	18.969	0.833
4.40	0	13.12	0.997	4.402	90.00	22.420	0.426
4.40	1	13.78	1.116	4.314	89.74	22.419	0.426
4.40	2	14.46	1.242	4.230	89.47	22.418	0.426
4.40	3	15.17	1.380	4.147	89.20	22.416	0.426
4.40	4	15.90	1.529	4.065	88.94	22.412	0.427
4.40	5	16.67	1.692	3.984	88.67	22.408	0.428
4.40	6	17.46	1.867	3.903	88.40	22.402	0.429
4.40	7	18.29	2.057	3.823	88.13	22.396	0.431
4.40	8	19.13	2.260	3.742	87.85	22.388	0.432
4.40	9	20.01	2.478	3.661	87.57	22.379	0.434
4.40	10	20.91	2.711	3.579	87.29	22.370	0.436
4.40	11	21.84	2.959	3.498	87.01	22.358	0.439
4.40	12	22.79	3.222	3.416	86.72	22.346	0.441
4.40	13	23.76	3.501	3.334	86.43	22.332	0.444
4.40	14	24.76	3.795	3.252	86.13	22.317	0.447
4.40	15	25.78	4.106	3.170	85.83	22.300	0.451
4.40	16	26.82	4.432	3.088	85.52	22.282	0.455
4.40	17	27.89	4.774	3.007	85.20	22.262	0.459
4.40	18	28.97	5.132	2.925	84.88	22.240	0.463
4.40	19	30.08	5.506	2.844	84.54	22.216	0.468
4.40	20	31.20	5.896	2.763	84.20	22.189	0.473
4.40	21	32.35	6.301	2.683	83.85	22.160	0.479
4.40	22	33.53	6.723	2.602	83.48	22.129	0.485
4.40	23	34.72	7.160	2.523	83.11	22.094	0.492
4.40	24	35.94	7.612	2.444	82.72	22.057	0.499

(*Contd.*)

Scanned by CamScanner

TABLE A3 Oblique Shock in Perfect Gas ($\gamma = 1.4$) (*contd.*)

		Weak solution			*Strong solution*		
M_1	θ	β	p_2/p_1	M_2	β	p_2/p_1	M_2
4.40	25	37.18	8.081	2.365	82.31	22.015	0.507
4.40	26	38.45	8.565	2.287	81.88	21.969	0.515
4.40	27	39.74	9.065	2.209	81.43	21.919	0.524
4.40	28	41.07	9.581	2.132	80.96	21.863	0.535
4.40	29	42.43	10.114	2.054	80.47	21.800	0.546
4.40	30	43.83	10.664	1.977	79.94	21.730	0.558
4.40	31	45.27	11.233	1.899	79.37	21.651	0.572
4.40	32	46.76	11.820	1.821	78.76	21.561	0.587
4.40	33	48.31	12.429	1.743	78.09	21.457	0.604
4.40	34	49.94	13.063	1.663	77.35	21.337	0.623
4.40	35	51.66	13.726	1.581	76.53	21.194	0.646
4.40	36	53.50	14.426	1.496	75.58	21.019	0.673
4.40	37	55.51	15.178	1.406	74.47	20.800	0.705
4.40	38	57.81	16.010	1.308	73.07	20.504	0.748
4.40	39	60.68	17.004	1.190	71.11	20.051	0.811
4.50	0	12.82	0.997	4.503	90.00	23.458	0.424
4.50	1	13.49	1.118	4.411	89.74	23.458	0.424
4.50	2	14.16	1.248	4.324	89.48	23.456	0.424
4.50	3	14.87	1.389	4.238	89.21	23.454	0.424
4.50	4	15.61	1.543	4.154	88.95	23.450	0.425
4.50	5	16.37	1.710	4.070	88.68	23.446	0.426
4.50	6	17.17	1.891	3.986	88.42	23.440	0.427
4.50	7	17.99	2.087	3.903	88.15	23.434	0.429
4.50	8	18.84	2.297	3.819	87.88	23.426	0.430
4.50	9	19.72	2.523	3.735	87.60	23.417	0.432
4.50	10	20.62	2.764	3.651	87.32	23.407	0.434
4.50	11	21.55	3.021	3.567	87.04	23.395	0.437
4.50	12	22.50	3.294	3.482	86.76	23.383	0.439
4.50	13	23.48	3.584	3.397	86.47	23.369	0.442
4.50	14	24.48	3.890	3.313	86.18	23.353	0.445
4.50	15	25.50	4.213	3.228	85.88	23.336	0.449
4.50	16	26.55	4.552	3.144	85.57	23.317	0.452
4.50	17	27.61	4.908	3.059	85.26	23.297	0.456
4.50	18	28.70	5.281	2.975	84.94	23.274	0.461
4.50	19	29.81	5.671	2.892	84.61	23.250	0.465
4.50	20	30.94	6.076	2.809	84.27	23.223	0.471
4.50	21	32.09	6.499	2.726	83.92	23.193	0.476
4.50	22	33.26	6.938	2.644	83.57	23.161	0.482
4.50	23	34.45	7.393	2.563	83.19	23.126	0.489
4.50	24	35.67	7.865	2.482	82.81	23.088	0.496

(*Contd.*)

Scanned by CamScanner

TABLE A3 Oblique Shock in Perfect Gas ($\gamma = 1.4$) (*contd.*)

		Weak solution			*Strong solution*		
M_1	θ	β	p_2/p_1	M_2	β	p_2/p_1	M_2
4.50	25	36.91	8.353	2.401	82.41	23.046	0.504
4.50	26	38.17	8.857	2.321	81.99	22.999	0.512
4.50	27	39.47	9.378	2.242	81.55	22.948	0.521
4.50	28	40.79	9.916	2.163	81.09	22.891	0.531
4.50	29	42.15	10.470	2.084	80.60	22.827	0.542
4.50	30	43.54	11.043	2.006	80.08	22.757	0.554
4.50	31	44.97	11.634	1.927	79.52	22.677	0.567
4.50	32	46.45	12.244	1.848	78.92	22.586	0.582
4.50	33	47.99	12.877	1.769	78.27	22.482	0.599
4.50	34	49.60	13.534	1.689	77.56	22.361	0.618
4.50	35	51.30	14.220	1.606	76.76	22.219	0.640
4.50	36	53.10	14.943	1.521	75.85	22.046	0.665
4.50	37	55.07	15.714	1.432	74.79	21.831	0.697
4.50	38	57.29	16.559	1.335	73.47	21.546	0.736
4.50	39	59.98	17.543	1.223	71.70	21.129	0.793
4.50	40	64.33	19.026	1.052	68.25	20.214	0.909
4.60	0	12.54	0.997	4.603	90.00	24.520	0.422
4.60	1	13.20	1.121	4.508	89.74	24.519	0.422
4.60	2	13.88	1.253	4.418	89.48	24.518	0.422
4.60	3	14.58	1.398	4.329	89.22	24.515	0.423
4.60	4	15.32	1.557	4.242	88.96	24.512	0.423
4.60	5	16.09	1.729	4.155	88.70	24.507	0.424
4.60	6	16.88	1.916	4.069	88.43	24.501	0.425
4.60	7	17.71	2.118	3.982	88.17	24.495	0.427
4.60	8	18.56	2.335	3.896	87.90	24.487	0.428
4.60	9	19.44	2.568	3.809	87.63	24.478	0.430
4.60	10	20.35	2.818	3.722	87.35	24.467	0.432
4.60	11	21.28	3.085	3.635	87.08	24.456	0.435
4.60	12	22.24	3.368	3.547	86.79	24.443	0.437
4.60	13	23.21	3.669	3.460	86.51	24.428	0.440
4.60	14	24.22	3.987	3.372	86.22	24.412	0.443
4.60	15	25.24	4.322	3.285	85.92	24.395	0.446
4.60	16	26.29	4.675	3.198	85.62	24.376	0.450
4.60	17	27.36	5.045	3.111	85.31	24.355	0.454
4.60	18	28.44	5.433	3.025	84.99	24.332	0.458
4.60	19	29.55	5.838	2.939	84.67	24.307	0.463
4.60	20	30.68	6.261	2.853	84.34	24.279	0.468
4.60	21	31.83	6.701	2.769	83.99	24.250	0.474
4.60	22	33.00	7.158	2.685	83.64	24.217	0.480
4.60	23	34.20	7.632	2.601	83.27	24.181	0.486

(*Contd.*)

Scanned by CamScanner

TABLE A3 Oblique Shock in Perfect Gas ($\gamma = 1.4$) (*contd.*)

		Weak solution			*Strong solution*		
M_1	θ	β	p_2/p_1	M_2	β	p_2/p_1	M_2
4.60	24	35.41	8.123	2.518	82.89	24.142	0.493
4.60	25	36.65	8.631	2.436	82.50	24.099	0.501
4.60	26	37.92	9.156	2.355	82.09	24.052	0.509
4.60	27	39.21	9.698	2.274	81.65	23.999	0.518
4.60	28	40.53	10.258	2.193	81.20	23.942	0.528
4.60	29	41.88	10.835	2.114	80.72	23.877	0.539
4.60	30	43.27	11.430	2.034	80.21	23.806	0.550
4.60	31	44.69	12.044	1.954	79.66	23.725	0.563
4.60	32	46.17	12.679	1.874	79.08	23.633	0.578
4.60	33	47.69	13.335	1.794	78.44	23.529	0.594
4.60	34	49.29	14.017	1.713	77.75	23.408	0.613
4.60	35	50.96	14.727	1.630	76.97	23.265	0.634
4.60	36	52.74	15.473	1.545	76.09	23.094	0.659
4.60	37	54.67	16.265	1.457	75.07	22.881	0.689
4.60	38	56.83	17.128	1.361	73.83	22.605	0.726
4.60	39	59.37	18.111	1.253	72.20	22.212	0.778
4.60	40	62.99	19.429	1.107	69.49	21.489	0.868
4.70	0	12.27	0.997	4.703	90.00	25.605	0.420
4.70	1	12.93	1.123	4.605	89.75	25.604	0.420
4.70	2	13.60	1.259	4.512	89.49	25.603	0.420
4.70	3	14.31	1.408	4.420	89.23	25.600	0.421
4.70	4	15.05	1.571	4.330	88.97	25.597	0.422
4.70	5	15.82	1.748	4.240	88.71	25.592	0.422
4.70	6	16.61	1.940	4.151	88.45	25.586	0.424
4.70	7	17.44	2.149	4.061	88.19	25.579	0.425
4.70	8	18.30	2.373	3.972	87.92	25.571	0.427
4.70	9	19.18	2.615	3.882	87.65	25.562	0.428
4.70	10	20.09	2.873	3.792	87.38	25.551	0.430
4.70	11	21.02	3.149	3.702	87.11	25.539	0.433
4.70	12	21.98	3.443	3.612	86.83	25.526	0.435
4.70	13	22.96	3.755	3.522	86.54	25.511	0.438
4.70	14	23.97	4.085	3.431	86.26	25.495	0.441
4.70	15	24.99	4.434	3.341	85.96	25.477	0.444
4.70	16	26.04	4.800	3.251	85.67	25.458	0.448
4.70	17	27.11	5.185	3.162	85.36	25.436	0.452
4.70	18	28.20	5.588	3.073	85.05	25.413	0.456
4.70	19	29.31	6.010	2.985	84.73	25.387	0.461
4.70	20	30.44	6.449	2.897	84.40	25.359	0.466
4.70	21	31.59	6.907	2.810	84.06	25.329	0.472
4.70	22	32.77	7.382	2.724	83.71	25.295	0.477
4.70	23	33.96	7.875	2.639	83.35	25.259	0.484

(*Contd.*)

Scanned by CamScanner

TABLE A3 Oblique Shock in Perfect Gas ($\gamma = 1.4$) (*contd.*)

		Weak solution			*Strong solution*		
M_1	θ	β	p_2/p_1	M_2	β	p_2/p_1	M_2
4.70	24	35.18	8.386	2.554	82.97	25.219	0.491
4.70	25	36.42	8.915	2.470	82.58	25.175	0.498
4.70	26	37.68	9.461	2.387	82.18	25.127	0.506
4.70	27	38.97	10.025	2.305	81.75	25.074	0.515
4.70	28	40.28	10.607	2.223	81.30	25.015	0.525
4.70	29	41.63	11.207	2.142	80.83	24.950	0.535
4.70	30	43.01	11.826	2.061	80.33	24.878	0.547
4.70	31	44.43	12.464	1.980	79.80	24.796	0.560
4.70	32	45.90	13.123	1.899	79.22	24.703	0.574
4.70	33	47.42	13.804	1.818	78.60	24.598	0.590
4.70	34	49.00	14.511	1.737	77.92	24.476	0.608
4.70	35	50.66	15.246	1.654	77.17	24.333	0.629
4.70	36	52.41	16.016	1.568	76.31	24.162	0.653
4.70	37	54.31	16.832	1.480	75.33	23.952	0.682
4.70	38	56.40	17.714	1.385	74.15	23.682	0.717
4.70	39	58.84	18.705	1.280	72.63	23.307	0.765
4.70	40	62.09	19.956	1.146	70.30	22.676	0.842
4.80	0	12.01	0.997	4.803	90.00	26.713	0.418
4.80	1	12.67	1.126	4.701	89.75	26.713	0.418
4.80	2	13.34	1.265	4.605	89.49	26.711	0.419
4.80	3	14.05	1.417	4.511	89.24	26.709	0.419
4.80	4	14.79	1.585	4.418	88.98	26.705	0.420
4.80	5	15.56	1.767	4.325	88.72	26.700	0.421
4.80	6	16.36	1.965	4.232	88.46	26.694	0.422
4.80	7	17.19	2.180	4.140	88.20	26.687	0.423
4.80	8	18.04	2.412	4.047	87.94	26.679	0.425
4.80	9	18.93	2.662	3.955	87.68	26.669	0.427
4.80	10	19.84	2.929	3.862	87.41	26.658	0.429
4.80	11	20.78	3.215	3.769	87.13	26.646	0.431
4.80	12	21.74	3.520	3.676	86.86	26.632	0.433
4.80	13	22.72	3.843	3.582	86.58	26.617	0.436
4.80	14	23.73	4.186	3.489	86.29	26.601	0.439
4.80	15	24.76	4.547	3.396	86.00	26.583	0.443
4.80	16	25.81	4.928	3.304	85.71	26.563	0.446
4.80	17	26.88	5.328	3.212	85.41	26.541	0.450
4.80	18	27.97	5.747	3.121	85.10	26.517	0.454
4.80	19	29.08	6.185	3.030	84.78	26.491	0.459
4.80	20	30.22	6.641	2.940	84.46	26.462	0.464
4.80	21	31.37	7.117	2.851	84.12	26.431	0.469
4.80	22	32.54	7.611	2.762	83.78	26.397	0.475
4.80	23	33.74	8.124	2.675	83.42	26.360	0.482
4.80	24	34.95	8.655	2.589	83.05	26.319	0.488
4.80	25	36.19	9.205	2.503	82.66	26.275	0.496
4.80	26	37.45	9.773	2.418	82.26	26.226	0.504
4.80	27	38.74	10.359	2.334	81.84	26.172	0.513

(*Contd.*)

Scanned by CamScanner

TABLE A3 Oblique Shock in Perfect Gas ($\gamma = 1.4$) (*contd.*)

		Weak solution			*Strong solution*		
M_1	θ	β	p_2/p_1	M_2	β	p_2/p_1	M_2
4.80	28	40.05	10.964	2.251	81.40	26.112	0.522
4.80	29	41.40	11.588	2.169	80.94	26.046	0.533
4.80	30	42.78	12.231	2.087	80.44	25.972	0.544
4.80	31	44.19	12.894	2.005	79.92	25.889	0.557
4.80	32	45.65	13.578	1.923	79.35	25.796	0.571
4.80	33	47.16	14.284	1.841	78.75	25.689	0.586
4.80	34	48.73	15.016	1.759	78.08	25.566	0.604
4.80	35	50.37	15.777	1.675	77.34	25.423	0.624
4.80	36	52.11	16.573	1.590	76.52	25.252	0.647
4.80	37	53.97	17.413	1.501	75.57	25.043	0.675
4.80	38	56.02	18.317	1.408	74.43	24.777	0.709
4.80	39	58.37	19.321	1.304	73.00	24.416	0.754
4.80	40	61.37	20.542	1.179	70.93	23.842	0.823
4.90	0	11.76	0.997	4.903	90.00	27.845	0.417
4.90	1	12.42	1.129	4.798	89.75	27.844	0.417
4.90	2	13.09	1.271	4.699	89.50	27.843	0.417
4.90	3	13.80	1.427	4.601	89.24	27.840	0.418
4.90	4	14.54	1.599	4.505	88.99	27.836	0.418
4.90	5	15.31	1.786	4.409	88.74	27.831	0.419
4.90	6	16.11	1.990	4.314	88.48	27.825	0.420
4.90	7	16.94	2.212	4.218	88.22	27.818	0.422
4.90	8	17.80	2.451	4.123	87.96	27.809	0.423
4.90	9	18.69	2.709	4.027	87.70	27.800	0.425
4.90	10	19.60	2.986	3.931	87.43	27.789	0.427
4.90	11	20.54	3.282	3.835	87.16	27.776	0.429
4.90	12	21.50	3.597	3.739	86.89	27.762	0.432
4.90	13	22.49	3.933	3.642	86.61	27.747	0.434
4.90	14	23.50	4.288	3.546	86.33	27.730	0.438
4.90	15	24.53	4.663	3.451	86.04	27.711	0.441
4.90	16	25.59	5.058	3.356	85.75	27.691	0.444
4.90	17	26.66	5.473	3.261	85.45	27.668	0.448
4.90	18	27.76	5.908	3.167	85.14	27.644	0.453
4.90	19	28.87	6.363	3.074	84.83	27.617	0.457
4.90	20	30.00	6.837	2.982	84.51	27.588	0.462
4.90	21	31.16	7.331	2.890	84.18	27.556	0.467
4.90	22	32.33	7.845	2.800	83.84	27.522	0.473
4.90	23	33.53	8.378	2.711	83.48	27.484	0.479
4.90	24	34.74	8.930	2.622	83.12	27.442	0.486
4.90	25	35.98	9.501	2.535	82.74	27.397	0.494
4.90	26	37.24	10.091	2.449	82.34	27.347	0.501

(*Contd.*)

Scanned by CamScanner

TABLE A3 Oblique Shock in Perfect Gas ($\gamma = 1.4$) (*contd.*)

		Weak solution			*Strong solution*		
M_1	θ	β	p_2/p_1	M_2	β	p_2/p_1	M_2
4.90	27	38.53	10.700	2.363	81.93	27.292	0.510
4.90	28	39.84	11.329	2.279	81.49	27.231	0.519
4.90	29	41.18	11.976	2.195	81.03	27.164	0.530
4.90	30	42.55	12.644	2.112	80.55	27.089	0.541
4.90	31	43.96	13.332	2.029	80.03	27.005	0.553
4.90	32	45.42	14.042	1.946	79.48	26.910	0.567
4.90	33	46.92	14.775	1.864	78.88	26.803	0.582
4.90	34	48.47	15.533	1.780	78.23	26.679	0.600
4.90	35	50.10	16.320	1.696	77.51	26.534	0.619
4.90	36	51.82	17.143	1.611	76.70	26.363	0.642
4.90	37	53.66	18.009	1.522	75.78	26.155	0.669
4.90	38	55.67	18.936	1.429	74.69	25.892	0.702
4.90	39	57.95	19.957	1.327	73.33	25.540	0.745
4.90	40	60.77	21.166	1.207	71.44	25.005	0.807
5.00	0	11.52	0.996	5.003	90.00	29.000	0.415
5.00	1	12.18	1.131	4.895	89.75	28.999	0.415
5.00	2	12.85	1.277	4.792	89.50	28.998	0.416
5.00	3	13.56	1.437	4.692	89.25	28.995	0.416
5.00	4	14.30	1.613	4.592	89.00	28.991	0.417
5.00	5	15.07	1.806	4.493	88.75	28.986	0.418
5.00	6	15.88	2.016	4.395	88.49	28.980	0.419
5.00	7	16.71	2.244	4.296	88.24	28.972	0.420
5.00	8	17.57	2.491	4.197	87.98	28.964	0.422
5.00	9	18.46	2.757	4.098	87.72	28.954	0.423
5.00	10	19.38	3.043	3.999	87.45	28.942	0.425
5.00	11	20.32	3.350	3.900	87.19	28.930	0.428
5.00	12	21.28	3.676	3.801	86.91	28.915	0.430
5.00	13	22.27	4.024	3.702	86.64	28.900	0.433
5.00	14	23.29	4.392	3.603	86.36	28.882	0.436
5.00	15	24.32	4.781	3.504	86.08	28.863	0.439
5.00	16	25.38	5.190	3.406	85.79	28.842	0.443
5.00	17	26.45	5.621	3.309	85.49	28.819	0.447
5.00	18	27.55	6.072	3.212	85.19	28.794	0.451
5.00	19	28.67	6.544	3.117	84.88	28.767	0.455
5.00	20	29.80	7.037	3.022	84.56	28.737	0.460
5.00	21	30.96	7.550	2.929	84.23	28.705	0.465
5.00	22	32.13	8.083	2.836	83.89	28.670	0.471
5.00	23	33.33	8.637	2.745	83.54	28.631	0.477
5.00	24	34.54	9.210	2.655	83.18	28.589	0.484
5.00	25	35.78	9.803	2.566	82.81	28.542	0.491
5.00	26	37.04	10.416	2.478	82.41	28.491	0.499
5.00	27	38.32	11.048	2.391	82.01	28.435	0.508
5.00	28	39.63	11.701	2.305	81.58	28.374	0.517
5.00	29	40.97	12.373	2.220	81.12	28.305	0.527

(*Contd.*)

Scanned by CamScanner

TABLE A3 Oblique Shock in Perfect Gas ($\gamma = 1.4$) (*contd.*)

		Weak solution			*Strong solution*		
M_1	θ	β	p_2/p_1	M_2	β	p_2/p_1	M_2
5.00	30	42.34	13.066	2.136	80.65	28.229	0.538
5.00	31	43.75	13.780	2.052	80.14	28.144	0.550
5.00	32	45.20	14.516	1.968	79.59	28.048	0.564
5.00	33	46.69	15.276	1.885	79.00	27.938	0.579
5.00	34	48.24	16.061	1.801	78.37	27.813	0.596
5.00	35	49.86	16.876	1.716	77.66	27.668	0.615
5.00	36	51.56	17.725	1.630	76.88	27.496	0.638
5.00	37	53.37	18.618	1.542	75.98	27.287	0.664
5.00	38	55.35	19.570	1.449	74.93	27.027	0.695
5.00	39	57.57	20.612	1.349	73.63	26.683	0.736
5.00	40	60.26	21.821	1.233	71.87	26.175	0.794
5.00	41	64.65	23.652	1.055	68.40	25.048	0.914

[Note: In Table A3 θ and β values are in degrees]

Scanned by CamScanner

TABLE A4 One-Dimensional Flow with Friction ($\gamma = 1.4$)

M	T/T^*	p/p^*	p_0/p_0^*	ρ^*/ρ	F/F^*	$4fL_{max}/D$
0.02	1.19990	54.77007	28.94214	0.02191	22.83364	1778.4498
0.04	1.19962	27.38175	14.48149	0.04381	11.43462	440.3522
0.06	1.19914	18.25085	9.66591	0.06570	7.64285	193.0311
0.08	1.19847	13.68431	7.26161	0.08758	5.75288	106.7182
0.10	1.19760	10.94351	5.82183	0.10944	4.62363	66.9216
0.12	1.19655	9.11559	4.86432	0.13126	3.87473	45.4080
0.14	1.19531	7.80932	4.18240	0.15306	3.34317	32.5113
0.16	1.19389	6.82907	3.67274	0.17482	2.94743	24.1978
0.18	1.19227	6.06618	3.27793	0.19654	2.64223	18.5427
0.20	1.19048	5.45545	2.96352	0.21822	2.40040	14.5333
0.22	1.18850	4.95537	2.70760	0.23984	2.20464	11.5961
0.24	1.18633	4.53829	2.49556	0.26141	2.04344	9.3865
0.26	1.18399	4.18506	2.31729	0.28291	1.90880	7.6876
0.28	1.18147	3.88199	2.16555	0.30435	1.79503	6.3572
0.30	1.17878	3.61906	2.03506	0.32572	1.69794	5.2993
0.32	1.17592	3.38874	1.92185	0.34701	1.61440	4.4467
0.34	1.17288	3.18529	1.82288	0.36822	1.54200	3.7520
0.36	1.16968	3.00422	1.73578	0.38935	1.47888	3.1801
0.38	1.16632	2.84200	1.65870	0.41039	1.42356	2.7054
0.40	1.16279	2.69582	1.59014	0.43133	1.37487	2.3085
0.42	1.15911	2.56338	1.52890	0.45218	1.33184	1.9744
0.44	1.15527	2.44280	1.47400	0.47293	1.29371	1.6915
0.46	1.15128	2.33256	1.42463	0.49357	1.25981	1.4509
0.48	1.14714	2.23135	1.38010	0.51410	1.22962	1.2453
0.50	1.14286	2.13809	1.33984	0.53452	1.20268	1.0691
0.52	1.13843	2.05187	1.30339	0.55483	1.17860	0.9174
0.54	1.13387	1.97192	1.27032	0.57501	1.15705	0.7866
0.56	1.12918	1.89755	1.24029	0.59507	1.13777	0.6736
0.58	1.12435	1.82820	1.21301	0.61501	1.12050	0.5757
0.60	1.11940	1.76336	1.18820	0.63481	1.10504	0.4908
0.62	1.11433	1.70261	1.16565	0.65448	1.09120	0.4172
0.64	1.10914	1.64556	1.14515	0.67402	1.07883	0.3533
0.66	1.10383	1.59187	1.12653	0.69342	1.06777	0.2979
0.68	1.09842	1.54126	1.10965	0.71268	1.05792	0.2498
0.70	1.09290	1.49345	1.09437	0.73179	1.04915	0.2081
0.72	1.08727	1.44823	1.08057	0.75076	1.04137	0.1721
0.74	1.08155	1.40537	1.06814	0.76958	1.03449	0.1411
0.76	1.07573	1.36470	1.05700	0.78825	1.02844	0.1145
0.78	1.06982	1.32606	1.04705	0.80677	1.02314	0.0917
0.80	1.06383	1.28928	1.03823	0.82514	1.01853	0.0723
0.82	1.05775	1.25423	1.03046	0.84335	1.01455	0.0559
0.84	1.05160	1.22080	1.02370	0.86140	1.01115	0.0423

(Contd.)

Scanned by CamScanner

TABLE A4 One-Dimensional Flow with Friction ($\gamma = 1.4$)

M	T/T^*	p/p^*	p_0/p_0^*	ρ^*/ρ	F/F^*	$4fL_{max}/D$
0.86	1.04537	1.18888	1.01787	0.87929	1.00829	0.0310
0.88	1.03907	1.15835	1.01294	0.89703	1.00591	0.0218
0.90	1.03270	1.12913	1.00886	0.91460	1.00399	0.0145
0.92	1.02627	1.10114	1.00560	0.93201	1.00248	0.0089
0.94	1.01978	1.07430	1.00311	0.94925	1.00136	0.0048
0.96	1.01324	1.04854	1.00136	0.96633	1.00059	0.0026
0.98	1.00664	1.02379	1.00034	0.98325	1.00014	0.0005
1.00	1.00000	1.00000	1.00000	1.00000	1.00000	0.0000
1.02	0.99331	0.97711	1.00033	1.01658	1.00014	0.0005
1.04	0.98658	0.95507	1.00130	1.03300	1.00053	0.0018
1.06	0.97982	0.93383	1.00291	1.04925	1.00116	0.0038
1.08	0.97302	0.91335	1.00512	1.06533	1.00200	0.0066
1.10	0.96618	0.89359	1.00792	1.08124	1.00305	0.0099
1.12	0.95932	0.87451	1.01131	1.09698	1.00429	0.0138
1.14	0.95244	0.85608	1.01527	1.11256	1.00569	0.0182
1.16	0.94554	0.83827	1.01978	1.12797	1.00726	0.0230
1.18	0.93861	0.82104	1.02484	1.14321	1.00897	0.0281
1.20	0.93168	0.80436	1.03044	1.15828	1.01081	0.0336
1.22	0.92473	0.78822	1.03657	1.17319	1.01278	0.0394
1.24	0.91777	0.77258	1.04323	1.18792	1.01486	0.0455
1.26	0.91080	0.75743	1.05041	1.20249	1.01705	0.0517
1.28	0.90383	0.74274	1.05810	1.21690	1.01933	0.0582
1.30	0.89686	0.72848	1.06630	1.23114	1.02170	0.0648
1.32	0.88989	0.71465	1.07502	1.24521	1.02414	0.0716
1.34	0.88292	0.70122	1.08424	1.25912	1.02666	0.0785
1.36	0.87596	0.68818	1.09396	1.27286	1.02925	0.0855
1.38	0.86901	0.67551	1.10419	1.28645	1.03189	0.0926
1.40	0.86207	0.66320	1.11493	1.29987	1.03459	0.0997
1.42	0.85514	0.65122	1.12616	1.31313	1.03733	0.1069
1.44	0.84822	0.63958	1.13790	1.32623	1.04012	0.1142
1.46	0.84133	0.62825	1.15015	1.33917	1.04295	0.1215
1.48	0.83445	0.61722	1.16290	1.35195	1.04581	0.1288
1.50	0.82759	0.60648	1.17617	1.36458	1.04870	0.1360
1.52	0.82075	0.59602	1.18994	1.37705	1.05162	0.1433
1.54	0.81393	0.58583	1.20423	1.38936	1.05456	0.1506
1.56	0.80715	0.57591	1.21904	1.40152	1.05752	0.1579
1.58	0.80038	0.56623	1.23438	1.41353	1.06049	0.1651
1.60	0.79365	0.55679	1.25023	1.42539	1.06348	0.1724
1.62	0.78695	0.54759	1.26662	1.43710	1.06647	0.1795
1.64	0.78028	0.53862	1.28355	1.44866	1.06948	0.1867
1.66	0.77363	0.52986	1.30102	1.46008	1.07249	0.1938
1.68	0.76703	0.52131	1.31904	1.47135	1.07550	0.2008
1.70	0.76046	0.51297	1.33761	1.48247	1.07851	0.2078
1.72	0.75392	0.50482	1.35673	1.49345	1.08152	0.2147
1.74	0.74742	0.49686	1.37643	1.50429	1.08453	0.2216

(*Contd.*)

Scanned by CamScanner

TABLE A4 One-Dimensional Flow with Friction ($\gamma = 1.4$)

M	T/T^*	p/p^*	p_0/p_0^*	ρ^*/ρ	F/F^*	$4fL_{max}/D$
1.76	0.74096	0.48909	1.39670	1.51499	1.08753	0.2284
1.78	0.73454	0.48149	1.41754	1.52555	1.09053	0.2352
1.80	0.72816	0.47407	1.43898	1.53598	1.09351	0.2419
1.82	0.72181	0.46681	1.46101	1.54626	1.09649	0.2485
1.84	0.71551	0.45972	1.48365	1.55642	1.09946	0.2551
1.86	0.70925	0.45278	1.50689	1.56644	1.10241	0.2616
1.88	0.70304	0.44600	1.53076	1.57633	1.10536	0.2680
1.90	0.69686	0.43936	1.55525	1.58609	1.10829	0.2743
1.92	0.69074	0.43287	1.58039	1.59572	1.11120	0.2806
1.94	0.68465	0.42651	1.60617	1.60523	1.11410	0.2868
1.96	0.67861	0.42030	1.63261	1.61460	1.11698	0.2929
1.98	0.67262	0.41421	1.65971	1.62386	1.11984	0.2990
2.00	0.66667	0.40825	1.68750	1.63299	1.12268	0.3050
2.02	0.66076	0.40241	1.71597	1.64200	1.12551	0.3109
2.04	0.65491	0.39670	1.74514	1.65090	1.12831	0.3168
2.06	0.64910	0.39110	1.77501	1.65967	1.13110	0.3225
2.08	0.64334	0.38562	1.80561	1.66833	1.13387	0.3282
2.10	0.63762	0.38024	1.83694	1.67687	1.13661	0.3339
2.12	0.63195	0.37498	1.86901	1.68530	1.13933	0.3394
2.14	0.62633	0.36982	1.90184	1.69362	1.14204	0.3449
2.16	0.62076	0.36476	1.93543	1.70182	1.14471	0.3503
2.18	0.61523	0.35980	1.96981	1.70992	1.14737	0.3556
2.20	0.60976	0.35494	2.00497	1.71791	1.15001	0.3609
2.22	0.60433	0.35017	2.04094	1.72579	1.15262	0.3661
2.24	0.59895	0.34550	2.07773	1.73357	1.15521	0.3712
2.26	0.59361	0.34091	2.11535	1.74125	1.15777	0.3763
2.28	0.58833	0.33641	2.15381	1.74882	1.16032	0.3813
2.30	0.58309	0.33200	2.19313	1.75629	1.16284	0.3862
2.32	0.57790	0.32767	2.23332	1.76366	1.16533	0.3911
2.34	0.57276	0.32342	2.27440	1.77093	1.16780	0.3959
2.36	0.56767	0.31925	2.31638	1.77811	1.17025	0.4006
2.38	0.56262	0.31516	2.35927	1.78519	1.17268	0.4053
2.40	0.55762	0.31114	2.40310	1.79218	1.17508	0.4099
2.42	0.55267	0.30720	2.44787	1.79907	1.17746	0.4144
2.44	0.54777	0.30332	2.49360	1.80587	1.17981	0.4189
2.46	0.54291	0.29952	2.54031	1.81258	1.18214	0.4233
2.48	0.53810	0.29579	2.58801	1.81921	1.18445	0.4277
2.50	0.53333	0.29212	2.63671	1.82574	1.18673	0.4320
2.52	0.52862	0.28852	2.68645	1.83219	1.18899	0.4362
2.54	0.52394	0.28498	2.73722	1.83855	1.19123	0.4404
2.56	0.51932	0.28150	2.78906	1.84483	1.19344	0.4445

(Contd.)

Scanned by CamScanner

TABLE A4 One-Dimensional Flow with Friction ($\gamma = 1.4$)

M	T/T^*	p/p^*	p_0/p_0^*	ρ^*/ρ	F/F^*	$4fL_{max}/D$
2.58	0.51474	0.27808	2.84197	1.85103	1.19563	0.4486
2.60	0.51020	0.27473	2.89597	1.85714	1.19780	0.4526
2.62	0.50572	0.27143	2.95108	1.86318	1.19995	0.4565
2.64	0.50127	0.26818	3.00733	1.86913	1.20207	0.4604
2.66	0.49687	0.26500	3.06471	1.87501	1.20417	0.4643
2.68	0.49251	0.26186	3.12327	1.88081	1.20625	0.4681
2.70	0.48820	0.25878	3.18300	1.88653	1.20830	0.4718
2.72	0.48393	0.25576	3.24394	1.89218	1.21033	0.4755
2.74	0.47971	0.25278	3.30611	1.89775	1.21235	0.4791
2.76	0.47553	0.24985	3.36951	1.90325	1.21433	0.4827
2.78	0.47139	0.24697	3.43417	1.90868	1.21630	0.4863
2.80	0.46729	0.24414	3.50012	1.91404	1.21825	0.4898
2.82	0.46324	0.24135	3.56736	1.91933	1.22017	0.4932
2.84	0.45922	0.23861	3.63593	1.92455	1.22208	0.4966
2.86	0.45525	0.23592	3.70584	1.92970	1.22396	0.5000
2.88	0.45132	0.23326	3.77711	1.93479	1.22582	0.5033
2.90	0.44743	0.23066	3.84976	1.93981	1.22766	0.5065
2.92	0.44358	0.22809	3.92382	1.94477	1.22948	0.5097
2.94	0.43977	0.22556	3.99931	1.94966	1.23128	0.5129
2.96	0.43600	0.22307	4.07625	1.95449	1.23307	0.5160
2.98	0.43226	0.22063	4.15465	1.95925	1.23483	0.5191
3.00	0.42857	0.21822	4.23456	1.96396	1.23657	0.5222
3.02	0.42492	0.21585	4.31598	1.96861	1.23829	0.5252
3.04	0.42130	0.21351	4.39894	1.97319	1.23999	0.5281
3.06	0.41772	0.21121	4.48347	1.97772	1.24168	0.5310
3.08	0.41418	0.20895	4.56958	1.98219	1.24334	0.5339
3.10	0.41068	0.20672	4.65730	1.98661	1.24499	0.5368
3.12	0.40721	0.20453	4.74666	1.99097	1.24662	0.5396
3.14	0.40378	0.20237	4.83768	1.99527	1.24823	0.5424
3.16	0.40038	0.20024	4.93038	1.99952	1.24982	0.5451
3.18	0.39703	0.19814	5.02480	2.00371	1.25139	0.5478
3.20	0.39370	0.19608	5.12095	2.00786	1.25295	0.5504
3.22	0.39041	0.19405	5.21886	2.01195	1.25449	0.5531
3.24	0.38716	0.19204	5.31855	2.01599	1.25601	0.5557
3.26	0.38394	0.19007	5.42006	2.01998	1.25752	0.5582
3.28	0.38075	0.18812	5.52342	2.02392	1.25901	0.5607
3.30	0.37760	0.18621	5.62863	2.02781	1.26048	0.5632
3.32	0.37448	0.18432	5.73574	2.03165	1.26193	0.5657
3.34	0.37139	0.18246	5.84478	2.03545	1.26337	0.5681
3.36	0.36833	0.18063	5.95576	2.03920	1.26479	0.5705
3.38	0.36531	0.17882	6.06872	2.04290	1.26620	0.5729
3.40	0.36232	0.17704	6.18368	2.04656	1.26759	0.5752

(*Contd.*)

Scanned by CamScanner

TABLE A4 One-Dimensional Flow with Friction ($\gamma = 1.4$)

M	T/T^*	p/p^*	p_0/p_0^*	ρ^*/ρ	F/F^*	$4fL_{max}/D$
3.42	0.35936	0.17528	6.30068	2.05017	1.26897	0.5775
3.44	0.35643	0.17355	6.41974	2.05374	1.27033	0.5798
3.46	0.35353	0.17185	6.54090	2.05727	1.27167	0.5820
3.48	0.35066	0.17016	6.66418	2.06075	1.27300	0.5842
3.50	0.34783	0.16851	6.78961	2.06419	1.27432	0.5864
3.52	0.34502	0.16687	6.91721	2.06759	1.27562	0.5886
3.54	0.34224	0.16526	7.04704	2.07094	1.27691	0.5907
3.56	0.33949	0.16367	7.17911	2.07426	1.27818	0.5928
3.58	0.33677	0.16210	7.31345	2.07754	1.27944	0.5949
3.60	0.33408	0.16055	7.45010	2.08077	1.28068	0.5970
3.62	0.33141	0.15903	7.58908	2.08397	1.28191	0.5990
3.64	0.32877	0.15752	7.73043	2.08713	1.28313	0.6010
3.66	0.32617	0.15604	7.87419	2.09026	1.28433	0.6030
3.68	0.32358	0.15458	8.02038	2.09334	1.28552	0.6049
3.70	0.32103	0.15313	8.16904	2.09639	1.28670	0.6068
3.72	0.31850	0.15171	8.32021	2.09941	1.28787	0.6087
3.74	0.31600	0.15030	8.47391	2.10238	1.28902	0.6106
3.76	0.31352	0.14892	8.63018	2.10533	1.29016	0.6125
3.78	0.31107	0.14755	8.78905	2.10824	1.29128	0.6143
3.80	0.30864	0.14620	8.95057	2.11111	1.29240	0.6161
3.82	0.30624	0.14487	9.11475	2.11395	1.29350	0.6179
3.84	0.30387	0.14355	9.28164	2.11676	1.29459	0.6197
3.86	0.30151	0.14225	9.45128	2.11954	1.29567	0.6214
3.88	0.29919	0.14097	9.62371	2.12228	1.29674	0.6231
3.90	0.29688	0.13971	9.79895	2.12499	1.29779	0.6248
3.92	0.29460	0.13846	9.97704	2.12767	1.29883	0.6265
3.94	0.29235	0.13723	10.15803	2.13032	1.29987	0.6282
3.96	0.29011	0.13602	10.34194	2.13294	1.30089	0.6298
3.98	0.28790	0.13482	10.52883	2.13553	1.30190	0.6315
4.00	0.28571	0.13363	10.71872	2.13809	1.30290	0.6331
4.02	0.28355	0.13246	10.91166	2.14062	1.30389	0.6346
4.04	0.28141	0.13131	11.10768	2.14312	1.30487	0.6362
4.06	0.27928	0.13017	11.30681	2.14560	1.30583	0.6378
4.08	0.27718	0.12904	11.50912	2.14804	1.30679	0.6393
4.10	0.27510	0.12793	11.71463	2.15046	1.30774	0.6408
4.12	0.27305	0.12683	11.92337	2.15285	1.30868	0.6423
4.14	0.27101	0.12575	12.13540	2.15522	1.30960	0.6438
4.16	0.26899	0.12467	12.35076	2.15756	1.31052	0.6452
4.18	0.26699	0.12362	12.56947	2.15987	1.31143	0.6467
4.20	0.26502	0.12257	12.79160	2.16215	1.31233	0.6481
4.22	0.26306	0.12154	13.01719	2.16442	1.31322	0.6495
4.24	0.26112	0.12052	13.24626	2.16665	1.31410	0.6509

(Contd.)

Scanned by CamScanner

TABLE A4 One-Dimensional Flow with Friction ($\gamma = 1.4$)

M	T/T^*	p/p^*	p_0/p_0^*	ρ^*/ρ	F/F^*	$4fL_{max}/D$
4.26	0.25921	0.11951	13.47888	2.16886	1.31497	0.6523
4.28	0.25731	0.11852	13.71505	2.17105	1.31583	0.6536
4.30	0.25543	0.11753	13.95487	2.17321	1.31668	0.6550
4.32	0.25357	0.11656	14.19835	2.17535	1.31752	0.6563
4.34	0.25172	0.11560	14.44554	2.17747	1.31836	0.6576
4.36	0.24990	0.11466	14.69648	2.17956	1.31919	0.6589
4.38	0.24809	0.11372	14.95123	2.18163	1.32000	0.6602
4.40	0.24631	0.11279	15.20983	2.18368	1.32081	0.6615
4.42	0.24453	0.11188	15.47233	2.18571	1.32161	0.6627
4.44	0.24278	0.11098	15.73875	2.18771	1.32241	0.6640
4.46	0.24105	0.11008	16.00916	2.18970	1.32319	0.6652
4.48	0.23933	0.10920	16.28361	2.19166	1.32397	0.6664
4.50	0.23762	0.10833	16.56215	2.19360	1.32474	0.6676
4.52	0.23594	0.10746	16.84483	2.19552	1.32550	0.6688
4.54	0.23427	0.10661	17.13165	2.19742	1.32625	0.6700
4.56	0.23262	0.10577	17.42273	2.19930	1.32699	0.6712
4.58	0.23098	0.10494	17.71807	2.20116	1.32773	0.6723
4.60	0.22936	0.10411	18.01775	2.20300	1.32846	0.6734
4.62	0.22775	0.10330	18.32179	2.20482	1.32919	0.6746
4.64	0.22616	0.10249	18.63027	2.20662	1.32990	0.6757
4.66	0.22459	0.10170	18.94323	2.20841	1.33061	0.6768
4.68	0.22303	0.10091	19.26071	2.21017	1.33131	0.6779
4.70	0.22148	0.10013	19.58277	2.21192	1.33201	0.6790
4.72	0.21995	0.09936	19.90947	2.21365	1.33269	0.6800
4.74	0.21844	0.09860	20.24085	2.21536	1.33338	0.6811
4.76	0.21694	0.09785	20.57698	1.21705	1.33405	0.6821
4.78	0.21545	0.09711	20.91790	2.21872	1.33472	0.6831
4.80	0.21398	0.09637	21.26365	2.22038	1.33538	0.6842
4.82	0.21252	0.09564	21.61431	2.22202	1.33603	0.6852
4.84	0.21108	0.09492	21.96992	2.22365	1.33668	0.6862
4.86	0.20965	0.09421	24.33055	2.22526	1.33732	0.6872
4.88	0.20823	0.09351	22.69624	2.22685	1.33796	0.6881
4.90	0.20683	0.09281	23.06705	2.22842	1.33859	0.6891
4.92	0.20543	0.09212	23.44304	2.22998	1.33921	0.6901
4.94	0.20406	0.09144	23.82427	2.23153	1.33983	0.6910
4.96	0.20269	0.09077	24.21077	2.23306	1.34044	0.6920
4.98	0.20134	0.09010	24.60265	2.23457	1.34104	0.6929
5.00	0.20000	0.08944	24.99994	2.23607	1.34164	0.6938

Scanned by CamScanner

TABLE A5 One-Dimensional Frictionless Flow with Change in Stagnation Temperature ($\gamma = 1.4$)

M	T_0/T_0^*	T/T^*	p/p^*	p_0/p_0^*	ρ^*/ρ
0.00	0.00000	0.00000	2.40000	1.26788	0.00000
0.02	0.00192	0.00230	2.39866	1.26752	0.00096
0.04	0.00765	0.00917	2.39464	1.26646	0.00383
0.06	0.01712	0.02053	2.38796	1.26470	0.00860
0.08	0.03022	0.03621	2.37869	1.26226	0.01522
0.10	0.04678	0.05602	2.36686	1.25915	0.02367
0.12	0.06661	0.07970	2.35257	1.25539	0.03388
0.14	0.08947	0.10695	2.33590	1.25103	0.04578
0.16	0.11511	0.13743	2.31696	1.24608	0.05931
0.18	0.14324	0.17078	2.29586	1.24059	0.07439
0.20	0.17355	0.20661	2.27273	1.23460	0.09091
0.22	0.20574	0.24452	2.24770	1.22814	0.10879
0.24	0.23948	0.28411	2.22091	1.22126	0.12792
0.26	0.27446	0.32496	2.19250	1.21400	0.14821
0.30	0.34686	0.40887	2.13144	1.19855	0.19183
0.32	0.38369	0.45119	2.09908	1.19045	0.21495
0.34	0.42056	0.49327	2.06569	1.18215	0.23879
0.36	0.45723	0.53482	2.03142	1.17371	0.26327
0.38	0.49346	0.57553	1.99641	1.16517	0.28828
0.40	0.52903	0.61515	1.96078	1.15658	0.31373
0.42	0.56376	0.65346	1.92468	1.14796	0.33951
0.44	0.59748	0.69025	1.88822	1.13936	0.36556
0.46	0.63007	0.72538	1.85151	1.13032	0.39178
0.48	0.66139	0.75871	1.81466	1.12238	0.41810
0.50	0.69136	0.79012	1.77778	1.11405	0.44444
0.52	0.71990	0.81955	1.74095	1.10588	0.47075
0.54	0.74695	0.84695	1.70425	1.09789	0.49696
0.56	0.77249	0.87227	1.66778	1.09011	0.52302
0.58	0.79648	0.89552	1.63159	1.08256	0.54887
0.60	0.81892	0.91670	1.59574	1.07525	0.57447
0.62	0.83983	0.93584	1.56031	1.06822	0.59978
0.64	0.85920	0.95298	1.52532	1.06148	0.62477
0.66	0.87708	0.96816	1.49083	1.05503	0.64941
0.68	0.89350	0.98144	1.45688	1.04890	0.67366
0.70	0.90850	0.99290	1.42349	1.04310	0.69751
0.72	0.92212	1.00260	1.39069	1.03764	0.72093
0.74	0.93442	1.01062	1.35851	1.03253	0.74392
0.76	0.94546	1.01706	1.32696	1.02777	0.76645
0.78	0.95528	1.02198	1.29606	1.02337	0.78853
0.80	0.96395	1.02548	1.26582	1.01934	0.81013
0.82	0.97152	1.02763	1.23625	1.01569	0.83125
0.84	0.97807	1.02853	1.20734	1.01241	0.85190

(Contd.)

Scanned by CamScanner

TABLE A5 One-Dimensional Frictionless Flow with Change in Stagnation Temperature ($\gamma = 1.4$)

M	T_0/T_0^*	T/T^*	p/p^*	p_0/p_0^*	ρ^*/ρ
0.86	0.98363	1.02826	1.17911	1.00951	0.87207
0.88	0.98828	1.02689	1.15154	1.00699	0.89175
0.90	0.99207	1.02452	1.12465	1.00486	0.91097
0.92	0.99506	1.02120	1.09842	1.00311	0.92970
0.94	0.99729	1.01702	1.07285	1.00175	0.94797
0.96	0.99883	1.01205	1.04793	1.00078	0.96577
0.98	0.99971	1.00636	1.02365	1.00019	0.98311
1.00	1.00000	1.00000	1.00000	1.00000	1.00000
1.02	0.99973	0.99304	0.97698	1.00019	1.01645
1.04	0.99895	0.98554	0.95456	1.00078	1.03245
1.06	0.99769	0.97756	0.93275	1.00175	1.04804
1.08	0.99601	0.96913	0.91152	1.00311	1.06320
1.10	0.99392	0.96031	0.89087	1.00486	1.07795
1.12	0.99148	0.95115	0.85078	1.00699	1.09230
1.14	0.98871	0.94169	0.85123	1.00952	1.10626
1.16	0.98564	0.93196	0.83222	1.01243	1.11984
1.18	0.98230	0.92200	0.81374	1.01573	1.13305
1.20	0.97872	0.91185	0.79576	1.01941	1.14589
1.22	0.97492	0.90153	0.77827	1.02349	1.15838
1.24	0.97092	0.89108	0.76127	1.02795	1.17052
1.26	0.96675	0.88052	0.74473	1.03280	1.18233
1.28	0.96243	0.86988	0.72865	1.03803	1.19382
1.30	0.95798	0.85917	0.71301	1.04366	1.20499
1.32	0.95341	0.84843	0.69780	1.04967	1.21585
1.34	0.94873	0.83766	0.68301	1.05608	1.22642
1.36	0.94398	0.82689	0.66863	1.06288	1.23669
1.38	0.93915	0.81613	0.65464	1.07007	1.24669
1.40	0.93425	0.80539	0.64103	1.07765	1.25641
1.42	0.92931	0.79469	0.62779	1.08563	1.26587
1.44	0.92434	0.78405	0.61491	1.09401	1.27507
1.46	0.91933	0.77346	0.60237	1.10278	1.28402
1.48	0.91431	0.76294	0.59018	1.11196	1.29273
1.50	0.90928	0.75250	0.57831	1.12154	1.30120
1.52	0.90424	0.74215	0.56677	1.13153	1.30945
1.54	0.89921	0.73189	0.55553	1.14193	1.31748
1.56	0.89418	0.72174	0.54458	1.15274	1.32530
1.58	0.88917	0.71168	0.53393	1.16397	1.33291
1.60	0.88419	0.70174	0.52356	1.17561	1.34031
1.62	0.87922	0.69190	0.51346	1.18768	1.34753
1.64	0.87429	0.68219	0.50363	1.20017	1.35455
1.66	0.86939	0.67259	0.49405	1.21309	1.36139
1.68	0.86453	0.66312	0.48472	1.22644	1.36806

(*Contd.*)

Scanned by CamScanner

TABLE A5 One-Dimensional Frictionless Flow with Change in Stagnation Temperature ($\gamma = 1.4$)

M	T_0/T_0^*	T/T^*	p/p^*	p_0/p_0^*	ρ^*/ρ
1.70	0.85971	0.65377	0.47562	1.24023	1.37455
1.72	0.85493	0.64455	0.46677	1.25447	1.38088
1.74	0.85019	0.63545	0.45813	1.26915	1.38705
1.76	0.84551	0.62649	0.44972	1.28428	1.39306
1.78	0.84087	0.61765	0.44152	1.29987	1.39891
1.80	0.83628	0.60894	0.43353	1.31592	1.40462
1.82	0.83174	0.60036	0.42573	1.33244	1.41019
1.84	0.82726	0.59191	0.41813	1.34943	1.41562
1.86	0.82283	0.58360	0.41072	1.36690	1.42092
1.88	0.81846	0.57540	0.40349	1.38486	1.42608
1.90	0.81414	0.56734	0.39643	1.40330	1.43112
1.92	0.80987	0.55941	0.38955	1.42224	1.43604
1.94	0.80567	0.55160	0.38283	1.44168	1.44083
1.96	0.80152	0.54392	0.37628	1.46163	1.44551
1.98	0.79742	0.53636	0.36988	1.48210	1.45008
2.00	0.79339	0.52893	0.36364	1.50309	1.45455
2.02	0.78941	0.52161	0.35754	1.52462	1.45890
2.04	0.78549	0.51442	0.35158	1.54668	1.46315
2.06	0.78162	0.50735	0.34577	1.56928	1.46731
2.08	0.77782	0.50040	0.34009	1.59244	1.47136
2.10	0.77406	0.49356	0.33454	1.61616	1.47533
2.12	0.77037	0.48684	0.32912	1.64044	1.47920
2.14	0.76673	0.48023	0.32382	1.66531	1.48298
2.16	0.76314	0.47373	0.31865	1.69076	1.48668
2.18	0.75961	0.46734	0.31359	1.71680	1.49029
2.20	0.75613	0.46106	0.30864	1.74344	1.49383
2.22	0.75271	0.45488	0.30381	1.77070	1.49728
2.24	0.74934	0.44882	0.29908	1.79858	1.50066
2.26	0.74602	0.44285	0.29446	1.82708	1.50396
2.28	0.74276	0.43699	0.28993	1.85622	1.50719
2.30	0.73954	0.43122	0.28551	1.88602	1.51035
2.32	0.73638	0.42555	0.28118	1.91647	1.51344
2.34	0.73326	0.41998	0.27695	1.94759	1.51646
2.36	0.73020	0.41451	0.27281	1.97938	1.51942
2.38	0.72718	0.40913	0.26875	2.01187	1.52232
2.40	0.72421	0.40384	0.26478	2.04505	1.52515
2.42	0.72129	0.39864	0.26090	2.07895	1.52793
2.44	0.71842	0.39352	0.25710	2.11356	1.53065
2.46	0.71559	0.38850	0.25337	2.14890	1.53331
2.48	0.71280	0.38356	0.24973	2.18499	1.53591
2.50	0.71006	0.37870	0.24615	2.22183	1.53846
2.52	0.70736	0.37392	0.24266	2.25943	1.54096

(Contd.)

Scanned by CamScanner

TABLE A5 One-Dimensional Frictionless Flow with Change in Stagnation Temperature ($\gamma = 1.4$)

M	T_0/T_0^*	T/T^*	p/p^*	p_0/p_0^*	ρ^*/ρ
2.54	0.70471	0.36923	0.23923	2.29781	1.54341
2.56	0.70210	0.36461	0.23587	2.33698	1.54581
2.58	0.69953	0.36007	0.23258	2.37695	1.54816
2.60	0.69700	0.35561	0.22936	2.41774	1.55046
2.62	0.69451	0.35122	0.22620	2.45934	1.55272
2.64	0.69206	0.34691	0.22310	2.50179	1.55493
2.66	0.68964	0.34266	0.22007	2.54509	1.55710
2.68	0.68727	0.33849	0.21709	2.58925	1.55922
2.70	0.68494	0.33439	0.21417	2.63428	1.56131
2.72	0.68264	0.33035	0.21131	2.68021	1.56335
2.74	0.68037	0.32638	0.20850	2.72703	1.56536
2.76	0.67815	0.32248	0.20575	2.77478	1.56732
2.78	0.67595	0.31864	0.20305	2.82345	1.56925
2.80	0.67380	0.31486	0.20040	2.87307	1.57114
2.82	0.67167	0.31114	0.19780	2.92365	1.57300
2.84	0.66958	0.30749	0.19525	2.97521	1.57482
2.86	0.66752	0.30389	0.19275	3.02775	1.57661
2.88	0.66550	0.30035	0.19029	3.08129	1.57836
2.90	0.66350	0.29687	0.18788	3.13585	1.58008
2.92	0.66154	0.29344	0.18552	3.19144	1.58177
2.94	0.65960	0.29007	0.18319	3.24808	1.58343
2.96	0.65770	0.28675	0.18091	3.30578	1.58506
2.98	0.65583	0.28349	0.17867	3.36457	1.58666
3.00	0.65398	0.28028	0.17647	3.42445	1.58824
3.02	0.65216	0.27711	0.17431	3.48544	1.58978
3.04	0.65037	0.27400	0.17219	3.54755	1.59129
3.06	0.64861	0.27094	0.17010	3.61081	1.59278
3.08	0.64687	0.26792	0.16806	3.67524	1.59425
3.10	0.64516	0.26495	0.16604	3.74084	1.59568
3.12	0.64348	0.26203	0.16407	3.80763	1.59709
3.14	0.64182	0.25915	0.16212	3.87564	1.59848
3.16	0.64018	0.25632	0.16022	3.94487	1.59985
3.18	0.63858	0.25353	0.15834	4.01536	1.60119
3.20	0.63699	0.25078	0.15649	4.08711	1.60250
3.22	0.63543	0.24808	0.15468	4.16014	1.60380
3.24	0.63389	0.24541	0.15290	4.23448	1.60507
3.26	0.63237	0.24279	0.15115	4.31013	1.60632
3.28	0.63088	0.24021	0.14942	4.38713	1.60755
3.30	0.62941	0.23766	0.14773	4.46548	1.60877
3.32	0.62795	0.23515	0.14606	4.54521	1.60996
3.34	0.62652	0.23268	0.14442	4.62634	1.61113
3.36	0.62512	0.23025	0.14281	4.70888	1.61228

(*Contd.*)

Scanned by CamScanner

TABLE A5 One-Dimensional Frictionless Flow with Change in Stagnation Temperature ($\gamma = 1.4$)

M	T_0/T_0^*	T/T^*	p/p^*	p_0/p_0^*	ρ^*/ρ
3.38	0.62373	0.22785	0.14123	4.79286	1.61341
3.40	0.62236	0.22549	0.13966	4.87829	1.61452
3.42	0.62101	0.22317	0.13813	4.96520	1.61562
3.44	0.61968	0.22087	0.13662	5.05361	1.61670
3.46	0.61837	0.21861	0.13513	5.14354	1.61776
3.48	0.61708	0.21639	0.13367	5.23500	1.61881
3.50	0.61581	0.21419	0.13223	5.32802	1.61983
3.52	0.61455	0.21203	0.13081	5.42263	1.62085
3.54	0.61331	0.20990	0.12942	5.51883	1.62184
3.56	0.61209	0.20780	0.12805	5.61666	1.62282
3.58	0.61089	0.20573	0.12670	5.71614	1.62379
3.60	0.60970	0.20369	0.12537	5.81729	1.62474
3.62	0.60853	0.20167	0.12406	5.92012	1.62567
3.64	0.60738	0.19969	0.12277	6.02467	1.62660
3.66	0.60624	0.19773	0.12150	6.13096	1.62750
3.68	0.60512	0.19581	0.12024	6.23900	1.62840
3.70	0.60401	0.19390	0.11901	6.34883	1.62928
3.72	0.60292	0.19203	0.11780	6.46046	1.63014
3.74	0.60184	0.19018	0.11660	6.57393	1.63100
3.76	0.60078	0.18836	0.11543	6.68925	1.63184
3.78	0.59973	0.18656	0.11427	6.80645	1.63267
3.80	0.59870	0.18478	0.11312	6.92555	1.63348
3.82	0.59768	0.18303	0.11200	7.04658	1.63429
3.84	0.59667	0.18131	0.11089	7.16956	1.63508
3.86	0.59568	0.17961	0.10979	7.29452	1.63586
3.88	0.59470	0.17793	0.10871	7.42149	1.63663
3.90	0.59373	0.17627	0.10765	7.55048	1.63739
3.92	0.59278	0.17463	0.10661	7.68154	1.63814
3.94	0.59184	0.17302	0.10557	7.81467	1.63888
3.96	0.59091	0.17143	0.10456	7.94991	1.63960
3.98	0.58999	0.16986	0.10355	8.08729	1.64032
4.00	0.58909	0.16831	0.10256	8.22683	1.64103
4.02	0.58819	0.16678	0.10159	8.36856	1.64172
4.04	0.58731	0.16527	0.10063	8.51250	1.64241
4.06	0.58644	0.16378	0.09968	8.65869	1.64309
4.08	0.58558	0.16231	0.09875	8.80716	1.64375
4.10	0.58473	0.16086	0.09782	8.95792	1.64441
4.12	0.58390	0.15943	0.09691	9.11101	1.64506
4.14	0.58307	0.15802	0.09602	9.26647	1.64570
4.16	0.58225	0.15662	0.09513	9.42431	1.64633
4.18	0.58145	0.15524	0.09426	9.58456	1.64696
4.20	0.58065	0.15388	0.09340	9.74726	1.64757

(*Contd.*)

Scanned by CamScanner

TABLE A5 One-Dimensional Frictionless Flow with Change in Stagnation Temperature ($\gamma = 1.4$)

M	T_0/T_0^*	T/T^*	p/p^*	p_0/p_0^*	ρ^*/ρ
4.22	0.57987	0.15254	0.09255	9.91244	1.64818
4.24	0.57909	0.15121	0.09171	10.08013	1.64878
4.26	0.57832	0.14990	0.09089	10.25035	1.64937
4.28	0.57757	0.14861	0.09007	10.42314	1.64995
4.30	0.57682	0.14734	0.08927	10.59851	1.65052
4.32	0.57608	0.14607	0.08847	10.77653	1.65109
4.34	0.51535	0.14483	0.08769	10.95721	1.65165
4.36	0.57463	0.14360	0.08691	11.14057	1.65220
4.38	0.57392	0.14239	0.08615	11.32666	1.65275
4.40	0.57322	0.14119	0.08540	11.51551	1.65329
4.42	0.57252	0.14000	0.08465	11.70714	1.65382
4.44	0.57183	0.13883	0.08392	11.90160	1.65434
4.46	0.57116	0.13767	0.08319	12.09891	1.65486
4.48	0.57049	0.13653	0.08248	12.29911	1.65537
4.50	0.56982	0.13540	0.08177	12.50222	1.65588
4.52	0.56917	0.13429	0.08107	12.70830	1.65638
4.54	0.56852	0.13319	0.08039	12.91737	1.65687
4.56	0.56789	0.13210	0.07971	13.12946	1.65735
4.58	0.56726	0.13102	0.07903	13.34460	1.65783
4.60	0.56663	0.12996	0.07837	13.56284	1.65831
4.62	0.56602	0.12891	0.07771	13.78422	1.65878
4.64	0.56541	0.12787	0.07707	14.00875	1.65924
4.66	0.56480	0.12685	0.07643	14.23648	1.65969
4.68	0.56421	0.12583	0.07580	14.46746	1.66014
4.70	0.56362	0.12483	0.07517	14.70170	1.66059
4.72	0.56304	0.12384	0.07456	14.93925	1.66103
4.74	0.56246	0.12286	0.07395	15.18016	1.66146
4.76	0.56190	0.12190	0.07335	15.42444	1.66189
4.78	0.56133	0.12094	0.07275	15.67216	1.66232
4.80	0.56078	0.12000	0.07217	15.92333	1.66274
4.82	0.56023	0.11906	0.07159	16.17798	1.66315
4.84	0.55969	0.11814	0.07101	16.43619	1.66356
4.86	0.55915	0.11722	0.07045	16.69797	1.66397
4.88	0.55862	0.11632	0.06989	16.96336	1.66437
4.90	0.55809	0.11543	0.06934	17.23241	1.66476
4.92	0.55758	0.11455	0.06879	17.50515	1.66515
4.94	0.55706	0.11367	0.06825	17.78162	1.66554
4.96	0.55655	0.11281	0.06772	18.06187	1.66592
4.98	0.55605	0.11196	0.06719	18.34592	1.66629
5.00	0.55556	0.11111	0.06667	18.63384	1.66667

Scanned by CamScanner

Appendix B

Listing of the Method of Characteristics Program

```
#include <stdio.h>
#include <math.h>

#define TRUE 1
#define FALSE 0

double gpm_mn(double m, double Gamma);
double gmn_pm(double neu, double Gamma);
double gar_mn(double m, double Gamma);
double tand(double x)
{
return tan(x*acos(-1.0)/180.0);
}

int main(int argc, char* argv[ ])
{
double  theta[200][200],   neu[200][200];
double  m[200][200],       a[200][200];
double m1, m2, Gamma, at, neu1, neu2, dneu, dtheta, theta0, theta1, x, y;
int i, j, k, count;
char  out[256];
FILE *fp;
count = 0;

mach_number:
printf("Mach numbers of input and output streams ?\n");
scanf("%lf %lf", &m1, &m2);
if((m1<1.0) || (m2<=m1)) goto mach_number;

// get specific heats ratio of the gas
heat_ratio:
```


Scanned by CamScanner

```
printf("Specific heat ratio of the gas (Cp/Cv) ?\n");
scanf("%lf", &Gamma);
if(Gamma<=0.0) goto heat_ratio;

// evaluate.....
neu1 = gpm_mn(m1,Gamma);
neu2 = gpm_mn(m2,Gamma);
dneu = (neu2-neu1)/2.0;

angle_dtheta:
printf("Angular separation among charateristics (0,%8.5f](deg.) ?\n", dneu);
scanf("%lf", &dtheta);
if((dtheta<=0.0)||(dtheta>dneu)) goto angle_dtheta;

net_area:
printf("Net area at inflow point \n");
scanf("%lf", &at);
if(at<=0.0) goto net_area;
at = at/gar_mn(m1,Gamma);

theta0 = 0.0;

printf("Output file name <\"file name\">250 chars, max.) ?\n");
scanf("%251s", out);
printf("output filename: %s\n", out);
fp = fopen(out, "wt");

k= (int)(dneu/dtheta)+1;
theta1 = dneu - (double)(k-1)*dtheta;

fprintf(fp,
"-------------------------------------------------------------------------------------------\n"
"                                Prandtl-Meyer\n"
"                  mach #         function\n"
"                                   neu\n"
"-------------------------------------------------------------------------------------------\n"
"inflow   %11.5f  %11.5f\n"
"outflow  %11.5f  %11.5f\n"
"-------------------------------------------------------------------------------------------\n"
"specific heats ratio (gamma = cp/cv)    :%11.5f\n"
"gas inlet point area                    :%11.5f\n"
"gas inlet & outlet angle                :%11.5f\n"
"total turning rquired for accn.         :%11.5f deg.\n"
"turning provided by one side            :%11.5f deg.\n"
"Total number of characteristics         :%5d\n"
"Angular separation between\n"
"vertical & first characteristics        :%11.5f deg.\n"
"two consecutive charateristics          :%11.5f deg.\n",
m1, neu1, m2, neu2, Gamma, at, theta0, dneu*2, dneu, k, theta1, dtheta);

for ( i = 1; i <= k+1 ; ++i ) {
for ( j = i; j <= k+1 ; ++j ) {
```

Scanned by CamScanner

```
if(i==1){
if(j==i){
theta[i][j] = theta0;
neu[i][j] = neu1;
} else {
if(j==i+1){
theta[i][j] = theta[i][j-1] + theta1;
neu[i][j] = neu[i][j-1] + theta1;
} else {
theta[i][j] = theta[i][j-1] + dtheta;
neu[i][j] = neu[i][j-1] + dtheta;
}
}
} else {
if(j==i){
theta[i][j] = theta0;
neu[i][j]   = theta[i-1][j] + neu[i-1][j];
} else {
neu[i][j] = neu[i-1][j] + theta[i-1][j] + neu[i][j-1] - theta[i][j-1];
neu[i][j] = neu[i][j]/2.0;
theta[i][j] = neu[i-1][j] + theta[i-1][j] - neu[i][j-1] + theta[i][j-1];
theta[i][j] = theta[i][j]/2.0;
}
}
m[i][j] = gmn_pm(neu[i][j], Gamma);
a[i][j] = gar_mn(m[i][j], Gamma);

if( ((count%66)==0) || (j==1)) {
fprintf(fp,
"-------------------------------------------------------------------------------------------\n"
"point      theta      Neu      Mach #  Area Ratio      X      Y\n"
"C +  C-\n"
"-------------------------------------------------------------------------------------------\n"
);
count = count + 4;
}

if( (j==1) || ((j==(k+1))&&(j!=i)) ) {
y = a[i] [j]*at/2.0;
if(j==1){
x= 0.0;
} else {
if(i==1){
x = x + ((a[i][j] - a[i][1]) * at /(2.0*tand(theta[i][j])));
} else {
x = x +((a[i][j] - a[i-1][j]) * at / (2.0*tand(theta[i][j])));
}
}
fprintf(fp,
"%4d,%4d %9.5f %9.5f %8.5f %10.5f %12.5f %12.5f\n",
i-1, j-i, theta[i][j], neu[i][j], m[i][j], a[i][j], x, y);
```

Scanned by CamScanner

```
} else {
fprintf(fp,
"%4d, %4d %9.5f %9.5f %8.5f %10.5f\n",
i-1, j-i, theta[i][j], neu[i][j], m[i][j], a[i][j]);
}
count = count + 1;
}
}

fclose(fp);

return 0;
        }

double gpm_mn(double m, double Gamma)
        {
double r, mm;
r = sqrt((Gamma + 1.0)/(Gamma - 1.0));
mm = sqrt(m*m - 1.0);
return ( (r*atan(mm/r) - atan(mm))*57.32 );
        }
double gmn_pm(double neu, double Gamma)
        {
double m, m1, m2, f, f1, f2, mmid, fmid, eps, r, mm, gmn, neu1, neu2, dm;
int found, n, i;
#define f(M) ( (sqrt((Gamma+1.0)/(Gamma-1.0))
              *atan(sqrt((Gamma-1.0)*(M*M-1.0)/(Gamma+1.0)))
                -atan(sqrt(M*M-1.0)))*57.32-neu )
eps = 1.0e-5;

neu1 = 0.0;
neu2 = (1.57*(sqrt((Gamma+1.0)/(Gamma-1.0)) - 1.0))*57.32;
if ((neu<neu1)||(neu>neu2)) {
printf("Error : Invalid value of Prandtl - Meyer function./"
        "Neu out of possible range for given gamma\n");
gmn = 0.0;
} else {
dm = 0.001;
m2 = 1.0;
f2 = f(m2);
found = FALSE;
while (found != TRUE) {
m1 = m2;
f1 = f2;
m2 = m1 + dm;
f2 = f(m2);
if(f1*f2<=0.0) found = TRUE;
}
if(fabs(f1)<eps) {
gmn = m1;
goto return_gmn;
```

Scanned by CamScanner

```
}
    if(fabs(f2)<eps) {
gmn = m2;
goto return_gmn;
}

n= (int)(log10((m2-m1)/eps)/log10(2.0)) +1;
for ( i = 1; i <= n; ++i) {
mmid = (m1 + m2) / 2.0;
fmid = f(mmid);
if (f1*fmid<=0.0) {
m2 = mmid;
f2 = fmid;
} else {
m1 = mmid;
f1 = fmid;
}
}
       gmn = (m1 + m2)/2.0;
                }
            return_gmn:
            return gmn;
}
double gar_mn(double m, double Gamma)
{
return ( pow(2.0*(1.0+(Gamma-1.0)/2.0*m*m)/(Gamma+1.0),(Gamma+1.0)/
(2.0*(Gamma-1.0)))/m );
}
\vskip5mm
\hrule
```

Scanned by CamScanner

Appendix C

Output for Mach 2.0 Nozzle Contour

	Mach #	Function Neu
Inflow	1.00000	0.00000
Outflow	2.00000	26.39091

Specific heats ratio (Gamma = c_p/c_v)	:	1.40000
Gas inlet point area	:	17.60000
Gas inlet and outlet angle		0.00000
Total turning required for accn.	:	26.39091 deg.
Turning provided by one side	:	13.19546 deg.
Total number of characteristics	:	14
Angular separation between		
vertical and first characteristic	:	0.19546 deg.
two consecutive characteristics	:	1.00000 deg.

Point C+	Point C−	Theta	Neu	Mach #	Area ratio	X	Y
0,	0	0.00000	0.00000	1.00000	1.00000	0.00000	8.80000
0,	1	0.19546	0.19546	1.02692	1.00060		
0,	2	1.19546	1.19546	1.09254	1.00681		
0,	3	2.19546	2.19546	1.14158	1.01560		
0,	4	3.19546	3.19546	1.18501	1.02619		
0,	5	4.19546	4.19546	1.22538	1.03831		
0,	6	5.19546	5.19546	1.26378	1.05182		
0,	7	6.19546	6.19546	1.30082	1.06665		
0,	8	7.19546	7.19546	1.33690	1.08278		
0,	9	8.19546	8.19546	1.37226	1.10018		
0,	10	9.19546	9.19546	1.40709	1.11885		
0,	11	10.19546	10.19546	1.44154	1.13883		

(Contd.)

Scanned by CamScanner

Point C+	Point C−	Theta	Neu	Mach #	Area ratio	X	Y
0,	12	11.19546	11.19546	1.47570	1.16012		
0,	13	12.19546	12.19546	1.50968	1.18277		
0,	14	13.19546	13.19546	1.54353	1.20681	7.76200	10.61991
1,	0	0.00000	0.39091	1.04302	1.00151		
1,	1	1.00000	1.39091	1.10280	1.00836		
1,	2	2.00000	2.39091	1.15039	1.01754		
1,	3	3.00000	3.39091	1.19310	1.02845		
1,	4	4.00000	4.39091	1.23301	1.04084		
1,	5	5.00000	5.39091	1.27111	1.05462		
1,	6	6.00000	6.39091	1.30794	1.06970		
1,	7	7.00000	7.39091	1.34386	1.08608		
1,	8	8.00000	8.39091	1.37911	1.10372		
1,	9	9.00000	9.39091	1.41385	1.12265		
1,	10	10.00000	10.39091	1.44823	1.14288		
1,	11	11.00000	11.39091	1.48236	1.16444		
1,	12	12.00000	12.39091	1.51630	1.18736		
1,	13	13.00000	13.39091	1.55014	1.21167	7.94751	10.66274
2,	0	0.00000	2.39091	1.15039	1.01754		
2,	1	1.00000	3.39091	1.19310	1.02845		
2,	2	2.00000	4.39091	1.23301	1.04084		
2,	3	3.00000	5.39091	1.27111	1.05462		
2,	4	4.00000	6.39091	1.30794	1.06970		
2,	5	5.00000	7.39091	1.34386	1.08608		
2,	6	6.00000	8.39091	1.37911	1.10372		
2,	7	7.00000	9.39091	1.41385	1.12265		
2,	8	8.00000	10.39091	1.44823	1.14288		
2,	9	9.00000	11.39091	1.48236	1.16444		
2,	10	10.00000	12.39091	1.51630	1.18736		
2,	11	11.00000	13.39091	1.55014	1.21167		
2,	12	12.00000	14.39091	1.58393	1.23745	9.01450	10.88953
3,	0	0.00000	4.39091	1.23301	1.04084		
3,	1	1.00000	5.39091	1.27111	1.05462		
3,	2	2.00000	6.39091	1.30794	1.06970		
3,	3	3.00000	7.39091	1.34386	1.08608		
3,	4	4.00000	8.39091	1.37911	1.10372		
3,	5	5.00000	9.39091	1.41385	1.12265		
3,	6	6.00000	10.39091	1.44823	1.14288		
3,	7	7.00000	11.39091	1.48236	1.16444		
3,	8	8.00000	12.39091	1.51630	1.18736		
3,	9	9.00000	13.39091	1.55014	1.21167		
3,	10	10.00000	14.39091	1.58393	1.23745		
3,	11	11.00000	15.39091	1.61772	1.26473	10.24975	11.12964
4,	0	0.00000	6.39091	1.30794	1.06970		
4,	1	1.00000	7.39091	1.34386	1.08608		
4,	2	2.00000	8.39091	1.37911	1.10372		
4,	3	3.00000	9.39091	1.41385	1.12265		

(Contd.)

Scanned by CamScanner

Point C+	C−	Theta	Neu	Mach #	Area ratio	X	Y
4,	4	4.00000	10.39091	1.44823	1.14288		
4,	5	5.00000	11.39091	1.48236	1.16444		
4,	6	6.00000	12.39091	1.51630	1.18736		
4,	7	7.00000	13.39091	1.55014	1.21167		
4,	8	8.00000	14.39091	1.58393	1.23745		
4,	9	9.00000	15.39091	1.61772	1.26473		
4,	10	10.00000	16.39091	1.65156	1.29358	11.68955	11.38352
5,	0	0.00000	8.39091	1.37911	1.10372		
5,	1	1.00000	9.39091	1.41385	1.12265		
5,	2	2.00000	10.39091	1.44823	1.14288		
5,	3	3.00000	11.39091	1.48236	1.16444		
5,	4	4.00000	12.39091	1.51630	1.18736		
5,	5	5.00000	13.39091	1.55014	1.21167		
5,	6	6.00000	14.39091	1.58393	1.23745		
5,	7	7.00000	15.39091	1.61772	1.26473		
5,	8	8.00000	16.39091	1.65156	1.29358		
5,	9	9.00000	17.39091	1.68550	1.32408	13.38433	11.65195
6,	0	0.00000	10.39091	1.44823	1.14288		
6,	1	1.00000	11.39091	1.48236	1.16444		
6,	2	2.00000	12.39091	1.51630	1.18736		
6,	3	3.00000	13.39091	1.55014	1.21167		
6,	4	4.00000	14.39091	1.58393	1.23745		
6,	5	5.00000	15.39091	1.61772	1.26473		
6,	6	6.00000	16.39091	1.65156	1.29358		
6,	7	7.00000	17.39091	1.68550	1.32408		
6,	8	8.00000	18.39091	1.71954	1.35629	15.40098	11.93537
7,	0	0.00000	12.39091	1.51630	1.18736		
7,	1	1.00000	13.39091	1.55014	1.21167		
7,	2	2.00000	14.39091	1.58393	1.23745		
7,	3	3.00000	15.39091	1.61772	1.26473		
7,	4	4.00000	16.39091	1.65156	1.29358		
7,	5	5.00000	17.39091	1.68550	1.32408		
7,	6	6.00000	18.39091	1.71954	1.35629		
7,	7	7.00000	19.39091	1.75375	1.39031	17.83881	12.23470
8,	0	0.00000	14.39091	1.58393	1.23745		
8,	1	1.00000	15.39091	1.61772	1.26473		
8,	2	2.00000	16.39091	1.65156	1.29358		
8,	3	3.00000	17.39091	1.68550	1.32408		
8,	4	4.00000	18.39091	1.71954	1.35629		
8,	5	5.00000	19.39091	1.75375	1.39031		
8,	6	6.00000	20.39091	1.78815	1.42621	20.84510	12.55067
9,	0	0.00000	16.39091	1.65156	1.29358		
9,	1	1.00000	17.39091	1.68550	1.32408		
9,	2	2.00000	18.39091	1.71954	1.35629		
9,	3	3.00000	19.39091	1.75375	1.39031		
9,	4	4.00000	20.39091	1.78815	1.42621		
9,	5	5.00000	21.39091	1.82277	1.46411	24.65715	12.88418

(Contd.)

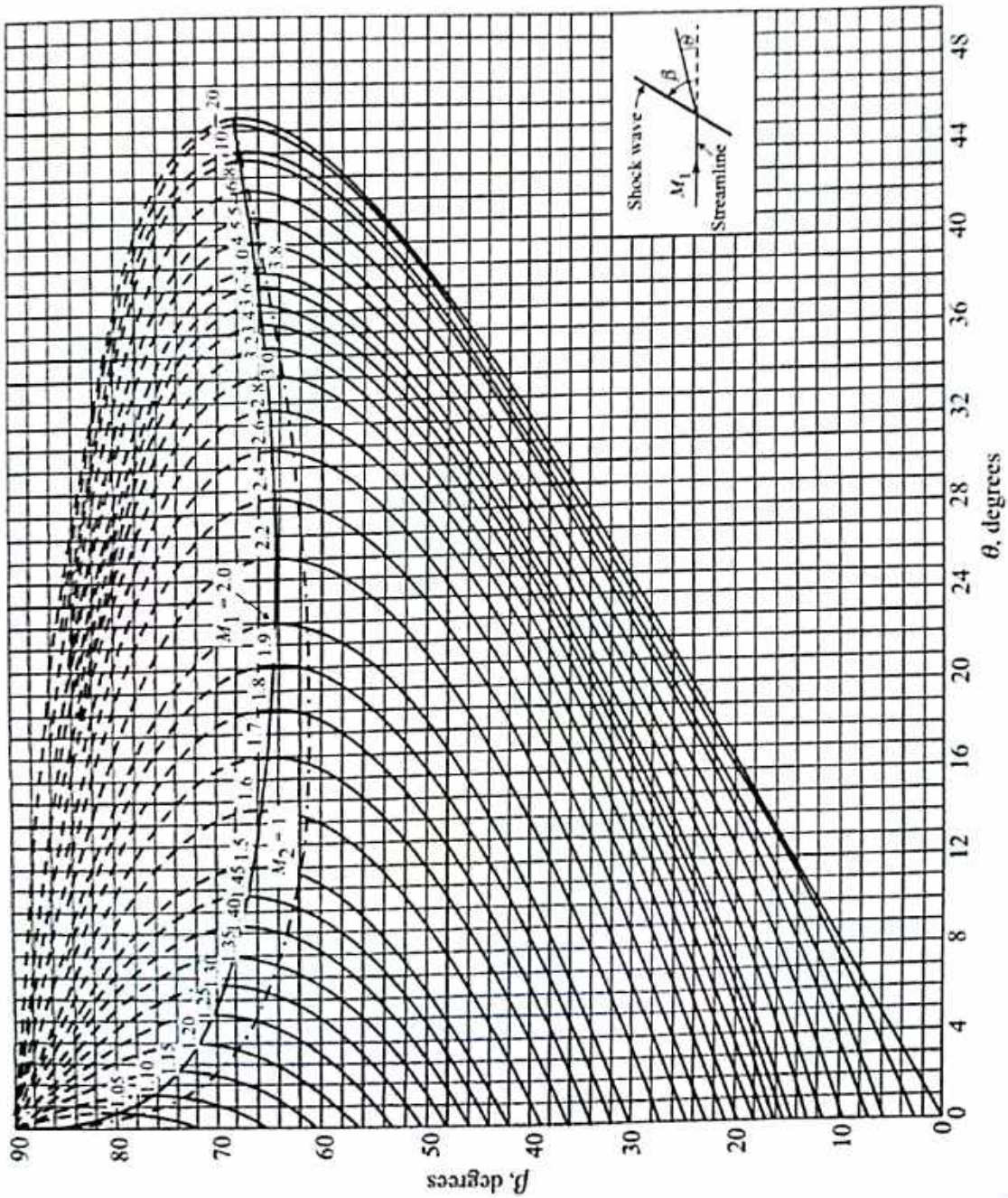
Scanned by CamScanner

Point C+	Point C−	Theta	Neu	Mach #	Area ratio	X	Y
10,	0	0.00000	18.39091	1.71954	1.35629		
10,	1	1.00000	19.39091	1.75375	1.39031		
10,	2	2.00000	20.39091	1.78815	1.42621		
10,	3	3.00000	21.39091	1.82277	1.46411		
10,	4	4.00000	22.39091	1.85763	1.50411	29.69031	13.23613
11,	0	0.00000	20.39091	1.78815	1.42621		
11,	1	1.00000	21.39091	1.82277	1.46411		
11,	2	2.00000	22.39091	1.85763	1.50411		
11,	3	3.00000	23.39091	1.89275	1.54631	36.77670	13.60752
12,	0	0.00000	22.39091	1.85763	1.50411		
12,	1	1.00000	23.39091	1.89275	1.54631		
12,	2	2.00000	24.39091	1.92818	1.59085	48.00141	13.99949
13,	0	0.00000	24.39091	1.92818	1.59085		
13,	1	1.00000	25.39091	1.96392	1.63787	71.70515	14.41324
14,	0	0.00000	26.39091	2.00000	1.68750		

Scanned by CamScanner

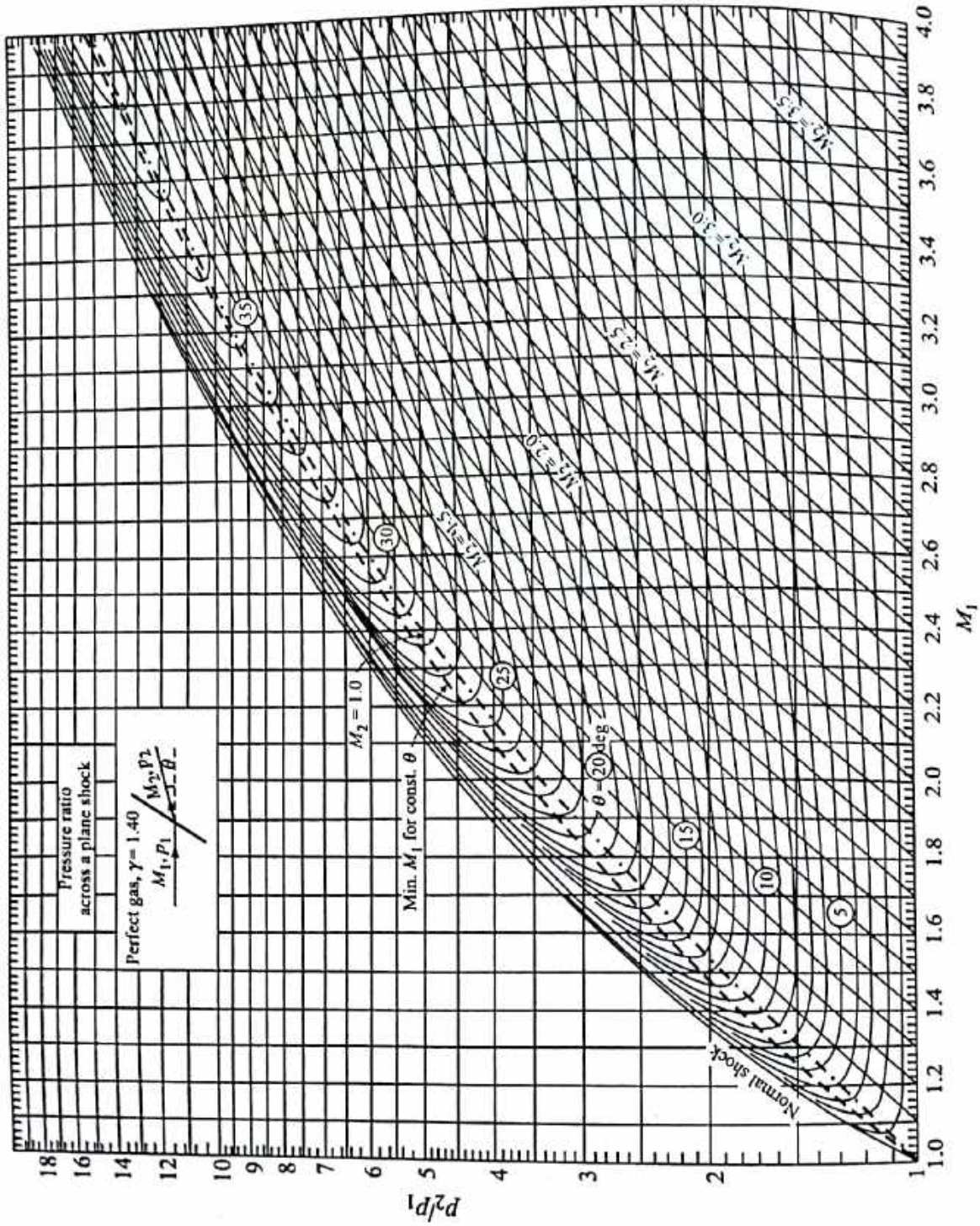
Appendix D

Oblique Shock Chart I



Scanned by CamScanner

Oblique Shock Chart 2



Scanned by CamScanner

Selected References

Allen, J.E., *Aerodynamics*, Granada, London, 1982.

Anderson, J.D., Jr., *Modern Compressible Flow*, McGraw-Hill, New York, 1982.

Anderson, J.D., Jr., *Hypersonic and High Temperature Gas Dynamics*, McGraw-Hill, New York, 1989.

Bird, G.A., *Molecular Gas Dynamics*, Clarendon Press, Oxford, 1976.

Courant, R. and Friedrichs, K.O., *Supersonic Flow with Shock Waves*, Springer-Verlag, New York, 1977.

Emmons, H.W. (Ed.), *Foundations of Gas Dynamics* (Vol. III of High Speed Aerodynamics and Jet Propulsion), Princeton, New Jersey, 1956.

Ferri, Antonio, *Elements of Aerodynamics of Supersonic Flows*, Macmillan, New York, 1949.

Hinze, J.O., *Turbulence*, McGraw-Hill, New York, 1975.

John, J.E.A., *Gas Dynamics*, Allyn and Bacon, Boston, 1984.

Ladenburg, R.W. (Ed.), *Physical Measurement in Gas Dynamics and Combustion*—Part I, Princeton University Series, Princeton, New Jersey, 1954.

Liepmann, H.W. and Roshko, A., *Elements of Gas Dynamics*, Wiley, New York, 1963.

Pankhurst, R.C. and Holder, D.W., *Wind Tunnel Technique*, Sir Isaac Pitman and Sons, London, 1982.

Patterson, G.N., *Molecular Flow of Gases*, Wiley, New York, 1956.

Pope, A. and Goin, K.L., *High-Speed Wind Tunnel Testing*, Wiley, New York, 1965.

Rathakrishnan, E., *Fundamentals of Engineering Thermodynamics*, Second edition, PHI Learning, Delhi, 2005.

Rathakrishnan, E., *Fluid Mechanics an Introduction*, Third edition, PHI Learning, Delhi, 2012.

Scanned by CamScanner

Rathakrishnan, E., *Gas Tables*, Second edition, Universities Press, India, 2004.

Rathakrishnan, E., *Instrumentation, Measurements, and Experiments in Fluids*, 2nd ed. CRC Press, Boca Raton, FL, USA, 2016.

Radhakrishnan, E., High Enthalgy Gas Dynamics, Wiley, 2015.

Schaaf, S.A. and Chambre, P.L., *Flow of Rarefied Gases*, Princeton Aeronautical Paperback, No. 8, Princeton University, New Jersey, 1961.

Shames, H., *Mechanics of Fluids*, McGraw-Hill, New York, 1962.

Shapiro, A.H., *Dynamics and Thermodynamics of Compressible Fluid Flow*, Vols. I & II, Ronald Press, New York, 1953.

Thompson, P.A., *Compressible Fluid Dynamics*, McGraw-Hill, New York, 1972.

Zucrow, M.J. and Hoffman, J.D., *Gas Dynamics*, Vols. I & II, Wiley, New York, 1976.

Scanned by CamScanner

Index

θ–β–M relation, 179

Action, zone of, 14, 16
Adiabatic process, 19, 22, 36
Adiabatic wall temperature, 392
Aerodynamic forces, 1, 223
Aerofoil
  circular arc, 224
  diamond wedge, 224
  in flow, 255, 263
Affine transformation, 271, 295
Area-Mach number relation, 65
Area-velocity relation, 62
Axially symmetric flows, 269

Barotropic fluid, 49
Barrel shock, 75
Basic potential equation for compressible flow, 255
Bernoulli's equation, 4, 22, 28, 49, 88
Blowdown tunnels, 416, 423
  operation, 434, 435
  running time, 439
Blunt body
  flow over, 110
  shock at, 218
Bodies of revolution, 255, 260
Boundary conditions, 263–265
Boundary layer, 31

Calorical properties, 24
Calorically perfect gas, 26, 27, 37, 466
Camber, effect on drag, 231, 232
Cancellation of wave reflection, 375, 383
Centred expansion waves, 144, 163, 193, 322
Characteristic Mach number, 59
Characteristics, 189
  method of, 359
Chemically reacting gas, 117, 124, 162
Choked flow, 68
Choked state, 74
Circulation, 252
Coefficient
  of friction (*see* Friction coefficient), 333
  of heat transfer, 396
  of pressure (*see* Pressure coefficient), 94
Compatibility relation, 360, 363
Compressibility, 2, 3, 4, 15
  correction to dynamic pressure, 91
  limiting conditions for, 4–5
Compressible Bernoulli's equation, 28, 98
Compressible flow, definition of, 3, 15
Compression, 189
  corner, 172
  front, 110
Conservation
  of energy, 35
  of mass, 4
Continuity equation, 2, 61, 145, 195, 253, 261
Continuum, 457
  flow, 459
Contoured nozzle, 76, 77

Scanned by CamScanner

Convergent-divergent
duct, 63
nozzle, 74
Cooling, flow with simple T_0 change, 342, 346
Corner flow, 187
Critical Mach number, 298
Critical values, 55, 58
Crocco's theorem, 249, 251, 267

D'Alembert's paradox, 225
De Laval nozzle, 64, 76
Density problems, 397
Detached shock, 89, 218
Diffusers, 85
isentropic efficiency of, 421
polytropic efficiency of, 421
of supersonic tunnels, 421
Discharge from a reservoir, 51
Dissimilar metals, 392
Disturbance, waves, propagation of, 12–14
Drag, 224
due to camber, 232
due to lift, 232
due to thickness, 232
due to wave, 239

Effects of second throat, 423
Elliptic equation, 258, 271, 288, 310
Energy equation, 21
for an adiabatic flow, 21, 22, 28, 36
isentropic flow, 11
for an open system, 21
Energy ratio of
continuous tunnels, 422
intermittent tunnels, 422
Enthalpy, 19
Entropy, 23
calculation of, 26
definition of, 23
equation, 23
Equation of state
calorical, 24, 26
for perfect or ideal gas, 26
thermal, 24, 26
Euler's equation, 195, 254
Expansion waves, 172, 189
Prandtl–Meyer, 194
reflected, 208

Fanno
curve, 331
flow, 329
line, 330
table of, 526–531
First law of thermodynamics, 19
Flow angularity, 395
determination of, 445
Flow with friction, 329
Flow with heat transfer, 309
Free molecular flow, 459–460
Friction coefficient, 335, 336
Frictional drag, 225, 239

Gas constant, 8, 24, 37
universal, 37
Gas dynamics
a brief history, 1
definition of, 2, 15
Gladstone–Dale
equation, 398
constant, 399
Gothert's rule, 273, 278, 281, 288, 290

Heat addition, flow with, 343, 346, 353
High-speed tunnels, 415
calibration of, 384, 441, 453
compressor-tunnel matching, 425
continuous tunnels, 418
definition of, 415
flow angularity, 442, 445
Mach number determination, 442
mass flow, 430
model mounting sting effects, 420, 447, 448
open circuit tunnels, 415
optimum conditions, 438
Reynolds number control, 435
Reynolds number effects, 447
starting loads, 447

Scanned by CamScanner

test-section noise, 445
turbulence level, 445
running time of, 439
Hodograph plane, 183
Hot wire anemometer, 397
Hugoniot
curve, 125
equation, 124, 162
Hyperbolic equation, 258, 271, 288, 310
Hypersonic
flow, 16, 17
similarity, 285

Ideal gas, 36
Incompressible flow, 3
Induction type tunnels, 417, 450
Interferometer, 397–399, 449
fringe-displacement method, 403
quantitative evaluation, 401
Irrotational flow, 251–253
Isentropic flow table, 469–481
Isentropic process
definition of, 8, 19, 24
equation for, 8
Isentropic relations, 29

King's law, 396
Knudsen number, 458

Laplace equation, 50, 54, 267, 288, 315
basic solutions of, 253, 267
Lift, 228, 231
coefficient of, 229, 232
Linearized potential flow equation, 257
Losses in supersonic tunnels, 419

Mach angle, 12, 16
Mach angle–Mach number relation, 188
Mach cone, 13, 14
Mach lines, 14, 16, 188, 189
Mach number
critical, 275
definition of, 5
relation to area, 65
relation to density, 70
relation to pressure, 70
relation to temperature, 70
relation to total pressure, 85, 117
behind shock wave, 114
Mach reflection, 219
Mach wave, 14, 16
Mass flow, 53, 73
Maximum velocity, 52
Method of characteristics, 359
axi-symmetric flow, 367
boundary points, 364–365
compatibility relations, 360, 363
concepts of characteristics, 359
design of supersonic nozzle, 377
nonisentropic flow, 370
numerical computation, 363, 373
program listing of, 538–546
theorems for 2-D flow, 371
Momentum equations, 111, 195, 254, 267
Moving shock wave, 126-128, 135

Natural coordinates, 249, 360, 362
Nonsimple regions, 201
characteristics in, 372
Normal shock, 110
in calorically perfect gas, 112
description of, 111
diffusers, 85
entropy increase, 115
equations for, 111
flow through, 112
Hugoniot equation of, 123
Prandtl relation of, 113
reflected, 135
relations, 112
speed of, 126, 127, 129
stagnation pressure ratio across, 117
strength of, 115
strong, 133
table for, 482–491
thickness of, 110, 164
weak, 132
Nozzle, 64
Area-Mach number relation, 65
converging, 96
converging–diverging operating characteristics of, 69

Scanned by CamScanner

De Laval, 64
isentropic expansion in, 67
overexpanded, 68
sharp cornered, 379
supersonic, 378
underexpanded, 69
Nusselt number, 396

Oblique shock, 171, 173
angle, 172
charts for, 179, 547–548
flow through, 173
intersection of, 203–205
limit as Mach wave, 180
maximum deflection for, 179, 180
reflections of, 202, 203, 207
relations, 172
strong, 180, 181
tables for, 492–525
transformed from normal shock, 173
wave drag, 225
weak, 180, 181
One-dimensional approximation, 47
One-dimensional flow
with area change, 61
with friction, 329–341
with heating, 341–350
Optical methods, 397

Perfect gas, 26
adiabatic flow of, 29
definition of, 26
entropy calculation of, 26
isentropic flow of, 29
isentropic relations, 29
specific heats of, 10, 26
specific heats ratio, 28
speed of sound in, 8
Perturbation
potential, 256
velocities, 256
Piston problem, 126
Pitot
pressure, 89, 90
pressure measurement, 443
probe, 89
tube, 89
Pitot-static tube, 91
Plane wave, 126
Potential equation for compressible flow, 255
Potential function, 253, 254, 261
Prandtl–Glauert rule
for subsonic flow, 271
for supersonic flow, 279
Prandtl–Meyer expansion, 194
Prandtl–Meyer flow, 322
Prandtl–Meyer function, 198
Prandtl number, 393
Prandtl relation
for normal shock, 113
for oblique shock, 174-176
Pressure
dynamic, 88
geometric, 88
Pitot, 89
static, 88
total, 88
transducers, 389
Pressure coefficient, 94
Pressure ratio, critical, 58
Process
adiabatic, 19, 22
irreversible, 24, 36
isentropic, 19, 29
reversible, 19, 23, 24, 36
Propagation of disturbance waves, 12–13
Propagating shock wave, 126

Quasi-one-dimensional flow, 47
Quick-operating valve, 446

Rayleigh line, 342, 344
flow, 341, 353
relation, 352
Rayleigh flow table, 532–537
Rayleigh supersonic Pitot formula, 90, 98
Recovery factor, 393, 394
Reflection
of an expansion fan, 202, 208
from free boundary, 207, 208
like, 207, 208

Scanned by CamScanner

Mach, 219
of normal shock, 135
of oblique shock, 202
unlike, 208
of waves, 374–375
Reservoir, discharge from a, 51
Reversible process, 19
Revolution
body of, 255, 260, 264
boundary condition for, 265
coefficient of pressure, 265
Reynolds number
control, 435
critical, 298
effects, 447
Rotation, 251

Schlieren system, 398, 404
colour, 408
optical components, 407
sensitivity of, 407, 411
Second law of thermodynamics, 23
Seebeck principle, 392
Separation drag, 225
Shadowgraph, 413
Shaft work, 21
Sharp cornered nozzle, 379
Shear stress, 332, 333
Shock cell, 75–76
Shock-expansion theory, 223
Shock polar, 183
relation of, 185–186
Shock tube, 149
applications, 152
diaphragm pressure ratio, 151
equation, 151, 163
flow motion in, 150
Shock wave
definition of, 110
detached, 218
normal (*see* Normal shock waves), 110
oblique (*see* Oblique shock waves), 171
Short duration light source, 409
Silence, zone of, 14, 16
Similarity rule (*see also* Prandtl–Glauert rule, Gothert rule), 271
Simple expansion, 193
Simple friction (*see also* Fanno line flow), 341
Simple region, 201–202, 238, 327
characteristics in, 372
Simple T_0 change, 342
relations for a perfect gas, 343
region, 239
Simple wave, 238, 371
Slip flow regime, 459
Slipstream, 204
Small perturbation theory, 256
Sonic circle, 185
Sonic velocity, 14
Sound, speed of, 6–8, 16, 44
Specific heats, 24
of calorically perfect gas, 24, 26
of perfect gas, 28
ratio, 28
ratio value range of, 28
of thermally perfect gas, 24, 26
Stagnation enthalpy, 21
Stagnation pressure (*see* Total pressure), 22
Stagnation temperature (*see* Total temperature), 116
Starting of supersonic tunnels, 446
starting loads, 447
Static pressure measurement, 444
Streamlines, 47
Strength of shock, 115
Subsonic flow, definition of, 13, 16, 44
Substantial acceleration, 48
Substantial derivative, 48
Supersonic flow, 2, 6, 16
in duct with friction, 329
in duct with simple T0 change, 342
general linear solution for, 310
over a wave-shaped wall, 315–316
Supersonic nozzle, 75–76, 378
design of, 377
Supersonic tunnel diffusers, 421, 447
Surface discontinuity (*see* Slipstream), 204
System
closed (or control mass), 35
open (or control volume), 35

Scanned by CamScanner

Temperature
adiabatic wall, 392
measurement of, 391
ratio of total to static, 31
rise, 11
stagnation, 11, 344
total, 11
Thermal properties, 24
Thermocouple, 392
Thermodynamics, 18, 35
first law of, 19, 21, 35
second law of, 23, 35
Thickness of normal shock, 110, 164
Thin aerofoil theory, 228
Total pressure, friction effect on, 334–336
Total temperature, 11
Transformation, affine, 271, 278, 283
Transonic flow, 16, 17, 44
von Karman rule for, 283, 298, 306

Underexpanded nozzle, 69
Upper critical Mach number, 298
Upper critical Reynolds number, 298

Velocity
critical, 55, 59
dimensionless, M^*, 59
maximum, 52
of shock C_s, 127, 129
of sound, 6–8
perturbation, 255, 256
Velocity plane, 184
Velocity potential, 254, 268
for bodies of revolution, 264
equation of, 260
linearized equation, 257
von Karman rule for transonic flow, 282, 297
Vorticity components, 252

Wave
cancellation of, 375, 383
centred (see Centred expansion waves), 143, 193
compression, 7
expansion (*see* Expansion waves), 143, 171
intersection of, 204, 219
left-running, 44, 45
Mach, 14
normal shock (*see also* Normal shock), 110
oblique (*see also* Oblique shock) , 171
reflection of, from free boundary, 207
reflection of, from rigid wall, 202, 374
right-running, 44-45
Wave drag, 225
Wave motion, 126
Wave-shaped wall
subsonic flow, 316
supersonic flow, 316
Wave speed, 126
Weak shock, 132, 181-182, 189
entropy change in, 191
solution, 180
Wedge
diamond, 224
double, 226
Wind tunnel nozzle, 77, 378

Zone of action, 14, 16
Zone of silence, 14, 16

Scanned by CamScanner

Sixth Edition

GAS DYNAMICS

Ethirajan Rathakrishnan

This revised and updated sixth edition continues to provide the most accessible and readable approach to the study of all the vital topics and issues associated with gas dynamic processes. At every stage, the physics governing the process, its applications and limitations are discussed in-depth.

With a strong emphasis on the basic concepts and problem-solving skills, this text is suitable for a course on Gas Dynamics/Compressible Flows/High-speed Aerodynamics at both undergraduate and postgraduate levels in aerospace engineering, mechanical engineering, chemical engineering and applied physics. The elegant and concise style of the book, along with illustrations and worked examples, makes it eminently suitable for self-study by students and also for scientists and engineers working in the field of gas dynamics in industries and research laboratories. The computer program to calculate the coordinates of contoured nozzle, with the method of characteristics, has been given in C-language. The program listing along with a sample output is given in the Appendix.

In this edition, detailed analytical derivations of the shock polar relation, expressions for the pressure and density ratio across an expansion fan, the relation between the Mach numbers of incident and reflected shocks and the mathematical steps in arriving at the $\theta-\beta-M$ relation of oblique shock are incorporated. Besides, the book includes several new solved examples on important analytical relations. New problems have been added in a number of chapters to help students practice applications of the theory studied.

Some of the Distinguishing Features of the Book

- Concise coverage of the thermodynamic concepts to serve as a revision of the background material.
- Logical and systematic treatment of fundamental aspects of gas dynamics, waves in the supersonic regime and gas dynamic processes.
- In-depth presentation of potential equations for compressible flows, similarity rule and two-dimensional compressible flows.
- Introduction to measurements in compressible flows and optical flow visualization techniques.
- Introduction to rarefied gas dynamics and high-temperature gas dynamics.
- Solutions Manual for instructors containing the complete worked-out solutions to chapter-end problems.

THE AUTHOR

ETHIRAJAN RATHAKRISHNAN, Ph.D., is Professor of Aerospace Engineering at the Indian Institute of Technology Kanpur. He is well known internationally for his research in the area of high-speed jets. The limit for the passive control of jets, called **Rathakrishnan Limit**, is his contribution to the field of jet research. The concept of breathing blunt nose (BBN), which reduces the positive pressure at the nose and increases the low pressure at the base simultaneously, is his contribution to drag reduction at hypersonic speeds. He has published a large number of research articles in many reputed international journals. He is a Fellow of many professional societies, including the Royal Aeronautical Society.

Professor Rathakrishnan serves as the Editor-in-Chief of the International Review of Aerospace Engineering (IREASE) and International Review of Mechanical Engineering (IREME) journals. He has authored two books, *Fundamentals of Engineering Thermodynamics*, 2nd ed. and *Fluid Mechanics: An Introduction*, 3rd ed., published by PHI Learning, Delhi. Besides, he has also authored eight other books, namely, *Gas Tables*; *Instrumentation, Measurements, and Experiments in Fluids*; *Theory of Compressible Flows*; *Gas Dynamics Work Book*; *Applied Gas Dynamics*; *Elements of Heat Transfer*; *Theoretical Aerodynamics*; *High Enthalpy Gas Dynamics*.

ISBN:978-81-203-5316-9

9 788120 353169

₹ 495.00

www.phindia.com

Scanned by CamScanner